

Archive ouverte UNIGE

https://archive-ouverte.unige.ch

Thèse 2013

Open Access

This version of the publication is provided by the author(s) and made available in accordance with the copyright holder(s).

Prediction of passive blood-brain barrier permeability with PAMPA: from small molecules to complex formulations

Le Bourdonnec Passeleu, Céline

How to cite

LE BOURDONNEC PASSELEU, Céline. Prediction of passive blood-brain barrier permeability with PAMPA: from small molecules to complex formulations. Doctoral Thesis, 2013. doi: 10.13097/archive-ouverte/unige:29071

This publication URL: https://archive-ouverte.unige.ch/unige:29071

Publication DOI: <u>10.13097/archive-ouverte/unige:29071</u>

© This document is protected by copyright. Please refer to copyright holder(s) for terms of use.

Prof. Pierre-Alain Carrupt

Prediction of Passive Blood-Brain Barrier Permeability with PAMPA: from Small Molecules to Complex Formulations

THÈSE

présentée à la Faculté des sciences de l'Université de Genève pour obtenir le grade de Docteur ès sciences, mention sciences pharmaceutiques

par

Céline Le Bourdonnec-Passeleu

de

Etaples-Sur-Mer (France)

Thèse n°4573

GENÈVE

Atelier d'impression ReproMail

2013



Doctorat ès sciences Mention sciences pharmaceutiques

Thèse de Madame Céline LE BOURDONNEC PASSELEU

intitulée:

"Prediction of Passive Blood-Brain Barrier Permeability with PAMPA: from Small Molecules to Complex Formulations"

La Faculté des sciences, sur le préavis de Messieurs P.-A. CARRUPT, professeur ordinaire et directeur de thèse (Section des sciences pharmaceutiques), E. ALLEMANN, professeur ordinaire (Section des sciences pharmaceutiques), Mesdames S. MARTEL, docteure (Section des sciences pharmaceutiques), N. ABLA (Merck Serono S.A., Genève) et Monsieur J.-M. SCHERMANN, professeur (Université Paris Descartes et Diderot, Hôpital Fernand Widal, Neuropsychopharmacologie des Addictions Vulnérabilité et Variabilité Expérimentale et Clinique, Paris, France), autorise l'impression de la présente thèse, sans exprimer d'opinion sur les propositions qui y sont énoncées.

Genève, le 24 juin 2013

Thèse - 4573 -

Le Doyen, Jean-Marc TRISCONE

« La science cherche le mouvement perpétuel. Elle l'a trouvé : c'est elle-même. » Victor Hugo

Remerciements

Ces 4 années de thèse ont été jalonnées de rencontres scientifiques, de collaborations fructueuses, de discussions enrichissantes, de réflexions et de partage. J'aimerais donc exprimer ma reconnaissance envers les personnes qui ont contribué de près ou de loin à l'aboutissement de ce travail.

Je tiens tout d'abord à remercier le Professeur Pierre-Alain Carrupt de m'avoir permis d'effectuer ce travail de thèse au sein du laboratoire de chimie thérapeutique et de m'avoir laissé une grande liberté tout au long de ces années de recherche. Merci également pour sa disponibilité et sa compréhension.

J'adresse une profonde reconnaissance au Docteur Sophie Martel, pour la supervision hors pair de ce travail, pour les discussions à la fois brillantes, enrichissantes et sources de nouvelles idées que nous avons pu avoir. Un grand merci pour son soutien, sa patience et sa grande disponibilité. Merci également pour le temps consacré à réviser ce manuscrit.

Je remercie le Professeur Pierre-Alain Carrupt, le Dr Sophie Martel, le Professeur Jean-Michel Scherrmann, le Professeur Eric Allémann et le Docteur Nada Abla, membres du jury, d'avoir accepté de juger ce travail de thèse, pour leur lecture du manuscrit ainsi que pour les remarques critiques qui en ont découlé.

J'adresse ma profonde gratitude au Docteur Florence Miller pour son initiation passionnante au monde de la biologie, de la culture cellulaire, pour les discussions captivantes que nous avons pu avoir. Un très grand merci pour tous ces moments passés ensemble, au travail comme en dehors, pour son amitié, son écoute, sa bonne humeur, les pauses "thés" ou les sorties sportives.

J'ai une pensée particulière pour le Docteur Julien Boccard, pour ses bons conseils, pour sa participation à l'optimisation de la nouvelle membrane artificielle, ainsi que pour ses connaissances inestimables en statistique et analyse de données. Je remercie également le Professeur Serge Rudaz pour son aide et ses connaissances en plans d'expérience.

Je tiens à exprimer ma sincère reconnaissance au Docteur Florence Délie et à Soura Challal pour leur relecture assidue et très enrichissante des chapitres concernant les nanovecteurs et les extraits phytothérapeutiques respectivement.

J'adresse un clin d'œil tout particulier à Céline Pascale, ancienne étudiante pour son excellent travail de Master ayant contribué à une partie du chapitre sur les extraits phytothérapeutiques. Un grand merci pour sa motivation, sa très grande maturité et sa rigueur scientifique, mais aussi pour son amitié et les bons moments passés.

Merci également à Kévin Nadin, ancien étudiant pour son travail de Master sur les nanoparticules polymériques pour son ingéniosité, ses réflexions pertinentes et scientifiques ayant contribué au travail sur les nanoparticules. Merci également à Laure Nicolet, ancienne étudiante ayant également participé au travail sur les nanoparticules.

J'adresse un grand merci aux collègues de pharmacochimie, en particuliers Charlotte Petit et Alban Bujard, avec qui j'ai eu la chance de partager le 418 durant cette dernière année, pour les bons moments passés, pour les discussions scientifiques ou un peu moins, pour leur bonne humeur et leur humour. Merci à Stéphanie Romand, Lucie Ryckewaert, Lionel Sacconay, Nathalie Deschamps, Olivier Cyclet, Vincent Zwick pour les bons moments partagés, en particuliers durant les repas!

Un grand merci aux Docteurs Delphine Cressend et Amandine Guillot pour les très bons moments passés durant les 2 premières années de ma thèse, que ce soit au labo ou en dehors.

Merci à Fabrice Gillérat, Irena Nikolova et Virginie Beyeler pour leur aide au laboratoire, ainsi qu'à Nils Oberhauser, Philippe Eugster, Christophe Francey, les docteurs Alessandra Nurisso, Claudia Avello-Simoes Pires, Karine Vuignier, Julietta Gradinaru, Antoine Daina, Liliana Sintra-Grilo et Elisabeth Favre pour les moments passés ou les discussions agréables que nous avons pu avoir ensemble.

Un grand merci à Sylvia Passaquay-Rion pour son efficacité, son écoute, sa gentillesse et ses précieux conseils.

Merci aux Docteurs Hansjorg Eder, Elisabeth Rivara-Minten et Davy Guillarme ainsi qu'à Jessica Ortelli pour ces excellents moments passés en salle de travaux pratiques! Merci également à Davy pour ses précieux conseils qui ont jalonnés mon travail de thèse.

J'adresse enfin une reconnaissance particulièrement émue à ma belle-famille, qui me soutient depuis tant d'années dans mes démarches, à ma maman, mais surtout à mon mari qui me supporte chaque jours, qui me guide, me soutient et m'encourage dans mes choix, et qui m'a permis de devenir la maman comblée d'une petite Cassandre qui me démontre chaque jour qu'il n'y a rien de plus important que la famille et l'amour de ses proches.

Résumé du travail de thèse

Abbreviations

Chapter 1: Introduction

1-1. Introduction	3
1-2. Physiology of the Blood-Brain Barrier	4
1-2.1. Endothelial cells and tight junctions	5
1-2.2. Astrocytes, pericytes and basal lamina	7
1-2.3. Physiology of the BBB during a pathological event	7
1-2.3.1. Brain tumors	7
1-2.3.2. Alzheimer's disease	8
1-2.3.3. Parkinson's disease	9
1-2.3.4. Epilepsy	9
1-2.3.5. HIV	9
1-2.3.6. Multiple sclerosis	10
1-2.3.7. Stroke	10
1-2.3.8. Diabetes	10
1-2.3.9. Sceptic encephalopathy	11
1-3. Mechanisms of transport through the BBB	11
1-3.1. Paracellular pathway	12
1-3.2. Transcellular pathway	13
1-3.2.1. Passive diffusion at the BBB	13
1-3.2.2. Carrier-mediated transport at the BBB	14
1-3.2.2.1. Carrier-mediated uptake	14
1-3.2.2.2. Efflux transport	14
1-3.2.3. Trans- and endocytosis mechanisms	15
1-4. Strategies for improving brain penetration	16
1-4.1. Invasive techniques	16
1-4.1.1. Direct injection into the cerebrospinal fluid	16
1-4.1.2. Therapeutic opening of the BBB	16
1-4.2. Non-invasive techniques	17
1-4 2 1. The nose-to-brain route	17

1-4.2.2. Inhibition of efflux transporters	17
1-4.2.3. Use of prodrugs	18
1-4.2.4. The Trojan horses or the BBB shuttles	18
1-4.2.5. Drug delivery with nanocarriers	19
1-5. Methods to assess BBB permeability information in drug research	20
1-5.1. In silico models that predict BBB permeability	20
1-5.2. In vitro models for prediction of BBB permeability	22
1-5.2.1. Immobilized artificial membrane	23
1-5.2.2. PAMPA models	23
1-5.2.2.1. Generalities on PAMPA	23
1-5.2.2.2. PAMPA-BBB	24
1-5.2.2.3. Compatibility of PAMPA with new drug delivery strategies	25
1-5.2.3. Cell culture models	25
1-5.2.3.1. Primary cultures	26
1-5.2.3.2. Immortalized cell lines	28
1-5.2.3.3. Cocultures	32
1-5.2.3.4. Cell lines of non-cerebral origin	37
The Madin-Darby Canine Kidney Cell line (MDCK)	37
Caco-2 cells	38
1-5.2.3.5. Adaptation of BBB cell models to new delivery strategies	38
Nanoparticles	38
Liposomes	39
1-5.2.4. Ex vivo experiments: transport across isolated brain microvessels	39
1-5.3. <i>In vivo</i> models	40
1-5.3.1. The brain/plasma ratio	40
1-5.3.2. The brain uptake index (BUI) technique	41
1-5.3.3. The <i>in situ</i> brain perfusion	42
1-5.3.4. The intravenous administration technique	42
1-5.3.5. The brain efflux index	43
1-5.3.6. The unbound brain/plasma ratio: K _{p,uu}	43
1-5.3.6.1. Intracerebral microdialysis	44
1-5.3.6.2. The <i>in vitro</i> brain slice uptake experiment combined with the <i>in vivo</i> K _p .	45
1-5.3.7. Non-invasive imaging techniques	46
1-6. Aim of the thesis	48
References	49

Chapter 2: Parallel Artificial Membrane Permeability Assay for the High-Throughput Prediction of Passive Blood-Brain Barrier Permeability

2-1. Introduction	69
2-2. Material and methods	72
2-2.1. Chemicals	72
2-2.2. PAMPA protocol	72
2-2.3. Permeability equations	74
2-2.4. Optimization of the membrane	74
2-3. Results and discussion	75
2-3.1. Hexadecane, n-octanol and o-nitrophenyloctyl ether as artificial membranes	76
2-3.1.1. Hexadecane	76
2-3.1.2. n-octanol	77
2-3.1.3. Ortho-nitrophenyloctyl ether (o-NPOE)	78
2-3.2. Mixture of solvents as artificial membrane	81
2-3.3. Optimization of the membrane: design of experiment	83
2-3.4. Correlation of HDC/NPOE PAMPA with PAMPA-BBB	87
2-3.5. Correlation of HDC/NPOE PAMPA with models expressing both active and pa	ssive
processes	88
2-3.5.1. Comparison of log P _e ^{HDC/NPOE} with <i>in vivo</i> log PS	88
2-3.5.2. Comparison of log $P_e^{HDC/NPOE}$ with log P_e^{BBCEC} for an extended dataset	90
2-3.5.3. Discussion	91
2-4. Conclusion	92
References	94
Chapter 3: PAMPA as a tool to understand the pharmacological act	ivity of
Hypericum perforatum	
3-1. Introduction	101
3-2. Materials and methods	105

3-2.1. Chemicals	105
3-2.2. HDM-PAMPA	105
3-2.3. HDC/NPOE PAMPA	106
3-2.4. Integrity of the membrane	107
3-2.5. UHPLC-TOF-MS measurements	107
3-2.6. UHPLC-UV measurements	108
3-2.7. Permeability equations	109
3-2.8. Acidic hydrolysis of the SJW extract	109
3-3. Results and discussion	110
3-3.1. Integrity of the membrane in presence of phyto extracts	110
3-3.2. SJW crude extracts and available isolated components	111
3-3.2.1. HDM PAMPA	114
3-3.2.2. HDC/NPOE PAMPA	119
3-3.3. Passive permeability of aglycones and hydrolyzed extract	121
3-4. Conclusion	124
References	126
Chapter 4: Similarities and differences between 4 PAMPA models: a comparative study	
4-1. Introduction	131
4-2. Material and methods	132
4-2.1. PAMPA-BBB	132
4-2.2. HDC/NPOE PAMPA	133
4-2.3. HDM-PAMPA	134
4-2.4. PAMPA-skin	134
4-2.5. Study in classes	135
4-3. Results and discussion	136

4-3.1. Prediction of in vitro passive permeation through the BBB, the GIT and the	e stratum
corneum	13
4-3.1.1. Comparison of PAMPA-BBB with HDC/NPOE PAMPA	14
4-3.1.2. Comparison between HDM-PAMPA and PAMPA predicting BBB permeability	14
4-3.1.3. Comparison of PAMPA-skin with the other models	14
4-3.2. Influence of the retention on the permeability coefficients	14
4-4- Conclusion	15
References	15
Chapter 5: Parallel Artificial Membrane Permeability Assay as a a describe the passive permeability of liposomes and polymeric nai	
through the Blood-Brain Barrier	
5-1. Introduction: nanocarriers as drug delivery systems	15
5-2. Liposomes and polymeric nanoparticles as drug delivery systems	15
5-2.1. Liposomes as drug delivery systems	15
5-2.2. Nanoparticles as drug delivery systems	16
5-2.3. Crossing the BBB with nanocarriers: how does it work?	16
5-3. Materials and methods	16
5-3.1. Chemicals	16
5-3.2. Liposomes	16
5-3.2.1. Formulations and characterization	16
5-3.2.1.1. Liposomes for the preliminary tests	16
Direct extrusion after liposome formation	16
Filtration, followed by extrusion	16
Sonication, followed by extrusion	16
Freeze-thaw procedure followed by extrusion	16
5-3.2.1.2. Liposomes for permeability determination with HDC/NPOE PAMPA	16
Formulation of rhodamine-labeled liposomes	16
Formulation of calcein-loaded liposomes	16
5-3.2.1.3. Liposomes for permeability determination with PAMPA-BBB	16
5-3.2.2. Determination of the entrapment yield	17

5-3.2.3. Drug release study	170
5-3.2.3.1. Drug release from the loaded-liposomes	170
5-3.2.3.2. Drug diffusion in unloaded liposomes	171
5-3.2.4. Permeability studies with HDC/NPOE PAMPA	171
5-3.2.4.1. HDC/NPOE PAMPA with non-loaded liposomes	172
5-3.2.4.2. HDC/NPOE PAMPA with non-loaded rhodamine-labeled liposomes	172
5-3.2.4.3. HDC/NPOE PAMPA with calcein-loaded liposomes	172
5-3.2.5. Permeability studies with PAMPA-BBB	173
5-3.2.6. Quantification with UHPLC-UV	173
5-3.2.7. Transmission Electron Microscopy (TEM)	174
5-3.3. Polymeric nanoparticles	174
5-3.3.1. Formulation	174
5-3.3.2. Entrapment efficiency and entrapment yield	175
5-3.3.3. Formulation of fluorescent-loaded or fluorescent labeled nanoparticles	175
5-3.3.4. Characterization	175
5-3.3.5. Permeability studies with HDC/NPOE PAMPA	176
5-3.3.6. Permeability studies with hCMEC/D3 cell line	176
5-3.4. Permeability equations	177
5-4. Results and discussions	178
5-4.1. Liposomes	178
5-4.1.1. Post formation treatments and liposome composition effects	178
5-4.1.2. Optimization of the extrusion process	180
5-4.1.3. Passive permeation study	181
5-4.1.3.1. HDC/NPOE PAMPA	182
Determination of the integrity of the artificial membrane	182
HDC/NPOE PAMPA with empty labeled liposomes	184
HDC/NPOE PAMPA with calcein-loaded liposomes	185
5-4.1.3.2. PAMPA-BBB	186
Entrapment yield and drug release from liposomes	187
Permeation study	191
5-4.1.4. Conclusion on the permeability of liposomes as drug carriers	196
5-4.2. Polymeric nanoparticles	197
5-4.2.1.Characterization of polymeric nanoparticles	197
5-4.2.2. Permeability studies	198
5-4.2.2.1. HDC/NPOE PAMPA	198
Determination of the integrity of the membrane	198

Permeability of loaded nanoparticles with HDC/NPOE PAMPA	199	
4-4.2.2.2. Permeability experiments with the hCMEC/D3 model	203	
5-5. Conclusion	205	
5-6. Acknowledgments	206	
References	207	
Conclusions and perspectives		
Conclusions	217	
Perspectives	219	
Supporting material		
Appendix 1: Permeability equations	223	
Appendix 2: Preparation of a SJW extract	225	
Appendix 3: Structures of the molecules employed for chapter 4	227	
Appendix 4: Publications	234	

Résumé du travail de thèse

Durant ces dernières décennies l'augmentation considérable de l'espérance de vie a conduit à l'émergence de nouvelles pathologies liées à la vieillesse, dont les maladies neurodégénératives telles qu'Alzheimer ou la démence sénile. Face à ces maladies, les traitements peinent à être développés ou ne parviennent pas à guérir les patients. Parallèlement à ce constat alarmant, les candidats médicaments visant à atteindre une cible au niveau du système nerveux central sont ceux qui subissent le plus haut taux d'échec lors des phases de développement clinique. En effet, lorsqu'environ 10% des candidats médicaments entrant en essais cliniques de phase I parviennent à entrer sur le marché, ce chiffre tombe à 3 à 5% dès lors que la cible thérapeutique est le système nerveux central. Ce constat est en partie dû à la présence de la barrière hémato-encéphalique (BHE), qui protège le cerveau de l'intrusion de composés exogènes grâce à sa structure particulière et la présence de nombreux transporteurs d'efflux. Une détermination de la perméabilité des candidats médicaments très tôt dans la phase de découverte du médicament est donc grandement appréciable, afin de sélectionner au mieux les composés présentant des caractéristiques pharmacocinétiques intéressantes. Dans cette optique, la PAMPA semble prometteuse, de part sa capacité à prédire de façon simple, reproductible et peu coûteuse la perméation passive de candidats médicaments avec un criblage à haut débit.

Durant ce travail de thèse, une nouvelle membrane artificielle composée de 75% d'hexadecane et 25% d'ortho nitrophenyloctyl ether a été développée. Les prédictions de perméation passive de cette nouvelle membrane corrèlent avec différents modèles *in vitro* et *in vivo* connus pour prédire le passage à la BHE. Cette méthode peut également être employée afin de déceler un éventuel transport actif, en établissant une corrélation entre un modèle cellulaire exprimant un transporteur spécifique et le modèle PAMPA pour des composés connus pour subir uniquement une diffusion passive au niveau de la BHE. Le positionnement d'un composé inconnu sur cette représentation permet d'en déduire la nature de son transport.

Cette nouvelle méthode PAMPA a ensuite été adaptée à des formulations plus complexe, telles que des solutions d'extraits phytothérapeutiques ou des suspensions de liposomes et de nanoparticules polymériques, afin de comprendre les modes de perméation de ces formulations. Il a été montré que l'extrait d'*Hypericum Perforatum*, plus connu sous le nom de millepertuis et utilisé dans le traitement de l'anxiété ou de la dépression moyenne, possède une activité pharmacologique similaire à celle de médicaments de synthèse comme l'imipramine, le moclobenide ou la fluoxetine, tout en ayant des effets secondaires moins

importants. Cependant, le véritable mode d'action des constituants de l'extrait, ainsi que l'identification des composés réellement responsables de l'effet anxiolytique observé ne sont pas encore clairement identifiés. Le postulat est que l'action thérapeutique serait due à l'hypéricine, à l'hyperforine, aux flavonoides, ou une combinaison de ces constituants. De plus, un effet synergique de l'extrait ne serait pas à exclure. La membrane artificielle HDC-NPOE PAMPA a donc été utilisée afin d'isoler une éventuelle composante passive du passage à travers la BHE. Les résultats ont montré une absence de perméation passive audelà de la limite de détection de la technique analytique employée, et ce pour l'ensemble des composés constituant l'extrait natif, incluant l'hypéricine, la pseudohypéricine et quelques flavonoides glycosylés. Une étude plus poussée effectuée avec des flavonoides aglycones a cependant montré un passage passif de certains de ces aglycones, comme le kaempferol. Il a donc été conclu que l'effet anxiolityque observé peut être dû à certains composés aglycones, capables de traverser la BHE de façon passive, ou à un transport actif de l'hypéricine ou des flavonoides, grâce notamment aux transporteurs du glucose. Aucune conclusion n'a cependant pu être tirée quant au rôle de l'hyperforine.

Les similitudes observées lors de l'étude de l'extrait d'hypericum perforatum sur les PAMPA estimant le passage passif à travers le tube intestinal et la BHE ont conduit à l'élaboration d'une étude comparative de 4 modèles PAMPA, prédisant la diffusion passive à la BHE (PAMPA-BBB et HDC/NPOE PAMPA), au niveau du tube intestinal (HDM-PAMPA) et à travers le stratum corneum (PAMPA-skin) sur une base de données de 88 composés. Cette étude a montré l'existence de ressemblances entre les PAMPA-BBB, HDC/NPOE PAMPA et HDM-PAMPA pour les composés ayant une diffusion rapide ou moyenne à travers la membrane artificielle. Une discrimination plus importante a été observée pour les composés les moins perméants. Ceci indique donc que ces 3 modèles ne sont pas très spécifiques pour les composés les plus aptes à diffuser de façon passive. De plus, une relation linéaire inverse a été montrée entre le pourcentage de passage et la rétention sur la membrane artificielle pour les PAMPA-BBB, HDC/NPOE PAMPA et PAMPA-skin, indiquant un effet réservoir de la membrane.

La technique PAMPA a également été utilisée pour tenter de comprendre le mécanisme de passage de nanovecteurs colloidaux au niveau de la BHE. La HDC-NPOE PAMPA a montré l'absence d'interactions entre les liposomes ou les nanoparticules et la membrane artificielle. La PAMPA-BBB, constituée de phospholipides, a alors été utilisée afin de déterminer un éventuel passage passif par échange de phospholipides entre les liposomes et la membrane artificielle. Cette étude a démontré une diminution de la perméation passive des composés hydrophobes, et aucune amélioration de perméation pour les composés hydrophiles. L'hypothèse de certains chercheurs prônant un perméation des vecteurs colloidaux par endocytose s'avère donc une piste des plus probables.

Abbreviations

ABC ATP-binding cassette family

AD Adherens junction

ADMET Absorption, distribution, metabolim, excretion, toxicity

AIDS Acquired immunodeficiency syndrom

ALP Alkaline phosphatase

AMT Adsorptive mediated transcytosis

ATP Adenosine triphosphate

BBB Blood-brain barrier

BBCEC Bovine brain capillary endothelial cell

BCRP Breast cancer resistant proteins

BMEC Brain microvascular endothelial cells

BUI Brain uptake index

CACO-2 Human colorectal adenocarcinoma cell line

cAMP Cyclic adenosine monophosphate

CAT Cationic acid transporter
CNS Central nervous system

CSF Cerebrospinal fluid CYP450 Cytochrome P 450 DMSO Dimethylsulfoxide

γ-GT Gamma glutamyl transpeptidase

GIT Gastro-intestinal tract
GLUT Glucose transporter

HIV Human immunodeficiency virus

HTS High-throughput screening

K_{p.uu} Unbound brain to plasma ratio

LAT Large neutral amino-acid transporter

LDL Low-density lipoprotein

log BB Logarithm of the brain to plasma ratio

log P Partition coefficient in the system octanol/water, for neutral molecules

log P_e Effective permeability coefficient

log PS Logarithm of the BBB permeability-surface area

MAO Monoamine oxidase

MCT Monocarboxylic acid transporter

MDCK Madin-Darby canine kidney cells

MDR Multidrug resistance gene mRNA Messenger ribonucleic acid

MRP Multi-drug resistance associated proteins

MS Mass spectrometry NCE New chemical entity

OATP Organic anion transporter

PAMPA Parallel artificial membrane permeability assay

PCR Polymerase chain reaction

PD Parkinson's disease PEG Polyethylene glycol

Pgp P-glycoprotein

PK pharmacokinetics

PVDF Polyvinylidene fluoride

RMT Receptor mediated transcytosis

RT-PCR Reverse transcription polymerase chain reaction

SJW St John's Wort

SLC Solute carrier family

TEER Trans-endothelial resistance

TJ Tight junction

TOF Time of flight detector, in mass spectrometry

UHPLC Ultra high pressure liquid chromatography

UWL Unstirred water layer

ZO Zonula occludens



Methodology to assess drug permeation through the Blood-Brain Barrier for pharmaceutical research

1-1. Introduction

The high attrition rate of drug candidates during all stages of the drug development process is a critical issue for both economic and treatment reasons (figure 1-1). It has been shown that the major factors leading to the attrition of new chemical entities (NCEs) during drug development results from inadequate ADMET (absorption, distribution, metabolism, excretion, toxicity) properties, especially poor pharmacokinetic (PK) properties ¹, together with a lack of potency and safety issues. Particularly for central nervous system (CNS) diseases, the lack of permeation through the blood-brain barrier (BBB) prevents the active compound from reaching its target. Because of the huge costs associated with bringing a drug to the market, it is important to generate information on the ADMET profile of candidate drugs as early as possible during the drug discovery process, in order to understand how the drug candidate would behave and distribute if administered in humans. A thorough ADMET evaluation decreases the risk of attrition during clinical phases or even possible withdrawal from the market ². ADMET issues are even more important for drug candidates that target the CNS. Only 3 to 5% of CNS drug candidates that enter phase I clinical trials are successfully launched compared to approximately 10% for all compounds ^{2, 3}. The particular organization of endothelial cells, which are connected by tight junctions and form the BBB, is a further obstacle to the CNS penetration of drug candidates. Combined with numerous transporters, such as efflux and uptake transporters, and drug-metabolizing enzymes present at the luminal side of the BBB, crossing the BBB is a big challenge when dealing with CNS diseases, such as Alzheimer's disease, Parkinson's disease and Huntington's disease. By contrast, when other organs are targeted, it is critical that BBB penetration is either null or reduced to limit adverse effects. Therefore, determining the distribution of a drug in and around the brain is important when developing a new compound.

Different methodologies exist to evaluate the permeation potential of new chemical entities. The choice of strategy relies primarily on the type of throughput (driven by the number of compounds that require testing) and the type of information needed. This implies that scientists should master these strategies to choose the proper methodology based on the information required, and they should be able to correctly interpret the results. Here, the different methods available for physicochemists, biologists and ADMET scientists at different stages of the drug discovery and development processes to select drug candidates that cross the BBB are reviewed. After describing the physiology of the blood-brain barrier, *in silico*, *in vitro* and *in vivo* approaches to determine BBB permeation will be explored. Drawbacks and advantages will be critically examined, and key experimental and/or

interpretation points will be highlighted. Finally, because an increasing number of strategies to enhance drug penetration require complex formulations, such as micro/nano-carriers, application of these different screening methods to modern drug development efforts will be discussed.

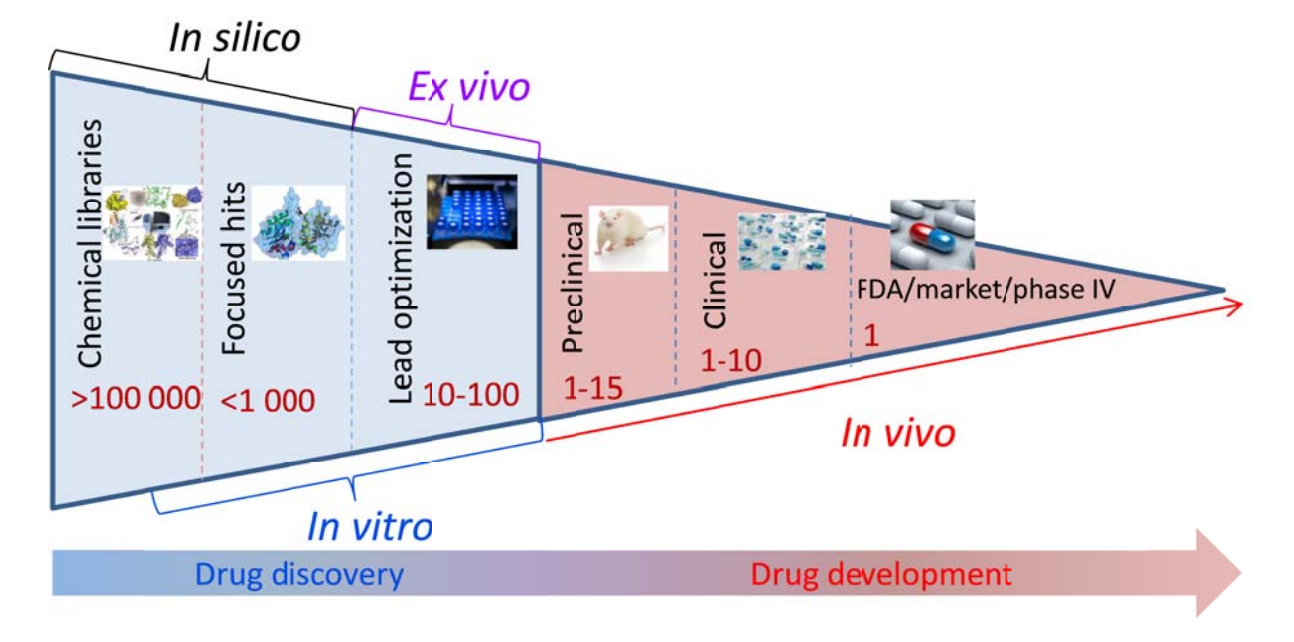


Figure 1-1: Drug discovery and development processes, associated with the number of compounds generally involved in each phase.

1-2. Physiology of the Blood-Brain Barrier

In 1885, the studies of Paul Ehrlich first highlighted the presence of the BBB. In his studies, Ehrlich intravenously injected various dyes, and he observed that almost the entire body was stained but not the brain ^{4, 5}. Edwin Goldman, a student of Ehrlich's, continued this research using the dye trypan blue. He found that after intravenous injection of the dye, the choroid plexus and meninges were stained; however, no dye was recovered in either the brain or cerebrospinal fluid (CSF) ⁶. In another experiment, he injected the dye directly into the CSF and found that the entire brain was stained but not the rest of the body ⁷. These experiments demonstrated the existence of a biological barrier between the brain and the rest of the systemic circulation, the blood-brain barrier.

Over many years of research, our knowledge of the BBB has increased, and scientists are now aware that the BBB is a structure with complex cellular organization that separates the brain parenchyma from the systemic circulation. It is of key importance for the

maintenance of brain homeostasis, which is essential for good neuronal and synaptic activities $^{8-12}$, and represents the main route by which compounds reach the CNS. Moreover, the BBB also acts as a metabolic barrier due to the presence of numerous enzymes $^{13, 14}$, including peptidases, γ -glutamyl transpeptidase (γ -GT), alkaline phosphatase (ALP), nucleotidases, cytochromes P450 (CYP450) and monoamine oxidase (MAO). These enzymes can metabolize potentially harmful drugs to inactive CNS compounds, convert an inactive drug to its active CNS metabolite or degrade them into metabolites or substrates of specific efflux transporters, such as the P-glycoprotein (Pgp/ABCB1) or multidrug resistance proteins.

The BBB consists of brain capillaries that support endothelial cells and are surrounded by astrocytic end-foot processes ¹⁵. It is the central part of the neurovascular unit, which is responsible for communication between endothelial cells, astrocytes, pericytes and neurons ¹⁴ (figure 1-2).

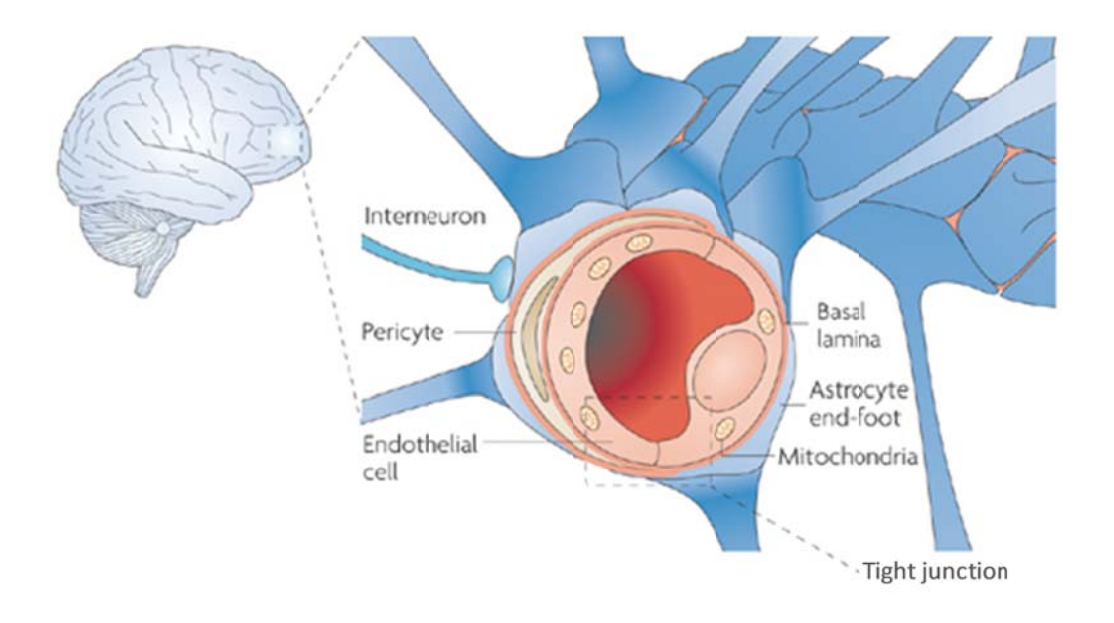


Figure 1-2: Section of a brain capillary ¹⁴

1-2.1. Endothelial cells and tight junctions

The specificity of the endothelial cells comprising the blood-brain barrier compared to the endothelial cells in the rest of the body is based on their organization. Cerebral endothelial cells are connected by intercellular proteins. Occludins, claudins and junctional adhesion molecules, together with cytoplasmic accessory proteins, including zonula occludens-1 (ZO-1), ZO-2, ZO-3 and others, are transmembrane proteins that are

responsible for the formation of tight junctions (TJs) 14 that seal the paracellular pathway $^{16-18}$ and make the brain nearly inaccessible to polar compounds that are not the substrates of specific transporters 19 . Adherens junctions (AJs) also contribute to the junction complex by joining the membrane proteins, cadherins, to the intermediary proteins, catenins, to form adhesive linkages between endothelial cells (figure 1-3) 20 . The TJs in cerebral capillaries are approximately 50 to 100 times tighter than the TJs in peripheral capillaries 21 and lead to a high transendothelial electrical resistance (TEER) of approximately 1500-2000 Ω .cm² compared to 3-33 Ω .cm² for other tissues $^{22, 23}$, which is due to the restriction of small ions, such as Na⁺ and Cl⁻, from passing through the TJs. Moreover, BBB endothelial cells differ from other endothelial cells in the low number of endocytotic invaginations at the luminal portion of the cell membrane, which leads to very limited pinocytic transcellular transport $^{12, 20, 24-28}$, a large number of mitochondria 29 and the polarized expression of transporters and receptors for active transport 30 . Indeed, the brain endothelium has only 3-6 pinocytic vesicles per µm³ compared to 82-93 per µm³ for the peripheral endothelium $^{31, 32}$.

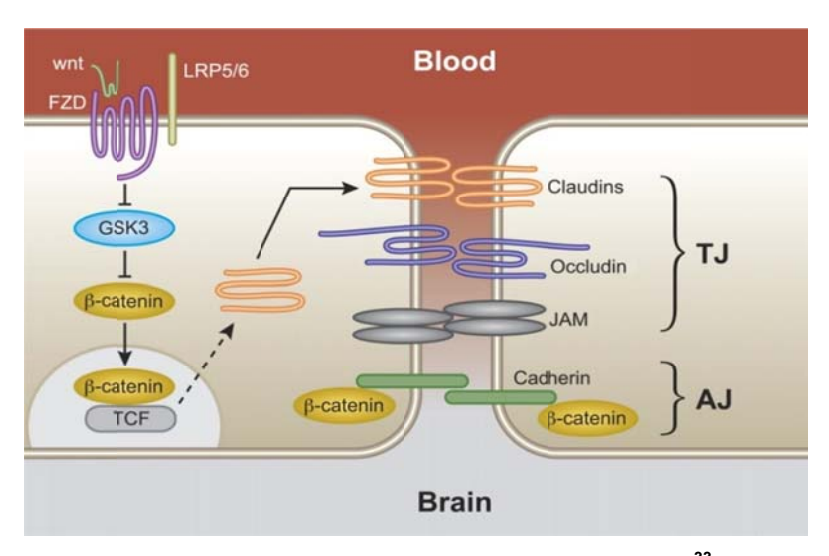


Figure 1-3: Proteins forming the tight-junctions at the BBB ³³.

Many transmembrane proteins are expressed on the luminal and/or abluminal membranes of the endothelium to transport nutrients that are essential for the brain and to eliminate waste products of metabolism. In particular, proteins, such as GLUT-1 (glucose transporters), transport polar nutrients; Na-ATPase and K-ATPase transport sodium and potassium ions respectively; insulin or transferrin receptors transport proteins ^{8, 24, 28, 34, 35}, and organic anion transporting proteins (OATP) ³⁶ transport hormones, opioids, steroids, statins, cardiac glycosides, anticancer drugs and antibiotics ¹⁵. These transporters all play important

roles in the maintenance of cerebral equilibrium. Moreover, efflux transporters, such as P-gp/ABCB1 ³⁷ or BCRP ³⁸ are highly expressed on the luminal side of endothelial cells.

1-2.2. Astrocytes, pericytes and basal lamina

Astrocytes are important cellular constituents of the neurovascular unit. They are linked to interneurons and thus to the entire cerebral microenvironment ¹⁹. Astrocytes represent approximately 50% of the total mammalian brain volume ³⁹. Moreover, some studies indicate that astrocytes play a role in the upregulation of BBB properties, such as tighter tight junctions ^{40, 41} and the expression of specific polarized transporters, such as P-gp/ABCB1 ¹⁴ and the enzymatic system ^{14, 19}, due to astrocyte-endothelial cell interactions. This upregulation of BBB properties by astrocytes is synergistic with pericytes, neurons and perivascular macrophages ⁴². Astrocytes also have different functions, such as the formation of an activity at synapses, energetic and redox metabolism, intercellular communication, homeostasis ³⁹ and glucose transport from the systemic circulation to the brain.

Similar to astrocytes and neurons, pericytes are part of the neurovascular unit and play a role in the maintenance of both BBB properties and cerebral homeostasis. Recent studies have also indicated a role for pericytes in hemostasis, as well as in immune and phagocytic processes ^{20, 43}. Pericytes surround endothelial cells and both cell types are supported by the basal lamina. The integrity of basal lamina allows the maintenance of BBB properties, due to its anchoring role, but the basal lamina does not have a significant impact on the permeability of the BBB. However, under specific pathological conditions or in response to an aggressive stimulus, its thickness can vary, which perturbs the normal function of the BBB ⁴³.

1-2.3. Physiology of the BBB during a pathological event

1-2.3.1. *Brain tumors*

Brain cancer regroups different forms of tumors developing in the brain. The most frequent brain tumor is the glioma, in half of the cases, originated from glial cells. Brain tumors can either be primary cancer, resulting from an abnormal growth of malignant cells

within the brain, or secondary, resulting from metastasis from a cancer initiated in another organ.

In brain tumors, the barrier property is altered, because of the leakier feature of tumor capillaries compared to healthy brain capillaries, with an altered basal lamina ³⁴, and the possible accumulation of growth factor and proinflammatory cytokines ⁴⁴. The vascular endothelial growth factor, endogenously produced in high amount in brain tumors, favors endocytosis of cadherin, leading to a disruption of the endothelial monolayer and higher transcellular permeability.

Moreover, the proteins claudin and occludins, governing the tightness of the tight junctions, are downregulated, implying larger intercellular tight junctions than in healthy patients ¹⁹. Paracellular pathway is therefore enhanced, homeostasis is not respected anymore, and vasogenic cerebral edema often occurred.

1-2.3.2. Alzheimer's disease

Alzheimer's disease is the most common neurodegenerative disease, characterized by a loss of cholinergic neurons, associated with a subsequent diminution of acetylcholine neurotransmittors.

On Alzheimer's disease patients, endothelial cells fail to fully limit the entry of leukocytes into the brain. Postmortem observations of brain tissue from Alzheimer's disease patients revealed an increased number of pinocytosis, enhancing the transendothelial entry of proteins or immune cells. Moreover, an alteration of the expression of mdr1 gene, coding for Pgp/ABCB1⁴⁵ leads to an alteration of the activity of Pgp/ABCB1. Additionally, an uptake of β -amyloids by the receptor for advanced glycosylation products in the brain is present. The clearance of these β -amyloids is provided by lipoprotein receptor protein on healthy subjects. In Alzheimer's disease patients, the expression of the receptor for advanced glycosylation products is enhanced, while the activity of the lipoprotein receptor protein is altered, leading to an accumulation of β -amyloids in senile plaques in the brain ³⁴.

Moreover, Alzheimer's disease patients exhibit functional and morphological alterations of astrocytes, leading to hypertrophic astrocytes as well as upregulation of filamentous proteins that aggregate ³⁹. Therefore, astrocytes do not fulfill their protective role anymore, which keep going inflammation.

1-2.3.3. Parkinson's disease

Parkinson's disease is the second most common neurodegenerative disease impairing the CNS. It is characterized by the progressive disappearance of dopaminergic neurons in *substancia nigra pars compacta* 46 . Additionally, expression of monoamine oxidase B, involved in the breakdown of dopamine, is increased. The level of produced dopamine is therefore diminished, leading to a deficit in nervous response. The disease is also characterized by intraneuronal inclusions, called Lewy bodies, consisting of a dense core mainly composed of α -synuclein fibrils. The direct consequence is the apparition of motility troubles (resting tremor, bradykinesia, muscle rigidity, instability).

The development of Parkinson's disease has been linked to polymorphisms of the gene coding for Pgp/ABCB1 (mdr1) ⁴⁷. Moreover, Parkinson's disease patients also suffer from transient BBB opening, even if the main critical events occur at the blood-cerebrospinal fluid barrier ⁴⁴.

1-2.3.4. Epilepsy

Epilepsy is a common neurological disorder, resulting from an abnormal and excessive neuronal activity and characterized by seizures.

On the epileptogenic sites, BBB is opened and does not assure its primordial functions as a barrier. A phenomenon of upregulation of ABC transporters, such as Pgp/ABCB1, is observed on astrocytes and endothelial cells, to counterbalance this opening ⁴⁸. This upregulation of efflux transporters have a direct influence on the bioavailability of the patient's treatment, limiting the penetration of substrates of these transporters.

1-2.3.5. HIV

Human Immunodeficiency Virus (HIV) is a retrovirus causing the Acquired Immunodeficiency Syndrom (AIDS). This virus impairs the immune system, allowing life-threatening opportunistic diseases to develop.

During HIV infection, expression of claudin-5 and occludins are reduced, leading to a loss of expression of the tight junctions. Moreover, morphological modifications such as the thinning of the basal lamina or the loss of endothelial glycoproteins are observed in HIV patients ⁴⁹. Thus, BBB is altered and HIV virus penetrates in the CNS generally *via*

macropinocytosis ³⁴, leading to neurological disorders, such as HIV induced encephalopathy. Moreover, permeability from brain to blood of this virus is very low, transforming the CNS in a viral reservoir for HIV ⁵⁰. HIV encephalopathy also promotes the activation of immune cells, which release toxins and cause neuronal disorders ²⁰.

1-2.3.6. Multiple sclerosis

Multiple sclerosis is an inflammatory disease of the CNS, characterized by a demyelination of axons and neuronal damages, perturbing the communication between neurons. During multiple sclerosis, adherens proteins constituting the tight junctions are degraded, generally by dephosphorylation of occludins, causing a BBB disruption and a loss of homeostasis that remove the brain protection against macromolecules. Therefore, activated immune cells have free access to the CNS, damaging the nervous cells and generally leading to apoptosis ^{12, 51, 52}.

1-2.3.7. Stroke

Stroke is the consequence of either ischemia or hemorrhage. In both cases, an insufficient blood flow supplied the brain. Under such circumstances, BBB is disrupted, which may lead to a vasogenic brain edema, as for brain tumor patients, with a rise of intracranial blood pressure during post-ischemic reperfusion ⁵³. During ischemia, pinocytic vesicles formation is enhanced, some may merged and form aqueous routes through the endothelial cell, enabling the transport of non-specific proteins. This vesicles formation is fuelled by an increased nitric oxide formation, inflammatory mediators occurring during the stroke event, as well as abnormal elevated level of neurotransmitters. Nitric oxide has been shown to enhance BBB permeability, while the elevated level of neurotransmitters augments pinocytosis ⁵³. All these pathological processes converge to the promotion of vasogenic brain edema.

1-2.3.8. Diabetes

Diabetes is a metabolic disease characterized either by a deficient production of insulin, or a resistance to insulin. Both cases lead to a high systemic sugar concentration.

Even if diabetes is often associated with renal, ocular and blood diseases, it also causes an increased risk of cerebrovascular diseases ³². Studies performed on diabetes induced rats indicated an increased paracellular permeation of small molecules, due to a decreased in tight-junction proteins, particularly occludin and zonula occludens-1. Moreover, Pgp/ABCB1 expression seems to be decreased, leading to an increased permeability of Pgp/ABCB1 substrates, potentially toxic for the brain ⁵⁴.

Diabetes and Parkinson's disease have often been associated and disclose common pathological features, such as inflammation, oxidative stress and apoptosis ⁴⁶. Inflammation was shown to be the main cause of destruction of both pancreatic islet and dopaminergic neurons.

1-2.3.9. Sceptic encephalopathy

Sceptic encephalopathy is associated with numerous events damaging the BBB: brain hypoxia, decreased cerebral blood flow and cerebral edema. These symptoms are thought to result from inflammatory mediators, abnormal neurotransmitters composition of the immune system, deficient astrocytes and neuronal degeneration ²⁰.

1-3. Mechanisms of transport through the BBB

The BBB is one of the most important barriers in the body. The permeation of drugs through the BBB is subject to a strong selection depending on the physicochemical properties of the compound, such as lipophilicity, molecular weight, permeability coefficient (log P_e), molecular volume, ionization state, and/or their affinity to specific transporters (efflux or uptake transporters) that are present in the cellular space ⁵⁵⁻⁵⁷. Therefore, the BBB may not be as impermeable as indicated by the first experiments with dyes. The cellular organization of the BBB and the presence of transmembrane proteins enable a selective regulation of the passage of molecules from the blood to the brain. This is of particular importance for the uptake of essential nutrients or active CNS drugs and protects the brain from undesirable compounds, which could be toxic to the CNS.

The specificities of brain capillaries make of the BBB an effective and efficient barrier that limits the entry of xenobiotics into the brain. Molecules present in the blood stream can

reach the CNS by two different pathways, the paracellular pathway, which is between 2 endothelial cells through the tight junctions, or the transcellular pathway, which is through an endothelial cell.

Molecules that reach the CNS via the transcellular pathway can diffuse passively, can be actively transported by specific transporters or can undergo endocytosis. For example, small lipophilic molecules, such as $\rm O_2$ and $\rm CO_2$, or very small compounds, such as ethanol, water or diverse lipophilic drugs, can freely diffuse through the lipid barriers of endothelial cells 19 .

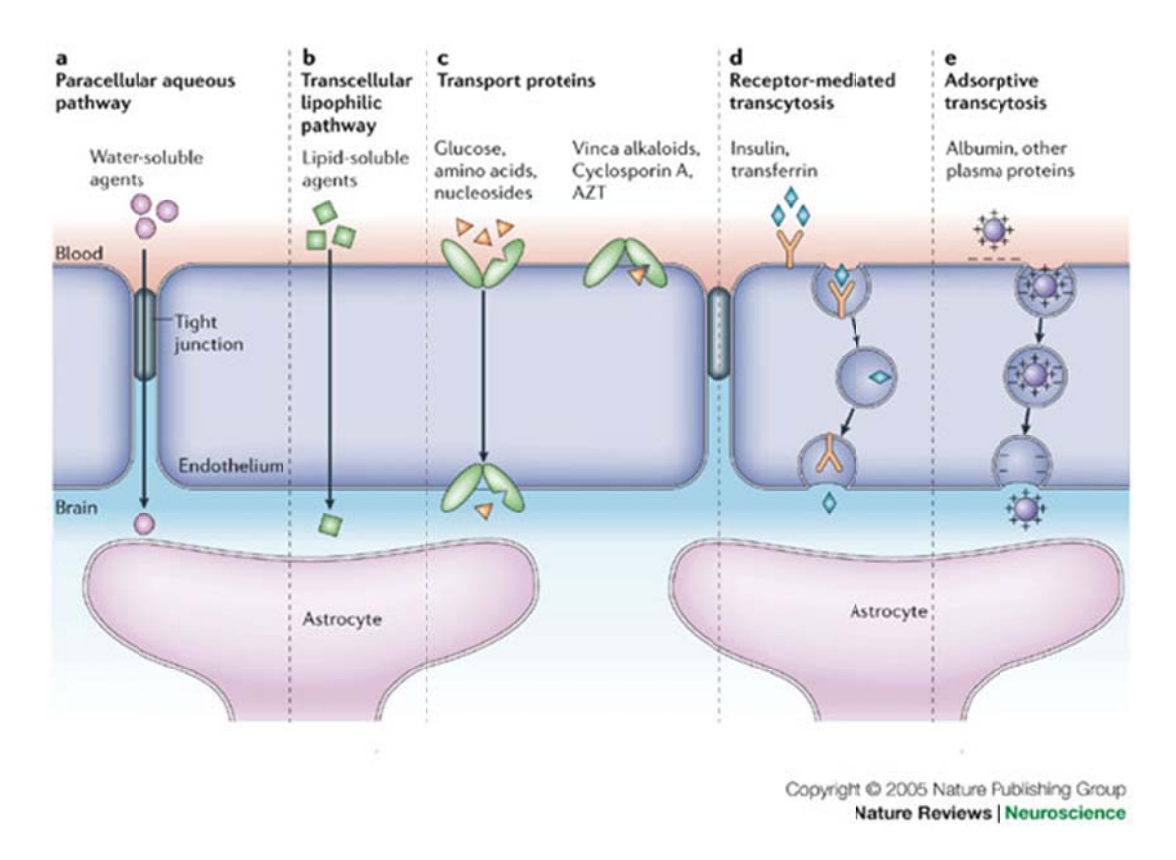


Figure 1-4: Schematic view of the different pathways that can be involved in the permeation of compounds through the BBB 19 .

1-3.1. Paracellular pathway

The paracellular pathway is a diffusion process that occurs between two cells. This pathway is limited to small hydrophilic molecules such as cimetidine, ranitidine, famotidine ^{58, 59} and furosemide ⁶⁰, which are hypothesized to be absorbed *via* the paracellular pathway in the intestinal tract, due to the aqueous surroundings of the cells ⁶¹. However, due to the presence of tight-junctions between two cerebral endothelial cells, this route is extremely limited and nearly non-existent at the BBB, although under some pathological conditions,

tight junctions and adherens junctions between endothelial cells may be altered. This alteration enables leakage, which can allow passage of plasma proteins, fluids or immune cells into the brain ^{12, 19, 44, 45, 48, 51, 52, 54}. The selectivity of this route is limited to either size or shape features.

1-3.2. Transcellular pathway

Due to the complex tight junctions, therapeutic molecules have to follow a transcellular pathway through the BBB to reach the CNS rather than the paracellular pathway as in most endothelia ¹⁹. Compounds may be transported throughout the endothelial cells either by passive diffusion or by active transporters.

1-3.2.1. Passive diffusion at the BBB

Passive diffusion is one of the most straightforward mechanisms of permeation. This process requires a concentration gradient but no energy and no specific protein carriers. Diffusion requires physicochemical interactions between the compound and the membrane that must be crossed ^{55, 56}. Moreover, because there is no specific binding site, passive transport is not affected by stereochemistry and there is no saturation and no possible inhibition of the diffusion process ⁶². These observations indicate that passive diffusion is concentration-independent: the process occurs till equilibrium between the blood and the brain.

Passive diffusion through the BBB is highly affected by lipophilicity and the size of the compound ⁶³⁻⁶⁵. It was demonstrated that compounds with a molecular weight greater than 500-600 Da poorly permeated the BBB ^{66, 67}. However, when combined with good lipid solubility, molecules with molecular weights greater than 500 Da have interesting BBB permeability characteristics ⁶⁸. Similarly, the lipophilicity of compounds should be high enough to allow for good affinity with lipidic membranes, but the lipophilicity should not be too high so as to avoid trapping of the compound within the membrane and bioaccumulation. By contrast, due to the amphiphilic nature of the membrane, ionization will greatly impact diffusion because ionized compounds are highly hydrophilic and therefore will have poor interactions with the hydrophobic part of the membrane ⁶⁹.

1-3.2.2. Carrier-mediated transport at the BBB

A certain number of uptake or efflux proteins are expressed at the BBB. These transporters are present on the luminal and/or abluminal membranes of the endothelium and regulate the entry of their specific substrates ^{19, 70}. Uptake proteins transport molecules from the blood to the brain. These transport systems allow the permeation of essential cerebral nutrients, such as glucose or amino acids, and either limit or prevent the passage of undesired or potentially toxic molecules. By contrast, efflux proteins, such as P-glycoproteins (P-gp/ABCB1), multidrug-resistance multidrug resistance associated proteins (MRP) or the breast cancer resistant protein (BCRP) ⁴⁹, excrete their substrates out of the brain by pumping the substrates into the blood stream. At the BBB, P-gp/ABCB1 are highly expressed and a certain number of NCEs are substrates for this protein ⁶².

1-3.2.2.1. Carrier-mediated uptake

Carrier-mediated transport can be either active or facilitated. When the transport of a substrate needs either direct energy which requires ATP binding and hydrolysis to mediate the primary active transport process, such as transporters of the ABC superfamily, or indirect energy, which is driven by ion gradients that result from ATP-dependent primary transport, such as many transporters of the SCL superfamily, that is an active carrier-mediated transport, whereas when transport requires only a concentration gradient and a transporter protein, it is a facilitated carrier-mediated transport. Both types of transport are saturable, competitive and stereospecific ⁶². Moreover, these transports imply a specific interaction between the carrier proteins and the substrate.

Some examples of transporters are the glucose transporter (GLUT-1), the monocarboxylic acid transporter (MCT1), the large neutral amino-acid transporter (LAT1) and the organic anion transporters (OATP) ^{32, 71}. Specific transporters are also present for small ions, such as Na⁺, K⁺ or Cl̄, in both the blood to brain and brain to blood directions. These ion transporters maintain brain homeostasis because ionic disequilibrium between the blood and brain can have serious effects, such as brain edema.

1-3.2.2.2. Efflux transport

Efflux transport is an energy-dependent, active process, which pumps metabolites out of the brain into the blood stream or prevent the entry of substrates of these efflux proteins.

The most well-known and studied efflux proteins belong to the ATP binding cassette (ABC) family, including the P-glycoproteins (P-gp/ABCB1), the MRP and the BCRP. These active transport processes are essential for brain protection because they prevent the cerebral penetration of potentially harmful drugs and also excrete waste products and metabolites. The expression of most efflux proteins is regulated by astrocytes or pericytes ⁷².

1-3.2.3. Trans- and endocytosis mechanisms

Brain penetration is not strictly limited to small lipophilic molecules or compounds shuttled by uptake proteins. Larger molecules, such as peptides, proteins or even viruses, which are too large for a carrier-mediated process, can also penetrate the BBB *via* the few pinocytic vesicles that are present in endothelial cells. These large molecules can be transported either by receptor-mediated transcytosis (RMT), adsorptive-mediated transcytosis (AMT) ¹⁰ or fluid phase endocytosis ³².

During RMT, the ligand specifically binds to the receptor protein and is transported through the cell. The best characterized and utilized RMT protein is most likely the transferrin receptor, which has also been extensively studied for the delivery of immunoliposomes ^{73, 74}. Other well-known receptors include the low-density lipoprotein (LDL) receptor and the insulin receptor ³².

During AMT, a non-specific interaction occurs between the solute and the surface protein. Peptides, glycopeptides, glycoproteins, and viruses are transported by this pathway ³².

During a fluid phase endocytosis event, there is no contact between the solute and the protein. The substrate is situated close to the membrane, which deforms and encircles both the solute and some extracellular fluid and transports the entire vesicle to the abluminal side. Lucifer yellow is transported in this manner ³².

1-4. Strategies for improving brain penetration

The BBB is a serious obstacle for the treatment of neurodegenerative diseases that require CNS action ⁵⁵. Because of its physical organization, the BBB prevents the passage of many drugs that target the CNS. Therefore, even if a potential drug has potent activity against its target, it may not be able to cross the BBB and will most likely be discarded during the drug development process. Moreover, metabolic features of the BBB may also prevent a CNS active drug from crossing the endothelial membrane because the therapeutic efficacy of the drug can be either inactivated or decreased by enzymes at the BBB. To circumvent the BBB and allow an active CNS compound to reach its target, many strategies exist, which may be either invasive or non-invasive with respect to the BBB.

1-4.1. Invasive techniques

1-4.1.1. Direct injection into the cerebrospinal fluid

Direct injection of drugs into the cerebrospinal fluid was the first strategy used to circumvent the BBB, primarily to target brain tumors. This technique is not very efficient because there is a poor diffusion between the cerebrospinal fluid and the brain and it is quite invasive ⁷⁵. Nau *et al.* demonstrated a 3-fold increase in the mortality of infants with Gramnegative meningitis treated with an intraventricular injection of aminoglycosides combined with intravenous injections of antibiotics compared to intravenous injection of antibiotics alone ⁷⁵, meaning that this technique should be employed as a last resort, when all possible therapeutic strategies have failed.

1-4.1.2. Therapeutic opening of the BBB

Therapeutic opening of the BBB is a reversible process. Because of specific molecules which generate a hyperosmolar environment, the BBB loses its barrier properties, thus enabling passage of the therapeutics into the brain before the BBB regains its functions. A transient brain opening is generally obtained by intra-carotid injection of mannitol or alkyl glycerol, which creates hyperosmolar conditions on the systemic circulation side of the BBB and causes a reversible shrinkage of the endothelial cells and a loss of adherens and junctional proteins, leading to a paracellular opening between endothelial cells $^{76, 77}$.

However, depending on the mediator used to momentarily disrupt the BBB, an increase in transcellular permeability can also occur, such as with tumor necrosis factor α , which leads to the permeation of opportunistic toxic compounds. Moreover, the duration of the opening of the BBB will depend on the mediator used. Histamine provides a rapid and temporary opening, whereas thrombin causes drastic modifications of the endothelial cytoskeleton resulting in prolonged opening of the BBB with difficulties in returning to the basal state 44 .

This difficult strategy must be handled with care and vigilantly monitored to prevent damage to the brain parenchyma and edema, which may be fatal. However, when performed properly, therapeutic opening of the BBB allows delivering active drugs into the CNS, which would not otherwise has reached the brain. This strategy is primarily used for the treatment of brain tumors or life-threatening diseases that have not been cured with less invasive treatments.

1-4.2. Non-invasive techniques

1-4.2.1. The nose-to-brain route

To circumvent the BBB and enter the brain parenchyma, alternative strategies for drug delivery such as the nose-to-brain route are useful. In the nose-to-brain pathway, the therapeutic compound can be directly transported to the brain by absorption in the nasal mucosa and transport *via* the olfactory routes ⁷⁸⁻⁸⁰. Therefore, localization of the olfactory route close to a brain region that is exempt from the BBB allows for the circumvention of the barrier, which allows the drug to reach the CNS ⁸¹. This route has been evaluated for the permeation of cocaine ⁸², as well as formulations such as the alprazolam-loaded solid lipid nanoparticles ⁸³ or even neuropeptides ⁸⁴. This strategy suffers primarily from poor bioavailability, which ranges from 0.01% to 0.1% ⁷⁹.

1-4.2.2. Inhibition of efflux transporters

The presence of numerous efflux transporters at the BBB prevents the entry of many CNS active compounds into the brain. In HIV treatment, the most efficient drugs, such as abacavir and efavirenz, are substrates of the ABC transporters. Therefore, an interesting strategy is to inhibit efflux transporter activity, saturating these transporters with substrates that have a higher affinity for the transporter than the potent drug ⁸⁵. This strategy is efficient

in HIV multi-therapy and improves the intracerebral concentration of HIV protease inhibitors ³⁴. However, this strategy may have several drawbacks because inhibition of efflux transporters will allow the penetration of other xenobiotics, which may be potentially toxic in the CNS and would have been effluxed under normal conditions. Therefore, adverse side effects may occur using this strategy.

1-4.2.3. *Use of prodrugs*

The formulation of prodrugs enables to mask inappropriate properties of an active compound, unable to cross biological barriers under its active form. Therefore, the active compound is chemically modified to enhance the lipophilicity of a drug candidate to favor its passive permeation ⁸⁶ or to mask the specific site recognized by efflux transporters. The primary goal of this strategy is to promote the permeation of compounds that have either low uptake or are substrates of efflux transporters in their native form. The addition of moieties to the drug, which are linked by covalent reversible bonds, allows for the physicochemical modification of the active compounds to cross the BBB. For example, dopamine, a treatment for Parkinson's disease, cannot cross the BBB and enter the central nervous system where its target is located. On the other hand, L-Dopa, which decarboxylation leads to the formation of dopamine, can be actively transported through the BBB. After the prodrug has entered the brain, DOPA decarboxylase activates L-Dopa into active dopamine. This strategy also permits the creation of a drug-reservoir, depending on the rate of release of the native active compound. This approach is therefore an asset for patient compliance. However, chemical modification of the native active drug may decrease its activity or bioavailability.

1-4.2.4. The Trojan horses or the BBB shuttles

The concept of Trojan horse consists of coupling the drug of interest, which cannot penetrate the BBB, to a moiety, such as a functional group, a peptide, a monoclonal antibody or transferrin. The BBB-penetrating moiety is recognized by the specific receptor, such as the glucose transporter (GLUT-1) or transferrin receptor, leading to the transport of the entire entity ⁸⁶. An extension of this concept was proposed by Malakoutikhah and co-workers ⁸⁷ who designed peptidic Trojan horses that were able to cross the BBB *via* passive diffusion. These compounds were defined as BBB shuttles. The challenge of both Trojan horses and BBB shuttles is to then liberate the active drug from the vector.

1-4.2.5. Drug delivery with nanocarriers

Liposomes, polymeric nanoparticles, solid lipid nanoparticles and micelles are all nanocarriers and have garnered great interest in recent pharmaceutical research. Because of the incorporation of a drug into the inside core of the nanocarrier, the drug bioavailability, physicochemistry and pharmacokinetics of the drug are changed ^{88, 89}. In pharmaceutical research, a well-known problem is the discovery and development of highly potent lead compounds, which can then be found to be either insoluble or poorly soluble. In most cases, either the molecule will be discarded from the drug development process, or a ligand strategy will be used to enhance the solubility of the potential drug, with the risk of decreasing its potency or bioavailability.

Drug delivery is a method of bypassing poor solubility, poor permeability or poor bioavailability by incorporating the compound of interest into either phospholipidic, polymeric or inorganic vesicles ⁹⁰.

Liposomes consist of a phospholipid bilayer forming a vesicle. The inner part of the liposome is full of aqueous medium, whereas the bilayer is highly hydrophobic. Therefore, they allow for the incorporation of either hydrophilic molecules, on the inside core, or lipophilic molecules, inside the bilayer ⁹⁰. Liposomes are extensively studied and highly promising nanocarriers, particularly for cancer therapy. Caelyx® (or Doxil®), a pegylated liposomal formulation of doxorubicin that targets breast and ovarian cancer cells, is a good representative of the success of these formulations ^{91, 92}.

Three generations of liposomes have now been developed. The first generation consists of a vesicle formed by a phospholipid bilayer. These types of liposomes are rapidly recognized by the reticuloendothelial system and eliminated. Therefore, their efficacy is very limited and not applicable for pharmaceutical purposes. The second generation of liposomes is surrounded by polyethylene glycol, which is covalently linked to the outer part of the vesicle. These pegylated liposomes have a longer circulation time in the body because PEG is not recognized as a pathogen by the immune system. The third generation of liposomes is the most potent generation of liposomes. These liposomes consist of the same pegylated liposomes as the second-generation liposomes but are functionalized with specific moieties, such as monoclonal antibodies, added to the PEG chain. Therefore, the modified liposome is recognized by the antibody-specific receptor and may be taken up by the cell. This strategy allows for specific targeting of cells. For example, immunoliposomes, grafted with OX26 monoclonal antibody are able to recognize transferrin receptor at the BBB, which transport it through the a rat BBB model *via* endocytosis ⁹³. Up to now, many immune-conjugated

nanocarriers are on clinical phases such as doxorubicin, anti-HER-2 ⁹⁴, but none has launched the market yet. Future years will probably disclose numerous new formulations aiming at treating CNS pathologies.

The major drawback of liposomes is their poor stability, which is due to their tendency to aggregate and their sensitivity to oxidation and hydrolysis. Some of these problems can be reduced by formulation strategies, such as the addition of α -tocopherol to decrease oxidation 95 . Other researchers have formulated liposomes as proliposomes, a dry granular product, which disperses to form multi-lamellar vesicles upon the addition of water 96 .

Nanoparticles as drug carriers have also been extensively studied recently. Their uptake into the brain is hypothesised to occur *via* receptor-mediated endocytosis ^{97, 98}. As liposomes, unmodified nanoparticles have been shown to be rapidly cleared by the reticuloendothelial system, within 5 minutes in a mouse model. The addition of surfactants or covalent binding of polyethylene glycol on the polymeric core led to a prolonged circulation time and improved bioavailability ⁹⁹. Only a few nanoparticle formulations of drugs are currently on the market, such as Rapamune®, an immunosuppressant drug. Promising results have been obtained in preclinical studies of a glioblastoma rat model, using doxorubicin-incorporated nanoparticles; however, no CNS-targeting nanoparticles are currently available in the market. Nanoparticles can either be polymeric, lipidic or inorganic. The safety profile of these vesicles is controversial, and much research is necessary to fully describe the mode of excretion, the possible accumulation of particles in organs and the side effects caused by these nanoparticles.

1-5. Methods to assess BBB permeability information in drug research

1-5.1. *In silico* models that predict BBB permeability

In silico models are used during the early stages of the drug discovery process when thousands of compounds must be screened for either interactions with a specific target or for the appropriate physicochemical properties (figure 1-1). For example, Lombardo *et al.* ¹⁰⁰ succeeded in predicting the blood-brain partitioning of compounds (log BB) using the calculated solvation free energy. Others correlated log BB with a combination of the molar

refraction, solute polarizability, hydrogen bond donor or acceptor capacity and molecular volume ^{101, 102}. *In silico* strategies can filter large databases to preselect compounds of interest and can predict whether a compound will be prone to BBB penetration or not ¹⁰³. These computational strategies can decrease the number of molecules to only few hit compounds, which are then tested with *in vitro* models to determine the pharmacokinetics and mechanism of action of the drug.

In silico models combine the measured brain penetration information that is available in the literature with molecular properties to build an algorithm that can predict BBB permeability. Using partial least squares regression, multiple regression analysis or neural networks, in silico models can generate pondered regressions consisting of different physicochemical properties, such as the lipophilicity (log P), standard free energy, H-bond donating capacity, H-bond accepting capacity, and molecular weight of the drug.

In practice, the initial data, which are obtained from libraries, are divided into 2 subtest sets, a training set, which is used to build the algorithm, and a test set, which allows for determination of the predictive ability of the algorithm. The experimental permeabilities of the test set are statistically compared to the predicted values that are generated by the algorithm to determine the predictive power ¹⁰³. The variety of algorithms that are able to build a predictive model is huge because many descriptors may be used to generate an equation. Some examples of *in silico* models to predict log BB are listed in a review of Abraham ¹⁰³. In general, the chosen descriptors are related to the size of the molecules and their physicochemical properties. As Abraham noted, an increase in size-related descriptors leads to an increased log BB (higher brain penetration), whereas an increase in the polarity-related descriptors leads to a decreased log BB. This characteristic is linked to the hydrophilic properties of both compartments, with the brain being more lipophilic than the blood. Moreover, Didziapetris *et al.* ¹⁰⁴ suggested that acids with a pKa > 4, containing greater than 8 oxygen and nitrogen atoms and a molecular weight greater than 400 Da were likely to be substrates of efflux proteins.

A major issue resulting from *in silico* models is the reliability of the chosen training sets and test sets. It is difficult to obtain experimental data that are homogeneous in terms of the experimental design, such as whether the perfusion was performed with whole blood, plasma or saline solutions, the reliability of descriptors, such as whether there was ionization, and the experimental know-how. The ideal situation would be to obtain the experimental data from the same laboratory, under the same conditions; however, that situation is utopist because the amount of data would be either too low to build the model or not diverse

enough. Therefore, attention should be paid when handling *in silico*-predicted data, and the user must also understand how the model was built.

1-5.2. In vitro models for prediction of BBB permeability

Different approaches have been proposed for the *in vitro* evaluation of whether a new chemical entity can cross the BBB. Significant differences exist from one method to another in terms of complexity and, consequently, cost and information obtained (figure 1-5). In this section, *in vitro* methods for predicting BBB permeability are ordered according to increasing complexity.

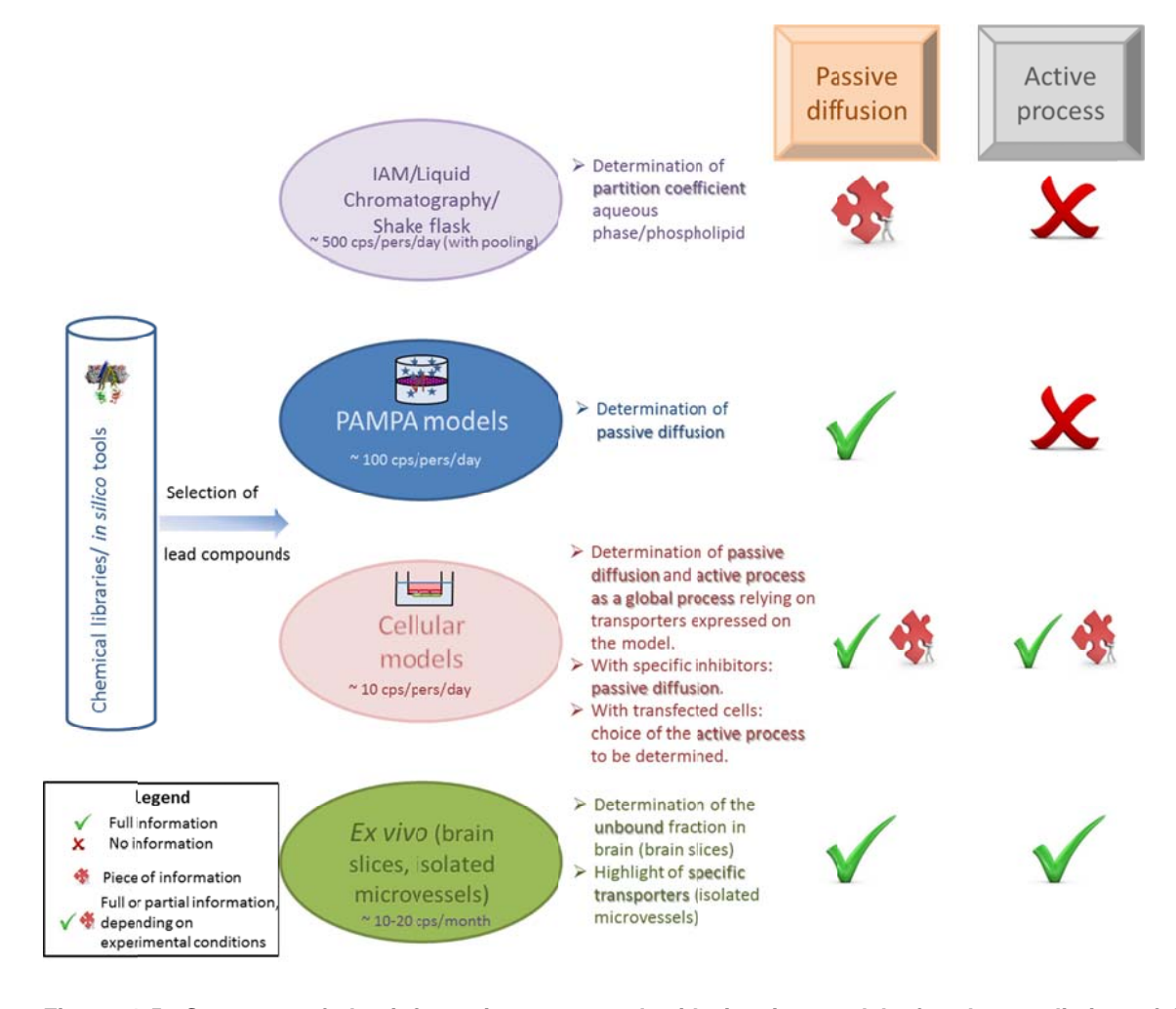


Figure 1-5: Summary of the information generated with *in vitro* models for the prediction of BBB permeability.

1-5.2.1. Immobilized artificial membrane

Lipophilicity (log P or log Poctanol/water) has long been reported to be a major parameter that influences CNS activity and the blood/brain concentration ratio (log BB) 105, 106. Because of its lipophilic feature, n-octanol was widely used for pharmacokinetic predictions. The small polar head of n-octanol and its hydrophobic carbonylated chain make it appear similar to phospholipidic membranes. However, the relationship between log P and log BB is not strong enough for the needs of CNS researchers. Therefore, immobilized artificial membranes (IAMs) were proposed as an alternative to log P predicted with shake-flask or liquid chromatography 107-110. Modified HPLC columns were prepared in which phospholipids were covalently bound to the silica ¹⁰⁶. Experiments showed a linear relationship between the retention factors on IAMs and the partition between an aqueous phase and liposomes ¹¹¹. Moreover, IAM chromatographic retention factors were shown to generate information on membrane permeability ¹¹². In some cases, these types of systems have shown reasonable results for permeability prediction, even if the retention time on the column does not reflect the transport across the membrane 113, 114. However, there are some limitations in terms of retention times for lipophilic compounds and stationary phase stability. Recently, short IAM columns appeared on the market. These columns (1-3 cm versus 10-12 cm) allow greater throughput but do not really offer any improvements in terms of reliability, and this approach is not widely used in drug discovery.

1-5.2.2. PAMPA models

1-5.2.2.1. Generalities on PAMPA

The parallel artificial membrane permeability assay (PAMPA) is a relatively recent technique developed in 1998 by Kansy *et al.* ¹¹⁵ to rapidly predict passive permeability through the gastrointestinal tract with high throughput efficiency. In this technique, a donor and an acceptor compartments are separated by a filter supporting a liquid artificial membrane. The assay is performed in 96-well plates. The 96-well acceptor plate contains a buffer of known pH, whereas the donor compartment contains the same buffer with a known amount of the drug to be tested. The donor and acceptor compartments and the filter plate are then assembled in a sandwich-like conformation, allowing an aqueous contact between the artificial membrane and the acceptor and donor solutions. Following a defined incubation time with or without stirring, the sandwich is disassembled and the concentration of the drug being tested is measured with either a UV-multiplate reader, (U)HPLC-UV or (U)HPLC-

MS(/MS) detector 116, 117 and compared to the initial donor drug concentration. The permeability coefficient is then determined in a straightforward manner with the permeability equation described by Avdeef 69. The artificial membrane that was originally made of phospholipids ^{62, 118} can also be as simple as an organic solvent ¹¹⁹ or a mixture of solvents ¹²⁰. PAMPA is gaining interest in the early drug discovery process because of the possibility to rapidly obtain straightforward transendothelial passive permeabilities of numerous compounds, it is a cost efficient technique with high inter- and intra-laboratory reproducibility and it can target different biological membranes. The major drawback of the PAMPA technique is that it can only predict passive diffusion and is therefore unable to generate a full description of the permeability process at the BBB. Hence, it is well admitted that numerous transporters and enzymes are expressed at the BBB level, greatly modifying the pharmacokinetics of the substrates of these transporters, such as verapamil, a P-qp/ABCB1 substrate. Therefore, for these specific compounds, PAMPA generates only a portion of the information regarding passive transcellular transport. PAMPA should not be used for compound selection purposes particularly for BBB penetration, because of the numerous transporters and metabolic enzymes that are present at the BBB.

1-5.2.2.2. PAMPA-BBB

Developed in 2003 by Li Di et al. 121, PAMPA-BBB has shown good prediction of BBB penetration for CNS classes of drugs. The drugs are described as CNS+ for compounds that have a high penetration through the BBB, CNS- for compounds that have a low permeability or are unable to penetrate the BBB, and CNS+/- for compounds with a medium permeability coefficient. A quantitative analysis correlating the permeability coefficients generated with PAMPA-BBB and in situ brain perfusion gave a poor correlation coefficient of $r^2 = 0.47^{122, 123}$ for a test set of 37 compounds. However, for 30 test compounds, this assay succeeded in predicting 25 compounds with the correct class of permeability, either CNS+ or CNS-. The only negative outlier was actively transported, whereas the 4 false positives were either substrates of efflux pumps or metabolised in vivo. One weak point of this assay is that it is performed under unstirred conditions, which maximises the unstirred water layer (UWL). UWL is a stagnant water layer at the two sides of the artificial membrane that has a distinct boundary with bulk water ⁶⁹. This layer can highly modify the permeation of compounds, in particular hydrophobic compounds, because passage through the UWL is governed by diffusion laws. Because of the blood flow and the very small size of the cerebral capillary, the in vivo UWL is nearly null. However, this is not the case for the in vitro UWL, particularly for the unstirred in vitro assay in which the UWL can be as thick as 1.5 to 2.5 mm ¹²⁴.

1-5.2.2.3. Compatibility of PAMPA with new drug delivery strategies

In 2009, Han et *al.* ¹¹⁸ used PAMPA to determine the intestinal permeation of ginsenoside, a hydrophilic molecule with very low membrane permeation, that was incorporated into a water-in-oil microemulsion. The objective was to obtain information on the mechanism of permeability of this carrier system. The original protocol of Kansy ¹¹⁵ using a phospholipidic-based membrane was used. Han *et al.* demonstrated an increased permeation of ginsenoside due to good permeation of the water-in-oil microemulsion through the PAMPA membrane. These results were corroborated by rat everted intestinal sac studies.

In 2007, Mathot *et al.* ¹²⁵ used the phospholipidic PAMPA developed by Kansy ¹²⁶ and commercialized by pION Inc. to evaluate the passive diffusion of polymeric micelles formed from polymeric surfactants through the gastrointestinal tract. They had already shown in the Caco-2 model that the polymers were able to cross the cells but did not know the possible mechanism of passage. Analysis of the acceptor compartment demonstrated the passage of the polymeric micelles through the lipid artificial membrane with a permeability coefficient of 1.0×10⁻⁶ cm.s⁻¹. To the best of our knowledge, no current study has evaluated the prediction of BBB permeation of these materials using the solvent-based PAMPA technique. However, the results obtained for the phospholipid-based PAMPA models for gastrointestinal tract passive transport predictions indicate that these models can be used to obtain information on the permeation of chemicals loaded in specific carriers. However, testing a new material on PAMPA is not obvious and requires particular attention regarding the reciprocal impact of carriers on the artificial membrane and *vice versa*. Therefore, preliminary tests must be performed before the permeability coefficients obtained from PAMPA tests can be interpreted.

1-5.2.3. Cell culture models

Cellular models that predict BBB permeability are extensively used during the early drug discovery process. A large panel of cellular models exists that differ in origin, the type of expressed transporters, the tightness of the tight junctions and affiliation with a primary or immortalized cell line. These factors greatly influence the reproducibility of the permeability experiments and the capacity of these models to predict *in vivo* BBB permeability. Therefore, all cellular models are different and generate specific information on permeability through the

BBB. Furthermore, none of the existing cellular models can fully predict the drug bioavailability *in vivo*.

The main advantages of cellular models are the throughput rate, which allows for the evaluation of a reasonable number of compounds even if this rate is only moderate. Additionally, cellular models have the capacity to evaluate transport mechanisms, which depends on the type of expressed transporters and the possible evaluation of metabolism and cytotoxicity. Furthermore, pathological conditions can be investigated choosing an appropriate model ¹²⁷. By contrast, homogeneity and reproducibility are difficult to obtain with cellular models, although these problems may be limited with the development of immortalized cell lines and standardized protocols.

To differentiate the wide variety of cellular models in existence since the 1970s, the following BBB parameters must be considered: the transendothelial electrical resistance (TEER), which indicates the tightness of transendothelial tight junctions and, therefore, restriction of the paracellular pathway; the endothelial permeability coefficient for paracellular markers such as sucrose, which indicates the integrity of the membrane 71 and the tightness of the tight junctions; the expression of specific BBB transporters, such as the carrier-mediated transporters, including glucose transporters (GLUT1), monocarboxylic acid transporter (MCT1), large amino-acid transporters (LAT1), and cationic acid transporters (CAT); the active efflux transporters, including the ATP binding cassette (ABC) gene family or solute carrier (SLC) gene family 128 ; and the presence of BBB markers, such as factor VIII, γ -glutamyl transpeptidase (γ -GT), alkaline phosphatase (ALP) and monoamine oxidase (MAO) 129 . Because the *in vivo* TEER of brain microvessels is approximately 1000-2000 Ω .cm² 130 , 131 and the permeation of sucrose can be as low as 0.03×10^{-6} cm.s⁻¹ 132 , the ideal cellular model should provide values as close as possible to the known values for these parameters.

1-5.2.3.1. Primary cultures

Cell biology research for the development of *in vitro* models of the human BBB began with primary bovine $^{41,\ 133-143}$ and porcine $^{144-148}$ cultures (table 1-1) because the brain size of these animals is large; leading to a high yield of cells per brain. However, rat $^{149-151}$, murine $^{152,\ 153}$ and human $^{50,\ 154-157}$ cell culture systems have also been developed. Compared to porcine or bovine cells, rat and mouse endothelial cells generate models with fewer BBB characteristics, such as a TEER value between 9 and 150 Ω .cm² and a P_e (sucrose) of

approximately 7.5×10⁻⁶ cm.s⁻¹ (table 1-1). Therefore, mouse brain endothelial cells are difficult to culture and lead to poor development of the endothelium ⁷². Additionally, because the number of cells per brain is limited, the batches of cells are always different even when the same protocol is used for extracting and seeding cells. This variability causes reproducibility issues because the cells used for permeability determinations are not the same from one day to the next. This is one reason why researchers have very little interest in using mouse primary cells for BBB permeability studies even if the best murine models can compete with some of the bovine models ^{150, 158}.

Bovine endothelial cells were the first *in vitro* BBB model and were developed by Bowman *et al.* as soon as 1983 136 . However, one of the primary bovine models expressing sufficient TEER for the prediction of BBB penetration was developed by Zenker *et al.* in 2003 159 . In this model, the TEER value reached 1350 Ω .cm², but values this high were rare and were dependent on the batch of cells. Furthermore, no paracellular permeability verification was performed, which makes an appropriate discussion of this model difficult. In general, the average TEER value generated with primary bovine endothelial cells is 150-200 Ω .cm², which is far from the *in vivo* TEER value of 1000 Ω .cm² $^{41, 133-143}$.

Porcine models display the best barrier properties (table 1-1). These models exhibit high TEER values ranging from 70 to 1800 Ω .cm² depending on the culture conditions and medium supplementation. Porcine models also have a low paracellular permeation of sucrose, with values ranging between 0.2 and 25×10⁻⁶cm.s⁻¹ 144-148, 160-167</sup>. Moreover, specific transporters, such as GLUT-1 or acetylated LDL are expressed and brain enzymes, such as the γ -GT or ALP, display an effective metabolic activity ¹⁴⁸ (table 1-1). The most efficient cellular model of the BBB was developed by Franke *et al.* ^{164, 168, 169} who grew primary porcine brain microcapillary endothelial cells in serum-free medium containing hydrocortisone. The result of this treatment was a monolayer of endothelial cells with very tight junctions, TEER values reaching 1500 Ω .cm² with an average of 700±100 Ω .cm², and sucrose permeation as low as 0.3×10^{-7} cm.s⁻¹. Further evaluations indicated that this model expressed several ATP-binding cassette (ABC) transporters, nutrient transporters and specific BBB receptors ¹⁷⁰. However, this model has not been used for any further permeability determinations.

Human brain cells are the gold standard for a human BBB *in vitro* model. However, for ethical reasons, the availability of this type of cell is very limited. The cells are generally obtained from biopsies of epileptic patients, and the number of cells obtained is very low. Rubin *et al.* and Bernas *et al.* developed primary human endothelial cell models with TEER

values of $339 \pm 107~\Omega.\text{cm}^2$ and $>1000~\Omega.\text{cm}^2$, respectively ^{41, 171}. No paracellular permeability was mentioned in these models, but the model developed by Bernas *et al.* was used in several studies to evaluate the effect of chemicals, such as cannabinoid receptor agonists, on the barrier function of BBB ¹⁷². Studies of these human models are limited and have instead focused on the generation of immortalized human cell lines, which should decrease the inter-individual, race, age and gender variations and increase the quality and reproducibility of the results obtained with human models.

Primary cell cultures may provide interesting information on human BBB permeability, but these models and culture conditions are not straightforward. Homogeneity and reproducibility of these models is not guaranteed because an animal brain cannot generate an infinite number of identical cells. Therefore, the variability of these models is due to interlaboratory and inter-individual factors, among others, and leads to large standard deviations. Finally, primary monocultures of brain endothelial cells were shown to rapidly lose their BBB properties, including tight junctions and specific transporters ¹⁷³.

1-5.2.3.2. Immortalized cell lines

To limit the drawbacks related to the handling of primary cells, researchers have immortalized their cultures to make cell lines. Immortalization is generally achieved with either gene or virus transfection ^{154, 174-176}, such as the SV40 large T-gene antigen ⁷² or the E1A adenovirus gene ¹⁷⁷ in the RBE4 model.

Few monoculture models of immortalized cell lines have been developed (table 1-1), however, bovine 178 , human $^{154, 156, 179-186, 186}$ mouse $^{187, 188}$ and rat $^{177, 188-193}$ endothelial cell lines have been established and tested for BBB properties. The model with the best BBB properties is a human brain endothelial cell line 156 , with TEER values ranging from 300 and 400 Ω .cm²; however, no sucrose permeation has been achieved, but inulin transport studies show low paracellular permeation. In 2005, Weksler *et al.* developed the hCMEC/D3 cell line, which displayed a TEER value below 40 Ω .cm² and a sucrose permeation of 27.10 $^{-6}$ cm.s $^{-1}$ 179, 194. Furthermore, many drug transporters, including most of the ABCB, ABCC and ABCG families found in the human BBB *in vivo* have been detected in the hCMEC/D3 cell line. Because of the existing BBB properties and its human origin, the hCMEC/D3 model has been used for many kinetic, pharmacological and permeability studies $^{74, 195-197}$.

In order to understand the predictive ability of primary cells and immortalized cell line, Steiner *et al.* ¹¹ compared primary mouse brain microvascular endothelial cells with

immortalized mouse brain endothelial cell lines and determined that the two types of endothelial cells exhibited different cytoskeletal morphologies. Moreover, the protein occludin, which plays a role in tight junction formation, was localized in the primary endothelial cells but not in the cell line, indicating a divergence in the junctional organization. This deviation leads to tighter junctions in the primary endothelial cells compared to the immortalized endothelial cells. Therefore, monocultures of immortalized cells are of limited interest for the prediction of BBB permeability, except the immortalized cell culture models derived from human cell lines.

Table 1-1: non exhaustive list of monoculture models aiming at predicting BBB permeability, their specificity and information provided. TEER stands for transendothelial electrical resistance BMEC is the brain microvascular endothelial cell; EC stands for endothelial cell; cAMP is the cyclic adenosine monophosphate; ALP is the alkaline phosphatase; γ-GT is the gamma glutamyl transpeptidase; P-gp/ABCB1 is the P-glycoprotein; MRP is the multiresistance drug protein, RT-PCR is the reverse transcription polymerase chain reaction, BCRP stands for breast cancer resistant protein; LDL are low density lipoproteins.

Cells origins	TEER (Ω.cm²)	Paracellular marker permeability P _e ×10 ⁻⁶ cm.s ⁻¹	Evidence of tight junctions	Pinocytic vesicles	Transporters	BBB receptors	BBB markers	In vitro/in vivo correlation	Author
Rat BMEC					acetylated LDL	factor VIII	ALP, γ-GT		Ichikawa N. <i>et al</i> ¹⁴⁹
Rat BMEC	100					factor VIII			Annunziata P. et al ¹⁵⁰
Immortalized rat RBE4		sucrose : 214±20				factor VIII	ALP, γ-GT		Roux F. et al ¹⁷⁷
Mouse BMEC		3kDa dextran : 2.2±0.3	immunostaining, western blot						Steiner O. et al ¹¹
Mouse BMEC	59.5±4.4					factor VIII	ALP, γ-GT		Imaizumi S. <i>et al</i> ¹⁵³
Immortalized mouse BMEC		3kDa dextran: 41±5	immunostaining, western blot						Steiner O. et al 11
Mouse endothelial cell line bEnd5 + astrocyte onditioned media	121	sucrose: 8; mannitol: 8	immunostaining, western blot		P-gp/ABCB1, GLUT1, sodium, potassium, chloride cotransporters, protein kinase C isoforms				Yang T. et al ¹⁵⁸
Immortalized mouse BMEC	40-50	inulin: 11			P-gp/ABCB1		ALP, γ-GT	low correlation (N=10)	Garberg P. et al ¹²⁹
Bovine brain EC		sucrose: 5.8±0.2	by immunostaining		P-gp/ABCB1, MRP1, MRP4, MRP5 by RT-PCR; presence of P-gp/ABCB1 by western				Culot M. et al ¹⁹⁸
Bovine brain EC	<9	sucrose: 25			hlot				Raub T. J. et al ¹⁴⁰
Bovine brain EC			by transmission electron micrograph	few					Bowman P. D. et al ¹³⁶
Bovine brain EC							ALP, γ-GT		Audus K. L. et al 135
Bovine brain EC		sucrose : 0.08							Smith K. R. et al ¹⁴¹
Bovine brain EC	61±2								Rubin L. L. <i>et al</i> ⁴¹
Bovine+astrocyte conditionned medium	115±11								Rubin L. L. <i>et al</i> ⁴¹
Bovine EC+ cAMP	305±50								Rubin L. L. <i>et al</i> ⁴¹

Table 1-1 (continued)

Cells origins	TEER (Ω.cm²)	Paracellular marker permeability P ×10 ⁻⁶ cm.s ⁻¹	Evidence of tight junctions	Pinocytic vesicles	Transporters	BBB receptors	BBB markers	In vitro/in vivo correlation	Author
Bovine EC+ astrocyte conditioned medium+cAMP	625±82	restricted paracellular efflux		low rate of endocytosis					Rubin L. L. et al ⁴¹
Bovine brain EC	500-600						γ-GT		Pirro J. P. et al 139
Bovine brain EC	160		immunostaining						Wang W. et al 143
Bovine brain EC	72-184	morphine: 8.8-16	electron microscopy		P-gp/ABCB1		ALP, γ-GT		Letrent S. P. et al 138
Bovine brain EC	200	sucrose : 8							Abbruscato T. J et al ¹³³
Bovine brain EC+astrocyte conditioned medium	175	sucrose : 8							Abbruscato T. J. et al ¹³³
Bovine brain EC+ astrocyte onditioned	>150	sucrose: 8; mannitol: 12	immunostaining, western blot		P-gp/ABCB1, GLUT1, sodium, potassium,				Yang T et al ¹⁵⁸
Human EC+astrocyte conditioned medium+cAMP	339±107	restricted paracellular efflux		low rate of endocytosis					Rubin L. L. <i>et al</i> ⁴¹
Immortalized human EC hCMEC/D3	<40	inulin: 12; sucrose: 27; lucifer yellow: 22			P-gp/ABCB1,BCRP, MDR1, MRP1, MRP3, MRP4, MRP5	human transferrin receptor			Weksler B. et al ¹⁷⁹
Immortalized human EC	300-400				acetylated low density lipoproteins	factor VIII	γ-GT, carbonic anhydrase IV, lectin UEA I		Stins M. F. et al ¹⁵⁶
Immortalized human EC (TY08)	35-43	inulin: 21			P-gp/ABCB1				Sano Y. et al ¹⁹⁹
Porcine brain EC	89.4±3.1								Fischer S et al 146
Porcine brain EC	700±100	Sucrose<1							Franke ^{164, 168} et al
MDCKII-MDR1	120-140	inulin: 0.2; sucrose: 0.3			P-gp/ABCB1			r ² = 0.40 (22 diverse compounds); r ² = 0.64(11 passive compounds)	Garberg P. et al ¹²⁹
MDCKII-MDR1		sucrose: 0.7±0.3						$r^2 = 0.72 (N=7)$, vs brain/blood ratio	Hakkarainen J. J. <i>et al</i> ²⁰⁰
CACO-2	600-1000	inulin: 0.08; sucrose: 1.4			P-gp/ABCB1, glut1, amino-acid transporters		ALP, γ-GT	$r^2 = 0.34$ (22 diverse compounds), $r^2 = 0.86$ (11 passive compounds)	Garberg P. et al ¹²⁹
CACO-2		sucrose : 2.4±1.4						$r^2 = 0.83$ (N=7), vs brain/blood ratio	Hakkarainen J. J. et al ²⁰⁰

1-5.2.3.3. Cocultures

Following the development of a variety of monoculture models and the determination that cerebral endothelial cells alone, do not express the appropriate BBB properties whatever their origin and also lose their specific characteristics when isolated from their environment ^{27,} cocultures became attractive models. In the human brain, there is constant communication between endothelial cells and other types of cerebral cells comprising the neurovascular unit, such as astrocytes, pericytes, neuroglia, and neurons ^{66, 201}. The action of surrounding cerebral cells on endothelial cells creates BBB properties and induces the production of junctional proteins and the expression of all the enzymes and transporters at the BBB ^{8, 9, 14, 19, 72, 78, 202}. Moreover, it was shown that astrocytes were able to reinduce BBB properties ²⁰³.

Megard et al. 50 noted several interesting observations in their research of human brain endothelial cells cocultured with human astrocytes. Primary human brain microvascular endothelial cells from normal human adult brain tissue were cultured to confluence for 7-10 days on a specific supplemented medium. Primary human astrocytes were also obtained from normal human adult brain tissue and cultured to confluence for 7-10 days on specific astrocyte growth medium. After several individual washes and treatments, a coculture was established with each type of cell grown on both sides of a collagen-coated membrane insert. The astrocytes were first grown for 1 to 2 days on the bottom of the collagen-coated membrane, and the endothelial cells were then added to the upper side and grown to confluence for 15 days. The resulting coculture exhibited specific barrier properties, such as a TEER value of 260 \pm 130 Ω .cm² (endothelial cells alone: 61 \pm 2 Ω .cm² and astrocytes alone: $37 \pm 5 \ \Omega.\text{cm}^2$) and a sucrose permeation of $(17 \pm 3).10^{-6} \ \text{cm.s}^{-1}$. To validate this BBB model, the authors selected the lipophilicity of a compound as a good indicator of BBB permeability. They demonstrated a good relationship between the in vitro BBB permeability of this model that was corrected with the molecular weight and the partition coefficients (r^2 = 0.88). Using flow cytometry and polymerase chain reaction (PCR), they showed that their model expressed P-qp/ABCB1 mRNA. A permeability determination with known P-qp/ABCB1 substrates, such as vincristine, verapamil or vinblastine, revealed a higher permeability from the basal to the apical compartments than from the apical to the basal compartments, indicating an efficient efflux process. These results underline the beneficial effect of cocultures on the expression of specific BBB properties in vitro models. The upregulation of P-gp/ABCB1 and the higher TEER value in cocultures compared to monocultures were also observed in several other studies ^{9, 159, 189, 202, 204, 205} (table 1-2).

These cocultures can be established with either primary cells or cell lines. As indicated in the review by Deli *et al.* ⁷¹ , many different cocultures have been developed but are usually established with endothelial cells and astrocytes from various animals. When the BBB properties of these cocultures were compared to the barrier properties of the corresponding endothelial monoculture, the resulting TEER values were generally improved, whereas the permeation of a paracellular tracer was decreased. Consequently, the expression of tight junction proteins is upregulated under coculture conditions, resulting in an improved *in vitro* BBB model ²⁰⁴.

To determine the reason why BBB properties are reinduced when endothelial cells are cocultured with astrocytes, Bénistant *et al.* ¹⁷³ evaluated the fatty acid composition of bovine brain capillary endothelial cells either monocultured or cocultured with rat astrocytes. They found that the phospholipid profiles of the endothelial cells were clearly different between the two culture conditions. The most significant differences were observed for palmitic acid, which was 13% of the total phospholipid proportion in the monoculture vs. 20% in the coculture, and for linoleic acid, which was 18% in the monoculture vs. 10% in the coculture. Therefore, these results indicated that the presence of astrocytes when culturing endothelial cells can modify the fatty acid composition of brain endothelial cells.

In 2009, Nakagawa *et al.* ²⁰¹ established a coculture model with three different types of cerebral cells, endothelial cells, pericytes and astrocytes, to provide a more realistic representation of the *in vivo* BBB. The pericytes were shown to have a similar positive influence as astrocytes on the tightness of the tight junctions ²⁰⁶. The TEER value of this triple coculture reached 400 Ω .cm², with a permeation of 3×10^{-6} cm.s⁻¹ for the non-permeant dye fluorescein. Moreover, specific BBB transporters, such as P-gp/ABCB1, glucose-transporter (GLUT1) and ABCC1, were expressed in the brain endothelial cells.

The BBB model displaying the best barrier features was developed by Dehouck *et al.* $^{27, 40, 127, 204, 207}$ and was called the bovine brain capillary endothelial cells model (BBCEC). This model, consisting of primary bovine endothelial cells cultured on one side of the filter and rat glial cells on the other side of the filter, exhibits high TEER values due to the presence of complex tight junctions. The TEER values range between 700 and 800 Ω .cm² ¹³, and the BBCEC model displays a low sucrose permeation between 5.4 and 32×10^{-6} cm.s⁻¹, a low rate of pinocytosis, the presence of P-gp/ABCB1 and metabolic enzymes, such as γ -GT, MAO, and the occurrence of LDL and transferrin receptors ²⁷. This combination of characteristics leads to interesting BBB properties. The original BBCEC model allowed for permeability determinations after three weeks of rat glial cell culture followed by twelve days of coculture ^{27, 40}. Further investigations and optimization permitted a ready-to-use model

after four days of culture ¹⁹⁸ with a four-fold increase in the number of compounds measured per plate due to an adaptation to 24-well plates instead of 6-well plates. The coculture step was replaced by the addition of BBB-inducing medium, which was hypothesized to promote the formation of BBB features. The permeability coefficient of sucrose measured in this optimized model was $(5.8 \pm 0.2) \times 10^{-6}$ cm.s⁻¹. Moreover, RT-PCR analysis indicated the mRNA expression of P-gp/ABCB1, ABCC1, ABCC4 and ABCC5, similar to the original coculture. The BBB-inducing medium appears to activate the ABCC1 gene that encodes ABCC1. When correlating *in vitro* BBB data, which are corrected by the molecular weight and a logarithmic function, with the corresponding BUI or *in vivo* BBB permeability, both of which are also corrected, good relationships were observed ($r^2 = 0.86$) ¹²⁷.

In conclusion, with regard to cellular models consisting of cerebral cells, primary cell cocultures generate the best models, although the reproducibility may not be optimal. The upregulation of tight junction proteins under coculture conditions allows for increased TEER values and decreased paracellular transport, which are characteristics of the BBB. The gold standard model would be a coculture of primary human cells, but this requires a constant renewal of the donor brain tissue, which causes ethical concerns.

Table 1-2: Non exhaustive list of coculture models aiming at predicting BBB permeability, their specificities and information provided.

Endothelial cell origin	Coculture cell type	TEER (Ω.cm²)	Paracellular marker permeability ×10 ⁻⁶ cm.s ⁻¹	Evidence of tight junctions	Pinocytic vesicles	Transporters	Receptors	Enzymes	in vitro/in vivo correlation	Author
Rat brain capillary EC (RBE4)	Rat astrocytes	500±20 ²⁰¹	sucrose :38±9	by immunostaining		P-gp/ABCB1, GLUT1, LAT1 ²⁰²	factor VIII, transferrin receptor	γ -GT , ALP		Roux et al ¹⁷⁷
Rat brain capillary EC	Rat astrocytes	438±75			few		factor VIII, transferrin receptor OX26	γ-GT		Demeuse P. et al ¹⁵¹
Puromycin purified rat EC	Rat astrocytes	>270	sucrose : <1.7	by immunostaining and RT-PCR		P-gp/ABCB1, Bcrp, Mrps, GLUT1			$r^2 = 0.88$	Perrière N. et al ¹⁵
Purified rat EC	Rat astrocytes		sucrose: 3.28±0.82	by confocal microscopy and immunostaining		abcg2, abcb1, abcc1, abcc4, abcc5			$r^2 = 0.67$	Lacombe O. et al ²⁰⁸
Rat brain capillary EC	Rat astrocytes	313±23	sucrose :16	by scanning electron microscopy and transmission electron microscopy						Lu W. et al ²⁰⁹
Rat brain capillary EC	Rat astrocytes and pericytes	354±15	fluorescein : 3.9±0.2	by western blot, electron microscopy		P-gp/ABCB1, GLUT1, Mrp1				Nakagawa S. et al ²⁰¹
Immortalized rat EC	Immortalized rat astrocytes	50-70	inulin: 5.3; sucrose: 8.6			acetylated LDL	factor VIII	γ-GT	low correlation	Garberg P. et al ¹²⁹
Puromycin purified mouse EC	Rat astrocytes	190	Na fluorescein: 3.5±0.1	immunocytochemistry and western blot		P-gp/ABCB1, GLUT1			r ² = 0.96 (N=7)	Shayan G. et al ²¹⁰
Primary mouse brain microvascular endothelial cell	Primary mouse glial cell	777.6±14.8	sucrose: 4.5±1.2; inulin: 1.2±0.3	by immunostaining		P-gp/ABCB1				Coisne C. et al ²¹¹

Table 1-2 (continued)

Endothelial cell origin	Coculture cell type	TEER (Ω.cm²)	Paracellular marker permeability ×10 ⁻⁶ cm.s ⁻¹	Evidence of tight junctions	Pinocytic vesicles	Transporters	Receptors	Enzymes	in vitro/in vivo correlation	Author
Bovine EC	Rat astrocytes	400-850	fluorescein: 6.0±1.0	by electron microscopy- presence of cadherin 5		P-gp/ABCB1 expression	α _v integrin, P- selectin receptor, transferrin receptor	γ-GT		Gaillard P.J. et al ²⁰²
Bovine EC	Rat astrocytes	700-800			Low rate	P-gp/ABCB1 ^{27, 204} ; LDL ²¹²	Transferrin receptor 213		$r^2 = 0.86^{-27}$, $r^2 = 0.86^{-27}$; $r^2 $	Dehouck M.P. et al ²¹⁴
Bovine aortic endothelial cells	Astrocytes	736±38	sucrose: 0.09							Stanness K. A. et al ⁸ (3D model)
Bovine EC	Rat astrocytes	400-800	inulin: 0.7; sucrose: 4.0			P-gp/ABCB1	factor VIII	γ -GT , MAO	22 (with log	Garberg P. et al ¹²⁹
Bovine EC	Rat C6 astrocytes	160±8	sucrose:24						BB)	Raub T. J. et al ¹⁴⁰
Bovine brain EC	Rat C6 astrocytes	210	sucrose: 10							Abbruscato T. J. et al
Purified human EC	Human astrocytes		lucifer yellow: 0.8; sucrose: 2.69±0.25			GLUT1, LAT1, LAT2, ABCB1, ABCC1, ABCC4, ABCC5, ABCG2			r ² = 0.90 (N = 6)	Mabondzo A. et al ³
Human EC	Human astrocytes		inulin: 12; sucrose: 22			LDL			no correlation	Garberg P. et al ¹²⁹
Human umbilical vein EC like cell line	Rat C6 glioma cell line	100	inulin: 0.6; sucrose: 8.1			GLUT1, leucine amino acid carrier, P- gp/ABCB1		γ-GT		Garberg P. et al ¹²⁹
Porcine brain microvascular EC	Rat astrocytes	104-219				GLUT1, acetylated LDL		γ-GT , ALP		Fischer S. et al ¹⁴⁸
Porcine brain microvascular EC	C6 glial cells	180±12				GLUT-1, acetylated LDL		$\gamma ext{-GT}$, ALP		Fischer S. et al ¹⁴⁸

1-5.2.3.4. Cell lines of non-cerebral origin

The Madin-Darby Canine Kidney Cell line (MDCK)

MDCK cells are cells of non-cerebral origin that are relatively easy to grow and can be transfected with specific gene transporters, particularly the MDR1 gene, which codes for polarized expression of P-gp/ABCB1 ⁷⁸. These transfected MDCK cells can then be used for the MDR1-MDCK (I or II) assay. MDCK cells can generate TEER values as high as 1800-2200 Ω .cm² ²¹⁵, indicating the existence of robust barrier properties with high expression of tight junctional proteins. Moreover, the in vitro/in vivo correlation obtained with this model is better than some of the existing in vitro models with cerebral cells, with $r^2 = 0.64^{129}$ or 0.72 ²⁰⁰ when passive compounds are selected for the correlation, depending on authors (table 1-1). However, in vitro/in vivo correlations with a diverse set of compounds (including compounds being actively transported or effluxed at the BBB) do not exhibit a significant correlation ($r^2 = 0.40$) ¹²⁹. The greatest limitation of these cells is the absence of transporter proteins other than P-gp/ABCB1 and their different morphology compared to endothelial cells because MDCK cells are epithelial cells ⁷⁸ ²⁰⁸. Moreover, these cells are derived from dog kidney cells ²¹⁵. However, transfection of the MDR1 gene allows for the determination of Pgp/ABCB1 substrates by measuring the permeability on both sides of the membrane. Another study conducted by Di Li et al. 123 did not generate an in vitro/in vivo correlation comparing the in vitro MDR1-MDCK permeation of a very diverse set of compounds with permeations obtained from *in situ* brain perfusion ($r^2 = 0.007^{123}$). This absence of correlation was most likely due to saturation of the P-gp/ABCB1 in vivo. The concentrations used for the in situ brain perfusion study were very high compared to the affinity constants of the compounds. These high concentrations lead to saturation of the efflux transport and use of the predominantly passive diffusion pathway, which overestimates the permeability in vitro. Moreover, differences in membrane characteristics, such as epithelial kidney cells for the MDR1-MDCK assay and cerebral endothelial cells for the in situ brain perfusion study, lead to a significant discrepancy in the predicted BBB permeability. Moreover, the phospholipid composition of both membranes is fundamentally different, with a higher proportion of cholesterol in the cerebral membrane than the MDCK cells. This composition leads to an increased fluidity of MDCK cells, which facilitates passive permeability in this model.

Caco-2 cells

Caco-2 cells are epithelial cells derived from a human colon carcinoma and are extensively used in the pharmaceutical industry to predict oral absorption through the intestinal epithelium. Moreover, the Caco-2 model is also used to predict BBB transport, even though the gastrointestinal tract is fundamentally different from the BBB, but as in vitro BBB models have evolved, the in vivo permeability predicted by the Caco-2 model became less and less useful 127 compared to other models. However, the Caco-2 assay remains an efficient method of identifying substrates of the P-gp/ABCB1 transporter from a set of test compounds because of the overexpression of P-qp/ABCB1 in cancer cells. More recently, Ball et al. 216 developed a physiologically based pharmacokinetics model to predict the fraction of unbound drug reaching the brain. They succeeded in generating an in vitro model that faithfully fits the in vivo unbound brain concentration of morphine, which is effluxed at the BBB, and oxycodone, which is taken up at the BBB. The K_{p.uu} was determined in Caco-2 cells expressing the P-gp/ABCB1 efflux transporters for morphine and in TR-BBB13 cells, which enable active uptake, for oxycodone. Both resulting distributions were corrected by a relative activity factor, which was estimated by a comparison between the in vitro model predictions and the in vivo data in rats.

1-5.2.3.5. Adaptation of BBB cell models to new delivery strategies

Some models were used to obtain information on nanocarrier transport across the BBB.

Nanoparticles

In 2006, the transcytosis of polyethylene glycol-polylactide (PEG-PLA) nanoparticles across the BBB was evaluated by Lu *et al.* using a rat syngeneic coculture of brain capillary endothelial cells and astrocytes 209 . The fluorescent compound 6-coumarin was incorporated inside these nanoparticles with a final size of 102.4 ± 6.8 nm. After transport study of the coumarin-loaded PEG-PLA nanoparticles across the coculture, a permeation of 4.8×10^{-6} cm.s⁻¹ was obtained. However, the permeation of the paracellular marker sucrose was higher than the permeation of the nanoparticles. Therefore, either a paracellular route or a transcytosis process may have occurred in this *in vitro* model.

Ragnaill *et al.* ²¹⁷ later described the transport of 50 nm silicium dioxide nanoparticles through the *in vitro* hCMEC/D3 BBB model ^{179, 194}. They succeeded in showing that nanoparticles were effectively taken up by the cells with the membrane enveloping the nanoparticles. Moreover, they also observed the nanoparticles in both the endosomes and

lysosomes and some on the basolateral side of the membrane. Therefore, they suggested that the silicium dioxide nanoparticles were endocytosed and that an exocytosis process also occurred.

<u>Liposomes</u>

The hCMEC/D3 cell line was also used to study the BBB penetration of an immunoliposome decorated with OX-26, an anti-transferrin monoclonal antibody ⁷⁴. The objective of the study was to target the transferrin-receptor for transport of the immunoliposome by a receptor-mediated transcytosis process. The mean diameter of the immunoliposomes was assessed with dynamic light scattering and was less than 200 nm. They demonstrated that the immunoliposomes were transported through the endothelial monolayer by receptor-mediated endocytosis.

In vitro cellular models can therefore be used for the permeability determination of more complex formulations, such as nanocarriers. However, adaptation of the model may not be straightforward because of the potential cell toxicity of the carriers, and a full assessment of the validity of the models is required before a discussion of the results, but promising data regarding the distribution of nanocarriers are emerging ^{74, 179, 194, 209}.

1-5.2.4. Ex vivo experiments: transport across isolated brain microvessels

Isolated brain microvessels are generally used to evaluate the gene expression of specific transporters at the BBB ²¹⁸, but permeability experiments may also be conducted to identify specific transporters. Fluorescent probes are tested in the presence or absence of known substrates of the transporters. A variation in the permeability indicates the presence of the specific transporter that is being assessed ^{219, 220}. Miller *et al.* used confocal microscopy to detect fluorescent xenobiotics, such as daunomycin and fluorescein labeled dextrans, within the lumen of isolated brain microvessels ²¹⁹. They succeeded in demonstrating a concentrative, specific and energy-driven transport process, indicating the expression of specific active transporters in isolated brain capillaries. Studies with specific substrates and immunostaining indicated that the active process was initiated by P-gp/ABCB1 and Mrps. The P-gp expression in isolated brain capillaries was corroborated by the studies of Durk *et al.* ²²⁰.

Transport across freshly isolated brain microvessels is a good alternative to cell culture because it is less time consuming; however, isolation of the brain microvessels

requires much skill and very clean manipulations to obtain microvessels that are extremely pure. Moreover, reproducibility issues may be more important in this model than for cellular models because fresh microvessels must be freshly prepared for each experiment.

1-5.3. In vivo models

In vivo models are the best models available to predict human *in vivo* permeabilities because of the combination of all biological aspects in the same model, such as physiological barriers, transporters, and metabolic pathways. However, these models are expensive, time-consuming, require the mastering of animal-based assays and often necessitate radiolabeled compounds. These factors ensure that *in vivo* models are used during the later stages of the drug discovery process, just prior to clinical investigations, for a limited number of lead compounds. Different *in vivo* models are available, which allows for determination of the permeation of the molecules tested and in particular the logarithm of the BBB permeability-surface area (log PS) or the logarithm of the brain to plasma ratio (log BB) (table 1-3). These models include *in situ* brain perfusion, single carotid injection (brain uptake index; BUI), intravenous injection and intracerebral microdialysis ⁷⁸. The log PS is considered the most relevant indicator of BBB permeability because it measures the clearance of a drug from the blood to the brain across the BBB ²²¹ and is not altered by either metabolism or protein binding ¹²³. The log PS is determined from the K_{in}, which is the clearance out of the brain. This determination better reflects BBB permeability.

Determination of the log BB requires several time point measurements, which requires animals at each time point and is costly. Moreover, several factors, such as metabolism and binding, interfere with brain penetration in the log BB determination; therefore, log BB is not an accurate measurement of BBB permeability.

1-5.3.1. The brain/plasma ratio

The brain/plasma ratio, established by Ohno *et al.* ²²², resulted in determination of the blood-brain distribution coefficient (BB), which is defined as the ratio between the concentration of the compound in the brain and in plasma. Therefore, this approach may be misleading because the partition parameter that is obtained is dependent on the affinity of the tested drug for circulating proteins in the blood stream ²²³. This method provides

determination of the drug partition between the plasma and brain but does not provide a pharmacokinetic profile. Determination of the brain/plasma ratio can be performed either at steady state or at different time points and requires sacrificing the animal and determining the concentration of the unbound drug in both the brain homogenate and plasma.

A brain/plasma ratio ≥ 1 indicates that a compound is able to cross the BBB, whereas a brain/plasma ratio < 1 reveals a poor distribution of the compound 223 . However, due to plasma protein binding, a brain/plasma ratio < 1 may also indicate a high affinity for circulating plasma proteins or an affinity for efflux proteins, both of which limit permeation of the compound through the barrier. Therefore, interpretation of the brain/plasma ratio must be performed cautiously.

Young *et al.* 224 used the brain/plasma ratio to design and select a CNS-active H₂ histamine receptor antagonist. More recently, Rohanova *et al.* used the brain/plasma ratio to study the brain penetration of a new illegal drug p-methoxymethamphetamine and its metabolites to better understand both the mode of action and the toxicity profile of these new drugs 225 .

1-5.3.2. The brain uptake index (BUI) technique

The brain uptake index model is appropriate for compounds that moderately to rapidly penetrate the BBB and is generally performed in rats. A rapid bolus injection of 200 µl buffered solution containing a known concentration of a radiolabeled reference compound and the tested drug is administered directly into the carotid artery of the rat. The brain is then removed after 5-15 s and analyzed for radiolabeled contents ⁷⁸ by scintillation counting. BUI allows for determination of the log PS, which is the permeability multiplied by the surface area. This technique is based on the following three hypotheses: the time between injection and decapitation is so short that no metabolism occurs before the brain is removed; the compound can diffuse from the blood to the brain; and when the compound is in the brain, it cannot go back into the blood ²²⁶. The main drawback of this technique is that extremely low concentrations of drug are present in the brain because of the very short analysis time, which causes sensitivity problems for compounds with low permeability. This technique is more appropriate for compounds with a high permeability through the BBB. For example, this technique has been used by Oldendorf *et al.*, who demonstrated modulation of the transporter activity under different pH conditions ²²⁷.

1-5.3.3. The in situ brain perfusion

In situ brain perfusion is suitable for low to high permeant compounds ⁵⁵ or substrates of an endogenous transport system. This model provides the same information as the BUI but with higher sensitivity. *In situ* brain perfusion is performed on an artificial cerebral circuit, resulting from the ligature of some cerebral arteries and catheterization of the external carotid artery. Therefore, the flow rate and duration of perfusion are known and can be controlled. The brain is then perfused with an oxygenated hydrogenocarbonate buffer containing a known amount of radiolabeled compound. Determination of the radioactivity at a predefined time, ranging from 5 s to 30 min, allows for the direct determination of pharmacokinetics parameters, particularly the volume of distribution and the rate of compound transfer, K_{in} ^{55, 228}.

Because the composition of the perfusate is controlled, *in situ* brain perfusion allows for the determination of PS values without considering either metabolism or plasma and brain protein binding. Only the intact form of the drug reaches the brain. This method provides information regarding the time required for the compound to cross the BBB. Moreover, the amount of drug reaching the brain is fully controlled. Compared to the BUI, the sensitivity of *in situ* brain perfusion is much higher because of a longer exposition time of the brain ¹³². This method is particularly interesting for determination of the kinetics of saturable transport at the BBB.

In situ brain perfusion was used by Cannon *et al.* ²²⁹ to study the modulation of P-gp/ABCB1 activity. They found that activation of the sphingosine-1-phosphate receptor by a specific ligand such as sphingosine-1-phosphate led to a decrease in P-gp/ABCB1 activity. The activity returned to the basal state after the administration of sphingosine-1-phosphate receptor antagonist. They concluded that this strategy could be used to increase the CNS bioavailability of P-gp/ABCB1 substrates, such as verapamil or loperamide.

1-5.3.4. The intravenous administration technique

Intravenous administration is one of the less invasive and most physiological methods of determining *in vivo* permeability. In this technique, the buffer containing radiolabeled solutes is injected inside a cannulated femoral vein or in the tail vein of the rat. The plasma concentration of the products is monitored for 10 s to several hours over various time points. The pharmacokinetic parameter obtained is the area under the curve of the drug concentration in the blood between time 0 and the time of the decapitation ²³⁰. Therefore, the

measured permeability will include the effective permeability, which is influenced by protein binding and metabolism. This technique has numerous advantages, such as the BBB remaining undisturbed and all transporters, enzymes and junctional proteins remaining intact, which enables metabolism. An entire pharmacokinetics profile can therefore be obtained. Moreover, because the evaluation can be performed for an extended period of time, both the plasma and brain pharmacokinetics can be determined. However, the study of specific influx transport is not possible with this intravenous administration technique.

1-5.3.5. The brain efflux index

The brain efflux index has been developed to determine the presence of a potential efflux pathway at the BBB when the compound is postulated to be transported from the brain to the blood. This technique is generally used to understand why a sufficiently lipophilic compound fails to penetrate the brain ²³⁰.

Briefly, the test and reference compounds are microinjected directly into the brain tissue. After a predefined time, the brain is removed and the tissues are analyzed to determine the concentration of the residual compounds.

This protocol requires the use of a highly sensitive method to determine the small amounts of compounds that may be present. Moreover, the researcher must be careful during the microinjection because a rapid or careless manipulation will irreversibly damage the BBB and confound the resulting measured permeability. The major drawback of this technique is the sacrifice of a large number of rats at different time points.

Kakee *et al.* ²³¹ used this technique to highlight the saturable efflux transport of paraaminohippuric acid at the BBB. A comparison of the apparent efflux clearance that was obtained in this study using the brain efflux index method with the apparent influx clearance obtained by BUI confirmed the selective transport of the carboxylic acid under investigation from the brain to the blood.

1-5.3.6. The unbound brain/plasma ratio: $K_{p,uu}$

To correct the errors that may be introduced by measurement of the brain/plasma ratio, a recent tendency consist in determining the unbound brain to plasma ratio ($K_{p,uu}$). This parameter may be obtained directly by intracerebral microdialysis or with a combination of *in*

vivo and *ex vivo* techniques. The last experiment is achieved measuring the quantity of drug that has reached the entire brain *in vivo* combined with an estimation of the unbound brain volume of distribution with *ex vivo* techniques such as the brain slice uptake experiment. The determination of $K_{p,uu}$ provides a better indication of the distribution of the active form of the drug. A $K_{p,uu}$ that is greater than unity indicates the presence of an active uptake process, whereas a $K_{p,uu}$ less than unity indicates the presence of an efflux process. A $K_{p,uu}$ near one indicates that the predominant pathway through the BBB is a passive diffusion process 232 .

1-5.3.6.1. Intracerebral microdialysis

Microdialysis allows for determination of the cerebral extracellular free drug concentration over a period of time with calculation of the K_{p,uu}. This free drug fraction represents the active form of the drug. Microdialysis requires the implantation of a dialysis probe in a selected area of the brain of the animal. This microdialysis probe consists of a semipermeable membrane that is continuously infused with physiological solution ²³³. Therefore, the compounds that are able to permeate through the membrane will diffuse according to the concentration gradient. This procedure does not require a specific mode of administration, and the permeation of the tested compound can be monitored after oral, intravenous, subcutaneous or infusion administration. Therefore, any drug entering the brain, which is always the unbound fraction of the drug, will be monitored over time in the extracellular fluid of the same animal ²³⁴ using HPLC, UHPLC or capillary electrophoresis. This technique requires a reduced number of animals for the pharmacokinetics determination compared to other techniques ⁷⁸. Moreover, because the same animal is monitored, there is no deviation due to variation in the population, gender or age of the animal. However, implantation of the dialysis system may locally disrupt the BBB, leading to a possible misinterpretation of the results. Moreover, highly lipophilic compounds can be adsorbed onto the probe, leading to mass-balance errors. This technique is more appropriate for moderately permeable compounds.

Intracerebral microdialysis was used by Gupta *et al.* 235 to compare the BBB transport and CNS distribution of two cetirizine enantiomers, the R and the S forms, to evaluate the stereoselectivity that occurs at the BBB. They compared the K_p (total brain to total plasma concentrations), $K_{p,u}$ (total brain to unbound plasma concentrations) and $K_{p,uu}$ (unbound brain to plasma concentrations) for both enantiomers. Whereas the K_p value could have led to the interpretation that brain penetration was stereoselective for both isomers ($K_p = 0.22$ for S-cetirizine and 0.04 for R-cetirizine), the $K_{p,u}$ (0.44 for S-cetirizine and 0.22 for R-cetirizine)

indicates that plasma protein binding greatly influences the biodistribution of both forms of the antihistamine. The unbound fraction was found to be 0.50 for S-cetirizine but only 0.15 for R-cetirizine. When considering both the plasma protein binding and brain tissue binding, they discovered that the $K_{p,uu}$ values were similar for both enantiomers ($K_{p,uu} = 0.17$ for S-cetirizine and 0.14 for R-cetirizine). These similar values indicate that both enantiomers are effluxed at the BBB ($K_{p,uu} < 1$) and that no significant difference occurs in their transport. The information generated by these *in vivo* methodologies that are able to distinguish between the active (unbound fraction) and inactive forms of the drugs are therefore able to reliably determine the biodistribution profile of a drug at the BBB.

1-5.3.6.2. The in vitro brain slice uptake experiment combined with the in vivo K_p .

Determination of the entire concentration of a drug in the brain in vivo, combined with the volume of distribution of the unbound drug determined by an in vitro brain slice uptake experiment, allows for calculation of the unbound brain to plasma concentration ratio K_{p,uu} ^{236,} ²³⁷. In the brain slice uptake experiment, the brain of a sacrificed animal is removed and immersed in ice-cold oxygenated pH 7.4 buffer ²³⁷. Brain slices (300 µm) of striatal areas are cut with a microslicer and preincubated with an extracellular fluid buffer before addition of the drug. At specific incubation times, the brain slices are removed from the solution of buffer containing the drug, dried, weighed and homogenized for determination of the amount of drug recovered in the brain slice. The main advantage of this technique is in the determination of the pharmacologically active unbound fraction of the drug in the brain. Moreover, the brain slices contain intact cerebral endothelial cells with their functional transporters as well as the same extra-to-intra-cellular pH gradient found in vivo 236. By contrast, the throughput of this model is limited due to the need for experimental animals and the minimum incubation time needed to reach drug equilibrium between the buffer and the brain slices, which is required to calculate $V_{u,\ brain}$ ²³⁶. As the incubation time to reach equilibrium increases with the V_{u, brain} and the V_{u, brain} increases with lipophilicity, the majority of compounds during the drug discovery phases require longer and longer incubation times, which cannot be supported by the limited life expectancy of the brain slices. Friden et al. evaluated this brain slice uptake assay to rapidly determine the unbound drug concentration in the brain ²³⁷. When they compared the results that were obtained for 15 diverse compounds with in vivo intracerebral microdialysis, they observed a reliable correlation between both techniques.

1-5.3.7. Non-invasive imaging techniques

Non-invasive imaging techniques have been developed to qualitatively and quantitatively determine the permeation of drugs in vivo. Moreover, imaging can also be used to identify P-gp/ABCB1 inhibitors or P-gp/ABCB1 substrates ²³⁸ or to determine the BCRP activity at the BBB ^{239, 239}. These techniques are primarily positron emission tomography (PET), magnetic resonance imaging or magnetic resonance spectroscopy. Because these techniques are non-invasive, they can be used in humans and allow for the determination of personalized pharmacokinetics. Imaging is also used to detect BBB damages in patients suffering from stroke, brain tumors or multiple sclerosis. However, these techniques require expensive equipment and labeled radiotracers. Sensitivity issues may be encountered, particularly with magnetic resonance imaging 132. Knight et al. used magnetic resonance imaging to localize and quantify the BBB opening in a rat model under ischemic conditions after the intravenous infusion of gadolinium-diethylenetriamine pentaacetic acid to achieve a blood concentration ²⁴⁰. Under normal conditions, this substance should not penetrate the brain. Other researchers, such as Serres et al., established a promising approach for the early diagnosis of brain tumors by targeting brain metastasis with iron oxide microparticles loaded with contrast agents ²⁴¹. Magnetic resonance imaging allowed for the visualization of brain metastases with 3-fold greater sensitivity than conventional tumor diagnostics. ¹³C magnetic resonance spectroscopy was used to assess the relationship between brain and plasma concentrations of glucose in patients suffering from diabetes type I during a hypoglycaemichypoglycemia event ²⁴².

Therefore, imaging is an efficient approach to determine personalized permeabilities during or after a pathological event. The main advantage of this technique is that it can be conducted in human for specific purposes and with safe drugs or dyes. Moreover, the distribution profile can be visualized, identifying the targeted regions of the brain.

Table 1-3 : Summary of the *in vivo* techniques in late drug discovery research

In vivo techniques	Characteristics	Experimental data			
Brain/plasma ratio	Study of low to rapid penetrating compounds; choice of variable exposure times; possible metabolism, protein binding and active transport.	A partition coefficient between plasma (or blood) and brain is generated. Be careful to misleading caused by protein binding.			
Brain uptake index	Study of moderate to rapid penetrating compounds; fast brain exposure (5 to 15 s between the injection and the sacrifice of the animal); no metabolism, no protein binding, no efflux transport.	log PS are generated. The extremely fast brain exposure time leads to sensitivity problems, due to very low concentration in the brain.			
In situ brain perfusion	Suitable for low to rapid penetrating compounds; fast to long exposure times (5 s to 1 hour); no metabolism, no protein binding, possible transport.	Data similar as Brain uptake index is generated. Sensitivity is much higher, thanks to a possible long brain exposure time.			
Intravenous administration technique	Study of low to rapid penetrating compounds; monitoring of the plasma concentration; existence of <i>in vivo</i> metabolism, protein binding and transport.	A whole pharmacokinetics profile is generated, on an intact BBB. This is the less ethically invasive and the most physiological method.			
Intracerebral microdialysis	More appropriate for medium permeant compounds. Drug monitoring of the unbound drug fraction after the choice of the mode of administration; existence of <i>in vivo</i> metabolism, protein binding and transport.	A whole pharmacokinetics profile is generated, but BBB can be damaged due to surgery. Monitoring is made on the same animal: decrease the number of experimental animals, no deviation due to variation in the origin, age, gender, weight of the animal.			
Imaging	Visualisation of the distribution in the body. Appropriate for medium to rapid penetrating compounds.	Non-invasive technique, which can be employed in humans. Existence of sensitivity issues, require expensive equipment.			

1-6. Aim of the thesis

The CNS drug discovery suffers from the highest attrition rate in early drug discovery, mainly caused by inappropriate pharmacokinetics and the presence of the Blood-Brain Barrier. However, the population worldwide is aging and by 2050, elderly people over the age of 65 will represent 16% of the population ⁵⁵. Along with this global aging, CNS disorders, such as Alzheimer's disease, are expected to increase exponentially, whereas treatments are lacking. Therefore, new reliable tools able to determine pharmacokinetics as early as possible in the drug discovery process need to be developed in order to decrease the attrition rate during the different phases and optimize the time expenditure.

The first part of this thesis was devoted to the development of a new in vitro technique able to predict passive permeation of drug candidates through the Blood-Brain Barrier with a high throughput efficiency in the early stages of the drug discovery process. Chapter 2 will therefore describe the development of a new artificial membrane using PAMPA, and exclusively constituted of solvents. This new artificial membrane and HDM-PAMPA, predicting GIT permeability, were employed to study the passive permeation of phyto-extracts (chapter 3) in order to understand the mechanisms leading to the anxiolytic effect of Hypericum perforatum. Similarities observed between the new artificial membrane and HDM-PAMPA lead to screen and compare the passive permeabilities of a larger dataset of compounds on 4 different PAMPA models: the HDC/NPOE PAMPA developed in chapter 2 and the PAMPA-BBB, both estimating passive permeation through the BBB, and HDM-PAMPA and PAMPA-skin, predicting passive permeation through the GIT and the stratum corneum respectively. The comparison of these 4 models allow to appreciate how different the artificial membranes are, and which information are generated on each model. Finally, the passive BBB permeation of formulations of liposomes and polymeric nanoparticles has been assessed with PAMPA (chapter 5). Hence, colloidal carriers appear as a promising strategy to improve the CNS targeting and find new ways of treatments. Due to the complexity of nanocarriers formulation, the experimental permeabilities generated with the new PAMPA technique were compared with other implemented in vitro models, such as PAMPA-BBB or the hCMEC/D3 cell line in order to provide information on their mode of transport at the BBB.

References

- 1. Kennedy, T. Managing the drug discovery/development interface. *Drug Discovery Today* **1997**, *2*, 436-444.
- 2. Tsaioun, K.; Bottlaender, M.; Mabondzo, A.; Alzheimer's Drug Discovery Fdn ADDME avoiding drug development mistakes early: central nervous system drug discovery perspective. *BMC Neurol.* **2009**, *9*.
- 3. Mabondzo, A.; Bottlaender, M.; Guyot, A. C.; Tsaouin, K.; Deverre, J. R.; Balimane, P. V. Validation of in vitro cell-based human blood-brain barrier model using clinical positron emission tomography radioligands to predict in vivo human brain penetration. *Mol. Pharmaceutics* **2010**, *7*, 1805-1815.
- 4. Davson, H. History of the blood-brain barrier concept. In Implications of the Blood-Brain Barrier and Its Manipulation. Volume 1: Basic Science Aspects.; Neuwelt, E. A. Ed.; Plenum Publishing Corp.: New York, **1989**; pp 27-52.
- 5. Ehrlich, P. Das Sauerstoff-Bedürfniss des Organismus: Eine farbenanalytische Studie; A. Hirschwald: **1885**.
- 6. Goldmann, E. E. Die aüssere und innere Sekretion des gesunden und kranken Organismus im Lichte der"vitalen Färbung"; H. Laupp: **1909**.
- 7. Goldmann, E. E. Vitalfärbung am Zentralnervensystem; Verl. der Akad. der Wiss.: 1913.
- 8. Stanness, K. A.; Westrum, L. E.; Fornaciari, E.; Mascagni, P.; Nelson, J. A.; Stenglein, S. G.; Myers, T.; Janigro, D. Morphological and functional characterization of an in vitro blood-brain barrier model. *Brain Res.* **1997**, *771*, 329-342.
- 9. Berezowski, V.; Landry, C.; Dehouck, M. P.; Cecchelli, R.; Fenart, L. Contribution of glial cells and pericytes to the mRNA profiles of P-glycoprotein and multidrug resistance-associated proteins in an in vitro model of the blood-brain barrier. *Brain Res.* **2004**, *1018*, 1-9.
- 10. Abbott, N. J. Prediction of blood-brain barrier permeation in drug discovery from in vivo, in vitro and in silico models. *Drug Discovery Today: Technologies* **2004**, *1*, 407-416.
- 11. Steiner, O.; Coisne, C.; Engelhardt, B.; Lyck, R. Comparison of immortalized bEnd5 and primary mouse brain microvascular endothelial cells as in vitro blood-brain barrier models for the study of T cell extravasation. *J. Cereb. Blood Flow Metab.* **2011**, *31*, 315-327.
- 12. Abbott, N. J.; Patabendige, A. A. K.; Dolman, D. E. M.; Yusof, S. R.; Begley, D. J. Structure and function of the blood-brain barrier. *Neurobiol. Dis.* **2010**, *37*, 13-25.
- 13. Dehouck, M. P.; Dehouck, B.; Fenart, L.; Cecchelli, R. Blood-brain barrier in vitro. Rapid evaluation of strategies for achieving drug targeting to the central nervous system. In Biology and *Physiology of the Blood-Brain Barrier*; Couraud, P. O.; Scherman, D. Eds.; Plenum Press: New York, **1996**; pp 143-146.

- 14. Cecchelli, R.; Berezowski, V.; Lundquist, S.; Culot, M.; Renftel, M.; Dehouck, M. P.; Fenart, L. Modelling of the blood-brain barrier in drug discovery and development. *Nat. Rev. Drug Discov.* **2007**, *6*, 650-661.
- Perrière, N.; Yousif, S.; Cazaubon, S.; Chaverot, N.; Bourasset, F.; Cisternino, S.; Declèves, X.; Hori, S.; Terasaki, T.; Deli, M.; Scherrmann, J. M.; Temsamani, J.; Roux, F.; Couraud, P. O. A functional in vitro model of rat blood-brain barrier for molecular analysis of efflux transporters. *Brain Res.* 2007, 1150, 1-13.
- Lanevskij, K.; Japertas, P.; Didziapetris, R.; Petrauskas, A. Ionization-Specific Prediction of Blood-Brain Permeability. J. Pharm. Sci. 2009, 98, 122-134.17.
 Stevenson, B. R.; Keon, B. H. The tight junction: morphology to molecules. *Ann. Rev. Cell Dev. Biol.* 1998, 14, 89-109.
- 18. Mitic, L. L.; Anderson, J. M. Molecular architecture of tight junctions. *Ann. Rev. Physiol.* **1998**, *60*, 121-142.
- 19. Abbott, N. J.; Ronnback, L.; Hansson, E. Astrocyte-endothelial interactions at the blood-brain barrier. *Nat. Rev. Neurosci.* **2006**, *7*, 41-53.
- 20. Ballabh, P.; Braun, A.; Nedergaard, M. The blood-brain barrier: an overview: structure, regulation, and clinical implications. *Neurobiology of Disease* **2004**, *16*, 1-13.
- 21. Abbott, N. J. Astrocyte-endothelial interactions and blood-brain barrier permeability. *J. Anat.* **2002**, *200*, 629-638.
- 22. Crone, C.; Christensen, O. Electrical-resistance of a capillary endothelium. *J. Gen. Physiol.* **1981**, 77, 349-371.
- 23. Butt, H. J.; Downing, K. H.; Hansma, P. K. Imaging the membrane-protein bacteriorhodopsin with the atomic force microscope. *Biophys. J.* **1990**, *58*, 1473-1480.
- 24. Wolburg, H.; Lippoldt, A. Tight junctions of the blood-brain barrier: Development, composition and regulation. *Vasc. Pharmacol.* **2002**, *38*, II.
- 25. Doan, K. M. M.; Humphreys, J. E.; Webster, L. O.; Wring, S. A.; Shampine, L. J.; Serabjit-Singh, C. J.; Adkison, K. K.; Polli, J. W. Passive permeability and P-glycoprotein-mediated efflux differentiate central nervous system (CNS) and non-CNS marketed drugs. *J. Pharmacol. Exp. Ther.* **2002**, *303*, 1029-1037.
- 26. Burns, E. M.; Buschmann, M. B. T.; Krukeberg, T. W.; Gaetano, P. K.; Meyer, J. N. Blood-brain barrier, aging, brain blood flow, and sleep. *Adv. Neurol.* **1981**, *30*, 301-306.
- 27. Cecchelli, R.; Dehouk, B.; Descamps, L.; Fenart, L.; Buéé-Scherrer, V.; Duhem, C.; Lundquist, S.; Rentfel, M.; Torpier, G.; Dehouck, M. P. In vitro model for evaluating drug transport across the blood-brain barrier. *Adv. Drug Deliv. Rev.* **1999**, *36*, 165-178.
- 28. Miller, D. S. Regulation of P-glycoprotein and other ABC drug transporters at the blood-brain barrier. *Trends Pharmacol. Sci.* **2010**, *31*, 246-254.
- 29. Weiss, N.; Miller, F.; Cazaubon, S.; Couraud, P. O. Biologie de la barrière hématoencéphalique: Partie I. *Rev. Neurol.* **2009**, *165*, 863-874.

- 30. Petty, M. A.; Lo, E. H. Junctional complexes of the blood-brain barrier: permeability changes in neuroinflammation. *Progr. Neurobiology* **2002**, *68*, 311-323.
- 31. Smith, M. W.; Gumbleton, M. Endocytosis at the blood-brain barrier: from basic understanding to drug delivery strategies. *J. Drug. Target.* **2006**, *14*, 191-214.
- 32. Hawkins, B. T.; Egleton, R. D. Pathophysiology of the blood-brain barrier: animal models and methods. In *Current Topics in Developmental Biology*, Volume 80 ed.; Gerald, P. S. Ed.; Academic Press: **2007**; pp 277-309.
- 33. Polakis, P. Formation of the blood-brain barrier: Wnt signaling seals the deal. *J. Cell. Biol.* 2008, 183, 371-373.
- 34. Weiss, N.; Miller, F.; Cazaubon, S.; Couraud, P. O. The blood-brain barrier in brain homeostasis and neurological diseases. *Biochim. Biophys. Acta* **2009**, *1788*, 842-857.
- 35. Löscher, W.; Potschka, H. Role of drug efflux transporters in the brain for drug disposition and treatment of brain diseases. *Prog. Neurobiology* **2005**, *76*, 22-76.
- 36. Gao, B.; Stieger, B.; Noé, B.; Fritschy, J. M.; Meier, P. J. Localization of the organic anion transporting polypeptide 2 (Oatp2) in capillary endothelium and choroid plexus epithelium of rat brain. *J. Histochem. Cytochem.* **1999**, *47*, 1255-1263.
- 37. Cordon-Cardo, C.; Obrien, J. P.; Casals, D.; Rittmangrauer, L.; Biedler, J. L.; Melamed, M. R.; Bertino, J. R. Multidrug-resistance gene (P-Glycoprotein) is expressed by endothelial-cells at blood-brain barrier sites. *Proc. Natl. Acad. Sci.* USA **1989**, *86*, 695-698.
- 38. Eisenblatter, T.; Galla, H. J. A new multidrug resistance protein at the blood-brain barrier. Biochem. *Biophys. Res. Commun.* **2002**, *293*, 1273-1278.
- 39. Salmina, A. B. Neuron-glia interactions as therapeutic targets in neurodegeneration. *J. Alzheimers Dis.* 2009, 16, 485-502.
- 40. Dehouck, M. P.; Meresse, S.; Delorme, P.; Fruchart, J. C.; Cecchelli, R. An easier, reproductible, and mass-production method to study the blood-brain barrier in vitro. *J. Neurochem.* **1990**, *54*, 1798-1801.
- 41. Rubin, L. L.; Hall, D. E.; Porter, S.; Barbu, K.; Cannon, C.; Horner, H. C.; Janatpour, M.; Liaw, C. W.; Manning, K.; Morales, J.; Tanner, L. I.; Tomaselli, K. J.; Bard, F. A cell-culture model of the blood-brain-barrier. *J. Cell. Biol.* **1991**, *115*, 1725-1735.
- 42. Ramsauer, M.; Krause, D.; Dermietzel, R. Angiogenesis of the blood-brain barrier in vitro and the function of cerebral pericytes. *FASEB J.* **2002**, *16*, 1274.
- 43. Sa-Pereira, I.; Brites, D.; Brito, M. A. Neurovascular unit: a focus on Pericytes. *Mol. Neurobiol.* **2012**, *45*, 327-347.
- 44. Stamatovic, S. M.; Keep, R. F.; Andjelkovic, A. V. Brain endothelial cell-cell junctions: How to "Open" the blood brain barrier. *Curr. Neuropharmacol.* **2008**, *6*, 179-192.
- 45. Cirrito, J. R.; Deane, R.; Fagan, A. M.; Spinner, M. L.; Parsadanian, M.; Finn, M. B.; Jiang, H.; Prior, J. L.; Sagare, A.; Bales, K. R.; Paul, S. M.; Zlokovic, B. V.; Piwnica-Worms, D.; Holtzman, D. M. P-glycoprotein deficiency at the blood-brain barrier increases amyloid-b

- deposition in an Alzheimer disease mouse model. J. Clin. Invest. 2005, 115, 3285-3290.
- 46. Lu, M.; Hu, G. Targeting metabolic inflammation in Parkinson's disease: implications for prospective therapeutic strategies. *Clin. Exp. Pharmacol. Physiol.* **2012**, *39*, 577-585.
- 47. Tan, E. K.; Chan, D. K. Y.; Ng, P. W.; Woo, J.; Teo, Y. Y.; Tang, K.; Wong, L. P.; Chong, S. S.; Tan, C.; Shen, H.; Zhao, Y.; Lee, C. G. L. Effect of MDR1 Haplotype on risk of Parkinson disease. *Arch. Neurol.* **2005**, *62*, 460-464.
- 48. Marroni, M.; Marchi, N.; Cucullo, L.; Abbott, N. J.; Signorelli, K.; Janigro, D. Vascular and parenchymal mechanisms in multiple drug resistance: a lesson from human epilepsy. *Curr. Drug Targets* **2003**, *4*, 297-304.
- 49. Varatharajan, L.; Thomas, S. A. The transport of anti-HIV drugs across blood-CNS interfaces: Summary of current knowledge and recommendations for further research. *Antiviral Research* **2009**, *82*, A99-A109.
- 50. Megard, I.; Garrigues, A.; Orlowski, S.; Jorajuria, S.; Clayette, P.; Ezan, E.; Mabondzo, A. A co-culture-based model of human blood-brain barrier: application to active transport of indinavir and in vivo-in vitro correlation. *Brain Res.* **2002**, *927*, 153-167.
- 51. Pittet, C. L.; Newcombe, J.; Prat, A.; Arbour, N. Human brain endothelial cells endeavor to immunoregulate CD8 T cells via PD-1 ligand expression in multiple sclerosis. *J. Neuroinflam.* **2011**, *8*.
- 52. Bennett, J.; Basivireddy, J.; Kollar, A.; Biron, K. E.; Reickmann, P.; Jefferies, W. A.; McQuaid, S. Blood-brain barrier disruption and enhanced vascular permeability in the multiple sclerosis model EAE. *J. Neuroimmunol.* **2010**, *229*, 180-191.
- 53. Cipolla, M. J.; Crete, R.; Vitullo, L.; Rix, R. D. Transcellular transport as a mechanism of blood-brain barrier disruption during stroke. *Frontiers in Biosc.* **2004**, *9*, 777-785.
- 54. Liu, H.; Xu, X.; Yang, Z.; Deng, Y.; Liu, X.; Xie, L. Impaired function and expression of P-glycoprotein in blood-brain barrier of streptozotocin-induced diabetic rats. *Brain Res.* **2006**, *1123*, 245-252.
- 55. Alavijeh, M. S.; Chishty, M.; Qaiser, M. Z.; Palmer, A. M. Drug metabolism and pharmacokinetics, the blood-brain barrier, and central nervous system drug discovery. *Neurotherapeutics* **2005**, *2*, 554-571.
- 56. Chancellor, M. B.; Staskin, D. R.; Kay, G. G.; Sandage, B. W.; Oefelein, M. G.; Tsao, J. W. Bloodbrain barrier permeation and efflux exclusion of anticholinergics used in the treatment of overactive bladder. *Drugs & Aging* **2012**, *29*, 259-273.
- 57. Summerfield, S. G.; Read, K.; Begley, D. J.; Obradovic, T.; Hidalgo, I. J.; Coggon, S.; Lewis, A. V.; Porter, R. A.; Jeffrey, P. Central nervous system drug disposition: the relationship between in situ brain permeability and brain free fraction. *J. Pharmacol. Exp. Ther.* **2007**, *322*, 205-213.
- 58. Lee, K.; Thakker, D. R. Saturable transport of H2-antagonists ranitidine and famotidine across Caco-2 cell monolayers. *J. Pharm. Sci.* **1999**, *88*, 680-687.

- 59. Zhou, S. Y.; Piyapolrungroj, N.; Pao, L. H.; Li, C.; Liu, G. Y.; Zimmermann, E.; Fleisher, D. Regulation of paracellular absorption of cimetidine and 5-aminosalicylate in rat intestine. *Pharm. Res.* **1999**, *16*, 1781-1785.
- 60. Flanagan, S. D.; Takahashi, L. H.; Liu, X. L.; Benet, L. Z. Contributions of saturable active secretion, passive transcellular, and paracellular diffusion to the overall transport of furosemide across adenocarcinoma (Caco-2) cells. *J. Pharm. Sci.* **2002**, *91*, 1169-1177.
- 61. Leontiadou, H.; Mark, A. E.; Marrink, S. J. Ion transport across transmembrane pores. *Biophys. J.* **2007**, *92*, 4209-4215.
- 62. Sugano, K.; Kansy, M.; Artursson, P.; Avdeef, A.; Bendels, S.; Di, L.; Ecker, G. F.; Faller, B.; Fischer, H.; Gerebtzoff, G.; Lennernaes, H.; Senner, F. Coexistence of passive and carrier-mediated processes in drug transport. *Nature Reviews Drug Discovery* 2010, 9, 597-614.
- 63. Waring, M. J. Lipophilicity in drug discovery. Expert Opin. Drug Discov. 2010, 5, 235-248.
- 64. Camenisch, G.; Alsenz, J.; van de Waterbeemd, H.; Folkers, G. Estimation of permeability by passive diffusion through Caco-2 cell monolayers using the drugs' lipophilicity and molecular weight. *Eur. J. Pharm. Sci.* **1998**, *6*, 313-319.
- 65. Johnson, T. W.; Dress, K. R.; Edwards, M. Using the golden triangle to optimize clearance and oral absorption. *Bioorg. Med. Chem. Lett.* **2009**, *19*, 5560-5564.
- 66. Pardridge, W. M. CNS drug design based on principles of blood-brain barrier transport. *J. Neurochem.* **1998**, *5*, 1781-1792.
- 67. Lipinski, C. A.; Lombardo, F.; Dominy, B. W.; Feeney, P. J. Experimental and computational approaches to estimate solubility and permeability in drug discovery and development settings. *Adv. Drug Deliv. Rev.* **1997**, *23*, 3-25.
- 68. Zhao, Y. H.; Abraham, M. H.; Ibrahim, A.; Fish, P. V.; Cole, S.; Lewis, M. L.; de Groot, M. J.; Reynolds, D. P. Predicting penetration across the blood-brain barrier from simple descriptors and fragmentation schemes. *J. Chem. Inf. Model.* **2006**, *47*, 170-175.
- 69. Avdeef, A. Absorption and Drug Development; John Wiley & Sons: Hoboken, 2003.
- 70. Kell, D. B.; Dobson, P. D.; Bilsland, E.; Oliver, S. G. The promiscuous binding of pharmaceutical drugs and their transporter-mediated uptake into cells: what we (need to) know and how we can do so . *Drug Discovery Today* **2012**.
- 71. Deli, M. A.; Abraham, C.; Kataoka, Y.; Niwa, M. Permeability studies on in vitro blood-brain barrier models: physiology, pathology, and pharmacology. *Cell. Mol. Neurobiol.* **2005**, *25*, 59-127.
- 72. Cecchelli, R.; Coisne, C.; Dehouck, L.; Miller, F.; Dehouck, M. P.; Buée-Scherrer, V.; Dehouck, B. Modeling the blood-brain barrier. In Blood-Brain Interfaces. From Ontogeny to Artificial Barriers; Dermietzel, R.; Spray, D. C.; Nedergaard, M. Eds.; Wiley-VCH Verlag GmbH: Weinheim, 2006; pp 337-355.

- 73. Ying, X.; Wen, H.; Yao, H. J.; Zhang, Y.; Tian, W.; Zhang, L.; Ju, R. J.; Wang, X. X.; Yu, Y.; Lu, W. L. Pharmacokinetics and tissue distribution of dual-targeting daunorubicin liposomes in mice. *Pharmacology* **2011**, *87*, 105-114.
- 74. Markoutsa, E.; Pampalakis, G.; Niarakis, A.; Romero, I. A.; Weksler, B.; Couraud, P. O.; Antimisiaris, S. G. Uptake and permeability studies of BBB-targeting immunoliposomes using the hCMEC/D3 cell line. *Eur. J. Pharm. Biopharm.* **2011**, *77*, 265-274.
- 75. Nau, R.; Soergel, F.; Eiffert, H. Penetration of drugs through the blood-cerebrospinal fluid/blood-brain barrier for treatment of central nervous system infections. *Clin. Microbiol. Rev.* **2010**, *23*, 858-883.
- 76. Kroll, R. A.; Neuwelt, E. A. Outwitting the blood-brain barrier for therapeutic purposes: osmotic opening and other means. *Neurosurgery* **1998**, *42*, 1083-1099.
- 77. Rapoport, S. I. Osmotic opening of the blood-brain barrier: principles, mechanism, and therapeutic applications. *Cell. Mol. Neurobiol.* **2000**, *20*, 217-230.
- 78. Nicolazzo, J. A.; Charman, S. A.; Charman, W. N. Methods to assess drug permeability across the blood-brain barrier. *J. Pharm. Pharmacol.* **2006**, *58*, 281-293.
- 79. Illum, L. Is nose-to-brain transport of drugs in man a reality? J. Pharm. Pharmacol. 2004, 56, 3-17.
- 80. Trivedi, J. B.; Upadhyay, P.; Shah, S.; Chauhan, N.; Patel, A. Intranasal liposomes: an approach for drug delivery to brain. *Int. J. Pharm. Res. Scholar.* **2012**, *1*, 79-91.
- 81. Deli, M. A. Potential use of tight junction modulators to reversibly open membranous barriers and improve drug delivery. *Biochim. Biophys. Acta* **2009**, *1788*, 892-910.
- 82. Zhang, H.; Prisinzano, T. E.; Donovan, M. D. Permeation and metabolism of cocaine in the nasal mucosa. *Eur. J. Drug Metabol. Pharmacokinet.* **2012**, *37*, 255-262.
- 83. Singh, A. P.; Saraf, S. K.; Saraf, S. A. SLN approach for nose-to-brain delivery of alprazolam. *Drug Deliv. and Transl. Res.* **2012**, *2*, 498-507.
- 84. Veronesi, M. C.; Kubek, D. J.; Kubek, M. J. Intranasal delivery of neuropeptides. *Neuropeptides* **2011**, *789*, 303-312.
- 85. Bousquet, L. Etude Comparative des Thérapies Anti-VIH: Rôle des Transporteurs d'Efflux sur le Passage Transmembranaire des Antirétroviraux au Niveau des Cellules CD4+ et de la Barrière Hémato-Encéphalique; Université Paris XI, 2008.
- 86. Drin, G.; Rousselle, C.; Scherrmann, J. M.; Rees, A. R.; Temsamani, J. Peptide delivery to the brain via adsorptive-mediated endocytosis: advances with SynB vectors. *AAPS Pharm. Sci.* **2002**, *4*.
- 87. Malakoutikhah, M.; Teixido, M.; Giralt, E. Toward an optimal blood-brain barrier shuttle by synthesis and evaluation of peptide libraries. *J. Math. Chem.* **2008**, *51*, 4881-4889.
- 88. Costantino, L.; Tosi, G.; Ruozi, B.; Bondioli, L.; Vandelli, M. A.; Forni, F. Colloidal systems for CNS drug delivery. In *Progress in Brain Research Nanoneuroscience and Nanoneuropharmacology*, Volume 180 ed.; Hari, S. S. Ed.; Elsevier: **2009**; pp 35-69.

- 89. Ruozi, B.; Tosi, G.; Forni, F.; Vandelli, M. A. Ketorolac tromethamine liposomes: encapsulation and release studies. *J. Liposome Res.* **2005**, *15*, 175-185.
- 90. Ali, M.; Kirby, D. J.; Mohammed, A. R.; Perrie, Y. Solubilisation of drugs within liposomal bilayers: alternatives to cholesterol as a membrane stabilising agent. *J. Pharm. Pharmacol.* **2010**, *62*, 1646-1655.
- 91. Gabizon, A. A. Pegylated liposomal doxorubicin: metamorphosis of an old drug into a new form of chemotherapy. *Cancer Investigation* **2001**, *19*, 424-436.
- 92. Working, P. K.; Dayan, A. D. Pharmacological-toxicological expert report Caelyx(TM) (Stealth(R) liposomal doxorubicin HCl) foreword. *Human Exp. Toxicol.* **1996**, *15*, 751-785.
- 93. Huwyler, J.; Wu, D.; Pardridge, W. M. Brain drug delivery of small molecules using immunoliposomes. *Proc. Natl. Acad. Sci. USA* **1996**, *93*, 14164-14169.
- 94. Mamot, C.; Ritschard, R.; Wicki, A.; Stehle, G.; Dieterle, T.; Bubendorf, L.; Hilker, C.; Deuster, S.; Herrmann, R.; Rochlitz, C. Tolerability, safety, pharmacokinetics, and efficacy of doxorubicin-loaded anti-EGFR immunoliposomes in advanced solid tumours: a phase 1 dose-escalation study. *Lancet Oncol.* **2012**, *13*, 1234-1241.
- 95. Mehlhorn, R. J.; Sumida, S.; Packer, L. Tocopheroxyl radical persistence and tocopherol consumption in liposomes and in vitamin-E-enriched rat-liver mitochondria and microsomes. *J. Biol. Chem.* **1989**, *264*, 13448-13452.
- 96. Hiremath, P. S.; Soppimath, K. S.; Betageri, G. V. Proliposomes of exemestane for improved oral delivery: Formulation and in vitro evaluation using PAMPA, Caco-2 and rat intestine. *Int. J. Pharm.* **2009**, *380*, 96-104.
- 97. Kreuter, J.; Alyautdin, R. N.; Kharkevich, D. A.; Ivanov, A. A. Passage of peptides through the blood-brain-barrier with colloidal polymer particles (nanoparticles). *Brain Res.* **1995**, *674*, 171-174.
- 98. Kreuter, J. Nanoparticulate systems for brain delivery of drugs. *Adv. Drug Deliv. Rev.* **2001**, *47*, 65-81.
- 99. Wohlfart, S.; Gelperina, S.; Kreuter, J. Transport of drugs across the blood-brain barrier by nanoparticles. *J. Control Release* **2012**, *161*, 264-273.
- 100. Lombardo, F.; Blake, J. F.; Curatolo, W. J. Computation of brain-blood partitioning of organic solutes via free energy calculations. *J. Med. Chem.* **1996**, *39*, 4750-4755.
- 101. Abraham, M. H.; Chadha, H. S.; Mitchell, R. C. Hydrogen bonding. 33. Factors that influence the distribution of solutes between blood and brain. *J. Pharm. Sci.* **1994**, *83*, 1257-1268.
- 102. Chadha, H. S.; Abraham, M. H.; Mitchell, R. C. Physicochemical analysis of the factors governing distribution of solutes between blood and brain. *Bioorg. Med. Chem. Lett.* **1994**, *4*, 2511-2516.
- 103. Abraham, M. H.; Hersey, A. In silico models to predict brain uptake. In *Comprehensive Medicinal Chemistry II*; Elsevier Ltd: **2007**; pp 745-766.

- 104. Didziapetris, R.; Japertas, P.; Avdeef, A.; Petrauskas, A. Classification analysis of P-glycoprotein substrate specificity. *J. Drug Targeting* **2003**, *11*, 391-406.
- 105. Timmermans, P. B. M. W. M.; Brands, A.; van Zwieten, N. S. Lipophilicity and brain disposition of clonidine and structurally related imidazolidines. *Arch. Pharm.* **1977**, *300*, 217-226.
- 106. Salminen, T.; Pulli, A.; Taskinen, J. Relationship between immobilised artificial membrane chromatographic retention and the brain penetration of structurally diverse drugs. J. Pharm. Biomed. Anal. 1997, 15, 469-477. 107. Taillardat-Bertschinger, A.; Carrupt, P. A.; Barbato, F.; Testa, B. Immobilized artificial membrane (IAM)-HPLC in drug research. J. Med. Chem. 2003, 46, 655-665.
- 108. Taillardat-Bertschinger, A.; Galland, A.; Carrupt, P. A.; Testa, B. Immobilized artificial membrane (IAM)-HPLC: proposed guidelines for technical optimization of retention measurements. *J. Chromatogr. A* **2002**, *953*, 39-53.
- 109. Taillardat-Bertschinger, A.; A Marca-Martinet, C.; Carrupt, P. A.; Reist, M.; Caron, G.; Fruttero, R.; Testa, B. Molecular factors influencing retention on immobilized artificial membranes (IAM) compared to partitioning in liposomes and n-octanol. *Pharm. Res.* **2002**, *19*, 729-737.
- 110. Taillardat-Bertschinger, A.; Barbato, F.; Quercia, M. T.; Carrupt, P. A.; Reist, M.; La Rotonda, M. I.; Testa, B. Structural properties governing retention mechanisms on immobilized artificial membrane (IAM) HPLC-columns. *Helv. Chim. Acta* **2002**, *85*, 519-532.
- 111. Ong, S.; Liu, H.; Qiu, X.; Bhat, G.; Pidgeon, C. Membrane partition coefficients chromatographically measured using immobilized artificial membrane surfaces. Anal. Chem. 1995, 67, 755-762. 112. Pidgeon, C.; Ong, S.; Liu, H.; Qiu, X.; Pidgeon, M.; Dantzig, M.; Dantzig, A. H.; Munroe, J.; Hornback, W. J.; Kasher, J. S.; Glunz, L.; Szczerba, T. IAM chromatography: an in vitro screen for predicting drug membrane permeability. J. Med. Chem. 1995, 38, 590-594.
- 113. Stenberg, P.; Norinder, U.; Luthman, K.; Artursson, P. Experimental and computational screening models for the prediction of instestinal drug absorption. *J. Med. Chem.* **2001**, *44*, 1927-1937.
- 114. Osterberg, T.; Svensson, M.; Lundahl, P. Chromatographic retention of drug molecules on immobilised liposomes prepared from egg phospholipids molecules and from chemically pure phospholipids. *Eur. J. Pharm. Sci.* **2001**, *12*, 427-439.
- 115. Kansy, M.; Senner, F.; Gubernator, K. Physicochemical high throughput screening: parallel artificial membrane permeation assay in the description of passive absorption processes. *J. Med. Chem.* **1998**, *41*, 1007-1010.
- 116. Zizzari, A.; Carrupt, P. A.; Martel, S. UHPLC for the determination of physicochemical parameters in drug discovery. In *Basics of UHPLC and Application in Life Science Analysis*, In press ed.; Guillarme, D.; Veuthey, J. L. Eds.; RSC publishing: **2012**.
- 117. Mensch, J.; Noppe, M.; Adriaensen, J.; Melis, A.; Mackie, C.; Augustijns, P.; Brewster, M. E. Novel generic UPLC/MS/MS method for high throughput analysis applied to permeability assessment in early Drug Discovery. *J. Chromatogr. B* **2007**, *847*, 182-187.

- 118. Han, M.; Fu, S.; Gao, J. Q.; Fang, X. L. Evaluation of intestinal absorption of Ginsenoside Rg(1) incorporated in microemulison using parallel artificial membrane permeability assay. *Biol. Pharm. Bull.* **2009**, *32*, 1069-1074.
- 119. Wohnsland, F.; Faller, B. High-throughput permeability pH profile and high-throughput alkane/water log P with artificial membranes. *J. Med. Chem.* **2001**, *44*, 923-930.
- 120. Ottaviani, G.; Martel, S.; Carrupt, P. A. Parallel artificial membrane permeability assay: a new membrane for the fast prediction of passive human skin permeability. *J. Med. Chem.* **2006**, *49*, 3948-3954.
- 121. Di, L.; Kerns, E. H.; Fan, K.; McConnell, O. J.; Carter, G. T. High throughput artificial membrane permeability assay for blood-brain barrier. *Eur. J. Med. Chem.* **2003**, *38*, 223-232.
- 122. Di, L.; Kerns, E. H.; Ma, X. J.; Huang, Y. P.; Carter, G. T. Applications of high throughput microsomal stability assay in drug discovery. *Comb. Chem. Highthroughput Screen.* **2008**, *11*, 469-476.
- 123. Di, L.; Kerns, E. H.; Bezar, I. F.; Petusky, S. L.; Huang, Y. P. Comparison of blood-brain barrier permeability assays: in situ brain perfusion, MDR1-MDCKII and PAMPA-BBB. *J. Pharm. Sci.* **2009**, *98*, 1980-1991.
- 124. Mensch, J.; Melis, A.; Mackie, C.; Verreck, G.; Brewster, M. E.; Augustijns, P. Evaluation of various PAMPA models to identify the most discriminating method for the prediction of BBB permeability. *Eur. J. Pharm. Biopharm.* **2010**, *74*, 495-502.
- 125. Mathot, F.; Schanck, A.; van Bambeke, F.; Ariën, A.; Noppe, M.; Brewster, M.; Préat, V. Passive diffusion of polymeric surfactants across lipid bilayers. *J. Control Release* **2007**, *120*, 79-87.
- 126. Kansy, M.; Fischer, H.; Kratzat, K.; Senner, F.; Wagner, B.; Parrilla, I. High-throughput artificial membrane permeability studies in early lead discovery and development. In Pharmacokinetic Optimization in Drug Research: Biological, Physicochemical and Computational Strategies; Testa, B.; van de Waterbeemd, H.; Folkers, G.; Guy, R. H. Eds.; Wiley-VHCA: Zurich, 2001; pp 447-464.
- 127. Lundquist, S.; Renftel, M.; Brillault, J.; Fenart, L.; Cecchelli, R.; Dehouck, M. P. Prediction of drug transport through the blood-brain barrier in vivo: A comparison between two in vitro cell models. *Pharm. Res.* **2002**, *19*, 976-981.
- 128. Pardridge, W. M. The blood-brain barrier and neurotherapeutics. *Neurotherapeutics* **2005**, *2*, 1-2.
- 129. Garberg, P.; Ball, M.; Borg, N.; Cecchelli, R.; Fenart, L.; Hurst, R. D.; Lindmark, T.; Mabondzo, A.; Nilsson, J. E.; Raub, T. J.; Stanimirovic, D.; Terasaki, T.; Öberg, J.-O.; Österberg, T. In vitro models for the blood-brain barrier. *Toxicol. in Vitro* **2005**, *19*, 299-334.
- 130. Gumbleton, M.; Audus, K. L. Progress and limitations in the use of in vitro cell cultures to serve as a permeability screen for the blood-brain barrier. *J. Pharm. Sci.* **2001**, *90*, 1681-1698.
- 131. Avdeef, A. How well can in vitro brain microcapillary endothelial cell models predict rodent in vivo blood-brain barrier permeability? *Eur. J. Pharm. Sci.* **2011**, *43*, 109-124.

- 132. Bickel, U. How to measure drug transport across the blood-brain barrier. *NeuroRx* **2005**, *2*, 15-26.
- 133. Abbruscato, T. J.; Davis, T. P. Combination of hypoxia/aglycemia compromises in vitro blood-brain barrier integrity. *J. Pharmacol. Exp. Ther.* **1999**, *289*, 668-675.
- 134. Audus, K. L.; Borchardt, R. T. Characteristics of the large neutral amino acid transport system of bovine brain microvessel endothelial cell monolayers. *J. Neurochem.* **1986**, *47*, 484-488.
- 135. Audus, K. L.; Borchardt, R. T. Characterization of an invitro blood-brain-barrier model system for studying drug transport and metabolism. *Pharm. Res.* **1986**, *3*, 81-87.
- 136. Bowman, P. D.; Ennis, S. R.; Rarey, K. E.; Betz, A. L.; Goldstein, G. W. Brain microvessel endothelial-cells in tissue-culture A model for study of blood-brain-barrier permeability. *Ann. Neurol.* **1983**, *14*, 396-402.
- 137. Eddy, E. P.; Maleef, B. E.; Hart, T. K.; Smith, P. L. In vitro models to predict blood-brain barrier permeability. Adv. Drug Deliv. Rev. 1997, 23, 185-198. 138. Letrent, S. P.; Polli, J. W.; Humphreys, J. E.; Pollack, G. M.; Brouwer, K. R.; Brouwer, K. L. R. P-glycoprotein-mediated transport of morphine in brain capillary endothelial cells. Biochem. *Pharmacol.* 1999, 58, 951-957.
- 139. Pirro, J. P.; Dirocco, R. J.; Narra, R. K.; Nunn, A. D. Relationship between in-vitro transendothelial permeability and in-vivo single-pass brain extraction. *J. Nucl. Med.* **1994**, *35*, 1514-1519.
- 140. Raub, T. J.; Kuentzel, S. L.; Sawada, G. A. Permeability of bovine brain microvessel endothelial cells in vitro: Barrier tightening by a factor released from astroglioma cells. *Exp. Cell. Res.* **1992**, *199*, 330-340.
- 141. Smith, K. R.; Borchardt, R. T. Permeability and mechanism of albumin, cationized albumin, and glycosylated albumin trans-cellular transport across monolayers of cultured bovine brain capillary endothelial-cells. *Pharm. Res.* **1989**, *6*, 466-473.
- 142. van Bree, J. B. M. M.; de Boer, A. G.; Danhof, M.; Ginsel, L. A.; Breimer, D. D. Characterization of an in vitro blood-brain barrier: effects of molecular size and lipophilicity on cerebrovascular endothelial transport rates of drugs. *J. Pharmacol. Exp. Ther.* **1988**, 247, 1233-1239.
- 143. Wang, W.; Dentler, W. L.; Borchardt, R. T. VEGF increases BMEC monolayer permeability by affecting occludin expression and tight junction assembly. Am. *J. Physiol. Heart Circ. Physiol.* **2001**, *280*, H434-H440.
- 144. Fischer, S.; Clauss, M.; Wiesnet, M.; Renz, D.; Schaper, W.; Karliczek, G. F. Hypoxia induces permeability in brain microvessel endothelial cells via VEGF and NO. *Am. J. Physiol. Cell. Physiol.* **1999**, *276*, C812-C820.
- 145. Fischer, S.; Renz, D.; Schaper, W.; Karliczek, G. F. In vitro effects of dexamethasone on hypoxia-induced hyperpermeability and expression of vascular endothelial growth factor. *Eur. J. Pharmacol.* **2001**, *411*, 231-243.

- 146. Fischer, S.; Renz, D.; Schaper, W.; Karliczek, G. F. Effects of barbiturates on hypoxic cultures of brain derived microvascular endothelial cells. *Brain Res.* **1996**, *707*, 47-53.
- 147. Fischer, S.; Renz, D.; Schaper, W.; Karliczek, G. F. Barbiturates decrease the expression of vascular endothelial growth factor in hypoxic cultures of porcine brain derived microvascular endothelial cells. *Mol. Brain Res.* **1998**, *60*, 89-97.
- 148. Fischer, S.; Wobben, M.; Kleinstuck, J.; Renz, D.; Schaper, W. Effect of astroglial cells on hypoxia-induced permeability in PBMEC cells. *Am. J. Physiol. Cell. Physiol.* **2000**, *279*, C935-C944.
- 149. Ichikawa, N.; Naora, K.; Hirano, H.; Hashimoto, M.; Masumura, S.; Iwamoto, K. Isolation and primary culture of rat cerebral microvascular endothelial cells for studying drug transport in vitro. *J. Pharmacol. Toxicol. Methods* **1996**, *36*, 45-52.
- 150. Annunziata, P.; Cioni, C.; Toneatto, S.; Paccagnini, E. HIV-1 gp120 increases the permeability of rat brain endothelium cultures by a mechanism involving substance P. *Aids* **1998**, *12*, 2377-2385.
- 151. Demeuse, P.; Kerkhofs, A.; Struys-Ponsar, C.; Knoops, B.; Remacle, C.; de Aguilar, P. V. Compartmentalized coculture of rat brain endothelial cells and astrocytes: a syngenic model to study the blood-brain barrier. *J. Neurosci. Meth.* **2002**, *121*, 21-31.
- 152. Sahagun, G.; Moore, S. A.; Hart, M. N. Permeability of neutral vs anionic dextrans in cultured brain microvascular endothelium. *Am. J. Physiol.* **1990**, *259*, H162-H166.
- 153. Imaizumi, S.; Kondo, T.; Deli, M. A.; Gobbel, G.; Joo, F.; Epstein, C. J.; Yoshimoto, T.; Chan, P. H.

 The influence of oxygen free radicals on the permeability of the monolayer of cultured brain endothelial cells. *Neurochem. Int.* **1996**, *29*, 205-211.
- 154. Muruganandam, A.; Herx, L. M.; Monette, R.; Durkin, J. P.; Stanimirovic, D. B. Development of immortalized human cerebromicrovascular endothelial cell line as in vitro model of the human blood-brain barrier. *FASEB J.* **1997**, *11*, 1187.
- 155. Mackic, J. B.; Stins, M.; Mccomb, J. G.; Calero, M.; Ghiso, J.; Kim, K. S.; Yan, S. D.; Stern, D.; Schmidt, A. M.; Frangione, B.; Zlokovic, B. V. Human blood-brain barrier receptors for Alzheimer's amyloid-beta 1-40 Asymmetrical binding, endocytosis, and transcytosis at the apical side of brain microvascular endothelial cell monolayer. *J. Clin. Invest.* 1998, 102, 734-743.
- 156. Stins, M. F.; Badger, J.; Sik Kim, K. Bacterial invasion and transcytosis in transfected human brain microvascular endothelial cells. *Microb. Pathogen.* **2001**, *30*, 19-28.
- 157. Jong, A. Y.; Stins, M. F.; Huang, S. H.; Chen, S. H. M.; Kim, K. S. Traversal of Candida albicans across human blood-brain barrier In vitro. *Infect. Immun.* **2001**, *69*, 4536-4544.
- 158. Yang, T.; Roder, K. E.; Abbruscato, T. J. Evaluation of bEnd5 cell line as an in vitro model for the blood-brain barrier under normal and hypoxic/aglycemic conditions. *J. Pharm. Sci.* **2007**, *96*, 3196-3213.
- 159. Zenker, D.; Begley, D.; Bratzke, H.; Rübsamen-Waigmann, H.; von Briesen, H. Human blood-derived macrophages enhance barrier function of cultured primary bovine and human brain capillary endothelial cells. *J. Physiol.* **2003**, *551*, 1023-1032.

- 160. Schulze, C.; Smales, C.; Rubin, L. L.; Staddon, J. M. Lysophosphatidic acid increases tight junction permeability in cultured brain endothelial cells. *J. Neurochem.* **1997**, *68*, 991-1000.
- 161. Gloor, S. M.; Weber, A.; Adachi, N.; Frei, K. Interleukin-1 modulates protein tyrosine phosphatase activity and permeability of brain endothelial cells. *Biochem. Biophys. Res. Commun.* **1997**, *239*, 804-809.
- 162. Hoheisel, D.; Nitz, T.; Franke, H.; Wegener, J.; Hakvoort, A.; Tilling, T.; Galla, H. J. Hydrocortisone reinforces the blood-brain barrier properties in a serum free cell culture system). *Biochem. Biophys. Res. Commun.* **1998**, *244*, 293-297.
- 163. Tilling, T.; Korte, D.; Hoheisel, D.; Galla, H. J. Basement membrane proteins influence brain capillary endothelial barrier function in vitro. *J. Neurochem.* **1998**, *71*, 1151-1157.
- 164. Franke, H.; Galla, H. J.; Beuckmann, C. T. An improved low-permeability in vitro-model of blood-brain barrier: transport studies on retinoids, sucrose, haloperidol, caffeine and mannitol. *Brain Res.* **1999**, *818*, 65-71.
- 165. Nitz, T.; Eisenblatter, T.; Psathaki, K.; Galla, H. J. Serum-derived factors weaken the barrier properties of cultured porcine brain capillary endothelial cells in vitro. *Brain Res.* **2003**, *981*, 30-40.
- 166. Igarashi, Y.; Utsumi, H.; Chiba, H.; Yamada-Sasamori, Y.; Tobioka, H.; Kamimura, Y.; Furuuchi, K.; Kokai, Y.; Nakagawa, T.; Mori, M.; Sawada, N. Glial cell line-derived neurotrophic factor induces barrier function of endothelial cells forming the blood-brain barrier. *Biochem. Biophys. Res. Commun.* **1999**, *261*, 108-112.
- 167. Yamagata, K.; Tagami, M.; Takenaga, F.; Yamori, Y.; Nara, Y.; Itoh, S. Polyunsaturated fatty acids induce tight junctions to form in brain capillary endothelial cells. *Neuroscience* **2003**, *116*, 649-656.
- 168. Franke, H.; Galla, H. J.; Beuckmann, C. T. Primary cultures of brain microvessel endothelial cells: a valid and flexible model to study drug transport through the blood-brain barrier in vitro. *Brain Res. Prot.* **2000**, *5*, 248-256.
- 169. Lohmann, C.; Hüwel, S.; Galla, H. J. Predicting blood-brain barrier permeability of drugs: evaluation of different in vitro assays. *J. Drug Targeting* **2002**, *10*, 263-276.
- 170. Smith, M.; Omidi, Y.; Gumbleton, M. Primary porcine brain microvascular endothelial cells: biochemical and functional characterisation as a model for drug transport and targeting. *J. Drug. Target.* **2007**, *15*, 253-268.
- 171. Bernas, M. J.; Cardoso, F. L.; Daley, S. K.; Weinand, M. E.; Campos, A. R.; Ferreira, A. J. G.; Hoying, J. B.; Witte, M. H.; Brites, D.; Persidsky, Y.; Ramirez, S. H.; Brito, M. A. Establishment of primary cultures of human brain microvascular endothelial cells to provide an in vitro cellular model of the blood-brain barrier. *Nat. Protocols* **2010**, *5*, 1265-1272.
- 172. Ramirez, S. H.; Hasko, J.; Skuba, A.; Fan, S.; Dykstra, H.; McCormick, R.; Reichenbach, N.; Krizbai, I.; Mahadevan, A.; Zhang, M.; Tuma, R.; Son, Y. J.; Persidsky, Y. Activation of cannabinoid receptor 2 attenuates leukocyte-endothelial cell interactions and bloodbrain barrier dysfunction under inflammatory conditions. *J. Neurosci.* **2012**, *32*, 4004-4016.

- 173. Benistant, C.; Dehouck, M. P.; Fruchart, J. C.; Cecchelli, R.; Lagarde, M. Fatty-acid composition of brain capillary endothelial-cells effect of the coculture with astrocytes. *J. Lipid Res.* **1995**, *36*, 2311-2319.
- 174. Edgell, C. J.; Mcdonald, C. C.; Graham, J. B. Permanent cell-line expressing human factor-Viiirelated antigen established by hybridization. *Proc. Natl. Acad. Sci. USA* **1983**, *80*, 3734-3737.
- 175. Shay, J. W.; Wright, W. E.; Werbin, H. Defining the molecular mechanisms of human cell immortalization. Biochim. *Biophys. Acta* **1991**, *1072*, 1-7.
- 176. Kirinaka, H.; Miyake, K.; Iijima, S. Isolation of immortal human endothelial cells. *Biosci. Biotech. Biochem.* **1995**, *59*, 912-914.
- 177. Roux, F.; Durieu-Trautmann, O.; Chaverot, N.; Claire, M.; Mailly, P.; Bourre, J. M.; Strosberg, A. D.; Couraud, P. O. Regulation of g-glutamyl transpeptidase and alkaline phosphatase activities in immortalized rat brain microvessel endothelial cells. *J. Cellul. Physiol.* **1994**, *159*, 101-113.
- 178. Sobue, K.; Yamamoto, N.; Yoneda, K.; Hodgson, M. E.; Yamashiro, K.; Tsuruoka, N.; Tsuda, T.; Katsuya, H.; Miura, Y.; Asai, K.; Kato, T. Induction of blood-brain barrier properties in immortalized bovine brain endothelial cells by astrocytic factors. *Neurosci. Res.* **1999**, *35*, 155-164.
- 179. Weksler, B. B.; Subileau, E. A.; Perriere, N.; Charneau, P.; Holloway, K.; Leveque, M.; Tricoire-Leignel, H.; Nicotra, A.; Bourdoulous, S.; Turowski, P.; Male, D. K.; Roux, F.; Greenwood, J.; Romero, I. A.; Couraud, P. O. Blood-brain barrier-specific properties of a human adult brain endothelial cell line. *FASEB J.* **2005**, *19*, 1872-+.
- 180. Kannan, R.; Chakrabarti, R.; Tang, D.; Kim, K. J.; Kaplowitz, N. GSH transport in human cerebrovascular endothelial cells and human astrocytes: evidence for luminal localization of Na+-dependent GSH transport in HCEC. *Brain Res.* **2000**, *852*, 374-382.
- 181. Gu, X.; Zhang, J.; Brann, D. W.; Yu, F. S. Brain and retinal vascular endothelial cells with extended life span established by ectopic expression of telomerase. *Invest. Ophtamol. Visual Sci.* **2003**, *44*, 3219-3225.
- 182. Hurst, R. D.; Fritz, I. B. Properties of an immortalised vascular endothelial/glioma cell co-culture model of the blood-brain barrier. *J. Cellul. Physiol.* **1996**, *167*, 81-88.
- 183. Hurst, R. D.; Heales, S. J. R.; Dobbie, M. S.; Barker, J. E.; Clark, J. B. Decreased endothelial cell glutathione and increased sensitivity to oxidative stress in an in vitro blood-brain barrier model system. *Brain Res.* **1998**, *802*, 232-240.
- 184. Dobbie, M. S.; Hurst, R. D.; Klein, N. J.; Surtees, R. A. H. Upregulation of intercellular adhesion molecule-1 expression on human endothelial cells by tumour necrosis factor-alpha in an in vitro model of the blood-brain. *Brain Res.* **1999**, *830*, 330-336.
- 185. Scism, J. L.; Laska, D. A.; Horn, J. W.; Gimple, J. L.; Pratt, S. E.; Shepard, R. L.; Dantzig, A. H.; Wrighton, S. A. Evaluation of an in vitro coculture model for the blood-brain barrier: comparison of human umbilical vein endothelial cells (ECV304) and rat glioma cells (C6) from two commercial sources. *In Vitro Cell Dev Biol Anim* **1999**, *35*, 580-592.

- 186. Easton, A. S.; Abbott, N. J. Bradykinin increases permeability by calcium and 5-lipoxygenase in the ECV304/C6 cell culture model of the blood-brain barrier. *Brain Res.* **2002**, *953*, 157-169.
- 187. Hosoya, K.; Tetsuka, K.; Nagase, K.; Tomi, M.; Saeki, S.; Ohtusuki, S.; Terasaki, T. Conditionally immortalized brain capillary endothelial cell lines established from a transgenic mouse harboring temperature-sensitive simian virus 40 large T-antigen gene. *AAPS Pharm. Sci.* **2000**, *2*, 1-11.
- 188. Youdim, K. A.; Dobbie, M. S.; Kuhnle, G.; Proteggente, A. R.; Abbott, N. J.; Rice-Evans, C. Interaction between flavonoids and the blood-brain barrier: in vitro studies. *J. Neurochem.* **2003**, *85*, 180-192.
- 189. Rist, R. J.; Romero, I. A.; Chan, M. W. K.; Couraud, P. O.; Roux, F.; Abbott, N. J. F-actin cytoskeleton and sucrose permeability of immortalised rat brain microvascular endothelial cell monolayers: effects of cyclic AMP and astrocytic factors. *Brain Res.* 1997, 768, 10-18.
- 190. Mertsch, K.; Blasig, I.; Grune, T. 4-Hydroxynonenal impairs the permeability of an in vitro rat blood-brain barrier. *Neuroscience Lett.* **2001**, *314*, 135-138.
- 191. Romero, I. A.; Rist, R. J.; Aleshaiker, A.; Abbott, N. J. Metabolic and permeability changes caused by thiamine deficiency in immortalized rat brain microvessel endothelial cells. *Brain Res.* **1997**, *756*, 133-140.
- 192. Romero, I. A.; Prevost, M. C.; Perret, E.; Adamson, P.; Greenwood, J.; Couraud, P. O.; Ozden, S. Interactions between brain endothelial cells and human T-cell leukemia virus type 1-infected lymphocytes: Mechanisms of viral entry into the central nervous system. *J. Virol.* **2000**, *74*, 6021-6030.
- 193. Romero, I. A.; Radewicz, K.; Jubin, E.; Michel, C. C.; Greenwood, J.; Couraud, P. O.; Adamson, P. Changes in cytoskeletal and tight junctional proteins correlate with decreased permeability induced by dexamethasone in cultured rat brain endothelial cells. *Neuroscience Lett.* **2003**, 344, 112-116.
- 194. Poller, B.; Gutmann, H.; Krahenbuhl, S.; Weksler, B.; Romero, I.; Couraud, P. O.; Tuffin, G.; Drewe, J.; Huwyler, J. The human brain endothelial cell line hCMEC/D3 as a human blood-brain barrier model for drug transport studies. *J. Neurochem.* **2008**, *107*, 1358-1368.
- 195. Kiss, L.; Walter, F. R.; Bocsik, A.; Veszelka, S.; Ozsvari, B.; Puskas, L. G.; Szabo-Revesz, P.; Deli, M. A. Kinetic analysis of the toxicity of pharmaceutical excipients cremophor EL and RH40 on endothelial and epithelial cells. *J. Pharm. Sci.* **2013**, *102* (4), 1173-1181.
- 196. Daniels, B. P.; Cruz-Orengo, L.; Pasieka, T. J.; Couraud, P. O.; Romero, I. A.; Weksler, B.; Cooper, J. A.; Doering, T. L.; Klein, R. S. Immortalized human cerebral microvascular endothelial cells maintain the properties of primary cells in an in vitro model of immune migration across the blood brain barrier. *J. Neurosci. Meth.* **2013**, *212*, 173-179.
- 197. Ohtsuki, S.; Ikeda, C.; Uchida, Y.; Sakamoto, Y.; Miller, F.; Glacial, F.; Decleves, X.; Scherrmann, J. M.; Couraud, P. O.; Kubo, Y.; Tachikawa, M.; Terasaki, T. Quantitative targeted absolute proteomic analysis of transporters, receptors and junction proteins for

- validation of human cerebral microvascular endothelial cell lne hCMEC/D3 as a human blood-brain barrier model. *Mol. Pharm.* **2012**, *10*, 289-296.
- 198. Culot, M.; Lundquist, S.; Vanuxeem, D.; Nion, S.; Landry, C.; Delplace, Y.; Dehouck, M. P.; Berezowski, V.; Fenart, L.; Cecchelli, R. An in vitro blood-brain barrier model for high throughput (HTS) toxicological screening. *Toxicol. in Vitro* **2008**, *22*, 799-811.
- 199. Sano, Y.; Shimizu, F.; Abe, M.; Maeda, T.; Kashiwamura, Y.; Ohtsuki, S.; Terasaki, T.; Obinata, M.; Kajiwara, K.; Fujii, M.; Suzuki, M.; Kanda, T. Establishment of a new conditionally immortalized human brain microvascular endothelial cell line retaining an in vivo blood-brain barrier function. *J. Cellul. Physiol.* **2010**, *225*, 519-528.
- 200. Hakkarainen, J. J.; Jalkanen, A. J.; Kääriäinen, T. M.; Keski-Rahkonen, P.; Venäläinen, T.; Hokkanen, J.; Mönkkönen, J.; Suhonen, M.; Forsberg, M. M. Comparison of in vitro cell models in predicting in vivo brain entry of drugs. *Int. J. Pharm.* **2010**, *402*, 27-36.
- 201. Nakagawa, S.; Deli, M. A.; Kawaguchi, H.; Shimizudani, T.; Shimono, T.; Kittel, A.; Tanaka, K.; Niwa, M. A new blood-brain barrier model using primary rat brain endothelial cells, pericytes and astrocytes. *Neurochem. Int.* **2009**, *54*, 253-263.
- 202. Gaillard, P. J.; Voorwinden, L. H.; Nielsen, J. L.; Ivanov, A.; Atsumi, R.; Engman, H.; Ringbom, C.; de Boer, A. G.; Breimer, D. D. Establishment and functional characterization of an in vitro model of the blood-brain barrier, comprising a co-culture of brain capillary endothelial cells and astrocytes. *Eur. J. Pharm. Sci.* **2001**, *12*, 215-222.
- 203. Janzer, R. C.; Raff, M. C. Astrocytes induce blood-brain barrier properties in endothelial cells. *Nature* 1987, 325, 253-257.
- 204. Fenart, L.; Buee-Scherrer, V.; Descamps, L.; Duhem, C.; Poullain, M. G.; Cecchelli, R.; Dehouck, M. P. Inhibition of P-glycoprotein: rapid assessment of its implication in blood-brain barrier integrity and drug transport to the brain by an in vitro model of the blood-brain barrier. *Pharm. Res.* **1998**, *15*, 993-1000.
- 205. Calabria, A. R.; Weidenfeller, C.; Jones, A. R.; De Vries, H. E.; Shusta, E. V. Puromycin-purified rat brain microvascular endothelial cell cultures exhibit improved barrier properties in response to glucocorticoid induction. *J. Neurochem.* **2006**, *97*, 922-933.
- 206. Dohgu, S.; Takata, F.; Yamauchi, A.; Nakagawa, S.; Egawa, T.; Naito, M.; Tsuruo, T.; Sawada, Y.; Niwa, M.; Kataoka, Y. Brain pericytes contribute to the induction and up-regulation of blood-brain barrier functions through transforming growth factor-beta production. *Brain Res.* 2005, 1038, 208-215.
- 207. Dehouck, M. P.; Jolliet-Riant, P.; Brée, F.; Fruchart, J. C.; Cecchelli, R.; Tillement, J. P. Drug transfer across the blood-brain barrier: correlation between in vitro and in vivo models. *J. Neurochem.* **1992**, *58*, 1790-1797.
- 208. Lacombe, O.; Videau, O.; Chevillon, D.; Guyot, A. C.; Contreras, C.; Blondel, S.; Nicolas, L.; Ghettas, A.; Benech, H.; Thevenot, E.; Pruvost, A.; Bolze, S.; Krzaczkowski, L.; Prevost, C.; Mabondzo, A. In vitro primary human and animal cell-based blood-brain barrier models as a screening tool in drug discovery. *Mol. Pharm.* **2011**, *8*, 651-663.

- 209. Lu, W.; Tan, Y. Z.; Jiang, X. G. Establishment of coculture model of blood-brain barrier in vitro for nanoparticle's transcytosis and toxicity evaluation. *Acta Pharm. Sinica* **2006**, *41*, 296-304.
- 210. Shayan, G.; Choi, Y. S.; Shusta, E. V.; Shuler, M. L.; Lee, K. H. Murine in vitro model of the blood-brain barrier for evaluating drug transport. *Eur. J. Pharm. Sci.* **2011**, *42*, 148-155.
- 211. Coisne, C.; Dehouck, L.; Faveeuw, C.; Delplace, Y.; Miller, F.; Landry, C.; Morissette, C.; Fenart, L.; Cecchelli, R.; Tremblay, P.; Dehouck, B. Mouse syngenic in vitro blood-brain barrier model: a new tool to examine inflammatory events in cerebral endothelium. *Lab. Invest.* **2005**, *85*, 734-746.
- 212. Dehouck, B.; Dehouck, M. P.; Fruchart, J. C.; Cecchelli, R. Upregulation of the low-density-lipoprotein receptor at the blood-brain-barrier Intercommunications between brain capillary endothelial-cells and astrocytes. *J. Cell Biol.* **1994**, *126*, 465-473.
- 213. Descamps, L.; Dehouck, M. P.; Torpier, G.; Cecchelli, R. Receptor-mediated transcytosis of transferrin through blood-brain barrier endothelial cells. *AM J. Physiol. Heart Circ. Physiol.* **1996**, *270*, H1149-H1158.
- 214. Dehouck, M. P.; Meresse, S.; Delbart, C.; Delorme, P.; Fruchart, J. C.; Cecchelli, R. Co-culture of astrocytes and brain endothelial cells: a potential model for in vitro studies of blood-brain barrier. *J. Neurochem.* **1989**, *52*(Supplement), 120.
- 215. Wang, Q.; Rager, J. D.; Weinstein, K.; Kardos, P. S.; Dobson, G. L.; Li, J. B.; Hidalgo, I. J. Evaluation of the MDR-MDCK cell line as a permeability screen for the blood-brain barrier. *Int. J. Pharm.* **2005**, *288*, 349-359.
- 216. Ball, K.; Bouzom, F.; Scherrmann, J. M.; Walther, B.; Declèves, X. Development of a physiologically based pharmacokinetic model for the rat central nervous system and determination of an in vitro-in vivo scaling methodology for the blood-brain barrier permeability of two transporter substrates, morphine and oxycodone. *J. Pharm. Sci.* 2012, 101, 4277-4292.
- 217. Ragnaill, M. N.; Brown, M.; Ye, D.; Bramini, M.; Callanan, S.; Lynch, I.; Dawson, K. A. Internal benchmarking of a human blood-brain barrier cell model for screening of nanoparticle uptake and transcytosis. *Eur. J. Pharm. Biopharm.* **2011**, *77*, 360-367.
- 218. Yousif, S.; Marie-Claire, C.; Roux, F.; Scherrmann, J. M.; Declèves, X. Expression of drug transporters at the blood-brain barrier using an optimized isolated rat brain microvessel strategy. *Brain Res.* **2007**, *1134*, 1-11.
- 219. Miller, D. S.; Nobmann, S. N.; Gutmann, H.; Toeroek, M.; Drewe, J.; Fricker, G. Xenobiotic transport across isolated brain microvessels studied by confocal microscopy. *Mol. Pharmacol.* **2000**, *58*, 1357-1367.
- 220. Durk, M. R.; Chan, G. N.; Campos, C. R.; Peart, J. C.; Chow, E. C.; Lee, E.; Cannon, R. E.; Bendayan, R.; Miller, D. S.; Pang, K. 1a,25-Dihydroxyvitamin D3-liganded vitamin D receptor increases expression and transport activity of P-glycoprotein in isolated rat brain capillaries and human and rat brain microvessel endothelial cells. *J. Neurochem.* 2012, 123, 944-953.

- 221. Pardridge, W. M. Log(BB), PS products and in silico models of drug brain penetration. Drug *Discovery Today* **2004**, *9*, 392-393.
- 222. Ohno, K.; Pettigrew, K. D.; Rapoport, S. I. Lower limits of cerebrovascular permeability to nonelectrolytes in the conscious rat. *Am. J. Physiol. : Heart Circ. Physiol.* **1978**, *235*, H299-H307.
- 223. Kalvass, J. C.; Maurer, T. S.; Pollack, G. M. Use of plasma and brain unbound fractions to assess the extent of brain distribution of 34 drugs: comparison of unbound concentration ratios to in vivo P-glycoprotein efflux ratios. *Drug Metab. Dispos.* **2007**, *35*, 660-666.
- 224. Young, R. C.; Mitchell, R. C.; Brown, T. H.; Ganellin, C. R.; Griffiths, R.; Jones, M.; Rana, K. K.; Saunders, D.; Smith, I. R.; Sore, N. E.; Wilks, T. J. Development of a new physicochemical model for brain penetration and its application to the design of centrally acting H2 receptor histamine antagonists. *J. Med. Chem.* **1988**, *31*, 656-671.
- 225. Rohanova, M.; Balikova, M. Studies on distribution and metabolism of paramethoxymethamphetamine (PMMA) in rats after subcutaneous administration. *Toxicology* **2009**, *259*, 61-68.
- 226. Bonate, P. L. Animal-models for studying transport across the blood-brain-barrier. *J. Neurosci. Meth.* **1995**, *56*, 1-15.
- 227. Oldendorf, W. H.; Stoller, B. E.; Tishler, T. A.; Williams, J. L.; Oldendorf, S. Z. Transient blood-brain barrier passage of polar compounds at low pH. *Am. J. Physiol. : Heart Circ. Physiol.* **1994**, *267*, H2229-H2236.
- 228. Takasato, Y.; Rapoport, S. I.; Smith, Q. R. An insitu brain perfusion technique to study cerebrovascular transport in the rat. *Am. J. Physiol.* **1984**, *247*, H484-H493.
- 229. Cannon, R. E.; Peart, J. C.; Hawkins, B. T.; Campos, C. R.; Miller, D. S. Targeting blood-brain barrier sphingolipid signaling reduces basal P-glycoprotein activity and improves drug delivery to the brain. *Proc. Natl. Acad. Sci.* **2012**, *109*, 15930-15935.
- 230. Boje, K. M. K. In vivo measurement of blood-brain barrier permeability. In *Current Protocols in Neuroscience*; John Wiley & Sons, Inc.: **2001**.
- 231. Kakee, A.; Terasaki, T.; Sugiyama, Y. Selective brain to blood efflux transport of paraaminohippuric acid across the blood-brain barrier: in vivo evidence by use of the brain efflux index method. *J. Pharmacol. Exp. Ther.* **1997**, *283*, 1018-1025.
- 232. Friden, M.; Ljungqvist, H.; Middleton, B.; Bredberg, U.; Hammarlund-Udenaes, M. Improved measurement of drug exposure in the brain using drug-specific correction for residual blood. *J. Cereb. Blood Flow Metab.* **2009**, *30*, 150-161.
- 233. Dash, A. K.; Elmquist, W. F. Separation methods that are capable of revealing blood-brain barrier permeability. *J. Chromatogr. B* **2003**, *797*, 241-254.
- 234. Elmquist, W. F.; Sawchuk, R. J. Application of microdialysis in pharmacokinetic studies. *Pharm. Res.* **1997**, *14*, 267-288.

- 235. Gupta, A.; Chatelain, P.; Massingham, R.; Jonsson, E. N.; Hammarlund-Udenaes, M. Brain distribution of cetirizin enantiomers: comparison of three different tissue-to-plasma partition coefficients: Kp, Kp,u, and Kp,uu. *Drug Metab. Dispos.* **2006**, *34*, 318-323.
- 236. Friden, M.; Ducrozet, F.; Middleton, B.; Antonsson, M.; Bredberg, U.; Hammarlund-Udenaes, M. Development of a high-throughput brain slice method for studying drug distribution in the central nervous system. *Drug Metab. Dispos.* **2009**, *37*, 1226-1233.
- 237. Friden, M.; Gupta, A.; Antonsson, M.; Bredberg, U.; Hammarlund-Udenaes, M. In vitro methods for estimating unbound drug concentrations in the brain interstitial and intracellular fluids. *Drug Metab. Dispos.* **2007**, *35*, 1711-1719.
- 238. Syvänen, S.; Eriksson, J. Advances in PET imaging of P-glycoprotein function at the blood-brain barrier. *ACS Chem. Neurosci.* **2012**.
- 239. Wanek, T.; Kuntner, C.; Bankstahl, J. P.; Mairinger, S.; Bankstahl, M.; Stanek, J.; Sauberer, M.; Filip, T.; Erker, T.; Muller, M.; Loscher, W.; Langer, O. A novel PET protocol for visualization of breast cancer resistance protein function at the blood-brain barrier. *J. Cereb. Blood Flow Metab.* **2012**, *32*, 2002-2011.
- 240. Knight, R. A.; Karki, K.; Ewing, J. R.; Divine, G. W.; Fenstermacher, J. D.; Patlak, C. S.; Nagaraja, T. N. Estimating blood and brain concentrations and blood-to-brain influx by magnetic resonance imaging with step-down infusion of Gd-DTPA in focal transient cerebral ischemia and confirmation by quantitative autoradiography with Gd-[lsqb]14C[rsqb]DTPA. J. Cereb. Blood Flow Metab. 2009, 29, 1048-1058.
- 241. Serres, S.; Soto, M. S.; Hamilton, A.; McAteer, M. A.; Carbonell, W. S.; Robson, M. D.; Ansorge, O.; Khrapitchev, A.; Bristow, C.; Balathasan, L.; Weissensteiner, T.; Anthony, D. C.; Choudhury, R. P.; Muschel, R. J.; Sibson, N. R. Molecular MRI enables early and sensitive detection of brain metastases. *Proc. Natl. Acad. Sci.* **2012**, *109*, 6674-6679.
- 242. van de Ven, K. C. C.; van der Graaf, M.; Tack, C. J.; Heerschap, A.; de Galan, B. E. Steady-state brain glucose concentrations during hypoglycemia in healthy humans and patients with type 1 diabetes. *Diabetes* **2012**, *61*, 1974-1977.

Chapter 2: Parallel Artificial Membrane
Permeability Assay for the High-Throughput
Prediction of Passive Blood-Brain Barrier
Permeability

2-1. Introduction

Blood-brain barrier (BBB) is a complex cellular organization separating the brain from the systemic circulation. It is therefore of key importance for the maintenance of brain homeostasis needed for a good neuronal activity ¹ and represents the main route followed by compounds to reach the central nervous system (CNS). The specificity of the BBB resides in the organization of the cerebral endothelial cells forming tight junctions and the absence of fenestration, compared with other endothelial cells in the body ^{2, 3}. These microvascular endothelial cells are responsible for the transport of metabolites and nutrients from blood to brain, the limited permeability of xenobiotics but also for the excretion of waste products or pathogens out of the brain ^{1, 2, 4, 5}. The tight junctions between endothelial cells imply a preferential transcellular pathway submitting drug to a strong selection, depending on their physicochemical properties (lipophilicity, molecular weight, molecular volume, ionization state), and on their possible interaction with specific transporters at the BBB.

To avoid inappropriate pharmacokinetics (PK) and decrease the attrition rate in CNS drug development, many compounds are screened during the early stages of drug discovery before matching one CNS drug candidate possessing satisfactory ADMET (absorption, distribution, metabolism, elimination, toxicity) properties. *In vitro* high throughput methods thus become important tools to assess PK properties and in particular the ability of candidates to penetrate biological membranes such as the BBB ⁶.

For years, *in vitro* permeability through the BBB was assessed by studying the permeability of drug candidates through CACO-2-cells ⁷⁻⁹ or Madin-Darby Canine Kidney (MDCK) cells ⁹. At present, other *in vitro* protocols using cells from various origins have been developed, involving endothelial cells from bovine, porcine, rat, mouse or human origin ¹⁰⁻¹⁹, as reviewed in the introduction of this manuscript. Relevant predictions of *in vivo* BBB permeability were obtained with cocultures, especially by combining endothelial cells and astrocytes, i.e. the Bovine Brain Capillary Endothelial Cells (BBCEC) model ^{10, 20, 21}. All these cellular models provide satisfactory predictions of *in vivo* permeability through the BBB with their own limitations (tightness of the tight junctions, paracellular pathway, transport and enzymatic deregulation...), but the success of the experiments resides on a real mastering of the cell culture and on the quality of the seeded cells.

Recently, a new high-throughput screening *in vitro* technique based on artificial membranes has gained importance in the field of drug discovery. PAMPA developments permitted the determination of passive permeability through biological membranes such as

the gastro-intestinal tract ²²⁻²⁴, the *stratum corneum* ^{25, 26} or the BBB ²⁷ in a rapid and reproducible way. In PAMPA, permeability studies are performed in 96-wells microfilter plates, between a donor (containing the compounds to test) and an acceptor compartments separated by an artificial membrane (figure 2-1). The artificial membrane is composed of the filter material coated by either a full solvent artificial membrane faller ^{24, 25}, or a combination of solvent and phospholipids ^{27, 28}.

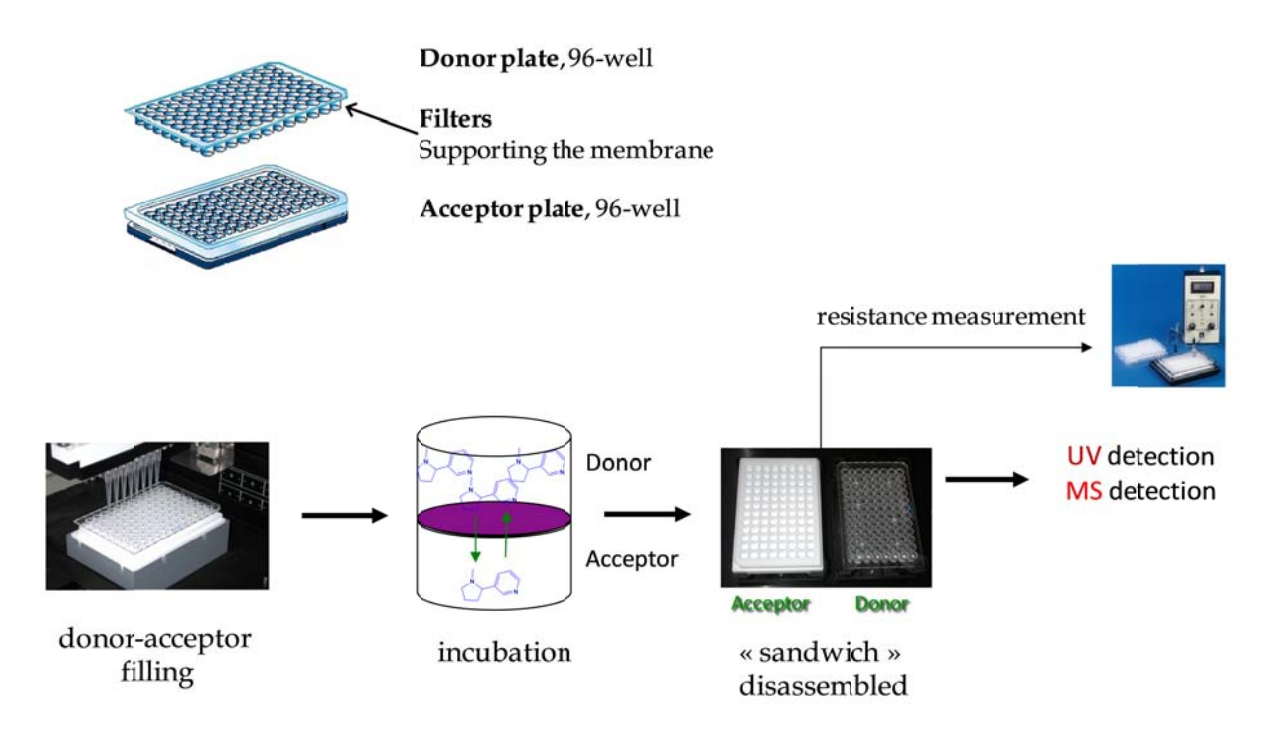


Figure 2-1: Schematic representation of the PAMPA technique and of the proceeding of the experiment. The position of the donor and acceptor compartments can be inversed depending on the literature.

The artificial membrane developed by Di *et al.* ²⁷ to predict BBB passive permeability was composed of porcine brain lipids (PAMPA-BBB). As phospholipids used as a membrane in PAMPA-BBB are biological material, consequent experimental results are highly dependent on the source and quality of the porcine lipids and reproducibility may be altered due to batch-to-batch variations and on the efficiency in the lipid layer formation ²⁴. Moreover, the tendency of phospholipids to oxidize adds a further source of variations between assays. The challenge of this present work was therefore to develop a simple non-biological artificial membrane able to overcome the limitations of systems based on biological material while predicting passive diffusion across the BBB.

Permeability through different artificial membranes of a set of compounds, believed to passively diffuse through the BBB, were thus compared to their permeability on the BBCEC model ¹⁰. This *in vitro* cellular model was initially chosen as an alternative to *in vivo* models

due to the specific BBB properties exhibited by this coculture model (tight junctions, enzymatic activity, transporters, limited paracellular pathway) $^{10, 20, 29-33}$. Its relative simplicity leads to the availability of a larger homogeneous data set compared to *in vivo* data. The relatively high ability of BBCEC to predict accurately *in vivo* BBB passive permeability thanks to its high transendothelial electrical resistance (TEER between 600 and 800 Ω .cm²) limits the cellular entry of molecules *via* a paracellular pathway. Therefore at a first glance the new artificial membrane was developed thanks to correlation with BBCEC permeabilities. At a second glance a comparison was performed with a reduced number of *in vivo* data (log PS obtained by brain perfusion in rats) or PAMPA-BBB data to support the fact that the new artificial membrane generates relevant results as cellular *in vitro* models could do.

The starting point for the artificial membrane development was based on previous relationships between lipophilicity and permeability predictions. Lipophilicity values in n-octanol/water system constitute one of the mostly used descriptors for the prediction of passive permeability across biological membranes due to the similarity of n-octanol with lipids ³⁴. However, due to significant differences between n-octanol and biological membranes regarding biophysical properties ³⁵, other authors experimented different solvent systems for quantitative structure-activity relationship (QSAR) and in vitro studies, such as dichloroethane/water (log P_{DCE}) alkane/water (log P_{alkane}) ²⁴ as well as differences of partition coefficients between n-octanol/water and either dichloroethane/water or alkane/water (\Delta\log P_{oct-DCE} ³⁵ or Δlog P_{oct-alkane} ³⁶). Ortho-nitrophenyloctyl ether(o-NPOE)/water system was also considered as an alternative to dichloroethane/water system with more appropriate physicochemical properties ³⁷. Even though relevant relationships between these descriptors and permeability through biological membranes could be underlined, partition coefficients were not sufficient to accurately predict membrane permeability. Hexadecane, n-octanol, and o-NPOE were therefore tested as artificial membrane in PAMPA due to their physicochemical properties. A design of experimental strategies optimizing the solvent proportion was then implemented in order to define an optimal membrane composition with the aim to obtain the closest correlation between the log Pe obtained with PAMPA and the log P_e obtained with the cellular model (log P_e BBCEC). Permeability values generated with the artificial membrane were also compared to the original PAMPA-BBB model 27 and to an in vivo log PS data set obtained by brain perfusion in rats.

On a secondary step, this work will try to apply PAMPA for the assessment of a hypothetic active transport. Actually, a non-negligible part of CNS-drugs is actively transported through BBB, either by efflux and/or uptake processes. As PAMPA is only able to describe passive diffusion, this tool will not be used as a filter in selecting CNS-hits during

early drug development. But when compared with the data obtained with a cellular *in vitro* model expressing biological transporters such as P-glycoproteins (Pgp/ABCB1), multidrug resistance-associated proteins (MRP), breast cancer resistant proteins (BCRP/ABCG2), it may help in describing and understanding the mode of permeation of the compounds through the BBB. The cellular model will give global information on permeability while the PAMPA model will isolate the diffusion information. By comparing both data, it may be possible to separate actively transported substances from compounds crossing the BBB *via* a diffusion process. This differentiation is of importance in optimization strategy and is a current preoccupation in the field of membrane permeability ³⁸.

2-2. Material and methods

2-2.1. Chemicals

Warfarin, pindolol, pirenzepine 2HCl, atropine sulfate, antipyrine, HCl, caffeine, carbamazepine, atenolol, imipramine HCl, theophylline, promazine, corticosterone, testosterone, ofloxacin, piroxicam, terbutaline, diclofenac, chlorambucil, theobromine, dopamine HCl, hydrocortisone, nicotine, chlorpromazine, methotrexate, quinidine, testosterone, hypoxanthine, hexane (purity grade >95%), o-NPOE (purity grade ≥ 99%) and hexadecane 99% were purchased from Sigma-Aldrich (St Louis, USA). n-octanol was purchased from Romil Ltd (Cambridge, United Kingdom), diazepam was purchased from Bufa, aldosterone and dimethylsulfoxide (DMSO) (purity grade >99.7%) were purchased from Acros Organics (Chemie Brunschwig AG, Basel, Switzerland). Buffers were prepared according to the Geigy tables.

2-2.2. PAMPA protocol

Stock solutions were prepared dissolving the test compounds in DMSO with concentration values depending on solubility and molar extinction coefficient (between 2 mM and 50 mM). Stock solutions were then diluted 20 times with a buffer to generate the reference solutions containing 5% DMSO.

Each well of a hydrophobic polyvinylidene fluoride (PVDF) 96-wells microtiter filter plate (Millipore AG, Volketswil, Switzerland) was impregnated with 15 μl of a 35% (v/v) liquid membrane (octanol, hexadecane, o-NPOE or a mixture of these solvents) dissolved in hexane. PVDF filters had 70% porosity, with a 0.45 μm diameter of pores and a 0.3 cm² cross-sectional area. This microtiter plate constitutes the donor compartment. The plate was left under the extractor hood for 15-20 minutes to completely evaporate hexane. A Teflon® 96-wells acceptor plate (Millipore MSSACCEPTOR) was filled with 280 μl of a buffer containing 5% DMSO. The donor plate was next placed upon the acceptor plate in a "sandwich-like conformation" and filled with 280 μl of the solution containing the compounds to test. The resulting sandwich was incubated during 7 hours at room temperature and under constant shaking at 150 rpm to minimize the unstirred water layer ²⁵. Permeability coefficients were determined in quadruplicate.

Following incubation, the sandwich was disassembled and 200 μ l of each well of the donor and acceptor compartments were transferred in a 96-wells UV-quartz plate (Hellma GmbH & Co, Müllheim, Germany). The UV absorption in each compartment was measured with a PowerWaveTM spectrometer (BioTek Instruments, Inc., Winooski, VT, USA). Since the limit of detection of the UV system did not allow the measurement of low concentrations, accurate log P_e determination was not possible for low-permeable compounds and the lowest detectable amount was fixed at 1% of passage, corresponding to a cut-off value of permeability of -6.3. In order to obtain more sensible data with minimal error, the concentration of these molecules was further measured with a HPLC Merck Hitachi apparatus equipped with a Discovery® RP amide C16 column (20 x 4 mm, ID 5 μ m) (Supelco, Bellefonte, PA, USA) for the most promising membranes.

Electrical resistance of each well of the microfilter plate was determined at the end of the incubation time to assess membrane integrity using an electrometer system designed for PAMPA (EVOMX and MULTI96, World Precision Instruments, Sarasota FL). Wells presenting an electrical resistance greater than 200 k Ω were kept for permeability calculations.

The PAMPA model was designed with iso-pH condition, (same pH in the donor and acceptor compartments) and physiological pH (pH 7.4) was used as in the BBCEC model. As each compound's permeability was determined in quadruplicate, the results are given as $log P_e \pm standard deviation$ (SD).

Alkane/water partition coefficients log P_{alk} were determined according to the published method of Wohnsland and Faller 24 .

2-2.3. Permeability equations

Appropriate permeability equations were selected according to the design of the PAMPA experimental protocol (equations 2-1 and 2-2). The presence of membrane retention and absence of sink conditions lead to define the effective permeability coefficient as follows ³⁹ (refer to appendix 1 for detailed calculations):

$$P_{e} = -\frac{2.303V_{D}}{A\left(t - \tau_{lag}\right)} \left(\frac{V_{A}}{V_{A} + V_{D}}\right) \log \left[1 - \left(\frac{V_{A} + V_{D}}{V_{D}\left(1 - R\right)}\right) \frac{C_{A}\left(t\right)}{C_{D}\left(0\right)}\right]$$
 (Equation 2-1)

where A is the accessible filter area in cm² (cross-sectional filter area multiplied by the porosity of the filter), t is the incubation time in seconds, V_A and V_D are the volume of the acceptor and donor compartments respectively (0.28 cm³), $C_A(t)$ is the concentration of solute in the acceptor compartment at time t and $C_D(0)$ the concentration of the reference solution, τ_{lag} is the steady-state time (s), that is the time needed for compounds gradient to be stabilized. The observed τ_{lag} are of the order of 20 minutes, which is relatively short compared to the incubation time of 7 hours. For this reason, the steady-state time was neglected for the calculations of the permeability coefficients. The retention factor R is defined as the quantity of solute which is not recovered in the acceptor or the donor compartments at the end of the incubation time. This quantity can either be retained at the membrane or adsorbed on the plate material:

$$R = 1 - \frac{C_D(t)}{C_D(0)} - \frac{V_A}{V_D} \frac{C_A(t)}{C_D(0)}$$
 (Equation 2-2)

The differentiation between the retained part at the membrane or the adsorbed part on the material cannot be achieved.

2-2.4. Optimization of the membrane

Experimental design and data analysis were performed using Modde 7.0 (Umetrics, Umea, Sweden).

A special cubic D-optimal simplex design was used to study the effect of membrane composition on the BBB permeability ability. The response to be minimized was defined as the standard deviation of the difference between PAMPA log P_e and *in vitro* BBCEC log P_e ,

knowing that the objective was the optimization of the membrane composition which would define the best proportions of n-octanol, o-NPOE and hexadecane.

The simplex design is able to evaluate properties of mixtures made of several components. It requires that the sum of the fractions of components making up any mixture equals unity ($\sum x_i=1$) and is able to reveal the three-component interaction, if any. A special-cubic simplex design is made by adding center points to the faces of the simplex. Since it possesses high prediction ability, such approach is one of the most efficient mixture optimization methods in terms of number of experiments.

Randomized experiments were generated and additional experiments were carried out at the center of the investigated domain to complete the experimental set-up. A set of fourteen experiments with three center points was carried out. The center points corresponded to a membrane composed of 72.5% hexacadecane, 10% n-octanol and 17.5% o-NPOE.

2-3. Results and discussion

Twenty six compounds (acidic, basic and neutral molecules), strongly believed to be transported $\it via$ passive diffusion only, were selected for the whole study. Among these twenty six compounds, a test set of eleven diversified drugs, covering a large range of log P_e values available from the BBCEC model $^{20, 33}$ (log P_e^{BBCEC}) were chosen from the literature, namely diazepam, atropine sulfate, antipyrine, warfarin, pirenzepine, pindolol, theobromine, dopamine, nicotine, carbamazepine and caffeine. This test set of eleven compounds has been employed for the development and optimization of the new PAMPA membrane. The permeability of these compounds was determined by PAMPA using different solvents as artificial membrane and the resulting permeability coefficients compared with log P_e^{BBCEC} . log P_e^{BBCEC} is derived from the clearance volume of the compound versus the time of the experiment and calculated as:

$$\frac{1}{PS_e} = \frac{1}{PS_t} - \frac{1}{PS_f}$$
 (Equation 2-3)

were PS is the permeability multiplied by the surface area of the well. The subscript e represents the endothelial layer, t is the total permeability (filter + endothelial layer) and f is the permeability on the filter alone, without the cell monolayer. The resulting P_e^{BBCEC} is

therefore obtained dividing PS_e by the surface area. Therefore, the scales are different between log P_e^{BBCEC} and log $P_e^{HDC/NPOE}$, but the meanings are the same: both represent the permeability of the compound, that is a flux between a donor and an acceptor compartments.

Following the optimization of the new artificial membrane, two new test sets have been selected: an *in situ* rat brain perfusion test set, composed of six passively transported compounds (antipyrine, caffeine, chlorambucil, dopamine, testosterone and theobromine), and three Pgp substrates (digoxine, quinidine and colchicine), and a PAMPA-BBB test set, composed of thirteen passively transported compounds (aldosterone, atenolol, caffeine, chlorpromazine, corticosterone, diazepam, dopamine, imipramine, ofloxacine, piroxicam, progesterone, promazine and testosterone). The original BBCEC test set was also supplemented with a passively transported drug (terbutaline) and two Pgp substrates (hydrocortisone and digoxine). Pgp substrates were added to assess the efficiency of PAMPA to highlight compounds subject to efflux transport by comparison with cellular or *in vivo* models. Table 2-4 shows the composition of the 3 test sets.

2-3.1. Hexadecane, n-octanol and o-nitrophenyloctyl ether as artificial membranes

Three different solvents (hexadecane, n-octanol, and o-NPOE) were tested as artificial membranes to evaluate their impact on solutes' permeability (log P_e^{HDC} , log P_e^{oct} and log P_e^{NPOE}) with respect to their physicochemical properties.

2-3.1.1. *Hexadecane*

Half of the eleven compounds of the BBCEC test set do not cross the hexadecane membrane, as highlighted in figure 2-2a and table 2-1. The response follows a bilinear profile: warfarine, pirenzepine, dopamine, antipyrine, pindolol and theobromine are not differentiated in PAMPA while the cellular model is able to discriminate them with around 1.2 log units. On the other hand, caffeine, carbamazepine, diazepam, atropine and nicotine are distributed along 2 log units of PAMPA permeability compared to 0.3 log units for the cellular model. Therefore, hexadecane membrane is able to differentiate the fast permeant compounds along a wide range of log P_e but this membrane is not able to discriminate medium to low permeant compounds. Regarding the retention, which corresponds to the

difference between the initial amount of drug tested and the quantity of drugs found in the donor and acceptor compartments at the end of the incubation time, almost no compound was retained in the hexadecane membrane nor on the material, as shown in table 2-1, excepted diazepam, presenting the highest $\log P_{alk}$ (table 2-4) which is only slightly retained. Hexadecane as artificial membrane is therefore not an ideal composition to predict passive permeation through the BBB with PAMPA.

2-3.1.2. n-octanol

n-octanol is a solvent usually employed to predict absorption ⁴⁰ *via* the determination of the partition coefficient of drug compounds, giving an idea of their lipophilicity. The structure of n-octanol is composed of a medium-length carbonated chain characterizing a hydrophobic part and the hydroxyle function, a small polar side. Unlike hexadecane, it possesses an acceptor and a H-bond donor capacity with the alcohol group.

Any improvement in permeability was observed for compounds which were already good permeants through the hexadecane membrane, an easier crossing of the n-octanol membrane was observed for all the other compounds when compared to the hexadecane one, as shown in figure 2-2b. Results indicate that log P_e^{oct} values vary from -4.40 for the most permeant solute (carbamazepine) to -5.38 for the least permeant (pirenzepine) (table 2-1), but n-octanol membrane does not allow a discrimination of the compounds along a large range of log P_e^{oct} values. Dopamine is the unique molecule that does not cross the membrane whereas seven compounds did not permeate through the hexadecane membrane. While compounds unable to cross the hexadecane membrane have a much higher permeability through n-octanol, permeability values for good permeants through hexadecane (nicotine, diazepam) were stable or slightly decreased.

It is admitted that the difference between partition coefficients in n-octanol/water system (log P_{oct}) and alkane/water system (log P_{alk}), Δ log $P_{oct-alk}$, evidences the H-donating capacity of the solutes and has been shown to be an important parameter to model the BBB permeability $^{41-44}$. When comparing the permeability coefficients through n-octanol and hexadecane membranes, it is not surprising that compounds having the smallest Δ log $P_{oct-alk}$ (when available, in table 2-4) correspond to permeability values that are not improved with n-octanol as a membrane (nicotine, diazepam), as these compounds have poor H-bond donating capacity. Therefore, the compounds that have H-bond donating sites are those disclosing the largest difference in permeability behaviors through n-octanol and hexadecane

artificial membranes. These results thus confirm that n-octanol membrane facilitates the permeability of the most H-donating molecules, as widely accepted in the field of PAMPA.

Table 2-1 indicates that most of the tested compounds are more retained in the n-octanol membrane compared to the hexadecane membrane, especially diazepam (R=79%) and carbamazepine (R=21%). As expected, the retention on n-octanol membrane increased with the lipophilicity of the solutes (table 2-1 and table 2-4), indicating that the resulting effective permeability is partly due to membrane retention in these cases.

2-3.1.3. Ortho-nitrophenyloctyl ether (o-NPOE)

Giving the graphical results with hexadecane and n-octanol as artificial membranes, the idea was to generate a compromise between the discrimination offered with hexadecane, and permeation through n-octanol as artificial membrane. o-NPOE was chosen due to its two different hydrophobic parts, an aromatic ring and a medium-length saturated chain, combined with a small H-accepting bond behavior on the ether group. Moreover, partition coefficients in the system o-NPOE/water have been extensively studied, especially for the partition on ionic compounds ^{37, 42, 45}. The permeability coefficients obtained with o-NPOE as artificial membrane are plotted on figure 2-2c. The profile of the curve can be divided in two parts, as with hexadecane: a group with no or slow permeant compounds, and another with a medium to fast permeability through the artificial membrane. Among the seven compounds that were not able to cross the hexadecane artificial membrane, all except antipyrine and warfarine still cannot permeate through the o-NPOE membrane. Moreover, two of the drugs able to cross hexadecane membrane failed to permeate through the o-NPOE one (carbamazepine, diazepam). This loss of permeability was associated with an increased retention at the membrane and/or on the material. These two compounds are among the most lipophilic ones, which can explains this net enhancement of retention. No additional discriminating ability was therefore obtained using o-NPOE as artificial membrane.

All these results indicated that none of the explored solvents can be used alone as an artificial membrane to predict passive diffusion through the BBCEC model and probably through BBB, but could have complementary influences when combined. The analysis of the results in table 2-1 and figures 2-2 indicates that each solvent has a different impact on the permeability of the test compounds. While the permeability follows a bilinear profile without retention for the hexadecane membrane, some compounds are moderately or strongly retained on the materials with n-octanol while their permeability is globally increased. The use of o-NPOE shows an intermediate profile, as some compounds are retained in the

membrane, similarly to the n-octanol artificial membrane, while the log P_e^{NPOE} vs. log P_e^{BBCEC} plot suggested a low discrimination between the compounds, as with hexadecane artificial membrane. Therefore, the next step of the study was to mix solvents and observe the behavior of the compounds through these new artificial membranes.

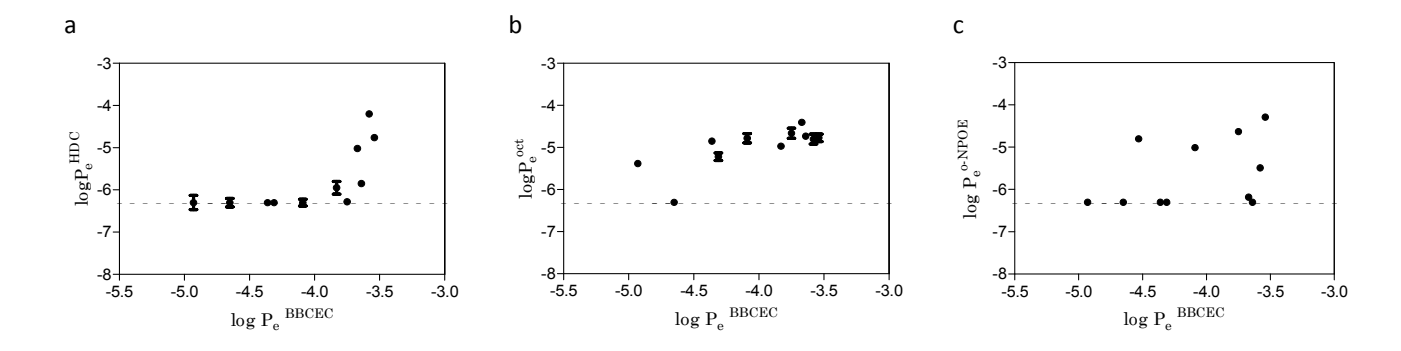


Figure 2-2: Comparison between log P_e obtained on different artificial membranes (hexadecane (a), n-octanol (b) and o-NPOE (c)) and log P_e^{BBCEC} . The dotted line is a cut-off, resulting from the limit of detection of UV-spectrometry. It corresponds to a permeability of 1% of the initial concentration on the acceptor compartment and a log P_e =-6.3.

Table 2-1: Experimental values of retention (R), proportion of compounds in the acceptor compartment (CA(t)/CD(0)) and permeability coefficients (log Pe) for the test set of compounds using pure hexadecane, pure octanol or pure o-NPOE as artificial membranes. A CA(t)/CD(0) value under 1%, was considered below the limit of detection of the UV-reader preventing exploitable results. A cut-off value of log P_e =-6.30, corresponding approximately to a passage of 1% of substance to the acceptor compartment was used.

	10	00% Hexadecane	e membrane	10	100% n-octanol membrane			100% o-NPOE membrane			
Commoundo	R	$C_A(t)/C_D(0)$	log P _e HDC	R	$C_A(t)/C_D(0)$	log P _e ^{HDC}	R	$C_A(t)/C_D(0)$	log P _e HDC		
Compounds	(%)	(%)		(%)	(%)		(%)	(%)			
Antipyrine	0	1 ± 1	-6.28 ± 0.06	6 ± 5	27 ± 6	-4.7 ± 0.1	0	35 ± 4	-4.63 ± 0.05		
Atropine sulfate	0	2 ± 1	-5.9 ± 0.2	1 ± 2	17 ± 2	-4.97 ± 0.04	ND	ND	ND		
Cafeine	0	3 ± 1	-5.85 ± 0.05	0	26 ± 1	-4.73 ± 0.03	16 ± 1	<1	-6.3		
Carbamazepine	0	18 ± 1	-5.02 ± 0.03	21 ± 3	31 ± 1	-4.40 ± 0.07	37 ± 1	5 ± 4	-5.4 ± 0.4		
Diazepam	5 ± 2	43 ± 2	-4.20 ± 0.07	79 ± 1	5 ± 1	-4.8 ±0.1	85 ± 1	<1	-5.5 ± 0.2		
Dopamine	0	<1	<-6.3	5 ± 2	<1	<-6.3	6 ± 1	<1	<-6.3		
Nicotine	0	31 ± 2	-4.76 ± 0.03	3 ± 5	23 ± 3	-4.77 ± 0.09	0	60 ± 8	-4.29 ± 0.07		
Pindolol	0	<1	<-6.3	0	21 ± 1	-4.85 ± 0.07	0	<1	<-6.3		
Pirenzepine	0	<1	<-6.3	0	7 ± 1	-5.38 ± 0.06	0	<1	<-6.3		
Theobromine	0	<1	<-6.3	0	11 ± 2	-5.22 ± 0.09	0	<1	<-6.3		
Warfarine	0	<1	<-6.3	6 ± 1	22 ± 4	-4.8 ± 0.1	13 ± 3	13 ± 1	-5.01 ± 0.02		

2-3.2. Mixture of solvents as artificial membrane

Regarding the results generated with a unique solvent as artificial membrane, a combination of n-octanol, which increases the permeability of the slow permeant compounds, and hexadecane, which promotes a higher discrimination, could lead to an interesting compromise. Therefore, further experiments were performed on the eleven compounds of the initial test set by mixing solvents to balance their respective advantages and drawbacks. Preliminary tests involving a membrane composed of hexadecane and n-octanol showed that the more n-octanol is added, the lower the discrimination between the compounds is obtained, as exposed in figures 2-3a and 2-3b and table 2-2. On the other hand, experiments also highlighted that a small addition of n-octanol (less than 30% in the mixture) was enough to greatly enhance the permeability of low-permeant molecules (warfarin, pirenzepine, antipyrine), while having only a slight influence on the most permeant ones. A small proportion of n-octanol in the membrane was therefore enough to observe its benefits.

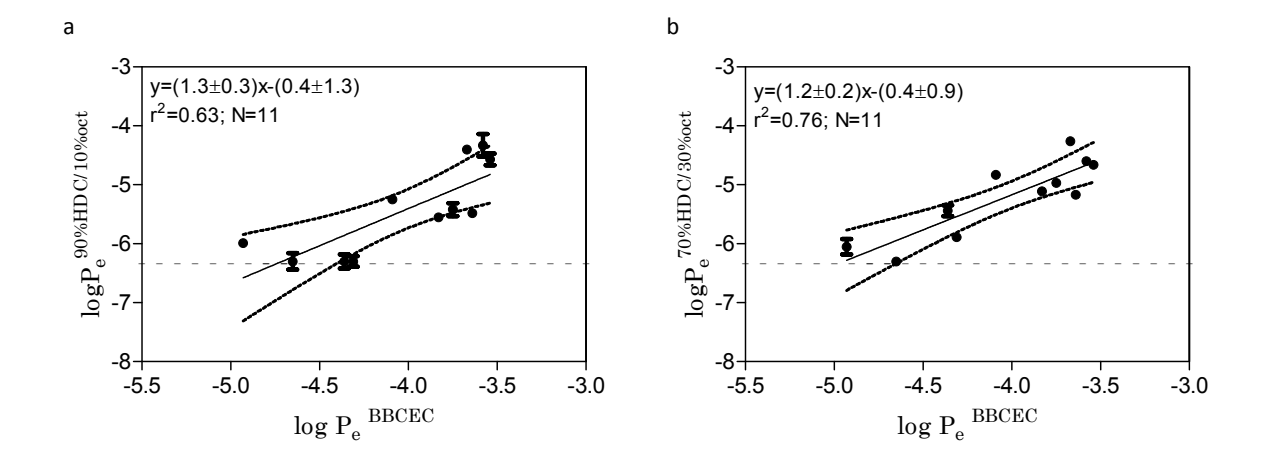


Figure 2-3: Comparison between log Pe obtained on mixtures of hexadecane and n-octanol as artificial membranes (hexadecane/n-octanol 90%/10% (a) and hexadecane/n-octanol 70%/30% (b)) and log P_e^{BBCEC} . The dotted line is a cut-off, resulting from the limit of detection of UV-spectrometry. It corresponds to a permeability of 1% of the initial concentration on the acceptor compartment and a log Pe=-6.3.

Table 2-2 : Retention values (R), percentage of passage in the acceptor compartment ($C_A(t)/C_D(0)$) and effective permeability coefficients generated with mixtures of hexadecane and n-octanol as artificial membranes.

	9	0% hexadecane	e/10% n-octanol	70%	70% hexadecane/30% n-octanol				
	R	$C_A(t)/C_D(0)$	log P _e ^{0.9HDC/0.1oct}	R	$C_A(t)/C_D(0)$	log P _e ^{0.7HDC/0.3oct}			
Compounds	(%)	(%)		(%)	(%)				
Antipyrine	< 1	7 ± 2	-5.4 ± 0.1	< 1	19 ± 1	-4.97 ± 0.04			
Atropine sulfate	< 1	5.1 ± 0.3	-5.55 ± 0.04	1±5	12 ± 1	-5.11 ± 0.05			
Cafeine	< 1	5.9 ± 0.4	-5.48 ± 0.03	< 1	1 ± 2	-5.17 ± 0.05			
Carbamazepine	< 1	43 ± 3	-4.40 ± 0.06	6±5	4 ± 2	-4.26 ± 0.02			
Diazepam	41 ± 4	24 ± 4	-4.3 ± 0.2	51 ± 1	15.1 ± 0.5	-4.60 ± 0.02			
Dopamine	< 1	< 1	< -6.3	3.9 ± 0.7	< 1	< -6.3			
Nicotine	< 1	44 ± 5	-4.53 ± 0.06	< 1	29 ± 2	-4.66 ± 0.05			
Pindolol	< 1	< 1	< -6.3	4 ± 2	6 ± 1	-5.44 ± 0.09			
Pirenzepine	< 1	2 ± 1	-5.99 ± 0.01	3 ± 2	1.6 ± 0.5	-6.1 ± 0.1			
Theobromine	< 1	< 1	<-6.3	2 ± 3	2.3 ± 0.2	-5.89 ± 0.04			
Warfarine	< 1	10 ± 1	-5.25 ± 0.07	< 1	22 ± 2	-4.83 ± 0.05			

The same preliminary tests were run with a membrane composed of hexadecane and o-NPOE, as shown on figures 2-4a, 2-4b and 2-4c and on table 2-3. The results indicated that small proportions of o-NPOE in the mixture enhanced the correlation between log $P_e^{HDC/x\% \ NPOE}$ (x corresponding to the percentage of o-NPOE in the membrane, completed up to 100% with hexadecane) and log P_e^{BBCEC} (r^2 between 0.78 and 0.81) (figures 2-4a and 2-4b) compared to hexadecane alone, while higher proportions degraded the correlation ($r^2 < 0.6$ (figure 2-4c)). Between 10 and 30% seem to be the best amount of o-NPOE together with hexadecane to observe the positive action of this solvent on the correlation.

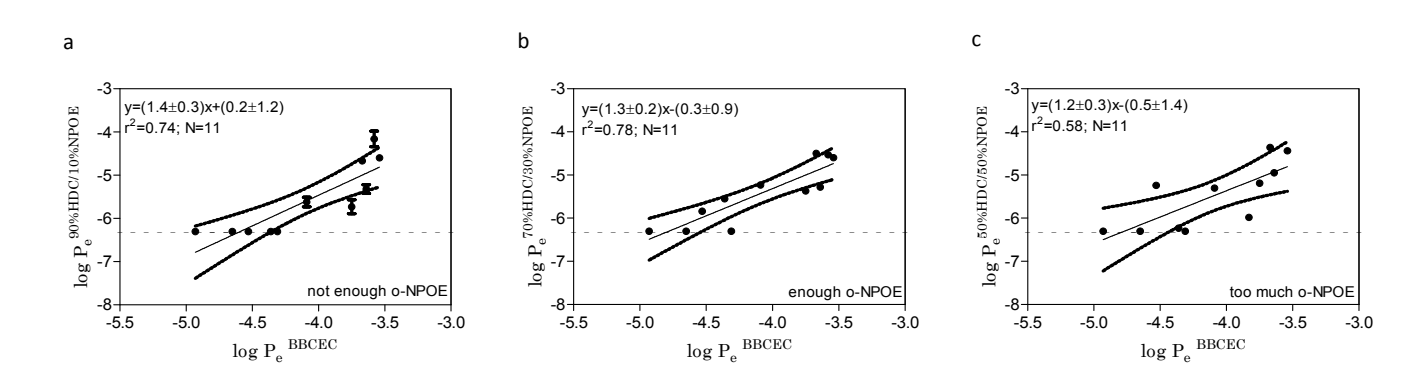


Figure 2-4: Comparison between log Pe obtained on mixtures of hexadecane and o-NPOE as artificial membranes (hexadecane/o-NPOE 90%/10% (a), hexadecane/o-NPOE 70%/30% (b) and hexadecane/o-NPOE 50%/50% (c)) and log $P_{\rm e}^{\rm BBCEC}$. The dotted line is a cut-off, resulting from the limit of detection of UV-spectrometry. It corresponds to a permeability of 1% of the initial concentration on the acceptor compartment and a log $P_{\rm e}$ =-6.3.

Table 2-3: Retention values (R), percentage of passage in the acceptor compartment (CA(t)/CD(0)) and effective permeability coefficients generated with mixtures of hexadecane and o-NPOE as artificial membranes.

•	90% Hexadecane/10%o-NPOE			70% hexadecane/30% o-NPOE			50% hexadecane/50% o-NPOE		
•	R	$C_A(t)/C_D(0)$	log P _e ^{0.9HDC/0.1NPOE}	R	$C_A(t)/C_D(0)$	log P _e ^{0.7HDC/0.3NPOE}	R	$C_A(t)/C_D(0)$	log P _e ^{0.5HDC/0.5NPOE}
Compounds	(%)	(%)		(%)	(%)		(%)	(%)	
Antipyrine	0	4 ± 1	-5.7 ± 0.2	0	7 ± 4	-5.6 ± 0.5	0	15 ± 1	-5.19 ± 0.08
Atropine sulfate	0	<1	<-6.3	0	<1	<-6.3	11 ± 4	2 ± 1	-5.98 ± 0.04
Cafeine	0	8 ± 3	-5.4 ± 0.2	0	10 ± 1	-5.28 ± 0.04	4 ± 3	17 ± 1	-4.95 ± 0.05
Carbamazepine	0	29 ± 1	-4.67 ± 0.03	0	36 ± 1	-4.50 ± 0.02	1 ± 4	40 ± 1	-4.36 ± 0.03
Diazepam	44 ± 7	26 ± 5	-4.2 ± 0.2	69 ± 4	10 ± 2	-4.53 ± 0.06	ND	ND	ND
Dopamine	0	<1	<-6.3	0	<1	<-6.3	0	<1	<-6.3
Nicotine	6 ± 4	33 ± 10	-4.5 ± 0.2	0	31 ± 3	-4.60 ± 0.09	11 ± 18	32 ± 3	-4.4 ± 0.1
Pindolol	2 ± 2	<1	<-6.3	0	4 ± 2	-5.7 ± 0.3	0	1 ± 1	-6.23 ± 0.06
Pirenzepine	0	<1	<-6.3	0	<1	<-6.3	0	<1	<-6.3
Theobromine	0	<1	<-6.3	0	<1	<-6.3	0	<1	<-6.3
Warfarine	0	5 ± 1	-5.6 ± 0.1	0	12 ± 2	-5.23 ± 0.08	0	20 ± 2	-4.9 ± 0.1

The results of the permeability experiments on PAMPA with mixtures of solvents as artificial membrane were promising compared to the results obtained with pure solvents. These preliminary tests led to the conclusion that the ideal artificial membrane should be mainly composed of hexadecane, to provide compound discrimination, and a small proportion of n-octanol and/or o-NPOE.

2-3.3. Optimization of the membrane: design of experiment

A significant model (ANOVA p = 0.023) characterized by a determination coefficient r^2 of 0.87 was obtained when performing the statistical analysis of the design of experiments. The predictive ability of the model was estimated by leave-one-out cross-validation and a satisfactory q^2 value of 0.67 was achieved. The analysis of the results generated by a design of experiments are represented as mixture contour plots (figure 2-5), where the most favorable solvents compositions are in the blue region and the least favorable in the red regions. From this representation of the results, it appears that n-octanol is not essential to enhance the prediction of BBB-permeability through the BBCEC model, and that a mixture of hexadecane and o-NPOE generated an efficient prediction of passive BBB permeability through the BBCEC model. As already revealed with preliminary experiments, the addition of 50% of o-NPOE degraded the correlation, as well as no o-NPOE in the membrane (red regions in figure 2-5).

Thanks to this design of experiments, an optimal membrane composition was highlighted corresponding to a mixture of 75% hexadecane and 25% o-NPOE (dark blue region in figure 2-5). This membrane composition was then assessed with PAMPA and the

experimental permeability values (log $P_e^{HDC/NPOE}$) obtained were compared with log P_e^{BBCEC} (figure 2-6, table 2-4). A determination coefficient of 0.88 (N = 12) was obtained, indicating a satisfactory membrane composition minimizing the standard deviation of the difference between *in vitro* PAMPA and BBCEC model values. A determination coefficient of 0.92 was even obtained when terbutaline, another compound that crosses the BBB *via* passive diffusion, was added in the initial test-set. The composition 75% hexadecane, 25% o-NPOE as artificial membrane in PAMPA model was therefore determined as an appropriate solvents' combination for the prediction of passive diffusion through BBCEC with high throughput efficiency. The higher deviation which can be observed for the drugs having very low permeability (figure 2-6) is explained by their position at the limit of detection. The linear relation between log $P_e^{HDC/NPOE}$ and log P_e^{BBCEC} is defined as:

$$\log P_e^{\text{HDC/NPOE}} = 2.2 (\pm 0.3) \log P_e^{\text{BBCEC}} + 3(\pm 1) (r^2 = 0.88, N = 11)$$
 (Equation 2-3)

Therefore, this new artificial membrane composed of 75% hexadecane and 25% o-NPOE is able to predict passive permeation through the BBCEC model.

In order to strengthen the capacity of this new PAMPA model to predict passive permeation through the BBB, experimental results generated with the new artificial membrane (log P_e^{HDC/NPOE}) have been correlated with standard procedures present in drug discovery and development to determine BBB permeation: the PAMPA-BBB *in vitro* model and the *in vivo* log PS determined with *in situ* rat brain perfusion.

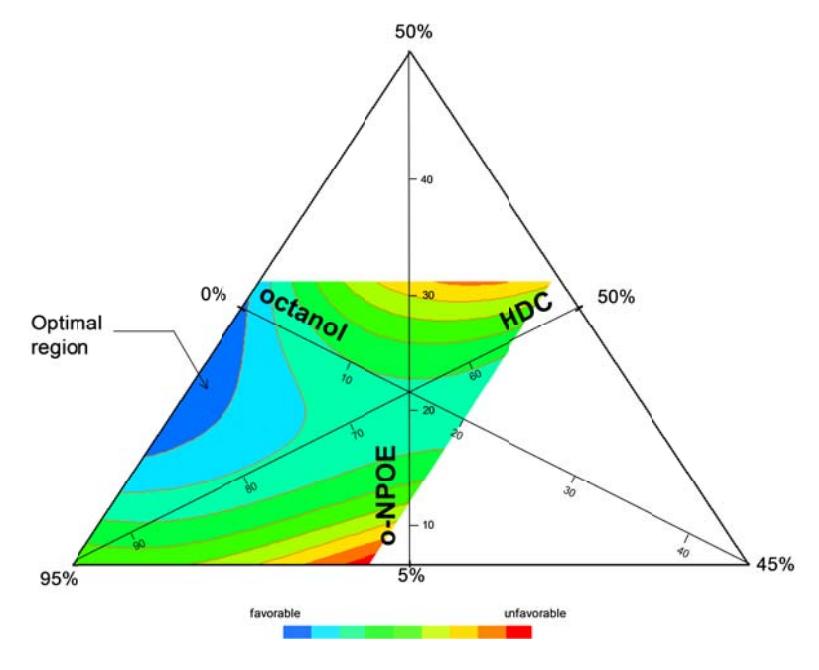


Figure 2-5: Mixture contour plot resulting from the analysis of the design of experiments. It reveals the compositions of artificial membranes showing the best correlations between the experimental log P_e and the cellular log P_e (dark blue region) and the ones which give bad prediction of passive permeability (red region).

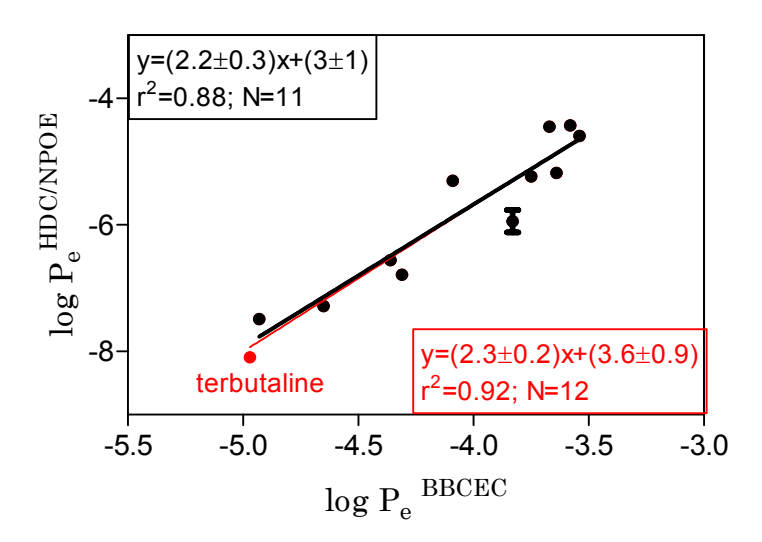


Figure 2-6: Comparison between log Pe obtained through hexadecane/o-NPOE (75% / 25%) as artificial membrane and log P_e^{BBCEC} . The black dots are the compounds constituting the initial test set of 11 compounds. The red dot is terbutaline, which was introduced in the initial test-set as a passive constituent.

Table 2-4: Physicochemical data of the test compounds and effective permeability coefficients obtained from BBCEC model (log P_e^{BBCEC}), PAMPA-BBB model (log P_e^{BBB}), in situ rat brain perfusion technique (log PS), and through the artificial membranes composed of 25% o-NPOE and 75% of hexadecane (log $P_e^{HDC/NPOE}$) ($\pm SD$).

Compounds	pKa ⁴⁶	log P _{oct} ⁴⁶	log P _{alk} ²⁴	Δlog P _{alk-oct}	log P _e ^{HDC/NPOE}	log P _e ^{BBCEC 20,}	log Pe ^{BBB 27}	log PS ⁴⁷
Antipyrine	1.44	0.56	-2.30 ⁴⁸	2.86	-5.23±0.02	-3.75		-2.0
Atropine sulfate	9.84	1.89	1.03	0.86	-5.9±0.2	-3.83		
Caffein	0.6	-0.07			-5.18±0.02	-3.64	-5.89	-2.0
Carbamazepine	-	2.45			-4.45±0.02	-3.67		
Diazepam	3.4	2.99 ⁴⁹	2.5	0.32	-4.43±0.05	-3.58	-4.80	
Dopamine	8.93 50	-0.98 ⁵¹			-7.28±0.01 (MS)	-4.65	-6.70	-2.1
Nicotine	8.11; 3.17	1.32	1.60	-0.28	-4.59±0.02	-3.54		
Pindolol	9.54	1.83	0.52	1.31	-6.56±0.02 (MS)	-4.36		
Pirenzepine	8.20 52	1.68 53			-7.49±0.01 (MS)	-4.93		
Theobromine	10.04 54	-0.78 ⁵¹			-6.79±0.02 (MS)	-4.31		-3.0
Warfarin	4.82	3.54	1.08	2.46	-5.14±0.03	-4.09		
Diclofenac	3.99	4.51			-5.33±0.02	-3.77		
Terbutaline	11.02; 9.97; 8.67	-0.08			-8.09±0.06 (MS)	-4.97		
Aldosterone	-	1.08 51			-5.66±0.07		-5.92	
Atenolol	9.54	0.22			-6.3±0.1		-6.10	
Chlorpromazine	9.24	5.40			-5.1±0.2		-5.19	

2-3.4. Correlation of HDC/NPOE PAMPA with PAMPA-BBB

Until now, PAMPA-BBB ²⁷ has been the method of choice to determine passive diffusion through the BBB with a high-throughput screening rate. Briefly, the diffusion of the tested compounds occurred through a filter membrane coated with porcine polar brain lipids dissolved in dodecane. This assay is successful in predicting *in vivo* permeability, classified by the authors in two classes: CNS+ and CNS- compounds. These classes have been determined thanks to one of the following methods: a kinetic method (fast permeation or not), the BBB distribution under steady state, a pharmacological activity or the brain to plasma ratio.

Thirteen compounds from the original test set of Li Di and coworkers 27 were tested with the new artificial membrane and the resulting permeability values were compared (figure 2-7 and table 2-4). The linear relationship obtained indicates that the new artificial membrane is able to give the same information than PAMPA-BBB ($r^2 = 0.80$, N = 13). This new assay allows to get rid off biological material, strongly decreasing the risks of poor reproducibility linked to the origins of the phospholipids and to the formation of the lipid layer, while significantly decreasing the time of analysis (7 hours instead of 18 hours with the original phospholipidic membrane based PAMPA). Therefore, experimental costs are consequently reduced. This significant decrease of the incubation time is partly due to the stirred conditions employed to run the new PAMPA experiment, to decrease the incidence of the unstirred water layer.

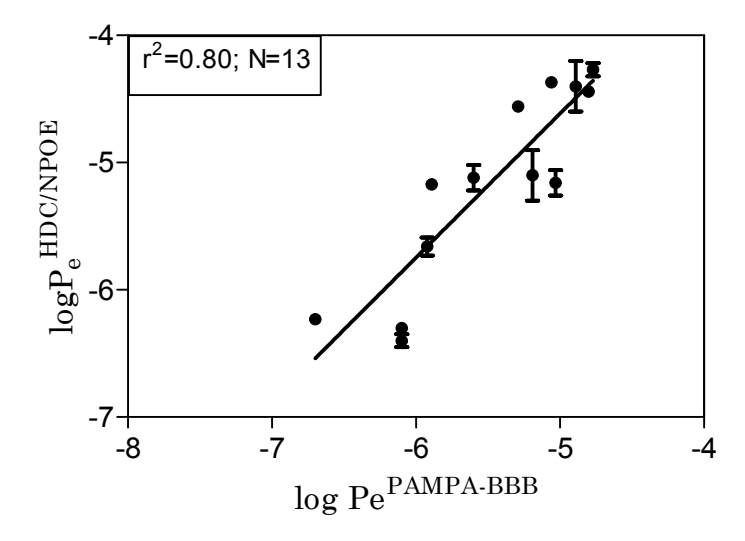


Figure 2-7: Correlation between the permeabilities determined with PAMPA-BBB ²⁷ and the new PAMPA membrane.

2-3.5. Correlation of HDC/NPOE PAMPA with models expressing both active and passive processes

2-3.5.1. Comparison of log $P_e^{HDC/NPOE}$ with in vivo log PS

In order to further evaluate the performance of the new artificial PAMPA membrane, comparisons with in vivo data were performed. The test set of 12 compounds of Liu et al. expressing log PS has been chosen ⁴⁷ (figure 2-8, table 2-4). These *in vivo* test set values have been determined using the in situ rat brain perfusion technique. In this technique, the composition of the perfusate is fully controlled. Therefore this methodology allows the determination of the permeability of the candidate without taking care of metabolism and protein binding, as PAMPA do. On the 12 compounds of the dataset, 8 were found to passively diffuse through the BBB and 4 undergone an efflux transport in vivo. Only the compounds supposed to cross the BBB via a passive diffusion process were correlated with the in vivo log PS. The 4 drug substrates of efflux transporters were then placed on the graph. In figure 2-8, all PAMPA permeability measurements with UV detection have been reported. Due to the limit of detection (LOD) of UV spectroscopy, and therefore the difficulty to determine very low concentrations in acceptor compartments for low permeants, a cut-off permeability of -6.3 had to be applied, corresponding approximately to the permeability of 1% of the initial concentration to the acceptor compartment. In order to improve the LOD and to refine some of the permeability values the concentrations of the cut-off compounds have been measured with UHPLC-MS. On the three cut-off compounds (hypoxanthine, theophylline, and theobromine), only theobromine was sufficiently ionized with the electrospray mode and reported on figure 2-8 (red dots) and table 2-4. The determination coefficient obtained with the 6 remaining compounds supposed to cross the BBB via passive diffusion indicates that the new artificial membrane is able to predict passive diffusion through the BBB with PAMPA ($r^2 = 0.81$, N = 6).

Four drugs strongly believed to be substrates of efflux transporters have also been introduced in figure 2-8, namely quinidine, digoxine, methotrexate and colchicine. Due to the capacity of PAMPA to only predict passive diffusion, when a substrate of a specific efflux transporter is tested on both models, PAMPA will overestimate the permeability of that compound. Results obtained for quinidine and digoxine (figure 2-8) indicate that permeability of these compounds through the HDC/NPOE artificial membrane is overestimated compared to *in vivo* permeability, corroborating their tendency as efflux substrates. On the other hand, colchicine did not permeate through our artificial membrane, even if it was considered as substrate of efflux transport at the BBB ^{57, 58}. Kerns and Di ⁵⁸ also indicated that colchicine

permeability on PAMPA-BBB was very low (P_e =0.025.10⁻⁶cm/s). Therefore this compound may be a substrate but still with a very low intrinsic passive permeation. In this specific case, the overestimation of the permeation in PAMPA could therefore not been observed. Methotrexate could not be sufficiently ionized with the electrospray mode in order to determine a permeability coefficient. As it is not a CNS compound *in vivo*, and less than 1% of this compound was able to cross the new PAMPA membrane, it was not possible to determine if PAMPA overestimates the permeability of methotrexate (figure 2-8).

Therefore, PAMPA is able to highlight an efflux process for substrates of efflux transporters that disclose a medium to fast passive permeation, by comparing *in vivo* permeability with PAMPA permeability. This operation only requires to build the linear relationship for known diffusing compounds and then to place the unknown compounds on the resulting graph. If the compounds with unknown behavior is on the linear relationship, this implies that this compound either diffuse or is slightly transported at the BBB. If the compound is clearly out of the linear relationship, with an overestimation with PAMPA, the compound is likely to be substrate of efflux transporters at the BBB.

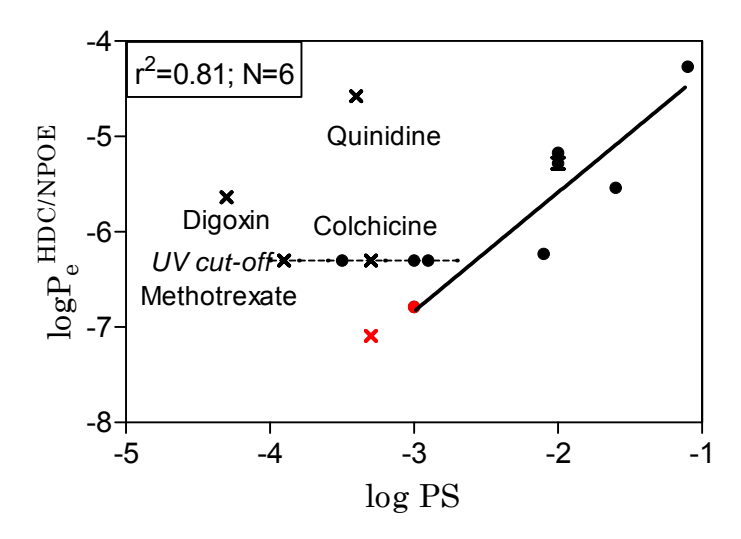


Figure 2-8: Comparison between *in vivo* log PS 47 and *in vitro* permeability with the HDC/NPOE PAMPA model using UV detection (black symbols) and MS detection (red symbols) for 11 compounds passively transported (circles) and 3 Pgp substrates (crosses). •represent the passively transported compounds, measured with UV detection, • represents salicylic acid, when permeability is measured with MS detection, × indicate the substrates of efflux transporters, measured with UV detection, × represents colchicine, a Pgp substrate measured with MS detection and * are the compounds at the cut-off when detected with UV. The solid black line is the correlation between log $P_e^{\text{HDC/NPOE}}$ and log PS for the compounds passively transported. The drugs having a permeability < -6.3, without an MS detection, have not been included in this correlation. The dotted line corresponds to the UV cut-off for log $P_e^{\text{HDC/NPOE}}$ determination.

2-3.5.2. Comparison of log $P_e^{HDC/NPOE}$ with log P_e^{BBCEC} for an extended dataset

BBCEC have also been described to express specific transporters such as Pgp/ABCB1 ¹⁰. Therefore, with the same idea of evaluating the ability of PAMPA to highlight efflux transport, digoxin and hydrocortisone were added to the initial set of thirteen compounds with known log P_eBBCEC. As Pgp substrates, these compounds should normally be out of the correlation. In figure 2-9, this is clearly the case for digoxin. Indeed, regarding the very low passage through BBCEC, digoxin should have a very poor permeability through the new artificial membrane if it crosses the membrane by diffusion. A digoxin permeability of -5.64 was obtained through the artificial membrane, meaning that the permeability of that compound was overestimated with PAMPA. This confirms the fact that PAMPA can highlight a global efflux transport.

Results for hydrocortisone were more ambiguous. The experiment revealed a log $P_e^{\text{HDC/NPOE}}$ of -5.83, which is quite closed of the linear correlation, as can be observed in figure 2-9. Considering the experimental errors on both *in vitro* models, overestimation of the PAMPA permeability is not evidenced. The categorization of this hormone as a Pgp substrate or not is subject to divergence between authors, as demonstrates references on the subject in ochem.eu. ⁵⁹. The PAMPA experimental result suggests that hydrocortisone is a poor substrate of Pgp. That could explain why hydrocortisone is so poorly out of the linear regression. Similarly, warfarin appeared to be out of the regression, even if the transport of this drug is currently expected to be purely passive. An indication of the error on the determination of the BBCEC permeability coefficient would surely have been useful for a complete interpretation.

Therefore, as for *in vivo* data, a comparison of the permeability coefficients determined with HDC/NPOE PAMPA and those determined with a cellular model can help in highlighting compounds probably substrates of efflux transporters *in vivo*.

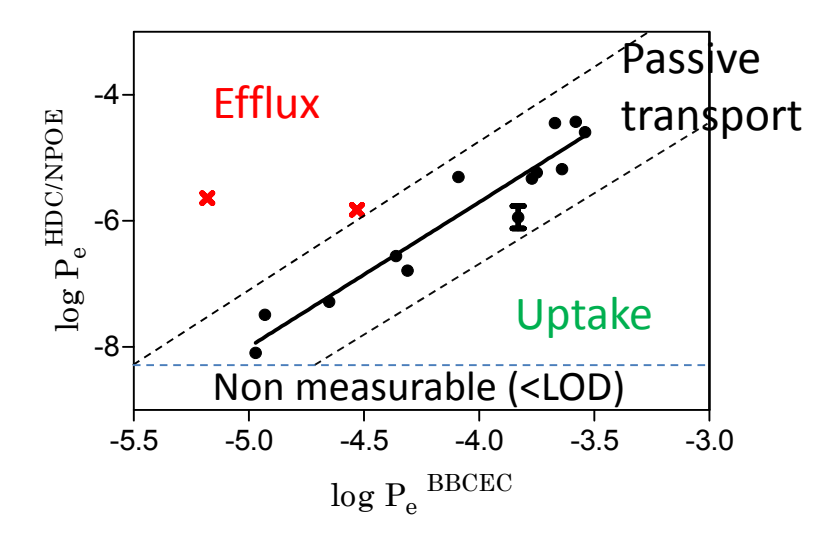


Figure 2-9: Comparison between log P_e^{BBCEC 33 20} and permeability with the new PAMPA model for 13 compounds passively transported (black circles) and 2 Pgp substrates, namely digoxine and hydrocortisone (red crosses). The blue dotted line at log P_e^{HDC/NPOE}=-8.2 is due to the limit of detection of the MS analyzer. The two black dotted lines surrounding the compounds crossing the BBB via passive diffusion are a speculative "barrier" separating the graph in 3 different zones: the zone where PAMPA estimates correctly the cellular permeability corresponds to the compounds which cross the BBB via passive diffusion; when PAMPA overestimates the cellular permeability, these compounds are prone to efflux transport, and when PAMPA underestimates the cellular data, the tested compounds are likely to be substrate of an uptake transporter.

2-3.5.3. Discussion

The promising results obtained when correlating log P_e^{HDC/NPOE} with both *in vivo* log PS and *in vitro* log P_e^{BBCEC} for passively transported compounds bring confidence on the new artificial membrane and on its capacity to predict passive BBB and BBCEC permeabilities. The main application of the optimized artificial membrane will therefore reside on the prediction of passive permeability through the BBB during the early drug discovery process. Indeed, due to the high throughput screening rate, the limited incubation time, the reproducibility of the method and thanks to the use of non-biological material, passive permeability through the BBB can be predicted in a straightforward way. Applying this model during the early drug discovery process, a hierarchy can be determined, as observed in figures 2-6, 2-7, 2-8 and 2-9. For the low permeant group, depending on the needs of the project, further cellular experiments can be undertaken for a possible uptake mechanism. For the fast permeants, in addition to the PAMPA experiment, permeability determination on cellular models expressing specific known transporters should be undertaken, in order to detect a potential efflux process.

As cellular models express a global permeability, composed of diffusion, an uptake and an efflux components, and since PAMPA can individualize the diffusion component, a

comparison of PAMPA and cellular permeabilities will give information on global efflux or influx transports, by considering the position of the tested molecule upon the linear relationship, and considering the limitation of the cellular model (transporters expressed, active or not) as illustrated in figure 2-9. Moreover, HDC/NPOE PAMPA is expected to provide help in the early investigation of potential active processes.

This strategy could be applied to different cellular models able to express specific active transporters, such as transfected cells. However, in each case, the passive permeability predicted with PAMPA model should correlates with the passive permeability through the considered cellular model. Of course, differences in the rate at which a compound will be able to cross the membrane can occur depending on the experimental strategy, especially when different stirring conditions are employed, but the linear relationship should subsist. Hence, stirred models will not disclose the same unstirred water layer (UWL) thickness as a stirred model. On unstirred conditions, UWL is thicker and the crossing of this aqueous layer is the limiting step for lipophilic compounds, whereas the permeability of the most hydrophilic ones will be favored. On a general concern, UWL is ordered by increasing thickness *in vivo* models < PAMPA < cell-based assays. Therefore, an evaluation of the correlations between *in vitro* passive permeability through artificial membrane and permeability through cellular model of interest should be carefully checked on well described passively transported compounds.

2-4. Conclusion

The present study led to the development of an original artificial membrane composed of 75% hexadecane and 25% o-NPOE, which revealed a good relationship between the experimental log P_e^{HDC/NPOE} and the permeability of passively transported compounds on different *in vitro* and *in vivo* models, for a limited number of compounds. Therefore, this new membrane appears as a promising tool to fast estimate passive permeability through the BBB in the early stages of drug discovery. Compared to permeabilities generated with PAMPA-BBB, this new artificial membrane allows an easier handling of the reproducibility, thanks to the use of organic solvents as artificial membrane. Moreover, the shorter incubation time allows the determination of passive BBB permeability within the working day.

A second application of this new artificial membrane could be the prediction of the mode of distribution of molecules at the BBB by combining results obtained with the artificial membrane and BBCEC model. Actually, when a NCE with unknown BBB distribution profile will be tested, both with a cellular and the artificial model, it will be possible to determine whether that compound will be prone to diffusion, influx, efflux or a combination of active and passive processes. The determination of the active process will be dependent on the type of cell model employed, as well as on the transporters expressed on these models.

Finally, the long-term perspective is to rate the proportion of passive diffusion and active transport of a drug compound, in order to fully understand its pharmacokinetics.

References

- Stanness, K. A.; Westrum, L. E.; Fornaciari, E.; Mascagni, P.; Nelson, J. A.; Stenglein, S. G.; Myers, T.; Janigro, D. Morphological and functional characterization of an in vitro blood-brain barrier model. *Brain Res.* 1997, 771, 329-342.
- 2. Wolburg, H.; Lippoldt, A. Tight junctions of the blood-brain barrier: Development, composition and regulation. *Vasc. Pharmacol.* **2002**, *38*, II.
- Doan, K. M. M.; Humphreys, J. E.; Webster, L. O.; Wring, S. A.; Shampine, L. J.; Serabjit-Singh, C. J.; Adkison, K. K.; Polli, J. W. Passive permeability and P-glycoprotein-mediated efflux differentiate central nervous system (CNS) and non-CNS marketed drugs. *J. Pharmacol. Exp. Ther.* 2002, 303, 1029-1037.
- 4. Weiss, N.; Miller, F.; Cazaubon, S.; Couraud, P. O. The blood-brain barrier in brain homeostasis and neurological diseases. *Biochim. Biophys. Acta* **2009**, *1788*, 842-857.
- 5. Löscher, W.; Potschka, H. Role of drug efflux transporters in the brain for drug disposition and treatment of brain diseases. *Prog. Neurobiology* **2005**, *76*, 22-76.
- 6. Tsaioun, K.; Bottlaender, M.; Mabondzo, A.; Alzheimer's Drug Discovery Fdn ADDME avoiding drug development mistakes early: central nervous system drug discovery perspective. *BMC Neurol.* **2009**, *9*.
- 7. Yazdanian, M.; Glynn, S. L.; Wright, J. L.; Hawi, A. Correlating partitioning and Caco-2 cell permeability of structurally diverse small molecular weight compounds. *Pharm. Res.* **1998**, *15*, 1490-1494.
- 8. Hakkarainen, J. J.; Jalkanen, A. J.; Kääriäinen, T. M.; Keski-Rahkonen, P.; Venäläinen, T.; Hokkanen, J.; Mönkkönen, J.; Suhonen, M.; Forsberg, M. M. Comparison of in vitro cell models in predicting in vivo brain entry of drugs. *Int. J. Pharm.* **2010**, *402*, 27-36.
- 9. Garberg, P.; Ball, M.; Borg, N.; Cecchelli, R.; Fenart, L.; Hurst, R. D.; Lindmark, T.; Mabondzo, A.; Nilsson, J. E.; Raub, T. J.; Stanimirovic, D.; Terasaki, T.; Öberg, J.-O.; Österberg, T. In vitro models for the blood-brain barrier. *Toxicol. in Vitro* **2005**, *19*, 299-334.
- Cecchelli, R.; Dehouk, B.; Descamps, L.; Fenart, L.; Buéé-Scherrer, V.; Duhem, C.; Lundquist, S.; Rentfel, M.; Torpier, G.; Dehouck, M. P. In vitro model for evaluating drug transport across the blood-brain barrier. Adv. Drug Deliv. Rev. 1999, 36, 165-178.
- Perrière, N.; Yousif, S.; Cazaubon, S.; Chaverot, N.; Bourasset, F.; Cisternino, S.; Declèves, X.; Hori, S.; Terasaki, T.; Deli, M.; Scherrmann, J. M.; Temsamani, J.; Roux, F.; Couraud, P. O. A functional in vitro model of rat blood-brain barrier for molecular analysis of efflux transporters. *Brain Res.* 2007, 1150, 1-13.
- 12. Coisne, C.; Dehouck, L.; Faveeuw, C.; Delplace, Y.; Miller, F.; Landry, C.; Morissette, C.; Fenart, L.; Cecchelli, R.; Tremblay, P.; Dehouck, B. Mouse syngenic in vitro blood-brain barrier model: a new tool to examine inflammatory events in cerebral endothelium. *Lab. Invest.* **2005**, *85*, 734-746.

- 13. Persidsky, Y.; Stins, M.; Way, D.; Witte, M. H.; Weinand, M.; Kim, K. S.; Bock, P.; Gendelman, H. E.; Fiala, M. Model for monocyte migration through the blood-brain barrier during HIV-1 encephalitis. *J. Immunol.* **1997**, *158*, 3499-3510.
- 14. Biernacki, K.; Antel, J. P.; Blain, M.; Narayanan, S.; Arnold, D. L.; Prat, A. Interferon beta promotes nerve growth factor secretion early in the course of multiple sclerosis. *Arch Neurol* **2005**, *62*, 563-568.
- 15. Durieu-Trautmann, O.; Foignant, N.; Strosberg, A. D.; Couraud, P. O. Coexpression of Beta-1-Adrenergic and Beta-2-Adrenergic receptors on bovine brain capillary endothelial-cells in culture. *J. Neurochem.* **1991**, *56*, 775-781.
- 16. Teifel, M.; Friedl, P. Establishment of the permanent microvascular endothelial cell line PBMEC/C1-2 from porcine brains. *Exp. Cell. Res.* **1996**, *228*, 50-57.
- Roux, F.; Durieu-Trautmann, O.; Chaverot, N.; Claire, M.; Mailly, P.; Bourre, J. M.; Strosberg, A. D.; Couraud, P. O. Regulation of γ-glutamyl transpeptidase and alkaline phosphatase activities in immortalized rat brain microvessel endothelial cells. *J. Cellul. Physiol.* 1994, 159, 101-113.
- 18. Laschinger, M.; Engelhardt, B. Interaction of alpha 4-integrin with VCAM-1 is involved in adhesion of encephalitogenic T cell blasts to brain endothelium but not in their transendothelial migration in vitro. *J. Neuroimmunol.* **2000**, *102*, 32-43.
- Dauchy, S.; Miller, F.; Couraud, P. O.; Weaver, R. J.; Weksler, B.; Romero, I. A.; Scherrmann, J. M.; De Waziers, I.; Declèves, X. Expression and transcriptional regulation of ABC transporters and cytochromes P450 in hCMEC/D3 human cerebral microvascular endothelial cells. *Biochem. Pharmacol.* 2009, 77, 897-909.
- Culot, M.; Lundquist, S.; Vanuxeem, D.; Nion, S.; Landry, C.; Delplace, Y.; Dehouck, M. P.;
 Berezowski, V.; Fenart, L.; Cecchelli, R. An in vitro blood-brain barrier model for high throughput (HTS) toxicological screening. *Toxicol. in Vitro* 2008, 22, 799-811.
- 21. Benistant, C.; Dehouck, M. P.; Fruchart, J. C.; Cecchelli, R.; Lagarde, M. Fatty-acid composition of brain capillary endothelial-cells effect of the coculture with astrocytes. *J. Lipid Res.* **1995**, *36*, 2311-2319.
- 22. Kansy, M.; Senner, F.; Gubernator, K. Physicochemical high throughput screening: parallel artificial membrane permeation assay in the description of passive absorption processes. *J. Med. Chem.* **1998**, *41*, 1007-1010.
- 23. Kansy, M.; Fischer, H.; Kratzat, K.; Senner, F.; Wagner, B.; Parrilla, I. High-throughput artificial membrane permeability studies in early lead discovery and development. In *Pharmacokinetic Optimization in Drug Research: Biological, Physicochemical and Computational Strategies*; Testa, B.; van de Waterbeemd, H.; Folkers, G.; Guy, R. H. Eds.; Wiley-VHCA: Zurich, 2001; pp 447-464.
- 24. Wohnsland, F.; Faller, B. High-throughput permeability pH profile and high-throughput alkane/water log P with artificial membranes. *J. Med. Chem.* **2001**, *44*, 923-930.

- 25. Ottaviani, G.; Martel, S.; Carrupt, P. A. Parallel artificial membrane permeability assay: a new membrane for the fast prediction of passive human skin permeability. *J. Med. Chem.* **2006**, *49*, 3948-3954.
- 26. Sinko, B.; Garrigues, T. M.; Balogh, G. T.; Nagy, Z. K.; Tsinman, O.; Avdeef, A.; Takacs-Novak, K. Skin–PAMPA: a new method for fast prediction of skin penetration. *Eur. J. Pharm. Sci.* **2012**, *45*, 698-707.
- 27. Di, L.; Kerns, E. H.; Fan, K.; McConnell, O. J.; Carter, G. T. High throughput artificial membrane permeability assay for blood—brain barrier. *Eur. J. Med. Chem.* **2003**, *38*, 223-232.
- 28. Avdeef, A.; Strafford, M.; Block, E.; Balogh, M. P.; Chambliss, W.; Khan, I. Drug absorption in vitro model: filter-immobilized artificial membranes. Studies of the permeability properties of lactones in *piper methysticum* forst. *Eur. J. Pharm. Sci.* **2001**, *14*, 271-280.
- 29. Dehouck, M. P.; Meresse, S.; Delorme, P.; Fruchart, J. C.; Cecchelli, R. An easier, reproductible, and mass-production method to study the blood-brain barrier in vitro. *J. Neurochem.* **1990,** *54*, 1798-1801.
- 30. Dehouck, M. P.; Jolliet-Riant, P.; Brée, F.; Fruchart, J. C.; Cecchelli, R.; Tillement, J. P. Drug transfer across the blood-brain barrier: correlation between in vitro and in vivo models. *J. Neurochem.* **1992**, *58*, 1790-1797.
- 31. Dehouck, M. P.; Dehouck, B.; Fenart, L.; Cecchelli, R. Blood-brain barrier in vitro. Rapid evaluation of strategies for achieving drug targeting to the central nervous system. In *Biology and Physiology of the Blood-Brain Barrier*; Couraud, P. O.; Scherman, D. Eds.; Plenum Press: New York, 1996; pp 143-146.
- 32. Fenart, L.; Buee-Scherrer, V.; Descamps, L.; Duhem, C.; Poullain, M. G.; Cecchelli, R.; Dehouck, M. P. Inhibition of P-glycoprotein: rapid assessment of its implication in blood-brain barrier integrity and drug transport to the brain by an in vitro model of the blood-brain barrier. *Pharm. Res.* **1998**, *15*, 993-1000.
- 33. Lundquist, S.; Renftel, M.; Brillault, J.; Fenart, L.; Cecchelli, R.; Dehouck, M. P. Prediction of drug transport through the blood-brain barrier in vivo: A comparison between two in vitro cell models. *Pharm. Res.* **2002**, *19*, 976-981.
- 34. Hansch, C.; Björkroth, J. P.; Leo, A. Hydrophobicity and central nervous system agents: on the principle of minimal hydrophobicity in drug design. *J. Pharm. Sci.* **1987**, *76*, 663-687.
- 35. Bouchard, G.; Carrupt, P. A.; Testa, B.; Gobry, V.; Girault, H. H. Lipophilicity and solvation of anionic drugs. *Chem. Eur. J.* **2002**, *8*, 3478-3484.
- 36. Caron, G.; Steyaert, G.; Pagliara, A.; Crivori, P.; Gaillard, P.; Carrupt, P. A.; Avdeef, A.; Box, K. J.; Girault, H. H.; Testa, B. Structure-lipophilicity relationships of the neutral and cationic forms of β-blockers. Part I. Partitioning in isotropic systems. *Helv. Chim. Acta* **1999**, *82*, 1211-1222.
- Liu, X.; Bouchard, G.; Müller, N.; Galland, A.; Girault, H. H.; Testa, B.; Carrupt, P. A. Solvatochromic analysis of partition coefficients in the o-nitrophenyloctylether (o-NPOE)/water system. Helv. Chim. Acta 2003, 86, 3533-3547.

- 38. Sugano, K.; Kansy, M.; Artursson, P.; Avdeef, A.; Bendels, S.; Di, L.; Ecker, G. F.; Faller, B.; Fischer, H.; Gerebtzoff, G.; Lennernaes, H.; Senner, F. Coexistence of passive and carrier-mediated processes in drug transport. *Nature Reviews Drug Discovery* **2010**, *9*, 597-614.
- 39. Avdeef, A. Permeability. In *Absorption and Drug Development*; Avdeef, A. Ed.; John Wiley & Sons: Hoboken, 2003; pp 116-246.
- 40. Henchoz, Y.; Bard, B.; Guillarme, D.; Carrupt, P. A.; Veuthey, J. L.; Martel, S. Analytical tools for the physicochemical profiling of drug candidates to predict absorption/distribution. *Anal. Bioanal. Chem.* **2009**, *394*, 707-729.
- 41. Caron, G.; Reymond, F.; Carrupt, P. A.; Girault, H. H.; Testa, B. Combined molecular lipophilicity descriptors and their role in understanding intramolecular effects. *Pharm. Sci. Technolog. Today* **1999**, *2*, 327-335.
- 42. Liu, X.; Bouchard, G.; Girault, H. H.; Testa, B.; Carrupt, P. A. Partition coefficients of ionizable compounds in o-nitrophenyl octyl ether/water measured by the potentiometric method. *Anal. Chem.* **2003**, *75*, 7036-7039.
- 43. Testa, B.; Crivori, P.; Reist, M.; Carrupt, P. A. The influence of lipophilicity on the pharmacokinetic behavior of drugs: concepts and examples. *Perspect. Drug Discovery Design* **2000**, *19*, 179-211.
- 44. Caron, G.; Ermondi, G. Calculating virtual log P in the alkane/water system (log P^{Nalk}) and its derived parameters $\Delta \log P^{Noct-alk}$ and $\log D^{pHalk}$. J. Med. Chem. **2005**, 48, 3269-3279.
- 45. Gulaboski, R.; Galland, A.; Bouchard, G.; Caban, K.; Kretschmer, A.; Carrupt, P. A.; Stojek, Z.; Girault, H. H.; Scholz, F. A comparison of the solvation properties of 2-nitrophenyloctyl ether, nitrobenzene, and n-octanol as assessed by ion transfer experiments. *J. Phys. Chem. B* **2004**, *108*, 4565-4572.
- 46. Avdeef, A. Absorption and Drug Development; John Wiley & Sons: Hoboken, 2003.
- 47. Liu, X.; Tu, M.; Kelly, K. S.; Chen, C.; Smith, B. J. Development of a computational approach to predict blood-brain barrier permeability. *Drug Metab. Dispos.* **2004**, *32*, 132-139.
- 48. El Tayar, N.; Testa, B.; Carrupt, P. A. Polar intermolecular interactions encoded in partition coefficients: an indirect estimation of hydrogen-bond parameters of polyfunctional solutes. *J. Phys. Chem.* **1992**, *96*, 1455-1459.
- 49. Millard, J. W.; Alvarez-Nunez, F. A.; Yalkowsky, S. H. Solubilization by cosolvents establishing useful constants for the log-linear model. *Int. J. Pharm.* **2002**, *245*, 153-166.
- 50. Winiwarter, S.; Bonham, N. M.; Ax, F.; Hallberg, A.; Lennernas, H.; Karlen, A. Correlation of human jejunal permeability (in vivo) of drugs with experimentally and theoretically derived parameters. A multivariate data analysis approach. *J. Med. Chem.* **1998**, *41*, 4939-4949.
- 51. Hansch, C.; Leo, A. *Exploring QSAR. Fundamentals and Applications in Chemistry and Biology*; ACS Professional Reference Book, American Chemical Society: Washington, 1995; pp 1-557.

- 52. Barlow, R. B.; Chan, M. The effects of pH on the affinity of pirenzepine for muscarinic receptors in the guinea-pig ileum and rat fundus strip. *British Journal of Pharmacology* **1982**, *77*, 559-563.
- 53. Greig, N. H.; Genka, S.; Daly, E. M.; Sweeney, D. J.; Rapoport, S. I. Physicochemical and pharmacokinetic parameters of seven lipophilic chlorambucil esters designed for brain penetration. *Cancer Chemother. Pharmacol.* **1990**, *25*, 311-319.
- 54. Dang, Q. X.; Yan, L. X.; Zeng-pei, S.; Da-kui, L. Separation and simultaneous determination of the active ingredients in theophylline tablets by micellar electrokinetic capillary chromatography. *J. Chromatogr. A* **1993**, *630*, 363-369.
- 55. Lin, C.-E.; Liao, W. S.; Chen, K.-H.; Lin, W. Y. Influence of pH on electrophoretic behavior of phenothiazines and determination of pK_a values by capillary zone electrophoresis. *Electrophoresis* **2003**, *24*, 3154-3159.
- 56. Geinoz, S. Assessment of Drug Permeation :Theory, Methods and Applications to Skin and Bacteria; Thesis: University of Lausanne, 2002.
- 57. Kerns, E. H.; Di, L. Physicochemical profiling: overview of the screens. *Drug Discovery Today: Technologies* **2004**, *4*, 343-348.
- 58. Kerns, E. H.; Di, L.; Petusky, S.; Farris, M.; Ley, R.; Jupp, P. Combined application of parallel artificial membrane permeability assay and Caco-2 permeability assays in drug discovery. *J. Pharm. Sci.* **2004**, *93*, 1440-1453.
- 59. Yoon, C. H.; Kim, S. J.; Shin, B. S.; Lee, K. C.; Yoo, S. D. Rapid screening of blood-brain barrier penetration of drugs using the immobilized artificial membrane phosphatidylcholine column chromatography. *J. Biomol. Screening* **2006**, *11*, 13-20.

<u>Chapter 3:</u> PAMPA as a tool to understand the pharmacological activity of Hypericum perforatum

3-1. Introduction

Phytotherapy is the most ancient form of medicine. The first traces indicating the use of plant extracts to treat human diseases have been found 3000 years b.c. Till the emergence of modern chemistry at the end of the XIXth century, plants or drugs extracted from plants are the main remedies employed to cure people. This ancient medicine is still largely employed in developing countries, where ancient believes are very strong. Nowadays in developed countries, new strategies coming from chemical synthesis and biotechnologies have emerged and constitute the majority of the prescriptions, but phytochemistry is still present and research areas focused on plant extracts are highly active, in order to find and isolate new active compounds from plants.

Hypericum perforatum L., best known as St John's Wort (SJW), is a popular yellow-flowering plant (figure 3-1) employed mainly to treat mild to moderate depression ¹⁻⁵. Compared to synthetic antidepressants such as imipramine (tricyclic antidepressant), moclobenide (MAO inhibitors) or fluoxetine (selective serotonine reuptake inhibitor) ¹, SJW was proved to be as efficient with fewer side effects ^{2, 6}. A meta analysis conducted by Kim *et al.* ⁷, analyzed the results of randomized, blinded and well conducted clinical trials of SJW extracts in patients suffering from depression. This analysis indicated a significantly higher response for the patients treated with SJW (73.2% *vs* 37.9% for placebo). Moreover, SJW was as efficient as tricyclic antidepressant (imipramine) (64%(SJW) *vs* 66.4%(tricyclic antidepressant)) while presenting a lower incidence of side effects (26.4%(SJW) *vs* 47% (tricyclic antidepressant)). SJW is also traditionally used as a multifunctional agent, to treat wounds, burns, muscle pain, and it can also be employed for its antiviral or anti-inflammatory properties ^{6, 8}. But despite its huge utilization in medicine, its exact mechanism of action is still not well understood and established, and the active molecules are still not well identified.



Figure 3-1: Photography of Hypericum perforatum (www.florafinder.com-29.04.2013)

Many compounds have been isolated from SJW, such as naphtodianthrones (hypericin, pseudohypericin...), phloroglucinols (hyperforin) or flavonoids (quercetin, rutin...) (figure 3-2) 2, but it is still not evidenced whether the CNS therapeutical effect is due to single compound or to a synergy of many constituents 9. Hypericin was originally thought to generate the antidepressant effect, due to inhibition of Monoamine oxidase A and B (MAO-A; MAO-B)¹⁰, but this assertion is now criticized ⁶. Clinical evidences now support the fact that the antidepressant effect may rather come from hyperforin ^{6, 11}, which acts on the reuptake of serotonin, dopamine and norepinephrin ⁴ and is thought to modify neurotransmitter storage in synaptic vesicles ¹. Moreover, SJW extracts as well as isolated hyperforin are thought to act on the uptake of γ-aminobutyric acid and L-glutamate, due to an increase in intracellular Na⁺ concentration ¹². But no clear evidence exists on the possible involvement of other SJW constituent in the pharmacological effect. In vivo data indicated a possible contribution of quercetin flavones in the antidepressant effect 1, 9. Hence, the Porsolt's force swin test made with rat treated with SJW extracts without rutin or with very low concentrations of rutin were inactive ^{1, 13}, implying a possible involvement of rutin in the pharmacological response. The same in vivo test, performed with fractions containing flavonoids or free from flavonoids lead to the conclusion that fractions free from flavonoids were inactive 14. Another study comparing the antidepressant activity of a SJW total extract, a fraction of hypericin and pseudo hypericin, and a fraction of protohypericin, indicated an anxiolytic effect of the extract, whereas no effect was observed for the isolated compounds 15. Therefore, hyperforin, hypericin or flavonoids are thought to play a role in the anxiolytic activity of SJW. A real understanding of the exact mechanism of action still needs to be clarified, since a synergy between the actions of combinations of constituents may occur to generate the therapeutical effect.

In order to exert a pharmacological activity, the constituents of SJW need to interact with disease receptors and cross biological barriers. As SJW extracts are traditionally orally administered, the constituents need to first cross the intestinal barrier, in order to reach the blood stream. The active molecules then need to penetrate through the BBB in order to exert their CNS action. This permeation can occur *via* different mechanisms among a diffusion process and/or active processes (carrier mediated transport, receptor mediated processes, transcytosis, endocytosis) ¹⁶. *In vivo* experiments performed by Keller *et al.* ¹² succeeded in demonstrating the presence of hyperforin in the blood and the brain of mice after oral administration of hyperforin salt and SJW extract. This clearly highlights the capacity of hyperforin to interact both with the gastro-intestinal tract (GIT) and the blood-brain barrier (BBB). On the other hand, no experimental data can affirm that hypericin and pseudohypericin are able to penetrate the BBB ¹, ¹⁷.

Parallel artificial membrane permeability assay (PAMPA) is a recent technique able to predict passive permeability through biological barriers with a high-throughput efficiency, a cost-efficiency and a reproducible way. Therefore, PAMPA can isolate the passive component in the permeation process, but cannot predict the active transport. The choice of the artificial membrane allows the assessment of passive permeability through specific biological barriers, such as the GIT 18, 19, the BBB 20, 21 or the stratum corneum 22. In the present study, PAMPA has therefore been employed to identify a possible passive permeation of extract constituents that could help in understanding the process leading to the CNS effect. As SJW is absorbed orally, a first evaluation of the passive permeation through the GIT was performed with HDM-PAMPA 19. Then, HDC/NPOE PAMPA 21 was used to evaluate a potential passive permeability through the BBB. This study has been performed with a standardized SJW extract and a home-made methanolic extract. The commercial extract acts as a standard, whereas the home-made extract allows a comparison of the extracted fractions of SJW with an in house extraction protocol (appendix 2). Furthermore because isolated hypericin and quercitrin (flavonoid) were easily available and probably involved in the antidepressant effect, these compounds were also tested in PAMPA assay and compared to SJW extract to try to evaluate a possible synergy effect which may be brought by other constituents of the extracts. Many constituents of SJW are flavonoid glycosides (rutin, epigallocatechin, hyperosid, isoguercetin, guercitrin, astilbin, miguelianin). Due to the weakness of the O-glucosidic bond, flavonoid glycosides can be hydrolyzed due to the pH conditions in the stomach and the enzymes present in the intestinal lumen. Therefore a hydrolysis of SJW extract has been performed and the permeation of the hydrolyzed extract, together with isolated aglycones compounds was also studied.

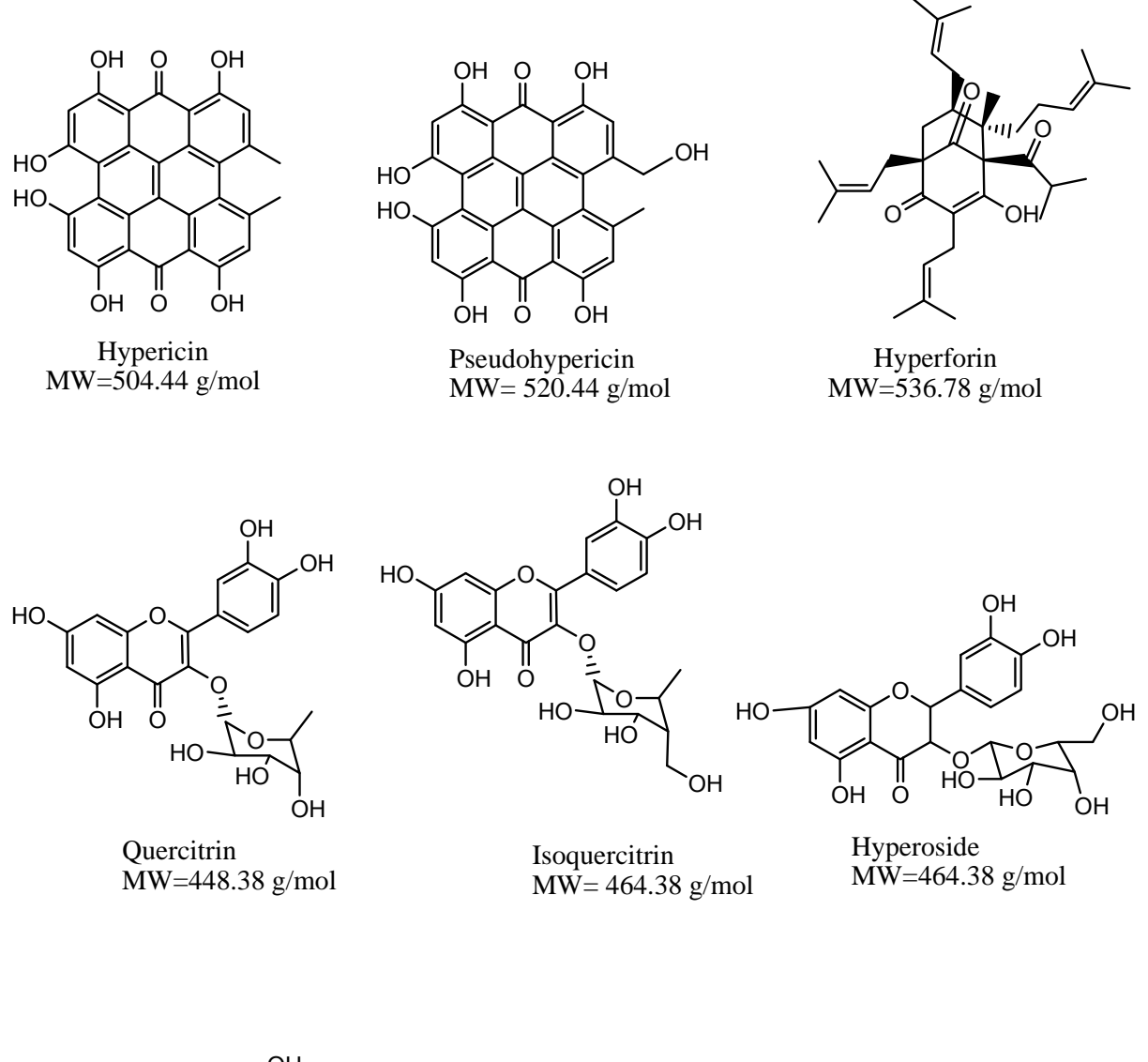


Figure 3-2: Structures of the main constituents of *Hypericum perforatum* (phloroglucinol(hyperforin), naphtodianthrones (hypericin, pseudohypericin), flavonoids (quercitrin, isoquercitrin, hyperoside, rutin, miquelianin)) and their respective molecular weight.

3-2. Materials and methods

3-2.1. Chemicals

Hexadecane 99% was provided by Sigma-Aldrich (St Louis, USA), hexane (purity grade > 95%), 2-nitrophenyl-octyl ether (purity grade ≥ 99%), disodium hydrogen phosphate and potassium dihydrogen phosphate were purchased from Fluka AG (Buchs, Switzerland), Dimethylsulfoxide was purchased from Acros Organics (Basel, Switzerland), hypericin 98%, from *Hypericum perforatum*, was purchased from Alfa Aesar (Karlsruhe, Germany), luteolin, kaempferol, quercetin, hyperoside, kaempferol, luteolin-7-glucoside and quercitrin were purchased from Carl Roth GmbH (Karlsruhe, Germany). St John's Wort home-made extract was kindly provided by Pr Wolfender, head of the Phytochemistry and Natural Products department of the University of Geneva, whereas the commercial extract was purchased from Indena (Milano, Italy). This extract, standardized in hypericin and hyperforin, contained between 0.1 and 0.3% hypericin and less than 6% hyperforin. The internal standards methotrexate and carbamazepine were obtained from Sigma-Aldrich (St Louis, USA).

3-2.2. HDM-PAMPA

HDM-PAMPA was developed in early 2000's to determine passive permeability of drug compounds through the GIT ¹⁹. Briefly, stock solutions were prepared dissolving the test compounds in DMSO with concentration values depending on their solubility in DMSO. For hypericin, the concentration of the stock solution in DMSO was 0.3 mg/ml, 26.6 mg/ml for the commercial SJW extract and 30 mg/ml for the home-made methanolic extract. For the study of isolated flavonoids, the concentrations were 1 mg/ml. Stock solutions of internal standards (methotrexate or carbamazepine) were prepared at a concentration of 10 mM in DMSO. Methotrexate was chosen as a slow permeant compound while carbamazepine was considered as a fast permeant compound. Reference solutions were prepared with 2.5% of DMSO stock solution of the extract or compound of interest and 2.5% DMSO stock solution of the internal standard dissolved in a phosphate buffer pH 6.8 (41 mM Na₂HPO₄ and 28 mM KH₂PO₄) supplemented with 100 mM KCI.

Each well of a hydrophobic polycarbonate 96-wells microtiter filter plate (MPC4NTR10 Millipore AG, Volketswil, Switzerland) was impregnated with 15 μ l of a 5% (v/v) hexadecane

membrane dissolved in hexane. Polycarbonate filters had 20% porosity, with a 0.4 μ m diameter of pores and a 0.26 cm² cross-sectional area. This microtiter plate constitutes the donor compartment. The plate was left under the extractor hood for 15-20 minutes to completely evaporate hexane. A Teflon® 96-wells acceptor plate (Millipore MSSACCEPTOR) was filled with 280 μ l of a pH 6.8 phosphate buffer containing 5% DMSO. The donor plate was next placed upon the acceptor plate in a "sandwich-like conformation" and filled with 280 μ l of the solution containing the compounds to test. The resulting sandwich was incubated for five hours at room temperature and under constant shaking at 75 rpm to minimize the unstirred water layer ²² without causing an overflowing between wells. Permeability coefficients were determined with equation 3-1.

At the end of the incubation time, 200 μ I of each well were transferred out of the donor and acceptor compartments for concentration determination with UHPLC-TOF-MS. A determination of the concentration of the donor compartment at time 0 (reference solutions) was also performed.

3-2.3. HDC/NPOE PAMPA

The details of this technique are described in chapter 2. Briefly, HDC/NPOE PAMPA was developed in house to predict the passive permeability of drug compounds through the BBB. In this technique, the artificial membrane is composed of 75% hexadecane and 25% ortho-nitrophenyl octyl ether dissolved in hexane, at a concentration of 35% artificial membrane for 65% hexane. 15 µl of the artificial membrane is laid down on a hydrophobic polyvinylidene fluoride (PVDF) 96-wells microfilter plate (Millipore, MAIPN4550). Donor solutions are prepared with 2.5% stock solution of the extract or compound of interest to be tested and 2.5% of a DMSO stock solution of an internal standard (either carbamazepine or methotrexate) in pH 7.4 phosphate buffer. Acceptor solutions are constituted of 5% DMSO in the same pH 7.4 phosphate buffer. The sandwich is incubated for 7 hours under constant shaking at 150 rpm.

At the end of the incubation time, 200 μ I of each well were transferred out of the donor and acceptor compartments for concentration determination with UHPLC-TOF-MS. A determination of the concentration at time 0 was also performed.

3-2.4. Integrity of the membrane

To check the integrity of the membrane in presence of phyto-extracts, control compounds (methotrexate (CNS-/GIT-) and carbamazepine (CNS+/GIT+)) have been added in each well containing either 670 μg/ml of commercial plant extract or 750 μg/ml of homemade plant extract in order to check the validity of the experiment. These reference solutions are prepared with 95% phosphate buffer, 2.5% DMSO stock solution of the control compound and 2.5% of DMSO stock solution of the extract (prepared at its maximum solubility capacity of 30 mg/ml for the home-made SJW and 26.6 mg/ml for the commercial SJW). The final DMSO concentration in the reference solution is thus 5%, as for the original PAMPA model. The resulting permeability of methotrexate and carbamazepine in presence and in absence of SJW were compared. When the artificial membrane is not modified by the presence of phyto-products, both permeability coefficients are identical.

3-2.5. UHPLC-TOF-MS measurements

The reference, donor and acceptor solutions generated after the PAMPA experiments with the extracts were analyzed with UHPLC-TOF-MS (Waters, Milford, USA). UHPLC column was an Acquity BEH Shield C 18, 100 mm×2.1 mm, 1.7µm pore size (Waters, Irland), calorifuged at 60°C. The flux of mobile phase was set to 500 µl/min. Mobile phases were constituted of a mixture of ammonium formate 10mM containing 0.1% formic acid (ULC/MS grade, Biosolve, Nederlands) and methanol supplemented with 0.1% formic acid (ULC/MS grade, Biosolve, Nederlands). The gradient mode exposed in table 3-1 was employed to determine the concentrations of active compounds in each compartment. MS detector was a Micromass-LCT Premier time-of-flight (Waters, Milford, USA). Compounds were ionized with the negative electrospray mode, a scan time of 0.3 s, a 40 V cone voltage for a mass detection between 100 and 1000 m/z in centroid mode. Due to the long UHPLC-TOF-MS runs (22 minutes per sample) and the very high number of wells to be analyzed, concentrations were measured once or in duplicate. That is why no standard deviation will be indicated with the AUC. This TOF-MS technique allows great sensitivity and specificity, but only qualitative measurements are achieved. Therefore, no precise quantification can be done with TOF-MS. The information generated will be either a detection or not on the acceptor compartment.

Table 3-1: Gradient applied for the analysis of SJW extracts.

Time (min)	% ammonium formate 10 mM (+0.1% formic acid)	% Méthanol (+0.1% formic acid)		
0	95	5		
4	50	50		
4.5	25	75		
13	0	100		
18	0	100		
18.5	95	5		
22	95	5		

3-2.6. UHPLC-UV measurements

The reference, donor and acceptor solutions obtained with isolated aglycones were analyzed with an Acquity UHPLC System PDA from Waters (USA). The maximum optical density was detected at 352.1 nm for luteolin, 364.1 nm for kaempferol and 370.1 nm for quercetin, thanks to the photodiode array (PDA) detector. The column was a BEH shield 50 mm× 2.1 mm, with 1,7 μ m pore size (Waters). The column was kept at 40°C, with a mobile phase flux of 500 μ l/min. The mobile phase is constituted of a mixture of 0.1% formic acid in 0.22 μ m filtered water and methanol. The gradient mode detailed in table 3-2 was employed as a standard method.

Table 3-2 : Details of the gradient employed in UHPLC-PDA for the analysis of the isolated glycosides and aglycones.

Time (min)	0.1% formic acid in water	% Méthanol		
0	95	5		
3	5	95		
4	5	95		
4.3	95	5		
6.3	95	5		

3-2.7. Permeability equations

Appropriate permeability equations were selected according to the design of the PAMPA experimental protocol. The presence of membrane retention and absence of sink conditions lead to define the permeability coefficient as follows 23 :

$$P_{e} = -\frac{2.303V_{D}}{A\left(t - \tau_{lag}\right)} \left(\frac{V_{A}}{V_{A} + V_{D}}\right) \log \left[1 - \left(\frac{V_{A} + V_{D}}{V_{D}\left(1 - R\right)}\right) \frac{C_{A}\left(t\right)}{C_{D}\left(0\right)}\right]$$
 (Equation 3-1)

where A is the accessible filter area in cm² (cross-sectional filter area multiplied by the porosity of the filter), t is the incubation time in seconds, V_A and V_D are the volume of the acceptor and donor compartments respectively (0.28 cm³), $C_A(t)$ is the concentration of solute in the acceptor compartment at time t and $C_D(0)$ the concentration of the reference solution, τ_{lag} is the steady-state time (s), that is the time needed for compounds gradient to be stabilized. The observed τ_{lag} are of the order of 20 minutes, which is relatively short compared to the incubation time of 5 or 7 hours. For this reason, the steady-state time was neglected for the calculations of the permeability coefficients. The retention factor R is defined as the quantity of solute which is not in the acceptor or the donor compartments at the end of the incubation time. This quantity can either be retained at the membrane or adsorbed on the plate material:

$$R = 1 - \frac{C_D(t)}{C_D(0)} - \frac{V_A}{V_D} \frac{C_A(t)}{C_D(0)}$$
 (Equation 3-2)

The differentiation between compound retained in the membrane and adsorbed the material cannot be achieved.

3-2.8. Acidic hydrolysis of the SJW extract

Flavonoids present in SJW extract are mainly flavonoid glycosides. Due to the hydrophilic nature of sugars, the interactions and the permeation of such glycosylated products is very limited both at the GIT and at the BBB ²⁴. But on the other hand, due to the strong acidic pH in the stomach, and the presence of glucosidases at the luminal side of the intestine, hydrolysis of those flavonoids is likely to occur before reaching the intestinal barrier, leading to the formation of aglycones. That is why an experimental hydrolysis of a SJW methanolic extract has been performed.

SJW was heated to reflux for one hour in HCl 2M. The resulting solution was extracted three times with ethyl acetate and washed two times with saturated NaCl solution. After dehydration of the organic phase with an anhydrous sulfate salt, the organic layer was evaporated with a Rotavapor® to generate a powder of the hydrolyzed extract.

3-3. Results and discussion

3-3.1. Integrity of the membrane in presence of phyto extracts

PAMPA was originally performed and validated for the determination of passive permeation of small isolated molecules. A phyto-extract is much more complex than isolated molecules. The whole extract may generate a matrix effect, and the extract is constituted of so many components that the physicochemical properties of the artificial membrane may be modified, resulting in incorrect prediction of permeability. Therefore, checking the integrity of the membrane is an important point before analyzing complex matrices such as phyto-extracts.

The permeability coefficients obtained for carbamazepine and methotrexate in presence and in absence of SJW were determined with HDM-PAMPA and HDC/NPOE PAMPA and are compiled in table 3-3. Permeability generated for carbamazepine and methotrexate in presence of SJW extract are equivalent to those obtained for the free drug. This indicates that the presence of the multiple constituents of the extract does not modify the physicochemical properties of both artificial membranes, which thus carry on predicting GIT passive permeability for HDM-PAMPA, and BBB passive permeability for HDC/NPOE PAMPA. Permeability of phyto-extracts can therefore be assessed with those two PAMPA models.

Table 3-3: PAMPA results for control compounds in presence or in absence of SJW extracts.

Control compound	Free drug	PAMPA	Extract	Free drug + extract
	-3.9 ± 0.1	CIT	commercial extract	-3.6
	-	GIT	home made extract	-3.9
carbamazepine -	-4.4 ± 0.1	DDD	commercial extract	-4.1
	-	BBB	home made extract	-4.1
	< -5.5	CIT	commercial extract	<-5.5
Methotrexate -	-	GIT	home made extract	< -5.5
	< -6.3	DDD	commercial extract	<-6.3
	-	BBB	home made extract	< -6.3

3-3.2. SJW crude extracts and available isolated components

A plant extract is composed of a multitude of constituents, from very hydrophilic to highly lipophilic molecules. Therefore, the apparent solubility of the total extract will be the solubility of the least soluble compound of the extract. In the case of the two SJW extracts studied in this chapter, the initial solubility in DMSO was acceptable (26.6 mg/ml for the commercial extract and 30 mg/ml for the in house methanolic extract). But within this dissolved quantity, only a very small percentage represents the compounds of interest. For example, hypericin counts for only 0.1 to 0.3% of the total extract, meaning that detection will be the limiting factor of this study. Moreover, some compounds within the plant extract may have the same molecular weight and the same retention time, such as the structural isomers hyperoside and isoquercitrin. Identification is therefore not an easy task. UHPLC-TOF-MS detection has been chosen to improve the selectivity of the detection.

Figure 3-3 and figure 3-4 represent the chromatograms of reference solutions (donor solution at t=0 min) of the home-made methanolic extract and of the commercial methanolic extract of SJW. Six constituents of SJW can be detected and quantified in the home made extract. Only naphtodianthrones (hypericin, pseudohypericin) and flavonoids (miquelianin, isoquercitrin, quercitrin and hyperoside) have been detected. The other chemical families which normally are present in SJW (phloroglucinol, phenolic acids) were not detected. Hyperoside and isoquercitrin, stuctural isomers, have the same molecular weight and very close physicochemical properties, due to a high degree of similarity in their structure. Therefore, the attribution of the 2 peaks at 3.4 minutes retention time was combined for both molecules ²⁵. Moreover, 2 peaks were identified at the mass corresponding to pseudohypericin, at retention times of 6.20 minutes and 7.35 minutes (corresponding to a difference of 3 % methanol in the mobile phase at the moment of elution). This second peak

is supposed to be a conformer of pseudohypericin, with a conformation a little bit more hydrophobic than the native conformation, but with the same m/z. The second conformer was nearly not detectable for the commercial extract in figure 3-4. This means that *Hypericum perforatum* employed to generate the home-made extract contained the conformer of pseudohypericin, whereas its quantity was negligible in the commercial extract.

The chromatogram of the commercial *Hypericum perforatum* shows a seventh constituent in the extract: rutin ([M-H]⁻ = 609 in negative ionisation mode). Rutin was not detected in the home-made extract. However, as both studied extracts are methanolic extracts, rutin is probably present in the home-made extract, but in low concentration. This fact may come from variability in plant chemical compositions that has an incidence on the abundance of some constituents of the extract ²⁶. Moreover, retention time of rutin is the same as hyperoside and isoquercitrin, even with a 22 minutes chromatographic method. An overlap may therefore occur between the species. On figure 3-4, the second peak of hyperoside and isoquercitrin observed in the home-made extract was not identified in the commercial extract. Here again, rutin may be more abundant in this commercial SJW than hyperoside and isoquercitrin, leading to this profile (figure 3-4).

It was surprising to note that hyperforin, which constitutes around 6% of the extract, was not detected in the 2 extracts. According to its structure, hyperforin should provide a high lipophilicity (log P estimated between 6 and 13 by ALogPS, ChemAxon and the US Estimation Program Interface) leading to a high retention time. Another explanation may also come from difficulties in ionizing this molecule during MS detection, regarding the structure of the molecule in figure 3-2.

The compounds detected in the reference solutions will therefore be followed during the PAMPA experiments. If passive permeation of these constituents occurs, they should also be detected in the acceptor compartment.

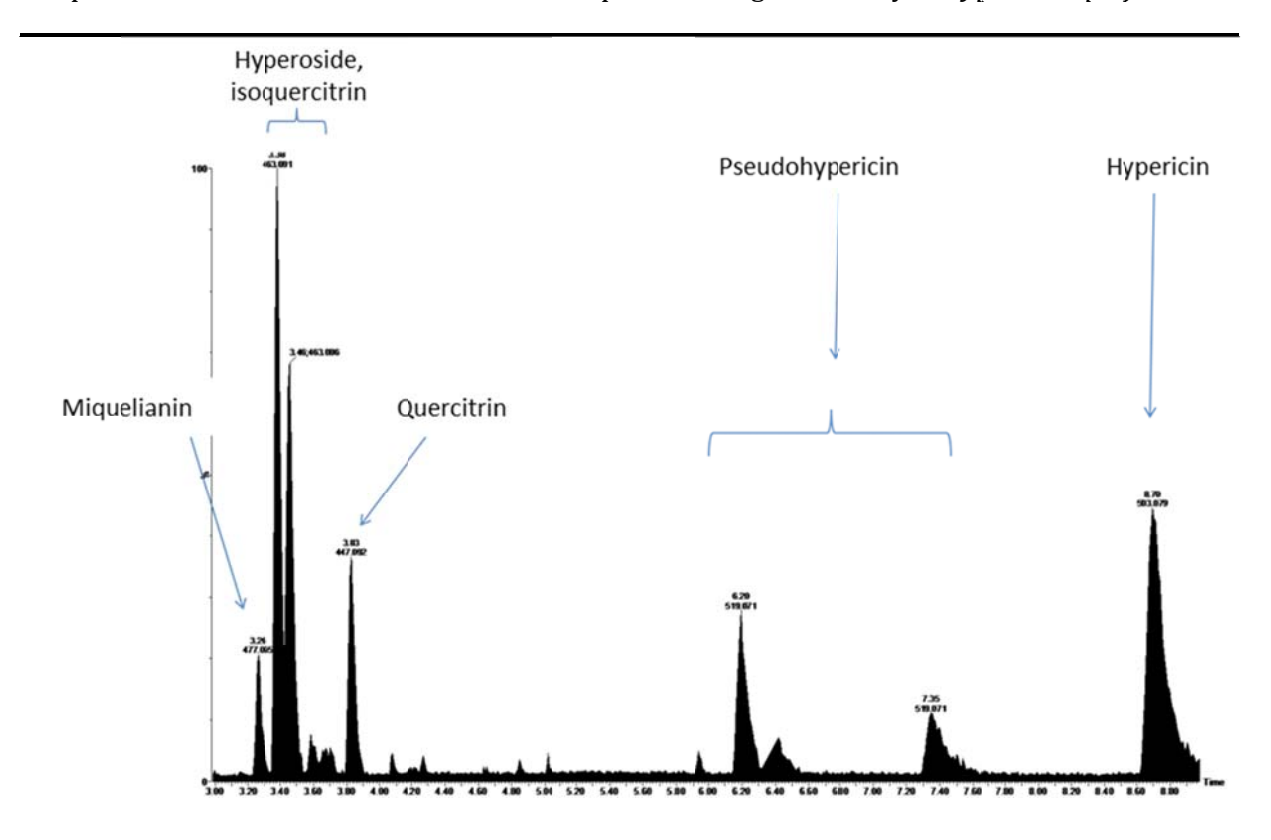


Figure 3-3 : UHPLC-TOF-MS profile of the reference solution of home-made methanolic SJW extract on HDM-PAMPA, with the gradient mode described in Table 3-1.

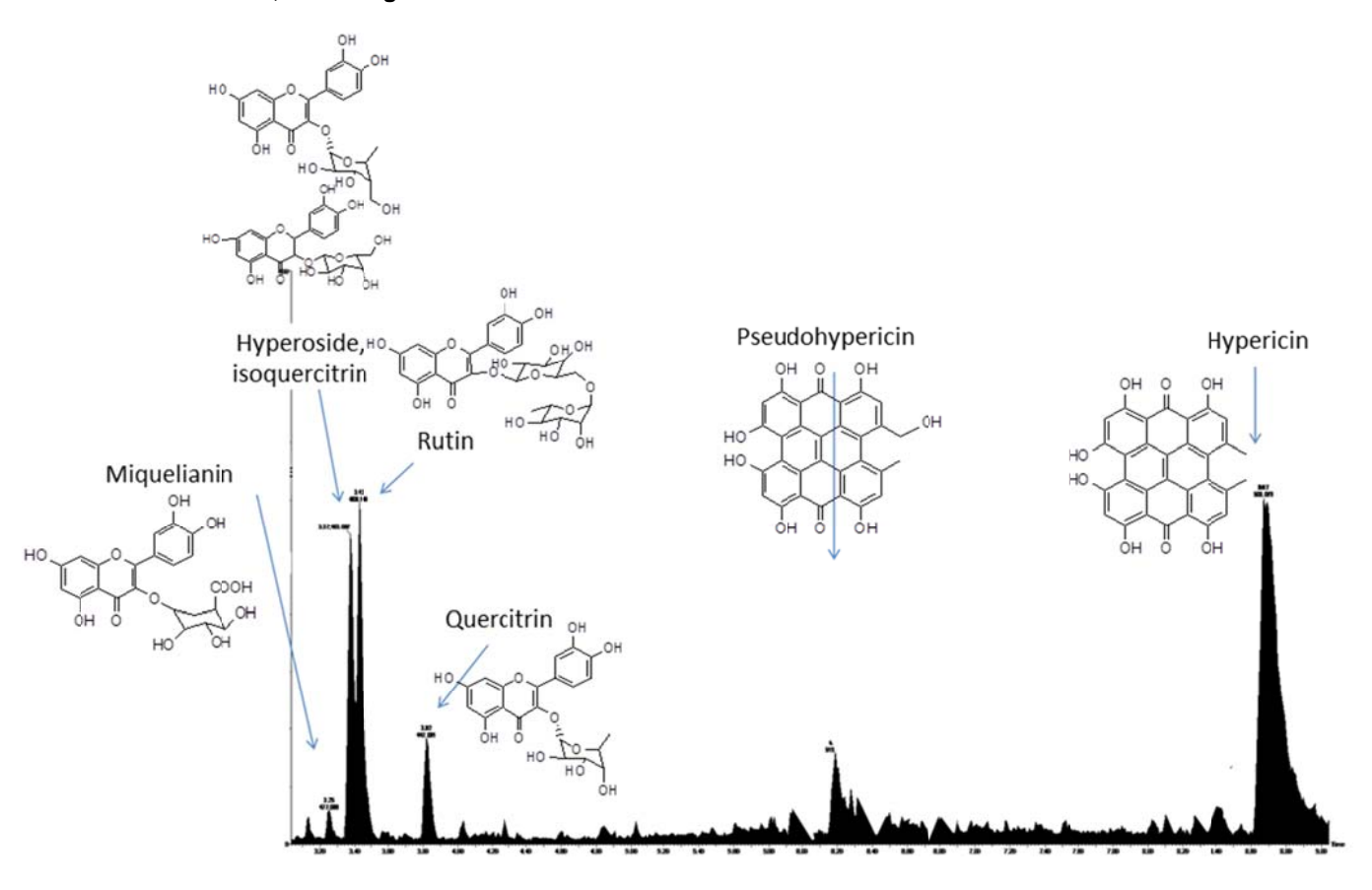


Figure 3-4: UHPLC-TOF-MS profile of the reference solution of commercial methanolic SJW extract on HDM-PAMPA, with the gradient mode described in table 3-1.

3-3.2.1. HDM PAMPA

In the original procedure exposed by Wohnsland and Faller ¹⁹, the best correlation between permeabilities measured with HDM-PAMPA (log P_e) and *in vivo* human absorption was obtained when considering the highest permeability coefficient determined at different pH between pH 4 and pH 8. Indeed, this maximum permeability corresponds to the permeability where the fraction of ionized compounds is the lowest between pH 4 and 8 ²⁷. However, the relationship between the log P_e measured at pH 6.8 and human absorption was considered acceptable in term of GIT permeability prediction. When dealing with extract, many compounds are in presence with different ionizable functions and hence ionization constants. Thus HDM-PAMPA was performed at pH 6.8 all along the study to harmonize the permeability assessment.

Permeability of isolated hypericin and quercitrin as well as commercial and homemade methanolic extracts were determined. Two internal standards (Carbamazepine or methotrexate) were added to verify the integrity of the membrane during PAMPA experiments.

Figure 3-5 shows the chromatograms acquired for commercial and home-made extract in the reference compartment (donor at time t=0) and in the donor and acceptor compartments after 5 hours incubation time. On figure 3-5a, residual peaks are observed in the acceptor, donor and reference compartments with the same AUC and the corresponding m/z cannot be attributed to a component of SJW. Furthermore, these specific peaks were also detected in blank wells and can thus be considered as artifact. Therefore, for the commercial extract, the blank profile was substracted to the chromatograms of the donor, acceptor and reference.

According to these considerations, figure 3-5 and table 3-4 indicate that no passive permeation of the compounds of interest of both commercial or home-made extracts occur through the hexadecane artificial membrane. Therefore, none of the constituents highlighted in figure 3-2 is predicted to cross the GIT by passive transcellular diffusion, or at least, none of them succeed in reaching the acceptor compartment at a concentration allowing the quantification. Moreover, no significant membrane retention was observed, which means that all the molecules remained in the donor compartment (table 3-4).

Table 3-4 : Permeability coefficients (log P_e) membrane retention (R %) and quantity of compounds that reached the acceptor compartment ($C_A(t)/C_D(t)$ %) obtained for isolated compounds (Hypericin and Quercitrin), methanolic commercial and home-made extract and standards (Carbamazepine and methotrexate) obtained using HDM-PAMPA.

	Compound	$C_A(t)/C_D(0)$ (%)	Retention (%)	log Pe
	Hypericin	0	<1	< -5.5
Isolated	Quercitrin	0	2	< -5.5
compounds	Carbamazepine (GIT+)	39	<1	-3.6
	Methotrexate (GIT -)	0	<1	< -5.5
	Miquelianin	0	<1	< -5.5
	Hyperoside/Isoquercitrin	0	<1	< -5.5
Standardized	Rutin	0	13	< -5.5
commercial extract	Quercitrin	0	13	< -5.5
extract	Pseudohypericin	0	<1	< -5.5
	Hypericin	0	<1	< -5.5
	Miquelianin	0	<1	< -5.5
	Hyperoside/Isoquercitrin	0	14	< -5.5
Home-made	Quercitrin	0	<1	< -5.5
extract	Pseudohypericin	0	<1	< -5.5
	Hypericin	0	<1	< -5.5

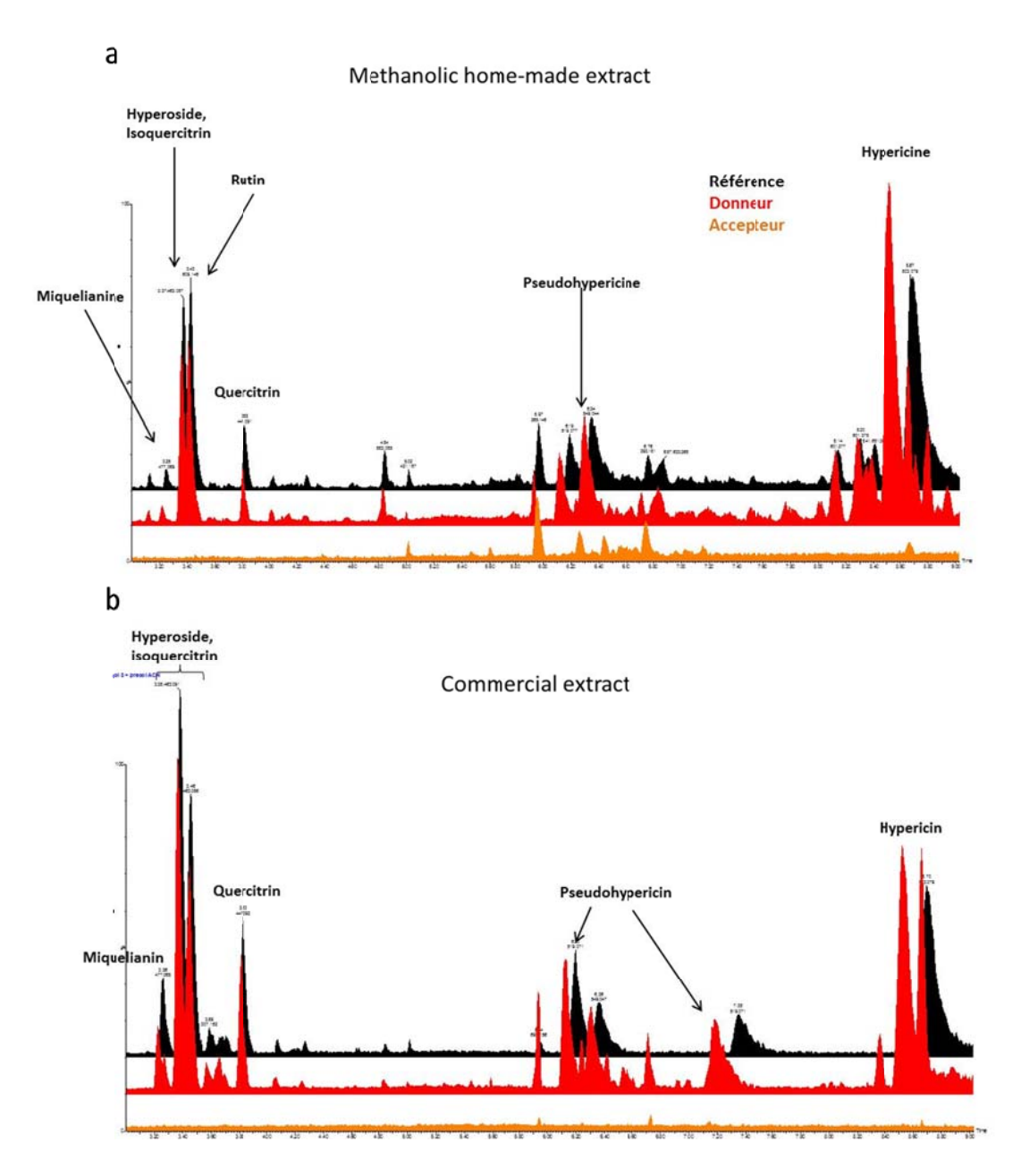


Figure 3-5: UHPLC-TOF-MS profiles of the reference (t=0), donor and acceptor compartments during the HDM-PAMPA experiment for the methanolic home-made extract (a) and the standardized commercial extract (b).

Knowing that the solubility of the commercial extract in DMSO is 26.6 mg/ml and that extract contains between 0.1% and 0.3% hypericin, the DMSO stock solution in commercial extract contains between 26.6 μ g/ml and 80 μ g/ml of hypericin. During the PAMPA experiment, this DMSO stock solution of extract is diluted 40 times in order to reach a final DMSO concentration of 5% (2.5% coming from the DMSO stock solution of extract and 2.5% coming from the DMSO stock solution of internal standard). Therefore, the concentration of hypericin in the donor compartment at the beginning of the PAMPA assay is between 665

ng/ml and 2 μ g/ml. The solubility of the home-made methanolic extract is 30 mg/ml and the same calculation as before lead to a concentration of pure hypericin in the donor compartment between 750 ng/ml and 2.25 μ g/ml. The limit of detection of hypericin was determined around 35 ng/ml. This corresponds to 1.5% to 4.5% of the initial concentration of hypericin in the plant extracts. As no peak was observable in the UHPLC-TOF-MS profile of the acceptor compartment, present results show that less than 4.5% of hypericin contained in the SJW extracts tested succeeded in crossing the artificial membrane.

Regarding the literature, Riedel et al. 28, Sattler et al. 29 and Schulz et al. 30 succeeded in dosing hypericin in plasma after in vivo experiments. After administration of 900 mg/day of SJW extract, corresponding to 750 µg hypericin, Riedel et al. measured a peak plasma concentration of 8.8 ng/ml, which corresponds to approximately 5.9% of the initial dose ²⁸. Schulz et al. administered 612 mg SJW extract, and found a peak plasma concentration of 3.14 ng/ml after 8.1 hours, which corresponds to 2.6% of the initial dose. After the administration of 1.2 mg hypericin to healthy volunteers. Sattler et al. 29 succeeded in dosing 9.5 ng/ml hypericin in plasma after 3 to 4 hours, which corresponds to 4% of the initial dose. Therefore, in these in vivo experiments in humans, hypericin is able to cross the GIT but in a limited way. However, the solubility of whole SJW extract and hypericin is probably an issue in this case. Therefore, present results tend to show that if passive diffusion of hypericin exists, as what was defended by Sattler et al. 29, this diffusion is very slow and not quantifiable with the analytical technique employed during this study. Moreover, if passive paracellular diffusion occurs in vivo, this phenomenon cannot be predicted with PAMPA, that isolates the passive transcellular component of the permeation process. On the other hand, it seems that this diffusion is not the major transport process as argued by Kamuhabwa et al. 31 when they highlighted a saturable uptake process of hypericin and protohypericin in Caco-2 cells, meaning that a possible active transport is at the origin of the permeation of hypericin through the GIT. Another issue regarding hypericin comes from its high photosensibility, leading to a fast degradation of the compound ³², and the suspected adsorption of hypericin on the material.

Concerning the other compounds of interest which were identified in the extract, no permeation through the artificial membrane was observed. All these compounds are flavonoid glycosides (miquelianin, isoquercitrin, hyperoside, rutin, quercitrin), and all are partially ionized at pH 6.8 (table 3-5). The glycosylation of the flavonoids makes them hydrophilic (log P between -1 and 1) and therefore decreases their ability to interact with a hydrophobic artificial membrane *in vitro*, or with a biological membrane *in vivo* ²⁴. These flavonoids glycosides are thought to be either transported with the organic anion transporting polypeptides ²⁴, that is the case for quercitrin, isoquercitrin, hyperoside and rutin ³³ or

hydrolyzed either in the intestinal lumen by lactase-phlorozin hydrolases ^{34, 35} or by glucosidase ²⁴. Experimental results with PAMPA corroborate the absence of passive transcellular permeation of flavonoid glycosides of the plant extract. Isolated quercitrin has also been tested on PAMPA, but, no quercitrin reached the acceptor compartment after the 5 hours incubation time. This corroborates the results generated with the extracts. Therefore, quercitrin is not able to permeate through the HDM membrane, whether on its isolated form or on the extract. Here again, as for hypericin, any synergy could be observed with the whole extract.

Table 3-5: Estimated pKa and log P of the constituents identified in the extract. Data are calculated with the caclulation tool chemicalize.org (Chemaxon, Budapest, Hungary).

Compound	lowest acidic pKa (estimated)			Calculated log P
Hypericin	6.97	58	20	7.70
Pseudohypericin	6.97	58	20	6.42
Miquelianin	2.65	0	0	0.18
Isoquercirin	6.43	30	9	-0.14
Hyperoside	6.43	30	9	-0.14
Rutin	6.43	30	9	-0.87
Quercitrin	6.43	30	9	0.90

To conclude, none of the identified constituents of both extracts tested with HDM-PAMPA was detected in the acceptor compartments, meaning that no quantifiable passive transcellular permeation of those components occurs. Therefore, the detection of some SJW constituents in the blood may either be a consequence of a paracellular process, as cells forming the GIT are not sealed with tight-junctions that prevent any paracellular permeation, or an active process *via* specific transporters ^{24, 31}.

3-3.2.2. HDC/NPOE PAMPA

To understand how SJW may exert its CNS effect, passive permeation of the constituents through the BBB was assessed using HDC/NPOE PAMPA. Results are presented in table 3-6 and figure 3-6.

Table 3-6 : Permeability coefficients (log P_e) membrane retention (R %) and quantity of compounds that reached the acceptor compartment ($C_A(t)/C_D(t)$ %) obtained for isolated compounds (Hypericin and Quercetrin), methanolic commercial and home-made extract and standards (Carbamazepine and methotrexate) obtained using HDC/NPOE PAMPA.

	Compounds	$C_A(t)/C_D(0)$ (%)	Retention (%)	log Pe
	Hypericin	0	< 1	<-6.3
Isolated	Quercitrin	0	5	<-6.3
compounds	Carbamazepine (CNS+)	43	< 1	-3.7
	Methotrexate (CNS-)	0	< 1	<-6.3
	Miquelianin	0	< 1	<-6.3
	Hyperoside/Isoquercitrin	0	< 1	<-6.3
Standardized	Rutin	0	< 1	<-6.3
commercial extract	Quercitrin	0	< 1	<-6.3
CATIGCT	Pseudohypericin	0	< 1	<-6.3
	Hypericin	0	13	<-6.3
	Miquelianin	0	48	<-6.3
Home-made extract	Hyperoside/Isoquercitrin	0	2	<-6.3
	Quercitrin	0	< 1	<-6.3
	Pseudohypericin	0	< 1	<-6.3
	Hypericin	0	5	<-6.3

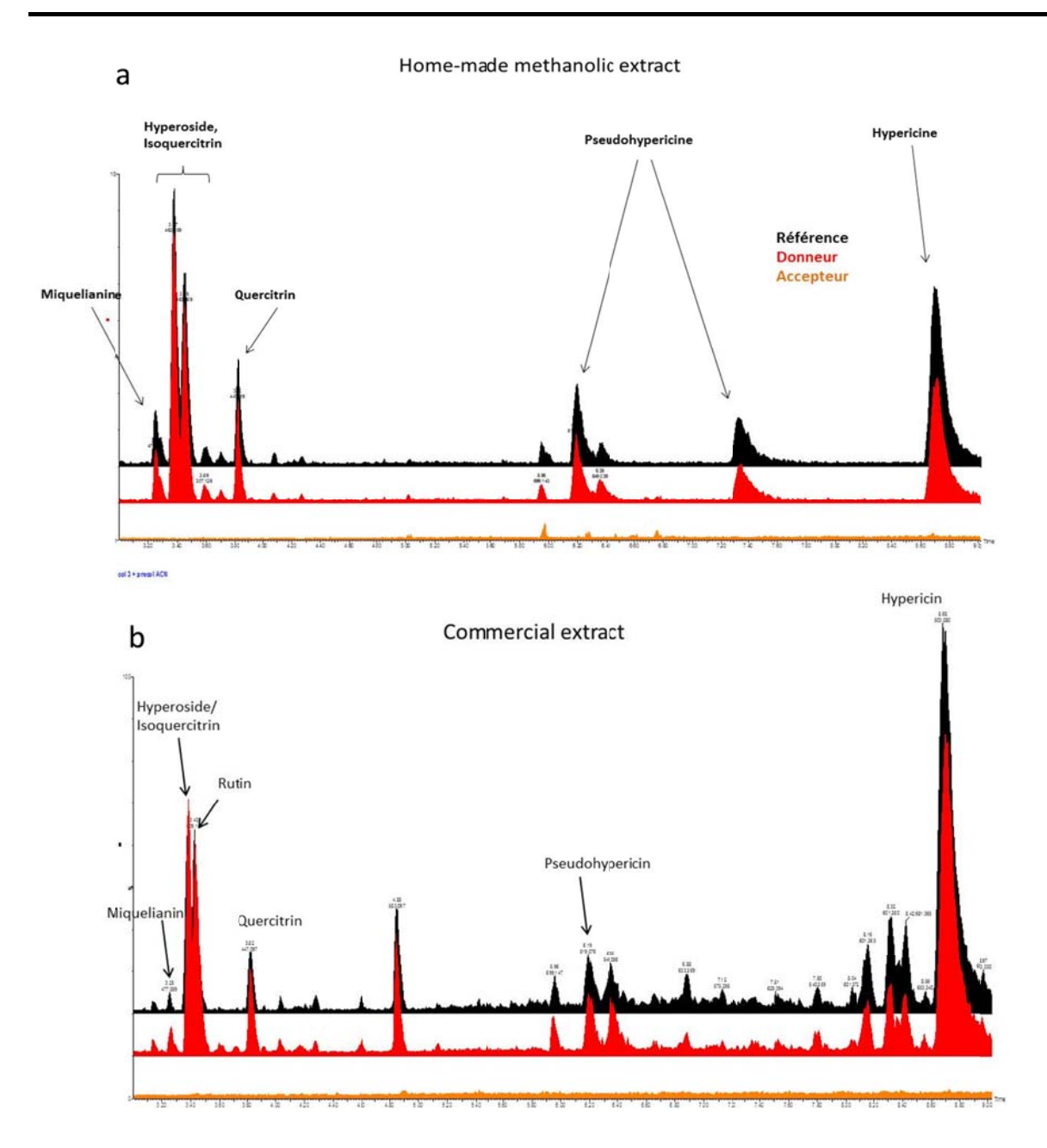


Figure 3-6: Overlays of the UHPLC-TOF-MS profiles of the reference, donor and acceptor compartments obtained during the HDC/NPOE PAMPA experiment for the home-made extract (a) and the commercial extract (b).

Figure 3-6 and table 3-6 bring to a similar conclusion than for the HDM-PAMPA: none of the identified constituents of the extracts is able to diffuse through the artificial membrane up to a detectable point, meaning that none of these molecules are predicted to follow a passive diffusion pathway through the Blood-Brain Barrier. Therefore, if hypericin is responsible for a part of the CNS effect of *Hypericum perforatum*, that is probably not due to a passive transport. This is consistent with recent *in vivo* observations made by Paulke *et al.* ¹, as developed in the introduction of this chapter. They found that the concentration of hypericin in the brain, if any, was below the limit of detection of the analytical technique

employed (8 ng/ml), whether after administration of SJW extract or pure hypericin. Therefore, three hypothesis subsist to clarify the pharmacological activity of *Hypericum perforatum*: i) the detection technique is not suitable for the analysis of the small amounts of solutes which may have diffused through the artificial membrane and the pharmacological potency is so important that very small quantity are sufficient to exert a CNS effect; ii) the active constituents of SJW are actively transported at the BBB; iii) the pharmacological activity is not due to the native constituents of the crude extract but to the metabolites, especially in the case of flavonoids.

3-3.3. Passive permeability of aglycones and hydrolyzed extract

Preliminary results all converge to the statement that no detectable passive permeation through the GIT and through the BBB occurs with the constituents of the crude extracts of *Hypericum perforatum*. Many authors suggest that the CNS effect observed with *Hypericum perforatum* was due to hyperforin and/or hypericin ^{1, 4, 6, 10-12}, but few others also stated that flavonoids may play a role on the antidepressant effect ^{1, 9, 13, 14}. Experimental results on hypericin lead to the conclusion that no passive diffusion occurs over the limit of detection of UHPLC-TOF-MS. Regarding the flavonoids, the gastric pH and the enzymes present in the intestinal lumen are known to potentially promote the deglycosylation of the flavonoids. The aglycones derivatives of flavonoids are more lipophilic than the glycosylated form and therefore physicochemically more prone to passively diffuse through biological membranes. Therefore second part of this study was focused on these compounds.

Isolated flavonoid glycosides (luteolin-7-glucoside, quercitrin, hyperoside), deglycosylated flavonoids (kaempferol, luteolin, quercetin) (figure 3-7) and an hydrolyzed SJW extract have been tested with HDC/NPOE- and HDM-PAMPAs in order to quantify a possible passive diffusion process. Table 3-7 compiles the results generated with HDM-PAMPA and HDC/NPOE PAMPA. As mentioned previously, results highlight that flavonoid glycosides are not able to cross both of the artificial membranes *via* passive diffusion when testing the extract.

On the other hand, aglycones showed important solubility issues within the experiment. Indeed, without the glucose moiety, their hydrophilicity has dropped down, as well as their solubility, leading to precipitation under aqueous conditions at the concentration needed to be detectable with the analytical technique. This phenomenon was much more important for quercetin and luteolin. Therefore, in those cases the observed passage is null

or very low (< 1%), but this is partly due to its poor solubility leading to very small amount of available compound for the permeability process than to a real slow permeation through the artificial membrane. Moreover, the very high retention of quercetin and luteolin in HDC/NPOE PAMPA (> 70%) carries on decreasing the available amount of free drug. When solubility of the aglycone was more important, which is the case of kaempferol, permeability coefficients could be determined and significant permeation was observed. The permeation of kaempferol was higher in the model predicting the passive BBB permeability than in the model predicting passive permeation through the GIT. When 10 ± 1% of initial concentration of kaempferol reached the acceptor compartment in HDC/NPOE PAMPA, only 1.6 ± 0.7% succeed to cross the hexadecane membrane in HDM-PAMPA. Therefore, the passive permeability of kaempferol through the GIT is the rate-limiting step, but when in the blood, a significant part of kaempferol will be able to reach the brain by passive diffusion. These results indicate that some of the aglycones are able to passively cross the artificial membrane, and consequently should be able to cross in vivo biological barrier via passive diffusion. Retention was very high for the 3 aglycones tested on HDC/NPOE PAMPA (> 50%) and non-negligible for HDM-PAMPA (6-17% compared to the glycosides. The increase in hydrophobicity resulting from the loss of the glucose moiety is responsible for this enhanced retention. The direct consequence is a decrease in the amount of aglycones available for the permeability assay, leading to detection issues.

An hydrolyzed extract was also tested with both PAMPA. A compound having its maximum absorbance at 245.5 nm was detected by UHPLC-UV in the acceptor compartment (figure 3-8). Moreover, the quantity of compound that reach the acceptor in HDM-PAMPA as well as in HDC/NPOE PAMPA were very close through the HDM and through the HDC/NPOE PAMPA was the very close (20 ± 1% for HDM-PAMPA after 5 hours and 28 ± 4% for HDC/NPOE PAMPA after 7 hours). UHPLC-TOF-MS was performed with the solutions of this hydrolyzed extract, to determine the molecular weight of this constituent. A peak with a retention time of 1.21 minute and at $[MH]^+$ = 180.1016 appears with the positive ionization mode, but not with the negative ionization. This indicates that the compound able to cross the artificial membrane has a 179 g/mol molecular weight. Moreover, the single mass analysis of this peak indicates that the molecule is monocationic. Integration of this peak for the donor, acceptor and reference solutions for HDC/NPOE PAMPA indicates that 28 ± 6% of this constituent diffuse through the HDC/NPOE artificial membrane after the 7 hours incubation of the experiment, which is consistent with the results obtained with the UV detection. However, no evident structure could be achieved and therefore no identification could be performed, since this m/z is too low for flavonoids (either glycosides or aglycones) or the other known constituents of *Hypericum perforatum*.

These experiments made with PAMPA led to the conclusion that passive transcellular transport exists for some of the deglycosylated flavonoids. Therefore, a CNS effect may be brought by flavonoids.

Figure 3- 7: Structure of the glycosylated flavonoids and aglycones tested with HDM PAMPA and HDC/NPOE PAMPA.

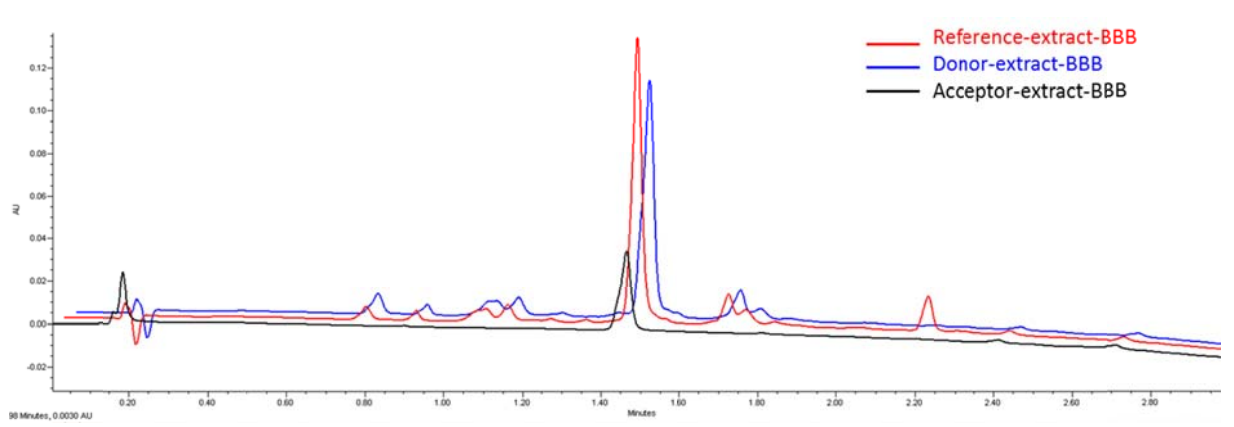


Figure 3-8: Overlays of the chromatograms obtained for the reference, donor and acceptor solutions with HDC/NPOE PAMPA, extracted at 245.5 nm.

Table 3-7 : HDM- and HDC/NPOE PAMPA results determined with flavonoid glycosides, aglycones and the hydrolyzed SJW extract.

	HDM-PAMPA		Н	HDC/NPOE-PAMPA		
Compounds	R	$C_A(t)/C_D(0)$	$Log\;P_{e}$	R	$C_A(t)/C_D(0)$	Log P _e
	(%)	(%)	(cm/s)	(%)	(%)	(cm/s)
		Flavor	oid glycosides			
Luteolin-7-glucoside	2 ± 2	< 0.1	< -5.5	4±2	< 0.1	< -6.3
Quercitrin	2 ± 1	< 0.1	< -5.5	5±1	< 0.1	< -6.3
Hyperoside	< 1	0.2 ± 0.1	< -5.5	5±2	< 0.1	< -6.3
Aglycones						
Kaempferol	6 ± 2	1.6 ± 0.7	-5.3 ± 0.2	57±5	10 ± 2	-4.80 ± 0.06
Luteolin	17 ± 1	0.5 ± 0.2	< -5.5	73±4	0.3 ± 0.1	-6.2 ± 0.2
Quercetin	16 ± 16	0.7 ± 0.6	< -5.5	77±14	< 0.1	< -6.3
Hydrolyzed extract						
λ=245.5 nm	< 1	20 ± 1	-4.13 ± 0.03	<1	28 ± 4	-4.68 ± 0.03
MS: m/z 180.10; tr=1.21 min	-	-	-	<1	28 ± 6	-4.73 ± 0.02

3-4. Conclusion

Hyperforin, hypericin and flavonoids are often cited as the compounds responsible for the antidepressant effect of *Hypericum perforatum*, but the way they interact with biological barriers, especially the GIT and BBB, is not elucidated yet. This present study allowed determining clues concerning the permeation process of 2 of these substances, at least concerning the passive permeation process part.

Hypericin, originally thought to be the constituent having a major role in the antidepressant activity of *Hypericum perforatum*, has never been detected *in vivo* in the brain ¹. The results of the PAMPA experiments performed in this study corroborate these *in vivo* observations and showed that no passive diffusion may occur whether through GIT or BBB biological membranes. Hyperforin, which is now thought to be the main responsible for the antidepressant effect, could unfortunately not been tested in our assays, because it was not detected in the tested extracts. This may be due to its unstability³⁶ or insufficient ionization for MS detection.

Flavonoids, mainly present under their glycoside form in the crude methanolic extract (quercitrin, hyperoside, rutin, isoquercitrin, miquelianin), are not able to passively diffuse

either through HDM or HDC/NPOE artificial membranes that could indicate that they will not pass through GIT nor BBB. But the native flavonoids can be metabolized by deglycosylation before reaching the biological barrier, and a passive permeability particularly through the HDC/NPOE PAMPA membrane was observed for kaempferol, indicating that a passive permeation of the BBB for these hydrolysates may occur *in vivo*. Aglycones could therefore be the active CNS molecules, rather than the native flavonoids. However, the intestinal endothelial cells are not sealed by the same tight junctions as the cerebral endothelial cells. The transendothelial resistances are much lower for intestinal cells than for cerebral cells. Therefore paracellular diffusion *in vivo* between intestine and blood for glycosides cannot be fully excluded, but this process cannot be modeled with PAMPA. Furthermore, an active transport may occur for some constituent of the extract and explain the antidepressant effect. Permeability measurements performed with cellular models could highlight a potential active transport and therefore complete the present study.

References

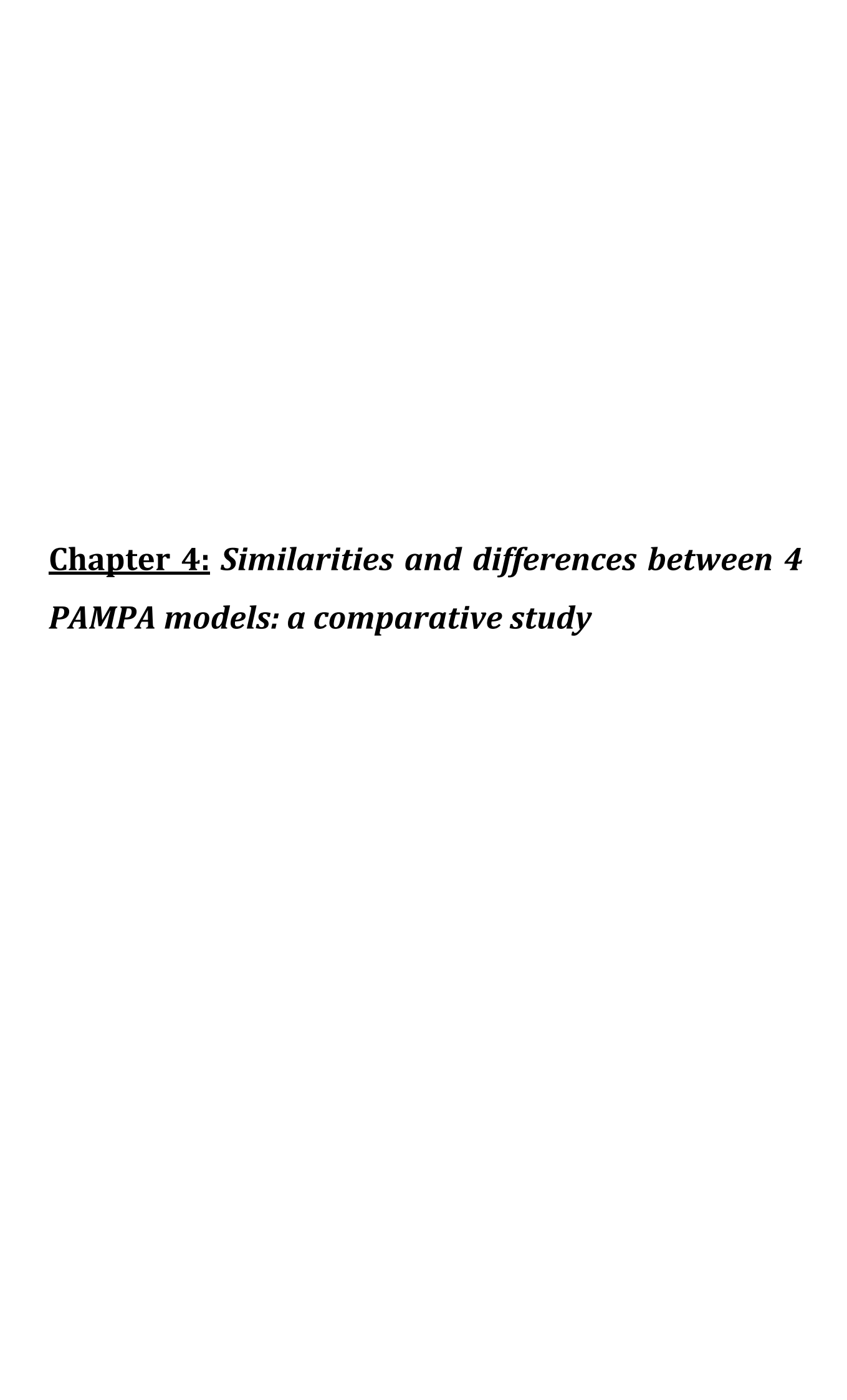
- 1. Paulke, A.; Schubert-Zsilavecz, M.; Wurglics, M. Determination of hypericin and pseudohypericin from *Hypericum perforatum* in rat brain after oral administration. *Monatsh. Chem.* **2008**, *139*, 489-494.
- 2. Valeri, A.; Capasso, R.; Valoti, M.; Pessina, F. Effects of St John's wort and its active constituents, hypericin and hyperforin, on isolated rat urinary bladder. *J. Pharm. Pharmacol.* **2012**, *64*, 1770-1776.
- 3. Grundmann, O.; Lv, Y.; Kelber, O.; Butterweck, V. Mechanism of St. John's wort extract (STW3-VI) during chronic restraint stress is mediated by the interrelationship of the immune, oxidative defense, and neuroendocrine system. *Neuropharmacol.* **2010**, *58*, 767-773.
- 4. Galeotti, N.; Vivoli, E.; Bilia, A. R.; Vincieri, F. F.; Ghelardini, C. St. John's Wort reduces neuropathic pain through a hypericin-mediated inhibition of the protein kinase C γ and ϵ activity. *Biochem. Pharmacol.* **2010**, *79*, 1327-1336.
- 5. McCue, P. P.; Phang, J. M. Identification of human intracellular targets of the medicinal herb St. John's wort by chemical-genetic profiling in yeast. *J. Agric. Food Chem.* **2008,** *56*, 11011-11017.
- 6. Barnes, J.; Anderson, L. A.; Phillipson, J. D. St John's wort (Hypericum perforatum L.): a review of its chemistry, pharmacology and clinical properties. *J. Pharm. Pharmacol.* **2001,** *53*, 583-600.
- 7. Kim, H. L.; Streltzer, J.; Goebert, D. St. John's wort for depression A meta-analysis of well-defined clinical trials. *J. Nerv. Ment. Dis.* **1999**, *187*, 532-538.
- 8. Vollmer, J. J.; Rosenson, J. Chemistry of St. John's wort: Hypericin and hyperforin. *J. Chem. Educ.* **2004**, *81*, 1450-1456.
- 9. Patocka, J. The chemistry, pharmacology, and toxicology of the biologically active constituents of the herb Hypericum perforatum L. J. Appl. Biomed. **2003**, *1*, 61-70.
- 10. Suzuki, O.; Katsumata, Y.; Oya, M.; Bladt, S.; Wagner, H. Inhibition of monoamine oxidase by hypercin. *Planta Med.* **1984**, *50*, 272-274.
- 11. Wonnemann, M.; Singer, A.; Siebert, B.; Muller, W. E. Evaluation of synaptosomal uptake inhibition of most relevant constituents of St. John's wort. *Pharmacopsychiat.* **2001**, *34*, S148-S151.
- 12. Keller, J. H.; Karas, M.; Müller, W. E.; Volmer, D. A.; Eckert, G. P.; Tawab, M. A.; Blume, H. H.; Dingermann, T.; Schubert-Zsilavecz, M. Determination of Hyperforin in mouse brain by high-performance liquid chromatography/tandem mass spectrometry. *Anal. Chem.* **2003**, *75*, 6084-6088.
- 13. Nöldner, M. M.; Schötz, K. K. Rutin is essential for the antidepressant activity of hypericum perforatum extracts in the forced swimming test. *Planta Med.* **2002**, *68*, 577-580.

- 14. Butterweck, V.; Jurgenliemk, G.; Nahrstedt, A.; Winterhoff, H. Flavonoids from Hypericum perforatum show antidepressant activity in the forced swimming test. *Planta Med.* **2000**, *66*, 3-6.
- 15. Vandenbogaerde, A.; Zanoli, P.; Puia, G.; Truzzi, C.; Kamuhabwa, A.; De Witte, P.; Merlevede, W.; Baraldi, M. Evidence that total extract of Hypericum perforatum affects exploratory behavior and exerts anxiolytic effects in rats. *Pharmacol. Biochem. and Behavior* **2000**, *65*, 627-633.
- 16. Sugano, K.; Kansy, M.; Artursson, P.; Avdeef, A.; Bendels, S.; Di, L.; Ecker, G. F.; Faller, B.; Fischer, H.; Gerebtzoff, G.; Lennernaes, H.; Senner, F. Coexistence of passive and carrier-mediated processes in drug transport. *Nature Reviews Drug Discovery* **2010**, *9*, 597-614.
- 17. Fox, E.; Murphy, R. F.; McCully, C. L.; Adamson, P. C. Plasma pharmacokinetics and cerebrospinal fluid penetration of hypericin in nonhuman primates. *Cancer Chemother Pharmacol* **2001**, *47*, 41-44.
- 18. Kansy, M.; Senner, F.; Gubernator, K. Physicochemical high throughput screening: parallel artificial membrane permeation assay in the description of passive absorption processes. *J. Med. Chem.* **1998**, *41*, 1007-1010.
- 19. Wohnsland, F.; Faller, B. High-throughput permeability pH profile and high-throughput alkane/water log P with artificial membranes. *J. Med. Chem.* **2001,** *44*, 923-930.
- 20. Di, L.; Kerns, E. H.; Fan, K.; McConnell, O. J.; Carter, G. T. High throughput artificial membrane permeability assay for blood—brain barrier. *Eur. J. Med. Chem.* **2003**, *38*, 223-232.
- 21. Passeleu Le Bourdonnec, C.; Boccard, J.; Rudaz, S.; Carrupt, P. A.; Martel, S. Evaluation of BBB permeation with PAMPA thanks to a new artificial membrane. Frontiers in medicinal chemistry FMC 2011 Stockholm Sweden June 19-21, 2011. 2011.

Ref Type: Conference Proceeding

- 22. Ottaviani, G.; Martel, S.; Carrupt, P. A. Parallel artificial membrane permeability assay: a new membrane for the fast prediction of passive human skin permeability. *J. Med. Chem.* **2006**, *49*, 3948-3954.
- 23. Avdeef, A. Absorption and Drug Development; John Wiley & Sons: Hoboken, 2003.
- 24. Németh, K.; Plumb, G. W.; Berrin, J. G.; Juge, N.; Jacob, R.; Naim, H. Y.; Williamson, G.; Swallow, D. M.; Kroon, P. A. Deglycosylation by small intestinal epithelial cell +¦-glucosidases is a critical step in the absorption and metabolism of dietary flavonoid glycosides in humans. *Eur. J. Nutr.* **2003**, *42*, 29-42.
- 25. Hölscher, D.; Shroff, R.; Knop, K.; Gottschaldt, M.; Crecelius, A.; Schneider, B.; Heckel, D. G.; Schubert, U. S.; Svatos, A. Matrix-free UV-laser desorption/ionization (LDI) mass spectrometric imaging at the single-cell level: distribution of secondary metabolites of Arabidopsis thaliana and Hypericum species. *The Plant J.* 2009, 60, 907-918.
- 26. Maffi, L.; Benvenuti, S.; Fornasiero, R. B.; Bianchi, A.; Melegari, M. Inter-population variability of secondary metabolites in Hypericum spp. (Hypericaceae) of the Northern Apennines, Italy. *Nord. J. Botanic* **2001**, *21*, 585-593.

- 27. Shore, P. A.; Brodie, B. B.; Hogben, C. A. M. The gastric secretion of drugs: a pH partition hypothesis. *J. Pharmacol. Exp. Ther.* **1957**, *119*, 361-369.
- 28. Riedel, K. D.; Rieger, K.; Martin-Facklam, M.; Mikus, G.; Haefeli, W. E.; Burhenne, J. Simultaneous determination of hypericin and hyperforin in human plasma with liquid chromatography-tandem mass spectrometry. *J. Chromatogr. B* **2004**, *813*, 27-33.
- 29. Sattler, S.; Schaefer, U.; Schneider, W.; Hoelzl, J.; Lehr, C. M. Binding, uptake, and transport of hypericin by Caco-2 cell monolayers. *J. Pharm. Sci.* **1997**, *86*, 1120-1126.
- 30. Schulz, H. U.; Schurer, M.; Bassler, D.; Weiser, D. Investigation of the bioavailability of hypericin, pseudohypericin, hyperforin and the flavonoids quercetin and isorhamnetin following single and multiple oral dosing of a hypericum extract containing tablet. *Arzneim. -Forsch.* **2005**, *55*, 15-22.
- 31. Kamuhabwa, A. R.; Augustijns, P.; de Witte, P. A. In vitro transport and uptake of protohypericin and hypericin in the Caco-2 model. *Int. J. Pharm.* **1999**, *188*, 81-86.
- 32. Wirz, A.; Meier, B.; Sticher, O. Stability of hypericin and pseudohypericin in extract solutions of Hypericum perforatum and in standard solutions. *Pharm. Ind.* **2001**, *63*, 410-415.
- 33. Hollman, P. C.; van Trijp, J. M.; Buysman, M. N.; van der Gaag, M. S.; Mengelers, M. J.; de Vries, J. H.; Katan, M. B. Relative bioavaibility of the antioxidant flavonoid quercetin from various foods in man. *FEBS* **1997**, *418*, 152-156.
- 34. Manach, C.; Donovan, J. L. Pharmacokinetics and metabolism of dietary flavonoids in humans. *Free Rad. Res.* **2004**, *38*, 771-785.
- 35. Passamonti, S.; Terdoslavich, M.; Franca, R.; Vanzo, A.; Tramer, F.; Braidot, E.; Petrussa, E.; Vianello, A. Bioavailability of flavonoids: a review of their membrane transport and the function of bilitranslocase in animal and plant organisms. *Curr. Drug Metab.* **2009**, *10*, 369-394.
- 36. Verotta, L.; Appendino, G.; Jakupovic, J.; Bombardelli, E. Hyperforin analogues from St. John's wort (Hypericum perforatum). *J. Nat. Prod.* **2000**, *63*, 412-415.



4-1. Introduction

Parallel Artificial Membrane Permeability Assay (PAMPA) is a technique initially developed by Kansy et al to predict oral absorption in high throughput screening 1. Historically, the partition coefficient between n-octanol and water (log P) was employed to estimate permeability ². However, the shake-flask techniques traditionally performed to determine log P were labor intensive and time-consuming for high throughput screening 3. With the setup in 96-wells microfilter plates, PAMPA therefore became very popular in early drug discovery, especially in industry, mainly due to its cost and time efficiency as well as its reproducibility 4. In the last decade, new declinations of PAMPA have been developed, optimizing artificial membrane composition (phospholipid or solvent-based artificial membrane), incubation time, stirring conditions taking into account the unstirred water layer, filter composition, pH conditions, or sink conditions ^{5, 6}. Nowadays, PAMPA assays can be used to predict passive permeability through the blood-brain barrier (BBB) 7, the gastrointestinal tract (GIT) 8-12 or the stratum corneum 13, 14. When performing a PAMPA assay, experimenter should keep in mind that only the passive transcellular permeation will be predicted. Therefore, critical discussion should be done regarding the results. In the specific case of BBB, PAMPA is rather a complementary method to cellular models, which enable the indirect highlight of possible active transport processes and metabolism.

The high throughput efficiency reached with PAMPA permits the generation of PAMPA permeability libraries, which can be sometimes employed to generate quantitative structure-activity relationships (QSAR). Modeling of PAMPA permeability has already been successfully performed using molecular descriptors such as the lipophilicity (log Poct), descriptors of hydrophilicity or hydrophobicity, descriptors of polarizability (polar surface area, etc.) or structural descriptors (molecular weight, molecular volume, etc.)¹⁵⁻²³. However the limited number of compounds used in QSAR models does not permit a real comparison between the different artificial membranes used.

In this part of the thesis, an enlarged data set of therapeutic compounds was selected. Their passive permeability across artificial membranes was measured using HDM-PAMPA ⁸, HDC/NPOE PAMPA explored during this thesis, PAMPA-BBB ⁷ and PAMPA-skin ¹³. The data generated were compared in order to identify the molecular properties governing the differences and similarities between the PAMPA studied.

4-2. Material and methods

1-chloro-2-nitrobenzene, 2-amino-4-nitrophenol, 2-naphtol, 2-naphtylamine, 4nitroaniline, 4-bromophenol, 4-phenylbutyric acid, 5-phenyl-n-valeric acid, acridine, alprenolol, aminopyrine, amitriptyline, antipyrine, benzidine, benzyl niotinate, caffein, cimetidine, chloramphenicol, chlorpromazine HCl, colchicine, corticosterone, coumarin, dexamethasone, diclofenac, diltiazem, dopamine, serine, flurbiprofen, hydrocortisone, hypoxanthine, ibuprofen, imipramine, indomethacine, ketoprofen, labetalol, L-dopa, lidocaine, methotrexate, methyl nicotinate, metoprolol, mianserine, nicotine, nifedipine, ofloxacin, oxprenolol, oxazepam, pindolol, pirenzepine, piroxicam, phenol, progesterone, promethazine, propranolol, pyridostigmine, salicylic acid, scopolamine, sulfabenzamide, sulfacarbamide, sulfadimethoxine, sulfanilamide, sulfasalazine, sulfathiazole, sulfisomidine, tenoxicam, terbutaline, testosterone, theobromine, theophyllin, thioridazine, thymol, tolbutamide, verapamil, warfarine, hexane, ortho nitrophenyloctyl ether and hexadecane 99% were purchased from Sigma-Aldrich Fluka (Sigma-Aldrich Chemie Gmbh, Buchs, Switzerland); 4-nitrophenol, doxycycline, paracetamol and dimethylsulfoxide (>99.7%) were obtained from Acros Organics (Chemie Brunschwig AG, Basel, Switzerland); diazepam was purchased from Büfa (Büfa Gmbh, Oldenburg, Germany); phenobarbital was purchased from Hänseler AG (Herisau, Switzerland); pyridine was obtained from Merck (Darmstadt, Germany).

Passive permeation of this test set of 88 compounds have been determined through different artificial membranes: the PAMPA-BBB and HDC/NPOE PAMPA, predicting passive transcellular permeability through the BBB, HDM-PAMPA, predicting passive permeability through the gastro-intestinal tract, and PAMPA-skin, predicting permeation through the *stratum corneum*. The experimental setups of these 4 PAMPA models are compiled in table 4-1.

4-2.1. PAMPA-BBB

PAMPA-BBB was developed by Di *et al* to predict passive permeability through the Blood-Brain Barrier 7 . With this PAMPA model, they successfully differentiated CNS compounds into 3 classes: CNS+ (high brain penetration); CNS- (low brain penetration) and CNS+/- (uncertain brain penetration). Moreover, this technique was shown to generate log P_e correlated to log BB obtained with *in situ* brain perfusion assay $^{24, 25}$. A 96 wells Teflon® plate

(Millipore MSSACCEPTOR, Zug, Switzerland) is filled with 280 μ l of a 0.5% DMSO pH 7.4 phosphate buffer containing the drug compound to be evaluated. Each well of a hydrophobic PVDF microfilter plate (MAIPN4550- Millipore AG, Zug, Switzerland) is filled with 4 μ l of 20 mg/ml porcine polar brain lipid extracts (ref 141101P- Aventi® Polar Lipids, Inc; Alabama, USA) in dodecane, which constitutes the artificial membrane. This microtiter plate is then placed upon the Teflon® acceptor plate on a "sandwich-like conformation" and each well is filled with 280 μ l pH7.4 phosphate buffer. The resulting "sandwich" is sealed with Parafilm®, covered with the microtiter lid to limit evaporation, and let undisturbed for 18 hours at 20°C.

After incubation, the concentration of drug compound in the donor, acceptor and reference (donor at time 0) solutions was determined with UV-spectrophotometry or UHPLC-PDA. The permeability coefficient was determined with equation 4-1.

$$P_{e} = -\frac{2.303V_{D}}{A\left(t - \tau_{lag}\right)} \left(\frac{V_{A}}{V_{A} + V_{D}}\right) \log \left[1 - \left(\frac{V_{A} + V_{D}}{V_{D}\left(1 - R\right)}\right) \frac{C_{A}\left(t\right)}{C_{D}\left(0\right)}\right]$$
 (Equation 4-1)

4-2.2. HDC/NPOE PAMPA

The protocol employed for HDC/NPOE PAMPA is described in chapter 2. Briefly, each well of a hydrophobic PVDF 96-wells microtiter filter plate (MAIPN 4550; Millipore, Zug, Switzerland) was impregnated with 15 μ l of a 35% (v/v) liquid membrane composed of 75% hexadecane and 25% o-NPOE dissolved in hexane. This donor plate was left under the extractor hood for 15-20 minutes to completely evaporate hexane. A Teflon® 96-wells acceptor plate was filled with 280 μ l of a pH 7.4 phosphate buffer containing 5% DMSO. The donor plate was next placed upon the acceptor plate in a "sandwich-like conformation" and filled with 280 μ l of the solution containing the compounds to test with 5% DMSO, called "donor solution". The resulting sandwich was sealed and incubated during 7 hours at 20°C and under constant shaking at 150 rpm to minimize the unstirred water layer. Permeability coefficients were determined in quadruplicate.

Following incubation, the sandwich was disassembled and 200 µl of each well of the donor and acceptor compartments were transferred in a 96-wells UV-quartz plate. The UV absorption in each compartment, as well as reference solutions (donor at time t=0) were measured. The permeability coefficient was calculated with equation 4-1.

4-2.3. HDM-PAMPA

HDM-PAMPA was developed by Wohnsland and Faller ⁸ to predict passive permeation through the GIT. The artificial membrane in this model is only composed of solvent, compared to the original method developed by Kansy ¹ which was composed of phosphatidylcholine dissolved in dodecane. This model was shown to predict the fraction of drug absorbed in human.

In this model, the artificial membrane is composed of 5% hexadecane dissolved in hexane. 15 µl of this artificial membrane is laid down on each well of a hydrophobic polycarbonate filter (MPC4NTR10; Millipore, Zug, Switzerland). The resulting microfilter plate is let under the extractor hood till a complete evaporation of hexane. A 96 wells Teflon® plate is filled with 280 µl of a pH 6.8 phosphate buffer containing 5% DMSO and constitutes the acceptor compartment. After the formation of a sandwich between the Teflon® acceptor plate and the microtiter plate (donor compartment), the donor solutions, constituted of 5% DMSO, 100 mM KCl and the drug compounds to be tested are poured on the donor compartment. The resulting sandwich is sealed with Parafilm®, covered with the microtiter lid and let incubate for 5 hours at 75 rpm and at 20°C.

After incubation, the concentration of drug compound in the donor, acceptor and reference (donor at time 0) solutions was determined with UV-spectrophotometry or UHPLC-PDA. The permeability coefficient was determined with equation 4-1.

4-2.4. PAMPA-skin

PAMPA-skin was developed by Ottaviani *et al* ¹³ to fast predict the *stratum corneum I* water partition coefficient and to screen for dermal delivery. The artificial membrane, composed of 70% silicon oil and 30% isopropylmyristate dissolved in hexane, was laid down on a 96-well hydrophobic PVDF microfilter plate (MAIPN4550, Millipore, Zug, Switzerland). In this PAMPA model, the buffer pH need to be adapted according to the pKa of the drug compounds tested, in order to assess the permeation of the neutral compound. Permeation occurs under iso-pH conditions. Similarly to HDC/NPOE PAMPA, incubation is performed for 7 hours at 20°C under constant shaking at 150 rpm.

After incubation, the concentration of drug compound in the donor, acceptor and reference (donor at time 0) solutions was determined with UV-spectrophotometry or UHPLC-PDA. The permeability coefficient was determined with equation 4-1.

Table 4-1: Experimental set up of the 4 PAMPA models under study.

Predicted barrier permeability	Filter support	Membrane composition	Buffer pH	Stirring conditions	Incubation time
GIT	Hydrophobic PC	100 % hexadecane	pH 6.8 (+100 mM KCl in donor buffer)	stirred (75 rpm)	5 hours
BBB	Hydrophobic PVDF	20 mg/ml porcine polar brain lipid extract in dodecane	pH 7.4	unstirred	18 hours
Skin	Hydrophobic PVDF	70 % silicon oil/30 % isopropyl myristate	dependent on pKa (neutral form of the drug candidates)	stirred (150 rpm)	7 hours
BBB	Hydrophobic PVDF	75 % hexadecane/25 % o- nitrophenyl octyl ether	pH 7.4	stirred (150 rpm)	7 hours
	GIT BBB Skin	GIT Hydrophobic PC BBB Hydrophobic PVDF Skin Hydrophobic PVDF	BBB Hydrophobic PVDF Hydrophobic PVDF BBB Hydrophobic PVDF T5 % hexadecane/25 % o-	BBB Hydrophobic PVDF BBB Hydrophobic PVDF T5 % hexadecane PH 6.8 (+100 mM KCl in donor buffer) PH 7.4	Filter support Membrane composition Buffer pH Stirring conditions

4-2.5. Study in classes

The experimental permeability data from the 4 PAMPA models were separated into 4 classes depending on their ability to cross the different artificial membranes. Class 0 corresponds to non permeant compounds (less than 5% of passage), class I groups the low permeant compounds (between 5 and 20% of passage), class II lists the medium permeant compounds (between 20 and 35% of passage) and class III sets the fast permeant compounds (> 35% passage). Due to the different incubation times in PAMPA, these passages correspond to the permeability coefficients exposed in table 4-2.

Table 4-2: Classification of the dataset according to the experimental log $P_{\rm e}$ in the different PAMPA models.

	Class 0	Class I	Class II	Class III
HDC/NPOE PAMPA	$\log P_{\rm e}$ < -5.5	$-5.5 \le \log P_e < -4.8$	$-4.8 \le \log P_e < -4.5$	$log P_e \ge -4.5$
PAMPA-BBB	$log P_e < -5.9$	$-5.9 \le \log P_e < -5.3$	$-5.3 \le \log P_e < -4.9$	$log P_e \ge -4.9$
HDM PAMPA	$log P_e < -4.8$	$-4.8 \le \log P_e < -4.2$	$-4.2 \le \log P_e < -3.8$	$log P_e \ge -3.8$
PAMPA-skin	$log P_e < -5.5$	$-5.5 \le \log P_e < -4.8$	$-4.8 \le \log P_e < -4.5$	$log P_e \ge -4.5$

4-3. Results and discussion

4-3.1. Prediction of *in vitro* passive permeation through the BBB, the GIT and the *stratum corneum*

PAMPA-BBB, HDC/NPOE PAMPA, HDM-PAMPA and PAMPA-skin allowed the determination of passive permeability values, compiled in table 4-3. Experimental issues such as precipitation resulted in a non-measurable data. UV spectrometry was employed to measure the concentrations of active compound on both sides of the membrane. Therefore, in order to be confident in the absorbance measured, an arbitrary cut-off was introduced on the quantification step. This cut-off corresponds to an effective passage of 1% of the reference solution. Therefore, when the passage of the tested drug was below 1%, no permeability coefficient was measured. This 1% cut-off corresponds to a permeability coefficient of -6.3 for HDC/NPOE PAMPA and PAMPA-skin (7 hours incubation time); -5.5 for HDM-PAMPA (5 hours incubation time) and -6.7 for PAMPA-BBB (18 hours incubation time). The cut-off operation concerns 30 compounds for the HDC/NPOE PAMPA, 27 for PAMPA-skin, 40 for HDM-PAMPA and 19 for PAMPA-BBB. This discrepancy is partly due to the design of each experiment (incubation time, stirring conditions). But differences observed between each models may rather result from the intrinsic nature of the artificial membrane, which interacts differently depending on the physicochemical properties of the tested compounds.

Table 4-3: Experimental data generated with HDC/NPOE PAMPA, PAMPA-BBB, HDM-PAMPA and PAMPA-skin.

Compound	HD	C/NPOE PAMPA			PAMPA-BBB		ŀ	IDM-PAMPA			PAMPA skin	
Compound	log Pe	C _A (t)/C _D (0) (%)	R (%)	log Pe	C _A (t)/C _D (0) (%)	R (%)	log Pe	C _A (t)/C _D (0) (%)	R (%)	log Pe	C _A (t)/C _D (0) (%)	R (%)
1-chloro-2-nitrobenzene	-4.55±0.07	9±1	73±1	-4.41±0.06	16.3±0.3	67±1	-3.78±0.07	20±3	41±9	-4.22±0.05	19.7±0.4	56±1
2-amino-4-nitrophenol	-5.8±0.04	1.6±0.1	<1	-	-	-	<-5.5	<1	1.2±0.3	-4.84±0.05	18.2±0.8	<1
2-aminonaphtalene	-4.4±0.2	21.2±0.9	42±7	-4.63±0.07	37.1±0.4	17±5	-3.50±0.01	42.3±0.7	3±1	-4.4±0.1	31±5	25±6
2-naphtol	-4.4±0.2	36.0±0.8	6±17	-4.53±0.01	38±1	20±3	-3.58±0.02	41±1	<1	-4.12±0.08	36.5±0.8	20±1
4-bromophenol	-4.2±0.3	41±1	<1	-4.56±0.05	46±2	2±2	-3.54±0.03	40±2	5±5	-3.90±0.08	44.1±0.8	10,9±0,9
4-nitroaniline	-4.21±0.01	43±1	4±2	-4.61±0.07	46±2	<1	-3.78±0.04	32±1	5±5	-4.38±0.02	39±1	2±1
4-nitrophenol	-4.76±0.01	23.0±0.5	4±1	-	-	-	-4.35±0.05	13±1	<1	-4.33±0.06	39.9±0.9	5±3
4-phenylbutyric acid	-5.5±0.3	7±5	<1	-6.16±0.06	2.9±0.1	9±10	-5.1±0.2	3±1	<1	-4.21±0.03	44.6±0.8	1.3±0.5
5-phenyl-n-valeric acid	-5.3±0.2	9±5	<1	-5.80±0.03	7.4±0.3	<1	-4.62±0.09	7±1	<1	-4.16±0.05	41±1	12.3±0.7
7-phenylheptanoic acid	-5.7±0.4	1±1	84±4	-	-	-	-4.6±0.1	7±2	7±3	-	-	-
Acebutolol HCl	<-6.3	<1	<1	-6.3±0.2	2.4±0.8	<1	<-5.5	<1	4±3	<-6.3	<1	<1
Acetylsalicylic acid	<-6.3	<1	<1	<-6,7	<1	<1	<-5.5	<1	<1	-5.05±0.06	15±2	<1
Acridine		precipitation			precipitation		-3.7±0.1	30±5	18±6	-4.6±0.1	13±2	57±2
Aldosterone	-5.73±0.01	3.2±0.1	4.6±0.4	-5.55±0.09	21±2	<1	-	-	-	-	-	-
Alprenolol HCl	-4.5±0.2	37±12	<1	-4.90±0.08	35±3	2±5	-4.20±0.01	17.2±0.2	<1	-4.42±0.02	30.3±0.8	20±4
Amiloride	<-6.3	<1	<1	<-6.7	<1	<1	<-5.5	<1	8±10	<-6.3	<1	<1
Aminopyrine	-4.62±0.03	32±2	<1	-4.85±0.02	38.6±0.8	<1	-3.86±0.02	30±1	<1	-5.20±0.05	11±1	<1
Amitriptyline	-4.89±0.08	4.5±0.6	77±3	-4.61±0.09	21±2	54±3	-3.76±0.03	31.5±0.8	8.0±0.9	<-6.3	<1	64±15
Amoxicillin	<-6.3	<1	5±2	<-6.7	<1	5	<-5.5	<1	<1	<-6.3	<1	27±3
Antipyrine	-5.28±0.06	8±1	<1	-5.89±0.02	6.0±0.2	<1	-4.81±0.02	4.9±0.2	<1	-6.2±0.2	1.2±0.5	<1
Atenolol	<-6.3	<1	<1	<-6.7	<1	<1	<-5.5	<1	<1	<-6.3	<1	<1
Benzidine	-4.37±0.07	36±2	10±10	-4.63±0.04	37±2	18±1	-3.89±0.05	29±2	<1	-4.69±0.04	26±1	8±2
Benzyl nicotinate	-4.4±0.2	17±5	55±4	-4.57±0.08	26±2	43±3	-3.63±0.02	34±1	6±2	-4.26±0.02	26±1	41±2
Caffein	-5.17±0.01	10.9±0.1	4±2	-	-	-	-	-	-	-5.63±0.02	4.30±0.02	<1
Chloramphenicol	<-6.3	<1	<1	-5.39±0.01	15.3±0.4	6±2	<-5.5	<1	<1	<-6.3	<1	<1
Chlorpromazine HCl	-5.1±0.2	1.6±0.7	87±9	-4.87±0.09	5.8±0.6	84,1±0,5	-3.87±0.04	30±2	14±2	<-6.3	<1	<1

Table 4-3 (continued)

Cimetidine Clonidine Codeine	log Pe <-6.3 -4.8±0.1 -5.2±0.2	C _A (t)/C _D (0) (%) <1 15±2	R (%)	log Pe	C _A (t)/C _D (0) (%)	R (%)		$C_A(t)/C_D(0)$		_	$C_A(t)/C_D(0)$	•
Clonidine	-4.8±0.1		<1		ν.,	11 (70)	log Pe	(%)	R (%)	log Pe	(%)	R (%)
		15±2		<-6.7	<1	<1	<-5.5	<1	<1	<-6.3	<1	<1
Codoino	-5.2±0.2		38±2	<-6.7	<1	<1	-	-	-	-5.03±0.04	15±1	<1
Codellie		10±4	12±2	-	-	-	<-5.5	<1	<1	-	-	-
Colchicine	<-6.3	<1	9±2	-	-	-	<-5.5	<1	4±1	<-6.3	<1	4±3
Corticosterone	ŗ	recipitation		-4.88±0.04	37±5	<1	-4.31±0.02	13±1	<1	-5.14±0.01	12.7±0.4	<1
Coumarin	-4.16±0.08	39±2	16±6	-4.6±0.1	39±5	16±7	-3.51±0.02	44±3	<1	-4.13±0.02	43.4±0.6	7.4±0.6
Dexamethasone	-5.89±0.01	2±1	<1	-5.02±0.07	30±2	<1	<-5.5	0	5±3	-5.85±0.05	2.6±0.4	<1
Diazepam	-4.43±0.05	14±1	63±3	-4.51±0.03	31±1	35±2	-3.66±0.07	38±3	4±2	-4.36±0.03	32±1	20±1
Diclofenac	-5.33±0.02	7.7±0.3	5±4	-5.37±0.09	20±3	<1	-4.21±0.02	17±1	<1	-4.3±0.1	11±2	72±4
Diltiazem*	-4.42±0.01	30±2	22±4	-	-	-	-3.78±0.04	34±2	<1	-4.44±0.07	39±4	<1
Dopamine HCl	<-6.3	<1	<1	<-6.7	<1	<1	<-5.5	<1	<1	<-6.3	<1	<1
Doxycycline	<-6.3	<1	<1	<-6.7	<1	<1	<-5.5	<1	8.6±0.7	<-6.3	<1	<1
Eserine	-4.79±0.03	22±1	5±2	-5.15±0.01	23.9±0.7	3±3	-	-	-	-5.9±0.2	2±1	13±2
Flurbiprofen	-5.31±0.03	8.4±0.7	<1	-5.40±.02	16.7±0.4	<1	-4.28±0.05	15±1	<1	-4.57±0.07	12.5±0.9	61±2
Hydrocortisone	<-6.3	<1	<1	-5.29±0.05	20±2	<1	<-5.5	<1	<1	-5.94±0.07	2.2±0.4	<1
Hypoxanthine	<-6.3	<1	2.4±0.6	<-6.7	<1	<1	<-5.5	<1	<1	<-6.3	<1	<1
Ibuprofen	-5.12±0.03	12.4±0.6	2±2	<-6.7	<1	<1	-3.81±0.03	32±2	<1	-4.50±0.02	11±1	70±2
Imipramine HCl	-4.47±0.05	12±1	68±3	-4.6±0.2	32±3	28±2	-3.67±0.04	38±2	<1	-5.1±0.2	3±1	81±3
Indomethacin	-5.59±0.06	4.1±0.8	12±8	-5.45±0.09	15±2	<1	-4.55±0.07	9±1	<1	-	-	-
Ketoprofen	-5.6±0.1	4±1	4±5	-6.43±0.04	1.7±0.2	6±6	<-5.5	<1	<1	-4.25±0.01	38.5±0.8	12±2
Labetolol HCl	<-6.3	<1	<1	-5.25±0.01	21.3±.4	<1	<-5.5	<1	<1	<-6.3	<1	<1
Levodopa	<-6.3	<1	<1	<-6.7	<1	<1	<-5.5	<1	<1	<-6.3	<1	<1
Lidocaine HCl	-4.47±0.01	32.5±0.3	9.4±0.6	-4.83±0.03	38±2	<1	-3.77±0.03	34±1	<1	-4.35±0.03	37±1	10±3
Methotrexate	<-6.3	<1	<1	<-6.7	<1	1	<-5.5	<1	<1	<-6.3	<1	<1
Metoprolol	-5.9±0.1	2.2±0.7	4±1	-5.34±0.05	12±2	32±5	<-5.5	<1	<1	-4.76±0.02	24±1	<1
Morphine	<-6.3	<1	10±13	-5.29±0.08	17±3	13±4	<-5.5	<1	<1	<-6.3	<1	<1

Table 4-3 (continued)

	HDC	NPOE PAMPA	<u> </u>	P	AMPA-BBB		Н	DM-PAMPA		F	PAMPA skin	
Compound	log Pe	$C_A(t)/C_D(0)$ (%)	R (%)	log Pe	C _A (t)/C _D (0) (%)	R (%)	log Pe	$C_A(t)/C_D(0)$ (%)	R (%)	log Pe	$C_A(t)/C_D(0)$ (%)	R (%)
Nicotinate methyl	-4.3±0.1	40±2	<1	-4.30±0.01	39.0±0.1	21.5±0.3	-3.58±0.02	38.8±0.9	8.6±0.8	-4.32±0.06	37±1	11±1
Nicotine	-4.54±0.02	32.5±0.6	3±2	-4.74±0.07	43±3	<1	-4.04±0.05	23±2	<1	-4.6±0.1	30±5	4±1
Ofloxacin	<-6.3	<1	13±1	-5.64±0.0.02	10.4±0.1	<1	<-5.5	<1	2±2	-6.0±0.2	1.9±0.8	<1
Oxazepam	-4.58±0.02	30.4±0.6	3±4	-4.60±0.05	44±2	2.6±0.4	-4.29±0.03	12.8±0.9	12±2	-4.81±0.03	22±1	<1
Oxprenolol HCl	-5.54±0.04	5.4±0.7	<1	-4.93±0.04	30±2	13±3	-5.15±0.09	2.4±0.5	<1	-4.49±0.02	36±2	<1
Paracetamol	<-6.3	<1	3.7±0.2	-6.56±0.04	1.3±0.1	<1	<-5.5	<1	8±2	<-6.3	<1	<1
Phenobarbital	-5.72±0.05	3.3±0.4	4±1	-5.44±0.07	15±1	1±7	<-5.5	<1	6±2	-5.15±0.02	11.7±0.4	<1
Phenol	-4.4±0.1	41±3	<1	-	-	-	-3.68±0.05	38±2	<1	-4.14±0.03	46.7±0.6	<1
Pindolol	<-6.3	<1	<1	-5.32±0.02	19.2±0.5	<1	<-5.5	<1	<1	-5.19±0.05	11±1	0
Pirenzepine 2HCl	<-6.3	<1	<1	-5.86±0.08	0.6±0.2	8±2	<-5.5	<1	<1	<-6.3	<1	<1
Piroxicam	-5.30±0.05	8.9±0.9	<1	-5.35±0.03	18.1±0.5	<1	-3.99±0.02	24.9±0.8	<1	-4.60±0.02	31.4±0.5	<1
Progesterone	-5.2±0.1	1.5±0.2	87±4	-4.74±0.01	10±1	77±2	-3.51±0.05	44±1	<1	-4.56±0.06	8.6±0.6	74±2
Promethazine	-4.71±0.09	6±1	76±3	-4.84±0.02	16±1	59±3	-3.71±0.01	33.4±0.3	8.3±0.5	-5.9±0.2	0.6±0.2	77±4
Propranolol HCl	-4.61±0.02	30.4±0.4	<1	-4.9±0.1	34±8	6±10	-4.26±0.04	15±1	<1	-4.06±0.04	37±2	15±2
Pyridine	-4.3±0.1	33±3	17±14	-	-	-	-3.4±0.1	32±3	30±3	-4.40±0.01	30±1	22±3
Pyridostigmine	-	-	-	<-6.7	<1	<1	<-5.5	<1	4±4	<-6.3	<1	<1
Salicylic acid	<-6.3	<1	4±1	<-6.7	<1	<1	<-5.5	<1	<1	-4.16±0.02	43±2	6±1
Scopolamine HCl	-5.52±0.03	4.7±0.3	13±3	-5.56±0.2	9.6±0.5	18±7	-5.39±0.08	1.4±0.2	<1	-5.7±0.2	4±2	<1
Sulfabenzamide	<6.3	<1	7±4	-	-	-	<-5.5	<1	<1	-5.71±0.05	2.4±0.3	<1
Sulfacarbamide	-5.98±0.08	2.3±0.1	<1	<-6.7	<1	7	<-5.5	<1	2±2	<-6.3	<1	<1
Sulfadimethoxine	<-6.3	<1	<1	<-6.7	<1	<1	<-5.5	<1	<1	-5.53±0.04	5.3±0.6	<1
Sulfanilamide	<-6.3	<1	<1	-6.14±0.02	3.3±0.1	<1	<-5.5	<1	11±1	<-6.3	<1	<1
Sulfasalazine	<-6.3	<1	6±2	<-6.7	<1	2	<-5.5	<1	2±2	<-6.3	<1	<1
Sulfathiazole	<-6.3	<1	<1	<-6.7	<1	<1	<-5.5	<1	<1	<-6.3	<1	<1
Sulfisomidine	<-6.3	<1	<1	<-6.7	<1	<1	<-5.5	<1	<1	<-6.3	<1	<1
Tenoxicam	-6.3±0.2	1.0±.4	2±3	-6.50±0.02	1.5±0.1	3±2	<-5.5	<1	3±5	-5.87±0.04	2.2±0.2	<1

Table 4-3 (continued)

	HDC,	/NPOE PAMPA		PA	AMPA-BBB		н	DM-PAMPA		ı	PAMPA skin	
Compound	log Pe	$C_A(t)/C_D(0)$ (%)	R (%)	log Pe	$C_A(t)/C_D(0)$ (%)	R (%)	log Pe $C_A(t)/C_D(0)$ R (%)		R (%)	log Pe	$C_A(t)/C_D(0)$ (%)	R (%)
Terbutaline	<-6.3	<1	6±4	<-6.7	<1	<1	<-5.5	<1	2±1	<-6.3	<1	<1
Terfenadine	<-6.3	<1	<1	-	-	-	<-5.5	<1	<1	<-6.3	<1	<1
Testosterone	-4.41±0.02	35±2	10±4	-4.55±0.07	46±3	<1	-	-	-	-4.11±0.04	43±1	9±2
Theobromine	<-6.3	<1	3±1	<6.7	<1	<1	<-5.5	<1	1.2±0.7	<-6.3	<1	<1
Theophylline	-5.9±0.1	2.7±0.7	<1	-6.60±0.05	1.4±0.1	<1	-	-	-	<-6.3	<1	<1
Thioridazine	-5.9±0.2	<1	84±4	-4.8±0.1	6±1	85±3	-3.99±0.07	17±1	30±3	-	-	-
Thymol	-4.5±0.1	21±9	49±9	-4.37±0.07	31±1	37±1	-3.64±0.09	36±4	9±3	-4.34±0.06	14±2	66±4
Tolbutamide	-5.7±0.2	3±2	<1	-	-	-	<-5.5	<1	<1	-4.47±0.04	42±2	<1
Verapamil HCl	-4.56±0.02	16.4±0.5	49±2	-4.8±0.1	36±5	6±9	-3.78±0.03	34±1	<1	-4.90±0.03	13±1	31±2
Warfarine	-5.19±0.02	10.6±0.5	3±1	-5.52±0.04	12.5±0.7	1±2	-4.38±0.05	12±1	<1	-4.38±0.05	37±3	8.3±0.1

4-3.1.1. Comparison of PAMPA-BBB with HDC/NPOE PAMPA

PAMPA-BBB and HDC/NPOE PAMPA both predict passive permeation through the BBB. The nature of the membrane differentiates both models. The artificial membrane in PAMPA-BBB is made of a dispersion of phospholipids in an organic solvent laid on a PVDF filter. Phospholipids of this membrane are extracted from porcine brain, and therefore, tend to mimic as close as possible the cerebral membrane. On the other hand, HDC/NPOE PAMPA aimed to get free from biological material and simplify the assay to improve reproducibility employing a full-solvent artificial membrane laid on a PVDF filter. Figure 4-1a highlights similarities between both models with the entire dataset. This observation is somewhat divergent from what was observed in chapter 2, which disclosed a relatively interesting correlation between both models (r² = 0.80; N = 13), but the correlation was estimated with only 13 compounds. Figure 4-1a shows that both models predict medium and high permeants in the same way, but that divergences appear for the slow permeants (log $P_{\rm e}^{\, HDC/NPOE}$ < -5.5). Indeed, experimental error made on the determination of permeability is more important for slow permeants than for fast permeants. Moreover, the longer incubation time in PAMPA-BBB may allow a better discrimination of the slow permeants. Additionnally, the phospholipidic nature of PAMPA-BBB artificial membrane creates a modified environment at the membrane, which tends to impact more on the slow permeants.

Outliers can be easily identified in figure 4-1a. Indeed, clonidine, that is a medium permeant in HDC/NPOE PAMPA (log $P_e = -4.80$), does not cross the phospholipid membrane at all. The cationic part of clonidine has been described to be actively transported by the H⁺-coupled reversible antiporter 26 , but the uncharged part, that exists at pH 7.4 rather distribute via passive diffusion. Therefore, the permeation observed for clonidine in HDC/NPOE PAMPA (15% of the amount of clonidine incorporated at time 0 on PAMPA succeed to reach the acceptor compartment after the 7 hours incubation) results from the permeation of the neutral drug. The absence of permeation in PAMPA-BBB is likely to be caused by a localized modification of pH at the phospholipid membrane. Hence, a small decrease of pH leads to a diminution of the uncharged clonidine (pKa = 8.05), and consequently to a decrease in passive permeability, according to the pH partition theory 27 . Moreover, the permeation observed in HDC/NPOE PAMPA is associated with a significant membrane retention. Indeed, if retention was not taken into account, clonidine would has been a class I compound in HDC/NPOE PAMPA.

Regarding the class study, 62% of the compounds are classified in the same class in the 2 PAMPA models (blue areas in figure 4-1a), and 84% are classified the same class \pm 1 (pink areas in figure 4-1a), meaning that strong similarities exist for those 2 artificial

membranes. The major discrepancy is observed for the prediction of steroids (dexamethasone, hydrocortisone, progesterone, aldosterone) and strong bases (labetalol, amitriptyline, chlorpromazine, oxprenolol, thioridazine). However, the majority of these highlighted compounds are prone to important retention at the membrane or on the material, especially for thioridazine, progesterone, amitryptilin, chlorpromazine, chloramphenicol and clonidine, highlighted as red crosses in figure 4-1. If the classification of these compounds had been based on the percentage of passage through the artificial membrane, the classification of these compounds would have been similar or in the neighboring class. However, the differences observed for dexamethasone, hydrocortisone, labetalol and aldosterone cannot be explained by retention, but rather to solubility issues that may occur, due to the lipophilicity of those compounds and the differences in experimental medium.

To conclude, HDC/NPOE PAMPA and PAMPA-BBB predict fast and medium permeant compounds the same way. When estimating passive permeation of slow permeants or compounds highly retained at the membrane, the differences between both model prediction become significant when comparing log $P_{\rm e}$, but less significant when looking at the effective percentage of passage through the membrane.

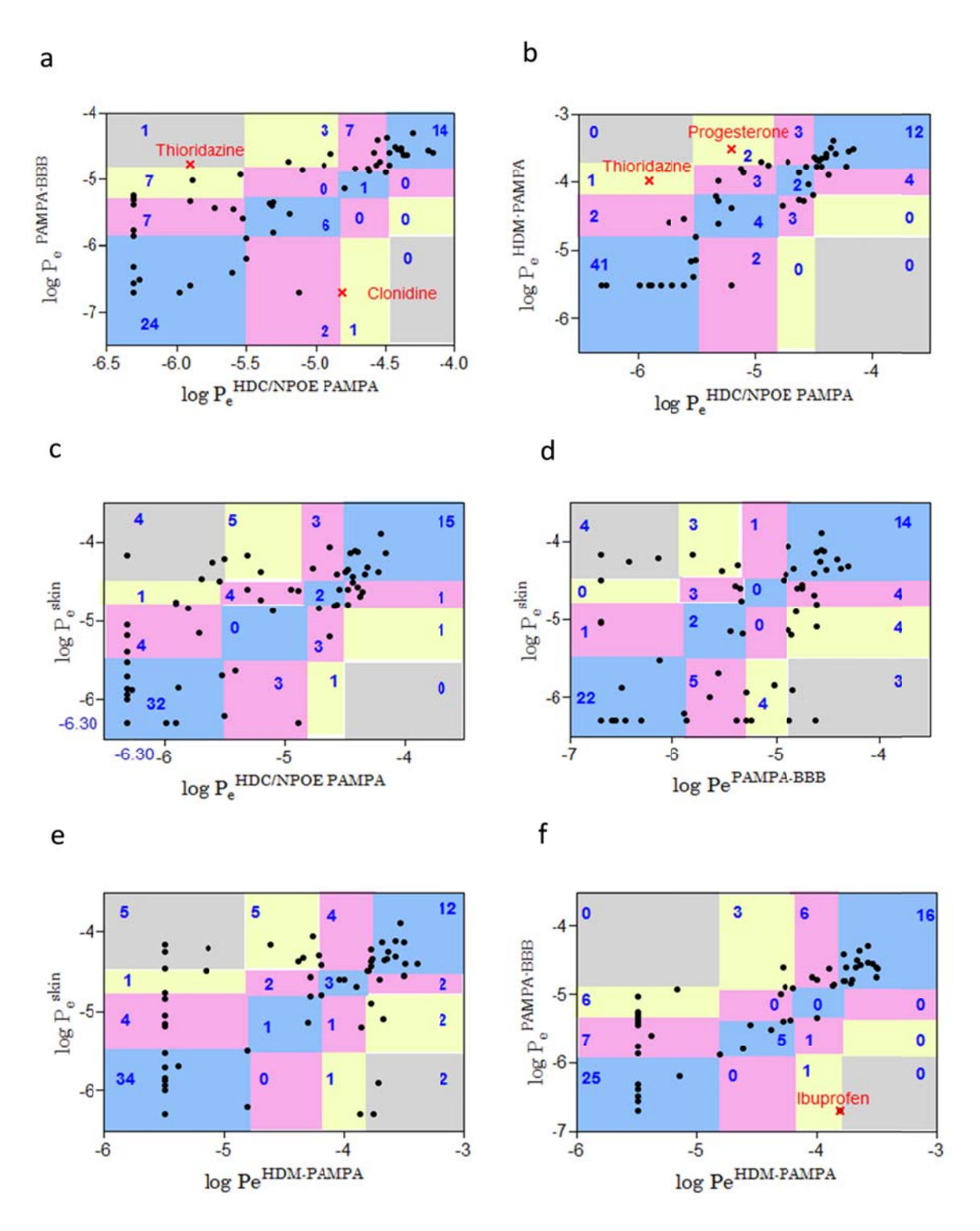


Figure 4-1: Comparisons of permeability coefficients obtained between the different PAMPA. Figure 4-1a represents the correlation between PAMPA-BBB and HDC/NPOE PAMPA; figure 4-1b represents the relation between HDM-PAMPA and HDC/NPOE PAMPA; figure 4-1c shows the comparison between PAMPA-skin and HDC/NPOE PAMPA; figure 4-1d plots PAMPA-skin vs PAMPA-BBB; figure 4-1e represents the correlation between PAMPA-skin and HDM-PAMPA and figure 4-1f plots the permeabilities generated with PAMPA-BBB in function of the permeabilities predicted in HDM-PAMPA. The blue areas represents the compounds that are classified in the same class on the 2 PAMPA models compared, pink areas indicate compounds that are classified in neighboring classes in the 2 PAMPA, and yellow and grey areas are the compounds that have very different profiles on the 2 compared models.

4-3.1.2. Comparison between HDM-PAMPA and PAMPA predicting BBB permeability

In figure 4-1b, plotting BBB permeabilities predicted with HDC/NPOE PAMPA and GIT permeabilities, strong similarities between both PAMPA appear. The figure indicates that 75% of the compounds are predicted in the same class, mainly medium to fast permeant compounds. The major deviation appears for the slow or non permeant compounds. Moreover, thioridazine and progesterone appear as outliers compared to the dataset, but these compounds are highly retained in HDC/NPOE PAMPA, biasing the resulting permeability coefficient. These similarities between the 2 artificial membranes mean that hexadecane as a membrane could be sufficient to give an idea of the BBB permeability for medium to fast permeants. The advantage of HDC/NPOE PAMPA could reside in a more precise determination of the permeability of the slow permeant compounds. When HDM-PAMPA is not able to evaluate the passive permeation of some of the very slow permeants (log $P_e^{HDM} < -5.5$), HDC/NPOE PAMPA is able to give a more precise determination of the permeability.

Regarding the 2 artificial membranes, HDM is constituted of 100% hexadecane whereas HDC/NPOE PAMPA is constituted of 75% hexadecane and 25% o-NPOE. As exposed in chapter 2, fast permeant compounds were able to permeate through hexadecane as artificial membrane. That could explain why fast permeant molecules seem to behave the same way through both artificial membranes, even if the targeted biological barrier is not the same. The addition of o-NPOE therefore has the most important impact on the slow permeant compounds.

Strong similarities are also observed when comparing the BBB permeability predicted with the phospholipid-based artificial membrane and with HDM-PAMPA (figure 4-1f). 66% of the compounds are classified on the same class in both PAMPA models. The major differences are caused by the compounds that are at the cut-off value on HDM-PAMPA. Indeed, PAMPA-BBB is able to discriminate these very slow permeant compounds whereas HDM-PAMPA cannot.

The similarities observed between the 3 PAMPA models indicate that the fast and medium permeant compounds are predicted the same way on the 3 artificial membranes, whereas more precision is obtained for the slow permeants with PAMPA-BBB and to a lesser extent with HDC/NPOE PAMPA.

This observation is not so surprising and was already pointed out with the human epithelial colon carcinoma cell line (caco-2 cells). This *in vitro* cellular model was originally

employed to predict intestinal permeability of drug candidates ²⁸⁻³¹, but more recently, interest rose for caco-2 as a predictive tool of BBB permeability ^{32, 33}. Caco-2 were shown to correlate in a good way with *in vivo* permeability measured with the mouse brain uptake assay for only passively transported compounds (r²=0.86, N=22) ³³.

4-3.1.3. Comparison of PAMPA-skin with the other models

Figure 4-1c, 4-1d and 4-1e indicate that poor similarities exist between the permeability predicted with PAMPA-skin and PAMPA-BBB (54% similitude) but that similarities exist with HDM-PAMPA and HDC/NPOE PAMPA (62 and 63% similarities). But regarding the graphical data, the dispersion is much more pronounced all around the experimental dataset as soon as comparison with PAMPA-skin occurred. The number of compounds that belong to the grey part, meaning that one model predict a very fast permeability while the other predicts a very slow permeability, is important when PAMPA-skin is compared to another model (between 4 and 7 compounds belong to these classes, compared to 0 or 1 when PAMPA-BBB, HDC/NPOE PAMPA and HDM-PAMPA are compared to each other). This divergence is likely to be due to structural differences in the cells constituting the skin barrier and those present in the intestine and in the cerebral capillaries, as well as differences in the lipid composition of the different cells ²⁸. Moreover, experimental pH conditions of PAMPA-skin are adapted in order to test drug candidates under their neutral form, whereas the 3 other PAMPA are run at fixed pH (pH 6.8 for HDM-PAMPA and 7.4 for HDC-NPOE PAMPA and PAMPA-BBB). This implies that depending on their pKa, the tested molecules can either be neutral or totally or partially ionized in HDM-PAMPA, HDC/NPOE PAMPA and PAMPA-BBB. According to the pH partition theory, which stands that in order to cross a biological lipidic membrane a drug needs to be under is neutral form ²⁷, molecules which are totally ionized should not be able to partition with the artificial membranes, which are hydrophobic. Therefore, the behavior of the tested molecules may be very different depending on their ionization state, since the hydrophobic surfaces will be different in a neutral molecule or in an ionized one. This fact explains why acidic molecules such as ketoprofen or salicylic acid, ionized at physiological pH, are able to fast permeate in PAMPA-skin but not on HDM-PAMPA, HDC/NPOE PAMPA and PAMPA-BBB.

4-3.2. Influence of the retention on the permeability coefficients

The passage through the artificial membrane is defined as the amount of compound that has reached the acceptor compartment after incubation ($C_A(t)/C_D(0)$). As most of the outliers highlighted with previous comparisons were retained at the membrane or on the material during the PAMPA experiments, comparisons of the different PAMPA models were performed using the percentage of passage as compared value. Results are exposed in figure 4-2 and table 4-4. Regarding the discrete data, there is much more dispersion when the percentages of passage are compared, rather than permeability coefficients, even if the percentage of similarities calculated in table 4-4 with the classes indicate that comparable results are obtained with log P_e and $C_A(t)/C_D(0)$. The dispersion appears less important for the comparison between the 2 models estimating the passive BBB permeation.

This fact highlights the importance of retention in the permeation process through artificial membranes. Hence, fast permeant compounds not retained at the membrane may have the same permeability coefficient as a compound retained at the membrane and having a poor passage through the membrane. Figure 4-3 exposes the relationship between the percentage of passage in HDC/NPOE PAMPA and the retention during the experiment. This figure indicates that there is a negative linear relationship between the passage and the retention for the class III compounds. Verapamil and 1-chloro-2-nitrobenzene, class II compounds, also belong to this linear correlation. But the permeability coefficient of these compounds is very closed to the threshold separating class II from class III (log $P_{\rm e}$ = -4.56 and log $P_{\rm e}$ = -4.55). 7-phenylheptanoic acid appears as an outlier, probably caused by its huge retention at the membrane (84%). Compounds belonging to classes 0, I and II are the one that are the less retained at the membrane (less than 20%).

The same conclusion can be taken with HDC/NPOE PAMPA and PAMPA-skin (figure 4-4 and figure 4-5): there is a linear relationship between the percentage of passage and the retention at the membrane for class III compounds, but no relationship exists for HDM-PAMPA (figure 4-6). Diclofenac was found as outlier with PAMPA-skin.

Similar conclusions have been obtained by Ottaviani et al 15 , who demonstrated a negative relationship between $C_A(t)/C_D(0)$ and the retention for fast permeant compounds and compounds retained at the membrane. They indicated that for these specific compounds, the membrane behave like a trap, or reservoir.

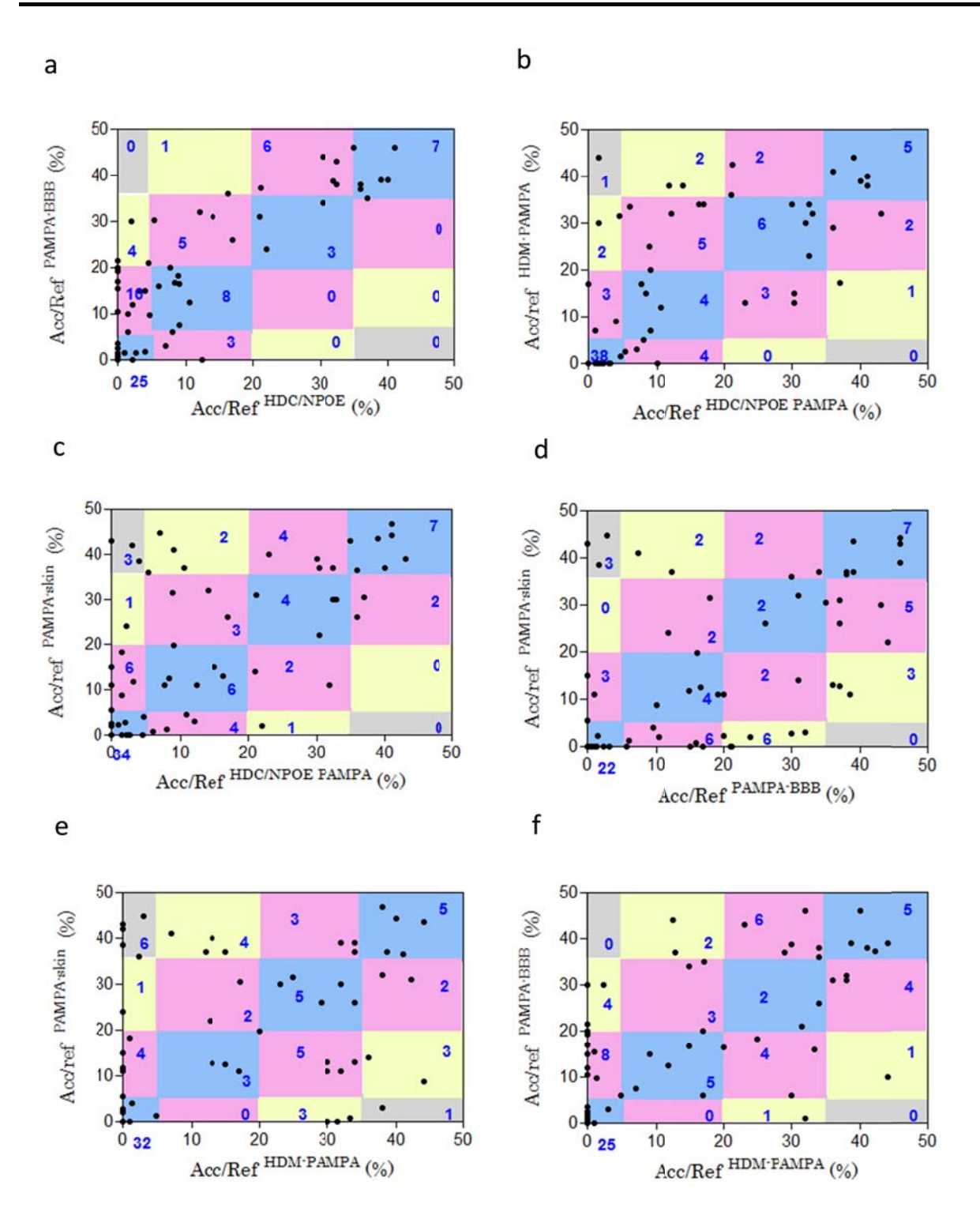


Figure 4-2: Comparisons of percentage of passage through the artificial membrane (Acc/Ref (%)) obtained between the different PAMPA. Figure 4-2a represents the correlation between PAMPA-BBB and HDC/NPOE PAMPA; figure 4-2b represents the relation between HDM-PAMPA and HDC/NPOE PAMPA; figure 4-2c shows the comparison between PAMPA-skin and HDC/NPOE PAMPA; figure 4-2d plots PAMPA-skin vs PAMPA-BBB; figure 4-2e represents the correlation between PAMPA-skin and HDM-PAMPA and figure 4-2f plots the permeabilities generated with PAMPA-BBB in function of the permeabilities predicted in HDM-PAMPA. The blue areas represents the compounds that are classified in the same class on the 2 PAMPA models compared, pink areas indicate compounds that are classified in neighboring classes in the 2 PAMPA, and yellow and grey areas are the compounds that have very different profiles on the 2 compared models.

Table 4-4 : Similarities between the different PAMPA assays, with log Pe and CA(t)/CD(0) as compared data.

		log I	P _e		C _A (t)/C _D (0) (%)			
	HDC/NPOE	PAMPA-	HDM-	PAMPA-	HDC/NPOE	PAMPA-	HDM-	PAMPA-
	PAMPA	BBB	PAMPA	skin	PAMPA	BBB	PAMPA	skin
HDC/NPOE PAMPA	-	62%	75%	62%	-	60%	69%	65%
PAMPA-BBB	-	-	66%	54%	-	-	53%	51%
HDM-PAMPA	-	-	-	63%	-	-	-	60%

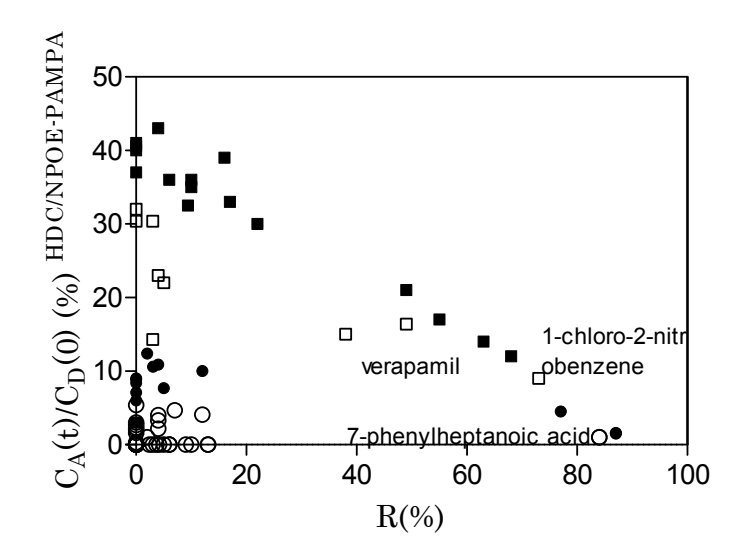


Figure 4-3 : Percentage of passage through the HDC/NPOE artificial membrane ($C_A(t)/C_D(0)$)) in function of the retention during PAMPA (R%). Open circles are the class 0 compounds, the dark circles are the class I compounds, the open squares are the class II compounds and the black squares are the class III compounds.

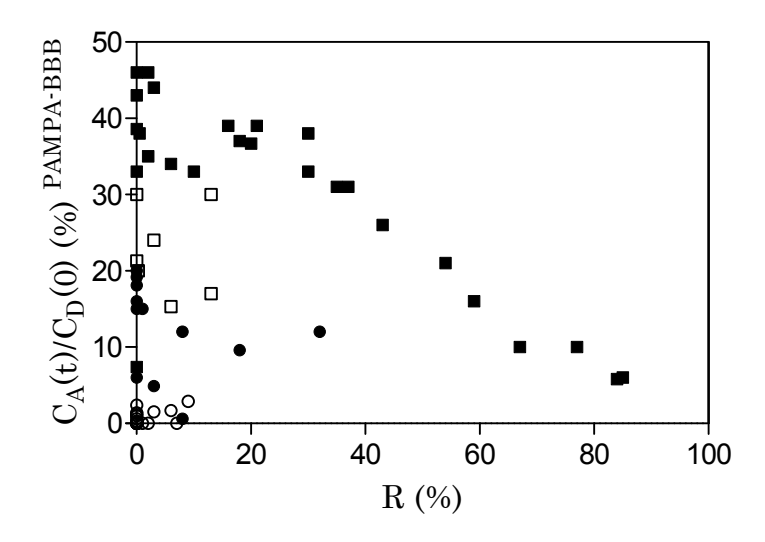


Figure 4-4 : Percentage of passage in PAMPA-BBB ($C_A(t)/C_D(0)$) in function of the retention during PAMPA (R%). Open circles are the class 0 compounds, the dark circles are the class I compounds, the open squares are the class II compounds and the black squares are the class III compounds.

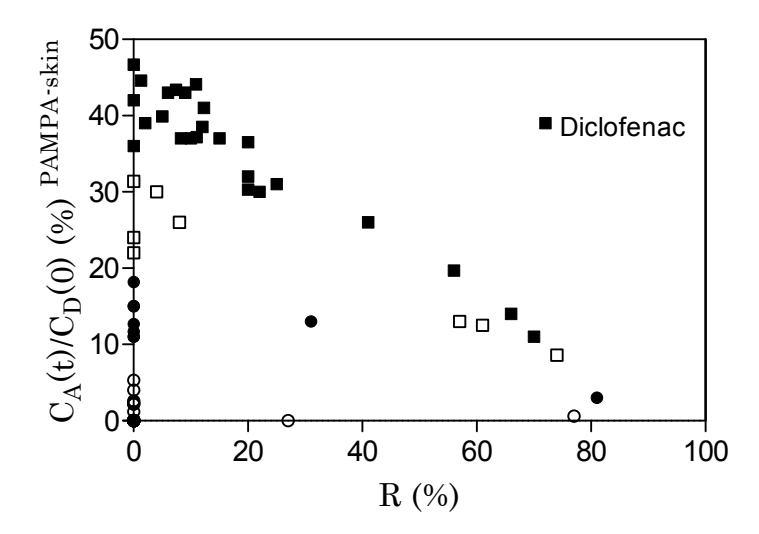


Figure 4-5 : Percentage of passage in PAMPA-skin ($C_A(t)/C_D(0)$) in function of the retention during PAMPA (R%). Open circles are the class 0 compounds, the dark circles are the class I compounds, the open squares are the class II compounds and the black squares are the class III compounds.

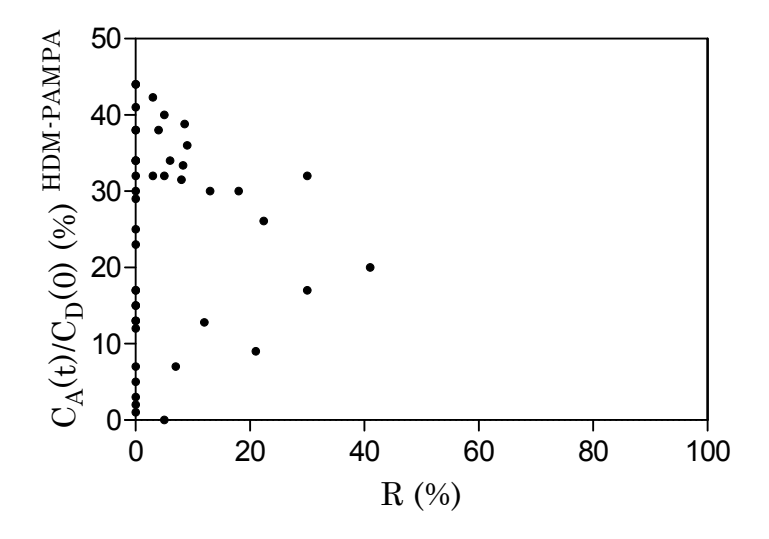


Figure 4-6 : Percentage of passage in HDM-PAMPA ($C_A(t)/C_D(0)$) in function of the retention during PAMPA (R%).

4-4- Conclusion

The various comparisons made in this chapter indicated that similarities exist between the 4 PAMPA models tested. Particularly, the high relationships between PAMPA-BBB, HDC-NPOE PAMPA and HDM-PAMPA demonstrated that the information generated by those 3 PAMPA models is similar. The same conclusion could be brought for PAMPA-skin with the study in classes, but when observing the discrete values, a strong dispersion could be observed. Therefore, PAMPA-skin is more specific than the 3 other models. This is consistent with strong differences in the physiology of *stratum corneum*, compared to the intestinal endothelium or the BBB.

When focusing on the retention at the membrane or on the material, this chapter led to the conclusion that HDC-NPOE PAMPA, PAMPA-BBB and PAMPA-skin behaved like drug reservoir for highly permeant compounds. Hence, due to their lipophilicity, these compounds are trapped at the membrane and are thought to distribute slowly from the membrane to the acceptor compartment (or the brain compartment *in vivo*).

References

- 1. Kansy, M.; Senner, F.; Gubernator, K. Physicochemical high throughput screening: parallel artificial membrane permeation assay in the description of passive absorption processes. *J. Med. Chem.* **1998**, *41*, 1007-1010.
- 2. Camenisch, G.; Alsenz, J.; van de Waterbeemd, H.; Folkers, G. Estimation of permeability by passive diffusion through Caco-2 cell monolayers using the drugs' lipophilicity and molecular weight. *Eur. J. Pharm. Sci.* **1998**, *6*, 313-319.
- 3. Leo, A.; Hansch, C.; Elkins, D. Partition coefficients and their uses. *Chem. Rev.* **1971,** *71,* 525-616.
- 4. Avdeef, A. The rise of PAMPA. Expert. Opin. Drug Metab Toxicol. 2005, 1, 325-342.
- 5. Avdeef, A.; Bendels, S.; Di, L.; Faller, B.; Kansy, M.; Sugano, K.; Yamauchi, Y. PAMPA critical factors for better predictions of absorption. *J. Pharm. Sci.* **2007**, *96*, 2893-2909.
- 6. Faller, B. Artificial membrane assays to assess permeability. *Curr. Drug Metab.* **2008,** *9*, 886-892.
- 7. Di, L.; Kerns, E. H.; Fan, K.; McConnell, O. J.; Carter, G. T. High throughput artificial membrane permeability assay for blood—brain barrier. *Eur. J. Med. Chem.* **2003**, *38*, 223-232.
- 8. Wohnsland, F.; Faller, B. High-throughput permeability pH profile and high-throughput alkane/water log P with artificial membranes. *J. Med. Chem.* **2001**, *44*, 923-930.
- 9. Sugano, K.; Hamada, H.; Machida, M.; Ushio, H.; Saitoh, K.; Terada, K. Optimized conditions of bio-mimetic artificial membrane permeation assay. *Int. J. Pharm.* **2001**, *228*, 181-188.
- Zhu, C.; Jiang, L.; Chen, T. M.; Hwang, K. K. A comparative study of artificial membrane permeability assway for high-throughput profiling of drug absoprtion potential. *Eur. J. Med. Chem.* 2002, 37, 399-407.
- 11. Avdeef, A.; Strafford, M.; Block, E.; Balogh, M. P.; Chambliss, W.; Khan, I. Drug absorption in vitro model: filter-immobilized artificial membranes. Studies of the permeability properties of lactones in *piper methysticum* forst. *Eur. J. Pharm. Sci.* **2001**, *14*, 271-280.
- 12. Bermejo, M.; Avdeef, A.; Ruiz, A.; Nalda, R.; Ruell, J. A.; Tsinman, O.; Gonzalez, I.; Fernandez, C.; Sanchez, G.; Garrigues, T. M.; Merino, V. PAMPA-a drug absorption in vitro model. Comparing rat in situ, Caco-2, and PAMPA permeability of fluoroquinolones. *Eur. J. Pharm. Sci.* **2004**, *in press*.
- 13. Ottaviani, G.; Martel, S.; Carrupt, P. A. Parallel artificial membrane permeability assay: a new membrane for the fast prediction of passive human skin permeability. *J. Med. Chem.* **2006**, *49*, 3948-3954.
- 14. Sinko, B.; Garrigues, T. M.; Balogh, G. T.; Nagy, Z. K.; Tsinman, O.; Avdeef, A.; Takacs-Novak, K. Skin–PAMPA: a new method for fast prediction of skin penetration. *Eur. J. Pharm. Sci.* **2012**, *45*, 698-707.

- 15. Ottaviani, G.; Martel, S.; Carrupt, P. A. In silico and in vitro filters for the fast estimation of skin permeation and distribution of new chemical entities. *J. Med. Chem.* **2007**, *50*, 742-748.
- 16. Verma, R. P.; Hansch, C.; Selassie, C. D. Comparative QSAR studies on PAMPA/modified PAMPA for high throughput profiling of drug absorption potential with respect to Caco-2 cells and human intestinal absorption. *J. Comput. Aided Mol. Des.* **2007**, *21*, 3-22.
- 17. Crivori, P.; Cruciani, G.; Carrupt, P. A.; Testa, B. Predicting blood-brain barrier permeation from three-dimensional molecular structure. *J. Med. Chem.* **2000**, *43*, 2204-2216.
- 18. Ano, R.; Kimura, Y.; Shima, M.; Matsuno, R.; Ueno, T.; Akamatsu, M. Relationships between structure and high-throughput screening permeability of peptide derivatives and related compounds with artificial membranes: application to prediction of Caco-2 cell permeability. *Bioorg. Med. Chem.* **2004**, *12*, 257-264.
- 19. Akamatsu, M.; Fujikawa, M.; Nakao, K.; Shimizu, R. In silico prediction of human oral absorption based on QSAR analyses of PAMPA permeability. *Chem. Biodivers.* **2009**, *6*, 1845-1866.
- Fujikawa, M.; Ano, R.; Nakao, K.; Shimizu, R.; Akamatsu, M. Relationships between structure and high-throughput screening permeability of diverse drugs with artificial membranes: application to prediction of Caco-2 cell permeability. *Bioorg. Med. Chem.* 2005, 13, 4721-4732.
- 21. Fujikawa, M.; Nakao, K.; Shimizu, R.; Akamatsu, M. QSAR study on permeability of hydrophobic compounds with artificial membranes. *Bioorg. Med. Chem.* **2007**, *15*, 3756-3767.
- 22. Nakao, K.; Fujikawa, M.; Shimizu, R.; Akamatsu, M. QSAR application for the prediction of compound permeability with in silico descriptors in practical use. *J. Comput. Aided Mol. Des.* **2009**, *23*, 309-319.
- 23. Abraham, M. H.; Hersey, A. In silico models to predict brain uptake. In *Comprehensive Medicinal Chemistry II*; Elsevier Ltd: 2007; pp 745-766.
- 24. Di, L.; Kerns, E. H.; Bezar, I. F.; Petusky, S. L.; Huang, Y. P. Comparison of blood-brain barrier permeability assays: in situ brain perfusion, MDR1-MDCKII and PAMPA-BBB. *J. Pharm. Sci.* **2009**, *98*, 1980-1991.
- 25. Mensch, J.; Melis, A.; Mackie, C.; Verreck, G.; Brewster, M. E.; Augustijns, P. Evaluation of various PAMPA models to identify the most discriminating method for the prediction of BBB permeability. *Eur. J. Pharm. Biopharm.* **2010**, *74*, 495-502.
- 26. Andre, P.; Debray, M.; Scherrmann, J. M.; Cisternino, S. Clonidine transport at the mouse blood-brain barrier by a new H+ antiporter that interacts with addictive drugs. *J. Cereb. Blood Flow Metab.* **2009**, *29*, 1293-1304.
- 27. Shore, P. A.; Brodie, B. B.; Hogben, C. A. M. The gastric secretion of drugs: a pH partition hypothesis. *J. Pharmacol. Exp. Ther.* **1957**, *119*, 361-369.
- 28. Hellinger, E.; Veszelka, S.; Toth, A. E.; Walter, F.; Kittel, A.; Bakk, M. L.; Tihanyi, K.; Hada, V.; Nakagawa, S.; Dinh Ha Duy, T.; Niwa, M.; Deli, M. A.; Vastag, M. Comparison of brain capillary endothelial cell-based and epithelial (MDCK-MDR1, Caco-2, and VB-Caco-2)

- cell-based surrogate blood—brain barrier penetration models. *Eur. J. Pharm. Biopharm.* **2012,** *82*, 340-351.
- 29. Artursson, P.; Palm, K.; Luthman, K. Caco-2 monolayers in experimental and theoretical predictions of drug transport. *Adv. Drug Deliv. Rev.* **1996,** *22*, 67-84.
- 30. Hubatsch, I.; Ragnarsson, E. G. E.; Artursson, P. Determination of drug permeability and prediction of drug absorption in Caco-2 monolayers. *Nat. Protocols* **2007**, *2*, 2111-2119.
- 31. Artursson, P.; Karlsson, J. Correlation between oral drug absorption in humans and apparent drug permeablity coefficients in human intestinal epithelial (Caco-2) cells. *Biochem. Biophys. Res. Commun.* **1991,** *175*, 880-885.
- 32. Hakkarainen, J. J.; Jalkanen, A. J.; Kääriäinen, T. M.; Keski-Rahkonen, P.; Venäläinen, T.; Hokkanen, J.; Mönkkönen, J.; Suhonen, M.; Forsberg, M. M. Comparison of in vitro cell models in predicting in vivo brain entry of drugs. *Int. J. Pharm.* **2010**, *402*, 27-36.
- 33. Garberg, P.; Ball, M.; Borg, N.; Cecchelli, R.; Fenart, L.; Hurst, R. D.; Lindmark, T.; Mabondzo, A.; Nilsson, J. E.; Raub, T. J.; Stanimirovic, D.; Terasaki, T.; Öberg, J.-O.; Österberg, T. In vitro models for the blood-brain barrier. *Toxicol. in Vitro* **2005**, *19*, 299-334.

Chapter 5: Parallel Artificial Membrane
Permeability Assay as a tool to describe the
passive permeability of liposomes and polymeric
nanoparticles through the Blood-Brain Barrier

5-1. Introduction: nanocarriers as drug delivery systems

The specific organization of cerebral capillaries makes the brain hardly accessible for most of drug compounds, leading to a high attrition rate during the drug discovery and development processes. When around 10% of the drugs entering clinical phase I succeed in launching, this figure falls to 3 to 5% as soon as central nervous system (CNS)-targeting drugs are concerned ^{1, 2}. This poor success in CNS drug discovery is mainly attributed to the presence of the blood-brain barrier (BBB). The organization of the cerebral endothelial cells, sealed together with tight-junctions and the existence of numerous efflux transporters at the BBB, prevent or limit the entry of many compounds into the brain. Therefore, drug attrition in CNS drug discovery is usually not associated with a lack of potency, but rather on poor biodistribution ³. Indeed, to interact with cell membrane, a molecule needs to disclose hydrophobicity. On the other hand, hydrophobicity often rhymes with poor water solubility, which is frequently a cause of withdrawal from the drug discovery ⁴.

When targeting the brain is needed in diseases such as Alzheimer's disease, Parkinson's disease, brain tumors or chronical pain, strategies have to be developed to make a drug reach the cerebral target, at a therapeutic concentration and for a defined period of time. Different approaches, either invasive or non-invasive, have been proposed.

Direct injections into the cerebrospinal fluid ⁵ or therapeutic opening of the BBB ⁶⁻⁸ suffer from many side effects linked to the degree of invasiveness of these techniques (increase in intracranial pressure, hemorrhage, cerebrospinal fluid leakage, neurotoxicity, infections). Therefore, non-invasive techniques are extensively studied in order to improve brain bioavailability. These strategies are mainly the use of prodrugs ⁹, the nose-to-brain route ¹⁰⁻¹⁶, the inhibition of efflux transporters ^{17, 18}, the usage of Trojan horses or BBB shuttles ^{9, 19}, and the nanocarriers ²⁰⁻²⁴, as developed in the introduction of this manuscript. Drug delivery systems such as liposomes and nanoparticles are a promising way to deliver active compounds at the CNS target. Their ability to bypass numerous limitations of traditional drug compounds such as poor aqueous solubility, poor bioavailability and affinity for efflux transporters made them valuable strategies to improve CNS drug delivery. Therefore, lead compounds that exhibit an efficient activity on a CNS target but would have been withdrawn from the drug development process due to incompatibility with *in vivo* conditions may be reconsidered under a nanocarrier form. Even if the development of

colloidal systems is growing, a clear understanding of the way nanovectors are able to cross the BBB is not achieved yet.

Nanoscale systems are carriers ranging from 1 to 1000 nm by definition, but most of the nanocarriers studied as drug delivery systems have a size ranging from 1 to 300 nm approximately 20, 25, 26. During the last decades, many types of nanocarriers have been developed and tested as drug carriers. The most promising colloidal vectors are the liposomes and the polymeric nanoparticles or polymeric micelles, even if other nanocarriers such as polymer-drug conjugates, dendrimers, solid lipid nanoparticles, microemulsions or inorganic nanoparticles ^{20, 27-34}. Compared to a free drug, the drug-loaded nanocarriers have the ability to circumvent poor bioavailability. The delivery of peptides or small proteins, which are very unstable in vivo but may have a high potency to treat certain CNS diseases ³⁵, becomes possible with nanoscale drug delivery. Moreover, one of the most important issues when targeting the CNS is linked to the presence of efflux proteins at the BBB. Hence, efflux transporters such as P-gp have a very low specificity. Many drug candidates can thus interact with these transporters and be pumped back into the blood stream. Therefore, the active compound will never reach a therapeutic concentration in the CNS. The incorporation of such substrates of efflux transporters inside nanocarriers may limit the action of the efflux protein.

Finally, the possible higher bioavailability gained with nanocarriers enables either the decrease of the administered dose, resulting in lower toxicity, or the administration of a higher quantity of encapsulated liposomes or nanoparticles, resulting in a better efficiency to maintain a therapeutic effect. Moreover, nanocarriers can act as drug reservoirs. Therefore, long-term treatments, requiring daily administration, may improve patient's compliance thanks to weekly or monthly administration of nanovectors formulations.

In addition to therapeutic purposes, liposomes as nanoparticles may also be employed for diagnostic applications allowing the identification of abnormal cells, viruses or disease markers ^{27, 29, 36, 37}.

This chapter aims to study nanocarriers with PAMPA, in order to understand the mode of distribution of such nanovectors, focusing on liposomes and polymeric nanoparticles. Following a general presentation of the liposomes and nanoparticles, as well as a review of the various hypotheses concerning the distribution of these nanocarriers at the BBB currently emitted, HDC/NPOE PAMPA will be employed to evaluate the presence of a passive permeation process at the BBB. The possible involvement of a flip-flop process between the phospholipids of the liposomes and those of the membrane will be assessed

with a phospholipid-based artificial membrane. Finally, in order to determine a possible active transport of the polymeric nanoparticles, a human cerebral cell-line has been employed for comparison.

5-2. Liposomes and polymeric nanoparticles as drug delivery systems

5-2.1. Liposomes as drug delivery systems

Liposomes are vesicular systems, formed of a phospholipids bilayer. They were first described by Bangham *et al.* in 1964, when he observed the rearrangement under hydration of a dried lipid film into spherical bilayers ³⁸. They are self-assembled structures that form spontaneously when phospholipids are dispersed in an aqueous environment. Liposomes have often been used as membrane permeability models due to their similar features with the cell membranes ³⁹⁻⁴⁸. Phospholipids are amphiphilic, therefore, when introduced in an aqueous environment, hydrophobic chains get together, while the polar sides face the aqueous medium. In order to decrease the free energy of such system, the optimal arrangement is the spherical bilayer (figure 5-1 and figure 5-2).

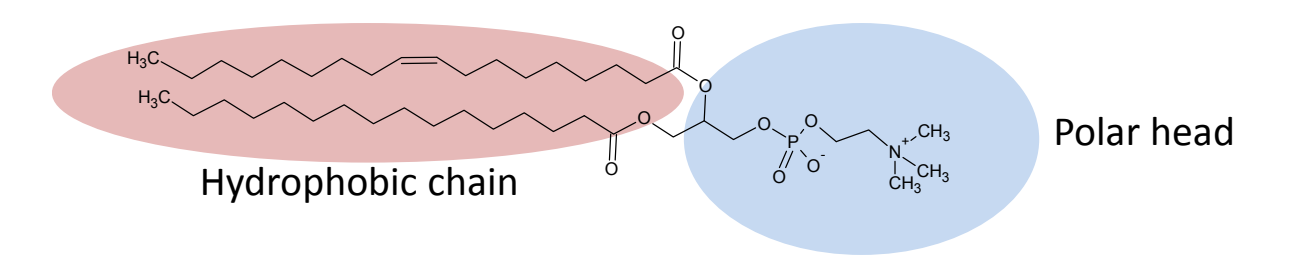


Figure 5-1: An example of phospholipid: a type of phosphatidylcholine

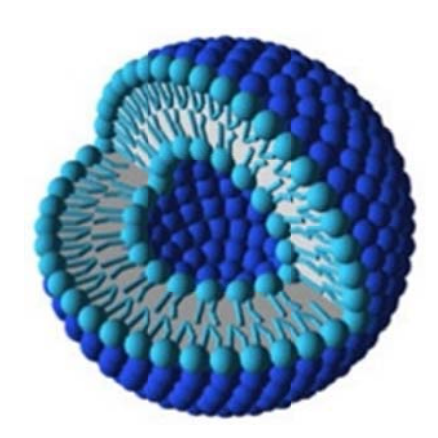


Figure 5-2: Section of a liposome, showing the lipid bilayer and the inner aqueous core (http://www.thescientist.com/?articles.view/articleNo/28888/title/Father-of-liposomes-dies/25.04.2013).

Liposomes have rapidly been considered as a revolution in drug development. Due to their biodegradability, bioavailability, and their ability to deliver their cargo to their biological target in a controlled manner ⁴⁹, they were fast used as drug delivery systems ⁵⁰⁻⁵³. Thanks to the amphiphilic property of phospholipids, liposomes possess two main domains with opposite properties: a hydrophilic core, and a hydrophobic bilayer (figure 5-2) with a hydrophilic outer surface. Consequently, hydrophilic drugs may be encapsulated on the inner aqueous core of liposomes or be adsorbed at the outer surface of the liposomes, while more hydrophobic drugs will incorporate in the bilayer ³⁶. The strength of a particular drug delivery system depends on its ability to modify the bioavailability/biodistribution of the encapsulated molecules and thus limit the problems associated with the clinical use of the free parent drug ²¹. For instance Doxil®, a liposomal formulation of doxorubicin, is used for the treatment of ovarian or breast cancers with lower cardiac toxicity compared to free doxorubicin ^{23, 24, 54, 55}. This decrease in cardiotoxicity allows increasing dosing, enhancing the efficacy of the treatment. In addition, such delivery systems enable the transport of new therapeutic entities such as RNA or peptides ⁵⁶.

Liposomes are generally classified into 3 classes, depending on their size and structure. Multilamellar vesicles (MLV) are liposomes generally obtained just after hydration of a lipid film. They are constituted of several phospholipid bilayers, separated by aqueous compartments (figure 5-3a). Their size is between 100 nm and 2 μ m. Unilamellar vesicules are constituted of a single bilayer delimiting a single aqueous core. Depending on their size, they are subdivided in large unilamellar vesicles (LUV), ranging from 100 nm to 1 μ m (figure 5-3b and in small unilamellar vesicules (SUV), sized between 20 and 100 nm (figure 5-3c). LUV and SUV are obtained from specific treatment of MLV, such as a freeze-thaw

procedure, several extrusions or sonication. Except their size, their aqueous volume differentiates them from each other, influencing their encapsulation capacity. Even if MLV are the largest liposomes, the aqueous compartments available for the encapsulation are very small.

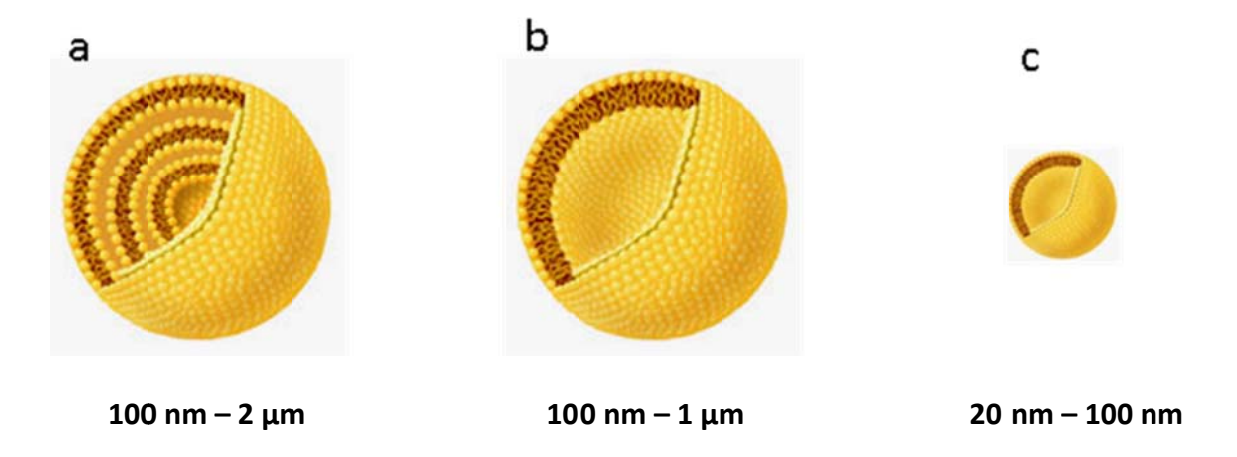


Figure 5-3: Schematic view of the 3 types of liposomes. (a) shows a multilamellar liposome; (b) represents a large unilamellar liposome, while (c) is a small unilamellar liposome.

Besides their structure, liposomes are also differentiated according to their functionality, as first, second or third generation liposomes.

Liposomes of first generation may be considered as native or conventional liposomes. They are constituted of phospholipids, with a possible addition of cholesterol. Their circulation time in blood is very short, due to their high uptake by the immune system. Plasma proteins, called opsonins, have a high affinity for the outer surface of liposomes, making them highly recognizable by the macrophages of the reticuloendothelial system (RES). Their circulation time hardly exceeds dozens of minutes ⁵⁷ and they are readily eliminated by the liver. These nanocarriers may have an interest in the treatment of liver cancer or infections, since the liposomes are absorbed by macrophages.

Also called pegylated liposomes, or long-circulating liposomes, liposomes of second generation are surrounded by long hydrophilic polymers, such as the polyethylene glycol (PEG) which sterically stabilizes the carriers. The pegylation limits the affinity of opsonins for the outer membrane, diminishing the recognition of liposomes by the RES, and therefore increasing the circulation time in the blood-stream ⁵⁸. Besides, cancer cells easily absorb polymers. These second generation of liposomes are therefore of interest in cancer therapy. Doxil® is such a long-circulating liposome ²⁴.

Liposomes of third generation are obtained by attaching a specific molecule (antibody, peptide, ligand) to the surface of the liposomes. Therefore, the functionalized liposomes have the ability to target a specific receptor or antigen of the diseased cells and increase the therapeutic response. The choice of coating will rely on the target, but also on its specificity, stability and availability ⁴. Such strategies may be employed to circumvent the BBB, grafting the surface of the liposome with antibodies ⁵⁹ or with a substrate of transporters present at the luminal side of cerebral endothelial cells, such as the transferrin receptor or the human insulin receptor ⁶⁰⁻⁶².

Liposomes have proved to be efficient in many pathological states, such as cancer therapy or infections (table 5-1). The main issue stays the release of the encapsulated drug at the desired place. Many strategies have been developed, such as the delivery upon pH or thermal variations ⁶³. For example, when intracellular drug delivery is wished, the incorporation of рΗ sensitive phospholipids into the bilayer such phosphatidylethanolamine allows an endosomal delivery. When these liposomes are stable in blood at physiological pH, they undergo phase transition under intracellular pH, which destabilizes the liposomal structure and allows the release of the free drug ³⁷.

Table 5-1 : Liposomal drugs in the market or in clinical phases $^{64}\,$

Active drug	Trade name	Company	Indication	Development phase
Amphotericin B	Abelcet	Enzon	infections	approved
Amphotericin B	AmBisone	Gilead sciences	infections	approved
Cytarabine	DepoCyt	SkyePharma	malignant lymphomatous meningitis	approved
Daunorubicin	DaunoXome	Gilead sciences	HIV-related Kaposi's sarcoma	approved
Doxorubicin	Myocet	Zeneus	Metastatic breast cancer	approved
influenza vaccine	Epaxal	Berna Biotech	Hepatitis A	approved
influenza vaccine	Inflexal V	Berna Biotech	Influenza	approved
Morphine	DepoPur	SkyePharma	Analgesia	approved
Verteprofin	Visudyne	Novartis	ARMD	approved
Doxorubicin	Doxil/Caelyx	Johnson&Johnson, Scherring-Plough	HIV-related Kaposi's sarcoma, metastatic breast and ovarian cancer	approved
Propofol	Diprivan	Zeneca Pharmaceutical	anesthetic	approved
Vincristine	Onco TCS	Inex. Enxon	leukemia	approved
Cisplatin	SLIT Cisplatin	Transave	osteogenic sarcoma metastatic to the lung	Phase II
Doxorubicin	Sarcodoxome	GP-Pharm	soft-tissue sarcoma	Phase II
Fentanyl	AeroLEF	Delex Therapeutics	Analgesic	Phase II/III
Lurtotecan	OSI-211	OSI Pharmaceuticals	Ovarian cancer	Phase II
Lidocaine	Maxilene		pain in pediatric population	phase IV
Cytarabine	Depocite		leukemia	phase III

5-2.2. Nanoparticles as drug delivery systems

In pharmaceutical sciences, nanoparticles are drug delivery systems typically ranging from 1 to 1000 nm. They can be composed of biocompatible polymers, lipids, or even metals. Transported molecule can be either incorporated in, adsorbed to or covalently bound to the nanoparticle ⁶⁵. Polymeric nanoparticles are formed mixing an organic phase of the polymer with an aqueous phase of surfactant ³⁷. Evaporation of the solvent leads to the precipitation of the nanoparticles, insoluble in aqueous environment (figure 5-4). Research made on nanoparticles is wide, since their properties will depend on i) their size; ii) the material to build the nanoparticle; iii) the physicochemical properties of the encapsulated drug; iv) the drug loading; v) the presence of polyethylene glycol; vi) the presence of antibodies or specific ligands on the outer membrane.

Release of the active compound is thought to occur *via* diffusion through the capsule, by erosion of the surface of the nanoparticle ⁶⁶, or by polymer swelling followed by diffusion ³⁷. Unlike liposomes, nanoparticles have a unique hydrophobic core allowing the incorporation of hydrophobic drugs. The incorporation of hydrophilic molecules requires an adaptation of the protocol of fabrication, and often leads to poor encapsulations ⁶⁷. As drug compounds suffering from poor water solubility are the most hydrophobic ones, nanoparticles are carriers of choice and compared to liposomes, polymeric nanoparticles are usually more stable.

Lots of researches are emerging on polymeric nanoparticles as drug delivery systems, especially for CNS targeting ^{20, 68-76}. Even if the pharmaceutical research considered that nanoparticles could be used as drug delivery systems to target the CNS after intravenous injection since 1995 ^{70, 72, 77}, only 5 polymeric nanoparticle formulations are on clinical trials and none of them aim to target the CNS ⁷⁸ (table 5-2). This report may be caused by toxicity issues resulting from administration of nanoparticles, and concerns about the excretion of the vesicle out of the brain, after drug release.

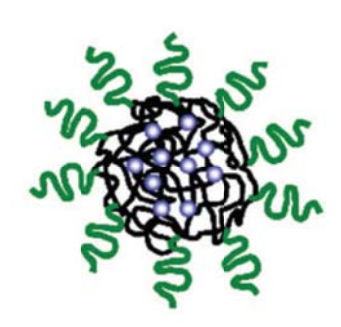


Figure 5-4: Schematic view of a polymeric nanoparticle. Black lines represent the hydrophobic polymers, while the green ones are the hydrophilic polymers. Dots represent the place where drugs are located. Picture from ³⁷.

Table 5-2: Polymeric nanoparticles on preclinical development, from Zhang et al. 37

Active drug	Polymer main component	Functionnalization	Indication	Compagny	Clinical phase
SiRNA	Cyclodextrin	Transferrin	Melanoma	Calando	1
Camptothecin	Cyclodextrin	-	Metastatic solid tumors	Insert Therapeutics	1
Doxorubicin	Cyanoacrylate	-	Hepatic tumors	BiioAlliance Pharma	II
Mitoxantrone	Cyanoacrylate	-	Hepatic tumors	Sichuan University	II
Docetaxal	Polyester	Prostate specific membrane antigen	Prostatic tumors	Bind Biosciences	I

5-2.3. Crossing the BBB with nanocarriers: how does it work?

The way colloidal nanocarriers cross the BBB is still unclear, even if hypothesis have been formulated. Moreover, the size of the nanocarriers and the material employed to form the particles also influence the distribution of the system ⁷⁹. Some researchers argued that the physicochemical properties of the nanoparticles, combined with their reduced size and their composition made them good candidates for BBB transport systems ⁸⁰.

The most widely assumed hypothesis on how nanocarriers interact with cell membranes and penetrate in the cerebral area is an active transport *via* receptor mediated transcytosis. In 1995, Kreuter *et al.* argued that the cerebral endothelial cells were not an inert barrier and were capable of both endocytosis and phagocytic processes ⁷². When demonstrating that long circulating doxorubicin-loaded liposomes selectively targeted the brain tumor area, Zara *et al.* hypothesized an increased retention of the nanocarriers in

cerebral capillaries that could create a higher concentration gradient, an enhanced transport *via* endocytosis or transcytosis through the cerebral endothelial cells, or a possible paracellular pathway ⁸¹. Indeed, the vasculature of solid tumors is leaky and contains gaps large enough (600-800 nm) for liposomes to extravasate in a passive way and in a size-dependent manner: that is the enhanced permeability and retention effect, often investigated in anticancer therapy ^{82, 83}. In addition, tumors have impaired lymph drainage and liposomes will thus accumulate within the tumor provided they stay long enough ^{63, 84}. In 2003, Koziara *et al.* suggested that either endocytosis and/or transcytosis were probable pathways for the BBB transport of nanoparticles, but that passive permeability may also have a role in this transport ⁶⁹. Alam *et al.* explained in 2010 that the nanocarriers may enter the brain thanks to various endocytotic, but non-phagocytic mechanisms ⁸⁵. Georgieva *et al.* explained this point showing that these processes were mostly caveolar endocytosis, adsorptive-mediated endocytosis, receptor-mediated endocytosis and clathrin-mediated endocytosis, but still non-phagocytic processes ⁸⁶.

To sum up, many hypotheses have been proposed concerning how nanocarriers can penetrate through biological membranes. Nearly all possible pathways have been suggested, including the paracellular way, the passive transcellular and the active transcellular ways. In this chapter, polymeric nanoparticles and liposomal formulations have been tested with PAMPA. Since only the passive component of permeability can be determined with artificial membranes, these tests will enable to corroborate or invalidate the hypothesis concerning a passive transcellular pathway.

For the purpose of this study, first generation liposomes have been formulated. Second generation liposomes have not been considered due to the important increase in hydrophilicity brought by the pegylation, as well as the significant increase in liposome size, not compatible with the pore size of the filters in PAMPA. Different compositions of phospholipids have been tested to prepare the liposomes, mainly composed of phosphatidylcholine (PC), with the incorporation or not of cholesterol, plus the addition of α -tocopherol to limit the oxidation of the phospholipids. The dowstream processes were optimized, in order to form liposomes suitable for PAMPA measurements. Once an optimized protocol of fabrication of liposomes has been achieved, incorporation of either fluorescent dyes or drug compounds was performed. Liposomal suspensions were tested with HDC/NPOE PAMPA and PAMPA-BBB in order to assess a possible passive process in the permeation of those drug delivery systems.

Polymeric nanocarriers were also prepared using protocols optimizing the entrapment efficiency of the drug studied. The copolymer poly(D,L-lactide-co-glycolide) was employed to structure the nanoparticles. HDC/NPOE PAMPA was employed to assess the passive permeation of nanoparticles. In order to corroborate the results, permeability of the nanoparticles was determined through a human cellular model mimicking BBB permeation (both active and passive processes): the hCMEC/D3 cell line ^{87, 88}.

5-3. Materials and methods

5-3.1. Chemicals

Phosphatidylcholine (PC) was purchased from Lipoid GmbH (Ludswighafen, Germany), α-tocopherol, cholesterol, antipyrine, caffeine, disodium calcein, carbamazepine, diazepam, dioctadecyloxacarbocyanine perchlorate (DIO), hydrocortisone, lidocaine, loperamide, Lucifer yellow, nicotine, pindolol, propranolol, verapamil, warfarin and chloroform were purchased from Sigma Aldrich (Saint Louis, USA); dimethylsulfoxide, acetonitrile UPLC grade and methanol UPLC grade were purchased from Acros Organics (Chemie Brunschwig AG, Basel, Switzerland); poly(D,L-lactide-co-glycolide) (PLGA) (resomer® RG502; MW=12000Da) was purchased from Boehringer Ingelheim, (Ingelheim am Rhein, Germany); polyvinylic alcohol (PVAL) (Mowiol 4-88) was obtained from Omya, (Oftringen, Switzerland). Rhodamine-labeled phosphatidylcholine was kindly synthesized by Pr Luca Costantino's lab (Modena, Italy).

5-3.2. Liposomes

5-3.2.1. Formulations and characterization

5-3.2.1.1. Liposomes for the preliminary tests

For preliminary tests, different compositions of liposomes have been formulated. Batches of liposomal suspensions were composed of PC (ranging from 80% to 100% of the

composition) and cholesterol (ranging from 0 to 20% of the composition). α -tocopherol was incorporated at a concentration of 230 μ M ⁸⁹.

PC, cholesterol and α -tocopherol are solubilized in chloroform, at a concentration of 10 mg/ml in total lipids The organic solution is evaporated overnight at 37°C with a rotavapor, under vacuum. Nitrogen is employed to come back to atmospheric pressure, to reduce lipid oxidation. The lipid film is then hydrated under mild stirring at 37°C with a preheated phosphate buffer pH 7.4 saturated in nitrogen to reach a suspension concentration of 10 mg/ml in lipids. Multilamellar vesicles are already formed as soon as hydration occurs. The resulting suspension is defined in this paper as the basic liposomal suspension. Liposomes used for experiments are then submitted to a treatment aiming at obtaining unilamellar liposomes, with a size ranging from 150 to 250 nm. These treatments are either the freeze-thaw procedure followed by extrusion, the direct extrusion process, the filtration followed by extrusion or the sonication followed by extrusion.

<u>Direct extrusion after liposome formation</u>

The basic liposomal suspension is extruded under pressure through 2 polycarbonate filters of 100 nm pore size, in order to achieve liposomes smaller than 450 nm. 6 successive cycles are provided. The passage of the liposomes through these filters causes a progressive diminution of the number of bilayers constituting the liposomes. This step allows the transformation of multilamellar vesicles to large or small unilamellar vesicles.

Filtration, followed by extrusion

A preliminary filtration with 450 nm filters is performed, followed by 6 cycles of extrusion through two 100 nm pore size filters.

Sonication, followed by extrusion

The basic liposomal suspension is sonicated during 15 minutes, with 15 seconds pulsations every 30 seconds. The sonicated liposomal suspension is then extruded 6 times through two 100 nm pore size filters.

Freeze-thaw procedure followed by extrusion

The basic liposomal suspension is frozen during 5 minutes in liquid nitrogen (-196°C) followed by thawing in a water bath during 15 minutes at 37°C. 5 cycles were applied. These freeze-thaw cycles allow a rearrangement of the phospholipids, diminishing the number of concentric bilayers to form unilamellar vesicles. 6 extrusion cycles were then applied through two 100 nm pore size filters.

The size and size distribution (polydispersity) of the liposomal suspensions were determined using dynamic light scattering with a Zetasizer® 3000 HSA (Malvern Instruments, Worcestershire, UK).

5-3.2.1.2. Liposomes for permeability determination with HDC/NPOE PAMPA

Formulation of rhodamine-labeled liposomes

The same protocol as above is applied to obtain the basic liposomal suspension, except that the phosphatidylcholine employed has been labeled with rhodamine. This suspension was then extruded 6 times through two 100 nm pore size filters.

Formulation of calcein-loaded liposomes

A mixture of 80% PC and 20% cholesterol is solubilized in chloroform and evaporated overnight under vacuum to obtain a lipid film. Calcein is solubilized in a pH 7.4 phosphate buffer saturated with nitrogen and prewarmed at 37°C, at a concentration of 1 mg/ml. The lipid film is then hydrated with the buffer containing calcein for 30 minutes under mild stirring. This suspension was then extruded 6 times through two 100 nm pore size filters.

5-3.2.1.3. Liposomes for permeability determination with PAMPA-BBB

Drug-loaded liposomes were employed for permeability assessment with PAMPA-BBB. A mixture of 80% PC, 20% cholesterol is dissolved in chloroform, in presence of 230 μ M α -tocopherol. The lipophilic drugs (diazepam and imipramine) are dissolved in this solution at a concentration of 1 mg/ml in the final liposomal suspension. Chloroform is evaporated overnight under vacuum at 37°C using a rotavapor (Buchi®). The resulting lipid

film is then hydrated with a pre-warmed phosphate buffer pH 7.4 saturated with nitrogen. Hydrophilic compounds (calcein, fluorescein and dopamine) are added during this hydration step. Calcein was added at a concentration of 2.5 mg/ml, fluorescein at a concentration of 15 mg/ml, and dopamine at a concentration of 1 mg/ml. The solution is mildly stirred for 30 minutes at 37°C. The liposomal suspension is then extruded 6 times through a 400 nm-pore size filter, and once through a 100 nm pore size filter. This adaptation of the extrusion process allows to form slightly bigger liposomes with an enhanced entrapment yield of the free drug.

5-3.2.2. Determination of the entrapment yield

The amount of drug incorporated in the liposomes was determined after separation of the loaded liposomes from the free drug by centrifugation at 30000 rpm (64400 g) for one hour at 4°C (Beckman, Avanti 30, CA, USA, rotor F1202). The supernatant is separated from the pellet (supernatant 1) and the pellet is resuspended with fresh buffer. 2 cycles of centrifugation were done. Following separation of supernatant 2 from the pellets, fresh buffer was slowly added on the pellet and immediately removed, to wash the traces of free drug (supernatant 3). The resulting pellet was dissolved with a mixture composed of 0.5% triton-X in buffer, to solubilize the phospholipids. The quantity of free drug was then determined by UHPLC-UV with the procedure described in paragraph 5-3.2.4.

Entrapment yield (EY) was determined according to Equation 5-1.

$$EY(\%) = \frac{\text{weight of free drug in the pellets}}{\sum \text{weight (supernatants and pellets)}}$$
(Equation 5-4)

5-3.2.3. Drug release study

5-3.2.3.1. Drug release from the loaded-liposomes

Diazepam-, calcein-, fluorescein- and imipramine- loaded liposomes composed of 80% PC and 20% cholesterol were prepared according to the standard procedure exposed above.

 $200~\mu l$ of liposomal suspension was washed twice to discard the free drug and resuspended in $200~\mu l$ of fresh buffer containing 0.5% DMSO. This determines the time 0. The drug release is then followed for 1 hour, 3 hours, 5 hours and 18 hours.

After incubation, the liposomal suspension is centrifuged for 1 hour at 30000 rpm (64400g) and 4°C. The pellets are separated from the supernatant and dissolved with buffer containing 0.5% DMSO and 0.5% triton X. The quantity of drug present in the dissolved liposomes and supernatant is determined with UHPLC-UV with the gradient mode exposed in table 5-3.

5-3.2.3.2. *Drug diffusion in unloaded liposomes*

A liposomal suspension of unloaded liposomes is centrifuged at 30000 rpm (64400g) for 1 hour at 4°C. The supernatant is discarded, while the pellet of liposomes is resuspended with a fresh buffer solution containing 0.5% of a DMSO stock solution of diazepam or imipramine, or a buffer solution of calcein or fluorescein additioned of 0.5% DMSO. This resulting solution was incubated for 1; 3; 5; 7 or 18 hours with the unloaded liposomes. After incubation, the liposomal suspension was centrifuged; the pellet was separated from the supernatant and dissolved with buffer containing 0.5% triton X. The quantity of drug in the dissolved pellets or supernatants was determined with UHPLC-UV with the gradient mode exposed in table 5-3.

5-3.2.4. Permeability studies with HDC/NPOE PAMPA

The procedure for PAMPA is the one described in chapter 2. Briefly, each well of a PVDF 96-wells microtiter filter plate was impregnated with 15 µl of a 35% (v/v) liquid membrane composed of 75% hexadecane and 25% o-NPOE dissolved in hexane. This donor plate was left under the extractor hood for 15-20 minutes to completely evaporate hexane. A Teflon® 96-wells acceptor plate was filled with 280 µl of a buffer containing 5% DMSO. The donor plate was placed upon the acceptor plate in a "sandwich-like conformation" and filled with 280 µl of the solution containing the compounds to test, called "donor solution". The resulting sandwich was incubated for 7 hours at 20°C and under constant stirring at 150 rpm. Each permeability determination was determined in quadruplicate. The donor solutions varied upon the test to be performed and are detailed in the following paragraphs.

5-3.2.4.1. HDC/NPOE PAMPA with non-loaded liposomes

The donor solutions were composed of various concentrations of 10 mg/ml non-loaded liposomes suspension (from 0.1% to 50%) in pH 7.4 phosphate buffer and in presence of free drug with a final concentration of 5% DMSO. The drugs tested were diazepam, hydrocortisone, warfarin, caffeine, carbamazepine, propranolol, lidocaine, nicotine, antipyrine and pindolol. Following incubation, the absorbance of the free drug was determined in 200 µl of the donor, acceptor and reference solutions, at their maximum wavelength of absorbance with a PowerWaveTM spectrometer (BioTek Instruments, Inc., Winooski, USA).

5-3.2.4.2. HDC/NPOE PAMPA with non-loaded rhodamine-labeled liposomes

The donor solution is constituted of various concentrations of labeled liposomes (Rholiposomes): 0.1%, 0.5%, 1%, 2% or 5% (v/v) of 10 mg/ml suspension of Rho-liposomes in pH 7.4 buffer, with a final concentration of 5% DMSO. All along the experiment, the sandwich was protected from light with aluminum, due to the fluorescent property of rhodamine.

Following incubation, 200 μ l of the donor, acceptor and reference (donor at time t = 0) solutions were transferred in a 96-wells MaxiSorp Nunc multiwell plate and treated with 0.5% triton X to solubilize the liposomes. The fluorescence was determined at λ_{exc} = 485 nm and λ_{em} = 560 nm with a Microplate fluorescence reader FLx800 (BioTek Instruments, Inc., Winooski, USA).

5-3.2.4.3. HDC/NPOE PAMPA with calcein-loaded liposomes

The donor solutions were constituted of either 10; 25; 50 or 95 % of 10 mg/ml suspension of calcein-loaded liposomes in pH 7.4 buffer, with a final concentration of 5% DMSO in pH 7.4 phosphate buffer. Following incubation that occurred protected from light, fluorescence was determined in 200 μ l of the donor, acceptor and reference solutions, previously treated with 0.5% triton X, at λ_{exc} = 485 nm and λ_{em} = 528 nm.

5-3.2.5. Permeability studies with PAMPA-BBB

Drug-loaded liposomes, as well as non-loaded liposomes in presence of free drugs. were tested on PAMPA-BBB 90. In this model, a Teflon® plate (Millipore) is filled with the donor solutions (either a buffered solution pH 7.4 containing 0.5% of a DMSO stock solution of free drug, or a buffered solution containing 0.5% of a DMSO stock solution of free drug and 50% v/v of 10 mg/ml suspension of unloaded liposomes, or a buffered solution containing 0.5% DMSO and 50% v/v of 10 mg/ml suspension of drug-loaded liposomes. A hydrophobic polyvinylidene fluoride microfilterplate (Millipore, MAIPN4550) was coated with 4µl of an artificial membrane composed of 20 mg/ml porcine brain lipids (Avanti Polar lipids,Inc) dissolved in dodecane and imbricated in the Teflon® plate to form the acceptor compartment. The acceptor solution is composed of a phosphate buffer pH 7.4. The sandwich was incubated for 18 hours without stirring. Following incubation, the sandwich was disassembled and 200 µl of each solution in the donor and acceptor compartments was transferred in a 96-wells multiplate. 10 µl of a 10% v/v triton X solution was added in each wells in order to solubilize the liposomes and liberate the incorporated drug in solution. The concentrations of the donor and acceptor compartments, as well as the concentration of the reference solutions (donor solution at time t=0min) were determined using an Acquity UHPLC-UV system (Waters, Milford, USA) coupled with a PDA detector with the method exposed in paragraph 5-3.2.6.

Permeability coefficients were determined with Equation 5-2.

5-3.2.6. Quantification with UHPLC-UV

UHPLC-UV was employed as a detection technique for the determination of the entrapment yield, the drug release and drug diffusion studies as well as the permeability assessments with PAMPA-BBB. A UHPLC system (Waters, Milford, USA) coupled with a PDA detector was employed to determine the concentrations of compounds in the supernatants and in the dissolved liposomes. The UHPLC column was a BEH shield $50 \text{mm} \times 2.1 \text{ mm}$, with $1.7 \mu \text{m}$ pore size. The column was kept at $40 \, ^{\circ}\text{C}$, with a mobile phase flux of $500 \mu \text{l/min}$. The mobile phase is constituted of a mixture of $0.1 \, ^{\circ}\text{M}$ formic acid in $0.22 \, \mu \text{m}$ filtered water and methanol. The gradient mode detailed in table 5-3 was employed as a standard method.

Table 5-3: Details of the gradient employed for the analysis of free drugs in liposomes.

Time (min)	0.1% formic acid in water	% Méthanol
0	95	5
3	5	95
4	5	95
4.3	95	5
6.3	95	5

5-3.2.7. Transmission Electron Microscopy (TEM)

TEM is a physical technique able to visualize very small particles or cells. In TEM, an electronic beam is transmitted through a very thin sample, stained with uranyl sulfate.

First of all, the thin layer of carbon coating the TEM copper grids (200 mesh) is ionized to generate a hydrophilic surface necessary for the analysis of aqueous samples. $5 \,\mu$ l of sample is then deposited as aqueous suspension on the pretreated grids and let absorbed for 30 seconds. The surplus of liquid is blotted off on a filter paper. The grid is then placed on a first drop of uranyl acetate 2% and let stained on a second drop of uranyl acetate for 30 seconds. The exceeding uranyl acetate is blotted off on a filter paper, and the resulting grid is analyzed with TEM (EM Tecnai G2, FEI Company, Hillsboro, USA).

5-3.3. Polymeric nanoparticles

5-3.3.1. Formulation

Nanoparticles were prepared by nanoprecipitation. Briefly, the organic phase, a solution of PLGA and the active compound in acetone was mixed in an aqueous solution of PVAL 0.4% w/w. In order to form the nanoparticles, the organic phase is added dropwise in the PVAL aqueous solution under stirring for 12 hours, in order to completely evaporate acetone. This leads to the precipitation of the nanoparticles, as the polymer is insoluble in water. The resulting nanoparticles are then washed 3 times with fresh MilliQ® water by centrifugation at 4°C during 20 minutes and at 12000 rpm (12200 g, Beckman rotor F1010). The resulting suspension can then be lyophilized for future experiments (Edwards, Modulyo K4, Oberwil, Switzerland).

The preparation of the loaded nanoparticles was performed in the School of Pharmaceutical Sciences in Geneva, in the Laboratories of Pharmaceutical Technology, and part of a Master thesis ⁹¹. 13 diversified drug compounds have been tested for incorporation inside polymeric nanoparticles, namely antipyrine, caffeine, carbamazepine, diazepam, dioctadecyloxacarbocyanine perchlorate (DIO), hydrocortisone, lidocaine, loperamide, lucifer yellow, nicotine, pindolol, propranolol and warfarine.

5-3.3.2. Entrapment efficiency and entrapment yield

Like liposomes, nanoparticles are characterized by their size and their polydiversity index, but also by the entrapment efficiency (EE) and the entrapment yield (EY). EE is defined as the amount of drug loaded experimentally by the initial amount of polymer ratio, whereas EY is the amount of recovered drug in the nanoparticles divided by the amount of drug initially used. A known amount of lyophilized nanoparticles is weighted and solubilized in 90% DMSO and 10% phosphate buffer pH 7.4, in order to solubilize the polymers and release the encapsulated drug. The concentration of drug compound in solution is measured with HPLC-UV described in paragraph 5-3.3.4.

5-3.3.3. Formulation of fluorescent-loaded or fluorescent labeled nanoparticles

Rhodamine-labeled polymer was employed to formulate a fluorescent labeled batch of nanoparticles, whereas DIO was employed as fluorescent cargo. The protocol is the same as for usual nanoparticles, except the addition of 5% w/w chemically-labeled polymers with RG502 kindly provided by Pr Luca Costantino (University of Modena, Italy) for the preparation of rhodamine-labeled nanoparticles. HDC/NPOE PAMPA is performed with different concentrations (from 0.5 to 5 mg/ml) of these rhodamine-labeled or DIO-loaded nanoparticles.

5-3.3.4. Characterization

The size and size distribution (polydispersity) of each suspension was determined with a Zetasizer® 3000 HSA (Malvern Instruments; Worcestershire, UK).

A high pressure liquid chromatography (HPLC) (Merck-Hitacki) system with a Xbridge C18 column (10 cm, internal diameter = 4.6 mm, particle size 3.5 μ m) was employed to determine the concentrations of free drug in each compartments of PAMPA. The 3 solutions were analyzed with an isocratic mode. Mobile phase was constituted of 50% acetonitrile / 50% water for diazepam, 35% acetonitrile / 65% water for carbamazepine, and 55% acetonitrile / 45% water for warfarin.

Scanning electron microscopy (SEM) was used to characterize the morphology of the nanoparticles. Samples were diluted in distilled water, dried and covered by a thin gold layer with Leica EM SCD 500 coater for 20 s at 44 mA. They were then observed with a JSM-6300 scanning electron microscope (JEAOL, Tokyo, Japan).

5-3.3.5. Permeability studies with HDC/NPOE PAMPA

Donor solutions were either composed of a free drug solution in pH 7.4 phosphate buffer, with a final concentration of 5% DMSO, or a solution composed of 2 mg/ml empty nanoparticles in presence of the drug to be tested, with 5% DMSO, or a suspension composed of 2 mg/ml drug-loaded nanoparticles in presence of 5% DMSO. Following incubation, the donor, acceptor and reference solutions were diluted with DMSO, to reach a final concentration of 90% v/v in DMSO. This composition of DMSO was shown to solubilize the polymers and liberate the incorporated active compound. The absorbance of the free drug was determined in 200 µl of the donor, acceptor and reference solutions, at their maximum wavelength of absorbance with a PowerWaveTM spectrometer (BioTek Instruments, Inc., Winooski, USA) or with the HPLC method described in paragraph 5-3.3.4.

For the fluorescent dye (rhodamine and DIO), the detection after incubation time is performed by fluorescence with a Microplate fluorescence reader FLx800 (BioTek Instruments, Inc., Winooski, USA) at λ_{exc} = 485 nm and λ_{em} = 560 nm for rhodamine, and at λ_{exc} = 485 nm and λ_{em} = 528 nm for DIO.

5-3.3.6. Permeability studies with hCMEC/D3 cell line

hCMEC/D3 cell line was a kind gift of Pierre-Olivier Couraud's lab (Institut Cochin, Paris, France). All experiments were conducted by Dr Florence Miller, from the Laboratories of Pharmaceutical Technology in the School of Parmaceutical Sciences of the University of

Geneva and University of Lausanne (Geneva, Switzerland) according to the protocol described by Weksler *et al.* ⁸⁸.

Concentration tested on the cells was of 1 mg/ml of drug-loaded nanoparticles. All concentrations were measured by UHPLC/MS (Thermo Fisher Scientific, CA, USA), with the gradient mode applied in table 5-3.

5-3.4. Permeability equations

Equation 5-2 employed to calculate the permeability coefficients are derived from the Fick's laws ⁹² and are consistent with the experimental setup of the experiment (isopH and no sink conditions).

$$P_{e} = -\frac{2.303V_{D}}{A\left(t - \tau_{lag}\right)} \left(\frac{V_{A}}{V_{A} + V_{D}}\right) \log \left[1 - \left(\frac{V_{A} + V_{D}}{V_{D}\left(1 - R\right)}\right) \frac{C_{A}\left(t\right)}{C_{D}\left(0\right)}\right]$$
(Equation 5-2)

Where V_A and V_D are the volume of the acceptor and donor solutions in the assay respectively (280 µI); $C_A(t)$ is the concentration in the acceptor compartment after incubation, while $C_D(0)$ is the concentration of the reference solution, which is the donor solution before the beginning of the assay; t is the incubation time in seconds; τ_{lag} is the lag-time, meaning the time needed for a molecule in solution to reach the artificial membrane. In PAMPA experiment, this lag time is expected to be less than 20 minutes, which is negligible compared to the duration of the assay. R is the retention, characterized as the mass balance between the amount of compounds introduced at the beginning of the experiment $(n_D(0))$ and the sum of the amounts retrieved after incubation in both donor and acceptor compartments $(n_A(t) + n_D(t))$ (equation 5-3).

$$R = 1 - \frac{C_D(t)}{C_D(0)} - \frac{V_A C_A(t)}{V_D C_D(0)}$$
 (Equation 5-3)

5-4. Results and discussions

5-4.1. Liposomes

The dry-lipid film technique was employed in this study as a standard method for the fabrication of liposomes, and an optimization of the composition in phospholipids and of the treatments applied to form the liposomes has been performed in order to select the appropriate protocol for PAMPA analysis. Phosphatidylcholine was employed to form the liposomes. As cholesterol was found to play a role in the stabilization of the vesicles and in the maintenance of the cargo inside the inner chore, a variation of the proportion of cholesterol among phosphatidylcholine was performed (from 0% to 20%) ^{50, 93}. Post formation treatments applied to reach a desired size of liposomes, as well as homogeneity in the population of liposomes were also submitted to study.

5-4.1.1. Post formation treatments and liposome composition effects

In order to form liposomes with size as homogeneous as possible, and with unilamellar features, different treatments may be applied. For this study, 4 possible treatments have been applied to the basement liposomal solution composed of 100% PC: the freeze-thaw procedure followed by extrusion, the direct extrusion process, the filtration followed by extrusion or the sonication followed by extrusion, as described in paragraph 5-3.2.1.1. Moreover, the PVDF microfilter plate employed for PAMPA experiments have 450 nm pore size, therefore the size of the liposomes has to be below this threshold.

Polydispersity index (PI) characterizes the distribution of size of the sample around the mean value. This index ranging from 0 to 1 represents the dispersity of the sample, 0 being monodisperse and 1 very polydisperse or non-uniform.

Table 5-4 lists the size and PI of the liposomes obtained after the various treatments applied to the same batch divided in 4 subparts.

When direct filtration was used, size measurement was not possible with dynamic light scattering due to an insufficient number of liposomes in the Zetasizer. This means that no or only few liposomes were able to cross the 450 nm filter pores. A hypothesis could be

that just after liposomal formation, all or nearly all MLV are bigger than 450 nm. Therefore, under filtration, all liposomes are stacked on the filter. Therefore, this technique was abandoned.

The freeze-thaw procedure as well as the direct extrusion led to low PI for liposomes composed of 100% PC, even if liposomes were larger when directly extruded. The sonication followed by extrusion procedure formed small liposomes, but the PI indicated that the size of liposomes was not homogeneous in solution. Thus, the freeze-thaw procedure followed by extrusion and direct extrusion were chosen for the downstream processes of liposomes composed of PC and cholesterol. Sonication followed by extrusion was applied to a formulation, in order to verify the trend observed with 100% PC liposomes.

Table 5-4: Average size and PI of liposomes depending on the proportion of cholesterol and of the post formation treatment applied.

Liposome	composition	Post formation	6 : ()	Number of	Polydispersity
% PC	% cholesterol	treatment	Size (nm)	populations	index
100	0	filtration+extrusion	NM	NM	NM
100	0	extrusion	159	1	0.17
100	0	sonication + extrusion	140	1	0.32
100	0	freeze-thaw+extrusion	138	1	0.11
80	20	extrusion	177	1	0.18
80	20	sonication + extrusion	222	1	0.40
80	20	freeze-thaw+extrusion	211	1	0.25
90	10	extrusion	259	2	0.25
90	10	freeze-thaw+extrusion	229	1	0.17

NM stands for non-measurable data.

From table 5-4, it appears that the incorporation of cholesterol slightly modifies the size of the resulting liposomes. When sonication is applied after formation of the MLV, the liposomal solution is heterogeneous, as highlighted by the high PI comprised between 0.3 and 0.4. This observation was consistent with the dispersion that was already highlighted with 100% PC liposomes. Once again, the direct extrusion and the freeze-thaw procedure followed by extrusion appear to generate the most homogeneous populations of liposomes, with acceptable size ranges.

Liposomes prepared with 100% phosphatidylcholine appear to generate smaller vesicles, with a very homogeneous population, but when looking at the literature, cholesterol could help in stabilizing the membrane and decreasing the release of incorporated drug compounds out of the bilayer ^{50, 93, 94}. Hence, cholesterol integrates the bilayer its axe

perpendicular to the membrane plane, with its hydroxyl part facing the aqueous medium and the hydrophobic rings parallel to the hydrocarbonated chains of phospholipids ⁹⁵. The –OH group of cholesterol interacts with the polar part of phospholipids forming H-bonds (figure 5-5) thus stabilizing the bilayer and decreasing the free motion of the bilayer. Moreover, cholesterol-free liposomes tend to interact with plasma proteins, leading to a destabilization of the liposomes ⁹⁶. Therefore, in a drug discovery point of view, cholesterol may be essential to keep the cargo inside the nanocarrier until it reaches its target.

For further study, liposomes have therefore been prepared with 80% PC, 20% cholesterol, and with the direct extrusion as a downstream process.

$$\begin{array}{c} H_3C \\ H_3C \\ H_3C \\ \end{array} \\ \begin{array}{c} H_3C \\ \end{array}$$

Figure 5-5: Incorporation of cholesterol in the phospholipid bilayer

5-4.1.2. Optimization of the extrusion process

The extrusion process is made of many successive cycles with a mini-extruder (figure 5-6), in order to decrease the number of concentric bilayers to go from multilamellar vesicles to unilamellar vesicles, but also to decrease the size of the liposomes. In this study, the ideal size of liposomes was between 150 and 250 nm, therefore inert polycarbonate filters of 100 nm pore size have been employed. These inert filters act as mechanic modifiers. As phospholipids are in constant motion in the fluidic bilayer, the passage through the filter under pressure forces the deformation and the rearrangement of the phospholipids. This deformation may be viewed as an elongation through the filter, till the formation of a "new" liposome, generally with a smaller size. Performing successive cycles through the filter allows the formation of smaller and smaller liposomes till a plateau is reached.

Figure 5-7 represents the evolution of the size and PI of a batch of liposomes. This figure discloses that right after two extrusion cycles, a significant decrease in the size of

liposomes is obtained, as well as a net improvement of the PI. After four passages, there is a plateau, where liposomes seem to have reached the smallest size possible with the filters employed (100 nm) and the optimal PI. Therefore, 6 extrusion cycles will be performed for further preparation of liposomes.

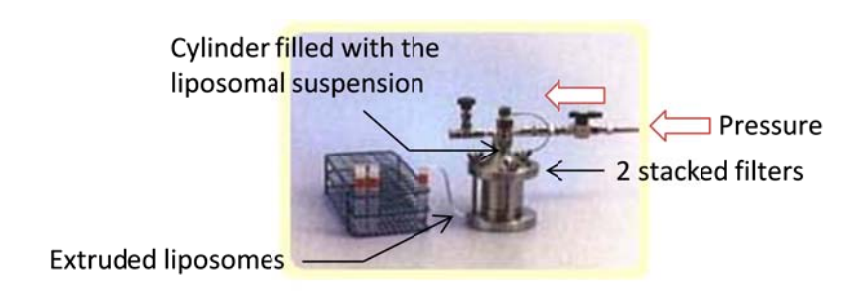


Figure 5-6: The Lipex biomembrane extruder, reproduced from www.lipex.com/extrusion.html (26.04.2013)

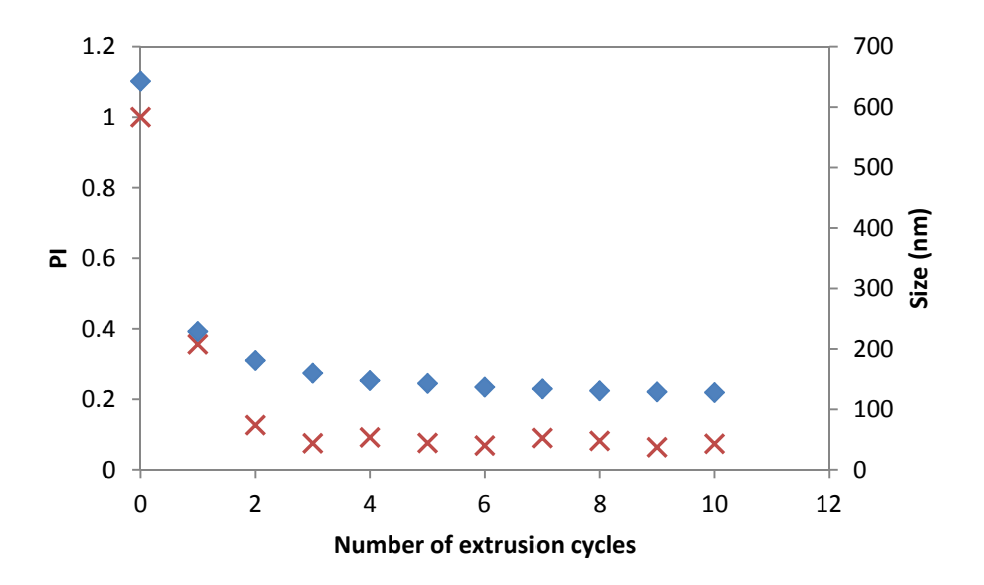


Figure 5-7: Evolution of the size and polydispersity index of liposomes right after formation (cycle 0) and after each cycle of extrusion. Red crosses represent the size of liposomes, blue squares are the PI.

5-4.1.3. Passive permeation study

The unclear mechanism of permeation of liposomes at the BBB exposed by many authors encouraged this study. Indeed, PAMPA is a tool that can clarify and isolate the passive transcellular diffusion part of colloidal formulations. Therefore, the HDC/NPOE PAMPA developed during this thesis has been employed to study a possible passive permeation of liposomes. In order to elucidate a possible exchange of phospholipids that can

occur *in vivo* between the biocompatible phospholipids of the liposomes and the phospholipids of cerebral endothelial cells, a further assessment of passive permeation with PAMPA-BBB, made with polar porcine brain phospholipids, has been performed.

5-4.1.3.1. HDC/NPOE PAMPA

<u>Determination of the integrity of the artificial membrane</u>

In order to be able to generate and discuss results with liposomes, an assessment of the integrity of the membrane was performed. Permeability of drug compounds in presence and in absence of unloaded liposomes are compared.

3 concentrations of unloaded liposomes have been tested: 1%, 0.5% and 0.1% v/v of 10 mg/ml liposomal suspension, in the presence of 10 compounds, namely diazepam, hydrocortisone, warfarin, caffeine, carbamazepine, propranolol, lidocaine, nicotine, antipyrine and pindolol. No permeability value could be determined for lidocaine, nicotine, diazepam and antipyrine in presence of 1% liposomes, and for diazepam in presence of 0.5% liposomes, due to experimental aberrant variations within the quadruplicates. The results are presented in figure 5-8.

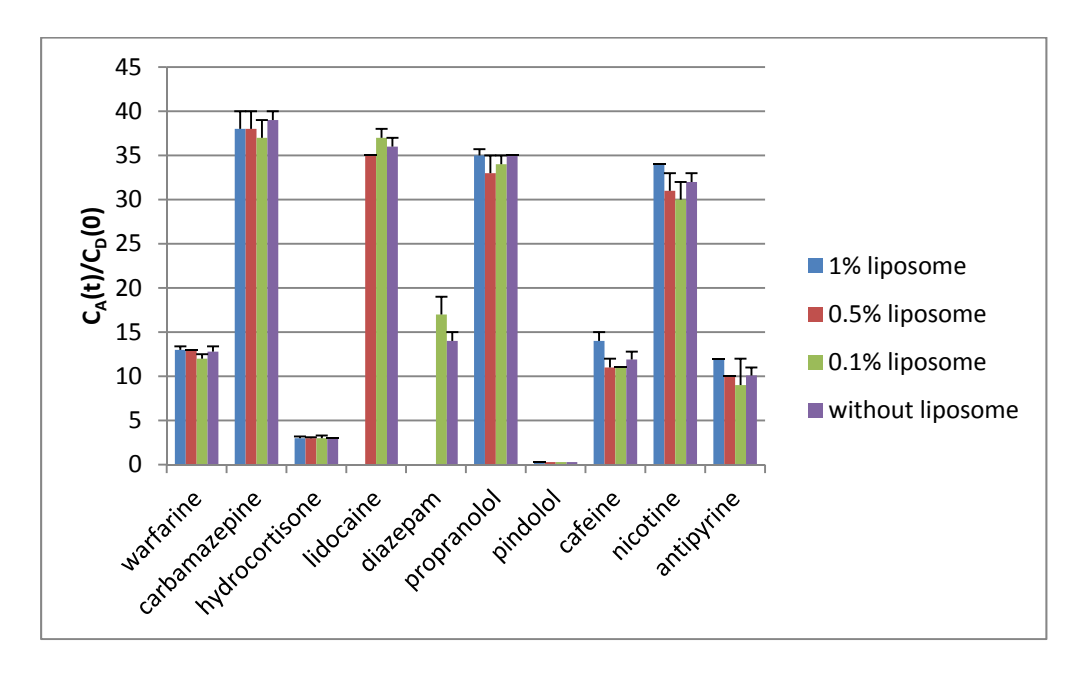


Figure 5-8 : Influence of the presence of different concentrations of unloaded liposomes on the passage $(C_A(t)/C_D(0))$ across HDC/NPOE PAMPA.

No significant differences in the percentages of passage generated in the presence of 0 to 1% empty liposomes in the medium was observed, as presented on figure 5-8. This means that liposomes do not damage the membrane, nor modify its properties up to 1% volumic concentration in the donor compartment. However, another test made with 6 compounds and the presence of 50% empty liposomes in the donor compartment leads to different conclusions. Indeed, figure 5-9 highlights that 50% empty liposomes in the donor compartment decrease the global permeability of the free drug which are known to cross the membrane (carbamazepine, diazepam, imipramine, verapamil), but it does not impact the compounds which did not cross the membrane (pindolol and dopamine). Hence, up to a certain percentage of liposomes in suspension, the free drug carries on crossing the membrane depending on its intrinsic physicochemical properties. As soon as the number of liposomes becomes non-negligible, new equilibria are created in the donor compartments: there is a competition between the affinity for the membrane (log Pe) and the affinity for the vesicle. Moreover, the time needed to reach the membrane through a suspension of liposomes may be higher. All these combined causes lead to slower permeation across the membrane, which is illustrated in figure 5-9. But this loss of permeability is not due to a degradation or modification of the membrane, since non-permeant compounds have the same behavior in presence or absence of unloaded liposomes (nearly 0% of passage).

Therefore, for the rest of the study, a limited percentage of liposomes have been introduced in the HDC/NPOE PAMPA model.

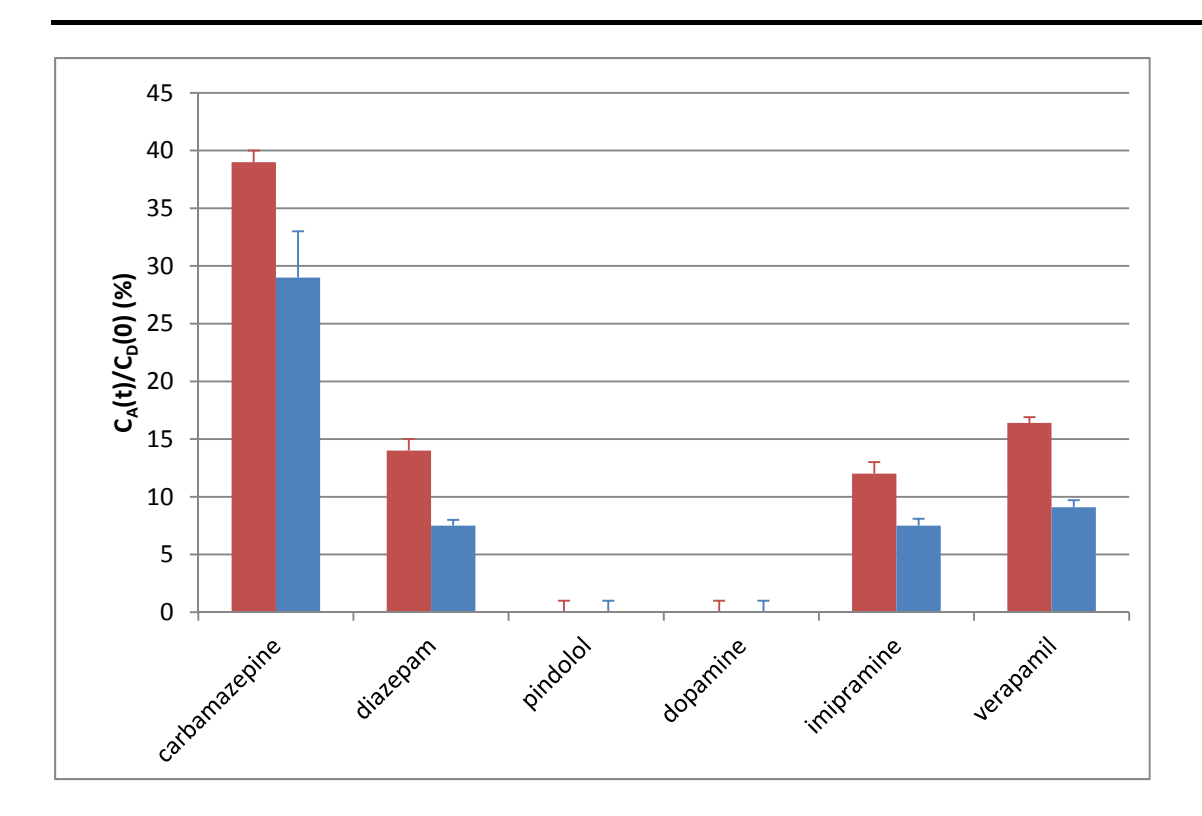


Figure 5-9: Comparison between $C_A(t)/C_D(0)$ obtained in presence or in absence of 50% empty liposomes. Red bars represent the percentage of passage of free carbamazepine, diazepam, pindolol, dopamine, imipramine and verapamil on HDC/NPOE PAMPA while the blue bars are the percentage of passage of the free drugs in presence of 5 mg/ml unloaded liposomes.

HDC/NPOE PAMPA with empty labeled liposomes

In order to evaluate the ability of liposomes to interact with the membrane, liposomes prepared with rhodamine tagged PC have been tested on PAMPA. Table 5-5 compiles the passages and retention measured for various concentrations of rhodamine-labeled liposomal suspensions in pH 7.4 phosphate buffer containing 5% DMSO.

The results indicate a minor passage of the liposomes through the membrane. The higher passage observed for the lowest concentrations of labeled liposomes is explained by very low fluorescence signals, leading to a higher experimental error of detection. When tested by dynamic light scattering, no signal was found in the acceptor wells. Therefore, it may be concluded that either the liposomes have not crossed the artificial membrane, or the concentration of liposomes was too low to be detected by dynamic light scattering. Moreover, the retention, characterized as the percentage of the reference solution which is not recovered in the donor and acceptor solutions after incubation, is important. This negative mass-balance may be explained by 3 hypotheses: i) liposomes may be trapped in the membrane; ii) liposomes may be adsorbed on the material constituting the donor compartment; iii) liposomes may deposit on the filter, creating a non-homogeneous suspension. The physicochemical nature of liposomes in one side (polar surface), and of the

artificial membrane in another side (hydrophobic), could influence to put aside the first hypothesis. But due to the fluidity of liposomes membrane, the exact mechanism by which liposomes interact with membranes and succeed in crossing biological barriers is not defined and unclear, the bilayer may still interact with the membrane with phospholipids changing their conformation and facing their hydrophobic part toward the hydrophobic membrane.

Table 5-5: Percentages of passage and retention measured for various concentration of rhodamine labeled liposomes by fluorescence.

concentration in Rho-liposomes	C _A (t)/C _D (0) (%)	Retention (%)
5%	0.86±0.03	69±1
2%	0.88±0.01	84±1
1%	0.82±0.02	83±1
0.5%	2.34±0.04	86±1
0.1%	3.3±0.9	79±1

HDC/NPOE PAMPA with calcein-loaded liposomes

Calcein has been readily employed as a marker of the internal aqueous volume of liposomes. This fluorescent probe is sensitive to the aqueous pH, and is soluble at physiological conditions ^{97, 98}. At pH 7.4, calcein is mostly negatively charged. Therefore, when encapsulated into liposomes and as a highly polar molecule, calcein should be maintained in the inner aqueous cavity of the liposome. The presence of 5% DMSO in the medium may also have an influence on the release of the cargo. But a study of the effect of DMSO on the release of calcein out of 100% PC liposomes made by Catherine a Marca Martinet during her PhD thesis concluded that 5% DMSO in the medium rather had a stabilizing effect, limiting calcein release compared to the absence of DMSO ⁹⁹. Moreover, the very high hydrophilicity of calcein limits the permeation of this molecule through the hydrophobic artificial membrane under its free form. Therefore, if calcein is recovered in the acceptor compartment after the 7 hours incubation time, this would be under a loaded-liposomal form.

Table 5-6 compiles the passages measured with different proportions of 10 mg/ml calcein-loaded liposomal suspension in the donor solutions. The tested concentrations are intentionally high to be able to detect very small amount of liposomes in the acceptor compartments. Nethertheless, no signal was observed, indicating that no calcein-loaded liposomes are detected in the acceptor compartment. This observation was corroborated with the absence of signal in dynamic light scattering. The non-negligible retention that are found may result from liposome trapping at the membrane

Table 5-6: Passages measured with calcein-loaded liposomes on HDC/NPOE PAMPA

% liposomes (v/v)	$C_A(t)/C_D(0)$ (%)	Retention (%)
10	<0.1	16±5
25	<0.1	16±3
50	<0.1	13±1
95	<0.1	12±9
free calcein	<0.1	9±1

The failure of rhodamine-labeled liposomes as well as calcein-loaded liposomes to cross the artificial membrane can be in part explained with the physicochemical properties of the liposomes. The artificial membrane is composed of hexadecane and o-nitrophenyloctyl ether, which are hydrophobic components, whereas the outer surface of liposomes is hydrophilic. Therefore, the interactions between the liposomes and the membrane may be limited and considered as the rate limiting step in the permeation of such liposomes.

To conclude, preliminary tests combining empty liposomes with free drugs indicated that liposomes do not modify the properties of the HDC/NPOE artificial membrane, as soon as less than 1% empty liposomes are in suspension in the medium. However, tests with labeled liposomes, as well as calcein-loaded liposomes exhibit no effective permeability of the nanocarriers through the artificial membrane. Therefore, this PAMPA model of estimation of the BBB permeability cannot be employed to understand the mode of penetration of liposomes through the BBB. This is likely to be caused by physicochemical incompatibility between the liposomes and the full solvent artificial membrane. A second PAMPA model has therefore been tested: PAMPA-BBB ⁹⁰, in order to assess a possible phospholipid exchange. In this model, the membrane contains porcine polar brain phospholipids. Therefore, phospholipids of the liposomes may interact with the phospholipids of the membrane, possibly exchanging each other with a flip-flop process or fusing with the membrane.

5-4.1.3.2. PAMPA-BBB

To assess a possible passive permeation of the liposomes at the BBB *via* membrane fusion, compounds with different BBB permeabilities will be loaded in liposomes composed of 80% PC and 20% cholesterol and tested with PAMPA-BBB. Diazepam, dopamine, imipramine, calcein and fluorescein have been selected for this study.

Calcein and fluorescein are considered as markers of the internal aqueous core of the liposomes. Diazepam was chosen due to its significant passive permeability through the BBB in its free form, as well as its high retention. The incorporation inside liposomes would thus decrease membrane retention and increase its bioavailability. The selection of dopamine was based on its importance as a neurotransmitter and its high potency for CNS treatments such as Parkinson's disease, but it fails to cross the BBB. The interest of the incorporation inside liposomes is therefore to increase the BBB permeability of dopamine. Imipramine was chosen because of its high passive permeability through the BBB, without disclosing retention. This compound can be considered as a positive control, and the incorporation may have either no impact, a negative impact or even increase the permeability, depending on how fast the imipramine-loaded liposome is able to cross the artificial membrane.

Entrapment yield and drug release from liposomes

Before performing PAMPAs experiments, a determination of the entrapment yield of each liposomal formulation has been performed to evaluate the feasibility of the permeability study. Indeed, liposomes have to be sufficiently loaded in order to be able to detect the free compound after PAMPA. A diffusion study was also executed in order to determine the amount of drug that freely cross the liposome bilayer (in or out) within the 18 hours incubation time of PAMPA-BBB.

Entrapment yield (EY)

Table 5-7 describes the entrapment yield of each drug-loaded batch of liposomes. EY varied from 0.4% to 42%. The compounds showing the lowest incorporation (dopamine and fluorescein) were the most hydrophilic compounds. Indeed, dopamine (log P = -0.9) and fluorescein (sodium salt) are prone either to incorporate on the aqueous inner core of the liposomes, or to stay outside the liposome. Therefore, if a large quantity of dopamine or fluorescein stays outside the liposomes, this amount will be washed out during the purification steps. Diazepam and imipramine are lipophilic molecules, which are dissolved with the phospholipids in the organic phase during the formulation of the liposomes. Therefore, when hydration occurs and liposomes are formed, their incorporation inside the liposomes is easier than for a molecule which would have been incorporated in the aqueous phase, especially if this phase highly dilutes the phospholipidic film. The high EY recovered for calcein is more surprising, since calcein was introduced in the aqueous phase during the

fabrication of the liposomes as fluorescein and dopamine were. But the complexity to wash out calcein during the various centrifugation step may have led to experimental variation. Residual calcein may stay adsorbed on the polar head of the phospholipids after centrifugation and therefore increase the concentration of calcein thought to be incorporated inside the liposomes. The very low EY of dopamine made it difficult to carry on investigations with these liposomes. Hence, the quantity of dopamine incorporated inside the liposomes is below the limit of detection of UHPLC-UV. Therefore, dopamine-loaded liposomes were not considered for further studies. Regarding fluorescein, even if a very low amount of entrapped drug was determined compared to the quantity initially added, this was sufficient for an efficient detection with UHPLC-PDA, since the amount contained inside the liposomes was superior to 10 times the limit of detection of fluorescein with UHPLC-UV.

Table 5-7: Average size and entrapment yield of the drug-loaded liposomes.

compounds	size (nm)	EY(%)
Calcein	171	42.4
Diazepam	190	11.0
Dopamine	190	0.4
Fluorescein	175	0.4
Imipramine	200	15.5

Drug release from the loaded-liposomes

A drug release study has been implemented to observe a potential leakage of drug outside the loaded-vesicle. Results of this study are compiled in figure 5-10.

When looking at the increase or decrease of the concentration of free drug in the supernatant (dashed bars), figure 5-10 indicates that there is no significant release of diazepam out of the loaded liposomes. When looking at the full bars for diazepam, a tendency appears, and it seems that the quantity of diazepam inside the liposomes is decreasing for the first 5 hours and then increase at 18 hours. But regarding the standard deviations, these variations are not statistically significant. This is corroborated by the evolution of the concentration of diazepam in the supernatant along the time.

On the other hand, a significant increase of the concentration of imipramine, calcein and fluorescein in the supernatant is observed after 18 hours. This increase of free drug in the supernatant is associated with a decrease of quantity in the pellets. This drop in the pellets is clearly visible for calcein and fluorescein. For calcein, it seems that the concentration of free drug found in the supernatant is constant for the first 5 hours, and that the increase in concentration is found after 18 hours. That tendency is also observed for

imipramine. Therefore, it seems that diffusion of imipramine and calcein is negligible for at least 5 hours, and that drug release begins to appear between 5 and 18 hours incubation. This observation can be corroborated by a decrease in the concentration of calcein in the pellets after 18 hours, but when looking at the full bars for imipramine, it seems that the quantity of imipramine in the pellets at 18 hours incubation increases, even if the concentration in the supernatant augments. This artifact may be due to a strong extinction coefficient of imipramine. Therefore, small errors of manipulation or in the determination of the absorbance may lead to a strong variation in the result. Experimental errors are likely to be more important in the determination of the concentration inside the liposomes, since the separation of the supernatant from the pellets is delicate. Therefore, for imipramine, the discussion was only based on the evolution of the concentration in the supernatant. Concerning fluorescein, it seems that a gradual release process exists as soon as the liposomes are in solution, illustrated by the constant increase of fluorescein concentration in the supernatant, in parallel with a constant decrease in the concentration inside the liposomes.

To conclude, diazepam, imipramine and calcein appear to stay incorporated inside the liposomes at least for the first 5 hours, but imipramine and calcein are found to slightly diffuse out of the liposomes after 18 hours. For fluorescein, the diffusion occurs constantly since the beginning of the incubation.

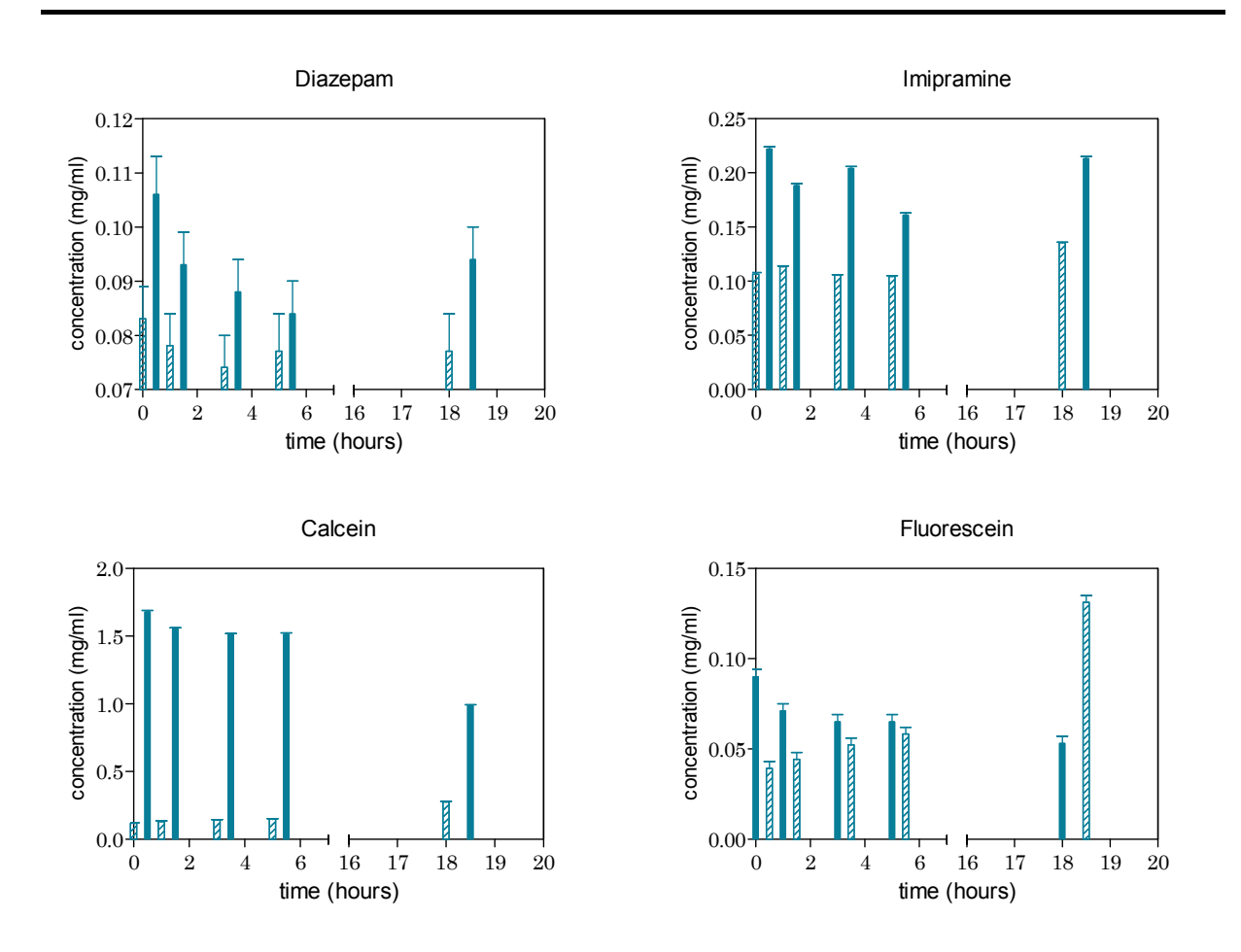


Figure 5-10: Results of the drug release study for diazepam, imipramine, calcein and fluorescein. The dashed bars correspond to the concentration of free drug in the supernatant while the full bars are the concentration of free drug in the pellets of liposomes.

Drug diffusion in unloaded liposomes

In order to explain a possible equilibrium between a free drug in solution and unloaded liposomes, buffering solution containing 0.5% DMSO and a known concentration of free drug was mixed with unloaded liposomes. Results are compiled in figure 5-11.

Results show that *a priori* no diffusion of free drug from the buffered solution to the inner core of the liposome occurs, since the concentration found in the pellet and in the supernatant is constant over time. However, a basal quantity of free drug seems to be either adsorbed or incorporated in the pellets rapidly within the first hour. This quantity corresponds to 5 to 10% of the initial concentration added (table 5-8 and figure 5-11).

Table 5-8: Numerical results of the diffusion study in the liposomes. For each active compound, the concentration of free drug was determined with UHPLC-PDA in the supernatant and in the pellets after various incubation times, and after centrifugation for 1 hour at 30000rpm and 4°C. The percentage of free drug contained in/on the pellets was also calculated.

	Concentration of diazepam (µg/ml)			Concentration of imipramine (µg/ml)			Concentration of calcein (µg/ml)		
Incubation time (hour)	supernatant	pellet	Percentage in pellets	supernatant	pellet	Percentage in pellets	supernatant	pellet	Percentage in pellets
0	276±12	-	-	85±1	-	-	455±8	-	-
1	263±12	17±4	6	85±1	5±1	6	486±8	39±6	7
3	275±12	15±4	5	78±1	7±1	8	451±8	30±6	6
5	259±12	11±4	4	78±1	6±1	7	438±8	35±6	7
7	227±11	19±4	8	81±1	8±1	9	447±8	30±6	6
18	242±11	19±4	7	80±1	7±1	8	427±8	41±6	9

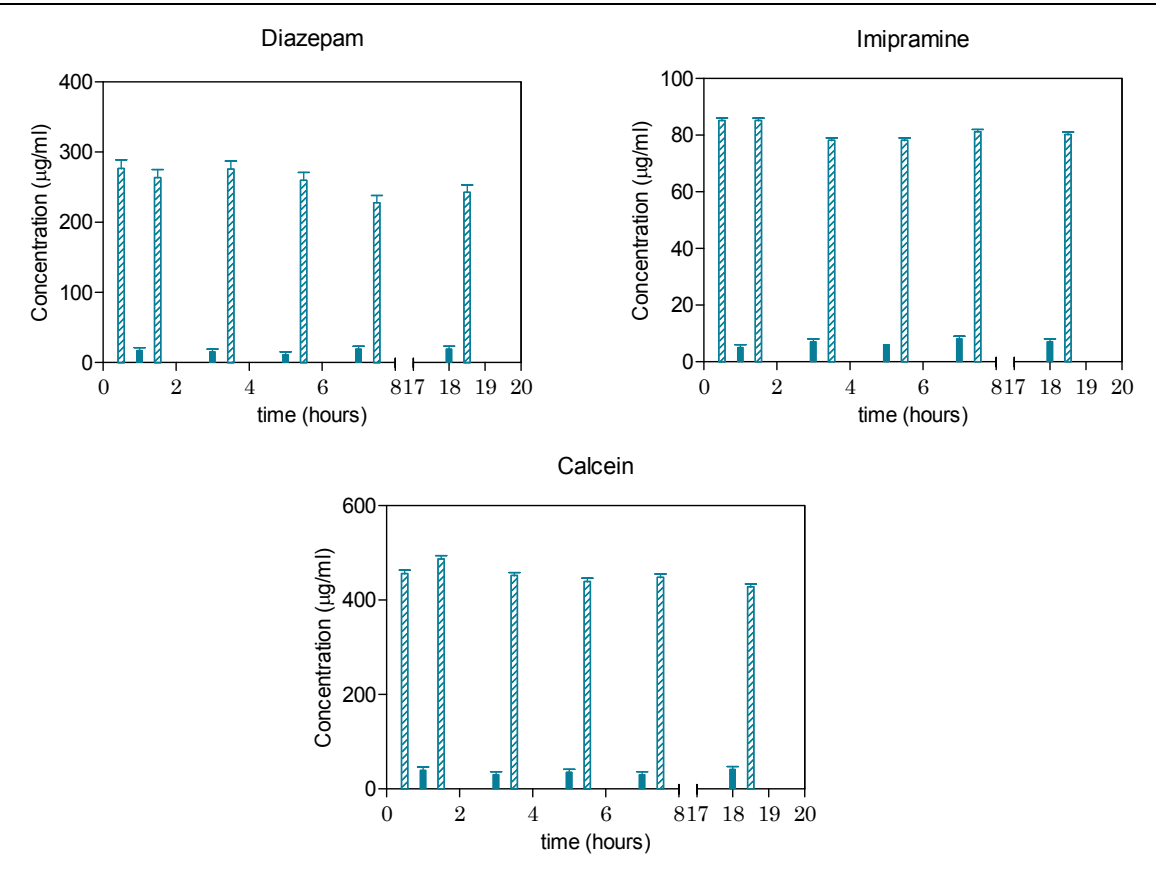


Figure 5-11: Graphical results of the drug diffusion in the unloaded liposomes. Dashed bars correspond to the weight of free drug in the supernatant while the full bars are the weight of free drug in the pellets of liposomes.

Permeation study

A comparison of the permeability of the free drugs in presence and in absence of unloaded liposomes allows an assessment of the integrity of the artificial membrane, as well

as possible interactions between the free drug and the unloaded liposomes. Moreover, the effect of the encapsulation in liposomes is determined with the measurement of the permeability of drug-loaded liposomes. If liposomes are able to interact with the artificial membrane, the permeability of the compound should vary in its free form and in its loaded form. As PAMPA-BBB is only able to predict passive permeation through the BBB, an enhanced permeability with the drug-loaded liposomes would be a sign of fusion or exchanges between liposomal and membrane phospholipids.

Integrity of the membrane

The permeation of the free drug is significantly decreased in presence of 50% v/v of 10 mg/ml unloaded liposomes (table 5-9 and figure 5-12). This indicates that interactions are occurring between the free drugs and the unloaded liposomes or that the properties of the artificial membrane are modified. When performing the diffusion study of the free drug from outside to inside empty liposomes, we concluded that no significant diffusion of the free drug occurred during the incubation, but a certain quantity, corresponding to 5 to 10% of the total amount of free drug, is recovered in the pellets after 1 hour incubation. This quantity can either be rapidly adsorbed at the surface or incorporated inside the liposomes. But even if this diffusion or adsorption is taken into account, the permeability of the free drugs in presence of empty liposomes is still decreased. Therefore, 50% empty liposomes tend to modify the phospholipid artificial membrane. We reached the same conclusion with the fullsolvent artificial membrane. It was hypothesized with HDC/NPOE PAMPA that the lag time was probably higher due to the concentration of empty liposomes in suspension, slowing down the overall permeability coefficient (equation 5-2). Moreover, liposomes in suspension may also interact with this artificial membrane, constituted of phospholipids. A fusion process may occur between phospholipids of the artificial membrane and phospholipids of the liposomes. This process may modify the properties of the artificial membrane and slow down the permeation process of the free drugs. Regarding calcein and fluorescein, hydrophilic compounds which do not diffuse through the BBB, the presence of non-loaded liposomes in the donor compartment do not enhance the permeability of the free drug, which stays null. This piece of information reveals that the membrane is not damaged by the presence of liposomes and carries on preventing the passage of hydrophilic drugs. But it also highlights that the permeation process is modified for the hydrophobic compounds.

Table 5-9: PAMPA-BBB results of the free drugs, the free drugs in presence of empty liposomes, and the drug-loaded liposomes expressed in terms of permeability (Pe.10-6 cm/s), percentage of passage (Acc/ref) and percentage of retention. Results are expressed with their standard deviations.

	Free drug			Free drug +	Free drug + empty liposomes			Drug-loaded liposomes		
	Pe	$C_A(t)/C_D(0)$	R	Pe	$C_A(t)/C_D(0)$	R	Pe	$C_A(t)/C_D(0)$	R	
	(×10 ⁻⁶ cm/s)	(%)	(%)	(×10 ⁻⁶ cm/s)	(%)	(%)	(×10 ⁻⁶ cm/s)	(%)	(%)	
Diazepam	21.0±0.6	32±1	28±3	3.9±0	14±0	11±0	5.5±0.2	17.0±0.9	18±2	
Imipramine	19±1	26±1	38±1	2.4±0.2	10±1	11±1	4.3±0.1	13±1	26±6	
Calcein	0	0	12±9	0	0	18±9	0	0	17±3	
Fluorescein	0.10±0.03	0.5±0.2	1±1	0.14±0.04	0.7±0.1	<1	0.14±0.01	0.7±0.1	<1	

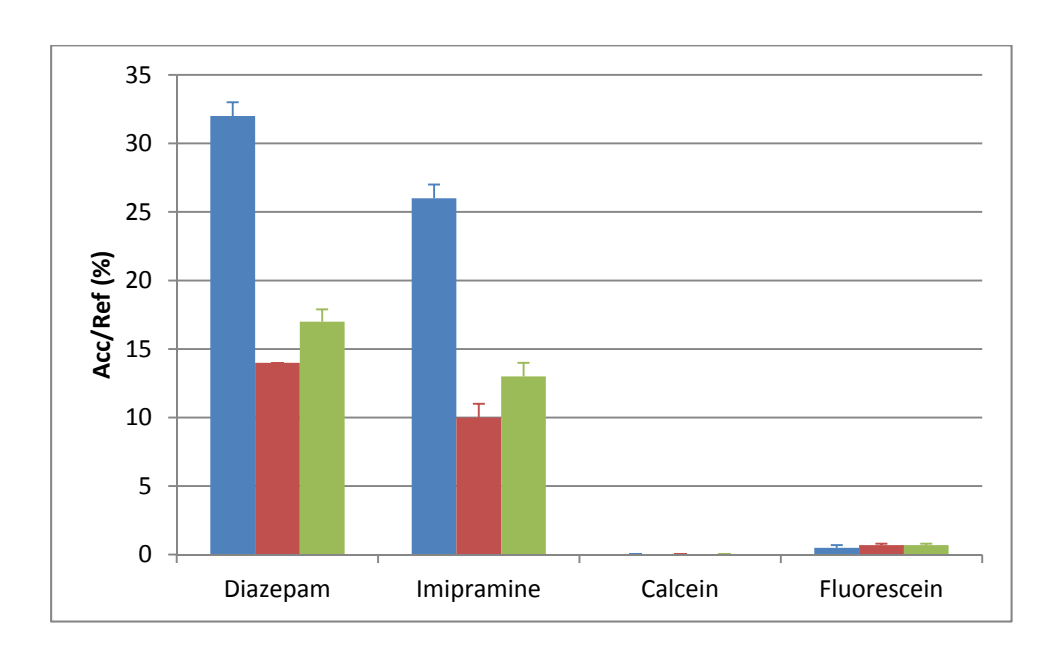


Figure 5-12: Percentage of passage of diazepam, imipramine, calcein and fluorescein through the phospholipid-based artificial membrane under their free form in presence (red bars) or in absence of unloaded liposomes (blue bars), and incorporated inside liposomes (green bars).

Effect of the encapsulation

When looking at the compounds that naturally diffuse through the BBB under their free form (diazepam, imipramine), encapsulation in liposomes has decreased their intrinsic permeability (figure 5-12 and table 5-9). When 32% of the free diazepam succeeds in crossing the phospholipid artificial membrane, only 17% of the diazepam incorporated inside the liposomes is able to permeate. The same report is made for imipramine: only half of the quantity that used to cross the membrane in its free form succeeds in reaching the acceptor compartment when incorporated inside the liposomes. On the other hand, permeability of non-permeant compounds (calcein, fluorescein) is not improved. The permeability observed

with diazepam- and imipramine-loaded liposomes may be caused by the permeation of the free drug that has diffused from the liposome, or by interactions between the phospholipids of the liposomes and those of the membrane, leading to a delivery of the free drug at the membrane.

The drug release study performed with drug-loaded liposomes in the same experimental conditions as PAMPA-BBB (pH 7.4 phosphate buffer, 0.5% DMSO) indicated that diazepam did not diffuse out of the liposomes, whereas imipramine presented a diffusion out of the liposomes (a 26% increase in the quantity of imipramine was found in the supernatant after 18 hours). Therefore, a part of imipramine permeation is due to this diffusion out of the liposome, but that cannot explain all the diffusion process. Moreover, a comparison of drug permeability under the free form in presence of empty liposomes and incorporated inside liposomes indicate a slight augmentation of permeation for the diazepam-and imipramine-loaded liposomes, associated with an increase in retention. Therefore, the permeation process of the drug-loaded liposomes cannot be reduced to the permeation of the free drug in presence of empty liposomes, meaning that another process than diffusion occurs at the membrane. This affirmation can be corroborated by the fact that diazepam did not diffuse out of the liposomes within the 18 hours of the incubation.

In order to understand what has happened at the phospholipidic artificial membrane, some solutions of acceptor compartments have been observed with transmission electron microscopy, in order to detect the presence of liposomal vesicles. Hence, the visualization of liposomes on the acceptor compartments would imply that liposomes were able to cross the phospholipid artificial membrane.

Transmission Electron Microscopy (TEM)

TEM is a physical technique able to visualize very small surfaces but also a difference on the composition of a particle. During the staining step, phospholipid bilayers will be marked by uranyl sulfate, enabling the vizualization of the successive bilayers.

Figure 5-13 represents a TEM image of the reference solution of diazepam-loaded liposomes. Vesicles with a homogeneous size are observed. Acceptor solutions corresponding to the permeability determination of diazepam-, calcein-, fluorescein- and imipramine-loaded liposomes have also been observed. Results are exposed in figure 5-14.

No vesicles were observed for imipramine- and calcein- loaded liposomes. For diazepam-loaded liposomes, amorphous conglomerates are observed, but no vesicles.

These agglomerates are thought to be fragments of liposomes, or assembly of phospholipids. Circular shapes have been observed only for fluorescein-loaded liposomes (figure 5-14b), but in very few amount. Regarding the size (~400nm), the identification of liposomes is questionable, since the measured size with Zetasizer® was between 200 and 250 nm. These vesicles may be the result of a reformation of liposomes after the passage through the artificial phospholipidic membrane.

The quantification after the PAMPA-BBB experiment indicate that passages of 13% and 17% imipramine and diazepam are observed when assessing permeation of diazepam and imipramine-loaded liposomes. That is far from what is observed on the TEM photos. Therefore, the permeability generated is likely to be the result of interactions between the phospholipids of the liposomes and those of the artificial membrane. An exchange between both types of phospholipids may have occurred, resulting in the delivery of the free drug at the membrane (either inside or out of the membrane). This whole process results in a slower permeation compared to the free drug.

Regarding fluorescein and calcein, even if interactions occur between the liposomes and the artificial membrane, the hydrophilic cargo will be liberated in the membrane or at the surface of the hydrophobic membrane. Therefore, permeation of such hydrophilic compounds is really slow or inexistant. If the whole liposome had been able to cross the artificial membrane, fluorescein or calcein permeation could have been identified, but in the absence of liposomes in the acceptor compartments, the present results are appropriate.

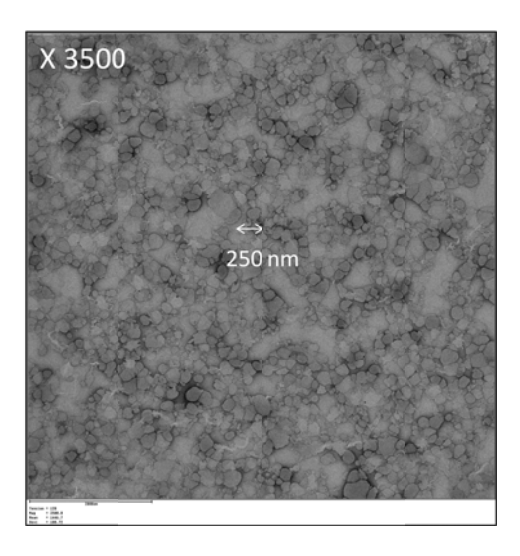


Figure 5-13: TEM photo of diazepam-loaded liposomes (reference suspension)

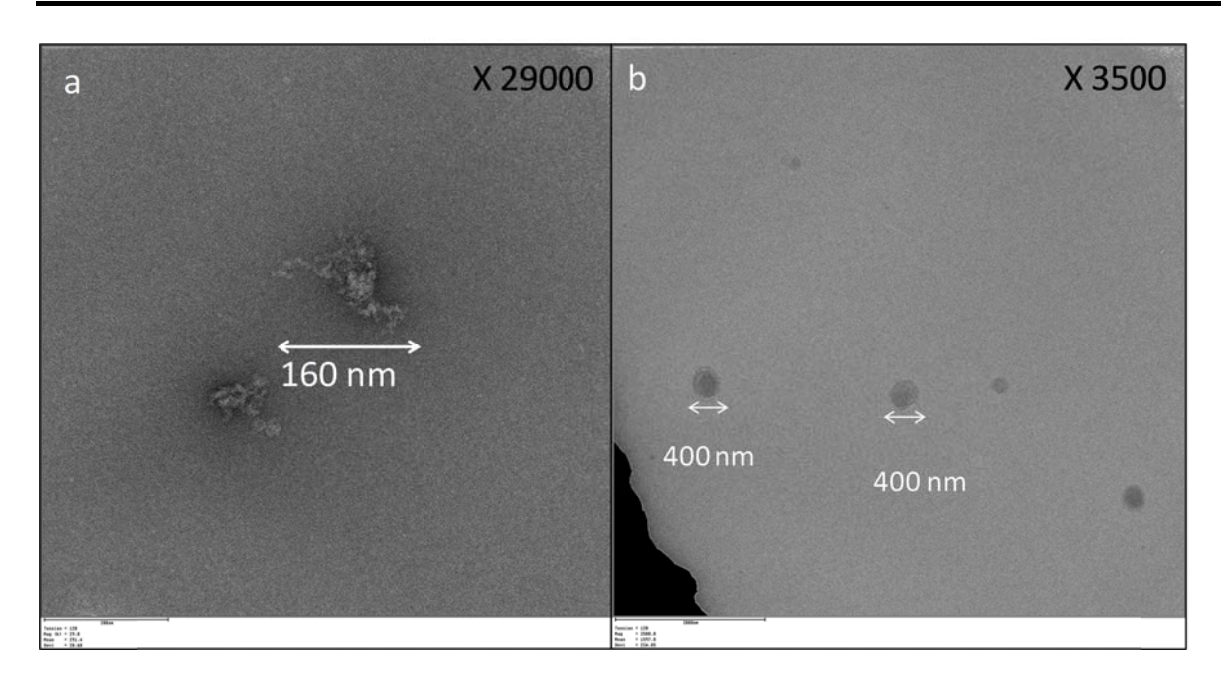


Figure 5-14: TEM of acceptor solutions after PAMPA-BBB. (a) represents the solution after permeation of diazepam-loaded liposomes, and (b) is for fluorescein-loaded liposomes.

5-4.1.4. Conclusion on the permeability of liposomes as drug carriers

The aim of this part of the chapter was to determine how liposomes may interact with biological barriers, with an attempt to understand how they can cross such membranes, as this point is still not clear. The starting point was the assumptions that liposomes could permeate through the BBB via either active processes such as endocytosis or passive processes $^{25, 69, 72, 81, 85, 86, 100, 101}$. PAMPA was therefore chosen to discuss on the passive part of the debate. Two different PAMPA assays have been employed. The first one, developed during this thesis, is a full-solvent artificial membrane, able to estimate the passive diffusion of compounds through the BBB. Analysis of the results generated with this tool highlights that there is no passive permeation of the liposomes through the artificial membrane. The equivalent phospholipid-based PAMPA was therefore employed to determine whether a phospholipid exchange could have occurred between the phospholipids of the liposomes, and those forming the artificial membrane. Results indicate that fusion, or at least interactions are occurring at the membrane. Indeed, phospholipids have been found in the acceptor solutions of some of the samples, and permeabilities have been calculated for diazepam and imipramine, but no intact liposome has been observed in acceptor solutions tested with TEM. Therefore, the hypothesis of a fusion of the liposomes with the membrane is privileged, with a delivery of the cargo either in the membrane or at the surface of the membrane. But this delivery results in a slower permeation through the artificial membrane of about 50% compared to the free drug. The expected increase of permeability of the free drug by incorporation inside liposomes has thus not been observed.

This piece of work leads to the conclusion that passive diffusion, with fusing of the liposomes at the biological membrane is not the major pathway taken by liposomes. Hence, a passive diffusion process cannot explain the increase in permeability observed in many studies ¹⁰²⁻¹⁰⁷. Therefore, active processes seem to be the privileged way of permeation for liposomal systems *in vivo*, as advanced by many researchers ^{69, 72, 81, 85, 86}. Endocytotic processes may be much more efficient to transport the entire liposomes than phospholipids fusion at the membrane, which degrade the vesicle, losing its reservoir capacity.

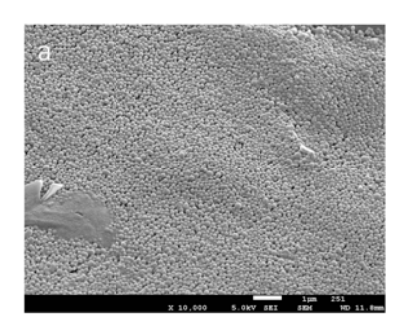
5-4.2. Polymeric nanoparticles

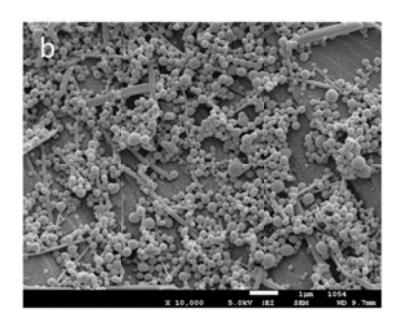
5-4.2.1.Characterization of polymeric nanoparticles

Carbamazepine, pindolol, diazepam and warfarin were successfully entrapped in the nanoparticles. The characteristics of these loaded nanoparticles are presented in table 5-10. Table 5-10: Characteristics of the nanoparticles with success loading. The morphology of the nanoparticles was observed with scanning electron microscopy (SEM) (figure 5-15).

Table 5-10: Characteristics of the nanoparticles with success loading 91

Active compound	Size(nm)	PI	EE(%)	EY(%)
Unloaded	262	0.2	-	-
Carbamazepine	498	0.6	0.6	7.9
Diazepam	345	0.6	3.7	47.9
Pindolol	259	0.4	0.2	2.3
Warfarin	445	0.6	5.2	67.4





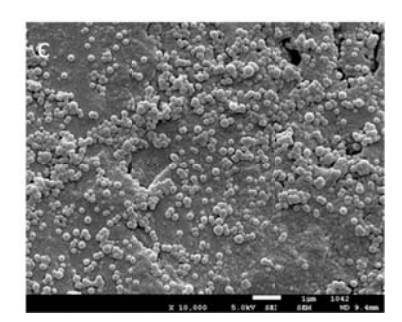


Figure 5-15: Scanning electron microscopy images of unloaded nanoparticles (a), warfarin-loaded nanoparticles (b) and diazepam loaded nanoparticles (c). The scale bar represents 1 μ m.

Images from figure 5-15 support the PI determined with Zetasizer: unloaded nanoparticles are generally homogeneous concerning size, shape and surface (figure 5-15a), whereas warfarin- and diazepam-loaded nanoparticles appear as more heterogeneous in size, with some needles (figure 5-15b), thought to be the free drug. Such differences between loaded and unloaded nanoparticles may indicate a modification of the nanoparticles, depending on the active compound incorporated. These modifications may either be an increase in the size, as exposed in table 5-10, a modification of the surface of the nanoparticles, and particularly of the physicochemistry at the surface, as well as a trend to aggregate, related to physicochemical modifications.

5-4.2.2. Permeability studies

The determination of the mechanism of permeation of nanoparticles through the BBB resides in a better understanding of the interactions and affinity of nanoparticles for the membrane. In order to try to elucidate the way nanoparticles may interfere with the barrier, two different *in vitro* models have been used: an artificial membrane with HDC/NPOE PAMPA, and a cellular model with a human immortalized cell line: the hCMEC/D3 cell line. A potential passive component of the permeability will be determined with PAMPA, while both active and passive processes can be investigated with the cellular model.

5-4.2.2.1. HDC/NPOE PAMPA

Determination of the integrity of the membrane

To be able to discuss results generated with PAMPA experiments, an assessment of the integrity of the membrane has to be performed, to make sure that the artificial membrane has not undergone significant modifications in the presence of the nanoparticles. Therefore, permeability of a set of active compounds has been tested, in the presence or in the absence of unloaded nanoparticles. Results are presented in figure 5-16.

Chapter 5: PAMPA as a tool to describe the passive permeability of liposomes and polymeric nanoparticles through the BBB

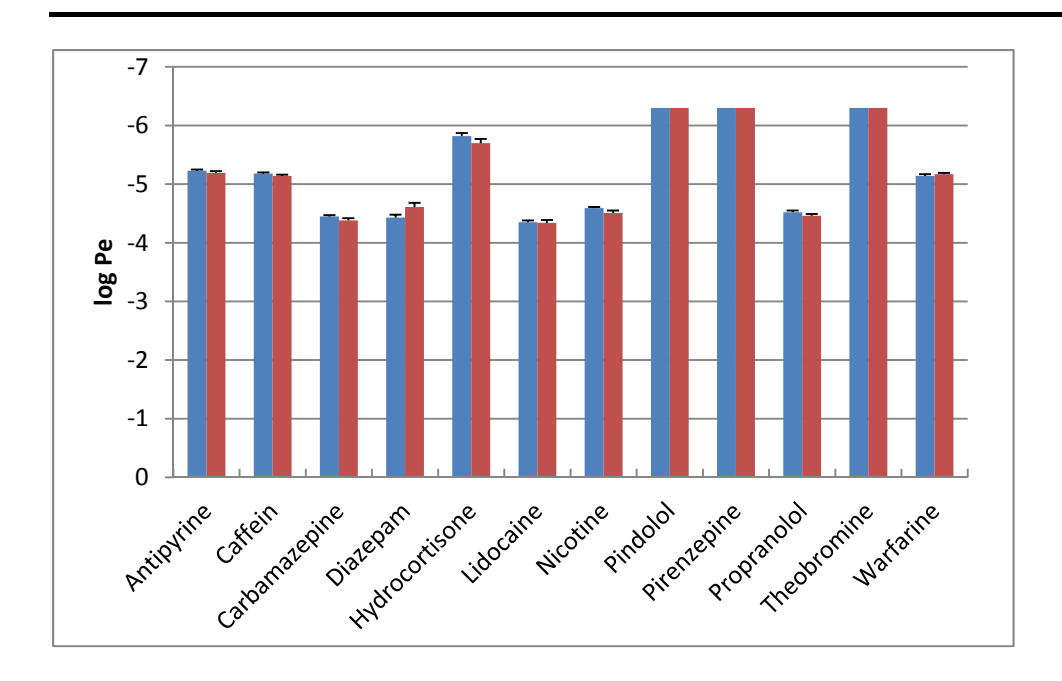


Figure 5-16 : $\log P_e$ of the free drug in the presence (red bars) or in the absence (blue bars) of 2 mg/ml non-loaded nanoparticles.

The passive permeations generated indicate no significant variations in the presence or in the absence of 2 mg/ml unloaded nanoparticles. Therefore, the presence of nanoparticles in the medium does not damage nor modify the properties of the artificial membrane, which carry on predicting passive permeability through the BBB. HDC/NPOE PAMPA can therefore be employed to predict the passive permeability of nanoparticles through the BBB.

Permeability of loaded nanoparticles with HDC/NPOE PAMPA

The permeability of diazepam-loaded nanoparticles, warfarin-loaded nanoparticles and carbamazepine-loaded nanoparticles through the HDC/NPOE PAMPA has been tested.

No significant differences between the data generated for the free drug and the incorporated nanoparticles was observed, as compiled in table 5-11.

Table 5-11: HDC/NPOE PAMPA results for the free drugs and the drug-loaded nanoparticles

Active compound	Free drug			Loaded nanoparticles		
	log P _e ±SD	$C_A(t)/C_D(0)$ (%)	R(%)	log P _e ±SD	$C_A(t)/C_D(0)$ (%)	R(%)
Diazepam	-4.43±0.05	14±1	63±3	-4.46±0.01	15.3±0.3	58.3±0.3
Warfarin	-5.14±0.03	12.8±0.6	<1	-5.17±0.04	11.0±0.8	3.4±0.4
Carbamazepine	-4.45±0.02	39±1	<1	-4.43±0.01	34±1	10±2

Hypotheses may be put forward concerning those results. Since passage through the artificial membrane is the same for the free drug or the nanoparticle, diffusion of the drug out of the nanoparticle may occur. Moreover, the free drug may not be inside but at the surface of the nanoparticle, enabling a rapid release. If the diffusion process from the copolymers occurs rapidly and the diffusion of the free drug through the artificial membrane is the rate limiting step, the permeability assessment of the drug-loaded nanoparticles will give the same information than a PAMPA assay of the free drugs. A second hypothesis could come from the structure of the loaded-nanoparticle itself. Hence, as displayed in the SEM pictures in figure 5-15, the morphology of loaded-nanoparticles and of the unloaded nanoparticles seems to differ. This may be caused by the position of the active compound on the nanoparticles, which may be adsorbed at the surface of the nanocarrier. Therefore, the drug at the surface may drive the interactions with the artificial membrane and promote the permeability of the unity {drug+nanoparticle}.

In order to understand what happened, the passive permeability of rhodamine-labeled nanoparticles or DIO-loaded nanoparticles has been assessed. As fluorescent tags, the detection of small amount of fluorescence will be easier in the acceptor compartment. Moreover, the assessment of the permeability of rhodamine-labeled nanoparticles will enable to track the behavior of the whole nanoparticle during the PAMPA assay, and determine a possible passage of the nanoparticles through the artificial membrane. Table 5-12 compiles the data generated by HDC/NPOE PAMPA for these nanoparticles. The data clearly indicate that no permeation occur, either for the nanoparticles, the rhodamine-labeled polymer or the free compounds. This experiment shows that the labeled nanoparticles are not able to reach the acceptor compartment. Similar results were obtained for DIO-loaded nanoparticles (table 5-12). Therefore, PLGA nanoparticles do not diffuse passively through the BBB. This tends to indicate that in the case of the drug-loaded nanoparticle (table 5-11) nanoparticles stay in the donor compartment and only the free drug permeate through the artificial membrane.

To verify this statement, SEM has been performed on acceptor solutions of carbamazepine-, diazepam- and warfarin-loaded nanoparticles, which were detected in the acceptor compartments. No nanoparticle was found. Therefore, the hypothesis claiming that free drug could diffuse through the copolymer vesicle is the most relevant. Attempting to visualize what could happen at the membrane, one can imagine interactions of the polymeric nanoparticles with the hydrophobic membrane, in the way that the free drug could diffuse from the nanoparticle core directly to the artificial membrane.

On the other hand, attention has been focused on the retention values exposed in table 5-12. With rhodamine-labeled nanoparticles, the retention increases with the concentration, meaning that the more nanoparticles are added in the reference, the less is recovered after incubation. This phenomenon can be a sign of aggregation of the labelednanoparticles or of adsorption at the membrane or on the material. In the case of DIO, retention decreases with concentration, which could be a sign of adsorption of the nanoparticles on the material or at the membrane. In order to demonstrate a possible sedimentation or adsorption of the nanoparticles, the same experiment has been run reversing the position of the donor and acceptor compartments. If aggregation of nanoparticles on the filter hampers the permeation through the membrane, reversing the donor and acceptor compartments should have an impact on the permeability and/or retention. Analysis of table 5-13 indicates that the trends are the same with both orientations and for both types of nanoparticles. This supports the hypothesis of an adsorption at the membrane for DIO-loaded nanoparticles and rhodamine-labeled nanoparticles, since material are different for the donor and acceptor compartments (Teflon® in one side and acrylic for the other side).

Table 5-12: Permeability coefficients (log P_e), ratio of passage in the acceptor compartment (Acc/Ref) and retention obtained with HDC/NPOE PAMPA for various concentrations of rhodamine-labeled nanoparticles, rhodamine-labeled polymer, fee rhodamine, DIO-loaded nanoparticles and free DIO.

	Rhodamine				DIO		
Concentration	log P _e ±SD	$C_A(t)/C_D(0)$ (%)	R(%)		log P _e ±SD	$C_A(t)/C_D(0)$ (%)	R(%)
	Rhodamine	-labeled nanopar	ticles		DIO-loaded nanoparticles		
5 mg/ml	<-6.3	<0.1	64±9		<-6.3	<0.1	58±1
2.5 mg/ml	<-6.3	<0.1	57±4		<-6.3	<0.1	59±2
2.0 mg/ml	<-6.3	<0.1	48±4		<-6.3	<0.1	64±1
1.5 mg/ml	<-6.3	<0.1	46±9		<-6.3	<0.1	65±2
1.0 mg/ml	<-6.3	<0.1	50±3		<-6.3	<0.1	69±1
0.5 mg/ml	<-6.3	<0.1	31±6		<-6.3	<0.1	77±1
0.25 mg/ml	-	-	-		<-6.3	0.4±0.3	82±2
Free tag or free labeled polymer							
Rho-polymer	<-6.3	0.20±0.01	<1		-	-	-
Rhodamine 50 μM	-6.10±0.04	1.50±0.02	<1		-	-	-
Free DIO	-	-	-		<-6.3	<0.1	42±1

Rho-polymer is the rhodamine-labeled polymer.

Table 5-13: Normal and reverse HDC/NPOE PAMPA performed with rhodamine-labeled nanoparticles and DIO-loaded nanoparticles.

		Standard sandwich			Reversed sandwich		
	Concentration	log P _e ±SD	$C_A(t)/C_D(0)$ (%)	R(%)	log P _e ±SD	$C_A(t)/C_D(0)$ (%)	R(%)
Rhodamine- labeled NP	2.0 mg/ml	<-6.3	<0.1	48±4	<-6.3	<0.1	42±4
	1.5 mg/ml	<-6.3	<0.1	46±9	<-6.3	<0.1	39±3
	1.0 mg/ml	<-6.3	<0.1	50±3	<-6.3	<0.1	37±4
	0.5 mg/ml	<-6.3	<0.1	31±6	<-6.3	<0.1	27±3
	5 mg/ml	<-6.3	<0.1	58±1	<-6.3	<0.1	43±2
DIO-loaded NP	2.5 mg/ml	<-6.3	<0.1	59±2	<-6.3	<0.1	49±1
	2.0 mg/ml	<-6.3	<0.1	64±1	<-6.3	<0.1	57±1
	1.5 mg/ml	<-6.3	<0.1	65±2	<-6.3	<0.1	60±1
	1.0 mg/ml	<-6.3	<0.1	69±1	<-6.3	<0.1	62±0
	0.5 mg/ml	<-6.3	<0.1	77±1	<-6.3	<0.1	71±1
	0.25 mg/ml	<-6.3	0.4±0.3	82±2	<-6.3	<0.1	74±2

NP stands for nanoparticles; SD stands for standard deviation; Acc/ref is the ratio between the concentration of the molecule in the acceptor and the concentration in the reference; R is the retention.

4-4.2.2.2. Permeability experiments with the hCMEC/D3 model

hCMEC/D3 is an immortalized cell line of human cerebral microvessels endothelial cells exhibiting most of the morphological and functional features of the cerebral endothelial cells $^{87, 88}$. hCMEC/D3 express many transporters and receptors, such as Pgp/ABCB1, ABCG2, ABCC1-5, human transferrin receptors, etc., and discloses interesting tight junction properties, even if the restriction of the paracellular pathway is not the strength of this model $(P_e(inulin)=12.10^{-6} \text{ cm.s}^{-1}; P_e(sucrose)=27.10^{-6} \text{ cm.s}^{-1}))$ $^{87, 88}$.

Permeability of some of the batches of polymeric nanoparticles were determined in hCMEC/D3 cell line in order to highlight a possible active transport of the vesicles, which cannot be modeled with PAMPA. This experiment was run with 2 batches of drug-loaded nanoparticles, namely diazepam and warfarin.

Table 5-14 discloses the passages obtained for free drugs, free drugs in presence of unloaded nanoparticles and diazepam- or warfarin-loaded nanoparticles through the hCMEC/D3 cell line model. Nanoparticles do not improve the passage of diazepam nor warfarin. For diazepam, it even seems that the drug-loaded nanoparticle formulation decreases the passage through the hCMEC/D3 cell line. For warfarin, the permeability of free warfarin and warfarin-loaded nanoparticle is statistically the same. These data reinforce the idea that the incorporated drug could fast escape from the polymeric matrix during incubation before reaching the cell membrane, and that the permeability observed could be related to the free drug released from the nanoparticles.

Table 5-14: Passage $(C_A(t)/C_D(0))$ of free drugs, free drugs in presence of non-loaded nanoparticles and warfarine- or diazepam- loaded particles through the hCMEC/D3 model.

Formulation	$C_A(t)/C_D(0)$ (%)		
Free diazepam	38±2		
Free diazepam + NP	36.8±0.5		
NP-diazepam	25±1		
Free warfarin	23±1		
Free warfarin+NP	32±2		
NP warfarin	21±3		

NP stands for nanoparticles

The comparison of the percentages of passage with the cellular model and with PAMPA (figure 5-17 and table 5-15) clearly indicates that the crossing is favored with the cellular model, whatever formulation. This fact can be due to a potential active process that

may occur with the cellular model, which may boost the resulting passage of the nanoparticles. On the other hand, diazepam and warfarin are drugs thought to only diffuse passively at the BBB. Therefore the comparison of the permeability of the free drugs between the cellular and the solvent-based models indicates that the passive diffusion processes are numerically different on those models. Moreover, the retention is not taken into account with hCMEC/D3 model due to the setup of the experiment, which can lead to variations between the 2 techniques compared, especially for diazepam that is highly retained in HDC/NPOE PAMPA.

For both *in vitro* models, incorporation of the active compound inside the nanoparticles does not enhance the final passive permeability of the drug.

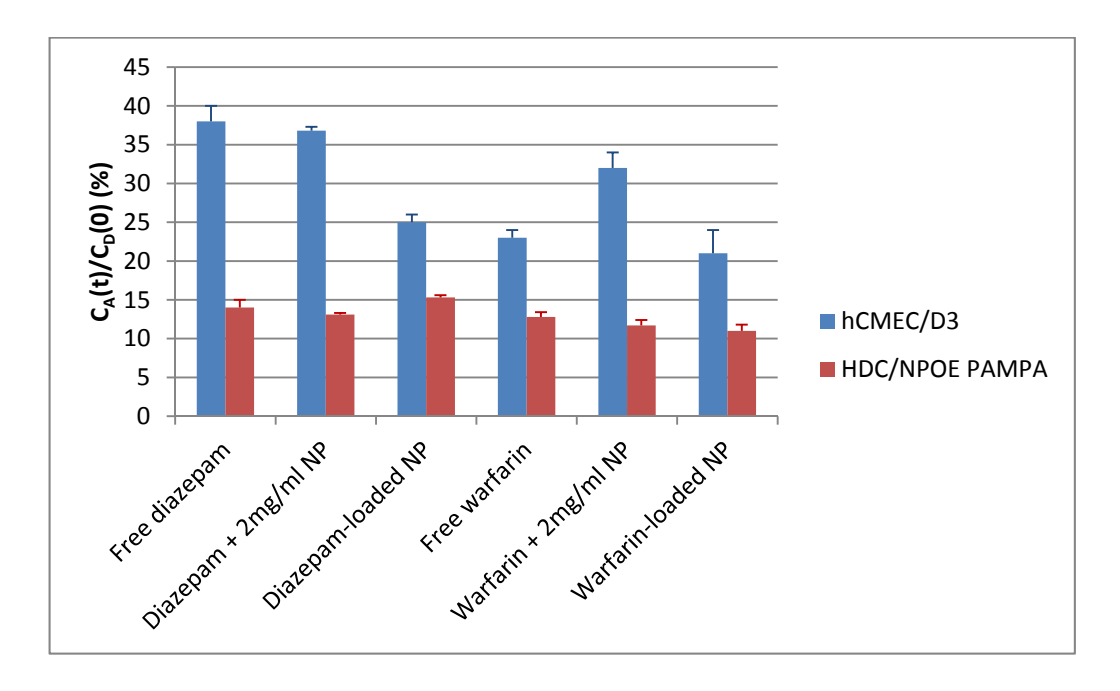


Figure 5-17: Ratio of compounds reaching the acceptor compartment in the HDC/NPOE PAMPA (red bars) and hCMEC/D3 cell line (blue bars).

Table 5-15: Comparison of the percentages of passage of different formulations of diazepam and warfarin through the PAMPA and the hCMEC/D3 models.

	hCMEC/D3	HDC/NPOE PAMPA
Formulation	$C_A(t)/C_D(0)$ (%)	$C_A(t)/C_D(0)$ (%)
Free diazepam	38±2	14±1
Free diazepam + NP	36.8±0.5	13.1±0.2
NP-diazepam	25±1	15.3±0.3
Free warfarin	23±1	12.8±0.6
Free warfarin+NP	32±2	11.7±0.7
NP warfarin	21±3	11.0±0.8

Results generated with PAMPA indicate that passive diffusion of the nanoparticle does not occur, and regarding the results generated with the cellular model, an active process can be suspected but not affirmed. Moreover, the hypothesis of a diffusion of the active compound from their polymeric vehicles is more and more plausible.

5-5. Conclusion

PAMPA is an easy and reproducible tool able to estimate passive permeability through biological membranes. Particularly, HDC/NPOE PAMPA has been shown to estimate the passive transendothelial permeability through the BBB with high throughput efficiency and in reproducible way. The experiments conducted in this chapter demonstrated that HDC/NPOE PAMPA was not able to estimate the passive BBB permeability of the formulated liposomes composed of 80% PC and 20% cholesterol due to physicochemical incompatibility between the liposomes and the artificial membrane. On the other hand, HDC/NPOE PAMPA was able to assess the passive permeability of polymeric nanoparticles.

Analysis of HDC/NPOE PAMPA with nanocarriers converged to the conclusion that no passive diffusion of the tested formulations occurred through the artificial membrane. With the liposomes, the membrane fusion process has been studied performing tests with the phospholipid membrane of PAMPA-BBB. Hence, due to the nature of the phospholipid of the artificial membrane in one hand, and those of the liposomes in a second hand, interactions and / or fusion between both parts are likely to occur. Fragments of liposomes have been observed with TEM in the acceptor compartments, while a very low amount of vesicles have been observed with fluorescein. Therefore, the hypothesis of interactions between the membrane and the vesicles is plausible, for these first generation liposomes. But the expected increase of permeability with drug-loaded liposomes has not been achieved.

Regarding the polymeric nanoparticles, permeabilities determined with HDC/NPOE PAMPA and the hCMEC/D3 cell line were compared and led to the conclusion that the drug-loaded nanoparticles did not improve the permeability of the incorporated drug. Imaging and dynamic light scattering indicated that no nanoparticle was able to cross the artificial membrane or the cell monolayer. Therefore, the drug may incorporate very close to the surface and be released rapidly form the PLGA nanoparticles.

Therefore, this work supports the hypothesis liposomes can fuse with the biological membrane, leading to drug release at the membrane, but that this process is not the

priviledged way of permeability. On the other hand, nanoparticles do not diffuse passively through the BBB. On the other hand, hCMEC/D3, which is able to perform active transport and endocytosis georgieva ^{86, 108} did not disclosed an increased permeability of the drugloaded nanoparticles compared to the free drug. These observations converged to the conclusion that the PLGA nanoparticles may generate a fast release of their cargo and that the permeabilities observed with both in vitro models are those of the free drug.

The most efficient way to circumvent the BBB with nanocarriers is therefore to employ functionalized-stealth liposomes, or coated nanoparticles. Antibody or transporter grafted on the outer surface of the vesicle will recognize a specific antigen or receptor, in order to selectively deliver its cargo. This strategy has already been successfully employed, grafting transferrin or ligands targeting the transferrin receptor on liposomes, naturally present at the BBB ^{26, 109}, but study of such complex nanocarriers are not able with simple models such as PAMPA.

5-6. Acknowledgments

A special attention is addressed to Pr Pierre-Olivier Couraud, from Institut Cochin (Paris), for having provided the hCMEC/D3 cell line used for some of the experiments, and Dr Florence Miller for all the cell culture and cell permeability experiments.

Thanks are also addressed to Pr Luca Costantino, from University of Modena (Italy), for the synthesis of rhodamine-labeled phosphatidylcholine.

Parts of this chapter resulted from Master's Thesis of Laure Nicolet (University of Geneva, Switzerland) and Kévin Nadin (University of Rouen, France). Deep acknowledgments are expressed for their seriousness and participation to the experimental results.

Thanks are also addressed to Dr Florence Délie for her in depth reviewing of this chapter.

References

- Tsaioun, K.; Bottlaender, M.; Mabondzo, A.; Alzheimer's Drug Discovery Fdn ADDME avoiding drug development mistakes early: central nervous system drug discovery perspective. BMC Neurol. 2009, 9.
- Mabondzo, A.; Bottlaender, M.; Guyot, A. C.; Tsaouin, K.; Deverre, J. R.; Balimane, P. V. Validation of in vitro cell-based human blood—brain barrier model using clinical positron emission tomography radioligands to predict in vivo human brain penetration. *Mol. Pharmaceutics* 2010, 7, 1805-1815.
- 3. Misra, A.; Ganesh, S.; Shahiwala, A.; Shah, S. P. Drug delivery to the central nervous system: a review. *J. Pharm. Pharmaceut. Sci.* **2003**, *6*, 252-273.
- 4. Kingsley, J. D.; Dou, H.; Morehead, J.; Rabinow, B.; Gendelman, H. E.; Destache, C. J. Nanotechnology: a focus on nanoparticles as a drug delivery system. *J. Neuroimmune Pharmacol.* **2006**, *1*, 340-350.
- Nau, R.; Soergel, F.; Eiffert, H. Penetration of drugs through the blood-cerebrospinal fluid/blood-brain barrier for treatment of central nervous system infections. Clin. Microbiol. Rev. 2010, 23, 858-883.
- 6. Stamatovic, S. M.; Keep, R. F.; Andjelkovic, A. V. Brain endothelial cell-cell junctions: How to "Open" the blood brain barrier. *Curr. Neuropharmacol.* **2008**, *6*, 179-192.
- 7. Kroll, R. A.; Neuwelt, E. A. Outwitting the blood-brain barrier for therapeutic purposes: osmotic opening and other means. *Neurosurgery* **1998**, *42*, 1083-1099.
- 8. Rapoport, S. I. Osmotic opening of the blood-brain barrier: principles, mechanism, and therapeutic applications. *Cell. Mol. Neurobiol.* **2000**, *20*, 217-230.
- 9. Drin, G.; Rousselle, C.; Scherrmann, J. M.; Rees, A. R.; Temsamani, J. Peptide delivery to the brain via adsorptive-mediated endocytosis: advances with SynB vectors. *AAPS Pharm. Sci.* **2002**, *4*.
- 10. Nicolazzo, J. A.; Charman, S. A.; Charman, W. N. Methods to assess drug permeability across the blood-brain barrier. *J. Pharm. Pharmacol.* **2006**, *58*, 281-293.
- 11. Illum, L. Is nose-to-brain transport of drugs in man a reality? *J. Pharm. Pharmacol.* **2004,** *56,* 3-17.
- 12. Deli, M. A. Potential use of tight junction modulators to reversibly open membranous barriers and improve drug delivery. *Biochim. Biophys. Acta* **2009**, *1788*, 892-910.
- 13. Singh, A. P.; Saraf, S. K.; Saraf, S. A. SLN approach for nose-to-brain delivery of alprazolam. *Drug Deliv. and Transl. Res.* **2012**, *2*, 498-507.
- 14. Zhang, H.; Prisinzano, T. E.; Donovan, M. D. Permeation and metabolism of cocaine in the nasal mucosa. *Eur. J. Drug Metabol. Pharmacokinet.* **2012**, *37*, 255-262.

- 15. Veronesi, M. C.; Kubek, D. J.; Kubek, M. J. Intranasal delivery of neuropeptides. *Neuropeptides* **2011**, *789*, 303-312.
- 16. Trivedi, J. B.; Upadhyay, P.; Shah, S.; Chauhan, N.; Patel, A. Intranasal liposomes: an approach for drug delivery to brain. *Int. J. Pharm. Res. Scholar.* **2012,** *1*, 79-91.
- 17. Bousquet, L. Etude Comparative des Thérapies Anti-VIH: Rôle des Transporteurs d'Efflux sur le Passage Transmembranaire des Antirétroviraux au Niveau des Cellules CD4+ et de la Barrière Hémato-Encéphalique; Université Paris XI, 2008.
- 18. Weiss, N.; Miller, F.; Cazaubon, S.; Couraud, P. O. The blood-brain barrier in brain homeostasis and neurological diseases. *Biochim. Biophys. Acta* **2009**, *1788*, 842-857.
- 19. Malakoutikhah, M.; Teixido, M.; Giralt, E. Toward an optimal blood—brain barrier shuttle by synthesis and evaluation of peptide libraries. *J. Math. Chem.* **2008**, *51*, 4881-4889.
- 20. Costantino, L.; Tosi, G.; Ruozi, B.; Bondioli, L.; Vandelli, M. A.; Forni, F. Colloidal systems for CNS drug delivery. In *Progress in Brain Research Nanoneuroscience and Nanoneuropharmacology*, Volume 180 ed.; Hari, S. S. Ed.; Elsevier: 2009; pp 35-69.
- 21. Ruozi, B.; Tosi, G.; Forni, F.; Vandelli, M. A. Ketorolac tromethamine liposomes: encapsulation and release studies. *J. Liposome Res.* **2005**, *15*, 175-185.
- 22. Ali, M.; Kirby, D. J.; Mohammed, A. R.; Perrie, Y. Solubilisation of drugs within liposomal bilayers: alternatives to cholesterol as a membrane stabilising agent. *J. Pharm. Pharmacol.* **2010**, *62*, 1646-1655.
- 23. Gabizon, A. A. Pegylated liposomal doxorubicin: metamorphosis of an old drug into a new form of chemotherapy. *Cancer Investigation* **2001,** *19*, 424-436.
- 24. Working, P. K.; Dayan, A. D. Pharmacological-toxicological expert report Caelyx(TM) (Stealth(R) liposomal doxorubicin HCl) foreword. *Human Exp. Toxicol.* **1996,** *15,* 751-785.
- 25. De Leeuw, J.; De Vijlder, H. C.; Bjerring, P.; Neumann, H. A. M. Liposomes in dermatology today. *J. Eur. Acad. Dermatol. Venerol.* **2009**, *23*, 505-516.
- 26. Wilner, S. E.; Wengerter, B.; Maier, K.; de Lourdes Borba Magalhaes, M.; Del Amo, D. S.; Pai, S.; Opazo, F.; Rizzoli, S. O.; Yan, A.; Levy, M. An RNA alternative to human transferrin: a new tool for targeting human cells. *Mol. Ther. Nucl. Acids.* **2012**, *1*, 1-14.
- 27. Doll, T. A. P. F.; Raman, S.; Dey, R.; Burkhard, P. Nanoscale assemblies and their biomedical applications. *J. R. Soc. Interface* **2013**, *10*.
- 28. Zhou, H.; Janghra, N.; Mitrpant, C.; Dickinson, R. L.; Anthony, K.; Price, L.; Eperon, I. C.; Wilton, S. D.; Morgan, J.; Muntoni, F. A novel morpholino oligomer targeting ISS-N1 improves rescue of severe spinal muscular atrophy transgenic mice. *Human Gene Ther.* **2013**, *24*, 331-342.
- 29. Li, F.; Pei, H.; Wang, L.; Lu, J.; Gao, J.; Jiang, B.; Zhao, X.; Fan, C. Nanomaterial-based fluorescent DNA analysis: a comparative study of the quenching effects of graphene oxide, carbon nanotubes, and gold nanoparticles. *Adv. Funct. Mater.* **2013**, n/a.

- 30. Kopecek, J. Polymer–drug conjugates: origins, progress to date and future directions. *Adv. Drug Del. Rev.* **2013**, *65*, 49-59.
- 31. Tong, R.; Gabrielson, N. P.; Fan, T. M.; Cheng, J. Polymeric nanomedicines based on poly(lactide) and poly(lactide-co-glycolide). *Curr. Opin. Solid State Mat. Sci.* **2012**, *16*, 323-332.
- 32. Chauhan, M. K.; Manchanda, A.; Khurana, J. K.; Jain, P.; Sharma, D.; Jain, S.; Bansal, S. Nanotechnology: The nano soldiers in the war against cancer. *J. Pharm. Res.* **2011**, *4*, 4420-4423.
- 33. Patel, P. A.; Patil, S. C.; Kalaria, D. R.; Kalia, Y. N.; Patravale, V. B. Comparative in vitro and in vivo evaluation of lipid based nanocarriers of Huperzine A. *Int. J. Pharm.* **2013**, *446*, 16-23.
- 34. Martins, S.; Tho, I.; Reimold, I.; Fricker, G.; Souto, E.; Ferreira, D.; Brandl, M. Brain delivery of camptothecin by means of solid lipid nanoparticles: Formulation design, in vitro and in vivo studies. *Int. J. Pharm.* **2012**, *439*, 49-62.
- 35. Egleton, R. D.; Davis, T. P. Devlopment of neuropeptide drugs that cross the blood-brain barrier. *Am. Soc. Experim. Neurother.* **2005,** *2*, 44-53.
- 36. Torchilin, V. P. Recent advances with liposomes as pharmaceutical carriers. *Nat. Rev. Drug Discov.* **2005**, *4*, 145-160.
- 37. Zhang, L.; Gu, F. X.; Chan, J. M.; Wang, A. Z.; Langer, R. S.; Farokhzad, O. C. Nanoparticles in medicine: therapeutic applications and developments. *Clin. Pharmacol. Ther.* **2007**, *83*, 761-769.
- 38. Bangham, A. D.; Horne, R. W. Negative staining of phospholipids and their structural modification by surface-active agents as observed in the electron microscope. *J. Mol. Biol.* **1964**, *8*, 660-668.
- 39. Avdeef, A.; Box, K. J.; Comer, J. E. A.; Hibbert, C.; Tam, K. Y. pH-metric log P. 10. Determination of vesicle membrane-water partition coefficients of ionizable drugs. *Pharm. Res.* **1998**, *15*, 209-215.
- 40. Balon, K.; Riebesehl, B. U.; Müller, B. W. Drug liposome partitioning as a tool for the prediction of human passive intestinal absorption. *Pharm. Res.* **1999,** *16*, 882-888.
- 41. Burns, S. T.; Khaledi, M. G. Rapid determination of liposome-water partition coefficients (Klw) using liposome electrokinetic chromatography (LEKC). *J. Pharm. Sci.* **2002,** *91*, 1601-1612.
- 42. Herbette, L. G.; Rhodes, D. G.; Mason, R. P. New approaches to drug design and delivery based on drug-membrane interactions. *Drug Design and Delivery* **1991,** *7*, 75-118.
- 43. Krämer, S. D.; Braun, A.; Jakits-Deiser, C.; Wunderli-Allenspach, H. Towards the predictability of drug-lipid membrane interactions: the pH-dependent affinity of propranolol to phosphatidylinositol containing liposomes. *Pharm. Res.* **1998**, *15*, 739-744.

- 44. Krämer, S. D.; Jakits-Deiser, C.; Wunderli-Allenspach, H. Free fatty acids cause pH-dependent changes in drug-lipid membrane interactions around physiological pH. *Pharm. Res.* **1997**, *14*, 827-832.
- 45. Surewicz, S. K.; Leyko, W. Interactions of propranolol with model phospholipid membranes. Monolayer, spin label and fluorescence spectroscopy studies. *Biochim. Biophys. Acta* **1981**, *643*, 387-397.
- 46. Alcorn, C. J.; Simpson, R. J.; Leahy, D. E.; Peters, T. J. Partition and distribution coefficients of solutes and drugs in brush border membrane vesicles. *Biochem. Pharmacol.* **1993**, 45, 1775-1782.
- 47. Choi, Y. W.; Rogers, J. A. The liposome as a model membrane in correlations of partitioning with α -adrenoreceptor agonist activities. *Pharm. Res.* **1990,** *7*, 508-512.
- 48. Austin, R. P.; Davis, A. M.; Manners, C. N. Partitioning of ionizing molecules between aqueous buffers and phospholipid vesicles. *J. Pharm. Sci.* **1995**, *84*, 1180-1183.
- 49. Nicolosi, D.; Scalia, M.; Nicolosi, V. M.; Pignatello, R. Encapsulation in fusogenic liposomes broadens the spectrum of action of vancomycin against Gram-negative bacteria. *Int. J. Antimicrob. Agents* **2010**, *35*, 553-558.
- 50. Puisieux, F.; Delattre, J. Les liposomes. Applications Thérapeutiques; Lavoisier: Paris, 1985.
- 51. Liposome Technology, 2nd Edition. Volume III. Interaction of Liposomes with Biological Milieu; CRC Press: Boca Raton, 1993.
- 52. Sato, T.; Sunamoto, J. Recent aspects in the use of liposomes in biotechnology and medicine. *Prog. Lip. Res.* **1992,** *31,* 345-372.
- 53. Sharma, A.; Sharma, U. S. Liposomes in drug delivery: progress and limitations. *Int. J. Pharm.* **1997**, *154*, 123-140.
- 54. Forssen, E. A.; Tokes, Z. A. In vitro and in vivo studies with Adriamycin liposomes. *Biochem. Biophys. Res. Commun.* **1979,** *91*, 1295-1301.
- 55. Rahman, A.; Kessler, A.; More, N.; Sikic, B.; Rowden, G.; Woolley, P.; Schein, P. S. Liposomal protection of Adriamycin-induced cardiotoxicity in mice. *Cancer Res.* **1980**, *40*, 1532-1537.
- 56. Pardridge, W. M. Intravenous, non-viral RNAi gene therapy of brain cancer. *Expert Opin. Biol. Ther.* **2004**, *4*, 1103-1113.
- 57. Lasic, D. D. Doxorubicin in sterically stabilized liposomes. *Nature* **1996**, *381*, 630.
- 58. Lasic, D. D. Liposomes: from Physics to Applications; Elsevier: Amsterdam, 1993.
- 59. Huwyler, J.; Wu, D.; Pardridge, W. M. Brain drug delivery of small molecules using immunoliposomes. *Proc. Natl. Acad. Sci. USA* **1996**, *93*, 14164-14169.

- 60. Ying, X.; Wen, H.; Yao, H. J.; Zhang, Y.; Tian, W.; Zhang, L.; Ju, R. J.; Wang, X. X.; Yu, Y.; Lu, W. L. Pharmacokinetics and tissue distribution of dual-targeting daunorubicin liposomes in mice. *Pharmacology* **2011**, *87*, 105-114.
- 61. Mamot, C.; Ritschard, R.; Wicki, A.; Stehle, G.; Dieterle, T.; Bubendorf, L.; Hilker, C.; Deuster, S.; Herrmann, R.; Rochlitz, C. Tolerability, safety, pharmacokinetics, and efficacy of doxorubicin-loaded anti-EGFR immunoliposomes in advanced solid tumours: a phase 1 dose-escalation study. *Lancet Oncol.* **2012**, *13*, 1234-1241.
- 62. Markoutsa, E.; Pampalakis, G.; Niarakis, A.; Romero, I. A.; Weksler, B.; Couraud, P. O.; Antimisiaris, S. G. Uptake and permeability studies of BBB-targeting immunoliposomes using the hCMEC/D3 cell line. *Eur. J. Pharm. Biopharm.* **2011**, *77*, 265-274.
- 63. Torchilin, V. Micellar nanocarriers: pharmaceutical perspectives. *Pharm. Res.* **2007**, *24*, 1-16.
- 64. Chang, H. I.; Yeh, M. K. Clinical development of liposome based drugs: formulation, characterization, and therapeutic efficacy. *Int. J. Nanomed.* **2012**, *7*, 49-0.
- 65. Pasha, S.; Gupta, K. Various drug delivery approaches to the central nervous system. *Exp. Opin. Drug. Del.* **2010**, *7*, 113-135.
- 66. Lockman, P. R.; Mumper, R. J.; Khan, M. A.; Allen, D. D. Nanoparticle technology for drug delivery across the blood-brain barrier. *Drug Dev. Ind. Pharm.* **2002**, *28*, 1-13.
- 67. Ogawa, Y.; Yamamoto, M.; Okada, H.; Yashiki, T.; Shimamoto, T. A new technique to efficiently entrap leuprolide acetate into microcapsules of polylactic acid or copoly(lactic glycolic) acid. *Chem. Pharm. Bull.* **1988**, *36*, 1095-1103.
- 68. Soppimath, K. S.; Aminabhavi, T. M.; Kulkarni, A. R.; Rudzinski, W. E. Biodegradable polymeric nanoparticles as drug delivery devices. *J. Control Release* **2001**, *70*, 1-20.
- 69. Koziara, J. M.; Lockman, P. R.; Allen, D. D.; Mumper, R. J. In situ blood-brain barrier transport of nanoparticles. *Pharm. Res.* **2003**, *20*, 1772-1778.
- 70. Alyautdin, R. N.; Petrov, V. E.; Langer, K.; Berthold, A.; Kharkevich, D. A.; Kreuter, J. Delivery of loperamide across the blood-brain barrier with polysorbate 80-coated polybutylcyanoacrylate nanoparticles. *Pharm. Res.* **1997**, *14*, 325-328.
- 71. Calvo, P.; Gouritin, B.; Chacun, H.; Desmaele, D.; D'Angelo, J.; Noel, J. P.; Georgin, D.; Fattal, E.; Andreux, J. P.; Couvreur, P. Long-circulating PEGylated polycyanoacrylate nanoparticles as new drug carrier for brain delivery. *Pharm. Res.* **2001**, *18*, 1157-1166.
- 72. Kreuter, J.; Alyautdin, R. N.; Kharkevich, D. A.; Ivanov, A. A. Passage of peptides through the blood-brain-barrier with colloidal polymer particles (nanoparticles). *Brain Res.* **1995**, *674*, 171-174.
- 73. Steiniger, S. C. J.; Kreuter, J.; Khalansky, A. S.; Skidan, I. N.; Bobruskin, A. I.; Smirnova, Z. S.; Severin, S. E.; Uhl, R.; Kock, M.; Geiger, K. D.; Gelperina, S. E. Chemotherapy of glioblastoma in rats using doxorubicin-loaded nanoparticles. *Int. J. Cancer* **2004**, *109*, 759-767.

- 74. Ulbrich, K.; Hekmatara, T.; Herbert, E.; Kreuter, J. Transferrin- and transferrin-receptor-antibody-modified nanoparticles enable drug delivery across the blood-brain barrier (BBB). Eur. J. Pharm. Biopharm. **2009**, 71, 251-256.
- 75. Vergoni, A. V.; Tosi, G.; Tacchi, R.; Vandelli, M. A.; Bertolini, A.; Costantino, L. Nanoparticles as drug delivery agents specific for CNS: in vivo biodistribution. *Nanomedicine: Nanotechnology, Biology and Medicine* **2009**, *5*, 369-377.
- 76. Costantino, L.; Gandolfi, F.; Tosi, G.; Rivasi, F.; Vandelli, M. A.; Forni, F. Peptide-derivatized biodegradable nanoparticles able to cross the blood-brain barrier. *J. Control Release* **2005**, *108*, 84-96.
- 77. Kreuter, J. Mechanism of polymeric nanoparticle-based drug transport across the blood-brain barrier (BBB). *J. Microencapsulation* **2012**, *30*, 49-54.
- 78. Costantino, L.; Boraschi, D. Is there a clinical future for polymeric nanoparticles as brain-targeting drug delivery agents? *Drug Discov. Today* **2012**, *17*, 367-378.
- 79. Gaumet; Vargas, A.; Gurny, R.; Delie, F. Nanoparticles for drug delivery: the need for precision in reporting particle size parameters. *Eur. J. Pharm. Biopharm.* **2008**, *69*, 1-9.
- 80. Podio, V.; Zara, G. P.; Carazzone, M.; Cavalli, R.; Gasco, M. R. Biodistribution of stealth and non-stealth solid lipid nanospheres after intravenous administration to rats. *J. Pharm. Pharmacol.* **2000**, *52*, 1057-1063.
- 81. Zara, G. P.; Cavalli, R.; Bargoni, A.; Fundaro, A.; Vighetto, D.; Gasco, M. R. Intravenous administration to rabbits of non-stealth and stealth doxorubicin-loaded solid lipid nanoparticles at increasing concentrations of stealth agent: pharmacokinetics and distribution of doxorubicin in brain and other tissues. *J. Drug. Target.* **2002**, *10*, 327-335.
- 82. Maeda, H.; Wu, J.; Sawa, T.; Matsumura, Y.; Hori, K. Tumor vascular permeability and the EPR effect in macromolecular therapeutics: a review. *J. Control Release* **2000**, *65*, 271-284.
- 83. Juillerat-Jeanneret, L. The targeted delivery of cancer drugs across the blood-brain barrier: chemical modifications of drugs or drug-nanoparticles? *Drug Discovery Today* **2008**, *13*, 1099-1106.
- 84. Allen, T. M.; Cullis, P. R. Drug delivery systems: entering the mainstream. *Science* **2004**, *303*, 1818-1822.
- 85. Alam, M. I.; Beg, S.; Samad, A.; Baboota, S.; Kohli, K.; Ali, J.; Ahuja, A.; Akbar, M. Strategy for effective brain drug delivery. *Eur. J. Pharm. Sci.* **2010**, *40*, 385-403.
- 86. Georgieva, J. V.; Kalicharan, D.; Couraud, P. O.; Romero, I. A.; Weksler, B.; Hoekstra, D.; Zuhorn, I. S. Surface characteristics of nanoparticles determine their intracellular fate in and processing by human blood-brain barrier endothelial cells in vitro. *Mol. Ther.* 2010.

- 87. Poller, B.; Gutmann, H.; Krahenbuhl, S.; Weksler, B.; Romero, I.; Couraud, P. O.; Tuffin, G.; Drewe, J.; Huwyler, J. The human brain endothelial cell line hCMEC/D3 as a human blood-brain barrier model for drug transport studies. *J. Neurochem.* **2008**, *107*, 1358-1368.
- 88. Weksler, B. B.; Subileau, E. A.; Perriere, N.; Charneau, P.; Holloway, K.; Leveque, M.; Tricoire-Leignel, H.; Nicotra, A.; Bourdoulous, S.; Turowski, P.; Male, D. K.; Roux, F.; Greenwood, J.; Romero, I. A.; Couraud, P. O. Blood-brain barrier-specific properties of a human adult brain endothelial cell line. *FASEB J.* **2005**, *19*, 1872-+.
- 89. Liebler, D. C.; Burr, J. A. Oxidation of vitamin E during iron-catalyzed lipid peroxidation: evidence for electron-transfer reactions of the tocopheroxyl radical. *Biochemistry* **1992**, *31*, 8278-8284.
- 90. Di, L.; Kerns, E. H.; Fan, K.; McConnell, O. J.; Carter, G. T. High throughput artificial membrane permeability assay for blood—brain barrier. *Eur. J. Med. Chem.* **2003**, *38*, 223-232.
- 91. Nicolet, L. Mise au point de vecteurs nanoparticulaires pour l'amélioration du passage à travers la barrière hémato-encéphalique in vitro; 2010.
- 92. Faller, B.; Wohnsland, F. Physicochemical parameters as tools in drug discovery and lead optimization. In *Pharmacokinetic Optimization in Drug Research: Biological, Physicochemical and Computational Strategies*; Testa, B.; van de Waterbeemd, H.; Folkers, G.; Guy, R. H. Eds.; Wiley-VHCA: Zurich, 2001; pp 258-273.
- 93. Lee, S. C.; Lee, K. E.; Kim, J. J.; Lim, S. H. The effect of cholesterol in the liposome bilayer on the stabilization of incorporated retinol. *J. Liposome Res.* **2005**, *15*, 157-166.
- 94. Thomas, G. *Medicinal Chemistry. An Introduction*; Wiley: Chichester, 2000.
- 95. Verkleij, A. J.; Ververgaert, P. H.; de Kruyff, B.; van Deenen, L. L. The distrivution of cholesterol in bilayers of phosphatidylcholines as visualized by freeze fracturing. *Biochim. Biophys. Acta* **1974**, *373*, 495-501.
- 96. Vemuri, S.; Rhodes, C. T. Preparation and characterization of liposomes as therapeutic delivery systems: a review. *Pharm. Acta Helv.* **1995,** *70*, 95-111.
- 97. Frézard, F.; Santaella, C.; Vierling, P.; Riess, J. G. Permeability and stability in buffer and in human serum of fluorinated phospholipid-based liposomes. *Biochim. Biophys. Acta* **1994**, *1192*, 61-70.
- 98. Ravily, V.; Santaella, C.; Vierling, P. Membrane permeability and stability in buffer and in human serum of fluorinated di-O-alkylglycerophosphocholine-based liposomes. *Biochim. Biophys. Acta* **1996**, *1285*, 79-90.
- 99. A Marca-Martinet, C. Les liposomes, un modèle dans l'étude des interactions entre médicaments et membranes biologiques; 2001; pp 1-223.
- 100. Kakar, R.; Rao, R.; Goswami, A.; Nanda, S.; Saroha, K. Pronosiomes: an emerging vesicular system in drug delivery and cosmetics. *Der Pharmacia Lettre* **2011**, *2*, 227-239.

- 101. Patlolla, R. R.; Desai, P. R.; Belay, K.; Singh, M. S. Translocation of cell penetrating peptide engrafted nanoparticles across skin layers. *Biomaterials* **2010**, *31*, 5598-5607.
- 102. Lv, Q.; Li, L. M.; Han, M.; Tang, X. J.; Yao, J. N.; Ying, X. Y.; Li, F. Z.; Gao, J. Q. Characteristics of sequential targeting of brain glioma for transferrin-modified cisplatin liposome. *Int. J. Pharm.* **2013**, *444*, 1-9.
- 103. Caraglia, M.; Luongo, L.; Salzano, G.; Zappavigna, S.; Marra, M.; Guida, F.; Lusa, S.; Giordano, C.; De Novellis, V.; Rossi, F.; Abbruzzese Saccardi, A.; De Rosa, G.; Maione, S. Stealth liposomes encapsulating zoledronic acid: a new opportunity to treat neuropathic pain. *Mol. Pharm.* **2013**, *10*, 1111-1118.
- 104. Ramos-Cabrer, P.; Campos, F. Liposomes and nanotechnology in drug development: focus on neurological targets. *Int. J. Nanomed.* **2013**, *8*, 951-960.
- 105. Ramos-Cabrer, P.; Campos, F.; Sobrino, T.; Castillo, J. Targeting the ischemic penumbra. *Stroke* **2011**, *42*, S7-S11.
- 106. Ramos-Cabrer, P.; Agulla, J.; Argibay, B.; Perez-Mato, M.; Castillo, J. Serial MRI study of the enhanced therapeutic effects of liposome-encapsulated citicoline in cerebral ischemia. *Int. J. Pharm.* **2011**, *405*, 228-233.
- 107. Rao Adibhatla, M.; Hatcher, J. F. Cytidine 5´-Diphosphocholine (CDP-Choline) in stroke and other CNS disorders. *Neurochem. Res.* **2005**, *30*, 15-23.
- 108. Chattopadhyay, N.; Zastre, J.; Wong, H. L.; Wu, X. Y.; Bendayan, R. Solid lipid nanoparticles enhance the delivery of the HIV protease inhibitor, atazanavir, by a human brain endothelial cell line. *Pharm. Res.* **2008**, *25*, 2262-2271.
- 109. Abdulkarim, M. F.; Heard, C.; Alany, R. G. An overview of recent patents on nanoparticles for drug delivery across the blood brain barrier. *Recent Patent Nanomed.* **2012**, *2*, 45-51.



Conclusions

Face to the increasing needs in CNS treatments, the drug discovery and development processes struggle to make CNS drugs from launching. Therefore, new techniques able to determine the pharmacokinetics of drug candidates as soon as possible in the drug discovery process, and in high-throughput screening are crucial. This present thesis reports the development of a new artificial membrane able to estimate passive transcellular permeation through the BBB in the early stages of the drug discovery process and with a high-throughput screening efficiency. This full-solvent based artificial membrane was shown to correlate with the standard PAMPA-BBB protocol while avoiding the use of biological material, which may cause reproducibility issues. The newly developed PAMPA technique enables the determination of 75 to 100 passive permeability values per day. Moreover, good relationships between the experimental log P_e^{HDC/NPOE} and the permeability of small dataset of passively transported compounds on different in vitro and in vivo models were observed. As drug candidates are transported passively and/or actively (either efflux or uptake transport) at the BBB, PAMPA appears as a complementary technique to cellular models able to determine a global process (passive + active pathways, depending on the transporters expressed in the cellular model). During the drug discovery process, the combination of these 2 techniques may generate an important response for the future of the lead compound. Hence, when a CNS active compound needs to be formulated, a first screening with PAMPA will enable to select the active compounds naturally diffusing through the BBB. These isolated compounds can then be tested with cellular models to determine a potential efflux process, which could prevent a sufficient amount of compound to reach its target. However, due to the large amount of uptake transporters that exist at the BBB, the compounds unable to diffuse through the BBB should not be fully discarded, especially if their structure contains a moiety easily recognized by a specific transporter. On the other hand, if a non-CNS drug need to be developed, it is crucial that no permeation through the BBB occurs to prevent cerebral toxicity or severe adverse side effects. Therefore, PAMPA will appear as an efficient tool to put aside compounds able to passively diffuse at the BBB.

The comparative study performed with a large home-made dataset separated into classes concluded that similarities exist between the passive permeabilities predicted with HDC/NPOE PAMPA, PAMPA-BBB and HDM-PAMPA. Therefore, the new artificial membrane is not as specific as what it was indicated with the correlations with restricted dataset, especially for the fast permeant compounds. This may also indicate that the passive

diffusion component of the permeation process is not significantly different on various biological membranes, even if their structure is basically not the same.

The ability of PAMPA to isolate the passive component of the permeation process led to the wish to understand the permeability of more complex matrices. Phyto-extracts, liposomes and polymeric nanoparticles were selected to explore these applications with the newly developed artificial membrane. PAMPA was found to be compatible with phyto extracts, meaning that passive permeation of the compounds forming a plant extract can be easily determined. Therefore, the new artificial membrane was employed to generate information that helps to understand the CNS action of an extract, or the molecule potentially responsible for a CNS activity. The main issue in handling phytochemistry extracts is the poor solubility. The multitude of components that constitutes a single extract has also to be carefully managed by employing an efficient method of detection.

Colloidal vectors are more complex to treat with PAMPA, since suspensions are studied, and no more solutions. Therefore, new equilibria are created in the PAMPA compartments. This work led to the conclusion that poor or no interactions exist between liposomes or nanoparticles and the new artificial membrane, highly caused by the physicochemical properties of the outer surface of those nanocarriers. To understand the mechanism of permeation of liposomes through the BBB, the phospholipidic-based PAMPA-BBB model was also performed with suspensions. It seems that interactions between the phospholipids forming the liposomes and those of the artificial membrane are occurring, and that the cargo is liberated at the membrane or in the membrane. Therefore, liposomes may also be prone to such interactions with the biological membranes *in vivo*. However, this mode of transport was found to slow down the passive permeation of the compounds naturally diffusing through the artificial membrane, and does not promote the transport of the most hydrophilic compounds.

To resume, PAMPA appears as an easy and fast tool enabling the determination of the passive permeability information. A combination with cellular models will enable to go further in the understanding of the permeability profile through biological barriers. But experimenter should keep in mind that *in vitro* models will never give the complete information of what will occur in a living human body. Moreover, new transporters are regularly discovered, meaning that understanding the complete permeation process is very difficult, and *in vitro* models always need to update, to give an information as close as possible of the *in vivo* information. However, they are good tools enabling a better selection of the lead compounds early in the drug discovery process, therefore decreasing the attrition

rate during the overall drug discovery and development processes and the costs associated with bringing an active drug to the market.

Perspectives

In order to protect the brain from exogenous and potentially toxic compounds, the BBB disposes of many mechanisms able to limit or prevent the passage of molecules from the blood to the brain. Particularly, the Pqp/ABCB1 efflux protein is abundant and lowspecific at the BBB, causing the failure of many drugs to reach the brain. On the other hand, to supply the needs in nutrients, uptake transport is available at the BBB. Therefore, for some compounds that are substrates of these active transport systems, PAMPA is a bit restrictive and does not fully explain the mode of permeation. Therefore, it would be interesting to develop a PAMPA assay in presence of transporter proteins, in order to determine the affinity for the protein on one side, and the resulting passive permeation on another side. Combining the information obtained in presence and in absence of protein, the rate of passive and/or active transport may be assessed. The implementation of such strategy early in the drug discovery process would limit the attrition rate later on the drug development process, understanding early the permeability of the candidates with a straightforward method. Moreover, as metabolism is also a crucial point in the pharmacokinetics of drug candidates, an implementation of the PAMPA with enzymes in solution (alkaline phosphatase, γ-qlutamyltranspeptidase, etc.) could also be developed, especially for the study of phyto-products, that can be very complex to understand. In order to create artificial conditions as closed as possible to in vivo conditions, buffering media may also be modified implementing experiments in plasma or in artificial media mimicking fed or fasted conditions. Such applications demand high adaptation of the protocol and specific method of detection that may decrease the high throughput efficiency of the current PAMPA methodology, but approaching the most the *in vivo* medium.

Regarding nanocarriers for CNS targeting, the future will rely on an enhanced specificity of the drug delivery systems. Hence, functionalized liposomes or nanoparticles are promoted, in order to target specific receptors or transporters at the BBB, such as the transferrin receptor, decreasing the toxicity to peripheral tissues while enhancing the potency. For these applications, PAMPA is not the adequate technique. Cellular models, able to perform active transport such as hCMEC/D3 are more reliable in order to predict what

could happen *in vivo*. However, the permeability of less hydrophilic nanocarriers such as the solid lipid nanoparticles may be determined with HDC-NPOE PAMPA and PAMPA-BBB, based on the same methodology exposed in this thesis for liposomes.

Phytochemical products were found to be good candidates for permeability assessment with PAMPA. The focus made on *Hypericum perforatum* in this thesis demonstrated that PAMPA can be employed to determine passive permeation of a total extract. On this specific topic, PAMPA may generate interesting information, isolating one or few compounds able to cross the artificial membrane *via* passive diffusion among the hundreds or thousands of components constituting a plant extract. This study could be extended to other PAMPA models, such as the phospholipid-based PAMPA-BBB, as well as cellular models able to predict both active and passive processes. Combination of such in vitro models may enable to fully understand the mode of penetration of natural products, whatever through the gastro-intestinal tract or through the blood-brain barrier, and extrapolate their potential effect at the central nervous system level.



Appendix 1: Permeability equations

Fick's first law is the starting point of the theory of diffusion. ¹. Depending on the design of the PAMPA assay, different equations can be deduced. When the retention of the compounds is considered negligible, the apparant permeability coefficient can be determined.

The Fick's first law indicates that the speed of diffusion of a molecule (J(t)) is directly linked to the concentration gradient existing on both sides of a membrane:

$$J(t) = P_a[C_D(t) - C_A(t)]$$
 (1) or $J(t) = \frac{-V_D}{A} \frac{dC_D(t)}{dt}$ (2)

Where P_a is the apparent permeability (cm/s); $C_D(t)$ and CA(t) are the concentrations of the solute in the donor and acceptor compartments at time t respectively (mol/cm³); V_D is the volume of the donor compartment (cm³), A is the surface area of the membrane (cm²), and t is the time (s). The diffusion flux is expressed in mol.cm⁻².s⁻¹.

As (1) and (2) are the same definition of Fick's first law, (1) = (2) leads to equation (3).

$$\frac{dC_D(t)}{dt} = \frac{-P_a A}{V_D} \left(C_D(t) - C_A(t) \right) \tag{3}$$

As the quantity of compounds added at time 0 will be distributed between the donor and the acceptor compartments, represented by equation (4), $C_A(t)$ can easily be expressed in function of $C_D(0)$ and $C_D(t)$ (equation (5)).

$$V_D C_D(0) = V_D C_D(t) + V_A C_A(t)$$
 (4) so $C_A(t) = \frac{V_D C_D(0) - V_D C_D(t)}{V_A}$ (5)

Equation (3) therefore becomes:

$$\frac{dC_D(t)}{dt} = \frac{-P_a A}{V_D} \left[C_D(t) - \frac{V_D C_D(0) - V_D C_D(t)}{V_A} \right]$$
 (6)

Solving this equation leads to the determination of the appararent permeability coefficient Pa:

$$P_{a} = \frac{-2.303 V_{D}}{A t} \cdot \frac{V_{A}}{V_{A} + V_{D}} log \left[1 - \frac{V_{A} + V_{D}}{V_{D}} \cdot \frac{C_{A}(t)}{C_{D}(0)} \right]$$
 (7)

However, some biological membrane are able to trap drug compounds, especially lipophilic molecules. Therefore, the retention parameter has to be introduced in the equations in order to correct the apparent permeability coefficient and determine the effective permeability coefficient P_e (cm/s).

The retention factor, which represents the quantity of compounds which is lost at the membrane or on the material, can therefore be introduced.

$$R = 1 - \frac{C_D(t)}{C_D(0)} - \frac{V_A C_A(t)}{V_D C_D(0)}$$
(8)

In these conditions, equation (4) has to introduced the quantity of compounds that may be retained at the artificial membrane or on the material:

$$V_D C_D(0) = V_D C_D(t) + V_A C_A(t) + V_D C_D(0) \cdot R \tag{9}$$

Introducing $C_A(t)$ in equation (3) and resolving the equation between τ_{lag} and t, τ_{lag} being the time needed for the first molecule to reach the artificial membrane (s), the effective permeability coefficient can be determined:

$$P_{e} = \frac{-2.303 \ V_{D}}{A \ (t - \tau_{LAG})} \cdot \left(\frac{V_{A}}{V_{A} + V_{D}}\right) \log \left[1 - \left(\frac{V_{A} + V_{D}}{V_{D} (1 - R)}\right) \cdot \frac{C_{A}(t)}{C_{D}(0)}\right]$$
(10)

This equation has been employed throughout the manuscript.

Reference

1. Avdeef, A.; Strafford, M.; Block, E.; Balogh, M. P.; Chambliss, W.; Khan, I. Drug absorption in vitro model: filter-immobilized artificial membranes. Studies of the permeability properties of lactones in *piper methysticum* forst. *Eur. J. Pharm. Sci.* **2001**, *14*, 271-280.

Appendix 2: Preparation of a SJW extract

Step 1: Soaking of the plant

In order to make an extract, part of the plant has to be soaked in appropriate solvent in order to isolate the compounds of interest. The extraction are generally performed in 2 to 4 solvent extractions, beginning with very apolar solvents such as hexane or dichloromethane, to finish with polar solvents such as methanol or water. This step lasts for 2 to 3 days.

For the purpose of the study, the aerial part of *Hypericum perforatum* is first immerged in 2 volumes of dichloromethane for 5 hours (1 volume being the volume of the dry plant). The mixture is then filtrated, and the operation is repeated twice. These extractions with dichloromethane aims to isolate the most apolar compounds of the plant.

3 cycles of solid-liquid extractions are then performed with methanol. Hypericin is extracted during this phase (a dark red solution is extracted).

Solvents are then evaporated to obtain a dry extract (either dichloromethanic or mathanolic).

Step 2: Size exclusion chromatography

The dry extract obtained in the previous step is solubilized in ethanol. The resulting solution is purified thanks to size exclusion through a column filled with Sephadex® LH-20, ethanol being the eluant.

Step 3: Fractionation of the extracts

Flash chromatography is employed for this step. Both extracts are solubilized either in dichloromethane or methanol. The resulting solutions are then separated in 5 parts (corresponding to the number of eluants that will be employed to perform the fractions). Silica is added in each part of the solubilized extract till the absorption of all the solvent. The resulting mixture is then stacked on a precolumn. A normal phase column is placed right after this precolumn. The eluants tested are dichloromethane, dichloromethane: ethyl acetate (75: 25 and 50: 50), ethyl acetate, and dichloromethane: ethyl acetate: methanol (45:45:10) for the dichloromethanic extract, and dichloromethane, dichloromethane: ethyl

acetate (75 : 25 and 50 : 50), ethyl acetate, ethyl acetate: water : formic acid (86 : 8 : 6) for the methanolic extract. This last solvent is the one recommended by the Swiss Pharmacopeia for the separation of hypericin in a methanolic extract by thin layer chromatography.

Each eluant is allowed to elute in the column for 20 minutes with a flux of 10 ml/min.

Appendix 3: Structures of the molecules employed for chapter 4

colchicine

verapamil

Appendix 4: Publications

Discovery of a Novel Class of Potent Coumarin MAO-B inhibitors: Development and Biopharmacological Profiling of 7-[(3-Chlorobenzyl)oxy]-4-[(methylamino)methyl]-2*H*-chromen-2-one methanesulfonate (NW-1772) as a Highly Potent, Selective, Reversible and Orally Active MAO-B inhibitor

Leonardo Pisani[†], Giovanni Muncipinto[†], Fabiola Miscioscia[†], Orazio Nicolotti[†], Francesco Leonetti[†], Marco Catto[†], Carla Caccia[§], Patricia Salvati[§], Ramon Soto-Otero[‡], Estefania Mendez-Alvarez[‡], Celine Passeleu[‡] and Angelo Carotti *[†]

Journal of Medicinal Chemistry, 2009, 52, 6685-6706

Methodologies to assess drug permeability through the blood-brain barrier for pharmaceutical research.

PASSELEU-LE BOURDONNEC Céline¹, CARRUPT Pierre-Alain¹, SCHERRMANN Jean Michel², MARTEL Sophie¹

Accepted for publication in Pharmaceutical Research. DOI 10.1007/s11095-013-1119-z



Discovery of a Novel Class of Potent Coumarin Monoamine Oxidase B Inhibitors: Development and Biopharmacological Profiling of 7-[(3-Chlorobenzyl)oxy]-4-[(methylamino)methyl]-2H-chromen-2-one Methanesulfonate (NW-1772) as a Highly Potent, Selective, Reversible, and Orally Active Monoamine Oxidase B Inhibitor

Leonardo Pisani, †, Giovanni Muncipinto, †, Teresa Fabiola Miscioscia, † Orazio Nicolotti, † Francesco Leonetti, † Marco Catto, † Carla Caccia, § Patricia Salvati, § Ramon Soto-Otero, † Estefania Mendez-Alvarez, † Celine Passeleu, and Angelo Carotti*,†

[†]Dipartimento Farmacochimico, Università degli Studi di Bari, Via Orabona 4, 70125-Bari, Italy, [§]Newron Pharmaceuticals Spa, Bresso (MI), Italy, [‡]Grupo de Neuroquímica, Departamento de Bioquímica y Biología Molecular, Facultad de Medicina, Universidad de Santiago de Compostela, Santiago de Compostela, Spain, and School of Pharmaceutical Sciences, University of Geneva, University of Lausanne, Switzerland. $^{\perp}L.P.$ and G.M. contributed equally to this work.

Received July 9, 2009

In an effort to discover novel selective monoamine oxidase (MAO) B inhibitors with favorable physicochemical and pharmacokinetic profiles, 7-[(m-halogeno)benzyloxy]coumarins bearing properly selected polar substituents at position 4 were designed, synthesized, and evaluated as MAO inhibitors. Several compounds with MAO-B inhibitory activity in the nanomolar range and excellent MAO-B selectivity (selectivity index SI > 400) were identified. Structure—affinity relationships and docking simulations provided valuable insights into the enzyme—inhibitor binding interactions at position 4, which has been poorly explored. Furthermore, computational and experimental studies led to the identification and biopharmacological characterization of 7-[(3-chlorobenzyl)oxy]-4-[(methylamino)methyl]-2H-chromen-2-one methanesulfonate 22b (NW-1772) as an in vitro and in vivo potent and selective MAO-B inhibitor, with rapid blood—brain barrier penetration, short-acting and reversible inhibitory activity, slight inhibition of selected cytochrome P450s, and low in vitro toxicity. On the basis of this preliminary preclinical profile, inhibitor 22b might be viewed as a promising clinical candidate for the treatment of neurodegenerative diseases.

Introduction

Monoamine oxidase (MAO, EC 1.4.3.4, amine—oxygen oxidoreductase) is a membrane-bound flavoenzyme responsible for the oxidative deamination of xenobiotic amines¹ and monoamine neurotransmitters such as serotonin (5-HT), norepinephrine (NE), and dopamine (DA).² Two distinct enzymatic isoforms, named MAO-A and MAO-B, have been identified; they differ in amino acid sequence, three-dimensional structure, organ and tissue distribution, substrate specificity, and sensitivity to inhibitors.³⁻⁹ Both enzymes oxidatively deaminate DA, whereas MAO-A preferentially deaminates 5-HT, epinephrine, and NE and is selectively inhibited by clorgyline. MAO-B preferentially metabolizes benzylamine and β -phenethylamine (PEA) and is selectively inhibited by selegiline and rasagiline (Chart 1).10,11 The involvement of MAO in the metabolism of key neurotransmitters has made it an attractive target for pharmacological

interventions in neurological disorders. The lack of selective inhibition, irreversible mechanism of action, severe side effects, e.g., hepatotoxicity and life-threatening hypertensive crisis, associated with the first-generation of antidepressant MAO-A inhibitors have stimulated further research aimed to the discovery of novel, less toxic drugs. 12,13 Several selective MAO-A inhibitors¹⁴ acting as antidepressants (i.e., moclobemide, 15 brofaromine, clorgyline, and toloxatone; Chart 1), and selective MAO-B inhibitors acting as anti-Parkinson agents (i.e., lazabemide, selegiline, safinamide, and rasagiline; Chart 1)^{16–18} have been discovered. Notably, rasagiline, approved by the U.S. Food and Drug Administration (FDA) as an anti-Parkinson drug, has been recently shown to be the first neuroprotective disease modifying drug for Parkinson's disease (PD). 19 In addition, selegiline has been recently approved as transdermal once-a-day patch formulation to treat major depressive disorders. The high doses of selegiline used in such a formulation may be responsible for MAO-A inhibition and, consequently, for the antidepressant effect.20

The MAO-B isoform is predominant in the human brain,²¹ and its level increases significantly in aging-related neurodegenerative diseases (NDs). ^{22–24} As a consequence, neurotransmitters levels are lowered and oxidative stress ^{25–27} may be induced by highly reactive hydroxyl radicals formed in the reaction between hydrogen peroxide, produced during amine

^{*}To whom correspondence should be addressed. Phone: +39-080-5442782. Fax: +39-080-5442230. E-mail: carotti@farmchim.uniba.it.

^a Abbreviations: AD, Alzheimer's disease; FAD, flavin adenine dinucleotide; HDM, hexadecane membrane; MAO, monoamine oxidase; MAO-A, monoamine oxidase A; MAO-B, monoamine oxidase B; PAMPA, parallel artificial membrane permeability assay; PD, Parkinson's disease; PDB, Protein Data Bank; PLS-DA, partial least-squares discriminant analysis; PSA, polar surface area; SAFIR, structure-affinity relationships; SSR, structure-selectivity relationships.

Chart 1. Chemical Structures of Nonselective and Selective MAO-A (A) and MAO-B (B) Inhibitors

Scheme 1. Synthesis of 7-Hydroxycoumarin Intermediates $\mathbf{1a} - \mathbf{d}^a$

 a Reagents and conditions: (method A) $\rm H_2SO_4$ conc (cat.), 120 °C, 1 h; (method B) $\rm H_2SO_4$ conc (large excess), 0 °C, 2 h; (method C) BF $_3$ · diethyl etherate, 90 °C, 24 h; (i) POCl $_3$, reflux, 4 h.

Chart 2. Starting 4-Substituted-7-hydroxycoumarin Derivatives **1a,b,d,e** and **5**

oxidation, and iron ion (Fenton's reaction). ²⁸ Selective MAO-B inhibitors have therefore attracted new interest also as neuroprotective agents in the elderly and as potential drugs in the therapy of Alzheimer's disease (AD). ^{29,30} Indeed a pronounced neuroprotective effect of selegiline and rasagiline has been claimed ^{31,32} but clinical trials of selegiline in combination with antioxidants or acetylcholinesterase inhibitors and alone in AD have shown contrasting results. ^{33–35}

Although significant advances in the design of selective MAO inhibitors (MAOIs) have been achieved in the past 2 decades, a veritable breakthrough in the field occurred only a few years ago with the publication of the X-ray crystal structures of human MAO-B (hMAO-B)^{5,36} and, to a lesser extent, rat MAO-A (rMAO-A).⁸ The high-resolution 3D structure of hMAO-B⁶ and, more recently, of hMAO-A³⁷ bound to selective, reversible, and irreversible inhibitors finally paved the way to the structure-based design of new and selective modulators of MAO activity. The wealth of information on structure and recently published methods for a medium throughput screening of MAOIs on cloned hMAOs^{38,39} might be particularly helpful for a more efficient and faster discovery of new MAOIs.

As a part of our ongoing research in this field, ^{40–47} herein we report the design, synthesis, and biochemical evaluation of a new series of coumarins that maintained the potent and selective MAO-B inhibition found for this class of compounds^{48–50} but that exhibited more appropriate physicochemical and pharmacokinetic properties for clinical applications as novel therapeutics of neurological disorders. In fact, most of the potent and selective MAO-B coumarin inhibitors studied so far have generally displayed too high lipophilicity and poor aqueous solubility, and this might strongly limit their investigations even at the level of experimental preclinical profiling. Guided by the wealth of information on structure-affinity and structureselectivity relationships (SAFIRs and SSRs, respectively) developed for coumarinic MAO inhibitors, ^{45–47,51–53} we designed a series of novel MAO-B inhibitors, maintaining the benzyloxy and m-fluorobenzyloxy or m-chlorobenzyloxy substituents at position 7 and introducing adequate polar moieties, that is, cyano, amido, amidoamino, and aliphatic amino groups, at position 4. These limited, albeit crucial, structural modifications, if tolerated, would have enabled us to identify new MAO-B inhibitors with an improved pharmacokinetic profile and a higher druggability.

The results of this investigation, which led to the discovery of an in vitro and in vivo very potent, reversible, and selective MAO-B inhibitor exhibiting appropriate pharmacologic

Scheme 2. Synthesis of Compound 3 and Aminoacidic Coumarin Derivatives 4a-h (Table 1)^a

1b or 1d
$$\stackrel{(i)}{\longrightarrow}$$
 R_3 $\stackrel{(i)}{\longrightarrow}$ R_3 $\stackrel{(iii)}{\longrightarrow}$ R_3 $\stackrel{(iii)}{\longrightarrow}$ R_3 $\stackrel{(iiii)}{\longrightarrow}$ R_3 $\stackrel{(iiiii)}{\longrightarrow}$ R_3 $\stackrel{(iiiii)}{\longrightarrow}$ R_3 $\stackrel{(iiii)}{\longrightarrow}$ R_3 $\stackrel{(iiii)}{\longrightarrow}$ R_3 $\stackrel{(i$

^a Reagents and conditions: (i) R₃C₆H₄CH₂Br, K₂CO₃, EtOH, reflux, 2 h; (ii) piperonyl alcohol, DIAD, PPh₃, dry THF, room temperature, 18 h; (iii) R₂NHCHR₁CONH₂⋅HCl, DIEA, dry DMF, 80 °C, 5 h.

Scheme 3. Synthesis of Amidoaminocoumarin Derivatives 8a-c (Table 2)^a

^a Reagents and conditions: (i) NH₂(CH₂)_nNHBoc, DCC, HOBt, dry DMF, room temperature, 5 h; (ii) R₃C₆H₄CH₂Br, dry K₂CO₃, absolute EtOH, reflux, 0.5 h; (iii) TFA, CH2Cl2, room temperature, 20 min.

Scheme 4. Solid-Phase Synthesis of Primary Amides 11a-d and 13a,b (Table 2)^a

Rink amide
$$R_3$$
 R_3 R_3

^a Reagents and conditions: (i) DIC, HOBt, dry DMF, room temperature, 15 h; (ii) DIEA, R₃C₆H₄CH₂Br or 17, dry DMF, 70 °C, 2.5 h; (iii) KHMDS, CH₃I, dry DMF, room temperature, 4 h; (iv) CH₃ONa, dry THF, room temperature, 4 h; (v) TFA/H₂O/TES, 9.5/0.25/0.25, room temperature, 1 h.

features to be progressed to clinical trials, will be presented and discussed in this paper, along with new SAFIRs, SSRs, and docking studies that provided a consistent picture of the main binding interactions modulating the MAO inhibitory potency and MAO-B isoform selectivity of this new class of coumarins. The data discussed in the present paper have been

anticipated in part in a patent⁴⁸ and at the ACS-EFMC meeting of medicinal chemistry.⁵⁴

Chemistry

The synthesis of the novel coumarin derivatives was performed according to the reaction pathways illustrated in Schemes 1–10. The starting 7-hydroxycoumarin intermediates **1a,b,d,e** and **5** depicted in Chart 2 were obtained through

Scheme 5. Synthesis of Benzoate 17^a

^a Reagents and conditions: (i) TEA, dry THF, room temperature, 0.5 h; (ii) NBS, AIBN, CCl₄, reflux, 1 h.

Scheme 6. Synthesis of 7-Pyridylmethoxycoumarin Derivatives **19a.b** (Table 2) a

^a Reagents and conditions: (i) aq NH₃, sealed tube, 90 °C, 60 h; (ii) 3- or 4-pyridinylmethanol, PBu₃, ADDP, dry THF, room temperature, 18 h.

the well-known von Pechmann reaction⁵⁵ with slight modifications^{56,57} depending on the stability and reactivity of the β -dicarbonyl reagent used (Scheme 1).

Chlorination of derivative **1c** in refluxing phosphorus oxychloride yielded regioselectively coumarin **1d**. The benzylation of **1b**,**d**,**e** with the appropriate benzyl bromide furnished target compound **3** and intermediate chlorides **2a**–**e** (Scheme 2).

Intermediate piperonyl chloride **2f** was prepared through a Mitsunobu reaction⁵⁸ starting from 7-hydroxycoumarin **1b** and piperonyl alcohol in the presence of diisopropyl azodicarboxylate (DIAD) and triphenylphospine (PPh₃). Chlorides **2a**–**f** were reacted with suitable, commercially available (*S*)-α-aminoamides, affording the target coumarins **4a**–**h** (Scheme 2).

DCC-HOBt mediated coupling of commercially available acid 5 and mono-Boc-protected hydrazine or ethylenediamine represented the first step for the synthesis of compounds 8a-c (Scheme 3). The resulting amides **6a**,**b** were benzylated at the 7-OH and then reacted with TFA in CH₂Cl₂ to remove the Boc protecting group. The selective benzylation of the 7-OH was problematic because of competitive alkylations at the acidic methylenic group at position 4 and at the amidic nitrogen of low sterically hindered secondary amides. The elimination of these undesired side reactions was accomplished by applying a solid-phase protocol to prepare primary amides 11a-d and the corresponding C-methylated analogues 13a,b (Scheme 4). 7-Hydroxycoumarinacetic acid 5 was loaded onto a Rink amide, followed by a benzylation reaction that proceeded cleanly, without the formation of byproduct, yielding the derivatized resins 10a-c. Regioselective methylation of the 4-CH₂ group was obtained using a strong and bulky base (potassium hexamethyldisilazane, KHMDS) and methyl iodide to afford resins 12a,b. The target amides 11a-d and

Scheme 7. Synthesis of Amidocoumarin Derivatives 21a-g (Table 2)

1a
$$\xrightarrow{(i)}$$
 R₃ $\xrightarrow{(ii)}$ R₃ $\xrightarrow{(iii)}$ R₃ $\xrightarrow{(iii)}$ R₃ $\xrightarrow{(iii)}$ 20a,b 21a-g

 a Reagents and conditions: (i) ADDP, PPh₃, R₃C₆H₄CH₂OH, dry THF, room temperature, 18 h; (ii) R₁R₂NH, dry THF, 90 °C, sealed tube, 24–60 h.

Scheme 8. Synthesis of Aminocoumarin Derivatives 22a-k and 24a,b (Table 3)^a

"Reagents and conditions: (i) R₁R₂NH, dry THF, 50 °C, 5 h; (ii) EtNH₂70% water solution, room temperature, 3 h; (iii) isopropylamine, reflux, 2 h; (iv) N-methylbenzylamine or benzylamine, K₂CO₃, EtOH, reflux, 2-5 h; (v) sodium azide, EtOH, reflux, 2 h; (vi) SnCl₂, MeOH, room temperature, 3 h.

Scheme 9. Synthesis of 4-Aminoethylcoumarin Derivative **26** (Table 3)^a

11a,b (i)
$$R_3 = CI$$
 $R_3 = CI$ $R_3 = CI$

Scheme 10. Synthesis of 4-Aminoethylcoumarin Derivatives 30a,b (Table 3)^a

13a,b were obtained upon cleavage from the resin with a TFA/ H₂O mixture containing triethylsilane as proton scavenger.

The preparation of amide 11d required different additional synthetic steps consisting of the removal of the benzoyl protecting group with sodium methoxide (from resin 10d) and of the separated synthesis of benzyl bromide 17 (Scheme 5) that began with the benzovlation of *m*-cresol followed by the bromination of ester 16 with NBS and AIBN.

The ammonolysis of ester 1a with aqueous NH₃ in a sealed tube afforded amide 18 in excellent yields. The introduction of 3- and 4-pyridinylmethoxy moiety at position 7 (compounds 19a,b; Scheme 6) was performed following a standard Mitsunobu protocol with tributylphosphine (PBu₃) and 1,1'-(azodicarbonyl)dipiperidine (ADDP), thus avoiding the use of relatively unstable pyridylmethyl bromides.

As described in Scheme 7, preliminary benzylation reaction of 7-hydroxycoumarin 1a under Mitsunobu conditions afforded the esters 20a,b that were reacted with a suitable aliphatic amine to yield secondary and tertiary amides 21a-g.

As outlined in Scheme 8, the substituted amines 22a-k were easily obtained by nucleophilic substitution of chlorides 2c-f with the appropriate amines. Primary amines 24a,b were synthesized from azides 23a,b obtained by refluxing chlorides 2c,d with sodium azide in ethanol, as illustrated in Scheme 8. In this case, despite the tedious and potentially toxic purification procedure, SnCl₂ proved to be the most effective method for reducing azides compared to the traditional Staudinger reduction with PPh₃/H₂O,⁵⁹ Sn(II)/thiophenol/triethylamine⁶⁰ reducing system, or catalytic hydrogenation.

The elongation of the aliphatic bridge linking the aminic moiety at position 4 to the coumarin ring was pursued according to the reaction pathway illustrated in Scheme 9. Amides 11a,b were converted into the corresponding nitriles 25a,b upon treatment with trifluoroacetic anhydride in pyridine according to an efficient method developed by some of us many years ago. 61 The reduction of nitrile 25b with sodium borohydride and CoCl₂ afforded the desired primary amine 26. An alternative synthetic pathway (Scheme 10) was followed to access secondary and tertiary amines.

The carboxylic group of compound 5 was selectively reduced by the BH₃-THF complex, and the resulting dihydroxylated derivative 27 was benzylated at the phenolic OH in the presence of potassium carbonate and a catalytic amount of KI in refluxing ethanol. The alcohols 28a,b underwent an Appel-type mild bromination with CBr₄ and PPh₃. The subsequent nucleophilic displacement of the bromide anion with the appropriate amine yielded the final amines 30a,b.

Physicochemical Assays

 $\log P$, p K_a , and Aqueous Solubility Measurements. The p K_a and octanol-water partition coefficient were measured by potentiometric methods⁶² with a Sirius GLpKa instrument. Aqueous solubility was determined with the DMSO-buffer dilution turbidimetric method⁶³ according to a reported procedure.64

PAMPA Permeation Assay. Selected MAO inhibitors were analyzed using PAMPA (parallel artificial membrane permeability assay), a method recently developed for the rapid determination of passive transport. 65 In PAMPA, an artificial liquid membrane is used to separate two compartments, one containing a buffer solution of compounds to be tested (defined as the donor compartment) and the other an initial fresh buffer solution (defined as the acceptor compartment) assembled in a "sandwich-like" configuration. The permeation of tested compounds through the artificial membrane is determined after a fixed incubation time by disassembling the "sandwich" and measuring sample concentrations in the donor and acceptor compartments.

^a Reagents and conditions: (i) TFAA, dry pyridine and dioxane, 0 °C to room temperature, 10 min; (ii) NaBH₄/CoCl₂, MeOH, room temperature, 1 h.

^a Reagents and conditions: (i) BH₃·THF complex, dry THF, room temperature, 6 h; (ii) R₃C₆H₄CH₂Br, K₂CO₃, EtOH, reflux, 45 min; (iii) CBr₄, PPh₃, dry CH₂Cl₂, room temperature, 1 h; (iv) R₁R₂NH, K₂CO₃, KI, dry THF, 50 °C, 15 h.

Chart 3. General Structures of Novel 4,7-Disubstituted Coumarin MAOIs (Tables 1-4)

Table 1. MAO Inhibitory Activity of (S)-Aminoamidocoumarin Derivatives **4a−h**

compd	n	R_1	R_2	R_3	$MAO-A^a$	$MAO-B^a$	SI^b
4a	0	CH ₃	Н	Н	100	0.68	147
4b	0	CH_3	Н	Cl	35%	0.21	
4c	0	$-CH_2CH_2C$	CH_2-	Н	99.8	16.1	6
4d	0	$-CH_2CH_2C$	CH_2-	Cl	5%	9.60	
4e	0	CH_2OH	Н	Cl	> 100	2.40	> 42
4f	1	CH_3	Н	Н	22.7	1.80	13
4g	1	$-CH_2CH_2C$	CH_2-	Н	35	0.38	92
4h	1	-CH ₂ CH ₂ C	CH ₂ -	F	> 100	0.85	> 117

 a IC₅₀ (μ M) or % inhibition at 10 μ M. b SI = [IC₅₀ MAO-A (μ M)]/[IC₅₀ MAO-B (μ M)].

The HDM-PAMPA (hexadecane membrane assay targeting GI track) assay developed by Wohnsland and Faller, 65 making use of an artificial liquid membrane composed of hexadecane supported on polycarbonate filters for the prediction of passive transcellular permeability, was used as a low cost and efficient alternative to the Caco-2 cell culture model. 66

Biological Assays

In Vitro MAO Inhibition. Rat brain mitochondria were used as the source for the two MAO isoforms. MAO enzymatic activities were assessed with a radioenzymatic assay using ¹⁴C-serotonin (5-HT) and ¹⁴C-phenylethylamine (PEA) as selective radiosubstrates for MAO-A and MAO-B, respectively, according to a well consolidated procedure. ⁶⁷ For compound **22b** the MAO-B radioenzymatic assay was performed also in human platelet rich plasma (PRP). ⁶⁸

In Vitro MAO B Reversibility Inhibition Studies. The reversible nature of MAO-B inhibition was assessed by evaluating the enzymatic activity upon different incubation time experiments. Time-dependent association kinetics were measured as the $\rm IC_{50}$ values after 0 and 30 min enzyme—inhibitor incubation in the assay medium.

Ex Vivo MAO Inhibition. Mice were treated with the test compound at different oral and intraperitoneal concentrations and sacrificed at different time intervals. The brains were removed, and crude homogenates were prepared in 0.1 M phosphate buffer, pH 7.40. Ex vivo MAO-A and MAO-B enzymatic activities were assessed according to the radioenzymatic assay described above.

In Vitro Human Recombinant Cytocrome P450 Isoform Assay. Inhibition of six key cytochrome P450 isoforms (CYP1A2, CYP2C9, CYP2C19, CYP2D6, CYP2E1, and

CYP3A4) was measured in distinct assays by using specific substrates that become fluorescent upon CYP-promoted metabolism (Gentest Kit assay, BD Biosciences, Bedford, MA).

In Vitro Cell Viability Assay. The SHSY-5Y continuous cell line from a human neuroblastoma was used and cell viability measured by the colorimetric MTS assay.⁶⁹

Computational and Molecular Modeling Studies

Building and optimization of small molecules and MAO homology modeling were performed with Sybyl (Tripos, St. Louis, MO) and Modeller (DBSPC, University of California—San Francisco, San Francisco, CA) software, respectively. Docking simulations were carried using the GOLD program (Cambridge Crystallographic Data Centre, Cambridge, U.K.).

Polar surface area (PSA), a molecular descriptor largely used to roughly estimate oral bioavailability of potential drugs, ⁷⁰ and LogBBB, a parameter related to the drug capability to cross the blood brain barrier (BBB)⁷¹ were calculated by using Volsurf+ (Molecular Discovery, Perugia, Italy).

Results and Discussion

4-Methyl-7-(*m*-chlorobenzyloxy)coumarin **3** was designed and synthesized as the compound bearing the simplest hydrophobic substituent at position 4. It was considered as an appropriate reference compound to which the biochemical, physicochemical, and pharmacokinetic properties of the newly designed 4,7-disubstituted coumarins, bearing polar groups at position 4, were to be compared.

Compound 3 exhibited high in vitro MAO-B affinity and a very low affinity to MAO-A (IC₅₀ of 0.007 and 5.2 μ M, respectively). Its estimated lipophilicity and aqueous solubility indicated a high octanol—water partition coefficient (P; log P=4.73, from Bioloom-BioByte Corp., Claremont, CA) and a poor aqueous solubility ($S=2.63\times10^{-5}$ M, from ACD, version 12, Advanced Chemistry Development, Toronto, Canada).

The chemical structures of the newly designed series of 4,7-disubstituted coumarins are shown in Chart 3, whereas their MAO-A and MAO-B affinities and selectivity indices are listed in Tables 1–4.

Inhibition data of both MAO isoforms are reported as IC_{50} (μ M) or as the percentage of inhibition at the indicated concentration for low-active inhibitors. Selectivity was expressed as selectivity index (SI), which is the ratio of the IC_{50} of MAO-A to the IC_{50} of MAO-B. For an immediate and more efficient analysis of SAFIRs and SSRs, inhibition data

Table 2. MAO Inhibitory Activity of Amidocoumarin Derivatives 8a-c, 11a-d, 13a,b, 19a,b, and 21a-g

compd	R_1	R_2	R_4	R_3	X	Y	MAO-A ^a	MAO-B ^a	SI^b
8a	Н	NH ₂	Н	Н	СН	СН	1.44	0.040	36
8b	Η	NH_2	Η	Cl	CH	CH	2.50	0.090	28
8c	Н	$(CH_2)_2NH_2$	Н	Cl	CH	CH	> 100	> 10	nd
11a	Η	H	Η	Η	CH	CH	8.0	0.20	40
11b	Η	H	Η	Cl	CH	CH	26	0.030	867
11c	Η	H	Η	F	CH	CH	70	0.050	1400
11d	Η	H	Η	OH	CH	CH	4.27	1.0	4
19a	Η	H	Η	Η	CH	N	21.0	1.30	16
19b	Η	H	Η	Η	N	CH	26.5	2.0	13
21a	Me	H	Η	Η	CH	CH	2.80	0.015	187
21b	Me	H	Η	Cl	CH	CH	0.50	0.024	21
21c	Bu	H	Н	Cl	CH	CH	> 100	> 10	nd
21d	Bn	H	Η	Cl	CH	CH	> 100	5.0	> 20
21e	Me	Me	Η	Η	CH	CH	23.1	0.40	58
21f	Me	Me	Н	Cl	CH	CH	> 100	0.040	> 2400
21g	Bu	Me	Η	Cl	CH	CH	> 100	> 10	nd
$13a^c$	Н	H	Me	Η	CH	CH	6.26	0.10	63
13b ^c	Н	Н	Me	F	CH	CH	2.0	0.10	20

 $^{^{}a}$ IC₅₀ (μ M). b SI = [IC₅₀ MAO-A (μ M)]/[IC₅₀ MAO-B (μ M)]. c Tested as racemate.

Table 3. MAO Inhibitory Activity of Aminocoumarin Derivatives 22a-k, 24a,b, 26, and 30a,b

compd	n	R_1	R_2	R_3	$MAO-A^a$	$MAO-B^a$	SI^b
22a	1	CH ₃	Н	Н	15.4	0.028	550
$22b^c$	1	CH_3	Н	Cl	5.94	0.013	457
$22c^c$	1	CH_3	Н	F	13.5	0.018	750
22d	1	CH_3	Н	e	5.40	0.020	270
$22e^c$	1	CH_2CH_3	Н	F	22.6	0.10	226
$22f^c$	1	$CH(CH_3)_2$	Н	F	91.0	3.80	24
22g	1	Bn	Н	Cl	> 100	3.60	> 28
22h	1	CH_3	CH_3	Η	100	1.80	56
22i	1	CH_3	CH_3	Cl	50.8	1.12	45
22j	1	CH_3	CH_3	F	> 100	0.51	> 196
22k	1	CH_3	Bn	Cl	> 100	8.0	> 13
24a	1	Н	Н	Η	4.40	0.021	210
24b	1	Н	Н	Cl	2.0	0.015	133
26^{d}	2	Н	Н	Cl	31.8	0.25	127
30a	2	CH_3	Н	Cl	74.0	0.30	247
30b	2	CH_3	CH_3	Η	25.9	0.46	56

 $[^]a\mathrm{IC}_{50}$ ($\mu\mathrm{M}$). $^b\mathrm{SI}=[\mathrm{IC}_{50}$ MAO-A ($\mu\mathrm{M}$)]/[IC_{50} MAO-B ($\mu\mathrm{M}$)]. $^c\mathrm{Tested}$ as mesylate. $^d\mathrm{Tested}$ as hydrochloride. $^e\mathrm{R}_{\mathrm{meta-para}}=-\mathrm{OCH}_2\mathrm{O}-$.

Table 4. MAO Inhibitory Activity of 4-Cyanomethylcoumarin Derivatives 25a,b

compd	R_3	MAO-A ^a	$MAO-B^a$	SI^b
25a	Н	0.20	0.23	0.9
25b	Cl	0.47	0.016	29

 $^{{}^{}a}IC_{50} (\mu M). {}^{b}SI = [IC_{50} MAO-A (\mu M)]/[IC_{50} MAO-B (\mu M)].$

are presented also in Figure 1 as a plot of pIC₅₀ of MAO-B (x-axis) versus pIC₅₀ of MAO-A (y-axis) using the same scale and range for both axes (square plot). For immediate location, the different classes of coumarin inhibitors, i.e., aminoamides (Table 1), carboxyhydrazides and amides (Table 2), amines (Table 3), nitriles (Table 4), and the reference compound 3 are indicated in the plot with differently colored circles. Unfortunately, the low MAO-A affinity, often associated with a limited solubility in the aqueous assay medium, did not permit the measurement of IC₅₀ (IC₅₀ > 100 μ M) for some compounds, and therefore, they are not shown in the plot. To avoid the loss of an important data point, compound 21f,

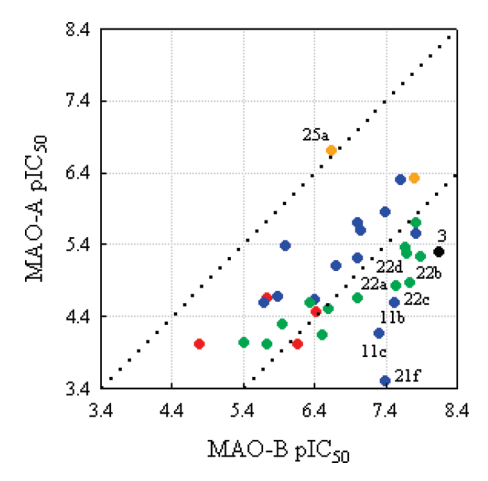


Figure 1. Square plot of rMAO affinity and selectivity. The different classes of coumarin inhibitors in Tables 1–4 and reference compound 3 are indicated with red, blue, green, orange, and black circles, respectively. Bottom-right corner contains potent and highly selective rMAO-B inhibitors. The most potent and selective MAO-B inhibitors are highlighted by black labels along with the only nonselective inhibitor 25a.

which is a potent and selective MAO-B inhibitor, was plotted with an estimated pIC₅₀ of MAO-A equal to 3.50.

Compounds with identical affinities at both isoenzymes lie on the bisector (y=x) of the graph, whereas highly selective MAO-B inhibitors lie well below the bisector, the distance of their pIC₅₀ values from the bisector being a direct measure of their degree of selectivity. A line traced at two pIC₅₀ unit distance below the bisector enables the straightforward location of inhibitors with a selectivity index—affinity ratio (SI) higher than 100 (i.e., Δ pIC₅₀ > 2).

At a first glance, the plot indicates that very potent and selective MAO-B inhibitors were discovered and that no apparent relationship exists between MAO-A and MAO-B inhibitory affinities. Only the cyano derivative **25a** lies on the bisector, exhibiting nearly equal affinity to both enzymes. MAO-A affinity was generally very low, and only in a very few cases, i.e., for the two cyanomethyl derivatives **25a,b** and the *N*-methlycarboxamidomethyl derivative **21b**, did affinities reach the submicromolar range.

Inhibitors endowed with both high MAO-B affinity and selectivity (i.e., both high pIC_{50} and SI values) are located at the bottom of the right-hand corner of the plot and belong mostly to the aminic and the amidic series (Tables 2 and 3, respectively). The most interesting compounds in terms of MAO-B affinity and selectivity, e.g., amides 22a-d and amines 11b,c, are highlighted in the plot.

A comparison of the MAO-B inhibition of 4-CH₂X-7-(m-chlorobenzyloxy)coumarins (Tables 1–4) revealed the following order of potency $24b \ge 25b > 11b > 8b > 4b > 26$, suggesting that the simple cyano, primary amino, and amido groups (X = CN, NH₂, and CONH₂, respectively) are highly preferred polar substituents at position 4 for an efficient binding to MAO-B.

A similar comparison of the MAO-B affinity of differently meta-substituted benzyloxy derivatives revealed that inhibitors bearing *m*-chloro and -fluoro substituents were generally more active than the corresponding benzyl-unsubstituted parent compounds. Moreover, the replacement of the 7-benzyloxy group with the 3- and 4-pyridylmethoxy isosteric substituents led to a significant decrease of affinity (compare **11a** vs **19a** and **19b**). These results are in full agreement with our previous

findings and confirm that the lipophilicity of the substituent at position 7 plays a crucial role in selective and efficient binding to MAO-B. 45,46,72

The most salient results emerging from a careful evaluation of the MAO-B affinity and selectivity variation within the different classes of coumarin derivatives reported in Tables 1–3 can be summarized as follows.

A dramatic reduction of MAO-B affinity, in comparison with reference compound 3, was observed for all the synthesized alanyl-, prolin-, and serin-amide derivatives 4 (Table 1) bearing the α -aminoamido moiety directly linked to the coumarin ring (i.e., 4a-e) or bridged to it through a methylenic unit (i.e., 4f-h). The less active MAO-B inhibitors were the more rigid prolinamide derivatives 4c,d, whereas alaninamide derivatives 4a,b and the more conformationally flexible prolinamide derivatives 4g,h exhibited submicromolar MAO-B affinities. The SIs ranged from 6 to 147, and no clear SSR emerged from their analysis.

Nanomolar MAO-B inhibitory potencies were shown by 4carboxyhydrazidomethylcoumarin derivatives 8a,b and by the 4-carboxamidomethylcoumarin, 4-N-methylcarboxamidomethylcoumarin, and 4-N,N-dimethylcarboxamidomethylcoumarin derivatives 11b,c, 21a,b, and 21f, respectively. MAO-B affinity of 7-m-chlorobenzyloxy derivatives remained high and nearly constant going from carboxamido (11b) to N-methylcarboxamido (21b) and to N,N-dimethylcarboxamido (21f) coumarin derivatives but dramatically diminished as the size of the N-alkyl substituent(s) increased as in compounds 21c,d,g. As previously anticipated, the isosteric substitution of the 7-benzyloxy group with the 3- and 4-pyridylmethoxy groups led to a significant decrease of affinity (compare 19a,b vs 11a). C-Methylated 7-m-chlorobenzyloxy and 7-m-fluorobenzyloxy racemates 13a,b displayed high and equal affinities to MAO-B. Compound 8c, an N-aminoethyl derivative of the 4-carboxamidomethylcoumarin 11b, was found completely inactive at both MAO isoforms. Potent and highly selective MAO-B inhibitors were found in the class of 4-carboxamidomethylcoumarins in Table 2. The 7-m-halogenobenzyloxy derivatives 11b,c and 21f exhibited IC₅₀/SI values equal to 0.030/867, 0.050/1400, and 0.040/2400, respectively. Very surprisingly, the Nmethylcarboxamide 21b was endowed with the highest MAO-A affinity of the entire series of tested inhibitors. Conversely, its close N,N-dimethyl analogue 21f was completely inactive at the same enzyme isoform (IC₅₀ > 100 μ M). This striking difference was quite unexpected and very difficult to interpret.

Affinity data of 4-aminomethyl- and 4-aminoethylcoumarins (Table 3) indicated that the most potent MAO-B inhibitors belong to this class of compounds and that high SIs are also associated with many of them. In fact, compounds **22a**—**d** can be seen in the region of highly potent and selective inhibitors (i.e., in the lower right-hand corner of the plot in Figure 1).

The 4-*N*-methylaminomethyl derivatives **22b** and **22c**, bearing at position 7 a *m*-halogenosubstituted benzyloxy group, and the 4-aminomethyl-7-(*m*-clorobenzyloxy)coumarin derivative **24b** exhibited the highest MAO-B inhibitory potencies (IC₅₀ of 13, 18, and 15 nM, respectively) and high SIs (457, 750, and 133, respectively). The presence of *N*-alkyl groups larger than the methyl group decreased the affinity (compare **22c** vs **22e** and **22f**, and **22b** vs **22g**). Similarly, *N*,*N*-dimethyl derivatives were less potent than the corresponding *N*-methyl analogues (compare **22a** vs **22h**, **22b** vs **22i**, and **22c** vs **22j**). A steric effect can be hypothesized around the position 4 as previously observed for the *N*-alkyl- and the *N*,*N*-dialkylcarboxamido

derivatives (Table 2). The finding that the most hindered N,N-dialkylamine (22k) and N,N-dialkylcarboxamide (21g) derivatives yielded the lowest MAO-B affinity (IC₅₀ of 8 and > 10 μ M) of the entire series of the two classes of examined inhibitors in Tables 2 and 3 might lend support to this hypothesis.

The short elongation of the aliphatic chain at position 4 of 7-*m*-chlorobenzyloxy derivatives **24b** and **22b** afforded compounds **26** and **30a**, respectively, exhibiting significantly lower MAO-B affinities.

Molecular Modeling Studies. The SAFIRs and SSRs discussed previously provided useful information on the main molecular determinants of the inhibitor potency and selectivity; however, a clear picture of the main interactions taking place at the binding sites of the two rat isoenzymes was still missing. A modeling study was therefore carried out through homology building and docking simulations for the purpose of (i) gaining insights on the nature and spatial location of the key interactions of the 4-substituents modulating the MAO-B affinity, (ii) explaining the excellent MAO-B selectivity observed for some classes of examined coumarins, and (iii) confirming, complementing, and better interpreting the results of previous studies conducted by our group on different sets of coumarin derivatives. 45,46

Analysis of crystal structures of hMAO-B in complex with several inhibitors^{6,36,56} revealed that the binding site consists of two cavities, the "substrate cavity" located near the FAD cofactor and the "entrance cavity", connected to the protein surface. The two cavities are separated by residues Tyr326, Ile199, Leu171 and Phe168, with Ile199 and Tyr326 behaving as gate-keeper residues. However, our attention was also drawn by other, apparently less important, structural features, i.e., the cocrystallized water molecules embedded in the reported X-ray complexes of hMAO-B. It is known that water molecules may become trapped in the protein crystal structure and, in addition, a number of them may contribute to the stabilization of the protein structure or of the protein-ligand complex through the formation of a network of hydrogen bonds bridging the ligand to specific binding site residues. 73,74 These structural water molecules are often conserved in crystallographic complexes of different ligands with the same macromolecular ligate and may play an important role in docking simulations and virtual screening. 75,76 Therefore, the detection of water molecules assuming a structural role in ligand binding is an important prerequisite to improve binding mode prediction of new ligands and the hit selection rate in docking virtual screening. 77,78 Accordingly, in a recent study of hMAO-B crystal structure (PDB code lojc),46 we designated as structural water those molecules intercepting the energetic hot spots mapped on a grid through a water molecule probe available in GRID.⁷⁹ A minimum of four water molecules were assumed to be critical in the ligand binding with MAO-B. To our satisfaction, our findings were recently largely confirmed in a study based on the structural sampling of water molecules occurring in different PDB crystals released for hMAO-B.³⁹ Starting with these observations, we carried out an accurate analysis of the hMAO-B complex (PDB code 2v60) that included 11 water molecules within a sphere of 6 Å around the cocrystallized inhibitor, the 4-formyl-7-m-chlorobenzyloxycoumarin (4-FCBC). Campaigns of molecular docking simulations were then conducted to select among the 11 water molecules those influencing inhibitor binding. Such a selection was done comparing the accuracy of docking simulations in successfully reproducing

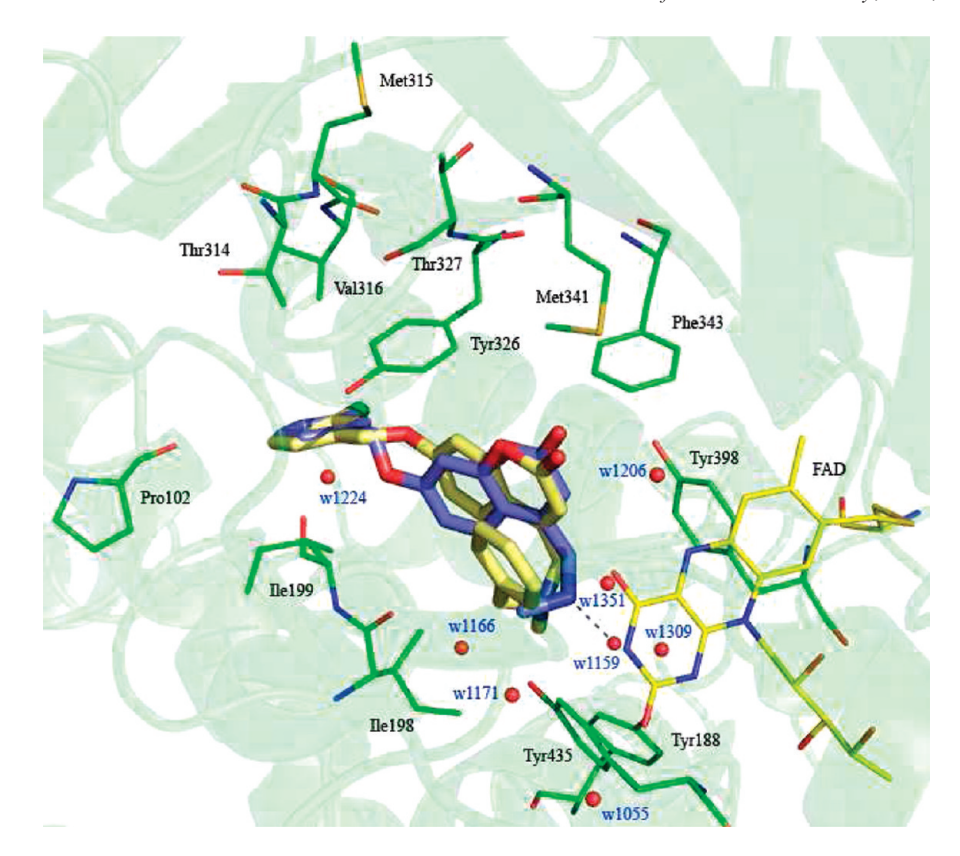


Figure 2. Docking poses of inhibitors 22b and 22k (rendered in yellow and cyan stick models, respectively) into rMAO-B binding site. Amino acid residues and FAD cofactor are represented in thin line form, colored according to the atom code (C atoms in green and yellow for amino acid residues and cofactor, respectively). Structural water molecules are represented as red balls. Hydrogen bonds are drawn as dark-blue dashed lines.

the binding mode of the cocrystallized 4-FCBC into hMAO-B binding site. As in previous studies, GOLD software was used in all the simulations. The best combination of water molecules, returning the lowest rmsd value of 0.578 Å with a docking score of 59.46 kJ/mol, included eight water molecules labeled as w1055, w1159, w1166, w1171, w1206, w1224, w1309, and w1351 according to the numbering reported in the cited hMAO-B X-ray complex. Given that our MAO inhibition data were determined on rat brain mitochondria assay, we first developed a 3D homology model of rat MAO-B for which no crystallographic data were available, starting from the rMAO-B sequence and the Cartesian coordinates of the PDB 2v60 complex. A proper fitting was also set for reconstructing the position in rMAO-B of both the FAD cofactor and the eight designated water molecules coming from the hMAO-B analysis. Confidence in the developed homology model was ensured by the high primary structure similarity (88%) and more so by the high degree of residue conservation into the binding site of rat and human enzymes. The cocrystallized 4-FCBC ligand of the 2v60 PDB structure did not exhibit appreciable binding differences with the hMAO-B when docked into the rMAO-B model. Only slight geometrical differences (rmsd = $0.855 \,\text{Å}$) were observed without any remarkable change in the binding topology. In light of these encouraging results, the chemical scaffold of the best ranked solution of the coumarin inhibitor 4-FCBC docked into the rMAO-B was used to physically constrain the docking simulations of selected inhibitors. The constraint was limited to the 7-benzyloxy substituents that were found to always assume a preferred binding conformation into the hydrophobic binding site composed of Val316, Pro102, Tyr 326, Ile198, and Ile199 side chains. A visual inspection of Figures 2 and 3 revealed that the selected and docked inhibitors 22b and 22k, and 22c and 22f, respectively, adopted a convergent binding mode with the coumarin ring facing the FAD moiety and the lactonic carbonyl generally involved in a hydrogen bond with the hydroxyl group of Tyr398. In addition, it was found that while amides or amines with small Nalkyl substituents at position 4 of the coumarin ring were well accommodated into the protein binding site and the protonated nitrogen atoms formed hydrogen bonds with water molecules w1351, w1166, and w1159 affording high Gold-Score values (59.86, 55.30, 53.35, and 65.70 kJ/mol, for 11b, **22b**, **22c**, and **24b**, respectively), the presence of bulkier Nalkyl groups such as isopropyl (22f), n-butyl (21c), or benzyl (22k) decreased the capability of establishing valuable binding interactions with specific amino acid side chains and water molecules into the protein binding site, leading to significantly lower GoldScores values (45.38, 46.56, and 44.44 kJ/mol, respectively).

Although docking score energy was mainly related to hydrophobic interactions that should be increasingly relevant for larger groups, in our analysis no significant difference occurred when comparing van der Waals terms of coumarins substituted at position 4 with small (22b and 22c) and large (22k and 22f) substituents. A major propensity to form hydrogen bonds was instead observed in 4-substituted coumarins bearing small (22b and 22c) rather than large (22k and 22f) substituents as denoted by the values of the external hydrogen bond term. As unequivocally shown in Figures 2 and 3, inhibitors with large groups at position 4 adopted folded conformations, and this may distort the correct geometry for a strong hydrogen bond interaction

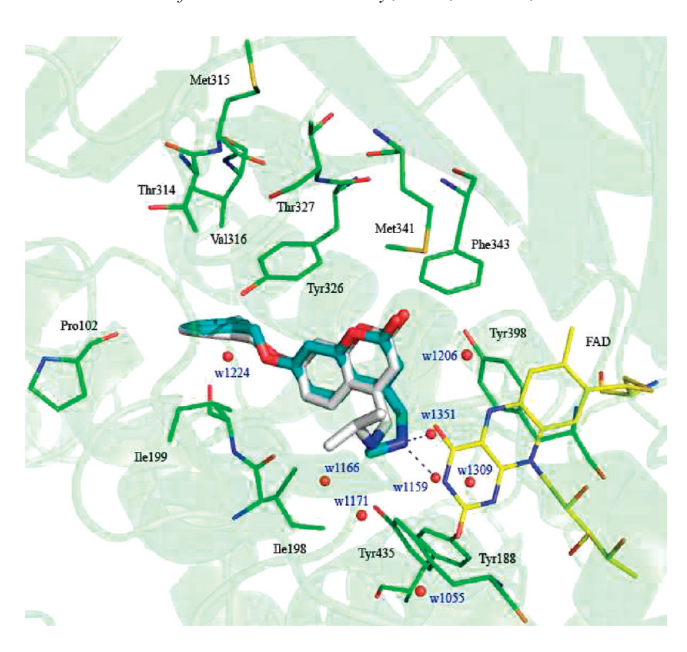


Figure 3. Docking poses of inhibitors **22c** and **22f** (rendered in light-blue and white stick models, respectively) into rMAO-B binding site. Amino acid residues and FAD cofactor are represented in thin line form, colored according to the atom code (C atoms in green and yellow for amino acid residues and cofactor, respectively). Structural water molecules are represented as red balls. Hydrogen bonds are drawn as dark-blue dashed lines.

between protonated nitrogens and surrounding water molecules. In addition, the analysis of GoldScore values attributed to each of the 10 top-scored poses per compound revealed a narrower standard deviation for both 22b and 22c (approximately $\pm 4\%$) compared to both 22k and 22f (approximately $\pm 6.5\%$). Finally, the energy gap between top and bottom scored docking solutions of 22b and 22c compared to 22k and 22f increased from about 13 to 29 kJ/mol. Taken together, all the above observations clearly indicated that large groups at position 4 can be accommodated only at the expense of high-energy inhibitor conformations unable to engage optimal ligand—protein interactions.

Interestingly, 4-substituted 7-(*m*-halogenobenzyloxy)coumarins exhibited generally higher docking scores compared to the corresponding unsubstituted benzyloxy derivatives, according to the experimental inhibition data.

Further analyses were carried out to investigate the reasons behind the pronounced selective inhibition of MAO-B exhibited by most of the coumarins analyzed. Given that only a low-resolution rMAO-A complex was available and water molecules were even missing (PDB code 1o5w), our investigation was focused on the hMAO-A/harmine complex (PDB code 2z5x). Rat and human MAO-A exhibited strong structural resemblance with an rmsd equal to 0.438 Å, a sequence similarity of 87%, and a binding site with identical amino acid residues. Interestingly, 7 out of the 8 selected water molecules for hMAO-B (w1055, w1159, w1166, w1171, w1206, w1309, and w1351) were also preserved in the hMAO-A binding site. These water molecules were therefore transferred into the rMAO-A crystal structure before running molecular docking simulations on a number of highly selective MAO-B inhibitors (i.e., 11c, 11b, 22a, and 22c). Because no MAO-A X-ray complex with coumarin ligands was available, the docking simulations were conducted without constraints. Not surprisingly, as shown in Figure 4, a diverse and somehow divergent binding

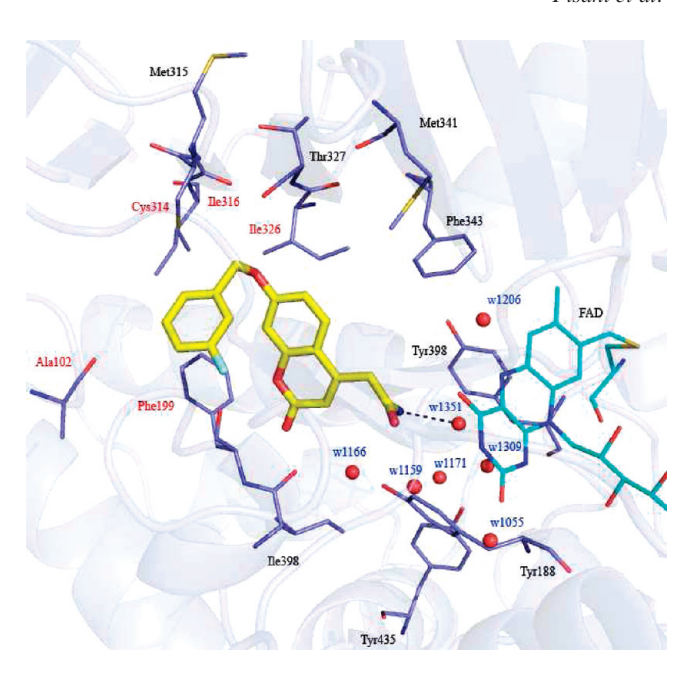


Figure 4. Top-score docking pose of inhibitor **11c**, rendered in yellow stick model, into rMAO-A binding site. Amino acid residues and FAD cofactor are represented in thin line form, colored according to the atom code (C atoms in blue and cyan for amino acid residues and cofactor, respectively). Structural water molecules are represented as red balls. Hydrogen bonds are drawn as darkblue dashed lines. The different amino acids with respect to rMAO-B residues are labeled in magenta according to the numbering of rMAO-B.

mode was observed in both rMAO-A and rMAO-B. Moreover, in rMAO-A, a remarkable lowering of docking scores was generally found. For instance, for inhibitor **11c** a Gold-Score of 19.92 kJ/mol was measured. The presence of diverse residues forming the entrance cavity of the rMAO-A compared to rMAO-B (i.e., Phe199Ile, Ala102Pro, Cys314Thr, Ile316Val and Ile326Tyr) is supposed to determine a different orientation of **11c**. As illustrated in Figure 4, a number of favorable hydrogen bonds and hydrophobic interactions was lost in rMAO-A compared to rMAO-B.

Binding, Physicochemical, and Biopharmacological Profiling of 22b Mesylate. Experimental MAO-B affinity and selectivity, as well as the estimated promising lipophilicity and aqueous solubility of the 7-(*m*-chlorobenzyloxy)-coumarin derivative 22b, prompted a deeper in silico and experimental investigation of its physicochemical and biopharmacological profiles. Indeed, the X-ray crystallographic structure of the complex of 22b with human MAO-B has been solved and published by the Mattevi group and our group 2 years ago⁵⁶ and the main inhibitor-enzyme binding interactions have been identified and discussed therein.

As for the physicochemical characterization of **22b**, aqueous solubility (S), pK_a , octanol—water partition coefficient (P), permeability coefficient (P_s) , for passive oral absorption), blood—brain barrier permeability coefficient (LogBBB), and PSA, all relevant physicochemical parameters for drug dissolution, absorption, and distribution were experimentally or computationally determined.

Aqueous solubility of **22b**, assessed by the DMSO-buffer dilution turbidimetric method⁶³ at pH 7.4 and 3.0 was 52 μ g/mL and 2.82 mg/mL, respectively, whereas p K_a and log P determined by potentiometric titration using the Sirius GLpKa instrument (Sirius Analytical Instruments Ltd.,

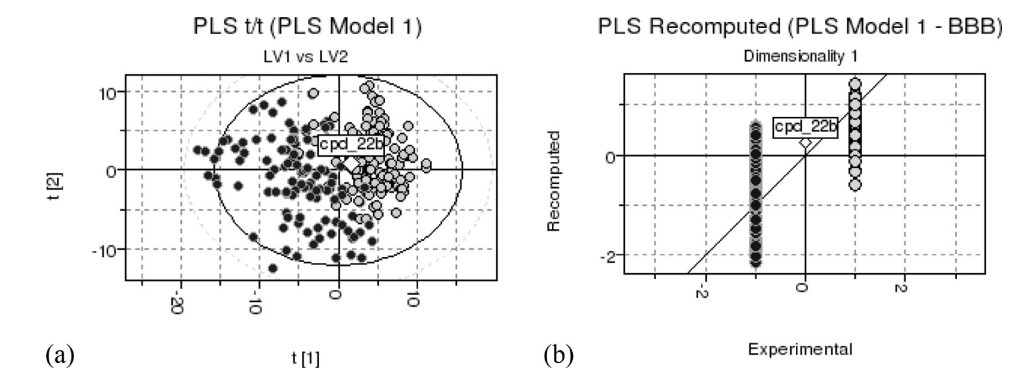


Figure 5. (a) Discriminant PLS t1-t2 analysis score plot for the BBB permeation model. BBB+ and BBB±/BBB- compounds are represented as dark and light solid gray circles respectively. Predicted compound 22b is indicated by the solid white diamond. (b) Experimental vs predicted BBB values for model compound along with projection for the predicted 22b.

Table 5. Permeability Data from HDM-PAMPA Assay

compd	$R^{a}(\%)$	$C_{\rm A}(t)/C_{\rm D}(0)^{b} (\%)$	log P _e ^c
22b	10 ± 3	33.8 ± 0.3	-3.48 ± 0.01
3	72 ± 1	3.7 ± 0.3	-4.13 ± 0.10

 $^{^{}a}R = \%$ of retention through the artificial membrane. $^{b}C_{A}(t)/C_{D}(0) =$ % of compound that reaches the acceptor compartment. $^{c}P_{e} = \text{effective}$ permeability coefficient expressed in cm/s.

Forest Row, East Sussex, U.K.) were 7.18 \pm 0.05 and 2.49 \pm 0.03, respectively. PSA, another computational parameter used along with the rule of five of Lipinski to roughly estimate oral drug absorption, 66 was 49.8 Å², a value compatible with good biovailability and BBB permeation.⁷

Passive oral absorption of 22b, was also evaluated experimentally by using the parallel artificial membrane permeability assay (PAMPA).65,80 Experimental values of the retention through the artificial membrane (R, %), the quantity of compound reaching the acceptor compartment $(C_{\rm A}(t)/C_{\rm D}(0), \%)$, and the effective permeability coefficient (P_e) of **22b** and **3** obtained using HDM-PAMPA are shown in Table 5. Both compounds presented a relatively high permeability coefficient through the hexadecane membrane. However, 3 was mostly retained in the membrane because of its notable affinity for hexadecane (as expected owing to its high log P predicted equal to 4.73 by Bioloom, Biobyte Corp., Claremont, CA). In contrast 22b largely reached the acceptor compartment and was slightly retained in the artificial membrane.

The ability of 22b to cross the BBB was assessed in silico through the estimation of the distribution parameter LogBBB from MIF-based Volsurf+ descriptors.81 A LogBBB value of 0.386 was calculated for 22b, a figure that was indicative of a good BBB permeation. Indeed, LogBBB values lower than -0.5 denote very poor brain permeation whereas values greater than 0.5 indicate high brain permeation.⁸² To lend further support to the potentially good BBB permeation ability of 22b, a knowledge-based approach was applied to a database containing a number of related, but chemically diverse, compounds exhibiting high, moderate, and poor BBB permeation (coded as BBB+, BBB±, and BBB-, respectively). After calculation of MIF-based Volsurf+ descriptors for the entire data set (245 compounds), y-response categorized variable was set to 1 for BBB+ compounds and to -1 for both BBB± and BBB- compounds. Partial least square discriminant analysis (PLS-DA)⁸³ was then carried out to develop a reliable BBB permeation model having confident statistics ($r^2 = 0.708$, $q^2 = 0.659$, SDEC = 0.538, SDEP =

0.582, PC = 3). As shown in Figure 5, the PLS t1-t2 score plot disclosed a good discrimination between the BBB+ on one side and BBB± and BBB- compounds on the other side. It was, in fact, immediately evident that the great majority of compounds was properly assigned to the correct class. On the basis of these solid statistics, the ability of 22b to cross the BBB was evaluated with much confidence. To our satisfaction, 22b, rendered as solid white diamond, was centered in the BBB+ region where CNS drugs are localized (Figure 5). It can therefore be assumed that 22b is endowed with physicochemical properties that are typical of CNS drugs and that its choice for a further experimental biological characterization was appropriate.

Compared to the reference compound 3, the aqueous solubility, lipophilicity, membrane and BBB permeability ($\log P_{\rm e}$ and LogBBB, respectively), and the PSA of 22b suggested a favorable profile for a CNS in vivo activity and prompted its in-depth biopharmacological profiling.

MAO-B inhibitory affinity of 22b was therefore measured also in human PRP with a radioenzymatic assay using [14C]PEA, a selective substrate already used in rat mitochondria. An IC₅₀ of 3 nM, very close to that determined in the rat mitochondria assay (13 nM), was measured.

The reversible nature of MAO-B inhibition by 22b was assessed in time-dependent inhibition experiments, by measuring the IC₅₀ after 0 and 30 min of inhibitor-enzyme incubation (PRP as enzyme source). No significant difference between the IC50 with or without incubation was observed (6 vs 3 nM, respectively), as is typically detected with reversible inhibitors.

Subsequently, 22b was also tested in ex vivo experiments as a selective MAO-B inhibitor. In C57Bl mice, 1 h after an oral or intraperitoneal dose of 22b (3 mg/kg), brain MAO-B activity was almost completely inhibited while MAO-A was not affected (Figure 6).

In time-course experiments, following a 0.5 mg/kg oral dose of 22b, MAO-B enzymatic activity was significantly inhibited at 30 min, 1 h, and 2 h (84%, 86%, and 90%, respectively), indicating a very rapid inhibition onset. Good MAO-B inhibition was maintained up to 8 h (nearly 60%), and full MAO-B activity was recovered after 16 h. During this timecourse, MAO-A activity remained unchanged (Figure 7), suggesting that compound 22b may be a tight binding inhibitor as lazabemide and safinamide. In a dose-response experiment, the ED₅₀ for brain MAO-B inhibition, calculated 1 h after dose administration, was 0.24 mg/kg po (Figure 8).

To evaluate potential drug-drug interaction effects of 22b, its inhibitory—induction activity on the selected series of

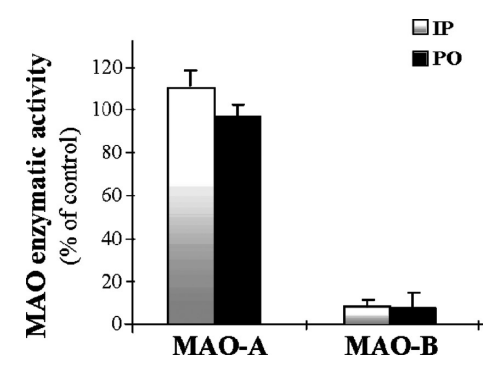


Figure 6. Ex vivo brain MAO activity after oral (po) and intraperitoneal administration (ip) of **22b** (3 mg/kg) in C57Bl mice. Mice (n = 6 per group) were treated (po or ip) with the test compound (3 mg/kg) and sacrificed after 1 h. The brains were removed, crude homogenates were prepared, and MAO enzyme activities were assessed with a radioenzymatic assay. Data were expressed as the mean \pm SEM and were analyzed by ANOVA followed by Dunnett's test.

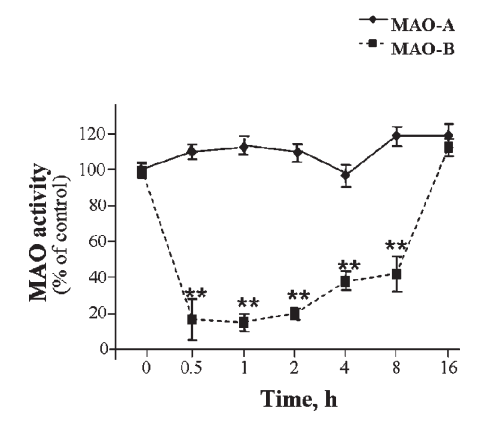


Figure 7. Ex vivo brain MAO activity after oral administration of **22b** (0.5 mg/kg) in C57Bl mice: time course experiment. Mice (n = 6 per group) were treated (po) with the test compound, and at different time intervals (0.5, 1, 2, 4, 8, and 16 h) they were sacrificed. The brains were removed, crude homogenates prepared and MAO enzyme activities assessed with a radioenzymatic assay. Data were expressed as the mean \pm SEM and were analyzed by ANOVA followed by Dunnett's test.

recombinant human CYP450s was evaluated. Data revealed that **22b** inhibited the CYP450 isoforms at high micromolar concentrations with IC₅₀ values between 5 and 50 μ M. These data were quite promising, since compounds exhibiting IC₅₀ > 5–10 μ M can be considered at low potential for drugdrug interaction because of the inhibition of CYP450 activity.

Finally, the in vitro effect of **22b** on SH-SY5Y cell viability was measured. As shown in Figure 9, incubation of cells for 24 h in a serumless medium containing **22b** did not induce any cellular damage up to $10 \,\mu\text{M}$ with $IC_{50} = 29.7 \,\mu\text{M}$, thus exhibiting very little in vitro toxicity.

Conclusions

A new class of higly potent and selective coumarin MAO-B inhibitors with an excellent biopharmacological profile was identified. SAFIRs and SSRs and modeling studies provided a clear picture of the main interactions taking place at position 4 of the newly designed 4,7-disubstituted coumarin derivatives and deepened our understanding of the structural requirements for high MAO-B affinity and selectivity. The determination or computational estimation of a number of physicochemical

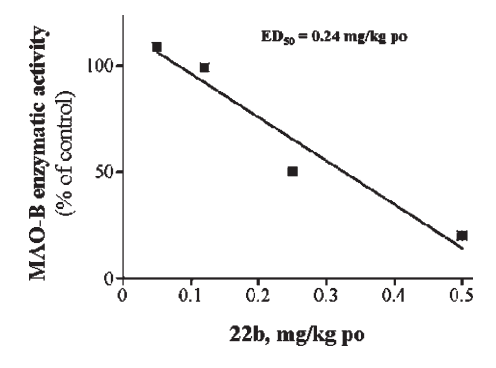


Figure 8. Ex vivo brain MAO activity after oral administration of **22b** (0.05, 0.1, 0.25, 0.5 mg/kg) in C57Bl mice: dose—response experiment. Mice (n = 6 per group) were treated with the test compound at different doses (0.05 - 0.5 mg/kg/po) and sacrificed after 1 h. The brains were removed, crude homogenates prepared, and MAO enzyme activities assessed with a radioenzymatic assay. Data were expressed as the mean \pm SEM and were analyzed by ANOVA followed by Dunnett's test.

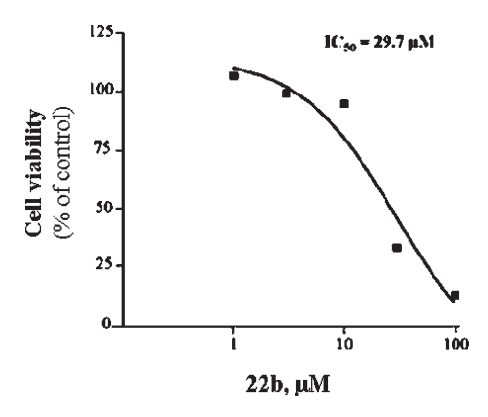


Figure 9. Effect of 22b on SH-SY5Y cell viability.

parameters relevant for drug activity in vivo led us to select compound **22b** for an in-depth biopharmacological profiling. In vitro radioenzymatic assays in rat brain mitochondria and in human PRP showed that **22b** was a strong MAO-B inhibitor (IC $_{50}$ of 13 and 3 nM, respectively) endowed with a high MAO-B selectivity (SI = 453, in rat brain mitochondria). The MAO-B inhibition of **22b** was not time-dependent as it would be for reversible inhibitors. In ex vivo experiments, **22b** showed an excellent BBB penetrating capacity when administered both parenterally and orally and behaved as a very potent (ED $_{50}$ = 0.24 mg/kg po), reversible, and short-acting (full recovery of the enzymatic activity at 16 h) MAO-B inhibitor with no significant effect on MAO-A. Moreover, compound **22b** exhibited no CYP isoform liabilities and was devoided of cytotoxic effects.

Because of its excellent in vitro and in vivo MAO-B inhibitory activity and appropriate pharmacokinetic properties, compound **22b** may be considered as a promising clinical candidate for the therapy of neurodegenerative diseases and, analogous to selegeline, ²⁰ for major depressive disorders.

Finally, we anticipate that compound **22b** also exhibits an interesting, albeit low, inhibitory activity toward acetylcholinesterase, an enzyme targeted by most of the anti-Alzheimer's drugs currently used in the therapy of this continuously growing neurodegenerative disease. An improvement of AChE inhibitory activity, while maintaining a sufficiently strong MAO-B inhibitory potency, is an important goal of

our ongoing research addressing the preparation of multipotent ligands for the therapy of neurological disorders. ^{54,85}

Experimental Section

Chemistry. Starting materials and reagents (including 1e and 5), the resin for solid phase synthesis and analytical grade solvents were from commercial sources. Melting points were determined by the capillary method on a Stuart Scientific SMP3 electrothermal apparatus and are uncorrected. Elemental analyses were performed on the Euroea 3000 analyzer only on the final compounds tested as MAO inhibitors. The measured values for C, H, and N agreed to within $\pm 0.40\%$ of the theoretical values. The purity of the intermediates, checked by ¹H NMR and HPLC, was always better than 95%. IR spectra were recorded using potassium bromide disks on a Perkin-Elmer Spectrum One FT-IR spectrophotometer; only the most significant IR absorption bands are reported. ¹H NMR spectra were recorded in the specified deuterated solvent at 300 MHz on a Varian Mercury 300 instrument. Chemical shifts are expressed in parts per million (δ) relative to the solvent signal and the coupling constants J in hertz (Hz). The following abbreviations were used: s (singlet), d (doublet), t (triplet), q (quadruplet), dd (double doublet), m (multiplet), br (broad signal); signals due to OH or NH protons were located by deuterium exchange with D₂O. Chromatographic separations were performed on silica gel (230–400 mesh, Merck) by using the flash methodology.

Ethyl (7-Hydroxy-2-oxo-2*H*-chromen-4-yl)acetate (1a). Resorcinol (2.2 g, 20 mmol), diethyl 1,3-acetonedicarboxylate (4.0 mL, 22 mmol), and few drops of 96% sulfuric acid were stirred at 120 °C for 1 h. The oily residue obtained was crystallized from absolute ethanol, yielding a red solid (2.48 g, 50% yield). ¹H NMR (300 MHz, DMSO- d_6) δ : 1.16 (t, J = 7.1 Hz, 3H), 3.91 (s, 2H), 4.09 (q, J = 7.1 Hz, 2H), 6.21 (s, 1H), 6.71 (d, J = 2.3 Hz, 1H), 6.78 (dd, $J_1 = 2.3$ Hz, $J_2 = 8.8$ Hz, 1H), 7.49 (d, J = 8.8 Hz, 1H), 10.55 (br s, 1H). IR cm⁻¹ (KBr): 3230, 1713, 1682, 1205, 1026, 849.

4-(Chloromethyl)-7-hydroxy-2*H***-chromen-2-one** (**1b**). Resorcinol (10 g, 91 mmol) was dissolved in 100 mL of 96% sulfuric acid at 0 °C. Then ethyl 4-chloroacetoacetate (10 mL, 74 mmol) was slowly added and the mixture was stirred at 0-5 °C for 2 h. The reaction mixture was then poured onto ice—water (1000 g) and the solid was filtered and washed with water, yielding the desired coumarin as white solid (12.2 g, 78% yield). ¹H NMR (300 MHz, acetone- d_6) δ : 4.92 (s, 2H), 6.40 (s, 1H), 6.80 (d, J = 2.5 Hz, 1H), 6.91 (dd, $J_1 = 2.5$ Hz, $J_2 = 8.8$ Hz, 1H), 7.73 (d, J = 8.8 Hz, 1H), 9.50 (s, 1H, dis. with D₂O). IR cm⁻¹ (KBr): 3283, 1686, 1235, 1136, 850.

4,7-Dihydroxy-2*H***-chromen-2-one (1c).** Resorcinol (8.8 g, 80 mmol), malonic acid (25 g, 240 mmol), and 40 mL of boron trifluoride—diethyl etherate complex (BF₃·Et₂O) were mixed at 90 °C for 24 h under magnetic stirring. The crude mixture was poured onto crushed ice (300 g), and the resulting precipitate was filtered, washed with diethyl ether (50 mL), and then purified by column chromatography using as eluent the mixture CHCl₃/CH₃OH, 9.5/0.5 (v/v). Yield: 23%. ¹H NMR (300 MHz, DMSO- d_6) δ : 5.36 (s, 1H), 6.64 (d, J = 2.2 Hz, 1H), 6.75 (dd, $J_1 = 2.2$ Hz, $J_2 = 8.8$ Hz, 1H), 7.62 (d, J = 8.8 Hz, 1H), 10.51 (s, 1H, dis. in D₂O), 12.23 (s, 1H, dis. in D₂O). IR cm⁻¹ (KBr): 1662, 1635, 1098, 802.

4-Chloro-7-hydroxy-2*H***-chromen-2-one (1d).** An amount of 2.0 g (11 mmol) of **1c** was refluxed in 12 mL of POCl₃ for 4 h. The mixture was poured onto crushed ice (100 g), and the aqueous layer was extracted with ethyl acetate (3×40 mL). The organic phases were collected and dried over sodium sulfate, and the solvent was evaporated under reduced pressure. The resulting red oil was purified by flash chromatography (eluent *n*-hexane/ethyl acetate, 8/2 v/v), furnishing a red solid (995 mg, 46% yield). ¹H NMR (300 MHz, DMSO- d_6) δ : 6.60 (s, 1H), 6.76 (d, J = 2.2 Hz, 1H), 6.88 (dd, $J_1 = 2.2$ Hz, $J_2 = 8.8$ Hz, 1H), 7.69 (d,

J = 8.8 Hz, 1H), 10.89 (s, 1H, dis. with D₂O). IR cm⁻¹ (KBr): 1706, 1624, 1272, 841.

General Procedure for the Synthesis of Chlorides 2a—e. An amount of 4.6 mmol of 1b or 1d was dissolved in 45 mL of hot ethanol. Then potassium carbonate (0.63 g, 4.6 mmol) and 5.5 mmol of the appropriate benzyl bromide (0.65 mL of benzyl bromide in the case of 2a and 2c, 0.72 mL of 3-chlorobenzyl bromide in the case of 2b and 2d, 0.68 mL of 3-fluorobenzyl bromide in the case of 2e) were added. The mixture was refluxed for 2 h and then cooled, and the inorganic residue was filtered off. The solvent was evaporated and the resulting solid was treated with diethyl ether and filtered, giving the desired products as off-white solids.

7-(Benzyloxy)-4-chloro-2*H***-chromen-2-one (2a).** Yield: 55%. ¹H NMR (300 MHz, CDCl₃) δ : 5.15 (s, 2H), 6.43 (s, 1H), 6.89 (d, J = 2.2 Hz, 1H), 6.99 (dd, $J_1 = 2.2$ Hz, $J_2 = 9.1$ Hz, 1H), 7.34–7.44 (m, 5H), 7.75 (d, J = 9.1 Hz, 1H). IR cm⁻¹ (KBr): 1735, 1359, 1126, 833.

4-Chloro-7-[(3-chlorobenzyl)oxy]-2*H***-chromen-2-one (2b).** Yield: 68%. ¹H NMR (300 MHz, CDCl₃) δ : 5.12 (s, 2H), 6.45 (s, 1H), 6.87 (d, J = 2.5 Hz, 1H), 6.99 (dd, $J_1 = 2.5$ Hz, $J_2 = 9.1$ Hz, 1H), 7.30–7.38 (m, 3H), 7.44 (s, 1H), 7.78 (d, J = 9.1 Hz, 1H). IR cm⁻¹ (KBr): 1721, 1365, 1275, 865, 838.

7-(Benzyloxy)-4-(chloromethyl)-2*H***-chromen-2-one (2c).** Yield: 69%. ¹H NMR (300 MHz, CDCl₃) δ : 4.62 (s, 2H), 5.14 (s, 2H), 6.40 (s, 1H), 6.92 (d, J=2.5 Hz, 1H), 6.97 (dd, $J_1=2.5$ Hz, $J_2=8.8$ Hz, 1H), 7.34–7.45 (m, 5H), 7.57 (d, J=8.8 Hz, 1H). IR cm⁻¹ (KBr): 1732, 1615, 1396, 1264, 1199, 1057, 1008.

7-[(3-Chlorobenzyl)oxy]-4-(chloromethyl)-2*H***-chromen-2-one (2d**). Yield: 78%. ¹H NMR (300 MHz, CDCl₃) δ : 4.62 (s, 2H), 5.11 (s, 2H), 6.41 (s, 1H), 6.88 (d, J = 2.5 Hz, 1H), 6.96 (dd, $J_1 = 2.5$ Hz, $J_2 = 8.8$ Hz, 1H), 7.27–7.37 (m, 3H), 7.43 (br s, 1H), 7.58 (d, J = 8.8 Hz, 1H). IR cm⁻¹ (KBr): 1699, 1611.

4-(Chloromethyl)-7-[(3-fluorobenzyl)oxy]-2*H***-chromen-2-one (2e**). Yield: 73%. ¹H NMR (300 MHz, CDCl₃) δ : 4.62 (s, 2H), 5.14 (s, 2H), 6.41 (s, 1H), 6.89 (d, J = 2.5 Hz, 1H), 6.97 (dd, $J_1 = 2.5$ Hz, $J_2 = 8.8$ Hz, 1H), 7.01–7.07 (m, 1H), 7.13–7.25 (m, 2H), 7.34–7.41 (m, 1H), 7.58 (d, J = 8.8 Hz, 1H). IR cm⁻¹ (KBr): 1718, 1611.

7-(1,3-Benzodioxol-5-ylmethoxy)-4-(chloromethyl)-2*H*-chromen**2-one (2f).** An amount of 1.0 mmol (0.21 g) of **1b** was dissolved in 10 mL of anhydrous THF. Piperonyl alcohol (0.46 g, 3.0 mmol), DIAD (0.59 mL, 3.0 mmol), and PPh₃ (0.79 g, 3.0 mmol) were added, and the mixture was stirred at room temperature for 18 h. The solvent was removed under vacuum, and the resulting crude oil was purified by column chromatography using as eluent a mixture of chloroform/petroleum ether, 1/1 (v/v). Yield: 76%. ¹H NMR (300 MHz, CDCl₃) δ: 4.62 (s, 2H), 5.03 (s, 2H), 5.98 (s, 2H), 6.40 (s, 1H), 6.79–6.84 (m, 2H), 6.87–6.91 (m, 2H), 6.93–6.96 (m, 1H), 7.55–7.58 (m, 1H). IR cm⁻¹ (KBr): 1731, 1614.

7-[(3-Chlorobenzyl)oxy]-4-methyl-2*H*-chromen-2-one (3). An amount of 0.81 g (4.6 mmol) of commercially available 1e was dissolved in 45 mL of hot ethanol. Then potassium carbonate (0.63 g, 4.6 mmol) and 3-chlorobenzyl bromide (0.72 mL, 5.5 mmol) were added. The mixture was refluxed for 2 h and then cooled. The inorganic residue was filtered off and the product crystallized from the resulting solution. Yield: 88%. Mp: 148–9 °C. ¹H NMR (300 MHz, CDCl₃) δ : 2.40 (d, J = 1.1 Hz, 3H), 5.10 (s, 2H), 6.15 (d, J = 1.1 Hz, 1H), 6.86 (d, J = 2.5 Hz, 1H), 6.93 (dd, $J_1 = 2.5$ Hz, $J_2 = 8.8$ Hz, 1H), 7.28–7.37 (m, 3H), 7.44 (s, 1H), 7.51 (d, J = 8.8 Hz, 1H). IR cm⁻¹ (KBr): 1713, 1614. Anal. (C₁₇H₁₃ClO₃) C, H.

General Procedure for the Synthesis of Coumarin Amines 4a—h. An amount of 0.50 mmol of the appropriate chloro derivative 2a—e was dissolved in 4.0 mL of dry DMF. Then 0.26 mL (1.5 mmol) of DIEA and 0.75 mmol of the appropriate amino acid (for compounds 4a,b,f, 0.093 g of L-alaninamide hydrochloride; for compound 4c,d,g,h, 0.086 g of L-prolinamide; for compound 4e, 0.11 g of L-serinamide hydrochloride) were added, and the mixture was stirred at 80 °C for 5 h. The solvent

was evaporated, and the resulting crude was purified by column chromatography (eluent CHCl₃/CH₃OH, 9.5/0.5 v/v).

 N^2 -[7-(Benzyloxy)-2-oxo-2*H*-chromen-4-yl]alaninamide (4a). Yield: 77%. Mp: 247–9 °C. ¹H NMR (300 MHz, DMSO- d_6) δ : 1.42 (d, J = 6.9 Hz, 3H), 3.97–4.01 (m, 1H), 4.88 (s, 1H), 5.19 (s, 2H), 6.94 (d, J = 2.2 Hz, 1H), 6.99 (dd, $J_1 = 2.2$ Hz, $J_2 = 9.1$ Hz, 1H), 7.30–7.47 (m, 6H), 7.17 (s, 1H), 7.61 (s, 1H), 8.12 (d, J = 9.1 Hz, 1H). IR cm⁻¹ (KBr): 3325, 1668, 1609. Anal. ($C_{19}H_{18}N_2O_4$) C, H, N.

 N^2 -{7-[(3-Chlorobenzyl)oxy]-2-oxo-2*H*-chromen-4-yl}alaninamide (4b). Yield: 82%. Mp: 237–9 °C. ¹H NMR (300 MHz, DMSO- d_6) δ : 1.42 (d, J=6.9 Hz, 3H), 3.97–4.01 (m, 1H), 4.88 (s, 1H), 5.21 (s, 2H), 6.95 (d, J=2.2 Hz, 1H), 7.00 (dd, $J_1=2.2$ Hz, $J_2=9.1$ Hz, 1H), 7.17 (s, 1H), 7.39–7.44 (m, 4H), 7.54 (s, 1H), 7.62 (s, 1H), 8.13 (d, J=9.1 Hz, 1H). IR cm⁻¹ (KBr): 3437, 3180, 1674, 1613. Anal. ($C_{19}H_{17}ClN_2O_4$) C, H, N.

1-[7-(Benzyloxy)-2-oxo-2*H***-chromen-4-yl]prolinamide (4c).** Yield: 59%. Mp: 203–5 °C. ¹H NMR (300 MHz, DMSO- d_6) δ : 1.82–1.99 (m, 3H), 2.26–2.30 (m, 1H), 3.78–3.79 (m, 1H), 3.92–4.00 (m, 1H), 4.29–4.34 (m, 1H), 4.91 (s, 1H), 5.20 (s, 2H), 6.92 (dd, $J_1 = 2.8$ Hz, $J_2 = 9.1$ Hz, 1H), 6.97 (d, J = 2.8 Hz, 1H), 7.21 (s, 1H), 7.31–7.47 (m, 5H), 7.67 (s, 1H), 7.95 (d, J = 9.1 Hz, 1H). IR cm⁻¹ (KBr): 3475, 3195, 1691, 1669, 1615. Anal. ($C_{21}H_{20}N_2O_4$) C, H, N.

1-{7-[(3-Chlorobenzyl)oxy]-2-oxo-2*H*-chromen-4-yl}prolinamide (4d). Yield: 73%. Mp: 222–3 °C. ¹H NMR (300 MHz, DMSO- d_6) δ : 1.82–1.99 (m, 3H), 2.26–2.27 (m, 1H), 3.73–3.78 (m, 1H), 3.94–3.97 (m, 1H), 4.29–4.32 (m, 1H), 4.91 (s, 1H), 5.22 (s, 2H), 6.93 (dd, $J_1 = 2.8$ Hz, $J_2 = 9.1$ Hz, 1H), 6.97 (d, J = 2.8 Hz, 1H), 7.19 (s, 1H), 7.40–7.44 (m, 3H), 7.53 (s, 1H), 7.66 (s, 1H), 7.95 (d, J = 9.1 Hz, 1H). IR cm⁻¹ (KBr): 3478, 3193, 1688, 1669, 1615. Anal. (C₂₁H₁₉ClN₂O₄) C, H, N.

 N^2 -{7-[(3-Chlorobenzyl)oxy]-2-oxo-2*H*-chromen-4-yl}serinamide (4e). Yield: 48%. Mp: 244 °C (dec). ¹H NMR (300 MHz, DMSO- d_6) δ : 3.75–3.80 (m, 2H), 3.96–4.02 (m, 1H), 4.94 (d, J = 1.9 Hz, 1H), 5.05–5.09 (m, 1H), 5.22 (s, 2H), 6.96 (d, J = 2.5 Hz, 1H), 7.02 (dd, $J_1 = 2.5$ Hz, $J_2 = 9.1$ Hz, 1H), 7.23 (d, J = 6.9 Hz, 1H), 7.26 (s, 1H), 7.38–7.43 (m, 3H), 7.54 (s, 1H), 7.64 (s, 1H), 8.08 (d, J = 9.1 Hz, 1H). IR cm⁻¹ (KBr): 3368, 3275, 3188, 1658, 1618. Anal. ($C_{19}H_{17}ClN_2O_5$) C, H, N.

 N^2 -{[7-(Benzyloxy)-2-oxo-2*H*-chromen-4-yl]methyl}alaninamide (4f). Yield: 63%. Mp: 151–3 °C. ¹H NMR (300 MHz, DMSO- d_6) δ : 1.23 (d, J=6.6 Hz, 3H), 3.23–3.33 (m, 1H), 3.98–4.01 (m, 2H), 5.21 (s, 2H), 6.37 (s, 1H), 7.01 (dd, $J_1=2.5$ Hz, $J_2=9.1$ Hz, 1H), 7.07 (d, J=2.5 Hz, 1H), 7.13 (br s, 1H), 7.33–7.47 (m, 6H), 7.73 (d, J=9.1 Hz, 1H), 1NH not detectable. IR cm⁻¹ (KBr): 3203, 1705, 1639, 1614. Anal. (C₂₀H₂₀N₂O₄) C, H N.

1-{[7-(Benzyloxy)-2-oxo-2*H*-chromen-4-yl]methyl} prolinamide (4g). Yield: 74%. Mp: 67–9 °C. 1 H NMR (300 MHz, DMSO- 4 6) δ : 1.72–1.78 (m, 3H), 2.02–2.06 (m, 1H), 2.25–2.30 (m, 1H), 3.02–3.10 (m, 2H), 3.63 (d, J=15.4 Hz, 1H), 3.93 (d, J=15.4 Hz, 1H), 5.21 (s, 2H), 6.44 (s, 1H), 6.98 (dd, $J_{1}=2.2$ Hz, $J_{2}=8.8$ Hz, 1H), 7.06 (d, J=2.2 Hz, 1H), 7.20 (s, 2H), 7.30–7.47 (m, 5H), 7.93 (d, J=8.8 Hz, 1H). IR cm $^{-1}$ (KBr): 3328, 3194, 1723, 1677, 1611. Anal. ($C_{22}H_{22}N_{2}O_{4}$) C, H, N.

1-({7-[(3-Fluorobenzyl)oxy]-2-oxo-2*H*-chromen-4-yl}methyl)prolinamide (4h). Yield: 61%. Mp: 162-4 °C. ¹H NMR (300 MHz, DMSO- d_6) δ : 1.72 (br s, 3H), 1.98–2.08 (m, 1H), 2.25–2.33 (m, 1H), 3.01–3.10 (m, 2H), 3.63 (d, J=15.4 Hz, 1H), 3.93 (d, J=15.4 Hz, 1H), 5.23 (s, 2H), 6.44 (s, 1H), 6.97–7.05 (m, 3H), 7.13–7.31 (m, 4H), 7.40–7.47 (m, 1H), 7.95 (d, J=8.8 Hz, 1H). IR cm⁻¹ (KBr): 3193, 1739, 1649, 1613. Anal. ($C_{22}H_{21}FN_2O_4$) C, H, N.

Synthesis of Amides 6a,b. The commercially available 7-hydroxycoumarin-4-acetic acid **5** (0.44 g, 2.0 mmol) and HOBt (0.63 g, 4.0 mmol) were dissolved in 12 mL of anhydrous DMF. DCC (0.8 g, 4.0 mmol) was added followed by an amount of 4.0 mmol of *tert*-butyl carbazate (for **6a**) or *N*-Boc-ethylene-

diamine (for **6b**). The mixture was then stirred at room temperature for 5 h.

tert-Butyl 2-[(7-Hydroxy-2-oxo-2*H*-chromen-4-yl)acetyl]hydrazinecarboxylate (6a). Yield: 98%. ¹H NMR (300 MHz, DMSO- d_6) δ : 1.40 (s, 9H), 3.60 (s, 2H), 6.22 (s, 1H), 6.70 (d, J=2.4 Hz, 1H), 6.77 (dd, $J_1=2.4$ Hz, $J_2=8.7$ Hz, 1H), 7.61 (d, J=8.7 Hz, 1H), 8.85 (s, 1H), 9.93 (s, 1H), 10.57 (s, 1H). IR cm⁻¹ (KBr): 3302, 3206, 1727, 1705, 1683, 1607.

tert-Butyl 2-{[(7-Hydroxy-2-oxo-2*H*-chromen-4-yl)acetyl]-amino}ethylcarbamate (6b). Yield: 65%. ¹H NMR (300 MHz, DMSO- d_6) δ : 1.35 (s, 9H), 2.96–3.05 (m, 4H), 3.60 (s, 2H), 6.14 (s, 1H), 6.69–6.78 (m, 3H), 7.57 (d, J=8.8 Hz, 1H), 8.19 (br s, 1H), 10.54 (br s, 1H). IR cm⁻¹ (KBr): 3360, 3335, 1695, 1680, 1656.

Synthesis of Amides 7a–c. The appropriate intermediate **6a,b** (1.5 mmol) was dissolved in absolute ethanol (10 mL) and K_2CO_3 (0.21 g, 1.5 mmol), and the suitable benzyl bromide (1.5 mmol) was added to the solution. The mixture was refluxed for 30 min. The solid was filtered off and the solution cooled at room temperature. The solvent was evaporated to give a solid that was purified by column chromatography (eluent $CHCl_3/MeOH$, 9.5/0.5 v/v).

tert-Butyl 2-{[7-(Benzyloxy)-2-oxo-2*H*-chromen-4-yl]acetyl}-hydrazinecarboxylate (7a). Yield: 30%. ¹H NMR (300 MHz, DMSO- d_6) δ: 1.37 (s, 9H), 3.68 (s, 2H), 5.22 (s, 2H), 6.30 (s, 1H), 7.01 (dd, $J_1 = 2.2$ Hz, $J_2 = 8.8$ Hz, 1H), 7.08 (d, J = 2.2 Hz, 1H), 7.30–7.46 (m, 5H), 7.70 (d, J = 8.8 Hz, 1H), 8.85 (s, 1H), 9.94 (s, 1H). IR cm⁻¹ (KBr): 3371, 3262, 1754, 1670.

tert-Butyl 2-{[7-(3-Chlorobenzyl)oxy)-2-oxo-2*H*-chromen-4-yl]-acetyl}hydrazinecarboxylate (7b). Yield: 56%. ¹H NMR (300 MHz, DMSO- d_6) δ : 1.37 (s, 9H), 3.68 (s, 2H), 5.22 (s, 2H), 6.30 (s, 1H), 7.01 (dd, $J_1 = 2.2$ Hz, $J_2 = 8.8$ Hz, 1H), 7.08 (d, J = 2.2 Hz, 1H), 7.39–7.40 (m, 3H), 7.51 (s, 1H), 7.70 (d, J = 8.8 Hz, 1H), 8.85 (s, 1H), 9.94 (s, 1H). IR cm⁻¹ (KBr): 3366, 3259, 1755, 1683.

tert-Butyl 2-[({7-[(3-Chlorobenzyl)oxy]-2-oxo-2*H*-chromen-4-yl}-acetyl)amino]ethylcarbamate (7c). Yield: 95%. ¹H NMR (300 MHz, DMSO- d_6) δ : 1.35 (s, 9H), 2.94–2.98 (m, 2H), 3.03–3.07 (m, 2H), 3.64 (s, 2H), 5.23 (s, 2H), 6.23 (s, 1H), 6.81 (br s, 1H), 7.03 (dd, $J_1 = 2.5$ Hz, $J_2 = 8.8$ Hz, 1H), 7.07 (d, J = 2.5 Hz, 1H), 7.39–7.41 (m, 3H), 7.53 (s, 1H), 7.67 (d, J = 8.8 Hz, 1H), 8.21 (br s, 1H). IR cm⁻¹ (KBr): 3356, 3290, 1729, 1685.

Synthesis of Amides 8a–c. The appropriate intermediate 7a–c (0.060 mmol) was dissolved in 1.0 mL of a 1/1 v/v mixture of $\text{CH}_2\text{Cl}_2/\text{CF}_3\text{COOH}$ and the solution stirred at room temperature for 20 min. The solvent was evaporated under vacuum and the oily residue obtained was treated with ether to give a precipitate that was filtered and crystallized from ethanol (8a,b) or chloroform/n-hexane (8c).

2-[7-(**Benzyloxy**)-**2-oxo-2***H*-**chromen-4-yl**]acetohydrazide (**8a**). Yield: 93%. Mp: 164 °C (dec). ¹H NMR (300 MHz, DMSO- d_6) δ : 3.60 (s, 2H), 4.29 (br s, 2H, dis. with D₂O), 5.22 (s, 2H), 6.23 (s, 1H), 7.02 (dd, $J_1 = 2.5$ Hz, $J_2 = 8.8$ Hz, 1H), 7.07 (d, J = 2.5 Hz, 1H), 7.30–7.47 (m, 5H), 7.70 (d, J = 8.8 Hz, 1H), 9.31 (s, 1H, dis. with D₂O). IR cm⁻¹ (KBr): 3303, 1716, 1644, 1615. Anal. (C₁₈H₁₆N₂O₄) C, H, N.

2-[7-(3-Chlorobenzyloxy)-2-oxo-2*H*-chromen-4-yl]acetohydrazide (**8b**). Yield: 86%. Mp 174–6 °C. ¹H NMR (300 MHz, DMSO- d_6) δ : 3.61 (s, 2H), 4.43 (br s, 2H, dis. with D₂O), 5.24 (s, 2H), 6.24 (s, 1H), 7.03–7.06 (m, 1H), 7.07 (br s, 1H), 7.41–7.42 (m, 3H), 7.53 (s, 1H), 7.71 (d, J = 8.8 Hz, 1H), 9.34 (s, 1H, dis. with D₂O). IR cm⁻¹ (KBr): 3309, 1719, 1646. Anal. (C₁₈H₁₅ClN₂O₄) C, H, N.

N-(2-Aminoethyl)-2-{7-[(3-chlorobenzyl)oxy]-2-oxo-2*H*-chromen-4-yl}acetamide (8c). Yield: 83%. Mp: 144−5 °C. ¹H NMR (300 MHz, DMSO- d_6) δ : 2.81−2.83 (m, 2H), 3.26−3.28 (m, 2H), 3.69 (s, 2H), 5.23 (s, 2H), 6.25 (s, 1H), 7.03 (dd, $J_1 = 2.5$ Hz, $J_2 = 8.8$ Hz, 1H), 7.09 (d, J = 2.5 Hz, 1H), 7.39−7.42 (m, 3H), 7.53 (s, 1H), 7.68 (d, J = 8.8 Hz, 1H), 7.74 (br s, 2H, dis. with D₂O), 8.33 (br s, 1H). IR cm⁻¹ (KBr): 3356, 3290, 1700, 1683. Anal. (C₂₀H₁₉ClN₂O₄) C, H, N.

Solid-Phase Synthesis of Amides 11a-d and 13a,b. Resin 9. An amount of 0.060 mmol (0.10 g) of Rink amide AM resin was suspended in 2.0 mL of anhydrous DMF and shaken for 20 min. The swelled resin was suspended in 2.0 mL of a 20% solution of piperidine in anhydrous DMF and shaken for 30 min, filtered, and washed with anhydrous DMF (3 \times 3.0 mL). The deprotected resin was suspended in 2 mL of anhydrous DMF, and 7-hydroxycoumarin-4-acetic acid 5 (0.070 g, 0.32 mmol), hydroxybenzotriazole (0.049 g, 0.32 mmol), and N,N-diisopropylcarbodiimide (0.050 mL, 0.32 mmol) were added. The mixture was shaken overnight. The resin was filtered and washed with DMF $(3 \times 2.0 \text{ mL})$ and THF $(3 \times 2.0 \text{ mL})$.

Resins 10a-d. An amount of 0.20 mmol (0.30 g) of resinbound 9 was suspended in 4.0 mL of anhydrous DMF and shaken for 20 min. The swelled resin was suspended in 3.0 mL of anhydrous DMF. Then 1.9 mmol of the appropriate benzyl bromide (benzyl bromide for 10a, 3-chlorobenzyl bromide for 10b, 3-fluorobenzyl bromide for 10c, and 17 for 10d) and 0.34 mL (1.9 mmol) of DIEA were added. The shaking was continued at 70 °C for 2.5 h. The mixture was cooled at room temperature, the resin was filtered, washed with anhydrous DMF ($3 \times 3.0 \text{ mL}$), and the coupling was repeated in the same conditions. The mixture was filtered, and the resin was washed with DMF (3 \times 3.0 mL), THF (3 \times 3.0 mL), and dichloromethane $(3 \times 3.0 \text{ mL})$.

Resin 10e. An amount of 0.17 mmol of swelled resin **10d** was suspended in 2.0 mL of anhydrous THF, and 0.13 mL of saturated solution in methanol of sodium methoxide was added. The mixture was shaken for 4 h, filtered, and washed with THF/ H_2O , $1/1 \text{ v/v} (3 \times 2.0 \text{ mL})$, THF/HCl 2.0 N, $1/1 \text{ v/v} (3 \times 2.0 \text{ mL})$, THF/H₂O, 1/1 v/v (3 × 2.0 mL), THF (3 × 2.0 mL), and CH₂Cl₂ $(3 \times 2.0 \text{ mL}).$

Resins 12a,b. An amount of 0.18 mmol of the resin 10a (for 12a) or 10c (for 12b) was suspended in 3.0 mL of anhydrous DMF and shaken for 20 min. The swelled resin was suspended in 2.0 mL of anhydrous DMF, and an amount of 1.1 mL (0.55 mmol) of a 0.5 M solution of KHMDS in toluene was added. The mixture was shaken for 10 min. The resin was filtered, washed with anhydrous DMF, resuspended in 2.0 mL of anhydrous DMF, and methyl iodide (0.23 mL, 3.7 mmol) was added. The resin was shaken for 4 h, filtered, and washed with DMF (3 \times 2.0 mL), THF (3 \times 2.0 mL), and CH₂Cl₂ (3 \times 2.0 mL).

General Procedure for the Cleavage of Amides 11a-d and 13a, b. The functionalized resin 12a,b or 10a-c or 10e was suspended in 3.0 mL of a 95% CF₃COOH, 2.5% H₂O, and 2.5% triethylsilane solution and shaken for 1 h. The resin was filtered and washed with the same solution $(3 \times 3.0 \text{ mL})$ and the solvent was evaporated under vacuum to give an oil that was treated with toluene, yielding a solid that was crystallized from ethanol or purified by column chromatography.

2-[7-(Benzyloxy)-2-oxo-2*H*-chromen-4-yl]acetamide Crystallized from ethanol. Yield: 53%. Mp: 218-221 °C (dec). ¹H NMR (300 MHz, DMSO- d_6) δ : 3.63 (s, 2H), 5.21 (s, 2H), 6.24 (s, 1H), 7.02-7.08 (m, 2H), 7.17 (s, 1H), 7.30-7.47 (m, 5H), 7.65-7.68 (m, 2H). IR cm⁻¹ (KBr): 3395, 3305, 1713, 1661, 1612. Anal. (C₁₈H₁₅NO₄) C, H, N.

2-{7-[(3-Chlorobenzyl)oxy]-2-oxo-2*H*-chromen-4-yl}acetamide (11b). Purified by column chromatography (eluent: CHCl₃/ MeOH, 9.5/0.5 v/v). Yield: 30%. Mp: 185-6 °C. ¹H NMR (300 MHz, DMSO-*d*₆) δ: 3.64 (s, 2H), 5.24 (s, 2H), 6.25 (s, 1H), 7.03-7.09 (m, 2H), 7.17 (s, 1H), 7.38-7.44 (m, 3H), 7.54 (s, 1H), 7.63 (s, 1H), 7.68 (d, J = 8.7 Hz, 1H). IR cm⁻¹ (KBr): 3447, 3341, 1733, 1693, 1618. Anal. (C₁₈H₁₄ClNO₄) C, H, N.

2-{7-[(3-Fluorobenzyl)oxy]-2-oxo-2*H*-chromen-4-yl}acetamide (11c). Purified by column chromatography (eluent: CHCl₃/MeOH, 9.5/0.5 v/v). Yield: 44%. Mp: 177-8 °C. ¹H NMR (300 MHz, DMSO- d_6) δ : 3.63 (s, 2H), 5.24 (s, 2H), 6.24 (s, 1H), 7.03–7.07 (m, 2H), 7.13-7.17 (m, 2H), 7.29 (d, J = 7.7 Hz, 2H), 7.40-7.47 (m, 1H), 7.64 (s, 1H), 7.68 (d, J = 8.8 Hz, 1H). IR cm⁻¹ (KBr): 3415, 1717, 1667, 1614. Anal. (C₁₈H₁₄FNO₄) C, H, N.

2-{7-[(3-Hydroxybenzyl)oxy]-2-oxo-2*H*-chromen-4-yl}acetamide (11d). Purified by column chromatography (eluent: CH₂Cl₂/ MeOH, 8.5/1.5 v/v). Yield: 30%. Mp: 190-1 °C (dec). ¹H NMR (300 MHz, DMSO-*d*₆) δ: 3.62 (s, 2H), 5.13 (s, 2H), 6.23 (s, 1H), 6.68–6.70 (m, 1H), 6.81–6.85 (m, 2H), 6.99–7.18 (m, 4H), 7.63–7.66 (m, 2H), 9.51 (s, 1H). IR cm⁻¹ (KBr): 3373, 3198, 1698, 1672, 1607. Anal. (C₁₈H₁₅NO₅) C, H, N.

2-[7-(Benzyloxy)-2-oxo-2*H*-chromen-4-yl]propanamide (13a). Crystallized from ethanol. Yield: 34%. Mp: 196 °C (dec), 204–6 °C. ¹H NMR (300 MHz, DMSO- d_6) δ : 1.38 (d, J =7.2 Hz, 3H), 3.99 (q, J = 7.2 Hz, 1H), 5.21 (s, 2H), 6.19 (s, 1H), $7.04 \, (dd, J_1 = 2.5 \, Hz, J_2 = 8.8 \, Hz, 1H), 7.08 \, (d, J = 2.5 \, Hz, 1H),$ 7.14 (s, 1H), 7.32-7.46 (m, 5H), 7.59 (s, 1H), 7.76 (d, J = 8.8 Hz, 1H). IR cm⁻¹ (KBr): 3398, 1716, 1667, 1618. Anal. (C₁₉H₁₇- NO_4) C, H, N.

2-{7-[(3-Fluorobenzyl)oxy]-2-oxo-2*H*-chromen-4-yl}propanamide (13b). Crystallized from ethanol. Yield: 24%. Mp: 168–9 °C. ¹H NMR (300 MHz, DMSO- d_6) δ : 1.38 (d, J = 6.9 Hz, 3H), 3.99 (q, J = 6.9 Hz, 1H), 5.24 (s, 2H), 6.20 (s, 1H), 7.03-7.19 (m, 4H), 7.28-7.30 (m, 2H), 7.44 (dd, $J_1 = 7.4$ Hz, $J_2 = 7.7 \text{ Hz}, 1\text{H}, 7.59 \text{ (s, 1H)}, 7.77 \text{ (d, } J = 8.5 \text{ Hz}, 1\text{H}). \text{ IR cm}^{-1}$ (KBr): 3422, 1723, 1655, 1618. Anal. (C₁₉H₁₆FNO₄) C, H, N.

3-Methylphenyl Benzoate (16). An amount of 1.0 mL (10 mmol) of m-cresol 14 and 7.0 mL (50 mmol) of anhydrous triethylamine were dissolved in 10 mL of anhydrous THF. Then 1.2 mL (10 mmol) of benzoyl chloride 15, previously dissolved in 10 mL of anhydrous THF, were added dropwise at 0 °C. The mixture was stirred at room temperature for 30 min. The obtained precipitate was filtered and the solvent was evaporated under vacuum to give an oil that was purified by flash chromatography (eluent CHCl₃/n-hexane, 1/1 v/v). Yield: 98%. ¹H NMR (300 MHz, CDCl₃) δ : 2.18 (s, 3H), 7.15–7.18 (m, 1H), 7.26–7.30 (m, 2H), 7.39-7.48 (m, 1H), 7.53-7.55 (m, 2H), 7.63-7.68 (m, 1H), 8.19-8.22 (m, 2H). IR cm⁻¹ (KBr): 1733, 1268, 1244.

3-(Bromomethyl)phenyl Benzoate (17). The intermediate 16 (1.3 g, 6.0 mmol), N-bromosuccinimide (1.3 g, 7.2 mmol), and 2,2'-azobis(2-methylpropionitrile) were dissolved in 6.0 mL of carbon tetrachloride. The solution was refluxed for 1 h, filtered, and added to n-hexane to give a precipitate that was filtered and washed with methanol. Yield: 53%. ¹H NMR (300 MHz, CDCl₃) δ : 4.51 (s, 2H), 7.16-7.18 (m, 1H), 7.25-7.32 (m, 2H), 7.39–7.46 (m, 1H), 7.52–7.55 (m, 2H), 7.63–7.68 (m, 1H), 8.19–8.22 (m, 2H). IR cm⁻¹ (KBr): 1728, 1270, 1240.

2-[7-(Hydroxy)-2-oxo-2H-chromen-4-yl]acetamide (18). In a glass vessel 0.80 g (3.2 mmol) of 1a was added to 8.0 mL (16 mmol) of a 2.0 M solution of ammonia in methanol. The ampule was sealed and placed in an oven at 90 °C for 60 h. The solution was evaporated under vacuum, and the solid obtained was crystallized from ethanol. Yield: 50%. ¹H NMR (300 MHz, DMSO- d_6) δ : 3.64 (s, 2H), 6.25 (s, 1H), 7.05 (dd, $J_1 = 2.4$ Hz, $J_2 = 8.8 \text{ Hz}, 1\text{H}, 7.08 \text{ (d}, J = 2.4 \text{ Hz}, 1\text{H}, 7.17 \text{ (s}, 1\text{H}), 7.63 \text{ (s}, 1\text{H})}$ 1H), 7.68 (d, J = 8.7 Hz, 1H), OH not detectable. IR cm (KBr): 3447, 3341, 3148, 1712, 1623.

Synthesis of Pyridyl Compounds 19a,b. Amounts of 0.11 g (0.50 mmol) of 18, 1.5 mmol of 3-(hydroxymethyl)pyridine (0.15 mL, in the case of 19a) or 4-(hydroxymethyl)pyridine (0.16 g, in the case of **19b**), 0.38 g (1.5 mmol) of 1,1'-(azodicarbonyl)dipiperidine (ADDP), and 0.38 mL (1.5 mmol) of tributylphosphine were dissolved in 5.0 mL of anhydrous THF, and the mixture was stirred at room temperature for 18 h. The obtained precipitate was filtered, washed with chloroform, and then crystallized from ethanol.

2-[2-Oxo-7-(pyridin-3-ylmethoxy)-2H-chromen-4-yl]acetamide (19a). Yield: 40%. Mp: 212 °C (dec). ¹H NMR (300 MHz, DMSO- d_6) δ : 3.63 (s, 2H), 5.26 (s, 2H), 6.25 (s, 1H), 7.05 $(dd, J_1 = 2.5 \text{ Hz}, J_2 = 8.8 \text{ Hz}, 1\text{H}), 7.11 (d, J = 2.5 \text{ Hz}, 1\text{H}),$ 7.17 (br s, 1H), 7.40 - 7.44 (m, 1H), 7.64 (br s, 1H), 7.67 (d, J = 8.8Hz, 1H), 7.88 (d, J = 8.0 Hz, 1H), 8.54 (d, J = 4.7 Hz, 1H), 8.68 (s, 1H). IR cm⁻¹ (KBr): 1714, 1667, 1615. Anal. (C₁₇H₁₄N₂O₄) C, H, N.

2-[2-Oxo-7-(pyridin-4-ylmethoxy)-2*H***-chromen-4-yl]acetamide** (**19b**). Yield: 71%. Mp: 193–4 °C. ¹H NMR (300 MHz, DMSO- d_6) δ : 3.63 (s, 2H), 5.30 (s, 2H), 6.25 (s, 1H), 7.04–7.07 (m, 2H), 7.16 (br s, 1H), 7.43 (d, J = 5.6 Hz, 2H), 7.63 (br s, 1H), 7.68 (d, J = 9.6 Hz, 1H), 8.57 (d, J = 5.6 Hz, 2H). IR cm⁻¹ (KBr): 3319, 1663, 1627. Anal. (C₁₇H₁₄N₂O₄) C, H, N.

Synthesis of Esters 20a,b. Amounts of 0.12 g (0.50 mmol) of **1a**, 1.5 mmol of the suitable benzyl alcohol, 0.38 g (1.5 mmol) of ADDP, and 0.39 g (1.5 mmol) of triphenylphosphine were dissolved in 5.0 mL of anhydrous THF, and the mixture was stirred at room temperature for 18 h. The precipitate was filtered off, the solvent evaporated under vacuum and the oily residue purified by flash chromatography (eluent CHCl₃).

Ethyl [7-(Benzyl)oxy-2-oxo-2*H*-chromen-4-yl]acetate (20a). Yield: 61%. 1 H NMR (300 MHz, DMSO- d_{6}) δ : 1.16 (t, J=7.1 Hz, 3H), 3.64 (s, 2H), 4.09 (q, J=7.1 Hz, 2H), 5.24 (s, 2H), 6.25 (s, 1H), 7.03–7.09 (m, 2H), 7.33–7.46 (m, 5H), 7.68 (d, J=8.7 Hz, 1H). IR cm⁻¹ (KBr): 1732, 1709, 1615.

Ethyl {7-[(3-Chlorobenzyl)oxy]-2-oxo-2*H*-chromen-4-yl}acetate (20b). Yield: 48%. ¹H NMR (300 MHz, DMSO- d_6) δ : 1.16 (t, J = 7.1 Hz, 3H), 3.64 (s, 2H), 4.09 (q, J = 7.1 Hz, 2H), 5.24 (s, 2H), 6.25 (s, 1H), 7.03–7.09 (m, 2H), 7.26–7.35 (m, 3H), 7.54 (s, 1H), 7.68 (d, J = 8.7 Hz, 1H). IR cm⁻¹ (KBr): 1736, 1712, 1615.

General Procedure for the Synthesis of Amides 21a-g. An amount of 2.0 mmol of a suitable ester 20a,b was placed in a glass vessel together with 20 mmol of the appropriate amine in a 2.0 N THF solution, commercially available or freshly prepared from the parent liquid amine. The vessel was sealed and placed in an oven at 90 °C for 24-60 h, until the starting ester was consumed as indicated by the TLC control. The solvent was then evaporated under vacuum, and the oily residue was purified by column chromatography or crystallized from absolute ethanol.

2-[7-(Benzyloxy)-2-oxo-2*H***-chromen-4-yl]-***N***-methylacetamide (21a). Crystallized from ethanol. Yield: 50%. Mp: 235-6 °C. ¹H NMR (300 MHz, DMSO-d_6) \delta: 2.57 (d, J=4.4 Hz, 3H), 3.64 (s, 2H), 5.22 (s, 2H), 6.22 (s, 1H), 7.02 (dd, J_1=2.5 Hz, J_2=8.8 Hz, 1H), 7.06 (d, J=2.5 Hz, 1H), 7.30–7.47 (m, 5H), 7.66 (d, J=8.8 Hz, 1H), 8.07 (br s, 1H). IR cm⁻¹ (KBr): 3303, 1716, 1635, 1614. Anal. (C₁₉H₁₇NO₄) C, H, N.**

2-{7-[(3-Chlorobenzyl)oxy]-2-oxo-2*H*-chromen-4-yl}-*N*-methylacetamide (21b). Purified by column chromatography (eluent: CHCl₃/MeOH, 9.5/0.5 v/v). Yield: 50%. Mp: 174–5 °C. ¹H NMR (300 MHz, DMSO- d_6) δ : 2.56 (s, 3H), 3.64 (s, 2H), 5.23 (s, 2H), 6.23 (s, 1H), 7.01–7.08 (m, 2H), 7.39–7.42 (m, 3H), 7.53 (s, 1H), 7.67 (d, J = 8.8 Hz, 1H), 8.07 (br s, 1H). IR cm⁻¹ (KBr): 3294, 1718, 1640, 1614. Anal. (C₁₉H₁₆ClNO₄) C, H, N.

N-Butyl-2-{7-[(3-chlorobenzyl)oxy]-2-oxo-2*H*-chromen-4-yl}-acetamide (21c). Crystallized from ethanol. Yield: 15%. Mp: 112-3 °C. ¹H NMR (300 MHz, CDCl₃) δ: 0.87 (t, J=7.2 Hz, 3H), 1.21–1.31 (m, 2H), 1.38–1.50 (m, 2H), 3.23 (q, J=6.7 Hz, 2H), 3.64 (s, 2H), 5.10 (s, 2H), 5.51 (br s, 1H), 6.23 (s, 1H), 6.87 (d, J=2.5 Hz, 1H), 6.91 (dd, $J_1=2.5$ Hz, $J_2=8.8$ Hz, 1H), 7.30–7.34 (m, 3H), 7.43 (br s, 1H), 7.60 (d, J=8.8 Hz, 1H). IR cm⁻¹ (KBr): 3287, 1718, 1638, 1613. Anal. (C₂₂H₂₂ClNO₄) C, H, N.

N-Benzyl-2-{7-[(3-chlorobenzyl)oxy]-2-oxo-2*H*-chromen-4-yl}-acetamide (21d). Crystallized from ethanol. Yield: 25%. Mp: 170–1 °C. ¹H NMR (300 MHz, CDCl₃) δ: 3.69 (s, 2H), 4.42 (d, J = 5.8 Hz, 2H), 5.10 (s, 2H), 5.90 (br s, 1H), 6.22 (s, 1H), 6.86 (d, J = 2.5 Hz, 1H), 6.92 (dd, $J_1 = 2.5$ Hz, $J_2 = 8.8$ Hz, 1H), 7.15–7.18 (m, 2H), 7.26–7.37 (m, 6H), 7.43 (br s, 1H), 7.60 (d, J = 8.8 Hz, 1H). IR cm⁻¹ (KBr): 3280, 1727, 1639, 1619. Anal. (C₂₅H₂₀ClNO₄) C, H, N.

2-[7-(Benzyloxy)-2-oxo-2*H*-chromen-4-yl]-*N*,*N*-dimethylaceta-mide (21e). Crystallized from ethanol. Yield: 55%. Mp: 162-3 °C. 1 H NMR (300 MHz, DMSO- d_{6}) δ : 2.83 (s, 3H), 3.07 (s, 3H), 3.93 (s, 2H), 5.21 (s, 2H), 6.15 (s, 1H), 6.99 (dd, $J_{1} = 2.5$ Hz, $J_{2} = 8.8$ Hz, 1H), 7.06 (d, J = 2.5 Hz, 1H), 7.30–7.47 (m, 5H), 7.55 (d, J = 8.8 Hz, 1H). IR cm⁻¹ (KBr): 1724, 1648, 1611. Anal. (C₂₀H₁₉NO₄) C, H, N.

2-{7-[(3-Chlorobenzyl)oxy]-2-oxo-2*H*-chromen-4-yl}-*N*,*N*-dimethylacetamide (21f). Purified by column chromatography (eluent: AcOEt). Yield: 62%. Mp: 159–160 °C. ¹H NMR (300 MHz, CDCl₃) δ : 3.02 (s, 3H), 3.10 (s, 3H), 3.79 (s, 2H), 5.10 (s, 2H), 6.14 (s, 1H), 6.87 (d, J = 2.5 Hz, 1H), 6.92 (dd, $J_1 = 2.5$ Hz, $J_2 = 8.8$ Hz, 1H), 7.29–7.34 (m, 3H), 7.43 (br s, 1H), 7.51 (d, J = 8.8 Hz, 1H). IR cm⁻¹ (KBr): 1717, 1644, 1617. Anal. (C₂₀H₁₈ClNO₄) C, H, N.

N-Butyl-2-{7-[(3-chlorobenzyl)oxy]-2-oxo-2*H*-chromen-4-yl}-*N*-methylacetamide (21g). Purified by column chromatography (eluent: CHCl₃/MeOH, 9.7/0.3 v/v). Yield: 25%. ¹H NMR (300 MHz, CDCl₃) δ: 0.90–1.03 (m, 3H), 1.25–1.67 (m, 4H), 2.98 (s, 3H) 3.06 (s, 3H), 3.32 (t, J = 7.4 Hz, 1H), 3.41 (t, J = 7.4 Hz, 1H) 3.78 (s, 2H), 5.10 (s, 2H), 6.15 (s, 1H), 6.86 (s, 1H), 6.91 (d, J = 8.8 Hz, 1H), 7.26–7.36 (m, 3H), 7.42 (br s, 1H), 7.49 (d, J = 8.8 Hz, 1H). IR cm⁻¹ (KBr): 2958, 2872, 1714, 1639, 1609. Anal. (C₂₃H₂₄ClNO₄) C, H, N.

General Procedure for the Preparation of Amines 22a,d,h-j and Free Amines of Mesylates 22b,c. The appropriate intermediate 2c-f (0.17 g, 0.50 mmol) and a 2.0 M solution of N-methylamine or N,N-dimethylamine in THF (5.0 mL, 10 mmol) were stirred at 50 °C under argon for 5 h. The mixture was then cooled to room temperature, and the inorganic precipitate was filtered off. The solvent was then evaporated, and the resulting solid was purified by column chromatography using AcOEt as eluent.

7-(Benzyloxy)-4-[(methylamino)methyl]-2*H***-chromen-2-one (22a).** Yield: 44%. ¹H NMR (300 MHz, DMSO- d_6) δ : 2.67 (s, 3H), 4.42 (s, 2H), 5.24 (s, 2H), 6.45 (s, 1H), 7.09 (dd, $J_1 = 2.2$ Hz, $J_2 = 8.8$ Hz, 1H), 7.13 (d, J = 2.2 Hz, 1H), 7.33–7.47 (m, 5H), 7.76 (d, J = 8.8 Hz, 1H), NH not detectable. IR cm⁻¹ (KBr): 1700, 1611. Anal. ($C_{18}H_{17}NO_3$) C, H, N.

7-(1,3-Benzodioxol-5-ylmethoxy)-4-[(methylamino)methyl]-2*H***-chromen-2-one** (**22d**). Yield: 40%. Mp: 168-170 °C. ¹H NMR (300 MHz, DMSO- d_6) δ : 2.33 (s, 3H), 3.81 (s, 2H), 5.09 (s, 2H), 6.01 (s, 2H), 6.28 (s, 1H), 6.89-6.99 (m, 3H), 7.02-7.04 (m, 2H), 7.72 (d, J = 8.8 Hz, 1H), NH not detectable. IR cm⁻¹ (KBr): 1705, 1614. Anal. ($C_{19}H_{17}NO_5$) C, H, N.

7-(Benzyloxy)-4-[(dimethylamino)methyl]-2*H***-chromen-2-one (22h). Yield:** 61%. ¹H NMR (300 MHz, CDCl₃) δ : 2.34 (s, 6H), 3.54 (s, 2H), 5.13 (s, 2H), 6.32 (s, 1H), 6.88 (d, J = 2.5 Hz, 1H), 6.93 (dd, $J_1 = 2.5$ Hz, $J_2 = 8.8$ Hz, 1H), 7.33–7.45 (m, 5H), 7.77 (d, J = 8.8 Hz, 1H). IR (cm⁻¹): 1723, 1611, 1392. Anal. (C₁₉H₁₉NO₃) C, H, N.

7-[(3-Chlorobenzyl)oxy]-4-[(dimethylamino)methyl]-2*H***-chromen-2-one (22i). Yield: 71%. Mp: 78-80 °C. ¹H NMR (300 MHz, CDCl₃) \delta: 2.33 (s, 6H), 3.53 (s, 2H), 5.10 (s, 2H), 6.33 (s, 1H), 6.86 (d, J = 2.5 Hz, 1H), 6.92 (dd, J_1 = 2.5 Hz, J_2 = 8.8 Hz, 1H), 7.28-7.34 (m, 3H), 7.43 (s, 1H), 7.78 (d, J = 8.8 Hz, 1H). IR cm⁻¹ (KBr): 1708, 1614, 1385. Anal. (C₁₉H₁₈ClNO₃) C, H, N.**

4-[(Dimethylamino)methyl]-7-[(3-fluorobenzyl)oxy]-2*H*-chromen-2-one (22j). Yield: 74%. Mp: 84–6 °C. ¹H NMR (300 MHz, CDCl₃) δ : 2.32 (s, 6H), 3.51 (s, 2H), 5.12 (s, 2H), 6.31 (s, 1H), 6.85 (d, J=2.5 Hz, 1H), 6.91 (dd, $J_1=2.5$ Hz, $J_2=8.8$ Hz, 1H), 7.00–7.06 (m, 1H), 7.13–7.20 (m, 2H), 7.33–7.40 (m, 1H), 7.79 (d, J=8.8 Hz, 1H). IR cm⁻¹ (KBr): 1704, 1615. Anal. (C₁₉H₁₈-FNO₃) C, H, N.

7-[(3-Chlorobenzyl)oxy]-4-[(methylamino)methyl]-2*H***-chromen-2-one** (Free Amine of 22b). Yield: 18%. ¹H NMR (300 MHz, CDCl₃) δ : 2.54 (s, 3H), 3.90 (s, 2H), 5.10 (s, 2H), 6.38 (s, 1H), 6.86 (d, J=2.8 Hz, 1H), 6.92 (dd, $J_1=2.8$ Hz, $J_2=8.8$ Hz, 1H), 7.31–7.34 (m, 3H), 7.43 (s, 1H), 7.60 (d, J=8.8 Hz, 1H), NH not detectable. IR cm⁻¹ (KBr): 1710, 1610. Anal. (C₁₈H₁₆ClNO₃) C, H, N.

7-[(3-Fluorobenzyl)oxy]-4-[(methylamino)methyl]-2*H***-chromen-2-one** (Free Amine of **22c**). Yield: 22%. Mp: 115–7 °C. ¹H NMR (300 MHz, DMSO- d_6) δ : 2.32 (s, 3H), 3.81 (s, 2H), 5.23 (s, 2H), 6.29 (s, 1H), 7.00 (dd, $J_1=2.5$ Hz, $J_2=8.8$ Hz, 1H), 7.05 (d, J=2.5 Hz, 1H), 7.12–7.19 (m, 1H), 7.28–7.31 (m, 2H), 7.40–7.47 (m, 1H), 7.73 (d, J=8.8 Hz, 1H), NH not detectable. IR cm⁻¹ (KBr): 1707, 1611. Anal. (C₁₈H₁₆FNO₃) C, H, N.

Mesylates 22b,c were prepared from the corresponding free amines following the general procedure reported below.

General Procedure for the Preparation of Methanesulfonate Salts. The suitable 4-aminoalkyl-7-benzyloxycoumarin derivative (1.1 mmol) was dissolved in dry THF (6.0 mL), and methanesulfonic acid (0.080 mL, 1.2 mmol) was slowly added. The resulting white solid was filtered, washed with dry THF, and crystallized from absolute ethanol.

7-[(3-Chlorobenzyl)oxy]-4-[(methylamino)methyl]-2H-chromen-2-one Methanesulfonate (22b). Mp: 213-5 °C. ¹H NMR (DMSO d_6) δ : 2.31 (s, 3H), 2.71 (s, 3H), 4.44 (s, 2H), 5.27 (s, 2H), 6.41 (s, 1H), 7.10 (dd, $J_1 = 2.5$ Hz, $J_2 = 8.8$ Hz, 1H), 7.14 (d, J = 2.5 Hz, 1H), 7.37–7.44 (m, 3H), 7.54 (s, 1H), 7.77 (d, J = 8.8 Hz, 1H), 9.01 (s, 2H, dis. with D_2O). IR cm⁻¹ (KBr): 1716, 1614. Anal. (C₁₉H₂₀ClNO₆S) C, H, N.

7-[(3-Fluorobenzyl)oxy]-4-[(methylamino)methyl]-2H-chromen-2-one Methanesulfonate (22c). Mp 215-6 °C. ¹H NMR (300 MHz, DMSO- d_6) δ : 2.28 (s, 3H), 2.70 (s, 3H), 4.43 (s, 2H), 5.27 $(s, 2H), 6.40 (s, 1H), 7.10 (dd, J_1 = 2.5 Hz, J_2 = 8.8 Hz, 1H), 7.15$ (d, J = 2.5 Hz, 1H), 7.16 (m, 1H), 7.28 - 7.31 (m, 2H), 7.41 - 7.45(m, 1H), 7.76 (d, J = 8.8 Hz, 1H), 8.96 (s, 2H, dis. with D_2O). IR cm⁻¹ (KBr): 1717, 1615. Anal. (C₁₉H₂₀FNO₆S) C, H, N.

4-[(Ethylamino)methyl]-7-[(3-fluorobenzyl)oxy]-2H-chromen-2-one Methanesulfonate (22e). Intermediate 2e (0.25 g, 0.80 mmol) and the commercially available 70% solution of ethylamine in water (3.0 mL) were stirred at room temperature under argon for 3 h. The mixture was then poured into ice-water, and a precipitated side product was filtered off. The solvent was evaporated to dryness and the resulting solid was purified by column chromatography using CHCl₃/n-hexane/AcOEt, 7/2/1 (v/v/v) as eluent, yielding a red oil that was further transformed into the corresponding mesylate salt according to the procedure described above. Yield: 35%. Mp: 242-4 °C. ¹H NMR (300 MHz, DMSO d_6) δ : 1.25 (t, J = 7.2 Hz, 3H), 2.28 (s, 3H), 3.11–3.12 (m, 2H), 4.42-4.46 (m, 2H), 5.27 (s, 2H), 6.45 (s, 1H), 7.11 (dd, J_1 $2.5 \text{ Hz}, J_2 = 8.8 \text{ Hz}, 1\text{H}, 7.15 \text{ (d}, J = 2.5 \text{ Hz}, 1\text{H}), 7.17 - 7.20 \text{ (m},$ 1H), 7.29-7.32 (m, 2H), 7.41-7.48 (m, 1H), 7.77 (d, J = 8.8 Hz, 1H), 8.88 (s, 2H, dis. with D_2O). IR cm⁻¹ (KBr): 1714, 1613. Anal. $(C_{20}H_{22}FNO_6S) C, H, N.$

7-[(3-Fluorobenzyl)oxy]-4-[(isopropylamino)methyl]-2H-chromen-2-one Methanesulfonate (22f). Intermediate 2e (0.25 g, 0.80 mmol) and the commercially available isopropylamine (2.7 mL, 31 mmol) were refluxed for 2 h. The solution was evaporated to dryness and the resulting oil was purified by column chromatography using CHCl₃/n-hexane/AcOEt 7/2/1 (v/v/v) as eluent, yielding a yellow oil that was further transformed into the corresponding mesylate derivative according to the procedure described above. Yield: 42%. Mp: 196–8 °C. ¹H NMR (300 MHz, DMSO- d_6) δ : 1.33 (d, J = 6.5 Hz, 6H), 2.29 (s, 3H), 3.47 (m, 1H), 4.43–4.47 (m, 2H), 5.29 (s, 2H), 6.47 (s, 1H), $7.12 \, (dd, J_1 = 2.4 \, Hz, J_2 = 8.9 \, Hz, 1H), 7.16 \, (d, J = 2.4 \, Hz, 1H),$ 7.21 (m, 1H), 7.30-7.33 (m, 2H), 7.42-7.49 (m, 1H), 7.81 (d, J = 8.9 Hz, 1H), 8.82 (s, 2H, dis. with D₂O). IR cm⁻¹ (KBr): 1713, 1612. Anal. (C₂₁H₂₄FNO₆S) C, H, N.

Synthesis of Amines 22g and 22k. 7-[(3-Chlorobenzyl)oxy]-4-(chloromethyl)-2*H*-chromen-2-one **2d** (0.40 g, 1.2 mmol), K₂CO₃ (0.17 g, 1.2 mmol), and benzylamine (0.66 mL, 6.0 mmol) or N-benzyl-N-methylamine (0.15 mL, 1.2 mmol) were stirred in refluxing absolute ethanol (10 mL) for 2-5 h, until the disappearance of the 2d spot as indicated by the TLC control. The reaction mixture was cooled to room temperature, the inorganic solid residue was filtered off, the solvent was evaporated, and the resulting oil was purified by column chromatography using CHCl₃/n-hexane/AcOEt 7/2/1 (v/v/v) as eluent, giving a solid, which was crystallized from absolute ethanol yielding a yellow solid.

4-[(Benzylamino)methyl]-7-[(3-chlorobenzyl)oxy]-2H-chromen-**2-one** (**22g**). Yield: 18%. Mp: 133–5 °C. ¹H NMR (300 MHz, CDCl₃) δ: 3.93 (s, 2H), 3.94 (s, 2H), 5.09 (s, 2H), 6.49 (s, 1H), 6.87 $(dd, J_1 = 2.5 \text{ Hz}, J_2 = 8.8 \text{ Hz}, 1\text{H}), 6.90 (d, J = 2.5 \text{ Hz}, 1\text{H}),$ 7.27-7.39 (m, 8H), 7.43 (s, 1H), 7.54 (d, J = 8.8 Hz, 1H), NH not detectable. IR cm⁻¹ (KBr): 3298, 1696, 1610. Anal. (C₂₄H₂₀-ClNO₃) C, H, N.

4-{[Benzyl(methyl)amino]methyl}-7-[(3-chlorobenzyl)oxy]-2Hchromen-2-one (22k). Yield: 46%. Mp: 107-8 °C. ¹H NMR $(300 \text{ MHz}, \text{DMSO-}d_6) \delta$: 2.13 (s, 3H), 3.58 (s, 2H), 3.67 (s, 2H), 5.23 (s, 2H), 6.35 (s, 1H), 7.02 (dd, $J_1 = 1.9$ Hz, $J_2 = 8.8$ Hz, 1H), 7.05 (d, J = 1.9 Hz, 1H), 7.20 - 7.39 (m, 5H), 7.41 - 7.44 (m, 3H),7.53 (s, 1H), 7.85 (d, J = 8.8 Hz, 1H). IR cm⁻¹ (KBr): 1708, 1619. Anal. (C₂₅H₂₂ClNO₃) C, H, N.

Synthesis of Azides 23a,b. The appropriate chlorides 2c,d (1.7 mmol) and NaN3 (0.44 g, 6.8 mmol) were refluxed in absolute ethanol (17 mL) for 2 h. The mixture was cooled to room temperature, and the solid residue was filtered off. The solvent was then evaporated and the resulting oil was purified by column chromatography using n-hexane/AcOEt, 8/2 (v/v), as eluent, yielding a yellow solid.

4-(Azidomethyl)-7-benzyloxy-2*H*-chromen-2-one (23a). Yield: 45%. ¹H NMR (300 MHz, CDCl₃) δ: 4.51 (s, 2H), 5.14 (s, 2H), 6.36 (s, 1H), 6.93 (br s, 1H), 6.96–6.97 (br s, 1H), 7.34–7.46 (m, 6H). IR cm⁻¹ (KBr): 2116, 1714, 1614.

4-(Azidomethyl)-7-[(3-chlorobenzyl)oxy]-2H-chromen-2-one (23b). Yield: 43%. ¹H NMR (300 MHz, CDCl₃) δ: 4.51 (s, 2H), 5.11 (s, 2H), 6.38 (s, 1H), 6.90 (d, J = 2.5 Hz, 1H), 6.94 (dd, $J_1 = 2.5 \text{ Hz}, J_2 = 8.8 \text{ Hz}, 1\text{H}, 7.30-7.35 \text{ (m, 3H)}, 7.43-7.47$ (m, 2H). IR cm⁻¹ (KBr): 2108, 1703, 1611.

Synthesis of Primary Amines 24a,b. To a clear solution of SnCl₂ dihydrate (0.66 g, 3.5 mmol) in dry methanol (5.0 mL) was added over 1 h the appropriate 4-(azidomethyl)-7-(benzyloxy)-2H-chromen-2-one 23a,b (0.40 mmol) in small portions. The mixture was then stirred at room temperature for 3 h. The solvent was then evaporated, the residue was poured into cold water, the pH was made strongly basic with 3 N NaOH, and then the resulting aqueous solution was extracted with AcOEt. The organic layers were collected, washed with brine, dried over Na₂SO₄, and evaporated in vacuum. The resulting solid was further purified by column chromatography using CHCl₃/ CH₃OH, 9.7/0.3 (v/v), as eluent, yielding the desired primary amines as white solids.

4-(Aminomethyl)-7-(benzyloxy)-2*H*-chromen-2-one Yield: 36%. Mp: 135-7 °C (dec). ¹H NMR (300 MHz, DMSO-d₆) δ: 3.90 (s, 2H), 5.21 (s, 2H), 6.38 (s, 1H), 6.99 (dd, $J_1 = 2.5 \text{ Hz}, J_2 = 8.8 \text{ Hz}, 1\text{H}, 7.07 (d, J = 2.5 \text{ Hz}, 1\text{H}),$ 7.30–7.47 (m, 5H), 7.67 (d, J = 8.8 Hz, 1H), 2 NHs not detectable. IR cm⁻¹ (KBr): 3391, 3320, 1703, 1611. Anal. $(C_{17}H_{15}NO_3)C, H, N.$

4-(Aminomethyl)-7-[(3-chlorobenzyl)oxy]-2*H*-chromen-2-one (24b). Yield: 39%. Mp: 166-7 °C. ¹H NMR (300 MHz, DMSO-*d*₆) δ: 3.90 (s, 2H), 5.23 (s, 2H), 6.39 (s, 1H), 7.00 (dd, $J_1 = 2.5 \text{ Hz}, J_2 = 8.8 \text{ Hz}, 1\text{H}), 7.07 \text{ (d, } J = 2.5 \text{ Hz}, 1\text{H}),$ 7.39 - 7.48 (m, 3H), 7.53 (s, 1H), 7.69 (d, J = 8.8 Hz, 1H), 2 NHs not detectable. IR cm $^{-1}$ (KBr): 3393, 1711, 1612. Anal. $(C_{17}H_{14}CINO_3)C, H, N.$

Synthesis of Nitriles 25a,b. An amount of 0.38 mmol of 11a or 11b and 0.061 mL (0.76 mmol) of anhydrous pyridine were dissolved in 4.0 mL of anhydrous dioxane. The mixture was cooled at 0 °C with an external ice bath, and trifluoroacetic anhydride (0.068 mL, 0.48 mmol) was added dropwise. The clear solution was allowed to reach room temperature and after 10 min was poured into ice. The aqueous solution was extracted with chloroform and the organic phase was dried over anhydrous Na₂SO₄, filtered, and evaporated under vacuum to give a white solid crystallized from ethanol.

(7-Benzyloxy-2-oxo-2*H*-chromen-4-yl)acetonitrile (25a). Yield: 86%. Mp: 178–9 °C. ¹H NMR (300 MHz, DMSO-*d*₆) δ: 4.37 (s, 2H), 5.23 (s, 2H), 6.32 (s, 1H), 7.09 (dd, $J_1 = 2.5$ Hz, $J_2 = 8.8$ Hz, 1H), 7.13 (d, J = 2.5 Hz, 1H), 7.30–7.46 (m, 5H), 7.66 (d, J = 8.8 Hz, 1H). IR cm⁻¹ (KBr): 2938, 1714, 1612, 1395, 1283. Anal. $(C_{18}H_{13}NO_3)C, H, N.$

{7-[(3-Chlorobenzyl)oxy]-2-oxo-2*H*-chromen-4-yl}acetonitrile (25b). Yield: 97%. Mp: 180-2 °C. ¹H NMR (300 MHz,

DMSO- d_6) δ : 4.37 (s, 2H), 5.25 (s, 2H), 6.33 (s, 1H), 7.09 (d, J = 2.5 Hz, 1H), 7.12–7.14 (m, 1H), 7.37–7.44 (m, 3H), 7.54 (s, 1H), 7.67 (d, J = 8.8 Hz, 1H). IR cm⁻¹ (KBr): 2936, 1716, 1613, 1396, 1268. Anal. (C₁₈H₁₂ClNO₃) C, H, N.

4-(2-Aminoethyl)-7-[(3-chlorobenzyl)oxy]-2H-chromen-2-one **Hydrochloride** (26). Amounts of $0.033 \,\mathrm{g} \,(0.10 \,\mathrm{mmol})$ of 25b and 0.048 g (0.20 mmol) of CoCl₂·H₂O were suspended in 2.0 mL of methanol. An amount of 0.038 g (1.0 mmol) of sodium borohydride was added to the suspension, and the reaction mixture was stirred at room temperature for 1 h. Then 1.0 mL of 2.0 N HCl was added and the organic solvent was evaporated under vacuum. The acid solution was cooled at 0 °C, and an amount of 5.0 mL of a solution of ammonia 30% in water was added. The basic solution was extracted with ethyl acetate and the organic phase dried over anhydrous Na2SO4, filtered, and evaporated to dryness, yielding a yellow solid which was dissolved in 2.0 mL of chloroform, and 1.0 mL of 3 N HCl was added. A precipitate was obtained and filtered, corresponding to the hydrochloric salt of the desired product. Yield: 20%. Mp: 113 °C (dec), 176–8 °C. 1 H NMR (300 MHz, DMSO- 2 d₆) δ: 3.08 (br, 4H), 5.26 (s, 2H), 6.27 (s, 1H), 7.07 (dd, $J_1 = 2.4$ Hz, $J_2 = 8.8$ Hz, 1H), 7.11 (d, J = 2.5 Hz, 1H), 7.42–7.44 (m, 3H), 7.54 (s, 1H), 7.78 (d, J = 8.8 Hz, 1H), 7.96 (br s, 3H, dis. with D₂O). IR cm⁻¹ (KBr): 3056, 1723, 1615. Anal. (C₁₈H₁₇Cl₂NO₃) C, H, N.

7-Hydroxy-4-(2-hydroxyethyl)-2*H*-chromen-2-one (27). An amount of 0.94 g (4.3 mmol) of commercially available 7-hydroxycoumarin-4-acetic acid 5 was dissolved in 25 mL of anhydrous tetrahydrofuran. The mixture was cooled at 0 °C with an external ice bath, and an amount of 13 mL (13 mmol) of a 1.0 M solution of borane in THF was added dropwise. The mixture was allowed to reach room temperature and stirred for 6 h. The mixture was cooled at 0 °C, and an amount of 20 mL of methanol was added. The solvent was evaporated under vacuum and the residue obtained was dissolved in ethyl acetate, washed with water, dried over anhydrous Na₂SO₄, filtered, and evaporated to give a solid that was purified by flash chromatography (eluent CHCl₃/MeOH, 9/1 v/v) to give a white solid of satisfactory purity. Yield: 54%. ¹H NMR (300 MHz, DMSO- d_6) δ : 2.86 (t, J = 6.3 Hz, 2H), 3.65–3.71 (m, 2H), 4.80 (t, J = 5.2 Hz, 1H), 6.09 (s, 1H), 6.70 (d, J = 2.2 Hz, 1H), 6.78 (dd, $J_1 = 2.2 \text{ Hz}$, $J_2 = 8.7 \text{ Hz}$, 1H), 7.63 (d, J = 8.7 Hz, 1H), 10.54 (s, 1H). IR cm⁻¹ (KBr): 1686, 1611.

Synthesis of Alcohols 28a,b. The intermediate **27** (0.21 g, 1.0 mmol) was dissolved in 10.0 mL of absolute ethanol, and K_2CO_3 (0.14 g, 1.0 mmol) and the corresponding benzyl bromide (2.0 mmol) were added to the solution, and the mixture was refluxed for 45 min. The precipitate was filtered off, and the organic solution was evaporated under vacuum. The oily residue was purified by flash chromatography (eluent $CHCl_3/MeOH$, 9.5/0.5 v/v) to give a white solid.

7-(Benzyloxy)-4-(2-hydroxyethyl)-2*H***-chromen-2-one (28a).** Yield: 53%. H NMR (300 MHz, DMSO- d_6) δ : 2.89 (t, J=6.3 Hz, 2H), 3.66-3.72 (m, 2H), 4.80 (t, J=5.5 Hz, 1H), 5.21 (s, 2H), 6.17 (s, 1H), 7.01 (dd, $J_1=2.5$ Hz, $J_2=8.8$ Hz, 1H), 7.06 (d, J=2.5 Hz, 1H), 7.30-7.47 (m, 5H), 7.73 (d, J=8.8 Hz, 1H). IR cm⁻¹ (KBr): 1697, 1614.

7-[(3-Chlorobenzyl)oxy]-4-(2-hydroxyethyl)-2*H*-chromen-2-one (28b). Yield: 67%. 1 H NMR (300 MHz, DMSO- d_{6}) δ : 2.89 (t, J = 6.3 Hz, 2H), 3.69 (t, J = 6.3 Hz, 2H), 4.78 (br s, 1H), 5.23 (s, 2H), 6.18 (s, 1H), 7.02 (dd, $J_{1} = 2.5$ Hz, $J_{2} = 8.6$ Hz, 1H), 7.06 (d, J = 2.5 Hz, 1H), 7.41-7.43 (m, 3H), 7.53 (s, 1H), 7.74 (d, J = 8.6 Hz, 1H). IR cm⁻¹ (KBr): 3068, 1718, 1610.

Synthesis of Bromides 29a,b. Amounts of 1.0 mmol of 28a (0.30 g, for 29a) or 28b (0.33 g, for 29b) and 0.73 g (2.2 mmol) of carbon tetrabromide were dissolved in 10 mL of anhydrous dichloromethane. The mixture was cooled at 0 °C with an external ice bath, and triphenylphosphine (0.53 g, 2.0 mmol) dissolved in 2.0 mL of anhydrous dichloromethane, was added dropwise. The mixture was allowed to reach room temperature and stirred for 1 h. The solvent was evaporated under vacuum

and the oily residue was purified by flash chromatography (eluent $CHCl_3/n$ -hexane, 8/2 v/v, for **29a** and $CHCl_3/n$ -hexane, 7/3 v/v, for **29b**) to give white solids.

7-(Benzyloxy)-4-(2-bromoethyl)-2*H***-chromen-2-one (29a).** Yield: 82%. ¹H NMR (300 MHz, DMSO- d_6) δ : 3.34 (t, J=6.8 Hz, 2H), 3.82 (t, J=6.8 Hz, 2H), 5.21 (s, 2H), 6.27 (s, 1H), 7.02 (dd, $J_1=2.2$ Hz, $J_2=9.0$ Hz, 1H), 7.08 (d, J=2.2 Hz, 1H), 7.30–7.47 (m, 5H), 7.75 (d, J=9.0 Hz, 1H). IR cm⁻¹ (KBr): 1727, 1609.

4-(2-Bromoethyl)-7-[(3-chlorobenzyl)oxy]-2*H***-chromen-2-one (29b). Yield: 59%. ¹H NMR (300 MHz, CDCl₃) \delta: 3.30 (t, J = 7.2 Hz, 2H), 3.64 (t, J = 7.2 Hz, 2H), 5.11 (s, 2H), 6.20 (s, 1H), 6.89 (d, J = 2.5 Hz, 1H), 6.95 (dd, J_1 = 2.5 Hz, J_2 = 8.8 Hz, 1H), 7.32–7.33 (m, 3H), 7.44 (s, 1H), 7.50 (d, J = 8.8 Hz, 1H). IR cm⁻¹ (KBr): 1718, 1610.**

Synthesis of Amines 30a,b. An amount of 0.51 mmol of the suitable bromide 29a,b was added to 3.8 mL (7.6 mmol) of a 2.0 M solution of methylamine (for 30a) or dimethylamine (for 30b) in THF, followed by anhydrous K_2CO_3 (0.070 g, 0.51 mmol) and KI (0.009 g, 0.051 mmol). The mixture was stirred at 50 °C overnight. The precipitate was filtered off and the solvent was evaporated under vacuum to give an oily residue that was purified by chromatography (eluent CHCl₃/MeOH, 9/1 v/v) and crystallized from ethanol.

7-[(3-Chlorobenzyl)oxy]-4-[2-(methylamino)ethyl]-2*H*-chromen-2-one (30a). Yield: 29%. Mp: 72 °C (dec), 137–9 °C. ¹H NMR (300 MHz, DMSO- d_6) δ : 2.34 (s, 3H), 2.84–2.92 (m, 4H), 5.24 (s, 2H), 6.19 (s, 1H), 7.04 (dd, $J_1 = 2.5$ Hz, $J_2 = 8.8$ Hz, 1H), 7.08 (d, J = 2.5 Hz, 1H), 7.42–7.44 (m, 3H), 7.54 (s, 1H), 7.76 (d, J = 8.8 Hz, 1H), NH not detectable. IR cm⁻¹ (KBr): 1719, 1609. Anal. (C₁₉H₁₈ClNO₃) C, H, N.

7-(Benzyloxy)-4-[2-(dimethylamino)ethyl]-2*H***-chromen-2-one (30b). Yield: 20%. Mp: 163-4 °C. ¹H NMR (300 MHz, DMSO-d_6) \delta: 2.84 (s, 6H), 3.17–3.25 (m, 2H), 3.32–3.40 (m, 2H), 5.23 (s, 2H), 6.28 (s, 1H), 7.06 (dd, J_1 = 2.5 Hz, J_2 = 8.8 Hz, 1H), 7.11 (d, J = 2.5 Hz, 1H), 7.31–7.48 (m, 5H), 7.84 (d, J = 8.8 Hz, 1H). IR cm⁻¹ (KBr): 1721, 1617. Anal. (C_{20}H_{21}NO_3) C, H, N.**

 pK_a and log P Determination of 22b. pK_a and octanol—water partition coefficient of compound 22b were determined by potentiometric titration using the Sirius GLpKa instrument implemented by the software RefinementPro (Sirius Analitical Ltd., Forest Row, East Sussex, U.K.). For pK_a determination, a 5×10^{-4} M concentration of the sample in a 0.15 M KCl solution was brought to pH 1.8 through the addition of 0.5 M HCl and then titrated up to pH 12.2 with carbonate-free 0.5 M KOH at a temperature of $25\pm0.5\,^{\circ}\text{C}$, under a slow argon flow to avoid CO $_2$ absorption at high pHs. An analogous measurement has been performed in the absence of compound, for the standardization of the instrument (blank curve). Detailed instrumental procedures can be found elsewhere. 86,87

The curves of sample and blank titrations were elaborated through a computerized mathematical algorithm with the software RefinementPro to get the differential curve of Bjerrum, that shows the number of free protons from the compound dissociation (n) versus pH. These calculations indicate a p K_a of 7.18 \pm 0.05, from three independent measurements.

The experimental $\log P$ values was determined through a potentiometric titration in a biphasic system constituted by a solution of 0.15 M KCl saturated with 1-octanol.

In a two-phases system, the dissociation of acids or bases is reduced because of the partitioning. This involves a shift of the Bjerrum plot, toward the right for acids and the left for bases. The new value of dissociation constant measured is an apparent pK_a (poKa).

The entity of pK_a shift allows the determination of the experimental value of $\log P$ through the following equations. For monoprotic acid, it is

$$P = \frac{10^{\text{poKa} - \text{p}K_a}}{r} - 1$$

For monoprotic basic, it is

$$P = \frac{10^{pK_a - poKa}}{r} - 1$$

The $\log P$ value of **22b** coming from these calculations was 2.48 ± 0.03 (from three separated experiments).

Aqueous Solubility Assay. Compound 22b was dissolved in DMSO at a concentration of 2 and 180 mg/mL. The appropriate solution was added in portions (2 μ L at a time) to 1 mL of a 50 mM Tris-HCl, pH 7.4, or of a 50 mM acetate buffer, pH 3.0, solution at room temperature. Typically a total of 10 additions were made so that the final volume of DMSO was well below 5%. The appearance of the precipitate was detected by an absorbance increase due to light scattering by particulate material, in a dedicated diode array UV spectrometer (GE Healthcare, Uppsala, Sweden). Increased UV absorbance was measured in the 600-820 nm range. In its simplest implementation, the precipitation point (i.e., the upper aqueous solubility limit) was calculated from a bilinear curve fit in a plot of the absorbance (y axis) versus μ L of DMSO (x axis). The solubility was $52 \pm 5 \,\mu g$ /mL and $2.82 \pm 0.35 \,m g$ /mL at pH 7.4 and pH 3.0, respectively, as the mean \pm SEM of three independent assays.

HDM-PAMPA Permeability Assay. Equation 1 below was used to calculate the *effective* permeability coefficient (P_e):

$$P_{e} = -\frac{2.303V_{D}}{A(t - \tau_{LAG})} \left(\frac{V_{A}}{V_{A} + V_{D}}\right) \log \left[1 - \left(\frac{V_{A} + V_{D}}{V_{D}(1 - R)}\right) \frac{C_{A}(t)}{C_{D}(0)}\right]$$
(1)

where A the accessible filter area (cm²) (i.e., filter area multiplied by filter porosity), t is incubation time (s), V_A and V_D are respectively the volumes in the acceptor and the donor wells (cm³), $C_A(t)$ is the concentration of the compound (mol cm⁻³) in the acceptor well at time t, and $C_D(0)$ is the concentration of the compound (mol cm⁻³) in the donor well at time t0. t1 is the retention factor, calculated by eq 2 and defined as the mole fraction that is lost in the membrane and in the microplates (i.e., filters and plate materials):

$$R = 1 - \frac{C_{\rm D}(t)}{C_{\rm D}(0)} - \left(\frac{V_{\rm A}}{V_{\rm D}}\right) \left(\frac{C_{\rm A}(t)}{C_{\rm D}(0)}\right) \tag{2}$$

 $au_{\rm LAG}$ is the steady-state time (s), i.e., the time needed for the permeant's concentration gradient to become stabilized. Mathematically $au_{\rm LAG}$ is the time at which Fick's second law has transformed into the limiting situation of Fick's first law. Steady-state times ($au_{\rm LAG}$) to saturate the membranes in PAMPA are short relative to the total permeation time (\sim 20 min with unstirred plates), and for this reason they are usually neglected.

Permeation experiments were carried out in polycarbonate (PC) 96-well microtiter filter plates (Millipore, Bellerica, MA). Filter specifications of PC filter plates were 3 μ m pore size, 10 μ m thickness, and 12.5% porosity (the manufacturer specifications were 5-20% porosity range; thus, the average porosity value was taken in this work). Each well was coated with $0.75 \,\mu\text{L}$ of hexadecane. Because of the high viscosity of hexadecane (HDC), hexane was used as a solvent (15 μ L of 5% (v/v) HDC in hexane was dispensed in each well), and after the application of the membrane, the resulting filter plates were placed under a hood for 20 min to completely evaporate the hexane. Subsequently, the donor plate was placed upon a Teflon acceptor plate (MSSACCEPTOR, Millipore, Bellerica, MA) which had been prefilled with 280 μ L of buffer containing 5% DMSO. The system was finally hydrated with $280 \,\mu\text{L}$ of tested compounds in buffer containing 5% DMSO, and the resulting sandwich was incubated for 5 h at room temperature under constant shaking (75 rpm). Reference compound concentrations were chosen according to their solubility (i.e., 2.5 mM for 22b and 617 μ M for 3). Each compound was measured in quadruplicate, and iso-pH conditions were used (same pH in donor and acceptor

compartments; 0.1 M phosphate buffer solution (pH 6.8) was used)

After 5 h, the sandwich was disassembled and both donor and acceptor compartments were transferred to a UV quartz plate (Hellma GmbH & Co., Mullheim, Germany). UV absorption was measured with a PowerWave (Bio-Tek Instruments, Inc., Winooski, VT), and the reading was performed at λ_{max} of the compounds.

The very low concentration (in both donor and acceptor compartments) of 3 renders the UV detection ineffective, and therefore, the detection was performed using HPLC Merck Hitachi apparatus with a Discovery RP amide C16 (20 mm \times 4 mm i.d., 5 μ m) (Supelco, Bellefonte, PA).

To assess membrane stability, electrical resistance measurements were conducted on the filter plate at the end of the incubation time, using an electrometer system especially designed for PAMPA assays (EVOMX and MULTI96, World Precision Instruments, Sarasota, FL).

Molecular Modeling. Molecular Building and Optimization. The coumarin inhibitors were built from the Sybyl (version 8.2) fragment libraries starting from the reference ligand (4-FCBC) cocrystallized with hMAO-B (PDB code 2v60). Geometrical optimization and charge calculation were made by means of a quantum mechanical method with the PM3 Hamiltonian. The starting conformation for docking of the 7-(*m*-halogeno)-benzyloxy substituents was recovered from the X-ray crystallographic structures of 4-FCBC and safinamide bound to hMAO-B. ⁵⁶

Homology Modeling. The 3D model of the rMAO-B (entry name of AOFB RAT; primary accession number of P19643 at the ExPASy proteomics server) was developed starting from the X-ray structure of the hMAO-B (PDB code 2v60) complexed with the 4-FCBC ligand. The two MAO-B from different species presented highly close amino acid sequences (520aa vs 520aa, 88% of sequence similarity) and almost identical amino acid residues in the binding site where the only difference was the substitution of Ile316 in human by Val316 in rat. The threedimensional model of rMAO-B was constructed through homology modeling within Modeller (version 9.2). Among the five best solutions derived from Modeller, the one provided with the lowest value of the Modeller objective scoring function was selected for the subsequent docking simulations. The stereochemical quality of this model, as well as the overall residue-byresidue geometry, was controlled with Procheck (version 3.5.4). By selection of a resolution value equal to 2.0 Å, the Ramachandran plot returned 99.5% of residues in the core regions that represent the most favorable and allowed combinations of φ and ψ angle values while only the remaining 0.5% of residues (Lys52) and Ala346) was located in disallowed regions. As expected, the fitting of the backbone α -carbons of theoretical (rMAO-B) and experimental (hMAO-B) models gave a very low deviation (rms 0.096 Å), indicating a substantial conservation of their spatial position. By Modeller modeling of all the heteroatoms, it was possible to rebuild the coordinates of FAD cofactor and the eight structural water molecules coming from hMAO-B 2v60.

The seven conserved water molecules in hMAO-A crystal structure (PDB code 2z5x) were transferred into the binding site of rMAO-A by using Sybyl.

Docking Simulations. GOLD (version 2.4), a genetic algorithm-based software, was used for a docking study selecting GoldScore as a fitness function. GoldScore is made up of four components that account for protein—ligand binding energy: protein—ligand hydrogen bond energy (external H-bond), protein—ligand van der Waals energy (external vdw), ligand internal vdw energy (internal vdw), and ligand torsional strain energy (internal torsion). Parameters used in the fitness function (hydrogen bond energies, atom radii and polarizabilities, torsion potentials, hydrogen bond directionalities, and so forth) were taken from the GOLD parameter file.

In the present study, the 3D coordinates of hMAO-B (PDB code 2v60), rat and human MAO-A (PDB codes 1o5w and 2z5x, respectively) were retrieved from the Protein Data Bank. The protein preparation for docking study was performed in Sybyl: the cocrystallized ligands were removed; the correct atom type and the bond orders were assigned to FAD cofactor; by use of the Biopolymer tool, hydrogen atoms were added. The structure model of rMAO-B from Modeller was prepared for docking simulation applying the same protocol described above. For each coumarin inhibitor, 10 conformations were generated in a sphere of a 12 Å radius centered on phenolic oxygen atom of Tyr435 and Tyr444 in rMAO-B and rMAO-A, respectively. In our docking runs, the molecular scaffold of the best ranked solution of the 2v60 reference ligand docked into the rMAO-B was set as physical constraint to favor the occurrence of the known binding mode of coumarin inhibitors.

Biological Assays. In Vitro MAO-A and MAO-B Inhibition. MAO Enzyme Source and Membrane Preparations (Crude Rat Brain Mitochondrial Fraction). Male Wistar rats (Harlan, Italy, 150–175 g) were sacrificed under light anesthesia, and brains were rapidly removed and homogenized in 10 volumes of icecold 0.32 M sucrose buffer containing 0.1 M EDTA, pH 7.40. The crude homogenate was centrifuged at 2220 rpm for 10 min and the supernatant recovered. The pellet was homogenized and centrifuged again, and the two supernatants were pooled and centrifuged at 9250 rpm for 10 min at 4 °C. The pellet was resuspended in fresh buffer and centrifuged at 11250 rpm for 10 min at 4 °C. The resulting pellet was stored at -80 °C until use.

Human Platelet Rich Plasma (PRP) Preparation. The human venous blood (3.8% sodium citrate as anticoagulant) was immediately centrifuged at 125g for 15 min at 4 °C. The supernatant was removed and stored in ice. The pellet was again centrifuged at 600g for 5 min at 4 °C. The two PRP supernatants were pooled and stored at -80 °C until assay.

In Vitro MAO-A and MAO-B Inhibition Assays in Rat Brain **Mitochondria.** The enzyme activities were assessed with a radioenzymatic assay using the selective substrates 14C-serotonin (5-HT) and ¹⁴C-phenylethylamine (PEA) for MAO-A and MAO-B, respectively. The mitochondrial pellet (500 μ g protein) was resuspended in 0.1 M phosphate buffer, pH 7.40, and $500 \,\mu\text{L}$ was added to $50 \,\mu\text{L}$ of the test compound or buffer for 30 min at 37 °C (preincubation). Then the substrate (50 μ L) was added. The incubation was carried out for 30 min at 37 °C ([14 C]5-HT, 5 μ M) or for 10 min at 37 °C ([14 C]PEA, 0.5 μ M). The reaction was stopped by adding 0.2 mL of 37% HCl or 0.2 M perchloric acid. After centrifugation, the deaminated metabolites were extracted with 3 mL of diethyl ether (5-HT) or toluene (PEA) and the radioactive organic phase was measured by liquid scintillation spectrometry at 90% efficiency. Radioactivity in the eluate indicates the production of neutral and acidic metabolites formed as a result of MAO activity. The enzymatic activity was expressed as nanomoles of substrate transformed per milligram of protein per minute. The activity of MAO in the sample was expressed as a percentage of control activity in the absence of inhibitors after subtraction of appropriate blank values.

In Vitro MAO-B Inhibition Assay in PRP Preparation. MAO-B enzyme activity was assessed with a radioenzymatic assay using [14 C]PEA as selective substrates (3). The PRP was diluted 1:5 in 0.1 M phosphate buffer, pH 7.40, and 500 μ L (in duplicate) was added to 50 μ L of buffer and to 50 μ L of substrate ([14 C]PEA, 0.5 μ M). The incubation was carried out for 10 min at 37 °C. The reaction was stopped by adding 0.2 mL of perchloric acid. After centrifugation, the acidic metabolites were extracted by 3.5 mL of toluene and an amount of 3 mL of the radioactive organic phase was added to 10 mL of scintillation cocktail Insta-Fluor and measured by liquid scintillation spectrometry at 90% efficiency.

In Vitro MAO-B Inhibition Reversibility Studies. The reversibility of MAO-B inhibition was assessed performing time-

dependent experiments. Time-dependent inhibition kinetics were measured as IC_{50} values after 0 or 30 min of enzyme—inhibitor preincubation. The absence of a significant difference between IC_{50} with or without preincubation was considered as indicative of reversible inhibition.

Ex Vivo MAO-A and MAO-B Inhibition. C57Bl mice were treated with the test compound at different concentrations (0.5 to 20 mg/kg po and ip), and at different time intervals (0.5, 1, 2, 4, 8, 16, and 24 h) they were sacrificed. The brains were removed, and crude homogenates were prepared in 0.1 M phosphate buffer pH 7.40. The enzyme inhibition were performed with a radioenzymatic assay as described above.

In Vitro Human Recombinant Cytocrome P450 Isoform Assay. Inhibition of the six most important P450 isoforms (CYP1A2, CYP2C9, CYP2C19, CYP2D6, CYP2E1, and CYP3A4) was measured in specific assays using suitable substrates that become fluorescent upon CYP metabolism (Gentest Kit assay, BD Biosciences, Bedford, MA). Compounds were tested in a 96-well plate containing incubation/NADPH regenerating buffer. Specific human recombinant isoenzymes (supersomes) and substrates were added and incubated at 37 °C. The specific substrates were the following: 3-cyano-7-ethoxycoumarin (CYP2C19 and CYP1A2), 7-methoxy-4-trifluoromethylcoumarin (CYP2C9), 3-[2-(N,N-diethyl-N-methylamonium)ethyl]-7-methoxy-4-methylcoumarin (CYP2D6), 7,8-benzoquinoline (CYP3A4), 7-methoxy-4-phenylcoumarin (2E1). The plates were read on a Victo3vr plate reader (Perkin-Elmer, Wellesley, MA) at the appropriate emission/excitation wavelengths. Known inhibitors from literature for each isoenzyme were tested in every assay as positive control.

In Vitro Cell Viability Assay. The SHSY-5Y continuous cell line from a human neuroblastoma (Istituto Zooprofilattico, Brescia, Italy) was chosen from the present study. Cells, showing a neuronal-like morphology and a growth adherent to the plastic culture surface, were routinely maintained in Dulbecco's modified essential medium (DMEM) supplemented with 10% of heat inactivated FBS plus 1% nonessential amino acid, 2 mM glutamine, and 100 U/mL penicillin + 100 μg/mL streptomycin and were grown at 37 °C in an atmosphere of 95% air and 5% CO₂. Culture medium was replaced every 24 h. Growth constituents unless otherwise stated were purchased from Life Technologies. Cells, routinely split 1:5, were transplanted by trypsin–EDTA solution (0.05–0.02% in PBS) and plated according to experimental needing.

The experimental protocol assay was as follows: at time 0 cells were seeded at $6.25 \times 10^4/\text{cm}^2$ in 96-well cell culture plates in complete growth medium, and after 72 h at subconfluent phase, growth medium was removed and neurobasal medium (with 2 mM glutamine and 100 U/mL penicillin + 100 μ g/mL streptomycin, without serum) was added 30 min before the addition of compound 22b. The assay proceeded with a 24 h incubation at 37 °C in serumless neurobasal medium (200 μ L/well) with or without 22b at 1, 3, 10, 30, and 100 μ M. At the end of incubation, cell viability was assessed by a colorimetric assay by using the MTS ([3-(4,5-dimethylthiazol-2-yl)-5-(3-carboxymethoxyphenyl)-2-(4-sulfophenyl)-2*H*-tetrazolium, inner salt]) kit by Promega (Promega Corp., Madison, WI).

Data Elaboration and Statistical Analysis. Enzyme inhibition curves were obtained from at least seven different concentrations, each in duplicate (from 10^{-10} to 10^{-4} M), and the IC₅₀ values with confidence intervals were determined using nonlinear regression analysis (GraphPad Prism). Data were expressed as the mean \pm SEM and were analyzed by ANOVA followed by Dunnett's test. Generally, SEM values were lower than 15% of the calculated mean.

Acknowledgment. We thank Dr. Sophie Martel and Prof. Pierre-Alain Carrupt from the School of Pharmaceutical Sciences, University of Geneva—University of Lausanne,

Switzerland, for helpful advice on the HDM-PAMPA assay and Dr. Piero Melloni from Newron Pharmaceuticals, Bresso, Italy, for helpful discussions and support in the execution of the present work. The experimental determinations of pK_a and log P by Filomena Fiorella, Dipartimento Farmacochimico, University of Bari, Italy, and of the aqueous solubility by Jose Manuel Brea Floriani, Department of Pharmacology, University of Santiago de Compostela, Spain, are kindly acknowledged. The Spanish authors thank the Ministerio de Ciencia e Innovación and the European Regional Development Fund (Madrid, Spain, Grant SAF2007-66114) for financial support.

References

- (1) Strolin-Benedetti, M.; Tipton, K. F.; Whomsley, R. Amine Oxidases and Monooxygenases in the in Vivo Metabolism of Xenobiotic Amines in Humans: Has the Involvement of Amine Oxidases Been Neglected? Fundam. Clin. Pharmacol. 2007, 21, 467-479.
- Shih, J. C.; Chen, K.; Ridd, M. J. Monoamine Oxidase: From Genes to Behaviour. Annu. Rev. Neurosci. 1999, 22, 197–217.
- (3) Edmondson, D. E.; Mattevi, A.; Binda, C.; Li, M.; Hubalek, F. Structure and Mechanism of Monoamine Oxidases. Curr. Med. Chem. 2004, 11, 1983-1993.
- Edmondson, D. E.; Binda, C.; Wang, J.; Upadhyay, A. K.; Mattevi, A. Molecular and Mechanistic Properties of the Membrane-Bound Mitochondrial Monoamine Oxidases. Biochemistry **2009**, 26, 4220-4230.
- (5) Binda, C.; Newton-Vinson, P.; Hubalek, F.; Edmondson, D. E.; Mattevi, A. Structure of Human Monoamine Oxidase B, a Drug Target for a Treatment of Neurological Disorders. Nat. Struct. Biol. 2002, 9, 22-26.
- Binda, C.; Li, M.; Hubalek, F.; Restelli, N.; Edmondson, D. E.; Mattevi, A. Insights into the Mode of Inhibition of Human Mitochondrial Monoamine Oxidase B from High-Resolution Crystal Structures. Proc. Natl. Acad. Sci. U.S.A. 2003, 100, 9750–9755.
- (7) De Colibus, L.; Li, M.; Binda, C.; Lustig, A.; Edmondson, D. E.; Mattevi, A. Three-Dimensional Structure of Human Monoamine Oxidase A (MAO A): Relation to the Structures of Rat MAO A and Human MÀO B. Proc. Natl. Acad. Sci. U.S.A. 2005, 102, 12684-12689.
- (8) Ma, J.; Yoshimura, M.; Yamashita, E.; Nakagawa, A.; Ito, A.; Tsukihara, T. Structure of Rat Monoamine Oxidase A and Its Specific Recognitions for Substrates and Inhibitors. J. Mol. Biol. **2004**, 338, 103-114.
- (9) Grimsby, J.; lan, N. C.; Neve, R.; Chen, K.; Shih, J. C. Tissue Distribution of Human Monoamine Oxidase-A and Oxidase-B Messenger-RNA. J. Neurochem. 1990, 55, 1166-1169.
- (10) Fowler, C. J.; Ross, S. B. Selective Inhibitors of Monoamine Oxidase A and B: Biochemical, Pharmacological, and Clinical Properties. Med. Res. Rev. 1984, 4, 323-358.
- (11) Youdim, M. B.; Bakhle, Y. S. Monoamine Oxidase: Isoforms and Inhibitors in Parkinson's Disease and Depressive Illness. Br. J. Pharmacol. **2006**, 147, S287–S296.
- (12) Yamada, M.; Yasuhara, H. Clinical Pharmacology of MAO Inhibitors: Safety and Future. Neurotoxicology 2004, 25, 215–221.
- (13) Lewitt, P. A. MAO-B Inhibitor Know-How: Back to the Pharm. Neurology 2009, 72, 1352-1357
- (14) Youdim, M. B.; Edmondson, D. E.; Tipton, K. F. The Therapeutic Potential of Monoamine Oxidase Inhibitors. Nat. Rev. Neurosci. **2006**, 7, 295–309.
- (15) Haefely, W. E.; Burkard, W. P.; Cesura, A. M.; Kettler, R.; Lorez, H. P.; Martin, J. R.; Richards, J. G.; Scherschlicht, R.; DaPrada, M. Biochemistry and Pharmacology of Moclobemide, a Prototype RIMA. Psychopharmacology 1992, 106, 6–14.
- (16) Fernandez, H. H.; Chen, J. J. Monoamine Oxidase-B Inhibition in the Treatment of Parkinson's Disease. Pharmacotherapy 2007, 27,
- (17) Onofrj, M.; Bonanni, L.; Thomas, A. An Expert Opinion on Safinamide in Parkinson's Disease. Expert. Opin. Invest. Drugs **2008**, 17, 1115–1125.
- (18) Chen, J. J.; Swope, D. M.; Dashtipour, K. Comprehensive Review of Rasagiline, a Second-Generation Monoamine Oxidase Inhibitor, for the Treatment of Parkinson's Disease. Clin. Ther. 2007, 29, 1825-1849
- (19) Olanow, C. W.; Hauser, R. A.; Jankovic, J.; Langston, W.; Lang, A.; Poewe, W.; Tolosa, E.; Stocchi, F.; Melamed, E.; Eyal, E.; Rascol, O. A. Randomized, Double-Blind, Placebo-Controlled, Delayed Start Study To Assess Rasagiline as a Disease Modifying Therapy in Parkinson's Disease (the ADAGIO Study): Rationale,

- Design, and Baseline Characteristics. Movement Disord. 2008, 23,
- (20) Lee, K. C.; Chen, J. J. Transdermal Selegiline for the Treatment of Major Depressive Disorder. Neuropsychiatr. Dis. Treat. 2007, 3, 527–537.
- (21) Thorpe, L. W.; Westlund, K. N.; Kochensperger, L. M.; Abell, C. W.; Denney, R. M. Immunocytochemical Localization of Monoamine Oxidases A and B in Human Peripheral Tissues and Brain. J. Histochem. Cytochem. 1987, 35, 23–32.
- (22) Strolin Benedetti, M.; Dostert, P. Monoamine Oxidase, Brain Aging and Degenerative Diseases. Biochem. Pharmacol. 1989, 38,
- Saura, J.; Andres, N.; Andrade, C.; Ojuel, J.; Eriksson, K.; Mahy, N. Biphasic and Region-Specific MAO-B Response to Aging in Normal Human Brain. Neurobiol. Aging 1997, 18, 497–507
- (24) Fowler, C. J.; Wiberg, A.; Oreland, L.; Marcusson, J.; Winblad, B. The Effect of Age on the Activity and Molecular Properties of Human Brain Monoamine Oxidase. J. Neural Transm. 1980, 49, 1-20.
- (25) Kovacic, P. Oxidative Stress. Curr. Med. Chem. 2001, 8, 721–863.
 (26) Barnham, K. J.; Masters, C. L.; Bush, A. I. Neurodegenerative
- Diseases and Oxidative Stress. Nat. Rev. 2004, 3, 205-214.
- Halliwell, B. Oxidative Stress and Neurodegeneration: Where Are We Now? J. Neurochem. 2006, 97, 1634-1658.
- (28) Hermida-Ameijeiras, A.; Mendez-Alvarez, E.; Sanchez-Iglesias, S.; Sanmartin-Suarez, C.; Soto-Otero, R. Autoxidation and MAO-Mediated Metabolism of Dopamine as a Potential Cause of Oxidative Stress: Role of Ferrous and Ferric Ions. Neurochem. Int. 2004, 45, 103-116.
- (29) Riederer, P.; Danielczyk, W.; Grunblatt, E. Monoamine Oxidase-B Inhibition in Alzheimer's Disease. Neurotoxicology 2004, 25, 271–277.
- (30) Thomas, T. Monoamine Oxidase-B Inhibitors in the Treatment of Alzheimers Disease. Neurobiol. Aging 2000, 21, 343–348.
- (31) Ebadi, M.; Sharma, S.; Shavali, S.; El Refaey, H. Neuroprotective Actions of Selegiline. J. Neurosci. Res. 2002, 67, 285–289.
- Eliash, S.; Dror, V.; Cohen, S.; Rehavi, M. Neuroprotection by Rasagiline in Thiamine Deficient Rats. Brain Res. 2009, 1256, 138-
- (33) Sano, M.; Ernesto, C.; Thomas, R. G.; Klauber, M. R.; Schafer, K.; Grundman, M.; Woodbury, P.; Growdon, J.; Cotman, C. W.; Pfeiffer, E.; Schneider, L. S.; Thal, L. J. A Controlled Trial of Selegiline, Alpha-Tocopherol, or Both as Treatment for Alzheimer's Disease. N. Engl. J. Med. 1997, 336, 1216–1222.
 (34) Schneider, L. S.; Olin, J. T.; Pawluczyk, S. A Double-Blind Cross-
- over Pilot Study of l-Deprenyl (Selegiline) Combined with Cholinesterase Inhibitor in Alzheimer's Disease. Am. J. Psychiatry 1993, 150, 321–323
- (35) Tolbert, S. R.; Fuller, M. A. Selegiline in Treatment of Behavorial and Cognitive Symptoms in Alzheimer's Disease. Ann. Pharmacother. 1996, 30, 1122-1129.
- (36) Binda, C.; Hubalek, F.; Li, M.; Herzig, Y.; Sterling, J.; Edmondson, D. E.; Mattevi, A. Crystal Structures of MAO B in Complex with Four Inhibitors of the N-Propargylaminoindan Class. J. Med. Chem. 2004, 47, 1767-1774.
- (37) Son, S. Y.; Ma, J.; Kondou, Y.; Yoshimura, M.; Yamashita, E.; Tsukihara, T. Structure of Human Monoamine Oxidase A at 2.2-A Resolution: The Control of Opening the Entry for Substrates/ Inhibitors. Proc. Natl. Acad. Sci. U.S.A. 2008, 105, 5739-5744.
- (38) Novaroli, L.; Reist, M.; Favre, E.; Carotti, A.; Catto, M.; Carrupt, P. A. Human Recombinant Monoamine Oxidase B as Reliable and Efficient Enzyme Source for Inhibitor Screening. Bioorg. Med. Chem. 2005, 13, 6212-6217.
- (39) Bravo, J. Development and Validation of Target-Based Drug Design Tools: Virtual Screening of Monoamine Oxidase Inhibitors. Ph.D. Thesis, Faculté des Sciences, Université de Genève, Switzerland, April 2009.
- (40) Kneubuhler, S.; Carta, V.; Altomare, C.; Carotti, A.; Testa, B. Synthesis and Monoamine Oxidase Inhibitory Activity of 3-Substituted 5H-Indeno[1,2-c]pyridazines. Helv. Chim. Acta 1993, 76, 1954-1963.
- (41) Kneubuhler, S.; Thull, U.; Altomare, C.; Carta, V.; Gaillard, P.; Carrupt, P.-A.; Carotti, A.; Testa, B. Inhibition of Monoamine Oxidase-B by 5*H*-Indeno[1,2-*c*]pyridazines. Biological Activities, Quantitative Structure-Activity-Relationships (QSARs) and 3D-QSARs. J. Med. Chem. 1995, 38, 3874-3883.
- (42) Altomare, C.; Cellamare, S.; Summo, L.; Catto, M.; Carotti, A.; Thull, U.; Carrupt, P. A.; Testa, B.; Stockli-Evans, H. Inhibition of Monoamine Oxidase-B by Condensed Pyridazines and Pyrimidines; Effects of Lipophilicity and Structure-Activity Relationships. J. Med. Chem. 1998, 41, 3812-3820.
- (43) Thull, U.; Kneubuhler, S.; Gaillard, P.; Carrupt, P.-A.; Testa, B.; Altomare, C.; Carotti, A.; Jenner, P.; McNaught, K. S. P.

- Inhibition of Monamine Oxidase by Isoquinoline Derivatives: Qualitative and 3D-Quantitative Structure-Activity Relationships. Biochem. Pharmacol. 1995, 50, 869-877.
- (44) Carotti, A.; Carrieri, A.; Chimichi, S.; Boccalini, M.; Cosimelli, B.; Gnerre, C.; Carotti, A.; Carrupt, P. A.; Testa, B. Natural and Synthetic Geiparvarins Are Strong and Selective MAO-B Inhibitors. Synthesis and SAR Studies. Bioorg. Med. Chem. Lett. 2002, *12*, 3551–3555.
- (45) Gnerre, C.; Catto, M.; Leonetti, F.; Weber, P.; Carrupt, P.-A.; Altomare, C.; Carotti, A.; Testa, B. Inhibition of Monoamine Oxidases by Functionalized Coumarin Derivatives: Biological Activities, QSARs, and 3D-QSARs. J. Med. Chem. 2000, 43, 4747-4758.
- (46) Catto, M.; Nicolotti, O.; Leonetti, F.; Carotti, A.; Favia, A. D.; Soto-Otero, R.; Mendez-Alvarez, E.; Carotti, A. Structural Insights into Monoamine Oxidase Inhibitory Potency and Selectivity of 7-Substituted Coumarins from Ligand- and Target-Based Approaches. J. Med. Chem. 2006, 49, 4912-4925.
- (47) Bruhlmann, C.; Ooms, F.; Carrupt, P.-A.; Testa, B.; Catto, M.; Leonetti, F.; Altomare, C.; Carotti, A. Coumarin Derivatives as Dual Inhibitors of Acetylcholinesterase and Monoamine Oxidase. J. Med. Chem. 2001, 44, 3195–3198.
- (48) Carotti, A.; Melloni, P.; Thaler, F.; Caccia, C.; Maestroni, S.; Salvati, P. Substituted Aminoalkyl and Amidoalkyl Benzopyran Derivatives. WO 2006/102958 A1, 2006.
- Rendenbach-Muller, B.; Schlecker, R.; Traut, M.; Weifenbach, H. Synthesis of Coumarins as Subtype-Selective Inhibitors of Monoamine Oxidase. Bioorg. Med. Chem. Lett. 1994, 4, 1195-1198
- (50) Rendenbach, B.; Weifenbach, H.; Teschendorf, H. J. Arylalkoxycumarine. Verfahren zu Ihre Herstellung und Diese Enthalende Therapeutische Mittel. Patent DE 3834861 A1, 1990 (BASF AG).
- (51) Chimenti, F.; Secci, D.; Bolasco, A.; Chimenti, P.; Granese, A.; Befani, O.; Turini, P.; Alcaro, S.; Ortuso, F. Inhibition of Monoamine Oxidases by Coumarin-3-acyl Derivatives: Biological Activity and Computational Study. Bioorg. Med. Chem. Lett. 2004, 14, 3697–3703.
- Chimenti, F.; Secci, D.; Bolasco, A.; Chimenti, P.; Bizzarri, B.; Granese, A.; Carradori, S.; Yáñez, M.; Orallo, F.; Ortuso, F.; Alcaro, S. Synthesis, Molecular Modeling, and Selective Inhibitory Activity against Human Monoamine Oxidases of 3-Carboxamido-7-substituted Coumarins. J. Med. Chem. 2009, 52, 1935–1942.
- (53) Santana, L.; Gonzalez-Diaz, H.; Quezada, E.; Uriarte, E.; Yanez, M.; Vina, D.; Orallo, F. Quantitative Structure-Activity Relationship and Complex Network Approach to Monoamine Oxidase A and B Inhibitors. J. Med. Chem. 2008, 51, 6740-6751.
- (54) Carotti, A. MAOs Long March: From Toxic First-Generation Drugs to Isoform-Selective, Reversible and Multi-Target Inhibitors. Presented at the Meeting of ACS-EFMC, Frontiers in CNS and Oncology Medicinal Chemistry, Siena, Italy, October 7–9, 2007.
- (55) v. Pechmann, H. Novel Synthesis of Coumarins. Ber. Dtsch. Chem.
- Ges. **1884**, *17*, 929–936. (56) Binda, C.; Wang, J.; Pisani, L.; Caccia, C.; Carotti, A.; Salvati, P.; Edmondson, D. E.; Mattevi, A. Structures of Human Monoamine Oxidase B Complexes with Selective Noncovalent Inhibitors: Safinamide and Coumarin Analogs. *J. Med. Chem.* **2007**, *50*, 5848–5852. (57) Campos-Toimil, M.; Orallo, F.; Santana, L.; Uriarte, E. Synthesis
- and Vasorelaxant Activity of New Coumarin and Furocoumarin Derivatives. Bioorg. Med. Chem. Lett. 2002, 12, 783–786
- (58) Mitsunobu, O. The Use of Diethyl Azodicarboxylate and Triphenylphosphine in Synthesis and Transformation of Natural Products. Synthesis 1981, 1, 1–29. Vaultier, M.; Knouzi, N.; Carrie, R. Reduction d'Azides en Amines
- Primaires par une Methode Generale Utilisant la Reaction de Staudinger. Tetrahedron Lett. 1983, 24, 763–764.
- (60) Bartra, M.; Romea, P.; Urpi, F.; Villarasa, J. A Fast Procedure for the Reduction of Azides and Nitro Compounds Based on the Reducing Ability of Sn(SR)3-Species. Tetrahedron 1990, 46, 587-594
- (61) Campagna, F.; Carotti, A.; Casini, G. A Convenient Synthesis of Nitriles from Primary Amides under Mild Conditions. Tetrahedron Lett. **1977**, 21, 1813–1816.
- (62) Martel S.; Gasparik, V.; Carrupt P. A. In Silico Tools and in Vitro HTS Approaches To Determine Lipophilicity during the Drug Discovery Process. In Hit and Lead Profiling; Faller, B., Urban, L., Eds.; Wiley-VCH: Weinheim, Germany, 2009.
- (63) Lipinski, C. A.; Lombardo, F.; Dominy, B. W.; Feeney, P. J. Experimental and Computational Approaches To Estimate Solubility and Permeability in Drug Discovery and Development Settings. Adv. Drug Delivery Rev. 2001, 46, 3–26.

- (64) Fernández, F.; Caamaño, O.; Nieto, M. I.; López, C.; García-Mera, X.; Stefanachi, A.; Nicolotti, O.; Loza, M. I.; Brea, J.; Esteve, C.; Segarra, V.; Vidal, B.; Carotti, A. 1,3-Dialkyl-8-N-substituted Benzyloxycarbonylamino-9-deazaxanthines as Potent Adenosine Receptor Ligands: Design, Synthesis, Structure-Affinity and Structure-Selectivity Relationships. Bioorg. Med. Chem. 2009, 17, 3618-3629.
- (65) Wohnsland, F.; Faller, B. High-throughput Permeability pH Profile and High-Throughput Alkane/Water log P with ArtificialMembranes. J. Med. Chem. 2001, 44, 923-930.
- (66) Henchoz, Y.; Bard, B.; Guillarme, D.; Carrupt, P. A.; Veuthey, J. L.; Martel, S. Analytical Tools for Physicochemical Profiling of Drug Candidates To Predict Absorption/Distribution. Anal. Bioanal. Chem. 2009, 394, 707-729.
- (67) Caccia, C.; Maj, R.; Calabresi, M.; Maestroni, S.; Faravelli, L.; Curatolo, L.; Salvati, P.; Fariello, R. G. Safinamide: From Molecular Targets to a New Anti-Parkinson Drug. Neurology 2006, 67, S18-S23.
- (68) Robinson, D. S.; Lovenberg, W.; Keiser, H.; Sjoerdsma, A. Effects of Drugs on Human Blood Platelet and Plasma Amine Oxidase Activity in Vitro and in Vivo. Biochem. Pharmacol. 1968, 17, 109-119.
- (69) Malich, G.; Markovic, B.; Winder, C. The Sensitivity and Specificity of the MTS Tetrazolium Assay for Detecting the in Vitro Toxicity of 20 Chemicals Using Human Cell Lines. Toxicology **1997**, *124*, 179–192.
- (70) Guba, W.; Roche, O. Computational Filters in Lead Generation: Targeting Drug-like Molecules. In Chemogenomics in Drug Discovery: A Medicinal Chemistry Perspective; Kubinyi, H., Folkers, G., Eds.; Wiley-VCH: Weinheim, Germany, 2004; pp 325-340.
- (71) Pajouhesh, H.; Lenz, G. R. Medicinal Chemical Properties of Successful Central Nervous System Drugs. NeuroRx 2005, 2, 541-553.
- Carotti, A.; Altomare, C.; Catto, M.; Gnerre, C.; Summo, L.; De Marco, A.; Rose, S.; Jenner, P.; Testa, B. Lipophilicity Plays a Major Role in Modulating the Inhibition of Monoamine Oxidase B by 7-Substituted Coumarins. Chem. Biodiversity 2006, 3, 134–149.
- (73) Amadasi, A.; Surface, J. A.; Spyrakis, F.; Cozzini, P.; Mozzarelli, A.; Kellogg, G. E. Robust Classification of "Relevant" Water Molecules in Putative Protein Binding Sites. J. Med. Chem. 2008, 51, 1063-1067
- (74) Barillari, C.; Taylor, J.; Viner, R.; Essex, J. W. Classification of Water Molecules in Protein Binding Sites. J. Am. Chem. Soc. 2007, 129, 2577-2587
- (75) Lu, Y.; Wang, R.; Yang, C. Y.; Wang, S. Analysis of Ligand-Bound Water Molecules in High-Resolution Crystal Structures of Protein-Ligand Complexes. J. Chem. Inf. Model. 2007, 47, 668-675.
- Cavasotto, C. N.; Orry, A. J. W. Ligand Docking and Structure-Based Virtual Screening in Drug Discovery. Curr. Top. Med. Chem. **2007**, 7, 1006–1014.
- Roberts, B. C.; Mancera, R. L. Ligand-Protein Docking with Water Molecules. J. Chem. Inf. Model. 2008, 48, 397–408.
- (78) Huang, N.; Shoichet, B. K. Exploiting Ordered Waters in Molecular Docking. J. Med. Chem. 2008, 51, 4862-4865.
- (79) Goodford, P. J. A Computational Procedure for Determining Energetically Favorable Binding Sites on Biologically Important Macromolecules. *J. Med. Chem.* **1985**, *28*, 849–857.
- (80) Avdeef, A. Absorption and Drug Development: Solubility, Permeability, and Charge State; John Wiley & Sons: Hoboken, NJ, 2003.
- (81) Cruciani, G.; Crivori, P.; Carrupt, P. A.; Testa, B. Molecular Fields in Quantitative Structure-Permeation Relationships: The VolSurf Approach. J. Mol. Struct.: THEOCHEM **2000**, 503, 17–30.
- Crivori, P.; Cruciani, G.; Carrupt, P. A.; Testa, B. Predicting Blood-Brain Barrier Permeation from Three-Dimensional Molecular Structure. J. Med. Chem. 2000, 43, 2204-2216.
- (83) Baker, M.; Rayens, W. Partial Least Squares for Discrimination. J. Chemom. 2003, 17, 166–173.
- (84) Munoz-Torrero, D. Acetylcholinesterase Inhibitors as Disease-Modifying Therapies for Alzheimer's Disease. Curr. Med. Chem. **2008**, *15*, 2433–2455.
- Cavalli, A.; Bolognesi, M. L.; Melchiorre, C.; Minarini, A.; Rosini, M.; Recanatini, M. Multi-Target-Directed Ligands To Combat Neurodegenerative Diseases. *J. Med. Chem.* **2008**, *48*, 347–372. Kramer, S. D.; Gautier, J. C.; Saudemom, P. Considerations on the
- Potentiometric Log P Determination. Pharm. Res. 1998, 15, 1310-1313.
- Avdeef, A.; Box, K. J.; Comer, J. E.; Gilges, M.; Hadley, M.; Hibbert, C.; Patterson, W.; Tam, K. Y. J. pH-metric log P 11. p K_a determination of water-insoluble drugs in organic solvent-water mixtures. J. Pharm. Biomed. Anal. 1999, 20, 631-641.

Methodologies to Assess Drug Permeation Through the Blood-Brain Barrier for Pharmaceutical Research

Céline Passeleu-Le Bourdonnec • Pierre-Alain Carrupt • Jean Michel Scherrmann • Sophie Martel

Received: 14 December 2012 / Accepted: 11 June 2013 © Springer Science+Business Media New York 2013

ABSTRACT The drug discovery process for drugs that target the central nervous system suffers from a very high rate of failure due to the presence of the blood-brain barrier, which limits the entry of xenobiotics into the brain. To minimise drug failure at different stages of the drug development process, new methodologies have been developed to understand the absorption, distribution, metabolism, excretion and toxicity (ADMET) profile of drug candidates at early stages of drug development. Additionally, understanding the permeation of drug candidates is also important, particularly for drugs that target the central nervous system. During the first stages of the drug discovery process, in vitro methods that allow for the determination of permeability using high-throughput screening methods are advantageous. For example, performing the parallel artificial membrane permeability assay followed by cell-based models with interesting hits is a useful technique for identifying potential drugs. In silico models also provide interesting information but must be confirmed by in vitro models. Finally, in vivo models, such as in situ brain perfusion, should be studied to reduce a large number of drug candidates to a few lead compounds. This article reviews the different methodologies used in the drug discovery and drug development processes to determine the permeation of drug candidates through the blood-brain barrier.

C. Passeleu-Le Bourdonnec · P.-A. Carrupt · S. Martel School of Pharmaceutical Sciences, University of Geneva University of Lausanne, Quai Ernest Ansermet 30 1211 Geneva, Switzerland

J. M. Scherrmann Neuropsychopharmacologie des Addictions (CNRS UMR 8206, INSERM U705), Université de Paris Descartes Université Paris Diderot, Paris, France

S. Martel (🖾) Quai Ernest Ansermet 30, 1211 Geneva 4, Switzerland e-mail: sophie.martel@unige.ch

Published online: 26 June 2013

KEY WORDS blood—brain barrier · central nervous system · drug delivery systems · pharmacokinetics

ABBREVIATIONS

ADMET Absorption, distribution, metabolism, excretion and toxicity AJ Adherens junctions **AMT** Adsorptive-mediated transcytosis ATP Adenosine triphosphate BBB Blood-brain barrier **BCRP** Breast cancer resistance protein **CNS** Central nervous system **CSF** Cerebrospinal fluid **GLUT** Glucose transporter LAT Large aminoacid transporter LDL Low density lipoprotein **MRP** Multidrug resistance associated protein NCE New chemical entities OATP Organic anion transporter protein **PAMPA** Parallel artificial membrane permeability assay PEG Polyethylene glycol P-gp/ABCB1 P-glycoprotein PΚ **Pharmacokinetics**

PVDF Polyvinylidene fluoride
RMT Receptor-mediated transcytosis
TEER Transendothelial resistance

TJ Tight junctions
UWL Unstirred water layer

INTRODUCTION

The high attrition rate of drug candidates during all stages of the drug development process is a critical issue for both economic and treatment reasons. It has been shown that



the major factor leading to the attrition of new chemical entities (NCEs) during drug development does not necessarily result from a lack of drug activity but is rather a result of inadequate pharmacokinetic (PK) properties (1). Particularly for central nervous system (CNS) diseases, the lack of permeation through the BBB prevents the active compound from reaching its target. Because of the huge costs associated with bringing a drug to market, it is important to fully characterise the ADMET (absorption, distribution, metabolism, excretion, toxicity) profile of candidate drugs as early as possible during the drug discovery process. A thorough ADMET evaluation decreases the risk of attrition during clinical phases or even possible withdrawal from the market (2). ADMET issues are even more important for drug candidates that target the central nervous system (CNS). Only 3 to 5% of CNS drug candidates that enter phase I clinical trials are successfully launched compared to approximately 10% for all compounds (2,3). The particular organisation of endothelial cells, which are connected by tight junctions and form the blood-brain barrier (BBB), is a further obstacle to the CNS penetration of drug candidates. Combined with numerous transporters, such as efflux and uptake transporters, and drug-metabolising enzymes present at the luminal side of the BBB, penetration of the BBB is a treatment issue for CNS diseases, such as Alzheimer's disease, Parkinson's disease and Huntington's disease. By contrast, when other organs are targeted, it is critical that BBB penetration is either null or reduced to limit adverse effects. Therefore, determining the distribution of a drug in and around the brain is important when developing a new compound.

Different methodologies exist to evaluate the permeation potential of new chemical entities. The choice of strategy relies primarily on the type of throughput (driven by the number of compounds that require testing) and the type of information needed. This implies that scientists should master these strategies to choose the proper methodology based on the information required, and they should be able to correctly interpret the results. Here, we review the different methods available for physicochemists, biologists and ADMET scientists at different stages of the drug discovery and development processes to select drug candidates that penetrate the BBB. After describing the physiology of the blood-brain barrier, in silico, in vitro and in vivo approaches to determine BBB permeation will be explored. Drawbacks and advantages will be critically examined, and key experimental and/or interpretation points will be highlighted. Finally, because an increasing number of strategies to enhance drug penetration require complex formulations, such as micro/nano-carriers, application of these different screening methods to modern drug development efforts will be discussed.



PHYSIOLOGY OF THE BLOOD-BRAIN BARRIER (BBB)

In 1885, the studies of Paul Ehrlich first highlighted the presence of the BBB. In his studies, Ehrlich intravenously injected various dyes, and he observed that almost the entire body was stained but not the brain (4,5).

Edwin Goldman, a student of Ehrlich's, continued this research using the dye trypan blue. He found that after intravenous injection of the dye, the choroid plexus and meninges were stained; however, no dye was recovered in either the brain or cerebrospinal fluid (CSF) (6). In another experiment, he injected the dye directly into the CSF and found that the entire brain was stained but not the rest of the body (7). These experiments demonstrated the existence of a biological barrier between the brain and the rest of the systemic circulation, the blood–brain barrier.

Over many years of research, our knowledge of the BBB has increased, and scientists are now aware that the BBB is a structure with complex cellular organisation that separates the brain parenchyma from the systemic circulation. It is of key importance for the maintenance of brain homeostasis, which is essential for good neuronal and synaptic activities (8–12), and represents the main route by which compounds reach the CNS. Moreover, the BBB also acts as a metabolic barrier due to the presence of numerous enzymes (13,14), including peptidases, γ-glutamyl transpeptidase (γ-GT), alkaline phosphatase (ALP), nucleotidases, cytochromes P450 (CYP450) and monoamine oxidase (MAO). These enzymes can either metabolise potentially harmful drugs to inactive CNS compounds, convert an inactive drug to its active CNS metabolite or degrade them into metabolites or substrates of specific efflux transporters, such as the P-glycoprotein or multidrug resistance proteins.

The BBB consists of brain capillaries that support endothelial cells and are surrounded by astrocytic end-foot processes (15). It is the central part of the neurovascular unit, which is responsible for communication between endothelial cells, astrocytes, pericytes and neurons (14).

Endothelial Cells and Tight Junctions

The specificity of the endothelial cells comprising the blood-brain barrier compared to the endothelial cells in the rest of the body is based on their organisation. Cerebral endothelial cells are connected by intercellular proteins. Occludins, claudins and junctional adhesion molecules, together with cytoplasmic accessory proteins, including zonula occludens-1 (ZO-1), ZO-2, ZO-3 and others, are transmembrane proteins that are responsible for the formation of tight junctions (TJs) (14) that seal the paracellular pathway (16–18) and make the brain nearly inaccessible to polar compounds that are not the substrates of specific transporters (19). Adherens

junctions (AJs) also contribute to the junction complex by joining the membrane proteins, cadherins, to the intermediary proteins, catenins, to form adhesive linkages between endothelial cells (20). The TJs in cerebral capillaries are approximately 50 to 100 times tighter than the TIs in peripheral capillaries (21) and lead to a high transendothelial electrical resistance (TEER) of approximately 1,500-2,000 Ω.cm² compared to $3-33\Omega$.cm² for other tissues (22,23), which is due to the restriction of small ions, such as Na⁺ and Cl⁻, from passing through the TJs. Moreover, BBB endothelial cells differ from other endothelial cells in the low number of endocytotic invaginations at the luminal portion of the cell membrane, which leads to very limited pinocytic transcellular transport (12,20,24–28), a large number of mitochondria (29) and the polarised expression of transporters and receptors for active transport (30). Indeed, the brain endothelium has only 3-6 pinocytic vesicles per µm³ compared to 82–93 per µm³ for the peripheral endothelium (31,32).

Many transmembrane proteins are expressed on the luminal and abluminal membranes of the endothelium to transport nutrients that are essential for the brain and to eliminate waste products of metabolism. In particular, proteins, such as GLUT-1 (glucose transporters), transport polar nutrients; Na-ATPase and K-ATPase transport sodium and potassium ions respectively; insulin or transferrin receptors transport proteins (8,24,28,33,34), and organic anion transporting proteins (OATP) (35) transport hormones, opioids, steroids, statins, cardiac glycosides, anticancer drugs and antibiotics (15). These transporters all play important roles in the maintenance of cerebral equilibrium. Moreover, efflux transporters, such as P-gp/ABCB1(36) or BCRP (37) are highly expressed on the luminal side of endothelial cells.

Astrocytes, Pericytes and Basal Lamina

Astrocytes are important cellular constituents of the neurovascular unit. They are linked to interneurons and thus the entire cerebral microenvironment (19). Astrocytes represent approximately 50% of the total mammalian brain volume (38). Moreover, some studies indicate that astrocytes play a role in the upregulation of BBB properties, such as tighter tight junctions (39,40) and the expression of specific polarised transporters, such as P-gp/ABCB1(14) and the enzymatic system (14,19), due to astrocyte-endothelial cell interactions. This upregulation of BBB properties by astrocytes is synergistic with pericytes, neurons and perivascular macrophages (41). Astrocytes also have different functions, such as the formation of and activity at synapses, energetic and redox metabolism, intercellular communication, homeostasis (38) and glucose transport from the systemic circulation to the brain.

Similar to astrocytes and neurons, pericytes are part of the neurovascular unit and play a role in the maintenance of both BBB properties and cerebral homeostasis. Recent studies have also indicated a role for pericytes in haemostasis, as well as in immune and phagocytic processes (20,42). Pericytes surround endothelial cells and both cell types are supported by the basal lamina. The integrity of basal lamina allows the maintenance of BBB properties, due to its anchoring role, but the basal lamina does not have a significant impact on the permeability of the BBB. However, under specific pathological conditions or in response to an aggressive stimulus, its thickness can vary, which perturbs the normal function of the BBB (42).

MECHANISMS OF TRANSPORT THROUGH THE BBB

The BBB is one of the most important barriers in the body. The permeation of drugs through the BBB is subject to strong selection depending on the physicochemical properties of the compound, such as lipophilicity, molecular weight, permeability coefficient (logP_e), molecular volume, ionisation state, and/or their affinity to specific transporters(efflux or uptake transporters) that are present in the cellular space (43–45). Therefore, the BBB may not be as impermeable as indicated by the first experiments with dyes. The cellular organisation of the BBB and the presence of transmembrane proteins enable a selective regulation of the passage of molecules from the blood to the brain. This is of particular importance for the uptake of essential nutrients or active CNS drugs and protects the brain from undesirable compounds, which could be toxic to the CNS.

The specificities of brain capillaries makes of the BBB an effective and efficient barrier that limits the entry of xenobiotics into the brain. Molecules present in the blood stream can reach the CNS by two different pathways, the paracellular pathway, which is between 2 endothelial cells through the tight junctions, or the transcellular pathway, which is through an endothelial cell.

Molecules that reach the CNS via the transcellular pathway can diffuse passively, can be actively transported by specific transporters or can undergo endocytosis. For example, small lipophilic molecules, such as O_2 and CO_2 , or very small compounds, such as ethanol, water or diverse lipophilic drugs, can freely diffuse through the lipid barriers of endothelial cells (19).

Paracellular Pathway

The paracellular pathway is a diffusion process that occurs between 2 cells. This pathway is limited to small hydrophilic molecules such as cimetidine, ranitidine, famotidine (46,47) and furosemide (48), which are hypothesised to be absorbed *via* the paracellular pathway in the intestinal track, due to the



aqueous surroundings of the cells (49). However, due to the presence of tight-junctions between two cerebral endothelial cells, this route is extremely limited and nearly non-existent at the BBB, although under some pathological conditions, tight junctions and adherens junctions between endothelial cells may be altered. This alteration enables leakage, which can allow passage of plasma proteins, fluids or immune cells into the brain (12,19,50–55). The selectivity of this route is limited to either size or shape features.

Transcellular Pathway

Complex tight junctions force therapeutic molecules to follow a transcellular pathway through the BBB rather than the paracellular pathway as in most endothelia (19).

Passive Diffusion at the BBB

Passive diffusion is one of the most straightforward mechanisms of permeation. This process requires a concentration gradient but no energy and no specific protein carriers. Diffusion requires physicochemical interactions between the compound and the membrane that must be crossed (43,44). Moreover, because there is no specific binding site, passive transport is not affected by stereochemistry and there is no saturation and no possible inhibition of the diffusion process (56). These observations indicate that passive diffusion is concentration-independent: the process occurs till equilibrium between the blood and the brain.

Passive diffusion through the BBB is highly affected by lipophilicity and the size of the compound (57–59). It was demonstrated that compounds with a molecular weight greater than 500–600 Da poorly permeated the BBB (60,61). However, when combined with good lipid solubility, molecules with molecular weights greater than 500 Da have interesting BBB permeability characteristics (62). Similarly, the lipophilicity of compounds should be high enough to allow for good affinity with lipidic membranes, but the lipophilicity should not be too high so as to avoid trapping of the compound in the membrane and bioaccumulation. By contrast, due to the hydrophobic nature of the membrane, ionisation will greatly impact diffusion because ionised compounds are highly hydrophilic and therefore have poor interactions with the membrane (63).

Carrier-Mediated Transport at the BBB

A certain number of uptake or efflux proteins are expressed at the BBB. These transporters are present on the luminal and abluminal membranes of the endothelium and regulate the entry of their specific substrates (19,64). Uptake proteins transport molecules from the blood to the brain. These transport systems allow the permeation of essential cerebral

nutrients, such as glucose or amino acids, and either limit or prevent the passage of undesired or potentially toxic molecules. By contrast, efflux proteins, such as P-glycoproteins (P-gp/ABCB1), multidrug-resistance multidrug resistance associated proteins (MRP) or the breast cancer resistant protein (BCRP) (65), excrete their substrates out of the brain by pumping the substrates into the blood stream. At the BBB, P-gp/ABCB1 are highly expressed and a certain number of NCEs are substrates for this protein (56).

Carrier-Mediated Uptake. Carrier-mediated transport can be either active or facilitated. When the transport of a substrate needs either direct energy which requires ATP binding and hydrolysis to mediate the primary active transport process, such as transporters of the ABC superfamily, or indirect energy, which is driven by ion gradients that result from ATP-dependent primary transport, such as many transporters of the SCL superfamily, it is active carrier-mediated transport, whereas when transport requires only a concentration gradient and a transporter protein, it is facilitated carrier-mediated transport. Both types of transport are saturable, competitive and stereospecific (56). Moreover, these types of transport imply a specific interaction between the carrier proteins and the substrate.

Some examples of transporters are the glucose transporter (GLUT-1), the monocarboxylic acid transporter (MCT1), the large neutral amino-acid transporter (LAT1) and the organic anion transporters (OATP) (32,66). Specific transporters are also present for small ions, such as Na⁺, K⁺ or Cl⁻, in both the blood to brain and brain to blood directions. These ion transporters maintain brain homeostasis because ionic disequilibrium between the blood and brain can have serious effects, such as brain oedema.

Efflux Transport. Efflux transport is an energy-dependant, active process, which pumps xenobiotics and metabolites out of the brain into the blood stream. The most well-known and studied efflux proteins belong to the ATP binding cassette (ABC) family, including the P-glycoproteins (P-gp/ABCB1), which are encoded by the multidrug resistance gene 1 (MDR1/ABCB1), the multidrug resistance associated protein (MRP) and the breast cancer resistance proteins (BCRP). These active transport processes are essential for brain protection because they prevent the cerebral penetration of potentially harmful drugs and also excrete waste products and metabolites. The expression of most efflux proteins is regulated by astrocytes or pericytes (67).

Trans- and Endocytosis Mechanisms

Brain penetration is not strictly limited to small lipophilic molecules or compounds shuttled by uptake proteins. Larger



molecules, such as peptides, proteins or even viruses, which are too large for a carrier-mediated process, can also penetrate the BBB via the few pinocytic vesicles that are present in endothelial cells. These large molecules can be transported either by receptor-mediated transcytosis (RMT), adsorptive-mediated transcytosis (AMT) (10) or fluid phase endocytosis (32).

During RMT, the ligand specifically binds to the receptor protein and is transported through the cell. The best characterised and utilised RMT protein is most likely the transferrin receptor, which has also been extensively studied for the delivery of immunoliposomes. Other well-known receptors include the low-density lipoprotein (LDL) receptor and the insulin receptor (32).

During AMT, a non-specific interaction occurs between the solute and the surface protein. Peptides, glycopeptides, glycoproteins, and viruses are transported by this pathway (32).

During a fluid phase endocytosis event, there is no contact between the solute and the protein. The substrate is situated close to the membrane, which deforms and encircles both the solute and some extracellular fluid and transports the entire vesicle to the abluminal side. Lucifer yellow is transported in this manner (32).

STRATEGIES FOR IMPROVING BRAIN PENETRATION

The BBB is a serious obstacle for the treatment of neurode-generative diseases that require CNS action (43). Because of its physical organisation, the BBB prevents the passage of many drugs that target the CNS. Therefore, even if a potential drug has potent activity against its target, it may not be able to cross the BBB and will most likely be discarded during the drug development process. Moreover, metabolic features of the BBB may also prevent a CNS active drug from crossing the endothelial membrane because the therapeutic efficacy of the drug can be either inactivated or decreased by enzymes at the BBB. To circumvent the BBB and allow an active CNS compound to reach its target, many strategies exist, which may be either invasive or non-invasive with respect to the BBB.

Invasive Techniques

Direct Injection into the Cerebrospinal Fluid

Direct injection of drugs into the cerebrospinal fluid was the first strategy used to circumvent the BBB, primarily to target brain tumours. This technique is not very efficient because there is a poor diffusion between the cerebrospinal fluid and the brain and it is quite invasive (68). Nau *et al.* demonstrated a 3-fold increase in the mortality of infants with Gram-

negative meningitis treated with an intraventricular injection of aminoglycosides combined with intravenous injections of antibiotics compared to intravenous injection of antibiotics alone (68).

Therapeutic Opening of the BBB

Therapeutic opening of the BBB is a reversible process. Because of specific molecules which generate a hyperosmolar environment, the BBB loses its barrier properties, thus enabling passage of the therapeutics into the brain before the BBB regains its functions. A transient brain opening is generally obtained by intra-carotid injection of mannitol or alkyl glycerol, which creates hyperosmolar conditions on the systemic circulation side of the BBB and causes a reversible shrinkage of the endothelial cells and a loss of adherens and junctional proteins, leading to a paracellular opening between endothelial cells (69,70). However, depending on the mediator used to momentarily disrupt the BBB, an increase in transcellular permeability can also occur, such as with tumour necrosis factor α , which leads to the permeation of opportunistic toxic compounds. Moreover, the duration of the opening of the BBB will depend on the mediator used. Histamine provides a rapid and temporary opening, whereas thrombin causes drastic modifications of the endothelial cytoskeleton resulting in prolonged opening of the BBB with difficulties in returning to the basal state (51).

This difficult strategy must be handled with care and vigilantly monitored to prevent damage to the brain parenchyma and oedema, which may be fatal. However, when performed properly, therapeutic opening of the BBB allows for the delivery of active drugs into the CNS, which would not otherwise reach the brain. This strategy is primarily used for the treatment of brain tumours or life-threatening diseases that have not been cured with less invasive treatments.

Non-Invasive Techniques

Brain penetration can be improved either using an alternative administration route, inhibiting efflux transporters, chemically modifying or encapsulating the active compound.

The Nose-to-Brain Route

To circumvent the BBB and enter the brain parenchyma, alternative strategies for drug delivery, such as the nose-to-brain route, are useful. In the nose-to-brain pathway, the therapeutic compound can be directly transported to the brain by absorption in the nasal mucosa and transport *via* the olfactory routes (71,72). Therefore, localisation of the olfactory route close to a brain region that is exempt of BBB allows for the circumvention of the barrier, which allows the



drug to reach the CNS (73). This route has been evaluated for the permeation of cocaine (74), as well as formulations such as the alprazolam-loaded solid lipid nanoparticles (75) or even neuropeptides (76). This strategy suffers primarily from poor bioavailability, which ranges from 0.01% to 0.1% (72).

Inhibition of Efflux Transporters

The presence of numerous efflux transporters at the BBB prevents the entry of many CNS active compounds into the brain. In HIV treatment, the most efficient drugs, such as abacavir and efavirenz, are substrates of the ABC transporters. Therefore, an interesting strategy is to inhibit efflux transporter activity and saturate these transporters with substrates that have higher affinity than the drug (77). This strategy is efficient in HIV multi-therapy and improves the intracerebral concentration of HIV protease inhibitors (33). However, this strategy may have several drawbacks because inhibition of efflux transporters will allow the penetration of other xenobiotics, which may be potentially toxic in the CNS. Therefore, adverse side effects may occur using this strategy.

Use of Prodrugs

Pharmacology-based strategies are methods to either enhance the lipophilicity of a drug candidate to favour its passive permeation (78) or to mask the specific site recognised by efflux transporters. The primary goal of this strategy is to promote the permeation of compounds that have either low uptake or are substrates of efflux transporters in their native form. The addition of moieties to the drug, which are linked by covalent reversible bonds, allows for the physicochemical modification of the active compounds to cross the BBB. For example, dopamine, a treatment for Parkinson's disease, cannot cross the BBB and enter the central nervous system where its target is located. Therefore, carbonylation of dopamine allows for the active transport of the inactive prodrug form through the BBB. After the prodrug has entered the brain, DOPA decarboxylase activates L-Dopa into active dopamine. This strategy also permits the creation of a drug-reservoir, depending on the rate of liberation of the native active compound. This approach is, therefore, an asset for patient compliance. However, chemical modification of the native active drug may decrease its activity or bioavailability.

The Trojan Horses or the BBB Shuttles

The concept of a Trojan horse consists of coupling the drug of interest, which cannot penetrate the BBB, to a compound, such as a molecule, peptide, or transferrin, that crosses the BBB *via* an active process uptake transporter, such as the

glucose transporter (GLUT-1) or transferrin receptor. The BBB-penetrating moiety is recognised by the specific receptor, leading to transport of the entire molecule, including the drug (78). An extension of this concept was proposed by Malakoutikhah and co-workers (79) who designed peptidic Trojan horses that were able to cross the BBB *via* passive diffusion. These compounds were defined as BBB shuttles. The challenge of both Trojan horses and BBB shuttles is to then liberate the active drug from the vector.

Drug Delivery with Nanocarriers

Liposomes, polymeric nanoparticles, solid lipid nanoparticles and micelles are all nanocarriers and have garnered great interest in recent pharmaceutical research. Because of the incorporation of a drug into the inside core of the nanocarrier, the drug bioavailability, physicochemistry and pharmacokinetics of the drug are changed (80,81). In pharmaceutical research, a well-known problem is the discovery and development of highly potent lead compounds, which are then found to be either insoluble or poorly soluble. In most cases, either the molecule will be discarded from the drug development process, or a ligand strategy will be used to enhance the solubility of the potential drug, with the risk of decreasing its potency.

Drug delivery is a method of bypassing poor solubility, poor permeability or poor bioavailability by incorporating the compound of interest into either phospholipidic, polymeric or inorganic vesicles (82).

Liposomes consist of a phospholipid bilayer; therefore, they allow for the incorporation of either hydrophilic molecules, on the inside core, or lipophilic molecules, inside the bilayer (82). These liposomes are extensively studied and highly promising nanocarriers, particularly for cancer therapy. Caelyx®, a pegylated liposomal formulation of doxorubicin that targets breast cancer cells, is a good representative of the success of these formulations (83,84).

Three generations of liposomes have now been developed. The first generation consists only of a vesicle formed by a phospholipid bilayer. These types of liposomes are rapidly recognised by the reticuloendothelial system and eliminated. Therefore, their efficacy is very limited and not applicable for pharmaceutical purposes. The second generation of liposomes is surrounded by polyethylene glycol, which is covalently linked to the outer part of the vesicle. These pegylated liposomes have a longer circulation time in the body because PEG is not recognised as a foreign body by the immune system. The third generation of liposomes is the most potent generation of liposomes. These liposomes consist of the same pegylated liposomes as the second-generation liposomes but are functionalised with specific moieties, such as monoclonal antibodies, added to the PEG chain. Therefore, the modified liposome is recognised by the



antibody-specific receptor and may be taken up by the cell. This strategy allows for specific targeting of cells. For example, immunoliposomes, grafted with OX26 monoclonal antibody are able to recognize transferrin receptor at the BBB, which transport it through the a rat BBB model *via* endocytosis (85). Up to now, many immune-conjugated nanocarriers are on clinical phases such as doxorubicin, anti-REH-2 (86), but none has launched the market yet. Future years will probably disclose numerous new formulations aiming at treating CNS pathologies.

The major drawback of liposomes is their poor stability, which is due to their tendency to aggregate and their sensitivity to oxidation and hydrolysis. Some of these problems can be reduced by formulation strategies, such as the addition of α -tocopherol to decrease oxidation (87). Other researchers have formulated liposomes as proliposomes, a dry granular product, which disperses to form multi-lamellar vesicles upon the addition of water (88).

Nanoparticles as drug carriers have also been extensively studied recently. Their uptake into the brain is hypothesised to occur via receptor-mediated endocytosis (89,90). Because unmodified nanoparticles have been shown to be rapidly cleared by the reticuloendothelial system, within 5 min in a mouse model, surfactants or covalent binding of polyethylene glycol on the polymeric core led to a prolonged circulation time and improved bioavailability (91). Only a few nanoparticle formulations of drugs are currently on the market (92), such as Rapamune®, an immunosuppressant drug. Promising results have been obtained in preclinical studies of a glioblastoma rat model, using doxorubicin-incorporated nanoparticles; however, no CNS-targeting nanoparticles are currently available in the market. Nanoparticles can either be polymeric, lipidic or inorganic. The safety profile of these vesicles is controversial, and much research is necessary to fully describe the mode of excretion, the possible accumulation of particles in organs and the side effects caused by these nanoparticles.

METHODS TO ASSESS BBB PERMEABILITY INFORMATION IN DRUG RESEARCH

In Silico Models That Predict BBB Permeability

In silico models are used during the early stages of the drug discovery process when thousands of compounds must be screened for either interactions with a specific target or for the appropriate physicochemical properties. For example, Lombardo *et al.* (93) succeeded in predicting the blood–brain partitioning of compounds (log BB) using the calculated solvation free energy. Others correlated log BB with a combination of the molar refraction, solute polarisability,

hydrogen bond donor or acceptor capacity and molecular volume (94,95). *In silico* strategies can filter large databases to preselect compounds of interest and can predict whether a compound will be prone to BBB penetration or not (96). These computational strategies can decrease the number of molecules to only few hit compounds, which are then tested with *in vitro* models to determine the pharmacokinetics and mechanism of action of the drug.

In silico models combine the measured brain penetration information that is available in the literature with molecular properties to build an algorithm that can predict BBB permeability. Using partial least squares regression, multiple regression analysis or neural networks, in silico models can generate ponderated regressions consisting of different physicochemical properties, such as the lipophilicity (log P), standard free energy, H-bond donating capacity, H-bond accepting capacity, and molecular weight of the drug.

In practice, the initial data, which are obtained from libraries, are divided into 2 subtest sets, a training set, which is used to build the algorithm, and a test set, which allows for determination of the predictive ability of the algorithm. The experimental permeabilities of the test set are statistically compared to the predicted values that are generated by the algorithm to determine this predictive power (96). The variety of algorithms that are able to build a predictive model is huge because many descriptors may be used to generate an equation. Some examples of in silico models to predict log BB are listed in a review of Abraham (96). In general, the chosen descriptors are related to the size of the molecules and their physicochemical properties. As Abraham noted, an increase in size-related descriptors leads to an increased log BB (higher brain penetration), whereas an increase in the polarity-related descriptors leads to a decreased log BB. This characteristic is linked to the physicochemistry of both compartments, with the brain being more lipophilic than the blood. Moreover, Didziapetris et al. (97) suggested that acids with a pKa>4, containing greater than 8 oxygen and nitrogen atoms and a molecular weight greater than 400 Da were likely to be substrates of efflux proteins.

A major issue resulting from *in silico* models is the reliability of the chosen training sets and test sets. It is difficult to obtain experimental data that are homogeneous in terms of the experimental design, such as whether the perfusion was performed with whole blood, plasma or saline solutions, the reliability of descriptors, such as whether there was ionisation, and the experimental know-how. The ideal situation would be to obtain the experimental data from the same laboratory, under the same conditions; however, that situation is utopic because the amount of data would be either too low to build the model or not diverse enough. Therefore, attention should be paid when handling *in silico*-predicted data, and the user must also understand how the model was built.



In Vitro Models for Prediction of BBB Permeability

Different approaches have been proposed for the *in vitro* evaluation of whether a new chemical entity can cross the BBB. Significant differences exist from one method to another in terms of complexity and, consequently, cost and information obtained (Fig. 1). In this section, *in vitro* methods for predicting BBB permeability are ordered according to increasing complexity.

Immobilised Artificial Membrane

Lipophilicity (log P or log Poctanol/water) has long been reported to be a major parameter that influences CNS activity and the blood/brain concentration ratio (log BB) (98,99). Because of its lipophilic feature, n-octanol was widely used for pharmacokinetic predictions. The small polar head of n-octanol and its hydrophobic carbonylated chain make it appear similar to phospholipidic membranes. However, the relationship between log P and log BB is not strong enough for the needs of CNS researchers. Therefore, immobilised artificial membranes (IAMs) were proposed as an alternative to log P predicted with shake flask or liquid chromatography (100-103). Modified HPLC columns were prepared in which phospholipids were covalently bound to the silica (99). Experiments showed a linear relationship between the retention factors on IAMs and the partition between an aqueous phase and liposomes (104). Moreover, IAM chromatographic retention factors were shown to generate information on membrane permeability (105). In some cases, these types of systems have shown reasonable results for permeability prediction, even if the retention time on the column does not reflect transport across the membrane (106,107). However, there are some limitations in terms of retention times for lipophilic compounds and stationary phase stability. Recently, short IAM columns appeared on the market. These columns (1–3 cm *versus* 10–12 cm) allow greater throughput but do not really offer any improvements in terms of reliability, and this approach is not widely used in drug discovery.

PAMPA Models

The parallel artificial membrane permeability assay (PAMPA) is a relatively recent technique developed in 1998 by Kansy et al. (108) to rapidly predict passive permeability through the gastrointestinal tract with high throughput efficiency. In this technique, a donor and an acceptor compartments are separated by a filter supporting a liquid artificial membrane. The drug to be tested, placed in the donor compartment, can then permeate between the donor and the acceptor compartments through the artificial membrane. The assay is performed in 96-well plates and thus enables high throughput screening. The permeability coefficient is then determined in a

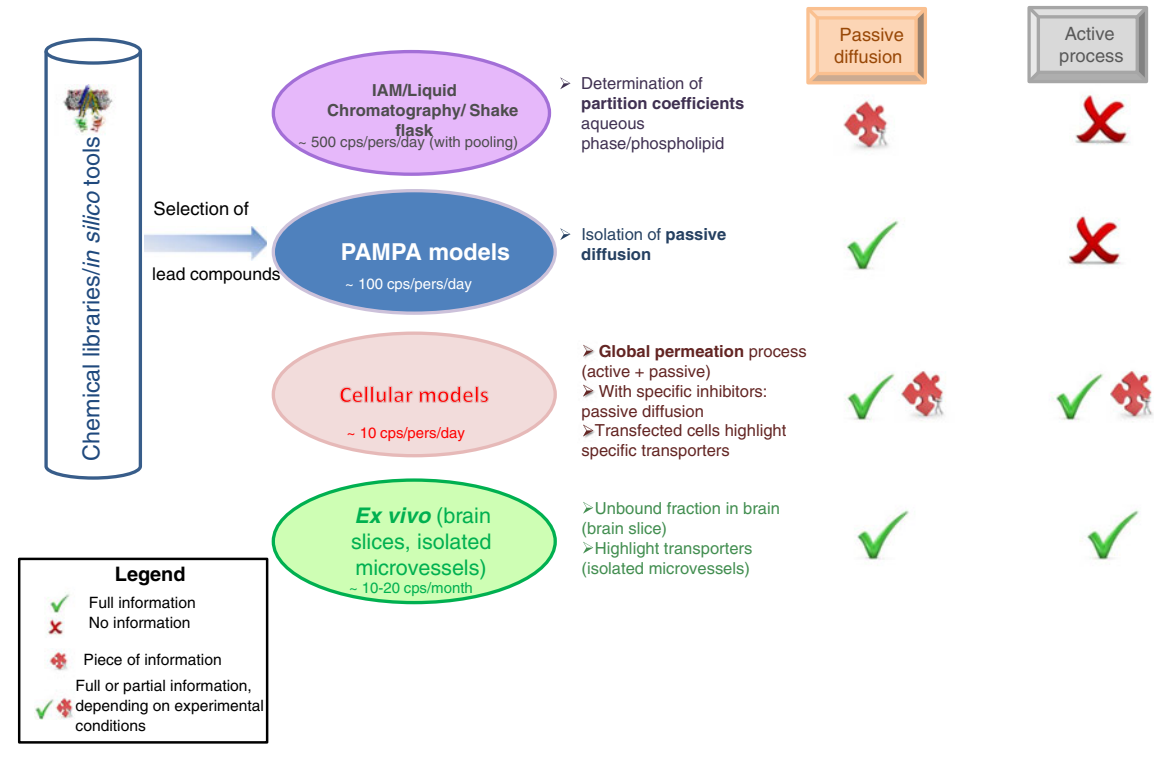


Fig. 1 Useful in vitro models to predict BBB permeability in early drug discovery process, and type of information generated.



straightforward manner with the permeability equation described by Avdeef (63). The artificial membrane that was originally made of phospholipids (56,109) can also be as simple as an organic solvent (110) or a mixture of solvents (111).

PAMPA is gaining interest in the early drug discovery process because it is possible to rapidly obtain the straightforward permeabilities of numerous compounds, it is cost efficient, it has high inter- and intra-laboratory reproducibility and it can target different biological membranes. The major drawback of the PAMPA technique is that it can only predict passive diffusion and is therefore unable to generate a full description of the permeability process at the BBB. It is wellknown that numerous transporters and enzymes are expressed at the BBB level, greatly modifying the pharmacokinetics of the substrates of these transporters, such as verapamil, a Pgp/ABAB1 substrate. Therefore, for these specific compounds, PAMPA generates only a portion of the information regarding passive transcellular transport. PAMPA should not be used for compound selection purposes particularly for BBB penetration, because of the numerous transporters and metabolic enzymes that are present at the BBB. P-gp/ABCB1 substrates more permeate in a PAMPA model compared to in vivo or in vitro cellular models.

Phospholipid-Based Membrane. Developed in 2003 by Li Di et al. (112), PAMPA-BBB has shown good prediction of BBB penetration for CNS classes of drugs. The drugs are described as CNS+ for compounds that have a high penetration through the BBB, CNS- for compounds that have a low permeability or are unable to penetrate the BBB, and CNS+/- for compounds with a medium permeability coefficient. In this assay, the artificial membrane is composed of porcine polar brain lipid extracts and the incubation last for 18 h. A quantitative analysis correlating the permeability coefficients generated with PAMPA-BBB and in situ brain perfusion gave a poor correlation coefficient of $r^2 = 0.47$ (113,114) for a test set of 37 compounds. However, for 30 test compounds, this assay succeeded in predicting 25 compounds with the correct class of permeability, either CNS+ or CNS-. The only negative outlier was actively transported, whereas the 4 false positives were either substrates of efflux pumps or metabolised in vivo. One weak point of this assay is that it is performed under unstirred conditions, which maximises the unstirred water layer (UWL). UWL is a stagnant water layer at the two sides of the artificial membrane that has a distinct boundary with bulk water (63). This layer can highly modify the permeation of compounds, in particular hydrophobic compounds, because passage through the UWL is governed by diffusion laws. Because of the blood flow and the very small size of the cerebral capillary, the in vivo UWL is nearly null. However, this is not the case for the *in vitro* UWL, particularly for the unstirred in vitro assay in which the UWL can be as thick as 1.5 to 2.5 mm (115).

Solvent-Based PAMPA. HDC-NPOE PAMPA is a high throughput screening method that has recently been developed to predict the passive transendothelial permeability through the BBB and is currently under study (116). The innovation of this PAMPA technique is in the use of nonbiological materials for the membrane, which allows for better reproducibility. In this new PAMPA model, the artificial membrane is composed of 75% hexadecane and 25% o-nitrophenyl octyl ether and incubation lasts for 7 h, enabling permeability determination within the working day. The experimental permeabilities determined by this new method demonstrated a good relationship with the permeabilities generated by a well-established cellular model BBCEC model from Cecchelli et al. (27,117) $(r^2=0.92)$: $\mathcal{N}=13$) and the PAMPA-BBB (112) ($r^2=0.80$: $\mathcal{N}=14$). Furthermore, a correlation was also established with an in vivo model of rat brain perfusion (118) ($r^2 = 0.81$; $\mathcal{N} = 6$) but only with a reduced number of compounds.

Compatibility of PAMPA with New Drug Delivery Strategies. In 2009, Han et al. (109) used PAMPA to determine the intestinal permeation of ginsenoside, a hydrophilic molecule with very low membrane permeation, that was incorporated into a water-in-oil microemulsion. The objective was to obtain information on the mechanism of permeability of this carrier system. The original protocol of Kansy (108) using a phospholipidic-based membrane was used. Han et al. demonstrated an increased permeation of ginsenoside due to good permeation of the water-in-oil microemulsion through the PAMPA membrane. These results were corroborated by rat everted intestinal sac studies.

In 2007, Mathot et al. (119) used the phospholipidic PAMPA developed by Kansy (120) and commercialised by pION Inc. to evaluate the passive diffusion of polymeric micelles formed from polymeric surfactants through the gastrointestinal tract. They had already shown in the Caco-2 model that the polymers were able to cross the cells but did not know the possible mechanism of passage. Analysis of the acceptor compartment demonstrated the passage of the polymeric micelles through the lipid artificial membrane with a permeability coefficient of 1.0×10^{-6} cm.s⁻¹. To the best of our knowledge, no current study has evaluated the prediction of BBB permeation of these materials using the solvent-based PAMPA technique. However, the results obtained for the phospholipid-based PAMPA models for gastrointestinal tract passive transport predictions indicate that these models can be used to obtain information on the permeation of chemicals loaded in specific carriers. However, testing a new material on PAMPA is not obvious and requires particular attention regarding the reciprocal impact of carriers on the artificial membrane and vice versa. Therefore, preliminary tests must be performed before the permeability coefficients obtained from PAMPA tests can be interpreted.



Cell Culture Models

Cellular models that predict BBB permeability are extensively used during the early drug discovery process. A large panel of cellular models exists that differ in origin, the type of expressed transporters, the tightness of the tight junctions and affiliation with a primary or immortalised cell line. These factors greatly influence the reproducibility of the permeability experiments and the capacity of these models to predict *in vivo* BBB permeability. Therefore, all cellular models are different and generate specific information on permeability through the BBB. Furthermore, none of the existing cellular models can fully predict the pharmacokinetic behaviour of drugs *in vivo*.

The main advantages of cellular models are the throughput rate, which allows for the evaluation of a reasonable number of compounds even if this rate is only moderate. Additionally, cellular models have the capacity to evaluate transport mechanisms, which depends on the type of expressed transporters and the possible evaluation of metabolism and cytotoxicity. Furthermore, pathological conditions can be investigated choosing an appropriate model (121). By contrast, homogeneity and reproducibility are difficult to obtain with cellular models, although these problems may be limited with the development of immortalised cell lines and standardised protocols.

To differentiate the wide variety of cellular models in existence since the 1970s, the following BBB parameters must be considered: the transendothelial electrical resistance (TEER), which indicates the tightness of transendothelial tight junctions and, therefore, restriction of the paracellular pathway; the endothelial permeability coefficient for paracellular markers such as sucrose, which indicates the integrity of the membrane (66); the expression of specific BBB transporters, such as the carrier-mediated transporters, including glucose transporters (GLUT1), monocarboxylic acid transporter (MCT1), large amino-acid transporters (LAT1), and cationic acid transporters (CAT); the active efflux transporters, including the ATP binding cassette (ABC) gene family or solute carrier (SLC) gene family (122); and the presence of BBB markers, such as factor VIII, γ-glutamyl transpeptidase (γ-GT), alkaline phosphatase (ALP) and monoamine oxidase (MAO) (123). Because the in vivo TEER of brain microvessels is approximately $1,000-2,000 \Omega$.cm² (124,125) and the permeation of sucrose can be as low as 0.03×10^{-6} cm.s⁻¹ (126), the ideal cellular model should provide values as close as possible to the known values for these parameters.

Primary Cultures. Cell biology research for the development of *in vitro* models of the human BBB began with primary bovine (40,127–137) and porcine (138–142) cultures (Table I) because the brain size of these animals is large;

leading to a high yield of cells per brain. However, rat (143-145), murine (146,147) and human (148-152) cell culture systems have also been developed. Compared to porcine or bovine cells, rat and mouse endothelial cells generate models with fewer BBB characteristics, such as a TEER value between 9 and 150Ω .cm² and a P_e (sucrose) of approximately 7.5×10⁻⁶ cm.s⁻¹ (Table I). Therefore, mouse brain endothelial cells are difficult to culture and lead to poor development of the endothelium (67). Additionally, because the number of cells per brain is limited, the batches of cells are always different even when the same protocol is used for extracting and seeding cells. This variability causes reproducibility issues because the cells used for permeability determinations are not the same from one day to the next. This is one reason why researchers have very little interest in using mouse primary cells for BBB permeability studies even if the best murine models can compete with some of the bovine models (144,153).

Bovine endothelial cells were the first *in vitro* BBB model and were developed by Bowman *et al.* as soon as 1983 (130). However, one of the primary bovine models expressing sufficient TEER for the prediction of BBB penetration was developed by Zenker *et al.* in 2003 (154). In this model, the TEER value reached $1,350\Omega.\text{cm}^2$, but values this high were rare and were dependent on the batch of cells. Furthermore, no paracellular permeability verification was performed, which makes an appropriate discussion of this model difficult. In general, the average TEER value generated with primary bovine endothelial cells is $150-200\Omega.\text{cm}^2$, which is far from the *in vivo* TEER value of $1,000\Omega.\text{cm}^2$ (40,127–137).

Porcine models display the best barrier properties (Table I). These models exhibit high TEER values ranging from 70 to $1,800\Omega$.cm² depending on the culture conditions and medium supplementation. Porcine models also have a low paracellular permeation of sucrose, with values ranging between 0.2 and 25×10^{-6} cm.s⁻¹ (138–142,155–162). Moreover, specific transporters, such as GLUT-1 or acetylated LDL, and brain enzymes, such as the y-GT or ALP, display efficient metabolic activity (142) (Table I). The most efficient cellular model of the BBB was developed by Franke et al. (159,163,164) who grew primary porcine brain microcapillary endothelial cells in serum-free medium containing hydrocortisone. The result of this treatment was a monolayer of endothelial cells with very tight junctions, TEER values reaching $1,500\Omega.\text{cm}^2$ with an average of $700\pm100\Omega.\text{cm}^2$, and a sucrose permeation as low as 0.3×10^{-7} cm.s⁻¹. Further evaluations indicated that this model expressed several ATP-binding cassette (ABC) transporters, nutrient transporters and specific BBB receptors (165). However, this model has not been used for any further permeability determinations.



 Table I
 Non Exhaustive List of Monoculture Models Aiming at Predicting BBB Permeability, Their Specificity and Information Provided

Author	Cells origins	TEER (Ω. cm²)	Paracellular marker permeability P × 10 ⁻⁶ cm.s ⁻¹	Evidence of TJ	Pinocytic vesides	Transporters	BBB receptors	BBB markers	In vitrolin vivo correlation
Ichikawa	rat BMEC					acetylated LDL	factor VIII	ALP, γ-GT	
Annunziata	rat BMEC	00					factor VIII		
F. et <i>al.</i> (144) Roux E et <i>al.</i> (172)	immortalized		sucrose: 214 ± 20				factor VIII	ALP, γ-GT	
Steiner (/ 2)	mouse BMEC		3 kDa dextran :	immunostaining,					
C. et <i>a</i> r. (11) Imaizumi S. <i>et a</i> l. (147)	mouse BMEC	59.5 ± 4.4	C: 0 - 7 - 7 - 7 - 7 - 7 - 7 - 7 - 7 - 7 -	western bloc			factor VIII	ALP, γ-GT	
Steiner	immortalized		3 kDa dextran:	immunostaining,					
O. et <i>al.</i> (11) Yang T , (15)	mouse biviec mouse endothelial	121	41 ± 5 sucrose: 8;	western blot immunostaining,		P-gp/ABCB1, GLUT1,			
l. et di. (153)	cell line bends + astrocyte conditioned		mannitol: 8	western blot		sodium, potassium, chloride cotransporters,			
Garberg P. et <i>al.</i> (123)	immortalized mouse BMEC	40–50	inulin: 11			P-gp/ABCB1		ALP, Y-GT	low correlation $(N=10)$
Culot M. et <i>al.</i> (232)	bovine brain EC		sucrose: 5.8 ± 0.2	immunostaining		P-gp/ABCB1, MRP1, MRP4, MRP5 by RT-PCR; presence of P-gp/ABCB1			
Raub T. J. et al. (134)	bovine brain EC	6 >	sucrose: 25			by western blot			
Bowman P. D. et al.(130)	bovine brain EC			transmission electron	few				
				micrograph					
Audus (129)	bovine brain EC			-				ALP, y-GT	
N. L. et al. (122) Smith (135) V. B. et el	bovine brain EC		sucrose : 0.08						
N. N. et al. Rubin	bovine brain EC	61±2							
L. L. et al. (40)									
Rubin L. L. et al. (40)	bovine+ astrocyte conditionned	5+							
S. S. S. S. S. S. S. S. S. S. S. S. S. S	medium bovine EC+ cAMP	305 + 50							
L. L. et al. (40)									
Rubin	bovine EC+ astrocyte	625 ± 82	restricted		low rate of				
L. L. et al. (40)	conditioned medium+ cAMP		paracellular efflux		endocytosis				
Pirro	bovine brain EC	200-600						γ-GT	
). r. et di. (155) Wang W. et el (155)	bovine brain EC	091		immunostaining					
v. e <i>t d</i> (137) Letrent S. P. <i>et d</i> . (133)	bovine brain EC	72–184	morphine:	electron microscopy		P-gp/ABCB1		ALP, γ-GT	
Abbruscato	bovine brain EC	200	sucrose:8						
Abbruscato T. J. et <i>al.</i> (127)	bovine brain EC+ astrocyte	175	sucrose:8						



Table I (continued)	ed)								
Author	Cells origins	TEER $(\Omega.cm^2)$	Paracellular marker permeability P × 10 ⁻⁶ cm.s ⁻¹	Evidence of TJ	Pinocytic vesicles	Transporters	BBB receptors	BBB markers	In vitrolin vivo correlation
	conditioned								
Yang T et <i>al.</i> (153)	Bovine brain EC+ astrocyte conditioned media	> 150	sucrose : 8; mannitol : 12	immunostaining, western blot		P.gp/ABCB1, GLUT1, sodium, potassium, choide corransporters, choice in the corransporters, contain the correspondence of the correspondence			
Rubin L. L. et al. (40)	Human EC+astrocyte conditioned	339 ± 107	restricted paracellular		low rate of endocytosis	protein kinase 🤇 isolornis			
Weksler B. et al. (174)	Immortalized human EC hCMEC/D3	> 40	inulin : 12; sucrose : 27; lucifer			P-gp/ABCB1,BCRP, MDR1, MRP1, MRP3, MPP4, MPP5	human transferrin receptor		
Stins M. F. et <i>al.</i> (150)	Immortalized human EC	300-400) calow . 22			acetylated low density lipoproteins	factor VIII	γ-GT, carbonic anhydrase IV,	
Sano Y. et <i>al.</i> (233) Fischer	Immortalized human EC (TY08) Porcine brain EC	35-43 89.4±3.1	inulin: 21			P.gp/ABCB1		ledin OttA	
S et <i>a</i> l. (140) Franke	Porcine brain EC	700 ± 100	Sucrose <						
(159,163) et al. Garberg P. et al. (123)	MDCKII-MDRI	120-140	inulin : 0.2; sucrose : 0.3			P.gp/ABCB1			$r^2 = 0.40$ (22 diverse compounds); $r^2 = 0.64$ (11 passive
Hakkarainen J. J. et <i>al.</i> (202)	MDCKII-MDRI		sucrose: 0.7 ± 0.3						$r^2 = 0.72 \ (N = 7)$, vs brain/blood ratio
Garberg P. et al. (123)	CACO-2	000'1-009	inulin : 0.08; sucrose : 1.4			P.gp/ABCB1, glut1, amino-acid transporters		ALP, Y-GT	$r^2 = 0.34$ (22 diverse compounds), $r^2 = 0.8611$ (11 passive compounds)
Hakkarainen J. J. et <i>di.</i> (202)	CACO-2		sucrose: 2.4 ± 1.4						$r^2 = 0.83(N = 7)$, vs brain/blood ratio

TEER transendothelial electrical resistance, BMEC brain microvascular endothelial cell, EC endothelial cell, cAMP cyclic adenosine monophosphate, ALP alkaline phosphatase, Y-GT gamma glutamyl transpeptidase, P-gp/ABCB1P-glycoprotein, MRP multiresistance drug protein, RT-PCR reverse transcription polymerase chain reaction, BCRP breast cancer resistant protein, LDL low density lipoprotein



Human brain cells are the gold standard for a human BBB in vitro model. However, for ethical reasons, the availability of this type of cell is very limited. The cells are generally obtained from biopsies of epileptic patients, and the number of cells obtained is very low. Rubin et al. and Bernas et al. developed primary human endothelial cell models with TEER values of $339 \pm 107 \Omega$.cm² and $>1,000 \Omega$.cm², respectively (40,166). No paracellular permeability was mentioned in these models, but the model developed by Bernas et al. was used in several studies to evaluate the effect of chemicals, such as cannabinoid receptor agonists, on the barrier function of BBB (167). Studies of these human models are limited and have instead focused on the generation of immortalised human cell lines, which should decrease the inter-individual, race, age and gender variations and increase the quality and reproducibility of the results obtained with human models.

Primary cell cultures may provide interesting information on human BBB permeability, but these models and culture conditions are not straightforward. Homogeneity and reproducibility of these models is not guaranteed because an animal brain cannot generate an infinite number of identical cells. Therefore, the variability of these models is due to inter-laboratory and inter-individual factors, among others, and leads to large standard deviations. Finally, primary monocultures of brain endothelial cells were shown to rapidly lose their BBB properties, including tight junctions and specific transporters (168).

Immortalised Cell Lines. To limit the drawbacks related to the handling of primary cells, researchers have immortalised their cultures to make cell lines. Immortalisation is generally achieved with either gene or virus transfection (148,169–171), such as the SV40 large T-gene antigen (67) or the E1A adenovirus gene (172) in the RBE4 model.

Few monoculture models of immortalised cell lines have been developed (Table I), however, bovine (173), human (148,150,174–181) mouse (182,183) and rat (172,183–188) endothelial cell lines have been established and tested for BBB properties. The model with the best BBB properties is a human brain endothelial cell line (150), with TEER values ranging from 300 to 400Ω .cm²; however, no sucrose permeation has been achieved, but inulin transport studies show low paracellular permeation. In 2005, Weksler et al. developed a model based in human cerebral cells: the hCMEC/D3 cell line, which displayed a TEER value below 40Ω .cm² and a sucrose permeation of 27.10⁻⁶ cm.s⁻¹ (174,189). Furthermore, many drug transporters, including most of the ABCB, ABCC and ABCG families found in the human BBB in vivo have been detected in the hCMEC/D3 cell line. Because of the existing BBB properties and its human origin, the hCMEC/D3 model has been used for many kinetic, pharmacological and permeability studies (190-193).

In order to understand the predictive ability of primary cells and immortalized cell line, Steiner *et al.* (11) compared primary mouse brain microvascular endothelial cells with immortalised mouse brain endothelial cell lines and determined that the two types of endothelial cells exhibited different cytoskeletal morphologies. Moreover, the protein occludin, which plays a role in tight junction formation, was localised in the primary endothelial cells but not in the cell line, indicating a divergence in the junctional organisation. This deviation leads to tighter junctions in the primary endothelial cells compared to the immortalised endothelial cells. Therefore, monocultures of immortalised cells are of limited interest for the prediction of BBB permeability, except the immortalised cell culture models derived from human cell lines.

Cocultures. Following the development of a variety of monoculture models and the determination that cerebral endothelial cells alone, whatever their origin, do not express the appropriate BBB properties and also lose their specific characteristics when isolated from their environment (27,145), cocultures became attractive models. In the human brain, there is constant communication between endothelial cells and other types of cerebral cells comprising the neurovascular unit, such as astrocytes, pericytes, neuroglia, and neurons (60,194). The action of surrounding cerebral cells on endothelial cells creates BBB properties and induces the production of junctional proteins and the expression of all the enzymes and transporters at the BBB (8,9,14,19,67,71,195). Moreover, it was shown that astrocytes were able to reinduce BBB properties (196).

Megard et al. (152) noted several interesting observations in their research on human brain endothelial cells cocultured with human astrocytes.

The resulting coculture exhibited specific barrier properties, such as a TEER value of $260 \pm 130 \Omega$.cm² (endothelial cells alone: $61\pm2\Omega$.cm² and astrocytes alone: $37\pm5\Omega$.cm²) and a sucrose permeation of 17 ± 3.10^{-6} cm.s⁻¹. To validate this BBB model, the authors selected the lipophilicity of a compound as a good indicator of BBB permeability. They demonstrated a good relationship between the in vitro BBB permeability of this model that was corrected with the molecular weight and the partition coefficients ($r^2 = 0.88$). Using flow cytometry and PCR, they showed that their model expressed P-gp/ABCB1 mRNA. A permeability determination with known P-gp/ABCB1 substrates, such as vincristine, verapamil or vinblastine, revealed a higher permeability from the basal to the apical compartments than from the apical to the basal compartments, indicating an efficient efflux process. These results underline the beneficial effect of cocultures on the expression of specific BBB properties in vitro models. The upregulation of P-gp/ABCB1 and the higher TEER value in cocultures compared to monocultures were also observed in several other studies (9,154,184,195,197,198) (Table II).



Table II Non Exhaustive List of Coculture Models Aiming at Predicting BBB Permeability, Their Specificities and Information Provided

Author	Endothelial cell origin	Coculture cell type	TEER ([].cm²)	Paracellular marker permeability × 10 ⁻⁶ cm.s ⁻¹	Evidence of T)	Pinocytic -vesicles	Transporters	Receptors	Enzymes	In vitrofin vivo correlation
Roux et al. (172) Demeuse P. et al. (145)	rat brain capillary EC (RBE4) rat brain capillary EC	rat astrocytes rat astrocytes	500 ± 20 (234) 438 ± 75	sucrose: 38 ± 9	immunostaining	Few	P-gp/ABCBI, GLUTI, LATI (235)	itor	γ-GT, ALP γ-GT	
Perrière N. et al. (15) Lacombe O. et al. (203) Lu W. et al. (205)	puromyain purified rat EC purified rat EC rat brain capillary EC	rat astrocytes rat astrocytes rat astrocytes	>270	sucrose: <1.7 sucrose: 3,28 ± 0.82 sucrose:16	immunostaining and RT-PCR confocal microscopy and immunostaining scanning electron microscopy and		P-gg/ABCB1, Bcrp, Mrps, GLUT1 abcg2, abcb1, abcc1, abcc4, abcc5	receptor OXZ6		$r^2 = 0.88$ $r^2 = 0.67$
Nakagawa S. et al. (194) Garberg	rat brain capillary EC immortalized	rat astrocytes and pericytes immortalized rat astrocytes	354 ± 15 50-70	fluorescein : 3.9 ± 0.2 inulin : 5.3;	transmission electron microscopy western blot, electron microscopy		P.gp/ABCB1, GLUT1, Mrp1 acetylated LDL	factor VIII	γ-GT	low correlation
Shayan G. et al. (236) Coisne C. et al. (237)	puromycin purified purified mouse EC primary mouse brain microvascular	rat astrocytes primary mouse glial cell	190 777.6 ± 14.8	.2;	immunocytochemistry and western blot immunostaining		P.gp/ABCBI, GLUTI P.gp/ABCBI			$r^2 = 0.96 (N = 7)$
Gaillard PJ. et al. (195) Dehouck M.R. et al. (117)	entotrellat cer bovine EC Bovine EC	rat astrocytes Rat astrocytes	400-850	fluorescein: 6.0 ± 1.0	electron microscopy- presence of cacherin 5	Fow rate	Pgp/ABCB1 expression Pgp/ABCB1 (27,197); LDL (238)	d, integrin, P-selectin receptor, transferrin receptor Transferrin receptor (239)	γ-GT	P = 0.86 (27, 121) $N = 20,$ $A = 10,$ $A =$
Stanness K. A. et al. (8) (3D model) Garberg P. et al. (123)	bovine aortic endothelial cells bovine EC	astrocytes rat astrocytes	736 ± 38 400–800	sucrose: 0.09 inulin: 0.7; sucrose: 4.0		_	P-gp/ABCB I	factor VIII	γ-GT, MAO	γ -GT, MAO $r^2 = 0.43 N = 22$ (with log BB)
Raub T. J. et al. (134) Abbruscato T. I. et al. (127)	bovine EC Bovine brain EC	rat C6 astrocytes rat C6 astrocytes	160 ± 8 210	sucrose: 24 sucrose: 10						
Mabondzo A. et al. (3) Garberg P. et al. (123)	purified human EC human EC	human astrocytes human astrocytes		lucifer yellow: 0.8; sucrose: 2.69 ± 0.25 inulin: 12; sucrose: 22		- -	GLUTI, LATI, LAT2, ABCBI, ABCCI, ABCC4, ABCC5, ABCG2 LDL			$r^2 = 0.90 (N=6)$ no correlation
Garberg P. et al. (123)	human umbilical vein EC like cell line	rat C6 glioma cell line	000	inulin: 0.6; sucrose: 8.1		-	GLUTI, leudine amino acid carrier, P-gp/ABCBI		γ-GT	



lable II (continued)	tinued)								
Author	Endothelial cell origin	Coculture cell type	TEER ([].cm ²)	Paracellular marker permeability × 10 ⁻⁶ cm.s ⁻¹	Evidence of TJ	Pinocytic Transporters vesicles	Receptors	Enzymes	In vitro/in vivo correlation
Fischer S. et al. (142)	porcine brain microvascular FC	rat astrocytes	104–219			GLUTI, acetylated LDL		γ-GT, ALP	
Fischer S. et al. (142)	porcine brain microvascular EC	C6 glial cells	180 ± 12			GLUT-1, acetylated LDL		γ-GT, ALP	

TER transendothelial electrical resistance, BMEC brain microvascular endothelial cell, EC endothelial cell, cAMP cyclic adenosine monophosphate, ALP alkaline phosphatase, y-GT gamma glutamyl transpeptidase, -gp/ABCB / P-glycoprotein, MRP multiresistance drug protein, RT-PCR reverse transcription polymerase chain reaction, BCRP breast cancer resistant protein, LDL low density lipoprotein, MAO monoamine

These cocultures can be established with either primary cells or cell lines. As indicated in the review by Deli *et al.* (66), many different cocultures have been developed but are usually established with endothelial cells and astrocytes from various animals. When the BBB properties of these cocultures were compared to the barrier properties of the corresponding endothelial monoculture, the resulting TEER values were generally improved, whereas the permeation of a paracellular tracer was decreased. Consequently, the expression of tight junction proteins is upregulated under coculture conditions, resulting in an improved *in vitro* BBB model (197).

To determine the reason why BBB properties are reinduced when endothelial cells are cocultured with astrocytes, Bénistant *et al.* (168) evaluated the fatty acid composition of bovine brain capillary endothelial cells either monocultured or cocultured with rat astrocytes. They found that the phospholipid profiles of the endothelial cells were clearly different between the two culture conditions. The most significant differences were observed for palmitic acid, which was 13% of the total phospholipid proportion in the monoculture *vs.* 20% in the coculture, and for linoleic acid, which was 18% in the monoculture *vs.* 10% in the coculture. Therefore, these results indicated that the presence of astrocytes when culturing endothelial cells can modify the fatty acid composition of brain endothelial cells.

In 2009, Nakagawa *et al.* (194) established a coculture model with three different types of cerebral cells, endothelial cells, pericytes and astrocytes, to provide a more realistic representation of the *in vivo* BBB. The pericytes were shown to have a similar positive influence as astrocytes on the tightness of the tight junctions (199). The TEER value of this triple coculture reached $400\,\Omega.\mathrm{cm}^2$, with a permeation of 3×10^{-6} cm.s⁻¹ for the non-permeant dye fluorescein. Moreover, specific BBB transporters, such as P-gp/ABCB1, glucose-transporter (GLUT1) and ABCC1, were expressed in the brain endothelial cells (Table II).

The BBB model displaying the best barrier features was developed by Dehouck *et al.* (27,39,121,197,200) and was called the bovine brain capillary endothelial cells model (BBCEC). This model, consisting of primary bovine endothelial cells cultured on one side of the filter and rat glial cells on the other side of the filter, exhibits high TEER values due to the presence of complex tight junctions. The TEER values range between 700 and 800Ω .cm² (13), and the BBCEC model displays a low sucrose permeation between 5.4 and 32×10^{-6} cm.s⁻¹, a low rate of pinocytosis, the presence of P-gp/ABCB1 and metabolic enzymes, such as γ -GT, MAO, and the occurrence of LDL and transferrin receptors (27). This combination of characteristics leads to interesting BBB properties.

When correlating *in vitro* BBB data, which are corrected by the molecular weight and a logarithmic function, with the



corresponding BUI or *in vivo* BBB permeability, both of which are also corrected, excellent relationships were observed ($r^2 = 0.86$) (121).

In conclusion, with regard to cellular models consisting of cerebral cells, primary cell cocultures generate the best models, although the reproducibility may not be optimal. The upregulation of tight junction proteins under coculture conditions allows for increased TEER values and decreased paracellular transport, which are characteristics of the BBB. The gold standard model would be a coculture of primary human cells, but this requires a constant renewal of the donor brain tissue, which causes ethical concerns.

Cell Lines of Non-Cerebral Origin

The Madin-Darby Canine Kidney Cell line (MDCK). MDCK cells are cells of non-cerebral origin that are relatively easy to grow and can be transfected with specific gene transporters, particularly the MDR1 gene, which codes for polarised expression of P-gp/ABCB1 (71). These transfected MDCK cells can then be used for the MDR1-MDCK (I or II) assay. MDCK cells can generate TEER values as high as 1,800- $2,200\Omega$.cm² (201), indicating the existence of robust barrier properties with high expression of tight junctional proteins. Moreover, the in vitro-in vivo correlation obtained with this model is better than some of the existing in vitro models with cerebral cells, with $r^2 = 0.64$ (123) or 0.72 (202) when passive compounds are selected for the correlation, depending on authors. However, in vitro/in vivo correlations with a diverse set of compounds (including compounds being actively transported or effluxed at the BBB) do not exhibit a significant correlation ($r^2 = 0.40$) (123). The greatest limitation of these cells is the absence of transporter proteins other than Pgp/ABCB1 and their different morphology compared to endothelial cells because MDCK cells are epithelial cells (71,203). Moreover, these cells are derived from dog kidney cells (201). However, transfection of the MDR1 gene allows for the determination of P-gp/ABCB1 substrates by measuring the permeability on both sides of the membrane. Another study conducted by Di Li et al. (114) did not generate an in vitro-in vivo correlation comparing the in vitro MDR1-MDCK permeation of a very diverse set of compounds with permeations obtained from in situ brain perfusion ($r^2 = 0.007$ (114)). This absence of correlation was most likely due to saturation of the P-gp/ABCB1 in vivo. The concentrations utilised for the in situ brain perfusion study were very high compared to the Michaelis-Menten constants of the compounds. These high concentrations lead to saturation of the efflux transport and use of the predominantly passive diffusion pathway, which overestimates the permeability in vitro. Therefore, attention should be paid to the experimental conditions when performing permeability assay with saturable transport. Moreover, differences in membrane characteristics, such as epithelial kidney cells for the MDR1-MDCK assay and cerebral endothelial cells for the *in situ* brain perfusion study, lead to a significant discrepancy in the predicted BBB permeability. Moreover, the phospholipid composition of both membranes is fundamentally different, with a higher proportion of cholesterol in the cerebral membrane than the MDCK cells. This composition leads to an increased fluidity of MDCK cells, which facilitates passive permeability in this model.

Caco-2 Cells. Caco-2 cells are epithelial cells derived from a human colon carcinoma and are extensively used in the pharmaceutical industry to predict oral absorption through the intestinal epithelium. Moreover, the Caco-2 model is also used to predict BBB transport, even though the gastrointestinal tract is fundamentally different from the BBB, but as in vitro BBB models have evolved, the in vivo permeability predicted by the Caco-2 model became less and less useful (121,123,202). compared to other models. However, the Caco-2 assay remains an efficient method of identifying substrates of the P-gp/ABCB1 transporter from a set of test compounds because of the overexpression of P-gp/ABCB1 in cancer cells. More recently, Ball et al. (204) developed a physiologically based pharmacokinetics model to predict the fraction of unbound drug reaching the brain. They succeeded in generating an in vitro model that faithfully fits the in vivo unbound brain concentration of morphine, which is effluxed at the BBB, and oxycodone, which is taken up at the BBB. The K_{p,uu} was determined in Caco-2 cells expressing the Pgp/ABCB1 efflux transporters for morphine and in TR-BBB13 cells, which enable active uptake, for oxycodone. Both resulting distributions were corrected by a relative activity factor, which was estimated by a comparison between the in vitro model predictions and the in vivo data in rats.

Adaptation of BBB Cell Models to New Delivery Strategies

Some models were used to obtain information on nanocarrier transport across the BBB.

Nanoparticles. In 2006, the transcytosis of polyethylene glycol-polylactide (PEG-PLA) nanoparticles across the BBB was evaluated by Lu *et al.* using a rat syngeneic coculture of brain capillary endothelial cells and astrocytes (205). The fluorescent compound 6-coumarin was incorporated inside these nanoparticles with a final size of 102.4±6.8 nm. After transport study of the coumarin-loaded PEG-PLA nanoparticles across the coculture, a permeation of 4.8×10^{-6} cm.s⁻¹ was obtained. However, the permeation of the paracellular marker sucrose was higher than the permeation of the nanoparticles. Therefore, either a



paracellular route or a transcytosis process may have occurred in this *in vitro* model.

Ragnaill et al. (206) later described the transport of 50 nm silicium dioxide nanoparticles through the in vitro hCMEC/D3 BBB model (174,189). They succeeded in showing that nanoparticles were effectively taken up by the cells with the membrane enveloping the nanoparticles. Moreover, they also observed the nanoparticles in both the endosomes and lysosomes and some on the basolateral side of the membrane. Therefore, they suggested that the silicium dioxide nanoparticles were endocytosed and that an exocytosis process also occurred.

Liposomes. The hCMEC/D3 cell line was also used to study the BBB penetration of an immunoliposome decorated with OX-26, an anti-transferrin monoclonal antibody (193). The objective of the study was to target the transferrin-receptor for transport of the immunoliposome by a receptor-mediated transcytosis process. The mean diameter of the immunoliposomes was assessed with dynamic light scattering and was less than 200 nm. They demonstrated that the immunoliposomes were transported through the endothelial monolayer by receptor-mediated endocytosis.

In vitro cellular models can therefore be used for the permeability determination of more complex formulations, such as nanocarriers. However, adaptation of the model may not be straightforward because of the potential cell toxicity of the carriers, and a full assessment of the validity of the models is required before a discussion of the results, but promising data regarding the distribution of nanocarriers are emerging.

Transport Across Isolated Brain Microvessels

Isolated brain microvessels are generally used to evaluate the gene expression of specific transporters at the BBB (207), but permeability experiments may also be conducted to identify specific transporters. Fluorescent probes are tested in the presence or absence of known substrates of the transporters. A variation in the permeability indicates the presence of the specific transporter that is being assessed (208,209). Miller et al. used confocal microscopy to detect fluorescent xenobiotics, such as daunomycin and fluorescein labeled dextrans, within the lumen of isolated brain microvessels (208). They succeeded in demonstrating a concentrative, specific and energy-driven transport process, indicating the expression of specific active transporters in isolated brain capillaries. Studies with specific substrates and immunostaining indicated that the active process was initiated by P-gp/ABCB1 and Mrps. The P-gp expression in isolated brain capillaries was corroborated by the studies of Durk et al. (209).

Transport across freshly isolated brain microvessels is a good alternative to cell culture because it is less time consuming; however, isolation of the brain microvessels requires much skill and very clean manipulations to obtain microvessels that are extremely pure. Moreover, reproducibility issues may be more important in this model than for cellular models because fresh microvessels must be freshly prepared for each experiment.

In Vivo Models

In vivo models are the best models available to predict human in vivo permeabilities because of the combination of all biological aspects in the same model, such as physiological barriers, transporters, and metabolic pathways. However, these models are expensive, time-consuming, require the mastering of animal-based assays and often necessitate radiolabelled compounds. These factors ensure that in vivo models are used during the later stages of the drug discovery process, just prior to clinical investigations, for a limited number of lead compounds. Different in vivo models are available, which allows for determination of the permeation of the molecules tested and in particular the logarithm of the BBB permeability-surface area (log PS) or the logarithm of the brain to plasma ratio (log BB) (Table III). These models include in situ brain perfusion, single carotid injection (brain uptake index; BUI), intravenous injection and intracerebral microdialysis (71). The log PS is considered the most relevant indicator of BBB permeability because it measures the clearance of a drug from the blood to the brain across the BBB (210) and is not altered by either metabolism or protein binding (114). The log PS is determined from the K_{in}, which is the clearance out of the brain. This determination better reflects BBB permeability..

Determination of the log BB requires several time point measurements, which requires animals a t each time point and is costly. Moreover, several factors, such as metabolism and binding, interfere with brain penetration in the log BB determination; therefore, log BB is not an accurate measurement of BBB permeability.

The Intravenous Administration Technique

Intravenous administration is one of the less invasive and most physiological methods of determining $in \ vivo$ permeability. In this technique, the buffer containing radiolabelled solutes is injected inside a cannulated femoral vein or in the tail vein of the rat. The plasma concentration of the products is monitored for 10 s to several hours over various time points. The pharmacokinetic parameter obtained is the area under the curve of the drug concentration in the blood between time 0 and the time of the decapitation (211). Therefore, the measured permeability will include the effective permeability, which is influenced by protein binding and metabolism. This technique has numerous advantages, such



Table III Summary of the In Vivo Techniques in Late Drug Discovery Research

In vivo techniques	Characteristics	Experimental data
Brain/plasma ratio	Study of low to rapid penetrating compounds; choice of variable exposure times; possible metabolism, protein binding and active transport.	A partition coefficient between plasma (or blood) and brain is generated. Be careful to misleading caused by protein binding.
Brain uptake index	Study of moderate to rapid penetrating compounds; fast brain exposure (5 to 15 s between the injection and the sacrifice of the animal); no metabolism, no protein binding, no efflux transport.	log PS are generated. The extremely fast brain exposure time leads to sensitivity problems, due to very low concentration in the brain.
In situ brain perfusion	Suitable for low to rapid penetrating compounds; fast to long exposure times (5 s to 1 h); no metabolism, no protein binding, possible transport.	Data similar as Brain uptake index is generated. Sensitivity is much higher, thanks to a possible long brain exposure time.
Intravenous administration technique	Study of low to rapid penetrating compounds; monitoring of the plasma concentration; existence of <i>in vivo</i> metabolism, protein binding and transport.	A whole pharmacokinetics profile is generated, on an intact BBB. This is the less ethically invasive and the most physiological method.
Intracerebral microdialysis	More appropriate for medium permeant compounds. Drug monitoring of the unbound drug fraction after the choice of the mode of administration; existence of <i>in vivo</i> metabolism, protein binding and transport.	A whole pharmacokinetics profile is generated, but BBB can be damaged due to surgery.
		Monitoring is made on the same animal: decrease the number of experimental animals, no deviation due to variation in the origin, age, gender, weight of the animal.
Imaging	Visualisation of the distribution in the body. Appropriate for medium to rapid penetrating compounds.	Non-invasive technique, which can be employed in humans. Existence of sensitivity issues, require expensive equipment.

as the BBB remaining undisturbed and all transporters, enzymes and junctional proteins remaining intact, which enables metabolism. An entire pharmacokinetics profile can therefore be obtained. Moreover, because the evaluation can be performed for an extended period of time, both the plasma and brain pharmacokinetics can be determined. However, the study of specific influx transport is not possible with this intravenous administration technique.

The Brain/Plasma Ratio

The brain/plasma ratio, established by Ohno *et al.* (212), resulted in determination of the blood–brain distribution coefficient (BB), which is defined as the ratio between the concentration of the compound in the brain and in plasma. Therefore, this approach may be misleading because the partition parameter that is obtained is dependent on the affinity of the tested drug for circulating proteins in the blood stream (213). This method provides determination of the drug partition between the plasma and brain but does not provide a pharmacokinetic profile. Determination of the brain/plasma ratio can be performed either at steady state or at different time points and requires sacrificing the animal and determining the concentration of the unbound drug in both the brain homogenate and plasma.

A brain/plasma ratio ≥1 indicates that a compound is able to cross the BBB, whereas a brain/plasma ratio <1 reveals a poor distribution of the compound (213). However, due to plasma protein binding, a brain/plasma ratio <1 may also

indicate a high affinity for circulating plasma proteins or an affinity for efflux proteins, both of which limit permeation of the compound through the barrier. Therefore, interpretation of the brain/plasma ratio must be performed cautiously.

Young et al. (214) used the brain/plasma ratio to design and select a CNS-active H_2 histamine receptor antagonist. More recently, Rohanova et al. used the brain/plasma ratio to study the brain penetration of a new illegal drug pmethoxymethamphetamine and its metabolites to better understand both the mode of action andas the toxicity profile of these new drugs (215).

The Unbound Brain/Plasma Ratio: $K_{b,uu}$

To correct the errors that may be introduced by measurement of the brain/plasma ratio, a recent tendency consist in determining the unbound brain to plasma ratio ($K_{p,uu}$). This parameter may be obtained directly by intracerebral microdialysis or with a combination of $in\ vivo$ and $ex\ vivo$ techniques. The last experiment is achieved measuring the quantity of drug that has reached the entire brain $in\ vivo$ combined with an estimation of the unbound brain volume of distribution with $ex\ vivo$ techniques such as the brain slice uptake experiment. The determination of $K_{p,uu}$ provides a better indication of the distribution of the active form of the drug. A $K_{p,uu}$ that is greater than unity indicates the presence of an active uptake process, whereas a $K_{p,uu}$ less than unity indicates the presence of an efflux process. A $K_{p,uu}$ near one indicates that the predominant pathway through the BBB is a passive diffusion process (216).



Intracerebral Microdialvsis. Microdialvsis allows for determination of the cerebral extracellular free drug concentration over a period of time with calculation of the K_{p,uu}. This free drug fraction represents the active form of the drug. Microdialysis requires the implantation of a dialysis probe in a selected area of the brain of the animal. This microdialysis probe consists of a semipermeable membrane that is continuously infused with physiological solution (217). Therefore, the compounds that are able to permeate through the membrane will diffuse according to the concentration gradient. This procedure does not require a specific mode of administration, and the permeation of the tested compound can be monitored after oral, intravenous, subcutaneous or infusion administration. Therefore, any drug entering the brain, which is always the unbound fraction of the drug, will be monitored over time in the extracellular fluid of the same animal (218) using HPLC, UHPLC or capillary electrophoresis. This technique requires a reduced number of animals for the pharmacokinetics determination compared to other techniques (71). Moreover, because the same animal is monitored, there is no deviation due to variation in the population, gender or age of the animal. However, implantation of the dialysis system may locally disrupt the BBB, leading to a possible misinterpretation of the results. Moreover, highly lipophilic compounds can be adsorbed onto the probe, leading to mass-balance errors. This technique is more appropriate for moderately permeable compounds.

Intracerebral microdialysis was used by Gupta et al. (219) to compare the BBB transport and CNS distribution of two cetirizine enantiomers, the R and the S forms, to evaluate the stereoselectivity that occurs at the BBB. They compared the K_p (total brain to total plasma concentrations), K_{p,u} (total brain to unbound plasma concentrations) and K_{p,uu} (unbound brain to plasma concentrations) for both enantiomers. Whereas the K_p value could have led to the interpretation that brain penetration was stereoselective for both isomers ($K_p = 0.22$ for S-cetirizine and 0.04 for R-cetirizine), the K_{p,u} (0.44 for S-cetirizine and 0.22 for R-cetirizine) indicates that plasma protein binding greatly influences the biodistribution of both forms of the antihistamine. The unbound fraction was found to be 0.50 for S-cetirizine but only 0.15 for R-cetirizine. When considering both the plasma protein binding and brain tissue binding, they discovered that the K_{p,uu} values were similar for both enantiomers (K_{p,uu}=0.17 for Scetirizine and 0.14 for R-cetirizine). These similar values indicate that both enantiomers are effluxed at the BBB (K_{p,uu}<1) and that no significant difference occurs in their transport. The information generated by these in vivo methodologies that are able to distinguish between the active (unbound fraction) and inactive forms of the drugs are therefore able to reliably determine the biodistribution profile of a drug at the BBB.

The In Vitro Brain Slice Uptake Experiment Combined with the In Vivo K_{p} . Determination of the entire concentration of a drug in the brain in vivo, combined with the volume of distribution of the unbound drug determined by an in vitro brain slice uptake experiment, allows for calculation of the unbound brain to plasma concentration ratio $K_{p,uu}$ (220,221). In the brain slice uptake experiment, the brain of a sacrificed animal is removed and immersed in ice-cold oxygenated pH 7.4 buffer (221). Brain slices (300 µm) of striatal areas are cut with a microslicer and preincubated with an extracellular fluid buffer before addition of the drug. At specific incubation times, the brain slices are removed from the solution of buffer containing the drug, dried, weighed and homogenised for determination of the amount of drug recovered in the brain slice. The main advantage of this technique is in the determination of the pharmacologically active unbound fraction of the drug in the brain. Moreover, the brain slices contain intact cerebral endothelial cells with their functional transporters as well as the same extra-to-intra-cellular pH gradient found in vivo (220). By contrast, the throughput of this model is limited due to the need for experimental animals and the minimum incubation time needed to reach drug equilibrium between the buffer and the brain slices, which is required to calculate $V_{u, \ brain}$ (220). As the incubation time to reach equilibrium increases with the $V_{u,\ \mathrm{brain}}$ and the $V_{u,\ \mathrm{brain}}$ increases with lipophilicity, the majority of compounds during the drug discovery phases require longer and longer incubation timestime, which cannot be supported by the limited life expectancy of the brain slices. Friden et al. evaluated this brain slice uptake assay to rapidly determine the unbound drug concentration in the brain (221). When they compared the results that were obtained for 15 diverse compounds with in vivo intracerebral microdialysis, they observed a reliable correlation between both techniques.

The Brain Uptake Index (BUI) Technique

The brain uptake index model is appropriate for compounds that moderately to rapidly penetrate the BBB and is generally performed in rats. A rapid bolus injection of 200 µl buffered solution containing a known concentration of a radiolabelled reference compound and the tested drug is administered directly into the carotid artery of the rat. The brain is then removed after 5–15 s and analysed for radiolabelled contents (71) by scintillation counting. BUI allows for determination of the log PS, which is the permeability multiplied by the surface area. This technique is based on the following three hypotheses: the time between injection and decapitation is so short that no metabolism occurs before the brain is removed; the compound can diffuse from the blood to the brain; and when the compound is in the brain, it cannot go back into the blood (222). The main drawback of



this technique is that extremely low concentrations of drug are present in the brain because of the very short analysis time, which causes sensitivity problems for compounds with low permeability. This technique is more appropriate for compounds with a high permeability through the BBB. For example, this technique has been used by Oldendorf *et al.*, who demonstrated modulation of the transporter activity under different pH conditions (223).

The In Situ Brain Perfusion

In situ brain perfusion is suitable for low to high permeant compounds (43) or substrates of an endogenous transport system. This model provides the same information as the BUI but with higher sensitivity. In situ brain perfusion is performed on an artificial cerebral circuit, resulting from the ligature of some cerebral arteries and catheterisation of the external carotid artery. Therefore, the flow rate and duration of perfusion are known and can be controlled. The brain is then perfused with an oxygenated hydrogenocarbonate buffer containing a known amount of radiolabeled compound. Determination of the radioactivity at a predefined time, ranging from 5 s to 30 min,) allows for the direct determination of pharmacokinetics parameters, particularly the volume of distribution and the rate of compound transfer, $K_{\rm in}$ (43,224).

Because the composition of the perfusate is controlled, *in situ* brain perfusion allows for the determination of PS values without considering either metabolism or plasma and brain protein binding. Only the intact form of the drug reaches the brain. This method provides information regarding the time required for the compound to cross the BBB. Moreover, the amount of drug reaching the brain is fully controlled. Compared to the BUI, the sensitivity of *in situ* brain perfusion is much higher because of a longer exposition time of the brain (126). This method is particularly interesting for determination of the kinetics of saturable transport at the BBB.

In situ brain perfusion was used by Cannon et al. (225) to study the modulation of P-gp/ABCB1 activity. They found that activation of the sphingosine-1-phosphate receptor by a specific ligand such as sphingosine-1-phosphate led to a decrease in P-gp/ABCB1 activity. The activity returned to the basal state after the administration of sphingosine-1-phosphate receptor antagonist. They concluded that this strategy could be used to increase the CNS bioavailability of P-gp substrates, such as verapamil or loperamide.

The Brain Efflux Index

The brain efflux index has been developed to determine the presence of a potential efflux pathway at the BBB when the compound is postulated to be transported from the brain to the blood. This technique is generally used to understand

why a sufficiently lipophilic compound fails to penetrate the brain (211).

Briefly, the test and reference compounds are microinjected directly into the brain tissue. After a predefined time, the brain is removed and the tissues are analysed to determine the concentration of the residual compounds.

This protocol requires the use of a highly sensitive method to determine the small amounts of compounds that may be present. Moreover, the researcher must be careful during the microinjection because a rapid or careless manipulation will irreversibly damage the BBB and confound the resulting measured permeability. The major drawback of this technique is the sacrifice of a large number of rats at different time points.

Kakee et al. (226) used this technique to highlight the saturable efflux transport of para-aminohippuric acid at the BBB. A comparison of the apparent efflux clearance that was obtained in this study using the brain efflux index method with the apparent influx clearance obtained by BUI confirmed the selective transport of the carboxylic acid under investigation from the brain to the blood.

Non-Invasive Imaging Techniques

Non-invasive imaging techniques have been developed to qualitatively and quantitatively determine the permeation of drugs in vivo. Moreover, imaging can also be used to identify P-gp/ABCB1 inhibitors or P-gp/ABCB1 substrates (227) or to determine the BCRP activity at the BBB (228). These techniques are primarily positron emission tomography (PET), magnetic resonance imaging or magnetic resonance spectroscopy. Because these techniques are noninvasive, they can be used in humans and allow for the determination of personalised pharmacokinetics. Imaging is also used to detect BBB damages in patients suffering from a stroke, brain tumours or multiple sclerosis. However, these techniques require expensive equipment and labelled radiotracers. Sensitivity issues may be encountered, particularly with magnetic resonance imaging (126). Knight et al. used magnetic resonance imaging to localise and quantify the BBB opening in a rat model under ischaemic conditions after the intravenous infusion of gadoliniumdiethylenetriamine pentaacetic acid to achieve a blood concentration (229). Under normal conditions, this substance should not penetrate the brain. Other researchers, such as Serres et al., established a promising approach for the early diagnosis of brain tumors by targeting brain metastasis with iron oxide microparticles loaded with contrast agents (230). Magnetic resonance imaging allowed for the visualisation of brain metastases with 3-fold greater sensitivity than conventional tumour diagnostics. 13C magnetic resonance spectroscopy was used to assess the relationship between brain and plasma concentrations of glucose in patients suffering from



diabetes type I during a hypoglycaemichypoglycemia event (231).

Therefore, imaging is an efficient approach to determine personalised permeabilities during or after a pathological event. The main advantage of this technique is that it can be conducted in human for specific purposes and with safe drugs or dyes. Moreover, the distribution profile can be visualised, identifying the targeted regions of the brain.

CONCLUSIONS

The specific organisation of the cerebral endothelial cells forming the BBB causes multiple problems for a drug that needs to reach the central nervous system. Additionally, the BBB is not only a physical barrier but also a pharmacological and a metabolic barrier due to the expression of numerous transporters and the presence of a variety of enzymes. These features are the reason why attrition rate is so high for CNS drug candidates. However, the population worldwide is aging and by 2050, elderly people over the age of 65 will represent 16% of the population (43). Along with this global aging, CNS disorders, such as Alzheimer's disease, increase exponentially, whereas treatments are lacking. Thus, there is a real need to either improve CNS drug discovery or to change the CNS drug delivery strategy by using colloidal vectorisation. The second option has garnered great interest during the last few decades. Vectorisation of active CNS drugs and mRNA or peptides with carriers that are able to recognise a specific target at the BBB are no longer impossibilities.

The main questions that remain to be answered in the early drug discovery and development processes are as follows: is the chemical CNS active? Is the drug a substrate of influx or efflux transporters? Is the drug bioavailable? Is it easily metabolised? As described in this review, many tools are available to predict and/or understand the mode of transport of a new chemical entity (NCE) through the BBB. These tools include computational sciences, in vitro and in vivo models and knowledge regarding new transporters. However, it is clear that a combination of methods, even in vitro models, should provide more relevant information regarding the potential of a drug to penetrate the BBB. Each method provides specific insight into the transport condition of NCEs, and only proper knowledge of the specificities of each model will help scientists to decrease the compound attrition rate. In vivo models provide much more global information regarding the BBB permeation of NCEs than other models. However, even simple models, such as artificial membranes, should not be neglected in the discovery process. Although these models provide neither a global view nor a realistic tool for the selection of compounds, they are useful for understanding the transport mechanism. The simplicity of these models isolates de facto unique or a limited number of aspects of the entire transport process. Similarly, although some cellular models do not provide sufficient relevancy in terms of BBB prediction, particularly regarding the tightness of the intercellular junctions as evaluated by TEER measurement and/or the permeation of sucrose, they constitute an extraordinarily predictive and sometimes selective tool for medicinal chemists if the data are well interpreted.

All of these models that are used for the evaluation of BBB penetration by NCEs may also provide information regarding the penetration of colloidal vectors and other nanocarriers. Currently during the drug discovery and development processes, an increasing number of delivery systems must be tested for efficacy; but, few models have been used and validated for the screening of new formulations. Moreover, kinetic parameters of carrier degradation that influence drug release should also be taken into consideration when evaluating a new model. Therefore, existing methods to predict or characterise BBB permeability need to adapt to these new drug delivery systems in order to fully understand their mode of action.

ACKNOWLEDGMENTS AND DISCLOSURES

Authors thank Professor Eric Allémann for useful discussions.

REFERENCES

- Kennedy T. Managing the drug discovery/development interface. Drug Discov Today. 1997;2:436

 –44.
- Tsaioun K, Bottlaender M, Mabondzo A, and Alzheimer's Drug Discovery Fdn. ADDME - avoiding drug development mistakes early: central nervous system drug discovery perspective. BMC Neurol. 2009;9(supll 1): S1.
- Mabondzo A, Bottlaender M, Guyot AC, Tsaouin K, Deverre JR, Balimane PV. Validation of in vitro cell-based human bloodbrain barrier model using clinical positron emission tomography radioligands to predict in vivo human brain penetration. Mol Pharm. 2010;7:1805–15.
- Davson H. History of the blood-brain barrier concept. In: Neuwelt EA, editor. Implications of the blood-brain barrier and its manipulation, Basic science aspects, vol. 1. New York: Plenum Publishing Corp; 1989. p. 27–52.
- Ehrlich P. Das sauerstoff-bedürfniss des organismus: eine farbenanalytische studie, A. Hirschwald; 1885, Berlin.
- Goldmann EE. Die aüssere und innere Sekretion des gesunden und kranken Organismus im Lichte der "vitalen Färbung", H. Laupp; 1909. Chir. 64 H. 1, 192.
- Goldmann EE. Vitalfärbung am Zentralnervensystem, Verl. der Akad. der Wiss.; 1913.
- 8. Stanness KA, Westrum LE, Fornaciari E, Mascagni P, Nelson JA, Stenglein SG, et al. Morphological and functional characterization of an in vitro blood-brain barrier model. Brain Res. 1997;771:329-42.
- Berezowski V, Landry C, Dehouck MP, Cecchelli R, Fenart L. Contribution of glial cells and pericytes to the mRNA profiles of Pglycoprotein and multidrug resistance-associated proteins in an



- in vitro model of the blood-brain barrier. Brain Res. 2004;1018:1-9.
- Abbott NJ. Prediction of blood-brain barrier permeation in drug discovery from in vivo, in vitro and in silico models. Drug Discov Today Technol. 2004;1:407–16.
- Steiner O, Coisne C, Engelhardt B, Lyck R. Comparison of immortalized bEnd5 and primary mouse brain microvascular endothelial cells as in vitro blood-brain barrier models for the study of T cell extravasation. J Cereb Blood Flow Metab. 2011;31:315-27.
- Abbott NJ, Patabendige AAK, Dolman DEM, Yusof SR, Begley DJ. Structure and function of the blood-brain barrier. Neurobiol Dis. 2010;37:13–25.
- Dehouck MP, Dehouck B, Fenart L, Cecchelli R. Blood-brain barrier in vitro. Rapid evaluation of strategies for achieving drug targeting to the central nervous system. In: Couraud PO, Scherman D, editors. Biology and physiology of the blood-brain barrier. New York: Plenum Press; 1996. p. 143–6.
- Cecchelli R, Berezowski V, Lundquist S, Culot M, Renftel M, Dehouck MP, et al. Modelling of the blood-brain barrier in drug discovery and development. Nat Rev Drug Discov. 2007;6:650– 61.
- Perrière N, Yousif S, Cazaubon S, Chaverot N, Bourasset F, Cisternino S, et al. A functional in vitro model of rat blood-brain barrier for molecular analysis of efflux transporters. Brain Res. 2007;1150:1–13.
- Lanevskij K, Japertas P, Didziapetris R, Petrauskas A. Ionization-Specific Prediction of Blood-brain Permeability. J Pharm Sci. 2009;98:122–34.
- Stevenson BR, Keon BH. The tight junction: morphology to molecules. Annu Rev Cell Dev Biol. 1998;14:89–109.
- Mitic LL, Anderson JM. Molecular architecture of tight junctions. Annu Rev Physiol. 1998;60:121–42.
- Abbott NJ, Ronnback L, Hansson E. Astrocyte-endothelial interactions at the blood-brain barrier. Nat Rev Neurosci. 2006;7:41–53.
- Ballabh P, Braun A, Nedergaard M. The blood-brain barrier: an overview: structure, regulation, and clinical implications. Neurobiol Dis. 2004;16:1–13.
- Abbott NJ. Astrocyte-endothelial interactions and blood-brain barrier permeability. J Anat. 2002;200:629–38.
- Crone C, Christensen O. Electrical-resistance of a capillary endothelium. J Gen Physiol. 1981;77:349–71.
- Butt HJ, Downing KH, Hansma PK. Imaging the membraneprotein bacteriorhodopsin with the atomic force microscope. Biophys J. 1990;58:1473–80.
- Wolburg H, Lippoldt A. Tight junctions of the blood-brain barrier: Development, composition and regulation. Vasc Pharmacol. 2002;38:II.
- Doan KMM, Humphreys JE, Webster LO, Wring SA, Shampine LJ, Serabjit-Singh CJ, et al. Passive permeability and Pglycoprotein-mediated efflux differentiate central nervous system (CNS) and non-CNS marketed drugs. J Pharmacol Exp Ther. 2002;303:1029–37.
- Burns EM, Buschmann MBT, Krukeberg TW, Gaetano PK, Meyer JN. Blood-brain barrier, aging, brain blood flow, and sleep. Adv Neurol. 1981;30:301–6.
- Cecchelli R, Dehouk B, Descamps L, Fenart L, Buéé-Scherrer V, Duhem C, et al. In vitro model for evaluating drug transport across the blood-brain barrier. Adv Drug Deliv Rev. 1999;36:165–78.
- Miller DS. Regulation of P-glycoprotein and other ABC drug transporters at the blood-brain barrier. Trends Pharmacol Sci. 2010;31:246-54.
- Weiss N, Miller F, Cazaubon S, Couraud PO. Biologie de la barrière hématoencéphalique: Partie I. Rev Neurol. 2009;165: 863–74.

- Petty MA, Lo EH. Junctional complexes of the blood-brain barrier: permeability changes in neuroinflammation. Prog Neurobiol. 2002;68:311–23.
- Smith MW, Gumbleton M. Endocytosis at the blood-brain barrier: from basic understanding to drug delivery strategies. J Drug Target. 2006;14:191–214.
- 32. Hawkins BT, Egleton RD. Pathophysiology of the blood–brain barrier: animal models and methods. In: Gerald PS, editor. Current topics in developmental biology. Academic Press; 2007. pp. 277–309. doi:10.1016/S0070-2153(07)80007-X
- 33. Weiss N, Miller F, Cazaubon S, Couraud PO. The blood–brain barrier in brain homeostasis and neurological diseases. Biochim Biophys Acta. 2009;1788:842–57.
- Löscher W, Potschka H. Role of drug efflux transporters in the brain for drug disposition and treatment of brain diseases. Prog Neurobiol. 2005;76:22–76.
- Gao B, Stieger B, Noé B, Fritschy JM, Meier PJ. Localization of the organic anion transporting polypeptide 2 (Oatp2) in capillary endothelium and choroid plexus epithelium of rat brain. J Histochem Cytochem. 1999;47:1255–63.
- Cordoncardo C, Obrien JP, Casals D, Rittmangrauer L, Biedler JL, Melamed MR, et al. Multidrug-tesistance hene (P-Glycoprotein) is rxpressed by rndothelial-cells at blood-brain barrier sites. Proc Natl Acad Sci USA. 1989;86:695–8.
- 37. Eisenblatter T, Galla HJ. A new multidrug resistance protein at the blood–brain barrier. Biochem Biophys Res Commun. 2002;293:1273–8.
- Salmina AB. Neuron-glia interactions as therapeutic targets in neurodegeneration. J Alzheimers Dis. 2009;16:485–502.
- Dehouck MP, Meresse S, Delorme P, Fruchart JC, Cecchelli R. An easier, reproductible, and mass-production method to study the blood-brain barrier in vitro. J Neurochem. 1990;54:1798–801.
- Rubin LL, Hall DE, Porter S, Barbu K, Cannon C, Horner HC, et al. A cell-culture model of the blood–brain-barrier. J Cell Biol. 1991;115:1725–35.
- Ramsauer M, Krause D, Dermietzel R. Angiogenesis of the blood-brain barrier in vitro and the function of cerebral pericytes. FASEB J. 2002;16:1274.
- Sa-Pereira I, Brites D, Brito MA. Neurovascular unit: a focus on Pericytes. Mol Neurobiol. 2012;45:327

 –47.
- Alavijeh MS, Chishty M, Qaiser MZ, Palmer AM. Drug metabolism and pharmacokinetics, the blood-brain barrier, and central nervous system drug discovery. Neurotherapeutics. 2005;2:554

 71.
- 44. Chancellor MB, Staskin DR, Kay GG, Sandage BW, Oefelein MG, Tsao JW. Blood–brain barrier permeation and efflux exclusion of anticholinergics used in the treatment of overactive bladder. Drugs Aging. 2012;29:259–73.
- 45. Summerfield SG, Read K, Begley DJ, Obradovic T, Hidalgo IJ, Coggon S, *et al.* Central nervous system drug disposition: the relationship between in situ brain permeability and brain free fraction. J Pharmacol Exp Ther. 2007;322:205–13.
- Lee K, Thakker DR. Saturable transport of H2-antagonists ranitidine and famotidine across Caco-2 cell monolayers. J Pharm Sci. 1999;88:680–7.
- Zhou SY, Piyapolrungroj N, Pao LH, Li C, Liu GY, Zimmermann E, et al. Regulation of paracellular absorption of cimetidine and 5-aminosalicylate in rat intestine. Pharm Res. 1999:16:1781–5.
- Flanagan SD, Takahashi LH, Liu XL, Benet LZ. Contributions of saturable active secretion, passive transcellular, and paracellular diffusion to the overall transport of furosemide across adenocarcinoma (Caco-2) cells. J Pharm Sci. 2002;91:1169–77.
- Leontiadou H, Mark AE, Marrink SJ. Ion transport across transmembrane pores. Biophys J. 2007;92:4209–15.
- 50. Cirrito JR, Deane R, Fagan AM, Spinner ML, Parsadanian M, Finn MB, et al. P-glycoprotein deficiency at the blood-brain



- barrier increases amyloid-b deposition in an Alzheimer disease mouse model. J Clin Invest. 2005;115:3285–90.
- Stamatovic SM, Keep RF, Andjelkovic AV. Brain endothelial cell-cell junctions: How to "Open" the blood brain barrier. Curr Neuropharmacol. 2008;6:179

 –92.
- Marroni M, Marchi N, Cucullo L, Abbott NJ, Signorelli K, Janigro D. Vascular and parenchymal mechanisms in multiple drug resistance: a lesson from human epilepsy. Curr Drug Targets. 2003;4:297–304.
- Pittet CL, Newcombe J, Prat A, Arbour N. Human brain endothelial cells endeavor to immunoregulate CD8 T cells via PD-1 ligand expression in multiple sclerosis. J Neuroinflam. 2011;8:155.
- Bennett J, Basivireddy J, Kollar A, Biron KE, Reickmann P, Jefferies WA, et al. Blood-brain barrier disruption and enhanced vascular permeability in the multiple sclerosis model EAE. J Neuroimmunol. 2010;229:180–91.
- Liu H, Xu X, Yang Z, Deng Y, Liu X, Xie L. Impaired function and expression of P-glycoprotein in blood-brain barrier of streptozotocin-induced diabetic rats. Brain Res. 2006;1123:245–52.
- Sugano K, Kansy M, Artursson P, Avdeef A, Bendels S, Di L, et al. Coexistence of passive and carrier-mediated processes in drug transport. Nat Rev Drug Discov. 2010;9:597–614.
- Waring MJ. Lipophilicity in drug discovery. Expert Opin Drug Discov. 2010;5:235–48.
- 58. Camenisch G, Alsenz J, van de Waterbeemd H, Folkers G. Estimation of permeability by passive diffusion through Caco-2 cell monolayers using the drugs' lipophilicity and molecular weight. Eur J Pharm Sci. 1998;6:313–9.
- Johnson TW, Dress KR, Edwards M. Using the golden triangle to optimize clearance and oral absorption. Bioorg Med Chem Lett. 2009;19:5560–4.
- Pardridge WM. CNS drug design based on principles of bloodbrain barrier transport. J Neurochem. 1998;5:1781–92.
- Lipinski CA, Lombardo F, Dominy BW, Feeney PJ. Experimental and computational approaches to estimate solubility and permeability in drug discovery and development settings. Adv Drug Deliv Rev. 1997;23:3–25.
- Zhao YH, Abraham MH, Ibrahim A, Fish PV, Cole S, Lewis ML, et al. Predicting penetration across the blood–brain barrier from simple descriptors and fragmentation schemes. J Chem Inf Model. 2006;47:170–5.
- Avdeef A. Absorption and drug development. Hoboken: John Wiley & Sons; 2003.
- 64. Kell DB, Dobson PD, Bilsland E, Oliver SG. The promiscuous binding of pharmaceutical drugs and their transporter-mediated uptake into cells: what we (need to) know and how we can do so. Drug Discov Today. 2013;18(5–6):218–39.
- Varatharajan L, Thomas SA. The transport of anti-HIV drugs across blood-CNS interfaces: Summary of current knowledge and recommendations for further research. Antivir Res. 2009;82:A99– 100
- Deli MA, Abraham C, Kataoka Y, Niwa M. Permeability studies on in vitro blood-brain barrier models: physiology, pathology, and pharmacology. Cell Mol Neurobiol. 2005;25:59–127.
- 67. Cecchelli R, Coisne C, Dehouck L, Miller F, Dehouck MP, Buée-Scherrer V, et al. Modeling the blood-brain barrier. In: Dermietzel R, Spray DC, Nedergaard M, editors. Blood-brain interfaces. From ontogeny to artificial barriers. Weinheim: Wiley-VCH Verlag GmbH; 2006. p. 337–55.
- Nau R, Soergel F, Eiffert H. Penetration of drugs through the blood-cerebrospinal fluid/blood-brain barrier for treatment of central nervous system infections. Clin Microbiol Rev. 2010;23:858. -+.
- Kroll RA, Neuwelt EA. Outwitting the blood-brain barrier for therapeutic purposes: osmotic opening and other means. Neurosurgery. 1998;42:1083–99.

- Rapoport SI. Osmotic opening of the blood-brain barrier: principles, mechanism, and therapeutic applications. Cell Mol Neurobiol. 2000;20:217–30.
- Nicolazzo JA, Charman SA, Charman WN. Methods to assess drug permeability across the blood-brain barrier. J Pharm Pharmacol. 2006;58:281–93.
- Illum L. Is nose-to-brain transport of drugs in man a reality? J Pharm Pharmacol. 2004;56:3

 –17.
- Deli MA. Potential use of tight junction modulators to reversibly open membranous barriers and improve drug delivery. Biochim Biophys Acta. 2009;1788;892–910.
- 74. Zhang H, Prisinzano TE, Donovan MD. Permeation and metabolism of cocaine in the nasal mucosa. Eur J Drug Metab Pharmacokinet. 2012;37:255–62.
- Singh AP, Saraf SK, Saraf SA. SLN approach for nose-to-brain delivery of alprazolam. Drug Deliv Transl Res. 2012;2:498–507.
- Veronesi MC, Kubek DJ, Kubek MJ. Intranasal delivery of neuropeptides. Neuropeptides. 2011;789:303–12.
- 77. Bousquet L. Etude comparative des thérapies anti-VIH: rôle des transporteurs d'Efflux sur le passage transmembranaire des antirétroviraux au niveau des cellules CD4+ et de la Barrière hémato-encéphalique, Université Paris XI; 2008.
- Drin G, Rousselle C, Scherrmann JM, Rees AR, Temsamani J. Peptide delivery to the brain via adsorptive-mediated endocytosis: advances with SynB vectors. AAPS Pharm Sci. 2002;4(4):61–7.
- Malakoutikhah M, Teixido M, Giralt E. Toward an optimal blood-brain barrier shuttle by synthesis and evaluation of peptide libraries. J Math Chem. 2008;51:4881–9.
- Costantino L, Tosi G, Ruozi B, Bondioli L, Vandelli MA, Forni F.
 Colloidal systems for CNS drug delivery. In: Hari SS, editor.
 Progress in Brain Research Nanoneuroscience and Nanoneuropharmacology. Elsevier; 2009. pp. 35–69.
- 81. Ruozi B, Tosi G, Forni F, Vandelli MA. Ketorolac tromethamine liposomes: encapsulation and release studies. J Liposome Res. 2005;15:175–85.
- Ali M, Kirby DJ, Mohammed AR, Perrie Y. Solubilisation of drugs within liposomal bilayers: alternatives to cholesterol as a membrane stabilising agent. J Pharm Pharmacol. 2010;62:1646– 55
- Gabizon AA. Pegylated liposomal doxorubicin: metamorphosis of an old drug into a new form of chemotherapy. Cancer Investig. 2001;19:424

 –36.
- 84. Working PK, Dayan AD. Pharmacological-toxicological expert report Caelyx(TM) (Stealth(R) liposomal doxorubicin HCl) foreword. Hum Exp Toxicol. 1996;15:751–85.
- Huwyler J, Wu D, Pardridge WM. Brain drug delivery of small molecules using immunoliposomes. Proc Natl Acad Sci USA. 1996;93:14164-9.
- 86. Mamot C, Ritschard R, Wicki A, Stehle G, Dieterle T, Bubendorf L, et al. Tolerability, safety, pharmacokinetics, and efficacy of doxorubicin-loaded anti-EGFR immunoliposomes in advanced solid tumours: a phase 1 dose-escalation study. Lancet Oncol. 2012;13:1234–41.
- 87. Mehlhorn RJ, Sumida S, Packer L. Tocopheroxyl radical persistence and tocopherol consumption in liposomes and in vitamin-Eenriched rat-liver mitochondria and microsomes. J Biol Chem. 1989;264:13448–52.
- 88. Hiremath PS, Soppimath KS, Betageri GV. Proliposomes of exemestane for improved oral delivery: Formulation and in vitro evaluation using PAMPA, Caco-2 and rat intestine. Int J Pharm. 2009;380:96–104.
- Kreuter J, Alyautdin RN, Kharkevich DA, Ivanov AA. Passage of peptides through the blood-brain-barrier with colloidal polymer particles (nanoparticles). Brain Res. 1995;674:171–4.
- Kreuter J. Nanoparticulate systems for brain delivery of drugs. Adv Drug Deliv Rev. 2001;47:65–81.



- Wohlfart S, Gelperina S, Kreuter J. Transport of drugs across the blood-brain barrier by nanoparticles. J Control Release. 2012;161:264-73.
- Costantino L, Boraschi D. Is there a clinical future for polymeric nanoparticles as brain-targeting drug delivery agents? Drug Discov Todav. 2012;17:367–78.
- Lombardo F, Blake JF, Curatolo WJ. Computation of brainblood partitioning of organic solutes via free energy calculations. J Med Chem. 1996;39:4750–5.
- Abraham MH, Chadha HS, Mitchell RC. Hydrogen bonding. 33.
 Factors that influence the distribution of solutes between blood and brain. J Pharm Sci. 1994;83:1257–68.
- Chadha HS, Abraham MH, Mitchell RC. Physicochemical analysis of the factors goverining distribution of solutes between blood and brain. Bioorg Med Chem Lett. 1994;4:2511–6.
- Abraham MH, Hersey A. In silico models to predict brain uptake.
 In: Comprehensive Medicinal chemistry II, Elsevier Ltd; 2007.
 pp. 745–766.
- Didziapetris R, Japertas P, Avdeef A, Petrauskas A. Classification analysis of P-glycoprotein substrate specificity. J Drug Target. 2003;11:391

 –406.
- Timmermans PBMWM, Brands A, van Zwieten NS. Lipophilicity and brain disposition of clonidine and structurally related imidazolidines. Arch Pharm. 1977;300:217–26.
- Salminen T, Pulli A, Taskinen J. Relationship between immobilised artificial membrane chromatographic retention and the brain penetration of structurally diverse drugs. J Pharm Biomed Anal. 1997;15:469–77.
- Taillardat-Bertschinger A, Carrupt PA, Barbato F, Testa B. Immobilized artificial membrane (IAM)-HPLC in drug research. J Med Chem. 2003;46:655–65.
- Taillardat-Bertschinger A, Galland A, Carrupt PA, Testa B. Immobilized artificial membrane (IAM)-HPLC: proposed guidelines for technical optimization of retention measurements. J Chromatogr A. 2002;953:39–53.
- 102. Taillardat-Bertschinger A, Marca-Martinet CA, Carrupt PA, Reist M, Caron G, Fruttero R, et al. Molecular factors influencing retention on immobilized artificial membranes (IAM) compared to partitioning in liposomes and n-octanol. Pharm Res. 2002;19:729–37.
- 103. Taillardat-Bertschinger A, Barbato F, Quercia MT, Carrupt PA, Reist M, La Rotonda MI, et al. Structural properties governing retention mechanisms on immobilized artificial membrane (IAM) HPLC-columns. Helv Chim Acta. 2002;85: 519–32.
- 104. Ong S, Liu H, Qiu X, Bhat G, Pidgeon C. Membrane partition coefficients chromatographically measured using immobilized artificial membrane surfaces. Anal Chem. 1995;67: 755–62.
- Pidgeon C, Ong S, Liu H, Qiu X, Pidgeon M, Dantzig M, et al. IAM chromatography: an in vitro screen for predicting drug membrane permeability. J Med Chem. 1995;38:590–4.
- Stenberg P, Norinder U, Luthman K, Artursson P. Experimental and computational screening models for the prediction of instestinal drug absorption. J Med Chem. 2001;44:1927–37.
- 107. Osterberg T, Svensson M, Lundahl P. Chromatographic retention of drug molecules on immobilised liposomes prepared from egg phospholipids molecules and from chemically pure phospholipids. Eur J Pharm Sci. 2001;12:427–39.
- 108. Kansy M, Senner F, Gubernator K. Physicochemical high throughput screening: parallel artificial membrane permeation assay in the description of passive absorption processes. J Med Chem. 1998;41:1007–10.
- 109. Han M, Fu S, Gao JQ, Fang XL. Evaluation of intestinal absorption of Ginsenoside Rg(1) incorporated in microemulison using parallel artificial membrane permeability assay. Biol Pharm Bull. 2009;32:1069–74.

- Wohnsland F, Faller B. High-throughput permeability pH profile and high-throughput alkane/water log P with artificial membranes. J Med Chem. 2001;44:923

 –30.
- 111. Ottaviani G, Martel S, Carrupt PA. Parallel artificial membrane permeability assay: a new membrane for the fast prediction of passive human skin permeability. J Med Chem. 2006;49:3948–54.
- 112. Di L, Kerns EH, Fan K, McConnell OJ, Carter GT. High throughput artificial membrane permeability assay for blood– brain barrier. Eur J Med Chem. 2003;38:223–32.
- 113. Di L, Kerns EH, Ma XJ, Huang YP, Carter GT. Applications of high throughput microsomal stability assay in drug discovery. Comb Chem High Throughput Screen. 2008;11:469–76.
- 114. Di L, Kerns EH, Bezar IF, Petusky SL, Huang YP. Comparison of blood-brain barrier permeability assays: in situ brain perfusion, MDR1-MDCKII and PAMPA-BBB. J Pharm Sci. 2009;98:1980–91.
- 115. Mensch J, Melis A, Mackie C, Verreck G, Brewster ME, Augustijns P. Evaluation of various PAMPA models to identify the most discriminating method for the prediction of BBB permeability. Eur J Pharm Biopharm. 2010;74:495–502.
- 116. Passeleu Le Bourdonnec C, Boccard J, Rudaz S, Carrupt PA, Martel S. Evaluation of BBB permeation with PAMPA thanks to a new artificial membrane. In: Frontiers in medicinal chemistry FMC 2011 Stockholm Sweden June 19–21, 2011, 2011. Poster presentation.
- 117. Dehouck MP, Meresse S, Delbart C, Delorme P, Fruchart JC, Cecchelli R. Co-culture of astrocytes and brain endothelial cells: a potential model for in vitro studies of blood-brain barrier. J Neurochem. 1989;52(Supplement):120.
- Liu X, Tu M, Kelly KS, Chen C, Smith BJ. Development of a computational approach to predict blood-brain barrier permeability. Drug Metab Dispos. 2004;32:132–9.
- 119. Mathot F, Schanck A, van Bambeke F, Aridn A, Noppe M, Brewster M, *et al.* Passive diffusion of polymeric surfactants across lipid bilayers. J Control Release. 2007;120:79–87.
- 120. Kansy M, Fischer H, Kratzat K, Senner F, Wagner B, Parrilla I. High-throughput artificial membrane permeability studies in early lead discovery and development. In: Testa B, van de Waterbeemd H, Folkers G, Guy RH, editors. Pharmacokinetic optimization in drug research: biological, physicochemical and computational strategies. Zurich: Wiley-VHCA; 2001. p. 447–64.
- 121. Lundquist S, Renftel M, Brillault J, Fenart L, Cecchelli R, Dehouck MP. Prediction of drug transport through the blood– brain barrier in vivo: a comparison between two in vitro cell models. Pharm Res. 2002;19:976–81.
- 122. Pardridge WM. The blood–brain barrier and neurotherapeutics. Neurotherapeutics. 2005;2:1–2.
- 123. Garberg P, Ball M, Borg N, Cecchelli R, Fenart L, Hurst RD, et al. In vitro models for the blood–brain barrier. Toxicol in Vitro. 2005;19:299–334.
- 124. Gumbleton M, Audus KL. Progress and limitations in the use of in vitro cell cultures to serve as a permeability screen for the blood-brain barrier. J Pharm Sci. 2001;90:1681–98.
- Avdeef A. How well can in vitro brain microcapillary endothelial cell models predict rodent in vivo blood–brain barrier permeability? Eur J Pharm Sci. 2011;43:109–24.
- 126. Bickel U. How to measure drug transport across the blood–brain barrier. NeuroRx. 2005;2:15–26.
- Abbruscato TJ, Davis TP. Combination of hypoxia/aglycemia compromises in vitro blood-brain barrier integrity. J Pharmacol Exp Ther. 1999;289:668-75.
- 128. Audus KL, Borchardt RT. Characteristics of the large neutral amino acid transport system of bovine brain microvessel endothelial cell monolayers. J Neurochem. 1986;47:484–8.
- Audus KL, Borchardt RT. Characterization of an invitro bloodbrain-barrier model system for studying drug transport and metabolism. Pharm Res. 1986;3:81–7.



- 130. Bowman PD, Ennis SR, Rarey KE, Betz AL, Goldstein GW. Brain microvessel endothelial-cells in tissue-culture - A model for study of blood-brain-barrier permeability. Ann Neurol. 1983;14:396–402.
- Eddy EP, Maleef BE, Hart TK, Smith PL. In vitro models to predict blood-brain barrier permeability. Adv Drug Deliv Rev. 1997;23:185–98.
- Letrent SP, Polli JW, Humphreys JE, Pollack GM, Brouwer KR, Brouwer KLR. P-glycoprotein-mediated transport of morphine in brain capillary endothelial cells. Biochem Pharmacol. 1999;58:951–7.
- Pirro JP, Dirocco RJ, Narra RK, Nunn AD. Relationship between in-vitro transendothelial permeability and in-vivo single-pass brain extraction. J Nucl Med. 1994;35:1514—9.
- 134. Raub TJ, Kuentzel SL, Sawada GA. Permeability of bovine brain microvessel endothelial cells in vitro: Barrier tightening by a factor released from astroglioma cells. Exp Cell Res. 1992;199:330–40.
- 135. Smith KR, Borchardt RT. Permeability and mechanism of albumin, cationized albumin, and glycosylated albumin trans-cellular transport across monolayers of cultured bovine brain capillary endothelial-cells. Pharm Res. 1989;6:466–73.
- 136. van Bree JBMM, de Boer AG, Danhof M, Ginsel LA, Breimer DD. Characterization of an in vitro blood–brain barrier: effects of molecular size and lipophilicity on cerebrovascular endothelial transport rates of drugs. J Pharmacol Exp Ther. 1988;247:1233–9.
- Wang W, Dentler WL, Borchardt RT. VEGF increases BMEC monolayer permeability by affecting occludin expression and tight junction assembly. Am J Physiol Heart Circ Physiol. 2001;280: H434–40.
- 138. Fischer S, Clauss M, Wiesnet M, Renz D, Schaper W, Karliczek GF. Hypoxia induces permeability in brain microvessel endothelial cells via VEGF and NO. Am J Physiol Cell Physiol. 1999;276:C812–20.
- 139. Fischer S, Renz D, Schaper W, Karliczek GF. In vitro effects of dexamethasone on hypoxia-induced hyperpermeability and expression of vascular endothelial growth factor. Eur J Pharmacol. 2001;411:231–43.
- Fischer S, Renz D, Schaper W, Karliczek GF. Effects of barbiturates on hypoxic cultures of brain derived microvascular endothelial cells. Brain Res. 1996;707:47–53.
- 141. Fischer S, Renz D, Schaper W, Karliczek GF. Barbiturates decrease the expression of vascular endothelial growth factor in hypoxic cultures of porcine brain derived microvascular endothelial cells. Mol Brain Res. 1998;60:89–97.
- 142. Fischer S, Wobben M, Kleinstuck J, Renz D, Schaper W. Effect of astroglial cells on hypoxia-induced permeability in PBMEC cells. Am. J Physiol Cell Physiol. 2000;279:C935–44.
- 143. Ichikawa N, Naora K, Hirano H, Hashimoto M, Masumura S, Iwamoto K. Isolation and primary culture of rat cerebral microvascular endothelial cells for studying drug transport in vitro. J Pharmacol Toxicol Methods. 1996;36:45–52.
- 144. Annunziata P, Cioni C, Toneatto S, Paccagnini E. HIV-1 gp120 increases the permeability of rat brain endothelium cultures by a mechanism involving substance P. AIDS. 1998;12:2377–85.
- 145. Demeuse P, Kerkhofs A, Struys-Ponsar C, Knoops B, Remacle C, de Aguilar PV. Compartmentalized coculture of rat brain endothelial cells and astrocytes: a syngenic model to study the bloodbrain barrier. J Neurosci Methods. 2002;121:21–31.
- 146. Sahagun G, Moore SA, Hart MN. Permeability of neutral vs anionic dextrans in cultured brain microvascular endothelium. Am.J Physiol. 1990;259:H162–6.
- 147. Imaizumi S, Kondo T, Deli MA, Gobbel G, Joo F, Epstein CJ, et al. The influence of oxygen free radicals on the permeability of the monolayer of cultured brain endothelial cells. Neurochem Int. 1996;29:205–11.
- 148. Muruganandam A, Herx LM, Monette R, Durkin JP, Stanimirovic DB. Development of immortalized human

- cerebromicrovascular endothelial cell line as in vitro model of the human blood–brain barrier. FASEB J. 1997;11:1187.
- 149. Mackic JB, Stins M, Mccomb JG, Calero M, Ghiso J, Kim KS, et al. Human blood-brain barrier receptors for Alzheimer's amyloid-beta 1–40 - Asymmetrical binding, endocytosis, and transcytosis at the apical side of brain microvascular endothelial cell monolayer. J Clin Invest. 1998;102:734–43.
- Stins MF, Badger J, Sik Kim K. Bacterial invasion and transcytosis in transfected human brain microvascular endothelial cells. Microb Pathog. 2001;30:19–28.
- 151. Jong AY, Stins MF, Huang SH, Chen SHM, Kim KS. Traversal of Candida albicans across human blood–brain barrier In vitro. Infect Immun. 2001;69:4536–44.
- 152. Megard I, Garrigues A, Orlowski S, Jorajuria S, Clayette P, Ezan E, et al. A co-culture-based model of human blood-brain barrier: application to active transport of indinavir and in vivo-in vitro correlation. Brain Res. 2002;927:153–67.
- 153. Yang T, Roder KE, Abbruscato TJ. Evaluation of bEnd5 cell line as an in vitro model for the blood–brain barrier under normal and hypoxic/aglycemic conditions. J Pharm Sci. 2007;96:3196–213.
- 154. Zenker D, Begley D, Bratzke H, Rübsamen-Waigmann H, von Briesen H. Human blood-derived macrophages enhance barrier function of cultured primary bovine and human brain capillary endothelial cells. J Physiol. 2003;551:1023–32.
- Schulze C, Smales C, Rubin LL, Staddon JM. Lysophosphatidic acid increases tight junction permeability in cultured brain endothelial cells. J Neurochem. 1997;68:991–1000.
- Gloor SM, Weber A, Adachi N, Frei K. Interleukin-1 modulates protein tyrosine phosphatase activity and permeability of brain endothelial cells. Biochem Biophys Res Commun. 1997;239:804–9.
- 157. Hoheisel D, Nitz T, Franke H, Wegener J, Hakvoort A, Tilling T, Galla HJ. Hydrocortisone reinforces the blood–brain barrier properties in a serum free cell culture system (vol 244, pg 312, 1998). Biochem Biophys Res Commun. 1998;247:536-+.
- Tilling T, Korte D, Hoheisel D, Galla HJ. Basement membrane proteins influence brain capillary endothelial barrier function in vitro. J Neurochem. 1998;71:1151–7.
- 159. Franke H, Galla HJ, Beuckmann CT. An improved low-permeability in vitro-model of blood-brain barrier: transport studies on retinoids, sucrose, haloperidol, caffeine and mannitol. Brain Res. 1999:818:65–71.
- 160. Nitz T, Eisenblatter T, Psathaki K, Galla HJ. Serum-derived factors weaken the barrier properties of cultured porcine brain capillary endothelial cells in vitro. Brain Res. 2003;981:30–40.
- 161. Igarashi Y, Utsumi H, Chiba H, Yamada-Sasamori Y, Tobioka H, Kamimura Y, et al. Glial cell line-derived neurotrophic factor induces barrier function of endothelial cells forming the bloodbrain barrier. Biochem Biophys Res Commun. 1999;261:108–12.
- 162. Yamagata K, Tagami M, Takenaga F, Yamori Y, Nara Y, Itoh S. Polyunsaturated fatty acids induce tight junctions to form in brain capillary endothelial cells. Neuroscience. 2003;116:649–56.
- 163. Franke H, Galla HJ, Beuckmann CT. Primary cultures of brain microvessel endothelial cells: a valid and flexible model to study drug transport through the blood–brain barrier in vitro. Brain Res Protocol. 2000;5:248–56.
- 164. Lohmann C, Hüwel S, Galla HJ. Predicting blood-brain barrier permeability of drugs: evaluation of different in vitro assays. J Drug Target. 2002;10:263–76.
- 165. Smith M, Omidi Y, Gumbleton M. Primary porcine brain microvascular endothelial cells: biochemical and functional characterisation as a model for drug transport and targeting. J Drug Target. 2007;15:253–68.
- 166. Bernas MJ, Cardoso FL, Daley SK, Weinand ME, Campos AR, Ferreira AJG, et al. Establishment of primary cultures of human brain microvascular endothelial cells to provide an in vitro cellular model of the blood–brain barrier. Nat Protoc. 2010;5:1265–72.



- 167. Ramirez SH, Hasko J, Skuba A, Fan S, Dykstra H, McCormick R, et al. Activation of cannabinoid receptor 2 attenuates leukocyteendothelial cell interactions and blood–brain barrier dysfunction under inflammatory conditions. J Neurosci. 2012;32:4004–16.
- 168. Benistant C, Dehouck MP, Fruchart JC, Cecchelli R, Lagarde M. Fatty-acid composition of brain capillary endothelial-cells effect of the coculture with astrocytes. J Lipid Res. 1995;36:2311–9.
- Edgell CJ, Mcdonald CC, Graham JB. Permanent cell-line expressing human factor-Viii-related antigen established by hybridization. Proc Natl Acad Sci USA. 1983;80:3734–7.
- 170. Shay JW, Wright WE, Werbin H. Defining the molecular mechanisms of human cell immortalization. Biochim Biophys Acta. 1991;1072:1–7.
- Kirinaka H, Miyake K, Iijima S. Isolation of immortal human endothelial cells. Biosci Biotechnol Biochem. 1995;59:912

 –4.
- 172. Roux F, Durieu-Trautmann O, Chaverot N, Claire M, Mailly P, Bourre JM, et al. Regulation of g-glutamyl transpeptidase and alkaline phosphatase activities in immortalized rat brain microvessel endothelial cells. J Cell Physiol. 1994;159:101–13.
- 173. Sobue K, Yamamoto N, Yoneda K, Hodgson ME, Yamashiro K, Tsuruoka N, et al. Induction of blood—brain barrier properties in immortalized bovine brain endothelial cells by astrocytic factors. Neurosci Res. 1999;35:155–64.
- 174. Weksler BB, Subileau EA, Perriere N, Charneau P, Holloway K, Leveque M, et al. Blood-brain barrier-specific properties of a human adult brain endothelial cell line. FASEB J. 2005;19:187. -+.
- 175. Kannan R, Chakrabarti R, Tang D, Kim KJ, Kaplowitz N. GSH transport in human cerebrovascular endothelial cells and human astrocytes: evidence for luminal localization of Na+-dependent GSH transport in HCEC. Brain Res. 2000;852:374–82.
- 176. Gu X, Zhang J, Brann DW, Yu FS. Brain and retinal vascular endothelial cells with extended life span established by ectopic expression of telomerase. Invest Ophthalmol Vis Sci. 2003;44:3219–25.
- 177. Hurst RD, Fritz IB. Properties of an immortalised vascular endothelial/glioma cell co-culture model of the blood–brain barrier. J Cell Physiol. 1996;167:81–8.
- 178. Hurst RD, Heales SJR, Dobbie MS, Barker JE, Clark JB. Decreased endothelial cell glutathione and increased sensitivity to oxidative stress in an in vitro blood–brain barrier model system. Brain Res. 1998;802:232–40.
- 179. Dobbie MS, Hurst RD, Klein NJ, Surtees RAH. Upregulation of intercellular adhesion molecule-1 expression on human endothelial cells by tumour necrosis factor-alpha in an in vitro model of the blood-brain. Brain Res. 1999;830:330-6.
- 180. Scism JL, Laska DA, Horn JW, Gimple JL, Pratt SE, Shepard RL, et al. Evaluation of an in vitro coculture model for the blood-brain barrier: comparison of human umbilical vein endothelial cells (ECV304) and rat glioma cells (C6) from two commercial sources. In Vitro Cell Dev Biol Anim. 1999;35(10):580–92.
- Easton AS, Abbott NJ. Bradykinin increases permeability by calcium and 5-lipoxygenase in the ECV304/C6 cell culture model of the blood-brain barrier. Brain Res. 2002;953:157–69.
- 182. Hosoya K, Tetsuka K, Nagase K, Tomi M, Saeki S, Ohtusuki S, et al. Conditionally immortalized brain capillary endothelial cell lines established from a transgenic mouse harboring temperature-sensitive simian virus 40 large T-antigen gene. AAPS Pharm Sci. 2000:2:1–11
- 183. Youdim KA, Dobbie MS, Kuhnle G, Proteggente AR, Abbott NJ, Rice-Evans C. Interaction between flavonoids and the bloodGÇôbrain barrier: in vitro studies. J Neurochem. 2003;85:180–92.
- 184. Rist RJ, Romero IA, Chan MWK, Couraud PO, Roux F, Abbott NJ. F-actin cytoskeleton and sucrose permeability of immortalised rat brain microvascular endothelial cell monolayers: effects of cyclic AMP and astrocytic factors. Brain Res. 1997;768:10–8.

- 185. Mertsch K, Blasig I, Grune T. 4-Hydroxynonenal impairs the permeability of an in vitro rat blood-brain barrier. Neurosci Lett. 2001;314:135–8.
- 186. Romero IA, Rist RJ, Aleshaiker A, Abbott NJ. Metabolic and permeability changes caused by thiamine deficiency in immortalized rat brain microvessel endothelial cells. Brain Res. 1997;756:133–40.
- 187. Romero IA, Prevost MC, Perret E, Adamson P, Greenwood J, Couraud PO, et al. Interactions between brain endothelial cells and human T-cell leukemia virus type 1-infected lymphocytes: Mechanisms of viral entry into the central nervous system. J Virol. 2000;74:6021–30.
- 188. Romero IA, Radewicz K, Jubin E, Michel CC, Greenwood J, Couraud PO, et al. Changes in cytoskeletal and tight junctional proteins correlate with decreased permeability induced by dexamethasone in cultured rat brain endothelial cells. Neurosci Lett. 2003;344:112–6.
- 189. Poller B, Gutmann H, Krahenbuhl S, Weksler B, Romero I, Couraud PO, et al. The human brain endothelial cell line hCMEC/D3 as a human blood-brain barrier model for drug transport studies. J Neurochem. 2008;107:1358–68.
- 190. Kiss L, Walter FR, Bocsik A, Veszelka S, Ozsvari B, Puskas LG, et al. Kinetic analysis of the toxicity of pharmaceutical excipients cremophor EL and RH40 on endothelial and epithelial cells. J Pharm Sci. 2013;102(4):1173–81.
- 191. Daniels BP, Cruz-Orengo L, Pasieka TJ, Couraud PO, Romero IA, Weksler B, et al. Immortalized human cerebral microvascular endothelial cells maintain the properties of primary cells in an in vitro model of immune migration across the blood brain barrier. J Neurosci Methods. 2013;212:173–9.
- 192. Ohtsuki S, Ikeda C, Uchida Y, Sakamoto Y, Miller F, Glacial F, et al. Quantitative targeted absolute proteomic analysis of transporters, receptors and junction proteins for validation of human cerebral microvascular endothelial cell line hCMEC/D3 as a human blood-brain barrier model. Mol Pharm. 2012;10:289–96.
- 193. Markoutsa E, Pampalakis G, Niarakis A, Romero IA, Weksler B, Couraud PO, et al. Uptake and permeability studies of BBBtargeting immunoliposomes using the hCMEC/D3 cell line. Eur J Pharm Biopharm. 2011;77:265–74.
- 194. Nakagawa S, Deli MA, Kawaguchi H, Shimizudani T, Shimono T, Kittel A, et al. A new blood–brain barrier model using primary rat brain endothelial cells, pericytes and astrocytes. Neurochem Int. 2009;54:253–63.
- 195. Gaillard PJ, Voorwinden LH, Nielsen JL, Ivanov A, Atsumi R, Engman H, et al. Establishment and functional characterization of an in vitro model of the blood–brain barrier, comprising a coculture of brain capillary endothelial cells and astrocytes. Eur J Pharm Sci. 2001;12:215–22.
- 196. Janzer RC, Raff MC. Astrocytes induce blood-brain barrier properties in endothelial cells. Nature. 1987;325:253–7.
- 197. Fenart L, Buee-Scherrer V, Descamps L, Duhem C, Poullain MG, Cecchelli R, et al. Inhibition of P-glycoprotein: rapid assessment of its implication in blood–brain barrier integrity and drug transport to the brain by an in vitro model of the blood–brain barrier. Pharm Res. 1998;15:993–1000.
- 198. Calabria AR, Weidenfeller C, Jones AR, De Vries HE, Shusta EV. Puromycin-purified rat brain microvascular endothelial cell cultures exhibit improved barrier properties in response to glucocorticoid induction. J Neurochem. 2006;97:922–33.
- 199. Dohgu S, Takata F, Yamauchi A, Nakagawa S, Egawa T, Naito M, et al. Brain pericytes contribute to the induction and upregulation of blood–brain barrier functions through transforming growth factor-beta production. Brain Res. 2005;1038:208–15.
- 200. Dehouck MP, Jolliet-Riant P, Brée F, Fruchart JC, Cecchelli R, Tillement JP. Drug transfer across the blood–brain barrier: correlation between in vitro and in vivo models. J Neurochem. 1992;58:1790–7.



- Wang Q, Rager JD, Weinstein K, Kardos PS, Dobson GL, Li JB, et al. Evaluation of the MDR-MDCK cell line as a permeability screen for the blood-brain barrier. Int J Pharm. 2005;288:349–59.
- Hakkarainen JJ, Jalkanen AJ, Kääriäinen TM, Keski-Rahkonen P, Venäläinen T, Hokkanen J, et al. Comparison of in vitro cell models in predicting in vivo brain entry of drugs. Int J Pharm. 2010;402:27–36.
- Lacombe O, Videau O, Chevillon D, Guyot AC, Contreras C, Blondel S, et al. In vitro primary human and animal cell-based blood-brain barrier models as a screening tool in drug discovery. Mol Pharm. 2011;8:651–63.
- 204. Ball K, Bouzom F, Scherrmann JM, Walther B, Declèves X. Development of a physiologically based pharmacokinetic model for the rat central nervous system and determination of an in vitroin vivo scaling methodology for the blood–brain barrier permeability of two transporter substrates, morphine and oxycodone. J Pharm Sci. 2012;101:4277–92.
- Lu W, Tan YZ, Jiang XG. Establishment of coculture model of blood-brain barrier in vitro for nanoparticle's transcytosis and toxicity evaluation. Acta Pharm Sin. 2006;41:296–304.
- 206. Ragnaill MN, Brown M, Ye D, Bramini M, Callanan S, Lynch I, et al. Internal benchmarking of a human blood–brain barrier cell model for screening of nanoparticle uptake and transcytosis. Eur J Pharm Biopharm. 2011;77:360–7.
- Yousif S, Marie-Claire C, Roux F, Scherrmann JM, Declèves X. Expression of drug transporters at the blood-brain barrier using an optimized isolated rat brain microvessel strategy. Brain Res. 2007;1134:1-11.
- 208. Miller DS, Nobmann SN, Gutmann H, Toeroek M, Drewe J, Fricker G. Xenobiotic transport across isolated brain microvessels studied by confocal microscopy. Mol Pharmacol. 2000;58:1357– 67.
- 209. Durk MR, Chan GN, Campos CR, Peart JC, Chow EC, Lee E, et al. 1a,25-Dihydroxyvitamin D3-liganded vitamin D receptor increases expression and transport activity of P-glycoprotein in isolated rat brain capillaries and human and rat brain microvessel endothelial cells. J Neurochem. 2012;123:944–53.
- Pardridge WM. Log(BB), PS products and in silico models of drug brain penetration. Drug Discov Today. 2004;9:392–3.
- Boje KMK. In vivo measurement of blood-brain barrier permeability. In: Current Protocols in Neuroscience. John Wiley & Sons, Inc.; 2001.
- Ohno K, Pettigrew KD, Rapoport SI. Lower limits of cerebrovascular permeability to nonelectrolytes in the conscious rat. Am J Physiol Heart Circ Physiol. 1978;235:H299–307.
- 213. Kalvass JC, Maurer TS, Pollack GM. Use of plasma and brain unbound fractions to assess the extent of brain distribution of 34 drugs: comparison of unbound concentration ratios to in vivo Pglycoprotein efflux ratios. Drug Metab Dispos. 2007;35:660–6.
- 214. Young RC, Mitchell RC, Brown TH, Ganellin CR, Griffiths R, Jones M, et al. Development of a new physicochemical model for brain penetration and its application to the design of centrally acting H₂ receptor histamine antagonists. J Med Chem. 1988;31:656–71.
- 215. Rohanova M, Balikova M. Studies on distribution and metabolism of para-methoxymethamphetamine (PMMA) in rats after subcutaneous administration. Toxicology. 2009;259:61–8.
- 216. Friden M, Ljungqvist H, Middleton B, Bredberg U, Hammarlund-Udenaes M. Improved measurement of drug exposure in the brain using drug-specific correction for residual blood. J Cereb Blood Flow Metab. 2009;30:150–61.
- Dash AK, Elmquist WF. Separation methods that are capable of revealing blood-brain barrier permeability. J Chromatogr B. 2003;797:241-54.
- Elmquist WF, Sawchuk RJ. Application of microdialysis in pharmacokinetic studies. Pharm Res. 1997;14:267–88.

- 219. Gupta A, Chatelain P, Massingham R, Jonsson EN, Hammarlund-Udenaes M. Brain distribution of cetirizin enantiomers: comparison of three different tissue-to-plasma partition coefficients: Kp, Kp, u, and Kp, uu. Drug Metab Dispos. 2006;34(2):318–23.
- 220. Friden M, Ducrozet F, Middleton B, Antonsson M, Bredberg U, Hammarlund-Udenaes M. Development of a high-throughput brain slice method for studying drug distribution in the central nervous system. Drug Metab Dispos. 2009;37:1226–33.
- 221. Friden M, Gupta A, Antonsson M, Bredberg U, Hammarlund-Udenaes M. In vitro methods for estimating unbound drug concentrations in the brain interstitial and intracellular fluids. Drug Metab Dispos. 2007;35:1711–9.
- 222. Bonate PL. Animal-models for studying transport across the blood–brain-barrier. J Neurosci Methods. 1995;56:1–15.
- Oldendorf WH, Stoller BE, Tishler TA, Williams JL, Oldendorf SZ. Transient blood-brain barrier passage of polar compounds at low pH. Am J Physiol Heart Circ Physiol. 1994;267:H2229-36.
- Takasato Y, Rapoport SI, Smith QR. An insitu brain perfusion technique to study cerebrovascular transport in the rat. Am J Physiol. 1984;247:H484–93.
- 225. Cannon RE, Peart JC, Hawkins BT, Campos CR, Miller DS. Targeting blood–brain barrier sphingolipid signaling reduces basal P-glycoprotein activity and improves drug delivery to the brain. Proc Natl Acad Sci. 2012;109:15930–5.
- 226. Kakee A, Terasaki T, Sugiyama Y. Selective brain to blood efflux transport of para-aminohippuric acid across the blood–brain barrier: in vivo evidence by use of the brain efflux index method. J Pharmacol Exp Ther. 1997;283:1018–25.
- Syvänen S, Eriksson J. Advances in PET imaging of Pglycoprotein function at the blood-brain barrier. ACS Chem Neurosci.; 2013;4(2):225–37.
- 228. Wanek T, Kuntner C, Bankstahl JP, Mairinger S, Bankstahl M, Stanek J, et al. A novel PET protocol for visualization of breast cancer resistance protein function at the blood–brain barrier. J Cereb Blood Flow Metab. 2012;32:2002–11.
- 229. Knight RA, Karki K, Ewing JR, Divine GW, Fenstermacher JD, Patlak CS, et al. Estimating blood and brain concentrations and blood-to-brain influx by magnetic resonance imaging with stepdown infusion of Gd-DTPA in focal transient cerebral ischemia and confirmation by quantitative autoradiography with Gd-[lsqb]14C[rsqb]DTPA. J Cereb Blood Flow Metab. 2009;29:1048–58.
- 230. Serres S, Soto MS, Hamilton A, McAteer MA, Carbonell WS, Robson MD, et al. Molecular MRI enables early and sensitive detection of brain metastases. Proc Natl Acad Sci. 2012;109: 6674–9.
- 231. van de Ven KCC, van der Graaf M, Tack CJ, Heerschap A, de Galan BE. Steady-state brain glucose concentrations during hypoglycemia in healthy humans and patients with type 1 diabetes. Diabetes. 2012;61:1974–7.
- 232. Culot M, Lundquist S, Vanuxeem D, Nion S, Landry C, Delplace Y, et al. An in vitro blood–brain barrier model for high throughput (HTS) toxicological screening. Toxicol in Vitro. 2008;22:799–811.
- 233. Sano Y, Shimizu F, Abe M, Maeda T, Kashiwamura Y, Ohtsuki S, et al. Establishment of a new conditionally immortalized human brain microvascular endothelial cell line retaining an in vivo bloodGÇôbrain barrier function. J Cell Physiol. 2010;225:519–28.
- 234. Balbuena P, Li W, Magnin-Bissel G, Meldrum JB, Ehrich M. Comparison of two blood-brain barrier in vitro systems: cytotoxicity and transfer assessments of malathion/oxon and lead acetate. Toxicol Sci. 2010;114:260–71.
- Roux F, Couraud PO. Rat brain endothelial cell lines for the study of blood–brain barrier permeability and transport functions. Cell Mol Neurobiol. 2005;25:41–57.



- 236. Shayan G, Choi YS, Shusta EV, Shuler ML, Lee KH. Murine in vitro model of the blood–brain barrier for evaluating drug transport. Eur J Pharm Sci. 2011;42:148–55.
- 237. Coisne C, Dehouck L, Faveeuw C, Delplace Y, Miller F, Landry C, et al. Mouse syngenic in vitro blood—brain barrier model: a new tool to examine inflammatory events in cerebral endothelium. Lab Investig. 2005;85:734–46.
- 238. Dehouck B, Dehouck MP, Fruchart JC, Cecchelli R. Upregulation of the low-density-lipoprotein receptor at the blood-brain-barrier Intercommunications between brain capillary endothelial-cells and astrocytes. J Cell Biol. 1994;126:465–73.
- Descamps L, Dehouck MP, Torpier G, Cecchelli R. Receptormediated transcytosis of transferrin through blood-brain barrier endothelial cells. Am J Physiol Heart Circ Physiol. 1996;270:H1149

 –58.

